THE ROLE OF RUVBL1/RUVBL2 AND THEIR POTENTIAL AS THERAPEUTIC TARGETS IN NON-SMALL CELL LUNG CANCER

APPROVED BY SUPERVISORY COMMITTEE

_____

John Minna, MD

_____

Ralf Kittler, PhD

_____

Ralph Deberardinis, MD, PhD

_____

David Mangelsdorf, PhD

_____

Lee Kraus, PhD

DEDICATION

To my mentors, my family, and my love

THE ROLE OF RUVBL1/RUVBL2 AND THEIR POTENTIAL AS THERAPEUTIC TARGETS IN NON-SMALL CELL LUNG CANCER

by

PAUL MATTHEW YENERALL

DISSERTATION

Presented to the Faculty of the Graduate School of Biomedical Sciences

The University of Texas Southwestern Medical Center at Dallas

In Partial Fulfillment of the Requirements

For the Degree of

DOCTOR OF PHILOSOPHY

The University of Texas Southwestern Medical Center at Dallas

Dallas, Texas

August 2019

ACKNOWLEDGEMENTS

They say it takes a village to raise a child. There is truth to this statement. In my case, it took two labs, two mentors, and whole bunch of lab mates to raise a graduate student. It is to these people that I will be forever grateful for passing along the gift of science, reasoning and curiosity.

Starting in chronological order, I'd like to especially thank Dr. Chunli Shao, who had the unfortunate luck of advising me during my rotation in the Minna lab. She is a wonderful scientist and teacher, but furthermore, even early on Chunli was my most adamant supporter and advocate. At a time in graduate school when I really needed someone to believe in me and reaffirm my ability to do science, Chunli was there. I will be forever grateful to Chunli for shepherding me into the Minna lab and giving me the confidence and skills I needed to tackle graduate school.

I'd like to thank and acknowledge my sounding board for all scientific ideas throughout graduate school, Dr. Mike Peyton. Mike's passion for science, discovery and the truth is immense, and the fact that so many people call Mike "our sounding board" is a testament to the type of scientist he is. Mike will steer your project, help you design a well-controlled experiment, or just shoot the breeze about a scientific idea or project at the drop of a dime. Our discussions have helped mold how I both view and approach science, especially translational science.

I'd like to take time to thank everyone here at UT Southwestern Medical Center who helped contribute directly to my paper. Dr. Amit Das played a huge role in shaping my manuscript and thesis by showing that inhibition of RUVBL1 or RUVBL2 radiosensitizes non-small cell lung cancer cell lines. Amit is fun, easy going guy with strong technical prowess, which makes him an amazing collaborator - he produces the smallest error bars you've ever seen in your life. Rahul Kollipara is a bioinformatician whose skill in analyzing the RNA-seq,

DNA-seq and other -omic's datasets was absolutely essential. Anyone can mix two ingredients in a test tube, but it takes supreme patience and intelligence to process and handle data large datasets flawlessly like Rahul. Dr. Long Shan Li is an extremely talented pathologist and bench scientist who knows and has done basically every experiment and whose advice and hands have helped me throughout graduate school. I'm starting to think I can make-up assays and Long Shan will say "I know how to do this. Easy". Dr. Brenda Timmons, the former Minna lab manager, is a seamless coordinator who is passionate about supporting and maximizing the potential of everyone. Her continued help, support, and food (she is a ridiculously good cook, like seriously) has literally fueled me through most of graduate school. Dr. Kenneth Huffman is a talented and witty scientist that contributed the idea that sparked my thesis project, and along with my friend Dr. Ryan Carstens, was a major driving force in shaping my project and my technical abilities early on in graduate school. Dr. Carstens and Dr. Huffman also performed the siRNA screen that is in this thesis and led to my project. Dr. Shan Wang is an immensely talented biochemist who has helped teach me various techniques and principles. He is my go-to troubleshooter, which says a lot about his technical and analytical abilities. I'd also like to thank all the individuals in Igancio Wistuba's lab at UT MD Anderson that were a tremendous help in performing immunohistochemistry– Jaime Rodrigeuz-Canales, Pamela Villabolos, Louisa Solis Maren and Barbara Mino.

Even when individuals didn't help me directly with my work, they helped me indirectly by providing a caring, supportive, fun and engaging work environment. My good friends Drs. Suzie Height and Patrick Dospoy, as well as the newer graduate students Josiah Flaming and Aiden Nguyen, were great examples of this – without them the Minna lab would not have had the same cheerful dynamics it has maintained, and I would not have enjoyed my time in the Minna lab so much. I'd also like to thank Drs. Boning Gao, Sam Huang, Luc Girard, Kim Avilla and Hyunsil Park. You are all awesome and I'm going to miss working with all of you.

My thesis committee members, Drs. Ralph Deberardinis, David Mangelsdorf and Lee Kraus, have been constant sources of friendly advice, encouragement, and wonderful ideas. It is humbling to interact with and get advice from such respected, accomplished and immensely intelligent scientists. Additionally, while some committee members tend to battle their students, my committee has been nothing but a positive guiding force, and for that I am extremely grateful.

Last but not least, I'd like to thank my mentors, Drs. John Minna and Ralf Kittler. While both are supremely intelligent, dedicated and collaborative scientists, their different strengths have taught me lessons I will never forget. Ralf has an immensely sharp wit, eye for technical details, and strong background in molecular biology. John, on the other hand, has tremendous people skills, great collaborative intuition and a strong background in treating and researching lung cancer - some may even say he's a giant in the field of lung cancer, although he is certainly the most friendly and supportive giant there could be. From Ralf, I've learnt about performing thorough, logic-based science, how to adapt, hone and utilize use my skills in molecular biology, and how to pay attention to all the details, big and small. From John, I've learned how to forge collaborations, navigate a politically hostile environment, and most importantly, how to handle myself professionally – I've never met a cooler operator than Dr. Minna. I feel that both of my mentors have done a tremendous job equipping me with the skills and support that I need to further both my career and myself personally, and for that I will be forever grateful. I only hope I can pass along the valuable skills they gave me to others.

THE ROLE OF RUVBL1/ RUVBL2 AND THEIR POTENTIAL AS THERAPEUTIC TARGETS IN NON-SMALL CELL LUNG CANCER

PAUL M. YENERALL, PhD

The University of Texas Southwestern Medical Center at Dallas, 2019

John D. Minna, MD and Ralf Kittler, PhD

Behind heart disease, cancer is the leading cause of death today in Americans. Among cancers, lung cancer is the deadliest, killing as many individuals as next 3 most lethal cancer types combined. Approximately 80% of lung cancers are a type known as non-small cell lung cancer (NSCLC), and despite numerous advances in the treatment of NSCLC, only 18% of all NSCLC patients live 5 years after their initial diagnosis. To identify new therapeutic targets in NSCLC, we performed a viability-based RNA interference (RNAi) screen targeting nuclear receptors,

their coregulators and chromatin remodelers. This screen identified RUVBL1 and RUVBL2 (collectively referred to as RUVBL1/2) as differentially required for the viability of NSCLC. We show that RUVBL1/2 require their ATPase activity to support NSCLC viability and have developed an orally bioavailable, potent and specific inhibitor of RUVBL1/2 ATPase activity, known as Compound B. Multiple unbiased analyses suggested that RUVBL1/2 may have roles in DNA replication in NSCLC, and inhibition or depletion of RUVBL1/2 in sensitive NSCLC lines delays S-phase progression and ultimately results in cancer cell death via replication catastrophe. While Compound B treatment *in vivo* produces modest anti-tumor activity, only a subset of NSCLC cell lines show a therapeutically meaningful response. To enhance the efficacy of Compound B, we searched for therapies that may synergize with Compound B. Various analyses indicated that RUVBL1/2 may have roles in the response to ionizing radiation (IR), and indeed, genetic depletion or pharmacological inhibition of RUVBL1/2 radiosensitized NSCLC cell lines and patient tumors both *in vitro* and *in vivo*. Interestingly, Compound B, did not radiosensitize models of non-transformed cells, potentially because key DNA damage proteins such as ATM and DNA-PK_{cs} were more stable after Compound B treatment in normal cells than in tumor cells. The combined necessity of RUVBL1/2 for NSCLC viability and the recovery from radiation, specifically in tumor cells, make RUVBL1/2 an attractive target for future preclinical development as a radiosensitizer in NSCLC.

TABLE OF CONTENTS

TITLE FLY i

DEDICATION ii

TITLE PAGE iii

ACKNOWLEDGEMENTS iv

ABSTRACT vii

TABLE OF CONTENTS ix

PRIOR PUBLICATIONS xiv

LIST OF FIGURES xv

LIST OF TABLES xvii

LIST OF APPENDICES xvii

LIST OF ABBREVIATIONS xix

CHAPTER ONE: Introduction 1

1.1 What is lung cancer? 1

1.2 Current treatments for non-small cell lung cancer 4

1.3 Nuclear receptors, their coregulators and chromatin remodelers in NSCLC 6

1.4 The AAA+ ATPases RUVBL1 and RUVBL2 8

1.5 The cell cycle, with an emphasis on DNA replication 14

1.6 DNA repair 21

1.7 Ionizing radiation 27

1.8 Goals of this study 30

CHAPTER TWO: Materials and Methods 31

2.1 Cell lines 31

2.2 Cell culture 31

2.3 Animal studies 32

2.4 Inhibitors/drugs used 32

2.5 Antibodies 33

2.6 esiRNA production 34

2.7 siRNA and esiRNA transfection in 6-well plates 34

2.8 siRNA and esiRNA transfections in 96-well plates 36

2.9 Immunohistochemistry (IHC) 37

2.10 Immunoblots 39

2.11 Plasmid transfection 40

2.12 Lentivirus generation and transduction 41

2.13 qPCR 41

2.14 PCR mutagenesis strategy to identify Compound B-resistance conferring mutations 42

2.15 Immunoprecipitation 44

2.16 Mass Spectrometry.....46

2.17 Chemical screening strategy for Compound B and RUVBL1/2 ATPase activity 48

2.18 Pharmacokinetics for Compound B.....49

2.19 Viability-based drug dose-response curves 49

2.20 RNA-sequencing 50

2.21 GSEA analysis.....50

2.22 Xenograft studies.....51

2.23 Isolation of proteins on nascent DNA (iPOND).....52

2.24 Flow cytometry experiments 54

2.25 Immunofluorescence 57

2.26 Surviving fraction curves.....58

CHAPTER THREE: Viability-Based RNAi Screening of NRs, Coregulators, and Chromatin Remodelers in NSCLC.....59

3.1 Introduction.....59

3.2 Results 61

3.2.1 A Viability-Based siRNA Screen of NRs, Their Coregulators and Chromatin Remodelers in NSCLC.....61

3.2.2 Validation of the siRNA Screen of NRs, Their Coregulators and Chromatin Remodelers using esiRNAs 66

3.3 Discussion 81

CHAPTER FOUR: The Identification and Exploration of RUVBL1 and RUVBL2 as Potential Therapeutic Targets in NSCLC 84

4.1 Introduction....84

4.2 Results 86

4.2.1 RUVBL1/2 are Overexpressed in NSCLC Patient Tumors and High Expression Correlates with Poor Overall Survival....86

4.2.2 RUVBL1/2 ATPase Activity are Required for NSCLC Growth *In Vitro* 90

4.2.3 Development and Validation of a RUVBL1/2 ATPase Inhibitor, Compound B 96

4.2.4 Validating the On-Target Activity of Compound B....103

4.2.5 Many of RUVBL1/2's Cellular Functions Likely Require ATPase Activity....109

4.2.6. Acute Inhibition of RUVBL1/2 ATPase Activity Inhibits PAQosome Maturation but not the INO80-family of Chromatin Remodelers....110

4.2.7 NSCLC Primarily Require RUVBL1/2 for Viability for Efficient DNA Replication 113

4.2.8 Inhibition of the ATPase Activity of RUVBL1/2 Radiosensitizes NSCLC, but not Normal Cells 128

4.3 Discussion....135

CHAPTER FIVE: Conclusions....141

APPENDIX A 147

APPENDIX B 183

APPENDIX C 225

APPENDIX D 268

APPENDIX E 289

BIBLIOGRAPHY 337

PRIOR PUBLICATIONS

M. Dalvi, L. Wang, R. Zhong, R. Kollipara, H. Park, J. Bayo, **P. Yenerall**, Y. Zhou, B. Timmons, J. Rodriguez-Canales, C. Behrens, B. Mino, P. Villalobos, E. Parra, M. Suraokar, A. Patae, S. Swisher, N. Kalhor, N. Bhanu, B. Garcia, J. Heymach, K. Coombes, Y. Xie, L. Girard, A. Gazdar, R. Kittler, I. Wistuba, J. Minna, E. Martinez. (2017) *Taxane-Platin-Resistant Lung Cancers Co-develop Hypersensitivity to JumonjiC Demethylase Inhibitors*. Cell Reports, 19(8):1669-1684.

S. Kasiri, C. Shao, B. Chen, A. Wilson, **P. Yenerall**, B. Timmons, L. Girard, H. Tian, C. Behrens, I. Wistuba, A. Gazdar, J. Kim. (2017) *GLI1 blockade potentiates the antitumor activity of PI3K antagonists in lung squamous cell carcinoma.* Cancer Research, in press.

P. Yenerall, R. Kittler (2015). *Familiar Faces in Unfamiliar Places: The Emerging Role of Nuclear Receptors in Lung Cancer*. Molecular Endocrinology, 29(12):1675-1683.

Leung W., …, **P. Yenerall**, …, Elgin SC. (2015) *Drosophila Muller F Elements Maintain a Distinct Set of Genomic Properties Over 40 Million Years of Evolution*. G3: Genes, Genomes, Genetics, 5(5):719-741

P. Yenerall, R. Kittler. (2014) *Harnessing the Nuclear Receptor PPARγ to Inhibit the Growth of Lung Adenocarcinoma by Rewiring Metabolic Circuitries*. Molecular and Cellular Oncology, 2(2).

C. Shao, J.P. Sullivan, L. Girard, A. Augustyn, **P. Yenerall**, J. Rodriguez, H. Liu, C. Behrens, J. Shay, I. Wistuba, J. Minna. (2014) *Essential role of the aldehyde dehydrogenase 1A3 (ALDH1A3) for the maintenance of non-small cell lung cancer stem cells is associated with the STAT3 pathway*. Clinical Cancer Research, 20(15):4154-66

LIST OF FIGURES

FIGURE 1.1. Schematic Depicting the Initiation of DNA Replication 16

FIGURE 3.1. Results of Viability-Based of siRNA Screen of NR + CoRegulator (Library 1) and Remodeler (Library 2) in Approximately 50 NSCLC Cell Lines and HBECs. 65

FIGURE 3.2. Results of Viability-Based of esiRNA Screen of NR + CoRegulator (Library 1) and Remodeler (Library 2) in Approximately 15 NSCLC Cell Lines and HBECs 75

FIGURE 3.3. Resynthesis of esiRNF4 Shows That This esiRNA Likely Triggers Cell Death via the Interferon Response.....76

FIGURE 3.4. Unsupervised Hierarchical Clustering of esiRNA and siRNA Phenotypes.....77

FIGURE 3.5. Pairwise Correlations of siRNA and esiRNA Phenotypes.....78

FIGURE 3.6. Comparison of Knock Down Efficiency of esiRNAs and siRNAs 79

FIGURE 3.7. esiRNAs Targeting the Same Targets as siRNAs do not Decrease Cell Viability .80

FIGURE 3.8. Deconvolution Analysis Fails to Identify Pools of Off-Target siRNAs.....81

FIGURE 4.1. Depletion of RUVBL1 or RUVBL2 in esiRNA and siRNA Screens Consistently Showed Toxicity in Some NSCLC Cell Lines. 86

FIGURE 4.2. RUVBL1/2 Expression in NSCLC is Elevated and High Expression Predicts Poor Patient Survival.....87

FIGURE 4.3. RUVBL1 Protein Expression in NSCLC is Higher in Squamous Cell Carcinoma and Patients with Smoking History.....90

FIGURE 4.4. Effect of RUVBL1/2 Depletion in 24 NSCLC Cell Lines.....92

FIGURE 4.5. Both esiRNAs and siRNAs Targeting RUVBL1 or RUVBL2 Kill NSCLC due to On-Target Activities. 93

FIGURE 4.6. Genetic Rescue Experiments Demonstrate the Necessity of RUVBL1/2 ATPase Activity for NSCLC Cell Growth.....95

FIGURE 4.7. Development of Compound B, a RUVBL1/2 ATPase Inhibitor 98

FIGURE 4.8. Compound B can be Administered Orally 101

FIGURE 4.9 Compound B Inhibits RUVBL1/2 in an On-Target Manner and Resistance Mutations Cluster on the 3D Structure of RUVBL1/2.....105

FIGURE 4.10. Mutations in RUVBL1/2 Identified in PCR-based Mutagenesis Screen as Compound B Resistance Mutations do Confer Resistance to Compound B.....108

FIGURE 4.11. RNA-seq Profiling Suggests Many of RUVBL1/2's Cellular Functions Likely Require ATPase Activity. 110

FIGURE 4.12. Inhibition of RUVBL1/2 ATPase Activity Causes Accumulation of PAQosome Components but not INO80-family of Chromatin Remodelers 111

FIGURE 4.13. Correlative Analyses Implicate RUVBL1/2 in DNA Replication in NSCLC 114

FIGURE 4.14. Inhibition or Depletion of RUVBL1/2 Interferes with S-phase Progression in NSCLC That are Sensitive to Compound B. 118

FIGURE 4.15. Compound B Hinders S-phase Progression 119

FIGURE 4.16. Compound B Treatment Dissociates Most Replisome Components, but not Polymerase Epsilon, Without Recruiting Replication Stress Factors. 120

FIGURE 4.17. RPA Hyperloading and Replication Catastrophe Occurs After Compound B Treatment due to ATR Loss 122

FIGURE 4.18. RUVBL1/2 Binds RPA3 After Compound B Treatment but does not Disturb RPA Complex Formation 124

FIGURE 4.19. RUVBL1/2 are Required for NSCLC Growth In Vivo but Afford a Small Therapeutic Window 126

FIGURE 4.20. RUVBL1/2 Inhibition or Depletion Enhances the Cell Killing Effect of Radiation In Vitro. 130

FIGURE 4.21. Compound B Delays the Resolution of DSBs in NSCLC, but not Normal Cells, In Vitro 132

FIGURE 4.22. Compound B can Radiosensitize Xenografted Tumors and Patient-Derived Explant Models 134

LIST OF TABLES

TABLE 1. 96-well Plate Transfection Conditions for all NSCLC and HBEC Cell Lines Used 62

TABLE 2. Primer Sequences for esiRNA Generation.....66

TABLE 3. IC_{50}'s of Compound B and Compound C in Viability-based Assays.....99

TABLE 4. List of Putative Compound B Resistance Conferring Mutations Identified by a PCR-based Mutagenesis Screen.....106

LIST OF APPENDICES

APPENDIX A. Sequence and Product ID of Qiagen siRNAs used in NR, Coregulator and Chromatin Remodeler Viability-Based Screen 147

APPENDIX B. DE Genes After Compound B Treatment in H2009 and H596.....183

APPENDIX C. RUVBL1 Co-Immunoprecipitating Proteins After Compound B Treatment.....225

APPENDIX D. RUVBL1/2 Co-Immunoprecipitating Proteins 268

APPENDIX E. List of Proteins Identified by iPOND-Mass Spec After Compound B Treatment289

LIST OF ABBREVIATIONS

NSCLC – non-small cell lung cancer
RNAi – RNA interference
RUVBL1/2 – RUVBL1 and RUVBL2
SCLC – small cell lung cancer
FDA – US Food and Drug Administration
NR – nuclear receptor
siRNA – small interfering RNA
esiRNA – endoribonuclease-prepared small interfering RNA
UTR – untranslated region
shRNA – short hairpin RNA
ssDNA – single stranded DNA
dsDNA – double stranded DNA
DSB – double strand break
HCC – hepatocellular carcinoma
ORC – origin of replication complex
CDK – cyclin-dependent kinase
pre-RC – pre-replication complex
DDK complex – CDC-DBF4
DDR – DNA damage response
ROS – Reactive oxygen species
BER – base excision repair
NER – nucleotide excision repair
NHEJ – non-homologous end joining
SSBR – single strand break repair
HR – homologous recombination
MMR – mismatch repair
IR – ionizing radiation
SBRT – stereotactic body radiotherapy
HBEC – human bronchial epithelial cells
RT-qPCR – reverse transcription followed by quantitative PCR
ddCt – delta delta Ct
HR – hazard ratio
Comp. B – Compound B (active RUVBL1/2 inhibitor)
Comp. C – Compound C (inactive Compound B control)
IHC – immunohistochemistry
DE – differentially expressed
iPOND – isolation of proteins on nascent DNA
TUNEL – terminal deoxynucleotidyl transferase dUTP nick end labeling
PDEx – patient-derived explants
FFPE – formalin-fixed paraffin-embedded
TMA – tissue microarrays

CHAPTER ONE:
Introduction

1.1 What is lung cancer?

Cancer, in general, is the rapid and abnormal growth and invasion of a host's own cells. The properties that confer these traits, chiefly abnormal growth and invasion, are believed to be caused by multi-step genetic mutations to the genome of the cell of origin, which is generally believed to be some type of stem cell. These genetic changes transform these stem cells into cancerous cells, and are referred to as "driver mutations", a term originally coined by Bob Weinberg in 1996 (Thiagalingam et al., 1996), as they are selected for and fuel or confer the properties that define malignancy, uncontrolled cellular growth and invasion into surrounding tissue. Driver mutations can be found in two types of genes, proto-oncogenes and tumor suppressors. Mutation of a proto-oncogene yields an oncogene, usually via a gain-of-function mutation. Oncogenes send strong, frequently constitutive signals to the cell to grow, divide, and invade into surrounding tissue. Mutation of a tumor suppressor, on the other hand, is usually a loss-of-function mutation. Because tumor suppressors usually act as checkpoints or "brakes" to malignant functions, these loss-of-functions mutations subvert these checkpoints and allow cancer cells to divide without recourse.

Driver genes have generally been identified by sequencing the DNA of large numbers of patient tumors and identifying genes that are recurrently mutated. This premise assumes that recurrently mutated genes are likely playing an active role in tumorigenesis. This is because the mutation of DNA is generally a random process, but the fixation and predominance of a mutation within a population (in this case, patient tumors) is a selective event, implying that the mutation caused some sort of selective advantage, enabling the malignant outgrowth of these cells. Additionally, it assumes there must be a limited number of genes that could function as

drivers, as only recurrently mutated genes are assumed to be drivers. This method has identified several important driver genes, all of which are now under active investigation.

Unfortunately, while these mutated driver genes are important for cancer growth and metastasis and their modulation may therefore be therapeutic, only some of these mutated driver genes can be leveraged therapeutically, at least easily. For instance, mutations in tumor suppressors are generally loss-of-function mutations and abolish the activity of the tumor suppressor. Therefore, drugs targeting these broken tumor suppressors may need to either restore their activity or enhance the activity of other proteins that have similar functions. While many groups are attempting to do this (Bauer et al., 2016; Wang and Fersht, 2017), it has proven challenging, and no treatments that directly target tumor suppressors are available for cancer patients. It should be noted, however, that mutations in tumor suppressors may create synthetic lethalities, and this property has been harnessed for anti-cancer treatment in the case of PARP inhibitors (Lord and Ashworth, 2017). A more straightforward therapeutic approach is to inhibit the aberrantly activated oncogenes using pharmacological inhibitors. For many oncogenes in specific tumor types, such as EGFR and ALK in NSCLC (Cohen et al., 2005; Shaw et al., 2013) and BRAF in melanoma (Chapman et al., 2011), this strategy has yielded clinical success. Additionally, by finding the same mutations across multiple tumor types, it has now been shown that drugs used to treat one type of cancer with a particular molecular alteration may be effective in other cancers sharing the same molecular alteration (Planchard et al., 2016). However, not all oncogenes can be therapeutically targeted. For instance, despite being frequently mutated in many cancer types and decades of research, there still exists no clinically approved therapy for patients with mutations in the oncogene KRAS (Ostrem and Shokat, 2016).

This simple view of curing or treating all cancer patients by identifying driver genes via sequencing and developing inhibitors/activators of them for clinical benefit, however, betrays the

bewildering complexity of the cell. In truth, the path to cancer development is different for each cancer type, and for some cancer types, different from patient to patient. Many tumors, especially in lung cancer, are sequenced and no known driver mutations are found, despite our belief of cancer being a genetic disease. Additionally, even in cases where an inhibitor against a driver gene is developed, resistance usually occurs, frequently without the creation of an obvious new driver gene. Whether this reflects a flaw in our model, or the need to sequence more tumor samples and identify more driver genes (i.e. identify driver genes mutated at a low frequency), is an area of active debate.

Lung cancer then, it follows, is the abnormal growth and invasion of stem cells within the lung, a process that is molecularly driven, at least in part, by the mutation of driver genes, which generally includes both the creation of oncogenes and the loss of tumor suppressors. Depending on the exact cell type and location of these mutated stem cells, which is discussed in further detail below, two main types of lung cancer may arise, small cell lung cancer (SCLC) or non-small cell lung cancer (NSCLC). In the United States in 2017, it is expected that ~225,000 people will be diagnosed with lung cancer; ~180,000 of these (80%) will be diagnosed with NSCLC, while the remaining ~45,000 (20%) will be diagnosed with SCLC (Siegel et al., 2017). NSCLC can then be further broken down into two main histological subtypes, adenocarcinoma and squamous cell carcinoma (Larsen and Minna, 2011). While these different subtypes of lung cancer all arise within the lung, they differ widely in their molecular and histological properties, as well as where they originate. SCLC is usually located in the central airway and is composed of highly proliferative cells with a flat shape and very little cytoplasm. SCLC is believed to originate from neuroendocrine stem cells within the central airway, as these tumors are frequently positive for neural markers such as synaptophysin, chromogranin and CD56 (Junker et al., 2000). Molecularly, these tumors show nearly uniform deletion of the tumor suppressors TP53 and RB1, with frequent inactivation of NOTCH pathway members (George et al., 2015).

NSCLC, on the other hand, consists of larger cells with more, but still reduced in comparison to non-transformed pulmonary epithelial cells, cytoplasm than SCLC. Adenocarcinomas are typically found in the more distal parts of the lung (alveolar sacs), form glandular structures, likely originate from club or type II alveolar cells (Hanna and Onaitis, 2013) and frequently have loss of function mutations in the tumor suppressors TP53, RB1 or CDKN2A and gain of function mutations in genes involved in MAPK signaling, such as KRAS, EGFR and BRAF, as well as fusions of ALK, RET, ROS and NTRK (Collisson EA, 2014). Squamous cell carcinomas are typically found in the more proximal parts of the lung, like adenocarcinomas may arise from club of type II alveolar cells, but generally have more stromal content (due at least in part to their high keratin positivity) with keratin pearls being a defining feature. These tumors frequently have inactivation of the tumor suppressors TP53 and CDKN2A, but do not display mutations in other genes at very high frequencies (Hammerman PS, 2012), making this an exceedingly hard cancer to treat with targeted therapies, such as small molecule inhibitors or antibodies.

1.2 Current treatments for non-small cell lung cancer

Currently, the type and course of treatment for NSCLC patients will depend upon a number of factors, such as tumor staging (i.e. has the tumor metastasized), tumor location, patient health performance status, histological subtype and molecular characteristics of the tumor (PD-L1 expression and EGFR, ALK, ROS, or BRAF mutation status). In patients without metastatic disease, and especially those with limited or no local tumor invasion and good health performance status, surgical removal of the tumor offers the best chance at survival, with surgery curing the majority of very early stage patients. In cases where surgery is not feasible for early stage patients, a new method of hypofractionated radiation referred to as stereotactic body radiotherapy (SBRT) (Baker et al., 2016) can also produce high rate of cures in early stage patients. The situation, however, is very different for later stage patients, i.e. patients whose disease has spread, such as extensive local, lymph node, or distant organ involvement. For

patients with this type of disseminated disease, <20% of patients will survive longer than 5 years as surgery is generally not beneficial for these patients. This is especially unfortunate as >50% of the patients that present clinically with NSCLC are late stage (Siegel et al., 2017).

Less than 20 years ago, nearly all metastatic NSCLC patients would receive their physician's choice of chemotherapy (generally pemetrexed, cisplatin, carboplatin, docetaxel, paclitaxel or gemcitabine), with or without radiation. However, research into the biology and treatment of NSCLC has yielded several novel therapeutic options to combat metastatic NSCLC. The first significant breakthrough was that of precision medicine, which matches mutations present in a patient's tumor to drugs specifically targeting these mutant proteins. In 2004, the FDA approved Tarceva (Erlotinib) for the treatment of EGFR-mutant NSCLC cancers (Cohen et al., 2005). Since then, Xalkori (Crizotinib) has been approved for ALK- and ROS1-rearranged lung cancers (Shaw et al., 2013; Shaw et al., 2014) and Zelboraf (Vemurafenib) has been approved for all BRAF V600E mutated cancers, which includes NSCLC (Planchard et al., 2016). Additionally, a new method of treating cancer which harnesses the patient's immune system to fight the tumor, broadly known as immunotherapies, has been approved by the FDA for use in NSCLC, with the first approval coming for Opdivo and then later for Keytruda, both of which are anti-PD-1 antibodies (Kazandjian et al., 2016; Sul et al., 2016).

Despite these advances, surgery or radiation remains one of the few ways to reliably cure an NSCLC patient. This therapy, however, is only beneficial in early stage patients, where the tumor has not metastasized or disseminated yet. For patients with metastatic disease, systemic treatments, utilizing small molecules or biologics, must be used. These treatments, however, are only marginally effective, at least in part because the differences between a malignant host cell and a normal host cell are, surprisingly, quite few and hard to target. As discussed above, the three main treatment types for metastatic disease are chemotherapy, precision medicine and immunotherapy. Chemotherapy works in a small percentage of patients,

generally only delays disease progression, and produces considerable side effects. Precision medicine provides an immediate and significant effect in the vast majority of patients that have a tumor harboring the mutated target, but these responses are transient and eventually nearly all patients will succumb to their disease. Immunotherapies offer the promise of a cure, but this only occurs in a small subset (~20%) of patients, and this therapy also has considerable side effects. Thus, new treatments for NSCLC are an urgent need.

1.3 Nuclear receptors, their coregulators and chromatin remodelers in NSCLC

Nuclear receptors (NRs) are a group of 48 structurally similar transcription factors whose activity is usually modulated via ligand binding. This means that for the majority of NRs, a ligand will bind the nuclear receptor and induce conformational changes that will result in activation or repression of the NR, which ultimately results in the expression or repression of the transcription of certain (target) genes. This action usually occurs at defined DNA sequences throughout the genome that the NR binds, and these defined DNA sequences generally have a motif that is specific for that NR (for instance, the androgen receptor binds to androgen response elements). NRs, however, do not act alone in stimulating or repressing transcription. Generally, the binding of agonistic ligands will cause conformational changes within the NR that will displace corepressors, recruit coactivators, or both. The loss of corepressors and the addition of coactivators produces an environment that is favorable to recruit the transcriptional machinery. This alone, however, may not be sufficient to initiate or increase gene expression. Because the DNA sequence that NRs bind are usually bound by histones, and these histones can occlude the binding of additional DNA-binding proteins, this chromatin environment may need to be directly remodeled or modified to permit recruitment of the NR, additional transcription factors, or to allow RNA polymerase to proceed. In the case of antagonistic ligands, the opposite of what was described for agonistic ligands usually applies – coactivators are displaced, corepressors are recruited, and the chromatin is modified to be both inaccessible and inhospitable to the

recruitment of additional transcription factors (Gronemeyer et al., 2004). Thus, while NRs play important roles in human physiology, their role in directing gene transcription requires the action of other proteins, chiefly coregulators and chromatin remodelers.

Because nuclear receptors are ligand-modulated transcription factors, and many of their ligands are small, cell permeable molecules, they can act as direct and rapid sensors and transducers of extracellular stimuli. A prime example of this is the ability of the estrogen receptor (ER) and the androgen receptor (AR) to sense female and male sex hormones, respectively. In normal physiology, the AR senses and responds to the male sex hormones testosterone and dihydrotestosterone, whereas the ER senses estrogen. The profound role of these NRs in sensing these ligands and directing important gene expression programs is apparent in the phenotype of knockout mice; AR knockout mice have reduced fertility, lack a prostate, have smaller testis and numerous female features (Yeh et al., 2002), whereas ER knockout mice are infertile and have underdeveloped mammary glands (Korach et al., 1996). Given the important role of NRs in normal physiology, it is no surprise that NRs and their coregulators are hijacked by cancerous cells to support their uncontrolled proliferation. For cancer, this hijacking normally, but not always, occurs in tissues that are reliant on these NRs. For instance, AR is an established driver of prostate cancer (Sharifi et al., 2005), whereas the ER in an established driver of ER^+ breast cancers (Cohen et al., 2001). Additionally, the importance of NRs in normal physiology and disease, as well as their ability to be modulated by small molecules, makes them excellent therapeutic targets. This is directly evident in the fact that 10-15% of FDA-approved drugs targets NRs (Overington et al., 2006).

While cancers driven by NRs, such as prostate and breast cancer, frequently arise in organs that are dependent on NRs for their development, there are examples of NRs driving cancer in other organs. For instance, the PML-RARA translocation (the NR is RARA, the retinoic acid receptor alpha) is a bonafide driver of acute promyelocytic leukemia (APL) (Cohen

et al., 2001). Research has suggested, however, that NRs may play important and underappreciated roles in other cancers. Interestingly, multiple lines of evidence suggest that NRs may play a role in the pathogenesis of lung cancer. At the global level, NR expression is frequently deregulated in lung cancer, and the expression level of some NRs can be used to form a robust prognostic signature for lung cancer patients undergoing surgical resection (Jeong et al., 2012; Jeong et al., 2010). This evidence is correlative, but other studies have shown a more causal role in the ability of NRs to support lung cancer proliferation. For instance, NSCLC cell lines that express PPARG are sensitive to the PPARG agonists of the thiazolidinedione class (pioglitazone, rosiglitazone and troglitazone) (Srivastava et al., 2014) and various NSCLC lines are sensitive to dexamethasone (Greenberg et al., 2002; Hofmann et al., 1995; Lu et al., 2006). The role of other NRs in NSCLC, however, has not been extensively studied, despite their expression being prognostic.

1.4 The AAA+ ATPases RUVBL1 and RUVBL2

RUVBL1 (originally called TIP49a, also known as pontin and RVB1) was first cloned in 1997 (Kanemaki et al., 1997) and RUVBL2 (originally called TIP49b, also known as reptin, RVB2 and TIP48) was later cloned by the same group in 1999 (Kanemaki et al., 1999). RUVBL1 and RUVBL2 are paralogous genes (i.e. likely the result of gene duplication) from the AAA+ ATPase family with high sequence similarity to the bacterial RuvB helicase, which utilizes ATP hydrolysis to help resolve Holliday junctions during DNA crossover reactions, hence their naming, RUVB-like 1 and RUVB-like 2 (Kanemaki et al., 1999). While bacterial RuvB may aid branch migration and resolution of Holliday junctions, eukaryotic RUVBL1/2 most likely do not function in the resolution of Holliday junctions, or at least not in the same way as bacterial RuvB (Qiu et al., 1998). In fact, the ability of RUVBL1/2 to hydrolyze ATP, unwind dsDNA, or be stimulated by DNA is controversial. One group found that purified RUVBL1 does not hydrolyze ATP or unwind dsDNA (Qiu et al., 1998). Another group found that RUVBL1 and RUVBL2 have

ATPase activity which is stimulated by ssDNA, and that RUVBL1 has helicase activity in the 5'-3' direction, whereas RUVBL2 has helicase activity in 3'-5' direction (Kanemaki et al., 1999; Makino et al., 1999). A different group found that the combination of RUVBL1 and RUVBL2 (herein referred to as RUVBL1/2) have ATPase activity, but this is not stimulated by ssDNA or dsDNA, and that RUVBL1/2 could potentially have helicase activity, but this was normally inhibited by a domain in the protein referred to as DII (Gorynia et al., 2011). This is similar to another group that found that RUVBL1/2 have stronger ATPase activity than either subunit alone, their ATPase activity was not stimulated by any type of DNA intermediate, and RUVBL1/2 had no helicase activity (Puri et al., 2007). Another group found that RUVBL1/2 have ATPase activity, but it is normally weak and stimulated by dsDNA with 5' or 3' overhangs (Gribun et al., 2008). Additionally, another group found that RUVBL1 had weak ATPase activity but no helicase activity (Matias et al., 2006). Some of the reasons for the differences between these studies may be due to the expression system utilized (i.e. yeast versus insect versus human cells), whether paralogs were expressed individually or together, and the sequence of the RUVBL1 or RUVBL2 proteins being expressed (i.e. full length versus truncated versus tagged). Since RUVBL1 and RUVBL2 are generally believed to be found in complexes together and the stability of one paralog depends on the presence of the other paralog (see below), it is also very likely that systems utilizing just one paralog do not recapitulate the physiological functions of RUVLB1/2 in the cell. Regardless, what is clear is that eukaryotic RUVBL1/2 do not function like the bacterial RuvB, and they likely have ATPase activity, which may or may not be stimulated by various ssDNA and dsDNA substrates.

Similar to the biochemical function of RUVBL1/2, the molecular architecture of RUVBL1/2 *in vivo* remains an area of active investigation. RUVBL1 and RUVBL2 physically interact and depend upon one another for stability (Haurie et al., 2009), strongly suggesting that they are almost always found in direct contact with each other *in vivo*. Despite this fact, purified

RUVBL1 or RUVBL2 alone *in vitro* will form a hexameric ring with a central cavity that is typical of members of the AAA+ ATPase family. This was first shown in the first crystal structure of human RUVBL1, which showed that human RUVBL1 formed a hexameric ring with a central opening of approximately 20 Angstroms (Matias et al., 2006). Subsequent crystal structures utilizing human RUVBL1/2 have also suggested that RUVBL1/2 form a hexamer with a central channel is likely ~20 Angstroms (Gorynia et al., 2011). Thus, it was a bit of a shock when the human RUVBL1/2 structure was solved by cryo-electron microscopy and shown to be a double hexamer (Puri et al., 2007). Additionally, this group showed that RUVBL1/2 required ATPase activity to assemble into a dodecamer, and the presence of one catalytically inactive member could abolish assembly (Puri et al., 2007). The same year another group published a paper showing that yeast RUVBL1/2 form a heterohexamer, not a dodecamer (Gribun et al., 2008), but only months later yet another group published a paper suggesting that yeast RUVBL1/2 form a dodecamer (Torreira et al., 2008). One study suggested that yeast RUVBL1/2 do indeed form hexamers, and that dodecamers were just an artifact of histidine tags (Cheung et al., 2010). However, this was followed by two studies showing that human RUVBL1/2 may form dodecamers, one using various low resolution techniques (Niewiarowski et al., 2010) and another using high-resolution crystal structures of human RUVBL1/2 lacking the D2 domain (Gorynia et al., 2011), with the latter paper suggesting that dodecamer formation was independent of the histidine tag (Gorynia et al., 2011). To complicate things further, electron microscopy performed using yeast proteins have suggested that yeast RUVBL1/2 is hexameric in the yeast SWR1 chromatin remodeling complex (SRCAP is the human counterpart) (Nguyen et al., 2013), but that yeast RUVBL1/2 is dodecameric in the yeast INO80 chromatin remodeling complex (Tosi et al., 2013). More recently, however, another group has suggested that the human INO80 chromatin remodeling complex contains hexameric RUVBL1/2 (Aramayo et al., 2018). Resolving these structural inconsistencies will help shed new light on RUVBL1/2 biology,

but it is our opinion that the majority of RUVBL1/2 within the cell is likely found in heterohexameric rings.

In humans RUVBL1/2 proteins are associated with a diverse array of protein complexes, and RUVBL1/2 are generally necessary for the assembly and/or stability of these complexes. For this reason, RUVBL1/2 have recently been labeled as chaperones (Nano and Houry, 2013; Zhou et al., 2017) or co-chaperones (Matias et al., 2015). Perhaps the most heavily studied RUVBL1/2-containing complexes are the INO80-family of ATP-dependent chromatin remodeling complexes Initially identified in a yeast screen looking for regulators of phospholipid biosynthesis, in humans the INO80-family of chromatin remodelers have been implicated in processes such as DNA repair, DNA replication, transcription, telomere stability and general cellular proliferation (Hargreaves and Crabtree, 2011). In addition, RUVBL1/2 and their ATPase activity have been shown to be important for the assembly of an active telomerase complex (Venteicher et al., 2008), although this important function of RUVBL1/2 remains understudied.

In addition to the INO80-family of chromatin remodelers and telomerase, another well described RUVBL1/2-containing complex with a multitude of important roles in the cell is the recently termed PAQosome complex, which consists of RUVBL1, RUVBL2, RPAP3, PIH1D1, HSP90 and the Prefoldin-like complex. RUVBL1 and RUVBL2 are essential for the formation of this complex, but their role in the complex is not well understood (Houry et al., 2018). Shortly after the discovery of RUVBL1/2, but before the PAQosome was identified, it was shown that depletion of RUVBL1/2 could impair the biogenesis of box C/D small nucleolar RNAs (snoRNAs) (Watkins et al., 2004), and later it was shown that this was due to interactions between the PAQosome complex and NUFIP1, a key component in the biogenesis of multiple ribonucleoproteins (Boulon et al., 2008). Keeping with the theme of small ribonucleoproteins, the PAQosome complex also controls U4 small nuclear ribonucleoproteins (snRNPs) through NUFIP1 (Boulon et al., 2008) and U5 snRNPs through ZNHIT2 (Cloutier et al., 2017). The

PAQosome has also been implicated in mediating the stability of phosphatidylinositol-3 kinase-related protein kinases (PIKKs), which includes ATM, ATR, DNA-PK_{cs} (PRKDC), MTOR, TRAPP and SMG1, through interactions with the Tel2 complex (TELO2-TTI1-TTI2). Depletion of RUVBL1/2 therefore leads to a decrease in the abundance of these PIKK-family proteins (Izumi et al., 2010). Additionally, one of the first identified RUVBL1/2 interacting proteins was RNA polymerase II (Qiu et al., 1998). Subsequent studies have shown that this is interaction is through the PAQosome complex, and that depletion of RUVBL1/2 impairs the assembly of cytoplasmic RNA polymerase II (Boulon et al., 2010), although the effect this has on global transcription is not well known. Interestingly, at least some of the functions of RUVBL1/2 in the PAQosome require their ATPase activity, such as PIKK stability (Izumi et al., 2010), however if this is true for all PAQosome clients, as well as the mechanism underlying this phenomenon, is not known.

The biological processes affected or regulated by RUVBL1/2 are diverse and numerous, likely a direct reflection of the wide range of protein complexes regulated by RUVBL1/2. On the gross phenotypical scale, RUVBL1/2 are essential for cellular proliferation, from yeast (Qiu et al., 1998) to mice (Rajendra et al., 2014), to a diverse set of human cancers (McDonald et al., 2017; Meyers et al., 2017), although the precise mechanism(s) underlying the essentiality of RUVBL1/2 is not known. RUVBL1/2 have been shown to have roles in DNA repair, both in studies that have directly interrogated the role of RUVBL1/2 in the response to double stand breaks (DSBs) (Jha et al., 2008; Raymond et al., 2015) and in studies that have interrogated the role of RUVBL1/2-controlled chromatin remodelers in the response to double stand breaks (Dong et al., 2014; Ikura et al., 2000; Morrison et al., 2004; Murr et al., 2006; Niida et al., 2010; Wu et al., 2007). Importantly, depletion of RUVBL2 has been shown to inhibit the ability of hepatocellular carcinoma cells to recover from DNA damage (Raymond et al., 2015), but RUVBL1 has not been directly interrogated. Additionally, whether this activity requires

RUVBL1/2's ATPase activity is unknown. RUVBL1/2 have also been shown to have roles in mitosis. For instance, recently a group has shown that RUVBL1/2 may be required for efficient chromatin decondensation following mitosis (Magalska et al., 2014). Other groups have shown that RUVBL1 may interact with tubulin and/or centrosomes during mitosis (Ducat et al., 2008; Gartner et al., 2003), whereas others have suggested that RUVBL1 interacts with the mitotic spindle apparatus and PLK1 during mitosis (Gentili et al., 2015). These groups have shown various mitotic defects following RUVBL1 or RUVBL2 depletion, such as lagging chromosomes following RUVBL1/2 knockdown (Gentili et al., 2015), or defects in spindle assembly and organization following RUVBL1, but not RUVBL2, knockdown (Ducat et al., 2008). A different group, however, has shown that RUVBL1/2 knockdown results in chromosomal abnormalities such as radial structures, chromosome gaps and chromosome breaks, which they believe is due to RUVBL1/2's role in stabilizing the Fanconi Anaemia family of proteins (Rajendra et al., 2014), and not due to its role in mitosis. Finally, RUVBL1/2 appear to play a role in cilia biology, possibly by promoting the stability of DNAI1 and DNAI2, which are necessary for axonemal dynein arm assembly. These motors arms are what cause the motile cilia to beat (Li et al., 2017; Zhao et al., 2013), although others have found that loss of RUVBL1/2 impairs ciliogenesis, rather than motile ciliary function (Tammana and Tammana, 2017).

Given their numerous and important roles in cellular processes, it is not surprising that RUVBL1/2 have been implicated in various types of cancers. RUVBL2 has been shown to be overexpressed in renal cell carcinoma in comparison to adjacent normal tissue, with high cytoplasmic, but not nuclear, staining predictive of poorer overall survival. Additionally, depletion of RUVBL2 resulted in diminished cell growth, invasion, and a G_1 arrest (Ren et al., 2013). In pancreatic cancer, one group reported that RUVBL1 is not required for cell viability, but is instead required for invasion and actin protrusion (Taniuchi et al., 2014); however, since many large-scale screening efforts have identified RUVBL1/2 as essential in pancreatic cancer

(McDonald et al., 2017; Meyers et al., 2017), it is unlikely that RUVBL1 was not required for viability in this cell line, although it may still be necessary for invasion (Taniuchi et al., 2014). Similar to these results, a different group in breast cancer found that RUVBL1 knockdown inhibited cell survival and migration. Additionally, they found that RUVBL1 mRNA was overexpressed in comparison to normal tissue and that high RUVBL1 mRNA predicted poor survival (Fan et al., 2017). An analysis of RUVBL1 protein expression in colorectal cancer found that 80% of patients had higher RUVBL1 staining in their tumor than in adjacent, normal tissue (Lauscher et al., 2007), and another group looking at colorectal cancer found that RUVBL2 may positively regulate hTERT expression (Flavin et al., 2011). Additionally, groups have shown that RUVBL1 in acute myeloid leukemia (Breig et al., 2014) and RUVBL2 in mixed lineage leukemia (Osaki et al., 2013) are essential for the proliferation of these cancers. While most of these reported roles for RUVBL1/2 in various cancer types are single studies, the role of RUVBL1/2 in hepatocellular carcinoma (HCC) is the most heavily researched and best characterized. HCC patient tumors overexpress both RUVBL1 and RUVBL2 in comparison to normal liver tissue (Haurie et al., 2009; Rousseau et al., 2007) and high mRNA expression of RUVBL1 is predictive of poor disease-free survival (Haurie et al., 2009). HCC cell lines require RUVBL1 and RUVBL2 for their growth *in vitro* (Grigoletto et al., 2013; Haurie et al., 2009) and forced overexpression of RUVBL2 could promote tumor growth *in vivo* (Rousseau et al., 2007). Additionally, it was shown that RUVBL2 is required for the growth of HCC *in vivo* in an ATPase-dependent manner (Grigoletto et al., 2013).

1.5 The cell cycle, with an emphasis on DNA replication

In order for cells to divide, they must undergo a series of highly organized and regulated steps referred to as the cell cycle, whereby cells replicate their DNA and much of their intracellular content during the G_1, S, and G_2 phases, then distribute these molecules into two daughter cells during the M phase. These steps must be tightly regulated for two reasons: one,

to ensure that the cell cycle proceeds accurately as to not produce damaged and/or cancerous cells; and two, so that proliferation only occurs when the correct conditions are present. The primary damages that can occur during cell division are changes to the DNA sequence of the cell, such as small base pair substitutions, deletions, inversion, duplications and translocations. These damages usually occur during DNA replication, although some occur during mitosis, and are the result of errors during DNA replication not being accurately resolved by the DNA repair machinery, both of which will be discussed in further detail below. Because one of the hallmarks of cancer is uncontrolled growth, and errors that occur normally during the cell cycle, especially during DNA replication, can lead to cancer, the cell cycle, cancer, DNA replication and DNA repair are intricately linked.

After development, during normal human physiology, most of the cells in the body do not divide. Instead, they are either quiescent or terminally differentiated. Quiescence is a state where a cell is not actively dividing, but it retains the capacity to divide. Stem cells are frequently quiescent until they receive a signal to divide, such as in the response to injury, where new cells need to be regenerated (Rumman et al., 2015). Terminally differentiated cells, on the other hand, are generally viewed as cells that have lost the capacity to divide (Buttitta and Edgar, 2007). The signals that drive progression from quiescence into the cell cycle are varied but in essence the cell will sense its extracellular environment, from mitogenic signals to the local nutrient composition, and make a decision to leave quiescence, generally referred to as G_0, and enter the first phase of the cell cycle, referred to as G_1 (Massague, 2004). Here, similar to G_0, the cell continues to sense its environment and signaling milieu before proceeding to the next step of the cell cycle; however, the cell also ensures the fidelity of its DNA before proceeding to the next stage of the cell cycle, S-phase, where DNA replication takes place. This checkpoint ensures that cells with damaged DNA do not proceed into S-phase, where pre-existing errors could cause catastrophic DNA damage, mutations, and/or cell death during DNA replication.

Strong p53-dependent DNA damage signaling, for instance, can result in the expression of p21, which ultimately prevents the cell from entering S-phase (Waldman et al., 1995). Once this checkpoint is passed and cells enter S-phase, the cell is fully committed to cell division, with the only outcomes being divide or die (Vermeulen et al., 2003).

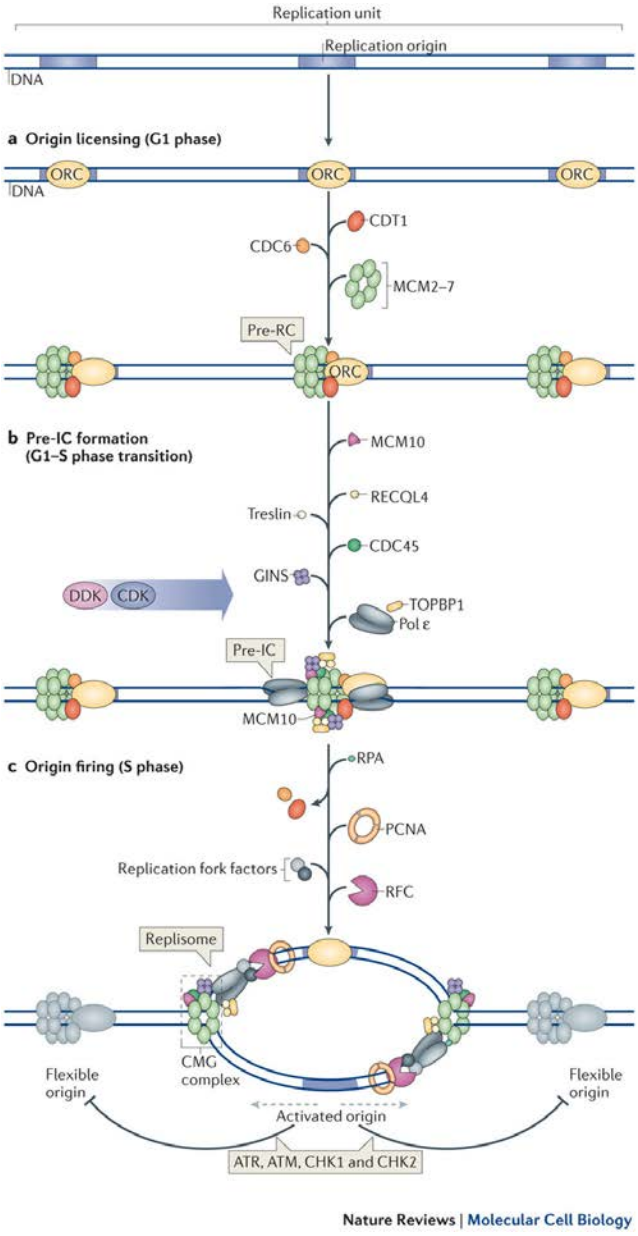


Figure 1.1. Schematic Depicting the initiation of DNA replication. A) Licensing of the origins occurs during early G_1 or late M-phase and is accomplished by the binding of ORC1-6, CDC6, CDT1 and MCM2-7 proteins, resulting in the formation of the pre-replication complex (pre-RC). B-C) Later, at the G_1-S phase transition, the CDC-DBF4 (DDK complex) and various CDKs

phosphorylate and recruit additional factors, such as MCM10, RECQL4, Treslin, CDC45, the GINS complex, TOPBP1 and DNA polymerases, to the pre-RC. Additional phosphorylations on the MCM2-7 complex, which occur during S-phase, result in its activation, causing it to unwind DNA, and allowing the origin to fire. Note that the additional, nearby licensed but unfired origins are suppressed by firing of the adjacent (middle) origin.

Modified from Fragkoss, Ganier, Coulombe and Mechali, Nature Reviews Molecular and Cell Biology, 2015.

S-phase, the phase of the cell cycle where DNA replication takes place, proceeds via two main steps: origin licensing / pre-replication complex (pre-RC) formation, and processive, bidirectional, semiconservative DNA replication (**Figure 1.1**). Origins are stretches of DNA where replication may begin – in lower eukaryotes, such as *Saccharomyces cerevisiae*, origins have a defined consensus sequence, whereas origins in higher eukaryotes, such as mammals have little, if any, consensus sequence (Fragkos et al., 2015). The licensing of origins involves the sequential and ordered loading of proteins of the pre-replicative complex, which is composed of the origin recognition complex (ORC – which in humans is composed of six members, ORC1-6), CDC6, CDT1, and MCM2-7, onto origins during late M or early G_1 phases of the cell cycle prior to the entrance into S-phase. At this point, the licensed origin is now referred to as a pre-replication complex (pre-RC). Eukaryotic cells actually form more pre-RCs on chromatin than will be fired (or activated) during normal S-phase progression, potentially to allow cells to fire alternative origins under conditions of replicative stress (Bell and Dutta, 2002; Masai et al., 2010). To begin DNA replication, these pre-RCs must be activated and made competent for DNA replication. This requires two key factors, both of which are regulated by the phase of the cell cycle: CDC7-DBF4 and cyclin-dependent kinases (CDKs). CDC7 is a kinase which is activated by DBF4A, a protein that is predominantly expressed during S-phase. The CDKs involved in DNA replication, such as CDK2, are activated by cyclins expressed specifically during S-phase, such as Cyclin E and Cyclin A (Woo and Poon, 2003). CDC7-DBF4 phosphorylates the N-terminal tail segments of MCM2, MCM4 and MCM6, members of the

MCM replicative helicase that unwinds dsDNA for DNA replication, likely after the phosphorylation of these MCMs by various CDKs (Masai et al., 2000). The coordinated phosphorylations of these MCMCs by CDC7-DBF4 and various CDKs activate the MCMs, cause dissociation of CDC6 and CDT1 from the pre-RC, and the MCMs to begin unwinding dsDNA. The order of events following activation of the MCM proteins is still controversial, but what is clear is that CDC45 is recruited, which causes recruitment of other factors necessary for replication, such as the GINS complex, DNA polymerases, RPA and fork stabilization factors (Bell and Dutta, 2002; Masai et al., 2010). The recruitment of these factors results in the "firing" of the origin, i.e. the formation of a competent replication complex (also known as the replisome). DNA replication then proceeds from the origin in a bi-directional "bubble", copying one strand of DNA in each direction and pairing it with the newly synthesized strand, a process known as semiconservative replication, since each newly replicated chromosome will contain one old and one new copy of the DNA.

As mentioned previously, more origins are licensed than will fire during S-phase. In fact, only 20-30% of the licensed origins are actually fired normally during S-phase. Additionally, in eukaryotes, and especially mammalian cells, all of the origins that will fire during S-phase are not activated at the same time. Instead, origin firing is a temporally regulated process which occurs throughout S-phase in Mb-scale domains. Some of these domains replicate early in S-phase, while others replicate later in S-phase. Early replicating domains tend to be in transcribed, euchromatic regions of the genome located in the interior of the nucleus, with a high density of licensed origins. Late replicating regions, on the other hand, tend to have low gene density, a low density of licensed origins, and are generally in heterochromatic regions of the genome located at the periphery of the nucleus. Additionally, late replicating regions sometimes contain DNA sequences that can form secondary structures that hinder the completion of DNA replication (Fragkos et al., 2015).

Once initiated, the process of DNA replication can be halted or stalled via various genomic insults and/or difficulties that may arise during replication, and the collective and varied insults that interfere with replication are referred to as replication stress (Zeman and Cimprich, 2014). These stressors, such as abnormal DNA structures, various types of DNA damage, or collisions between the DNA replication and DNA transcription machinery, lead to the stalling of a replication fork. When a replication fork stalls, the replicative helicase dissociates from the DNA polymerases, and producing a region of ssDNA. This ssDNA can then be coated by the heterotrimeric protein complex RPA, shielding it from degradation. This RPA-ssDNA intermediate is recognized by ATRIP, which recruits and activates ATR, which in turn phosphorylates and activates CHEK1 (Zou and Elledge, 2003). CHEK1 can then phosphorylate the CDC25 family of phosphatases, which are stimulators of CDK1, preventing mitotic entry until the replication problems can be resolved. Additionally, ATR/CHEK1 suppress origin firing globally (but not locally, as will be discussed later) to slow or halt overall DNA replication and prevent the exhaustion of RPA (Toledo et al., 2013). If the source of DNA replication stress is genomic (i.e. DNA damage, secondary DNA structures) and cannot be resolved by DNA repair mechanisms, the cell has a number of replication-based mechanisms to bypass or fix the lesion and thereby complete DNA replication. Most studied is the firing of nearby, dormant origins, which can help replicate the unreplicated DNA by replicating the DNA from a different direction (Ge et al., 2007), and this is the reason why ATR/CHEK1 suppress origin firing globally, but not locally, following replication stress. Additionally, the replication machinery can reprime and restart replication downstream of the lesion, leaving behind a ssDNA gap that can be filled using the lesion bypass pathway known as DNA damage tolerance (DDT) (Zeman and Cimprich, 2014). If these mechanisms of repair fail, the fork may collapse, and produce a double strand break (DSB), which can then be acted upon by the normal DNA damage response.

Upon the completion of S-phase, the cell undergoes a phase of the cell cycle referred to as G_2. While S-phase produces another copy of the genome so that each daughter cell can receive one copy, the G_2 phase of the cell cycle produces the rest of the cellular substituents necessary for creation of an additional cell, such as large amounts of protein, lipids and other macromolecules. Additionally, this is the final time for a cell to resolve DNA damage before progressing into mitosis, where certain types of DNA damage, such as persistent DSBs and unresolved replication forks, can result in mitotic catastrophe (Castedo et al., 2004). If sufficient macromolecules are present for division and there is minimal DNA damage, which is believed to be something similar to 20 DSBs or less per cell, the cell will enter mitosis (Lobrich and Jeggo, 2007).

Mitosis, the next stage of the cell cycle after the G_2 phase of the cell cycle, is a process in which the cell massively condenses both copies of its DNA (which were created during S-phase) into sister chromatids and segregates them evenly into two, identical daughter cells. Mitosis is traditionally broken down into five discrete stages, prophase, prometaphase, metaphase, anaphase and telophase. These stages are classically defined by the morphological changes that accompany these phases, and although newer ways have been proposed to classify mitosis (Pines and Rieder, 2001), these stages are still widely accepted. In mammalian cells, the first stage of mitosis, prophase, is defined by the condensation of the replicated sister chromosomes into smaller, discrete sister chromatids, which are physically linked at their centromeres by a ring-shaped protein complex known as cohesin (Pines and Rieder, 2001). Additionally, the two centrosomes, one of which was duplicated during late G_1/S-phase, separate and segregate to opposite ends of the cell (Fu et al., 2015). Prometaphase, the next phase of mitosis, is characterized the breakdown of the nuclear envelope and the searching of mictrotubules, which originate from the newly segregated centrosomes, for kinetochores on sister chromatids. Kinetochores are multi-protein structures located at the

centromere of each sister chromatid that serve as the anchoring site for microtubules originating from the centrosome (Pines, 2006). The two kinetochores on the two sister chromatids are arranged in a back-to-back orientation, allowing microtubules from opposite centrosomes to attach to only one chromatid (Hauf and Watanabe, 2004). Attachment of all 92 kinetechores to microtubules (originating from the centrosome) causes the onset of metaphase. During metaphase, the centrosome begins “pulling” chromatids towards the centrosome. Because the two centrosomes are located on opposites sides of the cell, and each chromatid within the pair of sister chromatids is attached to a different centrosome, this causes the sister chromatids to be pulled in two opposing directions at once, facilitating their alignment in the middle of the cell between the centrosomes. Once the cell senses that sister chromatid are properly aligned between the two centrosomes, via a process known as the spindle assembly checkpoint, the cell enters the next phase of mitosis, known as anaphase (Hauf and Watanabe, 2004). In anaphase, the cell activates a protein known as separase, which in turn cleaves cohesin, the protein found at centromeres that holds sister chromatids together, releasing the sister chromatids from each other. This allows the centrosomes to pull one of the 46 sister chromatids towards itself, resulting in the exact segregation of 23 pairs of chromosomes (or 46 chromatids) to each pole of the cell. This triggers the final phase of mitosis, telophase. In telophase, the cell begins to reform a nuclear membrane and nuclear envelope at each pole around the chromatids, and the chromatids begin to decondense. The cell then undergoes cytokinesis, in which a cleavage furrow contracts down the middle of the cell and pinches off the plasma membrane such that two, complete and identical daughter cells are created (Pines and Rieder, 2001).

1.6 DNA repair

The insults that damage DNA are varied in their source, their mechanism of action, and in the way the cell responds to such insults. If left unrepaired, these insults can cause genomic

instability and/or cell death; thus, their accurate repair is paramount. The response to these insults is collectively called the DNA damage response (DDR), and while the DDR attempts to accurately repair DNA, mistakes inevitably occur which lead to mutations. Some types of insults may primarily cause mutations such as single base pair changes, whereas other insults can cause large changes, such as deletions, duplications, inversions or translocations. As discussed below, the propensity of these insults to generate different types of mutations is due both to the nature of the insult and the repair pathway acting upon the insult.

DNA damage can come from endogenous or exogenous sources. Endogenous sources include the depurination, deamination, oxidation, and methylation of the DNA base, or attack of the DNA strand by reactive oxygen species (ROS), resulting in base oxidation or the generation of breaks in the phosphodiester backbone of DNA. Exogenous sources include toxins, such as cigarette smoke, or high energy photons, generally in the form of ionizing radiation (IR) or ultraviolet light (Ciccia and Elledge, 2010). It is important to note that for most types of mutations, especially endogenous, the damage itself usually does not directly result in DNA mutations (i.e. changes to the genetic code). Instead, it is the resolution of these damages by the DDR that can result in mutations.

Regardless of their source, DNA damage can be lumped into two classes: covalent and non-covalent modifications. The three main types of covalent damages are DNA base damages, DNA backbone damages, and DNA/DNA or DNA/protein cross-links. DNA base damages are covalent modifications of the base of the nucleotide and can be produced by ROS, IR, ultraviolet radiation, aberrant nucleotide metabolism or chemotherapeutics such as cisplatin, mitomycin C and Adriamycin. DNA backbone damages can result in abasic sites (sites where the DNA backbone is intact, but the purine or pyrimidine base is lost), single strand breaks, or double strand breaks, and can be caused by IR or ROS. The last class of covalent modifications, DNA/DNA and DNA/protein cross-links, come in a variety of flavors. Cross-links are either

between DNA and proteins or DNA and DNA, and DNA-DNA crosslinks may be inter- or intrastranded. Cross-links can be caused by IR, ROS, or reactive aldehydes. The other main class of DNA damage, non-covalent DNA damage, can result when the structure of DNA is changed such that errors may occur during normal cellular processes, such as DNA replication or transcription. Non-covalent changes generally result from abnormal base pairings (for instance, between DNA and RNA) or changes in the tertiary structure of DNA (Sancar et al., 2004).

A multitude of proteins sense various types of DNA damage, frequently by binding to the specific type of lesion (for instance, bulky base adducts or double strand breaks). The various proteins that identify these damages then recruit their own set of repair proteins to deal specifically with lesions of this nature. The main pathways of eukaryotic DNA repair include direct DNA repair, base excision repair (BER), nucleotide excision repair (NER), single-strand break repair (SSBR), mismatch repair (MMR), homologous recombination (HR), single-strand annealing (SSA), non-homologous end joining (NHEJ) and cross-link repair. It is important to note that while these are separate pathways, there is immense crosstalk between these pathways, and multiple pathways may act upon a single lesion (Sancar et al., 2004). For instance, a DNA damaging agent may create two single stranded nicks near each other on the same strand of DNA, one where the base is damaged and another where it is not. In this case, the damaged nucleotide must be removed by BER or NER, then the resulting single stranded gap must be filled by SSBR (Caldecott, 2008).

Direct DNA repair, SSBR, BER and NER all act upon damaged bases, generally covalently modified bases, or sites that are missing bases (abasic), within an intact DNA helix. In direct DNA repair, enzymes directly remove the covalent modification that occurred on the base. For instance, methylguanine-DNA methyltransferase (MGMT) removes the O^6-methyl group from O^6-methylguanine. SSBR, unlike direct DNA repair, is not a singular linear pathway,

but instead is composed of BER and NER (both described below), as well as a process by which single stranded regions of DNA, which can be formed when the same strand of DNA incurs two single stranded nicks in nearby locations, is directly filled by DNA polymerases (Caldecott, 2008). The process of BER begins when the cell recognizes an abasic site in the DNA, which can result either from direct DNA damage or the action of various DNA glycosylases, which are enzymes that remove damaged bases from DNA. Repair proteins induce a nick in the DNA backbone 5' to the abasic site to reveal a free 3' hydroxyl, and DNA polymerase adds new nucleotides up to the abasic site. The nucleotide at the abasic site is then filled either via a "short-patch" mechanism, in which just the abasic site is cleaved and filled by a single nucleotide, or a "long-patch" mechanism, in which the abasic site is cleaved but the polymerase adds 2-10 additional templated nucleotides, causing displacement of the 3' strand, and this displaced strand is then cut at the single- to double-strand junction (Krokan and Bjoras, 2013). NER is the main DNA repair pathway used for removing bulky covalent DNA lesions that can result from radiation, chemicals, or DNA/protein crosslinks. NER senses these bulky DNA lesions by the abnormal DNA backbone structure they create, then nicks both the 5' and 3' ends of a single strand of the duplex DNA molecule within a 12-13 nucleotide window surrounding the bulky lesion. This releases the single strand of DNA, a new strand of DNA is synthesized in its place, and this new strand of DNA is ligated in place (Sancar et al., 2004). SSBR acts directly on single stranded regions of DNA that occur when a single strand of the DNA molecule is nicked twice in nearby regions, which can be caused by DNA damaging agents such as ROS or IR. In this case, proteins such as PARP1 are loaded onto these regions, which then serve to recruit the various factors necessary for filling in this single stranded region (such as XRCC1, PCNA, and DNA polymerases) (Caldecott, 2008).

Mismatch repair is a process by which mismatched nucleotides and insertion/deletions that occur, primarily during replication, are sensed and repaired. The exact mechanism by which

mismatches are sensed is still not understood (Kunkel and Erie, 2015). However, once a mismatch is located, the cell determines which strand is the newly synthesized (and therefore incorrect strand) by a process known as strand discrimination. This is believed to occur by determining which strand is discontinuous (i.e. has a free 3' end) and is therefore newly synthesized. The discontinuous strand is then nicked on either the 3' or 5' end of the mismatched base. This nicked DNA segment is removed by the EXO1 endonuclease, and the resulting single-stranded gap is then filled in by DNA polymerase and ligated (Fukui, 2010; Kunkel and Erie, 2015).

HR, SSA and NHEJ generally act upon DSBs, rather than damaged bases. DSBs can be caused by reactive oxygen species (ROS), ionizing radiation, V(D)J recombination, replication fork collapse and some chemotherapeutics. The choice to use HR, SSA, or NHEJ to repair a DSB is believed to be determined by the type of proteins loaded at the DSB, the stage of the cell cycle, the resection length of the DSB and if there are homologous sequences flanking the DSB, although this is still an area of active investigation. The major determinant, however, may be the stage of the cell cycle, as HR requires a homologous sequence, which usually comes in the form of a sister chromatid, to operate (Symington and Gautier, 2011). HR is generally an error-free process, whereas SSA generally results in deletions between repeat sequences, and NHEJ may result in deletions, insertions, and translocations.

Both HR and SSA are initiated when the MRE11/RAD50/NBN (MRN) complex is loaded onto DSBs during the S, G_2, or M stages of the cell cycle. This primarily occurs during these stages of the cell cycle as HR and SSA require a sister chromatid, which is only present during these stages of the cell cycle. The MRN complex then promotes resection of the 5' strand on both DNA ends, in a process known as 5'-3' resection, leaving free 3' strand overhangs, which are coated by the heterotrimeric single-strand binding protein RPA. RAD51 is then recruited to this 3' RPA bound ssDNA and begins scanning for sequences with homology to this 3'

overhang. Upon finding homology, a process known as strand invasion occurs, whereby the 3' overhang invades the sister chromatid and forms a D-loop. This homologous sister chromatid is then used as a template for DNA polymerase to resynthesize the correct nucleotides on this invading strand, ultimately resulting in a cross-shaped structure known as a Holliday junction. The non-invading 3' overhang still needs to be synthesized, and this is where the HR and SSA pathways diverge. In the HR pathway, the non-invading 3' strand uses the sister chromatid DNA strand that was displaced by the invading 3' end as a template. This generates another Holliday junction, so that there are now two Holliday junctions. These Holliday junctions are then resolved by endonucleases, which depending upon how they nick these Holliday junctions may result in a crossover (i.e. one end of the originally damaged chromatid is fused to the other end of the undamaged chromatid, and vice-versa) or non-crossovers (i.e. the end of the originally damaged chromatid stays fused to its original end). The SSA pathway, instead of the HR pathway, may occur if there are repeats flanking the DSB. This is because during the process of 3' strand invasion, the homologous sequence that is found during the homology search is the repeat that was downstream from the DSB, and not the sister chromatid. These repeats anneal to each other, and the intervening sequence between this repeat, due to its lack of homology, is present as a flap. This flap, present on both strands, is then removed by endonucleases. The resulting product is ligated, resulting in a deletion on both strands between these two repeats (Bhargava et al., 2016; Ciccia and Elledge, 2010).

Like HR and SSA, NHEJ is also initiated when proteins are loaded onto the ends of DSBs. However, in NHEJ, Ku70 and Ku80 proteins bind free DNA ends, protecting them from MRN binding and subsequent extensive end resection that would lead to HR or SSA. Additionally, this process can begin in any phase of the cell cycle, unlike HR and SSA. Thus, nearly all DSBs in G_1 cells are repaired by NHEJ, as well as many DSBs in S, G_2 and M-phases of the cell cycle. Ku70/Ku80 binding to the ends of double strand breaks promotes recruitment

of DNA-PK_{cs}. Depending on the type of DSB, this Ku:DNA-PK_{cs} complex will then recruit different proteins. If the nucleotides at the end of the DSB are not damaged and can be directly religated (i.e. have undamaged blunt ends or undamaged ends with complementary overhangs), Ku:DNA-PK_{cs} will recruit proteins such as XRCC4, LIG4, and XLF to religate the break. In the event that the DSB ends are not compatible, for instance when there are overhangs of different lengths and/or damaged nucleotides at the DSB ends, Ku:DNA-PK_{cs} can recruit endonucleases such as ARTEMIS and APLF to process these ends, as well as both template-dependent or template-independent DNA polymerases such as POLL or POLM, respectively, to add nucleotides. After processing of these ends, to make them either have limited complementarity or ligatable blunt ends, Ku:DNA-PK_{cs} then recruits proteins such as PNK to phosphorylate these ends and/or XRCC4, LIG4 and XLF to religate these now compatible ends. While most DSBs processed by NHEJ are correctly repaired, if endonuclease activity is required, deletions of less than 25 nucleotides generally occur, although it is possible for NHEJ to make larger deletions. Furthermore, non-templated nucleotides can be introduced, resulting in insertions. Additionally, if multiple chromosomal breaks are present in the same cell and they are both being processed by NHEJ, NHEJ may result in chromosomal translocations, where two different chromosomes are fused to each other (Ciccia and Elledge, 2010; Lieber, 2010).

1.7 Ionizing radiation

Ionizing radiation (IR) is any form of radiation, such as gamma rays, X-rays and ultraviolet light, with sufficient energy to detach electrons from atoms of molecules. While IR damages many molecules within the cell, its best studied and most lethal effect is the ability of it to damage DNA. IR damages DNA via two mechanisms: radiation can directly ionize DNA itself, or more frequently, the ionization of water results in the generation of free radicals, which then damage DNA. These two types of damage can result in damage of the DNA base, crosslinking

of DNA and the breakage of the DNA backbone (both single- and double-stranded) (Lomax et al., 2013; Santivasi and Xia, 2014). These lesions may then be repaired by pathways such as NER, BER, SSBR, HR, NHEJ, or SSA (discussed above), depending on the exact nature of the lesion. However, IR should not be viewed as a creating one type of DNA damage at one or many loci throughout the genome. In fact, IR tends to create clusters of complex DNA damage near the track of the energetic particle, such that in one region there may be multiple damaged bases, single stranded breaks, and double stranded breaks. Additionally, these energetic particles are usually delivered throughout the cell's nucleus, such that there are many clusters of DNA damage throughout the cell's nucleus. This property may underlie why IR is particularly toxic to cells, whereas DNA damage from endogenous sources, such as ROS, tends to be less toxic (Lomax et al., 2013).

IR is used to treat about two-thirds of cancers in Western countries, and is generally used when surgery is not an option (Chen and Kuo, 2017). While it is believed that the cancer-killing effects of IR are due to its DNA damaging ability, the precise reasons underlying the enhanced cytotoxicity of cancer cells compared to normal cells following IR is only partially understood. Some of the cancer cell intrinsic effects may be due to cancer cells being less competent in the repair of their DNA than normal cells, their faster proliferation rate, which may allow cancer cells less time to repair their DNA, and their tendency to have faulty cell cycle / DNA repair checkpoints, which may fail to halt the progression of the cell cycle after DNA damage (Baskar et al., 2012). Additionally, the way in which radiation therapy is delivered, either by standard hyperfractionated doses or by hypofractionation in the case of SBRT, can help ensure that cancerous cells receive a higher dose of radiation than surrounding normal cells. Standard radiotherapy is delivered generally in hyperfractionated doses, meaning that a patient will only receive a small dose of radiation every day. Frequently in NSCLC up to 60 Gy of total radiation is given to patients; however, for standard radiotherapy this is given in a

hyperfractionated manner, such that the patient only receives 2 Gy for 5 days, with 2 days off, up to 60 Gy. Typically, radiation given in this manner is given from a few different angles, in an attempt to minimize the dose of radiation given to normal cells. SBRT is delivered via multiple beams of radiation with various intensities from many different angles, more so than standard radiotherapy, and such that the tumor is the center of all paths of radiation, and therefore receives much more radiation and subsequent DNA damage than surrounding, normal tissues. As such, SBRT can deliver the same total dose of radiation as conventional radiotherapy in far fewer doses (i.e. hypofractionated). With conventional radiotherapy, 60 Gy generally takes 30 doses, whereas the same amount of total radiation is delivered in just 3-4 doses with SBRT. This decreased treatment time is believed to allow less time for tumor cells to repopulate. Additionally, it allows patients to receive secondary treatments much faster. The combination of these factors is believed to contribute to the better outcomes of NSCLC patients treated with SBRT in comparison to conventional radiotherapy (Baker et al., 2016; Chi et al., 2010; Zappa and Mousa, 2016).

SBRT and conventional radiotherapy are frequently given to NSCLC patients with curative intent when there is only local, i.e. non-metastatic, disease, as both can extend patient life. SBRT and conventional radiotherapy may also be given in a palliative setting, or as a debulking strategy (Zappa and Mousa, 2016). While SBRT therapy is extremely effective in eradicating local NSCLC tumors, 9-20% of tumors will recur locally, with another 20% of patients developing distant metastasis (Baker et al., 2016). Thus, while SBRT has dramatically improved clinical outcomes for NSCLC patients, it is imperative that new treatments that enhance the efficacy of SBRT and conventional radiotherapy are developed.

1.8 Goals of this study

As outlined above, NSCLC patients desperately need new therapeutic options, NRs are good therapeutic targets in many diseases, and NRs may play an important role in NSCLC pathogenesis. For these reasons, we decided to investigate whether NRs, their coregulators, or their chromatin remodelers are necessary for the viability of NSCLC. To do this, we performed a viability-based small interfering RNA (siRNA) screen targeting 240 nuclear receptors, coregulators and chromatin remodelers. We then attempted to validate and follow up on hits from this screen. One of the most promising hits in this screen were the proteins RUVBL1 and RUVBL2, which are present within some of the chromatin remodelers that have been implicated in NR function. Our preliminary data showed that they were overexpressed in NSCLC and high expression was prognostic of poor patient outcomes. Thus, we chose to investigate both the biological functions of RUVBL1/2 in NSCLC, as well as their potential utility as therapeutic targets.

CHAPTER TWO:
Materials and Methods

2.1 Cell lines

The following cell lines were established by Drs. John Minna and Adi Gazdar at the NIH (referred to as Hxxxx) or UT Southwestern Medical Center (referred to as HCCxxxx or HBECxxKT) (1981-2019) (M = male, F = female) and are available through ATCC or the Hamon Center for Therapeutic Oncology at UT Southwestern Medical Center: H647 (M), H2009 (F), HBEC3KT (F), HBEC30KT (F), H1993 (F), H838 (M), H1703 (M), H727 (F), HCC4017 (F), H522 (M), H1648 (M), H460 (M), HCC1833 (F), H810 (M), H226 (M), HCC15 (M), HCC95 (M), HCC4019 (M), H1819 (F), H1155 (M), H1299 (M), H2073 (F), H1666 (F), H157 (M), H1650 (M), H596 (M), H1373 (M), H1048 (F) H1355 (M) H1473 (M), H1581 (M), H1693 (F), H1755 (F), H1944 (F), H1975 (F), H2030 (M), H2085 (M), H2087 (M), H2126 (M), H2347 (F), H2882 (F), H3122 (M), H358 (M), H661 (M), H820 (M), HCC1195 (M), HCC1719 (M), HCC193 (F), HCC2814 (M), HCC4190, HCC44 (F), HCC78 (M), HCC827 (F), and H1792 (M). DFCI-024 (F) was obtained from Dana-Farber Cancer Institute. OVCAR5 (F), PANC-1 (M), PC-3 (M), SK-LU-1 (F), MIA PaCa-2 (M), DU 145 (M), EBC-1 (M), ASPC-1 (F), A-427 (M), A549 (M), HOP-62 (F), Calu-1 (M), Calu-3 (M), Calu-6 (F) IMR-90 (F) and Ramos (M) were obtained from ATCC. Lenti-X 293T cells were obtained from Takara (catalog# 632180).

2.2 Cell culture

All cancer cell lines were grown in RPMI-1640 (MilliporeSigma, catalog# R8758) supplemented with 5% FBS (ThermoFisher Scientific, catalog# 26140079). HBECs were grown in KSFM-SFM (ThermoFisher Scientific, catalog # 17005042). To split cell lines and/or create single cell suspensions, both cancer cell lines and HBECs were first washed with 1X PBS (Sigma, catalog # P3813-1PAK) then trypsinized using .05% Trypsin-EDTA (Gibco, catalog #2530054). For

cancer cell lines, trypsin was neutralized using 2 volumes of R5. For HBECs, trypsin was neutralized using 1 volume of Trypsin Neutralizing Solution (Lifelife CM-0018). Cells were then spun at 1000rpm for 5 minutes and then used for subsequent analyses. All cells were maintained in a 37°C incubator (NuAire, model NU-5810) with 5% CO2 and 95% relative humidity. Cancer cell lines were frozen in a solution consisting of 10% DMSO, 10% fetal bovine serum and 80% RPMI-1640. HBECs were frozen in a solution consisting of 10% DMSO and 90% KSFM. Cell lines were routinely checked for mycoplasma contamination (E-myco, catalog # 25233, Bulldog Bio) and DNA fingerprinted for provenance (PowerPlex Fusion24, catalog# DC2402, Promega)

2.3 Animal studies

Mice were housed by the UTSW Animal Resource Center at 68-79°F, 30-70% humidity, in individually ventilated cages, with no more than 5 mice per cage on 12 hour on:off light:dark cycles. Mice were screened for and found free of MHV, Sendai virus, MPV, EDIM, MVM, PVM< TMEV-/GD-7, REO-3 virus, Mycoplasma pulmonis, pinworms, fur mites, LCMV, ECTRO, MAV, and K virus and had unrestricted access to RO chlorinated water and irradiated 2916 Teklab global diet (Envigo, catalog# 2916). For xenografts with Compound B monotherapy, NOD/SCID females (UTSW breeding core, NOD.CB17-Prkdcscid/J) aged 10-12 weeks, average weight ~21g, were used. For irradiation + Compound B experiments, female nude mice (Charles Rivers, Crl:NU-Foxn1nu, catalog# 553) aged 10-12 weeks, average weight ~23g, were used. For pharmacokinetic studies, 7-week-old male BALB/c mice were used. All protocols performed at UTSW were approved and monitored by the Institutional Animal Care and Use Committee.

2.4 Inhibitors/drugs used

Compound B (RUVBL1 inhibitor) and Compound C (Compound B control) were synthesized by Daiichi-Sankyo. VE-822 (ATR inhibitor) was purchased from Selleckchem (catalog # S7102).

LY2603618 (CHEK1 inhibitor) was purchased ApexBio (catalog # A8638). Puromycin was purchased from InvivoGen (catalog # ant-pr-1). Geneticin (G418) was purchased from ThermoFisher Scientific (catalog # 11811031). Doxycycline was purchased from MilliporeSigma (catalog # D9891).

2.5 Antibodies

Primary antibodies used include: RUVBL1 (MilliporeSigma Catalog # SAB4200194, Immunoblot 1:1000, IHC 1:1000), RUVBL2 (Abcam Catalog # ab36569, Immunoblot 1:1000), phosphoHistone H3 (Abcam Catalog # ab5176, Immunoblot 1:2000, Immunofluorescence 1:500), ATM (Abcam Catalog # ab201022, Immunoblot 1:1000), ATM (SantaCruz Catalog # sc-377293, Immunoblot 1:5000), phosphoATM (Santa Cruz Catalog # sc-47739, Immunoblot 1:5000), DNA-PK_{cs} (PRKDC) (Santa Cruz Catalog # sc-9051, Immunoblot 1:2000), phosphoDNA-PK_{cs} (PRKDC) (Abcam Catalog # ab18192, Immunoblot 1:1000), ATR (GeneTex Catalog # GTX70109, Immunoblot 1:1000), H2AX (Abcam Catalog # ab124781, Immunoblot 1:4000), phosphoH2AX or γH2AX (clone JBW301, MilliporeSigma Catalog # 16-193, Immunoblot 1:4000, Immunofluorescence 1:1000), phosphoH2AX or γH2AX (Cell Signaling Technology Catalog # D7T2V, IHC 1:1000), CHEK1 (SantaCruz Catalog # sc-8408, Immunoblot 1:1000), phosphoCHEK1 (Cell Signaling Technology Catalog # 2344, Immunoblot 1:1500), HSP90 (SantaCruz Catalog # sc-13119, Immunoblot 1:2000), BrdU (Santa Cruz Catalog # sc-32323, Flow cytometry 1:200), V5 (Genscript Catalog # A01724, Immunoprecipitation 15ug/20million cells, Immunoblot 1:2000), V5 (Bethyl Labs Catalog # A190-120A, Immunoblot 1:2000), Mouse IgG1 (Cell Signaling Technology Catalog # 5415, Immunoprecipitation 15ug/20million cells), a-Tubulin (Cell Signaling Technology Catalog # 3873, Immunoblot 1:2000), GAPDH (Cell Signaling Technology Catalog # 2118, Immunoblot 1:2000), PARP1 (Cell Signaling Technology Catalog # 9532, Immunoblot 1:2000), RPA1 (Abcam Catalog # ab79398, Immunoblot 1:1000), RPA2 (Abcam Catalog # ab2175, Immunoblot 1:1000, Flow Cytometry

1:100, Immunoprecipitation 1ug/2million cells), RPA3 (Abcam Catalog # ab97436, Immunoblot 1:1000), 53BP1 (Cell Signaling Technology Catalog # 4937, Immunofluorescence 1:500), RPAP3 (ProteinTech Catalog # 23741-1-AP, Immunoblot 1:1000), PIH1D1 (ProteinTech Catalog # 19427-1-AP, Immunoblot 1:1000), PFDN6 (ThermoFisher Catalog # PA5-61657, Immunoblot 1:1000), PDDRG1 (ProteinTech Catalog # 16968-1-AP, Immunoblot 1:1000), TTI1 (Bethyl Labs Catalog # A303-451A, Immunoblot 1:1000), TTI2 (Bethyl Labs Catalog # A303-476A, Immunoblot 1:1000), TELO2 (ProteinTech Catalog # 15975-1-AP, Immunoblot 1:1000).

Secondary antibodies used include: Goat anti-Rabbit HRP conjugate (Cell Signaling Technology Catalog # 7074, Immunoblot 1:2000), Horse anti-Mouse HRP conjugate (Cell Signaling Technology Catalog # 7076, Immunoblot 1:2000), Goat anti-Mouse IRDye 680RD conjugate (LiCor Catalog # 925-68070, Immunoblot 1:15000), Goat anti-Rabbit IRDye 800CW conjugate (LiCor Catalog # 925-3221, Immunoblot 1:15000), Goat anti-mouse Alexa Fluor 488 conjugate (ThermoFisher Catalog # A-11029, Flow Cytometry 1:200, Immunofluorescence 1:500), Donkey anti-Rabbit Alexa Fluor 555 conjugate (ThermoFisher Catalog # A-31572, Immunofluorescence 1:500), Goat anti-mouse IgG-Peroxidase polymer detection kit (Vector Laboratories Catalog # MP-7452, ready-to-use solution)

2.6 esiRNA production

To generate esiRNAs, we followed the protocol of (Kittler et al., 2005a).

2.7 siRNA and esiRNA transfection in 6-well plates

For all cell lines, for all assays involving siRNA or esiRNAs, cells were first trypsinized, spun down and resuspended as a single cell solution. For each well in a 6-well tissue culture treated plate, 2-3 μL of RNAiMAX (ThermoFisher Scientific, catalog # 13778150) was first incubated with 500 μL of serum-free RPMI 1640 for 5 minutes, then mixed with 3 μL of 20 mM siRNA or esiRNA (Kittler et al., 2007) for 15 minutes. From the single cell solution, 50,000-150,000 cells

(counted using a Beckman Coulter Z2 Particle Counter at >12 microns) in 2.5 mL of RPMI 1640 with 5% FBS were then mixed and left overnight. In the morning, media was changed. For cell growth assays, 5 days after transfection cells were trypsinized and counted using a Beckman Coulter Z2 particle counter at >12 microns and normalized to respective controls. For experiments mentioning RNAi-RUVBL1 or RNAi-RUVBL2, these values represent the average (mean) of the percent of cells remaining after siRUVBL1/2 knockdown and esiRUVBL1/2 knockdown (respectively), in comparison to control oligonucleotides (siNTC or esiGFP). For immunoblots, the cells were washed twice with ice-cold PBS, scraped on ice, and then treated and analyzed following the Immunoblots methods outlined in this manuscript. For RUVBL1/2 WT and ATPase dead rescue experiments, where endogenous RUVBL1/2 were depleted and exogenous WT or ATPase dead RUVBL1/2 was supplied, 2 μg/mL doxycycline (MilliporeSigma, catalog# D9891) was added immediately following transfection. When multiple siRNAs were transfected, final siRNA concentration was kept at 20 nM. The following siRNAs were used for all follow-up studies on RUVBL1/2: siRUVBL1 5'-CAGAGCTAACTCCGTGTGAGA-3' (Millipore Sigma, custom synthesis), siRUVBL2 5'-UAACAAGGAUUGAGCGAAU-3' (On-Target Plus, GE Healthcare, Catalog # J-012299-05) and siNTC (On-Target Plus, GE Healthcare, Catalog # D-001810-01). The following primers were used to generate esiRNAs used for all follow-up studies on RUVBL1/2: esiRUVBL1f 5'- TCACTATAGGGAGAGGAGGCATGTGGCGTCATAGT-3' esiRUVBL1r 5'- TCACTATAGGGAGAGTCAAGGTCGAATTCTGTGGCA-3', esiRUVBL2f 5'-TCACTATAGGGAGAGACGGAGATCATCGAAGGGGA-3' esiRUVBL2r 5'-TCACTATAGGGAGAGTCGTCGATGAACAGCACTCC-3', esiGFPf 5'-TCACTATAGGGAGAGACGTAAACGGCCACAAGTTC03' esiGFPr 5'-TCACTATAGGGAGACGCGGATCTTGAAGTTCACCT-3'.

2.8 siRNA and esiRNA transfections in 96-well plates

All transfections were performed with a final concentration of 20nM of oligonucleotides unless otherwise specified. For siRNAs, oligo libraries were purchased from Qiagen as pools of four siRNAs. For esiRNAs, target sequences were identified using DEQOR (primers listed in **Table 2**). The siRNA library from Qiagen was resynthesized by Dharmacon about halfway through screening and both libraries showed similar effects. Individual siRNAs utilized in follow up studies were sequences from the primary screen resynthesized by Sigma-Aldrich. Cell lines were optimized for transfection by varying lipid volume and cell number and measuring the proliferative difference between siNTC (Dharmacon) and toxic control oligo siPLK1 (Sigma). Because so many cell lines were to be screened in the 96-well format, a detailed, high-throughput methodology was developed to allow the accurate determination of transfection conditions for each cell line. Optimal transfection conditions for each cell line can be found in **Table 1**. Briefly, for transfection optimization, eight possible conditions were tested (2000, 4000, 6000, or 8000 cells per well and 0.2 or 0.4 uL of RNAiMAX transfection reagent per well), as well as controls consisting of: cells only, lipid only, scrambled control siRNA, and toxic control siRNA controls. Both transfection efficiency (inferred from the killing efficiency of the toxic control) and transfection toxicity (assessed by the comparison of the lipid control and the scrambled control to the cells only control) were considered in choosing the most appropriate transfection condition for each cell line tested. After optimization, the library was screened on each cell line. The siRNAs in each plate were arrayed and dispensed using UTSouthwestern's High-Throughput Robotics Core Facility at a concentration of 100nM in 20uL of RNAse/DNAse free water (Ambion). Edge wells were not used as testing wells to avoid effects caused by evaporation of the media. A solution of either 0.2 or 0.4 uL of RNAiMAX transfection reagent (depending on the predetermined optimal transfection conditions) per 20uL of RPMI 1640 serum free media was made and allowed to incubate at room temperature for 5 minutes to allow for

lipid complexes to form. Following incubation, 20uL of this mixture was added to each testing well of the 96-well plate using an eight-channel handheld repeating pipette gun (BioRad) and incubated for 20 minutes. Cells were trypsinized, spun down, resuspended as a single cell solution, cell numbers counted using a Beckman Coulter Z2 particle counter at >12 microns and after the 20 minute incubation, varying amounts of cells were seeded in 50uL of RPMI 1640 + 10%FBS, such that 2000-8000 cells/well were seeded in each well. The final volume of the well was brought to 100uL using serum free media resulting in a final media condition of 100uL of RMPI + 5% FBS.

2.9 Immunohistochemistry (IHC)

For IHC of RUVBL1 in patient tumors, two tissue microarrays (TMAs) were prepared using three 1.0-mm tissue cores obtained from the center, middle and periphery of formalin-fixed and paraffin-embedded (FFPE) histological sections from 752 surgically resected primary NSCLC tumors. All NSCLC tissues were evaluated, and patients underwent surgical resection at The University of Texas MD Anderson Cancer Center, following informed consent under protocols approved by the university's Institutional Review Board. From each FFPE sample, 4-micron sections were cut in a microtome and mounted on charged glass slides. All staining was performed automatically using the Leica Bond Max Autostainer system (Leica Biosystems). Antigen retrieval was performed with Epitope Retrieval Solution 1 BOND (Leica Biosystems, catalog# AR9961) and staining performed using the Bond Polymer Refine Detection kit (Leica Biosystems, catalog# DS9800) with RUVBL1 antibody at 1:1000 (MilliporeSigma, catalog# SAB4200194). Bond Polymer Refine Detection kit (Leica Biosystems) was employed as a detection system and diaminobenzidine (DAB) was used as chromogen for the visualization of the IHC staining. The slides were then counterstained with hematoxylin, dehydrated and coverslipped. Fallopian tube tissue was used as a positive control. After quality control on all slides, slides were scanned in an Aperio AT2 scanner (Leica Biosystems). IHC scoring was

performed by a pathologist (P.V.) using a brightfield microscope and the data was presented as the average of the H-scores (which ranges from 0 to 300 and incorporates both the intensity and percent of stained tumor cells) for both nuclear and cytoplasmic staining. The final data, images and report was reviewed by an independent pathologist (J.R.).

For ATM IHC, tumors were fixed in 10% neutral buffered formalin (VWR, catalog# 89497-305) for 48 hours. Tumors were then embedded in paraffin, sectioned into 4-micron slices and placed onto positively charged slides. All staining was performed automatically using the Leica Bond Max Autostainer system (Leica Biosystems). Antigen retrieval was performed with Epitope Retrieval Solution 2 BOND (Leica Biosystems, catalog# AR9640) and Bond Polymer Refine Detection kit (Leica Biosystems, catalog# Catalog# DS9800) was employed as a detection system with 1:300 ATM antibody (Abcam, catalog# ab32420). We used a modified protocol that removed the post-primary antibody step to avoid background from mouse tissue IgG. Diaminobenzidine (DAB) was used as chromogen for the visualization of the IHC staining. The slides were then counterstained with hematoxylin, dehydrated and coverslipped. Human breast cancers that were positive for ATM was used as a control. After quality control on all slides, slides were scanned in an Aperio AT2 scanner (Leica Biosystems) and scored using Aperio Toolbox Image Analysis software (Leica Biosystems) applying a nuclear algorithm by a pathologist (P.V.) and data was presented as a percentage of positive tumor cell nuclei. Final data, images and report was reviewed by an independent pathologist (J.R.).

For γH2AX IHC, tumors were fixed in ice-cold 4% paraformaldehyde (Electron Microscopy Sciences catalog # 15710) for 48 hours with slight agitation at 4°C, then embedded in paraffin, sectioned into 4-micron slices and placed onto positively charged slides. Slides were heated at 60°C for 10 minutes, deparaffinzed and rehydrated. Antigen retrieval was performed with a Biocare Medical Decloaking Chamber at 110°C for 17 minutes using 10 mM sodium citrate pH 6 then allowed to cool to room temperature for 30 minutes. Slides were washed for 5 minutes with

PBS, incubated in ice-cold 10% methanol for 10 minutes at room temperature, washed with de-ionized H20 for 5 minutes, then tissue was blocked for 30 minutes using SignalStain Antibody Diluent (Cell Signaling Technology, catalog # 8112). Blocking buffer was removed, then γH2AX antibody (Cell Signaling Technology, catalog # D7T2V) was diluted 1:1000 in SignalStain Antibody Diluent and added to samples at 4°C overnight with agitation. Samples were washed 3 times with .05% PBST for 5 minutes, once with PBS for 5 minutes, then secondary antibody solution (Vector Labs, ImmPRESS HRP Anti-Mouse IgG Polymer Detection Kit made in Goat, catalog # MP-7452) was added for 30 minutes with agitation at room temperature. Samples were washed once with .2% PBST for 5 minutes, twice with .5% PBST for 5 minutes, then a solution of 1:250 Opal570 (PerkinElmer, catalog # FP1488001KT) in 1X Plus Amplification Diluent (PerkinElmer, catalog # FP1498) was made and added to samples for 3 minutes. After 3 minutes, the solution was quickly aspirated and washed with .05% PBST 3 times, then washed with PBS + 2 mM EDTA for 10 minutes. Coverslips were mounted using Fluoroshield Mounting Medium with DAPI (Abcam, catalog # ab104139) and sealed with nail polish. Images were captured at 20X using a Keyence BZ-X710. For quantification, obvious debris and non-tumor tissue was first masked, then nuclear γH2AX signal was quantified using Fiji by splitting the multicolor images into three channels, selecting DAPI positive nuclei (“Find Edges”, “Make Binary”, “Close-“, “Fill Holes”, and “Create Selection”), applying this selection to the γH2AX channel, and measuring the median fluorescent intensity.

2.10 Immunoblots

Cells were washed twice with ice-cold PBS and then scraped on ice. Cells were lysed with a modified RIPA buffer (50 mM Tris, 150 mM NaCl, .1% SDS, 1% IGEPAL CA-630, 1% sodium deoxycholate, 2 mM $MgCl_2$, pH 8) with 1 unit/μL benzonase (MilliporeSigma, catalog # E1014), protease inhibitors (MilliporeSigma, catalog # P8340) and phosphatase inhibitors (MilliporeSigma, catalog # 4906845001) by rotating lysates at 4°C for 2 hours. Lysates were

then cleared by spinning at max speed for 10 minutes, quantified using BCA (ThermoFisher Scientific, catalog # 23225), mixed with 2X Laemmli buffer (BioRad, catalog # 1610737EDU) and boiled for 5 minutes immediately prior to loading. For ATR, ATM, and DNA-PKCS, 20-25 μg of protein was ran on a NuPAGE 3-8% Tris-Acetate gel (ThermoFisher Scientific, catalog # EA0375BOX) using NuPAGE Tris-Acetate SDS Running Buffer (ThermoFisher, catalog # LA0041) at 150V. For all other proteins, 20-25 μg of protein was ran on a 4-20% Mini-PROTEAN TGX gel (BioRad, catalog # 4561096) at 220 V. Samples were transferred using the Trans-Blot Turbo RTA Mini Nitrocellulose transfer kit (Biorad, catalog # 1704270) on the Trans-Blot Turbo Transfer System (Biorad, catalog # 1704150) using manufacturers suggested protocols. Some blots shown are chemiluminescent blots, and for these blocking/antibody incubation steps were done with 5% milk (Biorad, catalog # 1706404XTU) in .1% in PBST. Nearly all other blots were done using near infrared fluorescence, and blocking/antibody incubation steps were done with TBS Odyssey Blocking (LiCor, catalog # 927-50100) with 0% / .2% TBST, respectively, and imaged using a LiCor Odyssey Fc. Antibody information is listed under the **Antibodies** section in the **Materials and Methods** chapter.

2.11 Plasmid transfection

To establish H1299 and H2009 cells stably expressing RNAi-resistant wild type RUVBL1 and RUVBL2 proteins, rat RUVBL1 cDNA (Dharmacon, catalog # MRN1768-202782702, IMAGE Clone ID 7304521) and rat RUVBL2 cDNA (Dharmacon, catalog # MRN1768-202784379, IMAGE Clone ID 7457010) were mutated via site-directed mutagenesis at all wobble positions to share no homology to siRUVBL1 or siRUVBL2 and then cloned from start codon to stop codon into pIRESneo3 with an added C-terminal V5 tag. The resulting pIRESneo3-RUVBL1-RNAiR-V5 or pIRES-neo3-RUVBL2-RNAiR-V5 plasmids were forward transfected into 2 million H1299 or H2009 cells in a T75 using 2 μg plasmid DNA, 16 μL enhancer and 20 μL Effectene (Qiagen, catalog # 301425) following manufacturers protocol. Cells stably expressing the

constructs were selected for by adding .6 mg/mL G418 (ThermoFisher Scientific, Catalog# 11811031) for 2 weeks.

2.12 Lentivirus generation and transduction

To generate lentiviral particles, 2 million Lenti-X 293T cells (Clontech, catalog #632180) were forwarded transfected with 9 μg pCMV-dR8.91, 3 μg pMD2.G and 3 μg of LentiPlasmid-of-interest (i.e. pLVX-EF1A-TET3G, pLVX-TRE3G-IRES or pTRIPZ) using FuGene6 (Promega, catalog # E2691) following the manufacturers protocol. After 12 hours, media was changed and viral supernatant was collected every day for 3 days and filtered through a .45micron syringe filter (Corning, catalog # 431220). For each infection in each cell line, viral supernatant was titrated onto cells and mixed with 6 μg/mL polybrene (Santa Cruz, catalog # sc-134220) and incubated with cells overnight. Only cells receiving concentrations of viral supernatant that resulted in low infectivity (i.e. > 50% of the cells did not survive selection) were used to control for multiple integrations.

2.13 qPCR

Cells were lysed directly in 6-well plates and RNA was isolated using the RNeasy Plus Mini Kit (Qiagen, catalog# 74134) following manufacturers protocol. cDNA was synthesized from 1 μg of RNA using the iScript cDNA synthesis kit (Biorad, catalog# 1708890) following manufacturers protocols. qPCR was performed using iTaq Universal SYBR Green Supermix (Biorad, catalog# 1725120) using manufacturers protocols on an Applied Biosystems 7300 Real-Time PCR system (Thermo Fisher Scientific). All qPCR primers were verified for efficiency and their sequences are listed as follows: RUVBL1f 5'- AGAGCACTACGAAGACGCAG-3' RUVBL1r 5'-TATGACGCCACATGCCTCTC-3', RUVBL2f 5'- AACCGTTACAGCCACAACCA-3' RUVBL2r 5'-GCACCGATTCGCTCAATCCT-3', RNF4f 5'-AAGCTCAGAAGCGAACTCGG-3' RNF4r 5'-TCTCCAGCAGTTTCCACGAG-3', EP300f 5'-GCGATGGCACAGATTTTGGC-3' EP300r 5'-

CACCACCATTGGTTAGTCCCA-3', ESRRAf 5'-ACCACTATGGTGTGGCATCC-3' ESRRAr 5'-GTACTCGATGCTCCCCTGGA-3', PHBf 5'-AGTTCACAGAAGCGGTGGAA-3' PHBr 5'-CCTTTTTCTGTTGCTCAGCCTTT-3', SIN3Bf 5'-CCCGTGTCTGCACCCG-3' SIN3Br 5'-GGCGGACCTTGTCAAAGAAA-3', PIAS1f 5'-AGCCTTCCAGGTTACCTTCC-3' PIAS1r 5'-GTGGACAGTCGGACAAGTGA-3', CARM1f 5'-CCTTTAGCCAACACGGGGAT-3' CARM1r 5'-CGGAGGACCCTTGGACAATC-3', GAPDHf 5'-GAAGGTGAAGGTCGGAGTC-3' GAPDHr 5'-GAAGATGGTGATGGGATTTC-3'. Relative mRNA expression was determined using the delta delta Ct method (Schmittgen and Livak, 2008) and all primers were verified for efficiency.

2.14 PCR mutagenesis strategy to identify Compound B-resistance conferring mutations

RUVBL1 or RUVBL2 open reading frames were amplified from the pIRESneo3-RUVBL1-RNAiR or pIRESneo3-RUVBL2-RNAiR plasmids using standard error-prone Taq polymerase (Bioline MyTaq catalog # BIO-21105) and 30 cycles, with addition of flanking 5' NotI and 3' NdeI restriction sites added via primers. These conditions were chosen as 91% of PCR products should contain at least one mutation. PCR products were purified (Qiagen MinElute PCR Purification Kit catalog # 28004), digested with NotI and NdeI, then ligated into pLVX-TRE3G-IRES (digested with NotI and NdeI) using ElectroLigase (NEB catalog # M0369S). Ligated products were electroporated into ElectroMAX Stbl4 E. coli (Invitrogen catalog # 11635018) and allowed to grow for 60 minutes before 1/20th of the total volume was plated onto LB + carbenicillin (Sigma catalog # C1613) plates. All reactions were performed such that > 200 colonies were on this plate the next day, suggesting that there were at least 2000 individual transformants, and thus at least 1820 mutated RUVBL1/RUVBL2 alleles were made (2000 transformants * 91% PCR error rate). The remaining transformant mixture was grown overnight in LB + carbenicillin, then plasmid DNA was isolated (Qiagen Plasmid Midiprep catalog # 12145). Virus was packaged from these pLVX-TRE3G-RUVBL1/2-IRES plasmids and H2009 cells were transduced at .3 MOI, such that >100,000 cells received virus, and this number of

cells was maintained throughout passaging. For Compound B selection, 500,000 H2009 cells/dish were plated into 4 15 cm dishes. Two plates received 1 μg/mL doxycycline for two days, and after two days 500 nM Compound B +/- doxycycline (to respective plates) was added. Media was changed every three days until large resistant colonies emerged in the plates with doxycycline. These cells were harvested via trypsinization, genomic DNA prepared (Qiagen DNeasy Blood & Tissue Kit, catalog # 69504), and three ~500bp barcoded amplicons that covered the RUVBL1/RUVBL2 open reading frame were made via nested PCR (NEB Phusion, catalog # M0530S), pooled together, and these PCR products were isolated (Qiagen QIAquick PCR purification kit catalog # 28104). DNA was run with the D1000 ScreenTape on the Agilent Tapestation 4200 and quantified by Qubit. Libraries were prepared with the KAPA Hyper Prep Kit. Samples were end repaired, 3' ends adenylated and barcoded with multiplex adapters. Samples were then size selected prior to PCR to remove small fragments. Two cycles of PCR were used to amplify the libraries, which were then purified with AmpureXP beads and validated on the Agilent Tapestation 4200. Samples were normalized, pooled and then quantified by Qubit prior to being run on the MiSeq Reagent Kit v3 (600 cycle) chemistry. Reads obtained from pooled samples were separated into sample specific readIDs based on the barcode information. For each read in the pooled sample fastq file, 25bp containing the barcode and primer was trimmed from the 5’ end. Using the trimmed fastq file and readIDs obtained in the first step, sample specific fastq files were generated using BBMap (v 38.11). These reads were mapped to the RUVBL1 or RUVBL2 cDNA sequence using BWA (v. 0.7.15). Mismatched reads were separated from exact match reads using “NM:i:0” tag in the bam file. Read pileup information was obtained from these mismatched reads using the samtools (v.0.1.19) mpileup command. Finally, from the read pileup information, per base mismatch information was obtained using pileup2base tool. Per base error ratios were computed using an in-house Perl script. All sequencing data has been deposited under GEO accession number GSE107637.

2.15 Immunoprecipitation

For RUVBL1-V5 or RUVBL2-V5 immunoprecipitation, for each condition, 2 million H2009 cells stably expressing pIRESneo3-RUVBL1-RNAiR-V5 or pIRESneo3-RUVBL2-RNAiR-V5 were reverse transfected with 50 μL Lipofecatmine RNAiMAX and 20 nM (final concentration) siRUVBL1 or 20nM siRUVBL2 (per dish) in 4 15cm dishes following manufacturer's incubation times. For immunoprecipitation experiments involving drug treatment, 3 days after siRNA transfection cells were treated with 100 nM Compound B or Compound C for 12 hours, cells were washed twice with ice-cold PBS, scraped on ice and technical replicates were combined. For immunoprecipitation experiments without drug, cells were harvested as above 3 days after siRNA treatment. After scraping cells, all subsequent steps were performed on ice or at 4°C. Cells were lysed in 1 mL high salt NP-40 buffer (25 mM HEPES, 420 mM NaCl, 5 mM EDTA, .4% IGEPAL CA-630, 10% glycerol, pH 7.5) with protease inhibitors (MilliporeSigma, catalog # P8340) and phosphatase inhibitors (MilliporeSigma, catalog # 4906845001) for 1 hour while rotating at 4°C, then spun at max speed for 15 minutes. For Compound B and Compound C treated samples, protein concentrations were determined and normalized using BCA (ThermoFisher Scientific, catalog # 23225), 5% of the sample was saved for an Input sample, then the normalized lysate was mixed with 3 volumes dilution buffer (25 mM HEPES, 2% glycerol, pH 7.5) and filtered through a .45 micron PVDF filter (MilliporeSigma, catalog # SLHV033RS). For samples involving an IgG control (no drug treatment), 1/3rd volume from siRUVBL1 and 1/3rd volume from siRUVBL2 samples were mixed together for the IgG sample. For samples involving drug treatment and mass spectrometry, no IgG control was used as immunoprecipitated proteins from Compound B were normalized to Compound C. 100 μL of Protein G-Gamma Sepharose beads (GE Healthcare, catalog # 17088501) per sample were washed 3 times with 1 mL of 3:1 dilution:lysis buffer, resuspended in 200 μL 3:1 dilution:lysis buffer and then added for 30 minutes for pre-clearing. 15 μg V5 antibody (Genscript catalog #

A01724) or 15 μg Mouse IgG (Cell Signaling, catalog # 5415) was incubated with respective samples overnight. In the morning, 50 μL of Protein G-Gamma Sepharose beads per sample were washed 3 times in 1 mL 3:1 dilution:lysis buffer and then resuspended in 100 μL 3:1 dilution:lysis buffer, added to each sample, and rotated for 2 hours. Beads were then washed 3 times for 5 minutes using 1 mL 3:1 dilution:lysis buffer, and proteins were eluted using 50 μL of 500 μg/mL V5 peptide (MiliporeSigma, catalog# V7754) by shaking at 12°C at 900 RPM for 3 hours. Beads were pelleted, supernatant collected, and supernatant was passed through an insulin syringe (BD Biosciences, catalog# 324909). Samples were spun again, and supernatant was mixed with 4X Laemmli buffer (BioRad, catalog #1610747), boiled for 5 minutes, loaded onto a 4-20% Mini-PROTEAN TGX gel (BioRad, catalog # 4561096) and ran a distance of 2 cm. The gel was washed 3 times for 5 minutes with deionized water, stained with Coommassie (Biorad, catalog# 1610436) for 15 minutes and destained (45% methanol, 10% acetic acid, 45% deionized water) for 1 hour. Gels were imaged using the Licor Odyssey Fc. Lanes were cut, cubed into 1 mm3 pieces, then prepped for mass spectrometry (below).

For RPA2 immunoprecipitation, 6 million H2009 cells were plated into 4 15 cm dishes, allowed to attach overnight, 2 dishes were treated with 100 nM Compound B or Compound C for 24 hours, then 2 dishes were treated with 2 mM hydroxyurea for 2 hours. All subsequent steps were performed on ice or at 4°C. Cells were scraped in ice-cold PBS, washed twice with ice-cold PBS, then lysed in 300 μL of high salt NP-40 buffer (25 mM HEPES, 420 mM NaCl, 5 mM EDTA, .4% IGEPAL CA-630, 10% glycerol, pH 7.5) with protease inhibitors (MilliporeSigma, catalog # P8340), phosphatase inhibitors (MilliporeSigma, catalog # 4906845001) and 1 unit/μL benzonase (MilliporeSigma, catalog # E1014) for 2 hours, then spun at max speed for 15 minutes. For input samples, 15 μL (5%) of this supernatant was put aside. To create an IgG control, 59 μL (20%) of each sample's supernatant was combined. Each sample was then mixed with 3 volumes (236 μL) dilution buffer (25 mM HEPES, 2% glycerol, pH 7.5 with

protease and phosphatase inhibitors) and filtered through a .45-micron PVDF filter (MilliporeSigma, catalog# SLHV033RS). 100 μL of Protein G-Gamma Sepharose beads (GE Healthcare, catalog# 17088501) per sample were washed 3 times with 1 mL of 3:1 dilution:lysis buffer, resuspended in 100 μL 3:1 dilution:lysis buffer and then added to samples for 30 minutes for pre-clearing. Samples were spun, then supernatant was combined with either 6 μg RPA2 antibody (Abcam ab2175) or 6 μg Mouse IgG (Cell Signaling, catalog# 5415) and incubated overnight. In the morning, 50 μL of Protein G-Gamma Sepharose beads per sample were washed 3 times in 1 mL 3:1 dilution:lysis buffer and then resuspended in 100 μL 3:1 dilution:lysis buffer, added to each sample, and rotated for 2 hours. Beads were then washed 3 times for 5 minutes using 1 mL 3:1 dilution:lysis buffer and proteins were eluted by adding 2X Laemmli buffer (BioRad, catalog # 1610737EDU) and boiling for 5 minutes. Supernatant was passed through an insulin syringe (BD, catalog # 328438), then ran on a 4-20% Mini-PROTEAN TGX gel (BioRad, catalog # 4561096) at 220 V and subjected to standard immunoblotting procedures (see above).

2.16 Mass Spectrometry

For all samples, mass spectrometry was performed at UTSW's proteomics core using the following protocol: gel pieces were digested overnight with trypsin (Pierce) following reduction and alkylation with DTT and iodoacetamide (MilliporeSigma). The samples then underwent solid-phase extraction cleanup with an Oasis HLB microelution plate (Waters) and the resulting samples were analyzed by liquid chromatograph followed by tandem mass spec (LC-MS/MS) using an Orbitrap Fusion Lumos mass spectrometer (ThermoElectron) coupled to an Ultimate 3000 RSLC-Nano liquid chromatography system (Dionex). Samples were injected onto a 75 μm i.d., 50-cm long EasySpray column (Thermo), and eluted with a gradient from 1-28% buffer B over 60 min. Buffer A contained 2% (v/v) ACN and 0.1% formic acid in water, and buffer B

contained 80% (v/v) ACN, 10% (v/v) trifluoroethanol, and 0.1% formic acid in water. The mass spectrometer operated in positive ion mode with a source voltage of 2.4 kV and an ion transfer tube temperature of 275 °C. MS scans were acquired at 120,000 resolution in the Orbitrap and up to 10 MS/MS spectra were obtained in the ion trap for each full spectrum acquired using higher-energy collisional dissociation (HCD) for ions with charges 2-7. Dynamic exclusion was set for 25 seconds after an ion was selected for fragmentation. Raw MS data files were converted to a peak list format and analyzed using the central proteomics facilities pipeline (CPFP), version 2.0.3 (Trudgian and Mirzaei, 2012). Peptide identification was performed using the X!Tandem (Craig and Beavis, 2004) and Open MS Search Algorithm (OMSSA) (Geer et al., 2004) search engines against the human protein database from Uniprot, with common contaminants and reversed decoy sequences appended (Elias and Gygi, 2007). Fragment and precursor tolerances of 20 ppm and 0.6 Da were specified, and three missed cleavages were allowed. Carbamidomethylation of Cys was set as a fixed modification and oxidation of Met was set as a variable modification. Label-free quantitation of proteins across samples was performed using SINQ normalized spectral index Software (Trudgian et al., 2011).

To identify true RUVBL1/2 interacting proteins in Figure S4A we required co-immunoprecipitating proteins in both IP:RUVBL1-V5 and IP:RUVBL2-V5 samples to have an average enrichment of >3 fold over IgG samples (“Selected” genes) using SINQ normalized spectral indices (Trudgian et al., 2011). We then called the overlapping proteins from these two lists (IP:RUVBL1-V5 and IP:RUVBL2-V5) as true RUVBL1/2 interacting proteins. RUVBL1/2 co-immunoprecipitating proteins were ran through the gene enrichment program Enrichr (Kuleshov et al., 2016) using default settings, and gene sets were called as enriched if they were found using both the KEGG and Reactome databases.

2.17 Chemical screening strategy for Compound B and RUVBL1/2 ATPase activity

The ATPase activity of RUVBL1/RUVBL2 were evaluated using recombinant RUVBL1 and RUVBL2 proteins. For screening, RUVBL1 and RUVBL2 cDNAs were purchased from Open Biosystems and cloned into the pGEX-6P-1 plasmid (GE Healthcare, catalog # 28-9546-48) for expression in BL21 STAR (DE3) E. coli (ThermoFisher Scientific, catalog # C601003). To express and purify RUVBL1 mutant proteins, rat RNAi-resistant RUVBL1 cDNA from the pIRESneo3-RUVBL1-RNAiR plasmid were cloned via PCR into pGEX-6P-1. E. coli were sonicated in 20 mM Tris-HCl (pH 8), 1 mM EDTA, 1% Triton X-100, 1mM PMSF, 5 mM DTT, with a protease inhibitor cocktail (MilliporeSigma, catalog # P8340), and then supernatants were mixed with Glutathione Sepharose 4 Fast Flow beads for 2 hours while stirring at 4°C (GE Healthcare, catalog # 17513201). Beads were loaded onto a column, washed with 20 mM Tris-HCl (pH 8), 1% Triton X-100 and 500 mM NaCl, and then washed with PreScission Buffer (50 mM Tris-HCl, 150 mM NaCl and 1 mM DTT, pH 7). The column was then incubated with PreScission Buffer with PreScission Protease (GE Healthcare, catalog # 27-0843-01) overnight at 4°C with shaking. The column was then eluted with PreScission Buffer, reloaded onto the column, and eluted again. For chemical screening, a 2-fold assay buffer (100 mM Tris-HCl pH 7.5, 100 mM NaCl, 40 mM $MgCl_2$, 2 mM DTT, 20 μM ATP, and 0.2 mg/mL BSA) was dispensed at 24.5 μL/well to a 384-well assay plate. Various concentrations of the test compound solution was dispensed thereto at 1 μL/well. Recombinant RUVBL1 and RUVBL2 were diluted to a concentration of 50 μg/mL using sterilized water. The diluted solution was dispensed at 24.5 μL/well to the 384-well assay plate, mixed using a plate mixer, and left standing at room temperature for 1.5 hours. 5 μL of the solution in each well was transferred to a white assay plate, and ADP-Glo Reagent (Promega Corp., catalog # V9101) was dispensed thereto at 5 μL/well. After the completion of the reaction, the plate was left standing at room temperature for 40 minutes. Kinase Detection Reagent was further dispensed thereto at 5 μL/well, the plate was

left standing at room temperature for 30 minutes, and luminescence intensity was measured using a plate reader.

The % ATPase inhibitory activity for each compound was calculated according to the expression given below for luminescent intensities, where A = luminescence in well with recombinant RUVBL1/2 protein and test compound, B = luminescence in well with recombinant RUVBL1/2 protein, and C = luminescence in well with neither test compound nor recombinant RUVBL1/2 protein

$$\% \text{ ATPase inhibitory activity} = 100 * [(A - C) / (B - C)]$$

Curve fitting was performed using GraphPad Prism 4 from the concentration of each of serially diluted test compound and the % ATPase inhibitory activity at this concentration. This curve was then used to determine the concentration at which the ATPase activity was inhibited by 50% (IC_{50} value).

2.18 Pharmacokinetics for Compound B

Compound B suspended in 0.5% methylcellulose was administered orally to 7-week-old male BALB/c mice purchased from CLEA Japan, Inc and housed by Daiichi-Sankyo. Plasma samples were obtained from blood collected from each animal into tubes containing sodium heparin at 0.5, 1, 2, 4, 7 and 23 hours after administration. The concentration of Compound B in mice plasma samples was determined using API4000 LC-MS/MS system (Applied Biosystems/MDX SCIEX). Pharmacokinetic parameters of Compound B were calculated by non-compartmental analysis using the computer software BioBook (Ver. 9.4.0, ID Business Solutions Ltd.).

2.19 Viability-based drug dose-response curves

For all experiments involving dose-response curves of drugs with viability readouts, 1000-2000 cells were plated into each well of a 96-well tissue culture treated plate. After 24 hours, drugs

were added as 8-point serial dilutions. After 4 more days, viability was determined using CellTiter 96 Aqueous One Solution Cell Proliferation Assay (MTS) (Promega, catalog# G3582) on a Molecular Devices SpectraMax 190 microplate reader. Curve fitting was performed in GraphPad Prism using “[inhibitor] vs normalized response with variable slope”.

2.20 RNA-sequencing

For H2009 siRUVBL1 experiments, RNA was harvested 2.5 days after transfection; RNA for H596 siRUVBL1 experiments was harvested 3 days after transfection to ensure similar levels of protein knockdown and cell doublings. For Compound B experiments, RNA was extracted 24 hours after treatment in both cell lines. RNA was extracted and genomic DNA discarded using the RNeasy Plus Mini Kit (Qiagen, catalog # 74134). All RNA had a RIN score >9 prior to sequencing as determined by an Agilent Tapestation 4200. Libraries were assembled using 4 μg of poly adenylated RNA with Illumina’s TruSeq Stranded mRNA library prep kit (Illumina, catalog # RS-122-2101) following manufacturers protocols. Libraries were sequenced on the Illumina NextSeq 500 using V2 reagents and 75 nucleotide single end reads for an average of 30-40 million reads. TopHat (v 2.0.12), Cufflinks (v 2.2.1) and Cuffdiff (v2.2.1) were used for read mapping (using hg19), transcript calling, and differential expression analysis, respectively. For all differential expression analyses, Compound B was compared to Compound C, Compound C was compared to untreated cells, and siRUVBL1 was compared to siNTC. All RNA-seq datasets have been deposited under GEO accession number GSE107637.

2.21 GSEA analysis

For GSEA of RNA-seq data, RPKM values for genes with RPKM >1 in treated and untreated samples were fed into GSEA (V 2.2.2). For GSEA of RUVBL1/2 correlated genes and GSEA of genes correlated to RUVBL1/2 RSA scores in Project DRIVE, rank ordered correlation values

were fed into GSEA (v 2.2.2). The following gene sets from MSigDB were used in all GSEA analyses: H, C1, C2 (CGP, CP, CP:KEGG, CP:Reactome), C5, and C6.

2.22 Xenograft studies

For studies involving Compound B alone, 1 million H2009 or H596 cells in 100 μL ice-cold PBS were injected subcutaneously through a 25G needle into the right rear flank of ~10-week-old female NOD/SCID (NOD.CB17-PrkdcSCID/J) mice under isoflurane. All mice were pre-conditioned to oral gavage (gavaged orally without drug) twice prior to treatment, and the gavage tip was always dipped in a 10% sucrose solution to reduce animal stress (Hoggatt et al., 2010). Once average tumor size of all mice reached ~150 mm^3, (calculated length * $width^2$ * .52, where length is the longest axis), mice were randomized into equal groups, weighed routinely and treated via oral gavage with 175 mg/kg/day Compound B using flexible gavage tips (Instech, catalog # FTP-20-38). The treatment schedule was as follows: 4 days on treatment, 9 days off, 3 days on, 7 days off, 3 days on. On treatment days, mice were orally gavaged in the morning (9 A.M.) and evening (5 P.M.) with 100uL of vehicle (Polyethylene glycol 200, MilliporeSigma, catalog # 88440) or Compound B twice per day, such that the total dose per day was 175 mg/kg Compound B. Compound B was dissolved in polyethylene glycol 200 by douncing vigorously using a PFTE pestle and glass tube (MilliporeSigma, catalog # P7859). Tumor tissue for immunoblot, H&E and IHC was harvested after 3 days of treatment.

For studies involving Compound B and IR, 2 million H1299 cells in 100 μL ice-cold PBS were injected subcutaneously through a 25G needle into the right leg/low hip of ~10-week-old female Nude (Nu/Nu) mice under isoflurane. Mice were pre-conditioned to oral gavage, tumors measured, mice weighed, orally gavaged and treated with vehicle or Compound B as stated above for Compound B alone treatment, except that the total dose was 125 mg/kg/day on treatment days, and using the following treatment schedule: mice were treated at 9 A.M. with

drug or vehicle, irradiated with 2 Gy at 12 P.M. (if applicable), then given drug or vehicle at 5 P.M. for four days. The fifth day, mice received only 2 Gy irradiation (if applicable). Irradiation was delivered specifically to the tumor using a PXI Precision X-ray X-RAD 320 Series machine while mice were under isoflurane.

For studies involving shRUVBL1 and shNTC, 1 million H1299 cells transduced with pTRIPZ doxycycline-inducible shNTC or shRUVBL1 in 100 μL ice-cold PBS were injected subcutaneously through a 25G needle into the right rear flank of ~8-week-old female NOD/SCID (NOD.CB17-PrkdcSCID/J) mice under isoflurane. Once average tumor volume reached ~150 mm^3, 2 mg/mL doxycycline (MilliporeSigma, catalog # D9891) and 2% sucrose was added to mice drinking water until the time of sacrifice. Tumor tissue was harvested for immunoblots after 14 days of doxycycline treatment.

2.23 Isolation of proteins on nascent DNA (iPOND)

We modified the protocol of (Sirbu et al., 2012) to increase sonication efficiency and ensure equal amounts of protein lysate were utilized for pull down. For each condition, 7 million H2009 cells were plated into 6 15cm dishes, as well as one additional plate for cell counting. Cells attached overnight and were then treated with 100 nM of Compound B or Compound C for 12 hours. After 12 hours, cells on the extra plate were trypsinized and counted to determine cell numbers in each condition. EdU (Cayman Chemicals, catalog # 20518) was added to Compound C and Compound B treated cells to a final concentration of 10 μM for 10 minutes, cells were cross-linked with 1% formaldehyde (Sigma-Aldrich catalog # 252549) in PBS for 20 minutes, cross-links were quenched using 1.25 M glycine (Sigma-Aldrich catalog # 50046), washed once with ice-cold PBS, scraped in ice-cold PBS on ice and technical replicates were combined. Cells were washed twice in ice-cold PBS, then resuspended in 1 mL nuclear release buffer (pH 7.9 25 mM HEPES, 10 mM KCl, 1.5 mM $MgCl_2$, .5 mM DTT and protease inhibitors,

MilliporeSigma, catalog # P8340), rotated at 4°C for 30 minutes, then dounced 10 times in a 2 mL Kontes Dounce Homogenizer (VWR catalog # KT885300-0002). Nuclei were pelleted, supernatant aspirated, and cells were resuspended in permeabilization buffer (.25% Triton X-100 in PBS) such that there were 10 million cells/mL. Cells were slowly agitated at room temperature for 30 minutes, spun down, supernatant discarded, resuspended in ice-cold .5% BSA (Jackson ImmunoResearch, catalog # 001-000-173) in PBS and spun down. Supernatant was aspirated, cells were washed with PBS, then resuspended in click solution at 100 million cells / 5 mL, which consists of 10 μM biotin azide (Click Chemistry Tools, catalog # 1265-6), 10 mM sodium ascorbate (SantaCruz catalog # sc-215877) and 2 mM CuSO4 (SantaCruz, catalog # sc-203009A), added to PBS in that order, for 2 hours at room temperature with agitation. Cells were spun down, supernatant aspirated, cells resuspended in ice-cold .5% BSA in PBS, spun down, washed with PBS, spun down, and supernatant aspirated. Cells were resuspended in lysis buffer (1% SDS in 50mM Tris, pH 8 with protease inhibitors) at a concentration of 10 million cells / 100 μL, moved to a 15 mL polystyrene conical, rotated for 15 minutes at 4°C, then sonicated 3 times for 15 minutes each on HIGH using a Diagenode Bioruptor Plus water bath sonicator, with fresh ice-cold water added after each 15 minute run. Lysate was transferred to a 1.5 mL eppindorf tube, spun at 16000g for 10' at 4°C, the top lipid bilayer was aspirated, then supernatant was passed through a 70 μm nylon filter (Sigma-Aldrich, catalog # CLS431751). Protein lysate was quantified and normalized using BCA (ThermoFisher Scientific, catalog # 23225). From this protein lysate, 5 μL was decrosslinked by adding 90 μL H2O and 4 μL 5 M NaCl, incubating at 65°C overnight, adding 1 μL RNase A, incubating at 37°C for 30 minutes, adding 2 μL .5 M EDTA, 4 μL 1 M Tris and 1 μL proteinase K and incubating at 45°C for 2 hours. De-crosslinked DNA was isolated using QIAquick PCR purification kit (Qiagen, catalog # 28104), then ran on a .75% agarose gel to ensure that sonication yielded 100-300bp fragments. To the normalized protein lysate, 1 mL ice-cold PBS with protease inhibitors was added. Per

condition, 100 μL streptavidin agarose beads (Millipore, catalog # 161-0436) were prepared by washing beads twice with 1 mL ice-cold lysis buffer and once with 1 mL ice-cold PBS + protease inhibitors. Streptavidin agarose beads were resuspended in 100 μL PBS + protease inhibitors, added to protein lysates, and rotated at 4°C for 20 hours. Beads were washed with ice-cold lysis buffer for 5 minutes, spun down, washed with room temperature 1 M NaCl for 5 minutes, spun down, then washed two more times with ice-cold lysis buffer as done previously. Beads were collected, supernatant aspirated, 60 μL of 2X Laemmli Sample Buffer (Biorad, catalog # 1610737) added, and beads were boiled for 25 minutes to elute proteins. Eluted proteins were collected and loaded onto a 4-20% Mini-PROTEAN TGX gel (BioRad, catalog # 4561096) and ran a distance of 2 cm. The gel was washed 3 times for 5 minutes with deionized water, stained with Coommassie (Biorad, catalog# 1610436) for 15 minutes and destained (45% methanol, 10% acetic acid, 45% deionized water) for 1 hour. Gels were imaged using the Licor Odyssey Fc, then lanes were cut, cubed into 1 mm^3 pieces, and prepped for mass spectrometry as described above.

2.24 Flow cytometry experiments

Cell cycle analyses by DNA content were performed by pelleting 400,000 cells and washing twice with ice-cold PBS. Cells were resuspsended in 1 mL of ice-cold PBS, then 2.5 mL of 100% ice-cold ethanol was added dropwise while vortexing cells slowly. The sample was then stored at -20°C at least overnight, pelleted, washed with ice-cold PBS, and then resuspended in 500 μL of PI staining solution consisting of .1% Triton X-100 in PBS, 50 μg/mL propidium iodide (ThermoFisher Scientific, catalog# P3566), 100 μg/mL RNase A (Qiagen, catalog# 19101), and 2% FBS (ThermoFisher Scientific, catalog# 26140079) and placed in a 37°C waterbath for 1 hour protected from light. Samples were washed once with ice-cold PBS+2% FBS, resuspended in 500 μL ice-cold PBS+2% FBS, then filtered into a polystyrene flow tube with a

35 μm strainer (Corning, catalog# 352235) and analyzed with a BD LSRFortessa flow cytometer using BD FACSDIVA software, such that 10,000 single, live cells were gated and collected per run. The resulting gated FCS2 files were then analyzed using FlowJo software.

For BrdU incorporation assays, 250,000 H2009 cells were plated in a T75 and allowed to adhere overnight, before 2 mM thymidine (MilliporeSigma, catalog # T1895) was added for 18 hours. Cells were then washed with PBS and allowed to grow in normal media for 9 hours, after which 2 mM thymidine was added for 10 hours. After 10 hours, 100 nM Compound B or Compound C was added for 6 hours, then cells were washed with PBS (released from thymidine block) and kept in 100 nM Compound B or Compound C for the duration of the assay. At indicated time points post release (0, 3, 6, 12, 18 hours), 50 μM BrdU (MilliporeSigma, catalog # B5002) was added for 30 minutes to media before harvesting cells. Cells were harvested by pelleting 1,000,000 cells, washing twice with ice-cold PBS, resuspending the pellet in 1 mL ice-cold PBS, and then 2.5 mL 100% ice-cold ethanol was added drop wise while gently vortexing cells. Samples were stored at -20°C at least overnight, then pelleted and washed with PBS. Cells were permeabilized and DNA denatured by resuspending in 1 mL of 2 M HCl + .5% Triton X-100 for 30 minutes, then spun down and resuspended in 1mL of .1 M sodium tetraborate (MilliporeSigma, catalog # 221732). Cells were washed with .1% TBST, then blocked in 500 μL 5% BSA (Jackson ImmunoResearch, catalog # 001-000-173) in .1% TBST for 1 hour, and resuspended in 250 μL 5% BSA + 5 μL anti-BrdU antibody (Santa Cruz, catalog # sc-13119) overnight at 4°C. In the morning, cells were washed 3 times with .1% TBST, then resuspended in 250 μL BSA + 1.25 μL anti-mouse Alexa Fluor 488 (ThermoFisher Scientific, catalog # A-11029) and rotated protected from light for 1 hour. Cells were washed 3 times with .1% TBST for 5 minutes, then stained with propidium iodide and analyzed using the cell cycle protocol outlined above (starting at the addition of 500 μL PI staining solution), except that at

least 30,000 single, live cells were gated and collected per sample and overlapping fluorescent signals were mitigated via compensation.

RPA loading assays were performed by pelleting 3,000,000 cells and washing twice with ice-cold PBS. Cells were pre-extracted on ice by permeabilizing with 1 mL of ice-cold .2% Triton X-100 in PBS for 1 minute. This solution was then immediately diluted with 10 mL ice-cold PBS and spun down at 4°C. Cells were resuspended in 1 mL 4% paraformaldehyde (Fischer Scientific, catalog # 50-980-487), fixed in a 37°C waterbath for 10 minutes, kept on ice for 1 minute, and then spun down at 4°C. Cells were resuspended in 1 mL ice-cold PBS, then 9 mL of 100% ice-cold methanol was added drop wise while gently vortexing cells. This solution was stored at least overnight at -20°C, spun down, transferred to a polypropylene tube, washed with 1 mL .1% TBST, and blocked using 500 μL of 5% BSA (Jackson ImmunoResearch, catalog# 001-000-173) in .1% TBST for 1 hour while rotating. Cells were resuspended in 250 μL 5% BSA + 2.5 μL anti-RPA2 antibody (Abcam, catalog # ab2175) and rotated overnight at 4°C. Cells were washed 3 times for 5 minutes with .1% TBST, then resuspended in 250 μL 5% BSA + 1.25 μL anti-mouse Alexa Fluor 488 (ThermoFisher Scientific, catalog # A-11029) and rotated protected from light for 1 hour. Cells were washed 3 times with .1% TBST for 5 minutes, then stained with propidium iodide and analyzed using the cell cycle protocol outlined above (starting at the addition of 500 μL PI staining solution), except that at least 30,000 single, live cells were gated and collected per sample and overlapping fluorescent signals were mitigated via compensation.

For TUNEL assays, cells were synchronized and treated the same as the BrdU incorporation assay (above), except that 100 nM of the CHEK1 inhibitor LY2603618 (ApexBio, catalog # A8638) was added following the second (final) release from thymidine. At specified time points, cells were harvested by pelleting 500,000 cells, washing twice with ice-cold PBS and fixing with

1% paraformaldehyde (Fischer Scientific, catalog # 50-980-487) for 15 minutes on ice. Cells were then resuspended in 1 mL ice-cold PBS, and 2.5 mL of ice-cold 100% ethanol was added dropwise while slowly vortexing cells. This was stored at least overnight at -20°C, spun down, washed with PBS, and then stained using the APO-BrdU TUNEL Assay Kit, with Alexa Fluor 488 Anti-BrdU (ThermoFisher Scientific, catalog # A23210) only using polypropylene tubes and following manufacturers protocol with the following modifications: PBS + 2% BSA (Jackson ImmunoResearch, catalog # 001-000-173) was used instead of wash buffer to prevent cell sticking, and DNA staining and analysis was performed using the protocol outlined above for cell cycle analyses, instead of the kits solution, starting at the addition of 500 μL PI staining solution. At least 30,000 single, live cells were gated and collected per sample and overlapping fluorescent signals were mitigated via compensation.

2.25 Immunofluorescence

Cells were plated into glass chamberslides (ThermoFisher Scientific, catalog # 154526) and allowed to adhere overnight. Cells were then treated as indicated, media was aspirated, cells were fixed with 4% paraformaldehyde (Fischer Scientific, catalog # 50-980-487) for 10 minutes, washed 3 times with TBS, then permeabilized with .5% Triton-X 100 on ice for 10 minutes. After 3 TBS washes, cells were blocked with 5% BSA (Jackson ImmunoResearch, catalog# 001-000-173) in .1% TBST for 1 hour. Following blocking, cells were incubated with primary antibody + 5% BSA, using anti-γH2AX (1:1000, MilliporeSigma, catalog # 16-193), anti-phospho-Histone H3 (1:500, Abcam, catalog # ab5176), or anti-53BP1 (1:500, Cell Signaling, catalog # 4937) antibodies, for 2 hours. Cells were then washed 3 times for 5 minutes with .1% TBST and incubated with secondary antibody + 5% BSA, either anti-mouse Alexa Fluor 488 (1:500, ThermoFisher Scientific, catalog # A-11029) or anti-rabbit Alexa Fluor 555 (1:500, ThermoFisher Scientific, catalog # A-31572), for 1 hour protected from light. Chambers were then washed 3 times for 5 minutes with .1% TBST, chambers were removed, and glass

coverslips (VWR, catalog # 48404-133) were mounted using Vectashield with DAPI (Vector Laboratories, catalog # H-1200). Images were captured at 40X using a Leica DM5500 or a Keyence BZ-X710 and analyzed for foci using Cell Profiler (1.0.9717) or BZ-X Analyzer (v1.3.1.1, Keyence), respectively, with similar results. Pan-γH2AX quantification was performed manually on 10X magnification.

2.26 Surviving fraction curves

NSCLC and HBEC cells were trypsinized and re-suspended as single cell suspensions. Cells were counted (Z2 Particle Counter, Beckman Coulter) and a fixed number of cells was plated for individual doses of radiation across experimental groups, with increasing number of cells for higher levels of radiation. Counted cells were seeded in 60 mm tissue culture dishes in triplicate for each dose of radiation, allowed to attach to the dish for 6-8 hours, then irradiated at various doses using a 137Cs irradiator (Mark 1-68 irradiator, J.L. Shepherd and associates). Irradiated plates were then incubated until colonies formed, where a colony is defined as ~50 cells. The colonies were fixed and stained with 4% formaldehyde (Fischer Scientific, catalog # 50-980-487) in PBS containing 0.05% crystal violet (MilliporeSigma, catalog # C6158), and colonies were counted manually using a light microscope. The surviving cell fraction was calculated as: (Mean colony counts) / [(cells plated) X (plating efficiency)], in which plating efficiency was defined as (Mean colony counts) / (cells plated for unirradiated control). Curve fitting was performed using the Liner Quadratic equation in SigmaPlot (Systat Software Inc.), and SF2 values are from this fitted curve.

CHAPTER THREE:
Viability-Based RNAi Screening of NRs, Coregulators, and Chromatin Remodelers in NSCLC

3.1 Introduction

NRs are liganded transcription factors that control diverse pathways within cells by acting as master regulators of the transcription of these pathways. Due to their ligand-modulated nature, as well as their importance in cellular processes, many NRs have important roles in human health and disease and represent important drug targets (Gronemeyer et al., 2004). In fact, nearly 15% of all FDA approved drugs target NRs (Overington et al., 2006), and multiple NRs have FDA approved inhibitors with oncology indications (Cohen et al., 2001; Sharifi et al., 2005). However, while many NRs have highly specific and potent synthetic agonists and antagonists, some do not. Additionally, NRs do not act alone. They require coregulators to help stimulate or repress transcription, as well as chromatin remodelers to provide access to their target sequences in DNA (Gronemeyer et al., 2004). Thus, while NRs already have many synthetic ligands that can target them, the chromatin remodelers and coregulators they utilize may also represent important therapeutic targets. We recently found that NRs may play an unexpected role in the growth and/or pathogenesis NSCLC (Jeong et al., 2012; Jeong et al., 2010; Srivastava et al., 2014). Therefore, interrogating the necessity of all NRs in NSCLC for cellular growth, as well as their coregulators and chromatin remodelers, may provide new potential therapeutic targets for the treatment of NSCLC.

The discovery that in eukaryotic cells the endogenous miRNA machinery could be hijacked by exogenous siRNAs (small, double stranded RNAs 20-25 nucleotides in length) to deplete target mRNAs in a sequence-specific manner (Fire et al., 1998), revolutionized the ability of researchers to inhibit gene function, especially in mammalian cells. Before long, researchers were screening increasingly complex siRNA libraries, targeting hundreds to

thousands of genes, and examining the effect that these knockdowns had on various phenotypes, such as viability (Aza-Blanc et al., 2003). While siRNAs are an indispensable tool for quickly and easily downregulating a gene product, they are not without significant caveats. Right around the time that the first siRNA screens were being published, researchers began to realize that siRNAs could downregulate unintended or non-target genes, a phenomenon known as an off-target effect (Jackson et al., 2003), and that these off-target effects could have serious phenotypic consequences (Fedorov et al., 2006). Similar to the action of endogenous microRNAs, off-target effects are generally the result of interactions between bases 2-8 of the 5' end of an siRNA and the 3' untranslated region (UTR) of an endogenous gene (Jackson et al., 2006). These off-target effects can have strong and consistent enough phenotypic effects to obfuscate siRNA screens by producing high false-positive rates (Lin et al., 2007). While this is a significant problem with siRNAs, as well as short hairpin RNAs (shRNAs) (Jackson et al., 2006), the problem has not received the attention and scrutiny it deserves. Even when multiple RNAi reagents per gene are used in large scale screening methods, the lists of hits that are returned from these screens are essentially unusable, as the off-targets, not the on-targets, are frequently responsible for the phenotype that is being screened for (Schultz et al., 2011; Sudbery et al., 2010). On a more global and rigorous scale, multiple shRNAs targeting the same gene in a large-scale shRNA drop out screen performed on many cell lines have little to no concordance. In contrast, shRNAs with similar seed sequences, which are believed to drive the off-target effects, have highly similar phenotypes. Recently an algorithm has been deduced to help alleviate these effects, DEMETER, but use of this algorithm requires a very large dataset and was only developed recently (Tsherniak et al., 2017). Because of these wide-spread and potent off-target activities of RNAi reagents, a number of RNAi screens are now infamous for their irreproducibility and discordance (Barbie et al., 2009; Luo et al., 2009; Scholl et al., 2009), and off-target effects continue to plague the RNAi literature.

To help circumvent the off-target effect of siRNAs, researchers have developed an alternative referred to as endonuclease-prepared siRNAs (esiRNAs). These esiRNAs are prepared by digesting a 500-700 base pair double-stranded RNA molecule into small 20-25 nucleotide fragments using recombinant Escherichia coli RNase III (Kittler et al., 2004; Yang et al., 2002). As such, esiRNAs consist of a pool of siRNAs with different sequences targeting the same gene. Interestingly, this pooling effect helps retain on-target activity (i.e. esiRNAs have similar knock down efficiency as siRNAs) while mitigating off-target activity (Kittler et al., 2007).

Here, a viability-based siRNA screen targeting 240 NRs, coregulators and chromatin remodelers in NSCLC was performed. A secondary screen was then performed using esiRNAs targeting the same genes as in the siRNA in an attempt to validate hits from the siRNA screen.

3.2 Results

3.2.1 A Viability-Based siRNA Screen of NRs, Their Coregulators and Chromatin Remodelers in NSCLC

In order to determine if the downregulation of any NR, their coregulators or chromatin remodelers would impact the viability of NSCLC, 2 custom siRNA libraries from Qiagen were purchased. The first library targeted all 48 human NRs as well as 72 coregulators, referred to as the NR+CoReg library. The second library targeted 120 chromatin remodelers, referred to as the Remodeler screen. Each siRNA library was arrayed in 96-well plates, with each gene targeted in a single well by a pool of 4 different siRNAs to ensure efficient knockdown. Additionally, each plate contained one positive control (an siRNA against PLK1) and one negative control (a non-targeting siRNA) on each plate. The sequence and Qiagen Product ID for all siRNAs can be found in **Appendix A**. Transfections conditions were optimized for each cell line by testing various amounts of lipids (the transfection reagent) and cell numbers. Cell lines were only used if transfections were non-toxic (< 10 % viability loss from lipid alone) and

efficient (> 60% efficiency, read out as viability loss from an siRNA targeting PLK1, a known essential gene). Optimized transfection conditions for each cell line can be found in **Table 1**.

Cell Line	Cells/well	Lipid/well	Efficiency
A427	4000	0.2	84%
A549	2000	0.4	74%
Calu-6	2000	0.2	83%
DFCI 024	2000	0.2	66%
DFCI 032	2000	0.2	86%
EKVX	2000	0.2	77%
H1155	2000	0.2	67%
H1184	8000	0.2	60%
H1299	2000	0.2	88%
H1355	4000	0.2	67%
H1373	8000	0.2	67%
H1437	2000	0.2	81%
H1568	8000	0.2	65%
H157	2000	0.2	65%
H1573	4000	0.4	65%
H1607	8000	0.2	71%
H1650	8000	0.4	72%
H1693	2000	0.2	81%
H1703	8000	0.2	80%
H1792	2000	0.2	74%
H1819	2000	0.2	69%
H1944	2000	0.2	77%
H1975	8000	0.2	67%
H1993	2000	0.2	66%
H2009	4000	0.2	68%
H2030	4000	0.2	71%
H2073	2000	0.2	81%
H2087	8000	0.2	73%
H2122	4000	0.4	67%
H2228	2000	0.2	71%
H226	2000	0.2	69%
H23	8000	0.2	83%
H2887	8000	0.2	73%
H3122	8000	0.4	80%
H358	2000	0.2	70%
H446	2000	0.2	60%
H460	2000	0.2	84%

H522	2000	0.2	72%
H647	2000	0.2	63%
H650	8000	0.2	75%
H661	4000	0.4	77%
H838	8000	0.4	87%
H841	2000	0.2	80%
H920	2000	0.2	68%
HCC15	2000	0.2	64%
HCC1806	2000	0.2	67%
HCC1954	2000	0.2	79%
HCC2185	8000	0.2	66%
HCC3051	8000	0.2	79%
HCC3153	8000	0.2	78%
HCC4006	4000	0.4	73%
HCC4017	2000	0.2	68%
HCC4019	8000	0.2	70%
HCC461	4000	0.2	68%
HCC827	2000	0.2	82%
HCC95	2000	0.2	80%
PC9	2000	0.2	81%
HBEC3KT	4000	0.3	72%
HBEC12KT	4000	0.4	58%
HBEC15KT	2000	0.2	69%
HBEC31KT	2000	0.2	59%
HBEC34KT	4000	0.4	79%
HBEC3KT	4000	0.3	65-75%
HBEC3KT-S6Z-L6R	4000	0.3	65-75%
HBEC3KT-53	4000	0.3	65-75%
HBEC3KT-RL53	4000	0.3	65-75%
HBEC3KT-RL53-shL	4000	0.3	65-75%
HBEC30KT	4000	0.3	65-75%
HBEC30KT-S6Z-L6R	4000	0.3	65-75%
HBEC30KT-53	4000	0.3	65-75%
HBEC30KT-RL53	4000	0.3	65-75%
HBEC30KT-RL53-shL	4000	0.3	65-75%
HBEC24KT	8000	0.4	74%
H2405	2000	0.2	66%

HCC1833	2000	0.4	66%
H2347	2000	0.2	63%
H2444	4000	0.2	69%
HCC515	2000	0.2	64%
HCC1395	2000	0.2	63%
H810	4000	0.2	69%
H2250	2000	0.2	73%
H2258	2000	0.2	76%
H727	2000	0.2	75%

Table 1. 96-well Plate Transfection Conditions for all NSCLC and HBEC Cell Lines Used. Cells were reverse transfected using the following conditions (lipid = LifeTechnologies RNAiMAX) and 20 nM siPLK1 for 5 days, then cellular viability was measured using the MTS assay and a plate reader. Efficiency refers to the percent loss of viability observed following transfection of an siRNA targeting PLK1, in comparison to a control non-targeting siRNA.

Following transfection optimization, transfections were performed in NSCLC and human bronchial epithelial cells (HBECs) with three technical replicates and at least 2 biological replicates. In total, 54 NSCLC cell lines and 7 normal HBECs that were immortalized with CDK4 + hTERT expression were screened with the NR+CoReg library, whereas 51 NSCLC cell lines and 4 HBECs were screened with the Remodeler library. Additionally, the NR+CoReg library was screened on 14 HBEC cell lines with various oncogenic mutations (such as TP53 knockdown, mutant EGFR/KRAS expression, or LKB1 knockdown) and the Remodeler library was screened on 4 of these manipulated HBEC cell lines (**Figure 3.1**). The Minna lab has extensively profiled most of the cell lines utilized in this siRNA screen, and has clinical information such as the histology, smoking status and patient treatments, as well as molecular data, such as RNA-sequencing, exome sequencing and whole genome sequencing, on most of the cell lines utilized in this siRNA screen. This, coupled with the wealth of phenotypic responses from the siRNA screen alone, affords a multitude of correlative and clustering based analyses, many of which were performed and yielded interesting results. For instance, by hierarchical clustering, these siRNAs distinguished NSCLC cell lines from HBEC cell lines, and HBEC cell lines from the HBEC cell lines with oncogenic manipulations. There were also

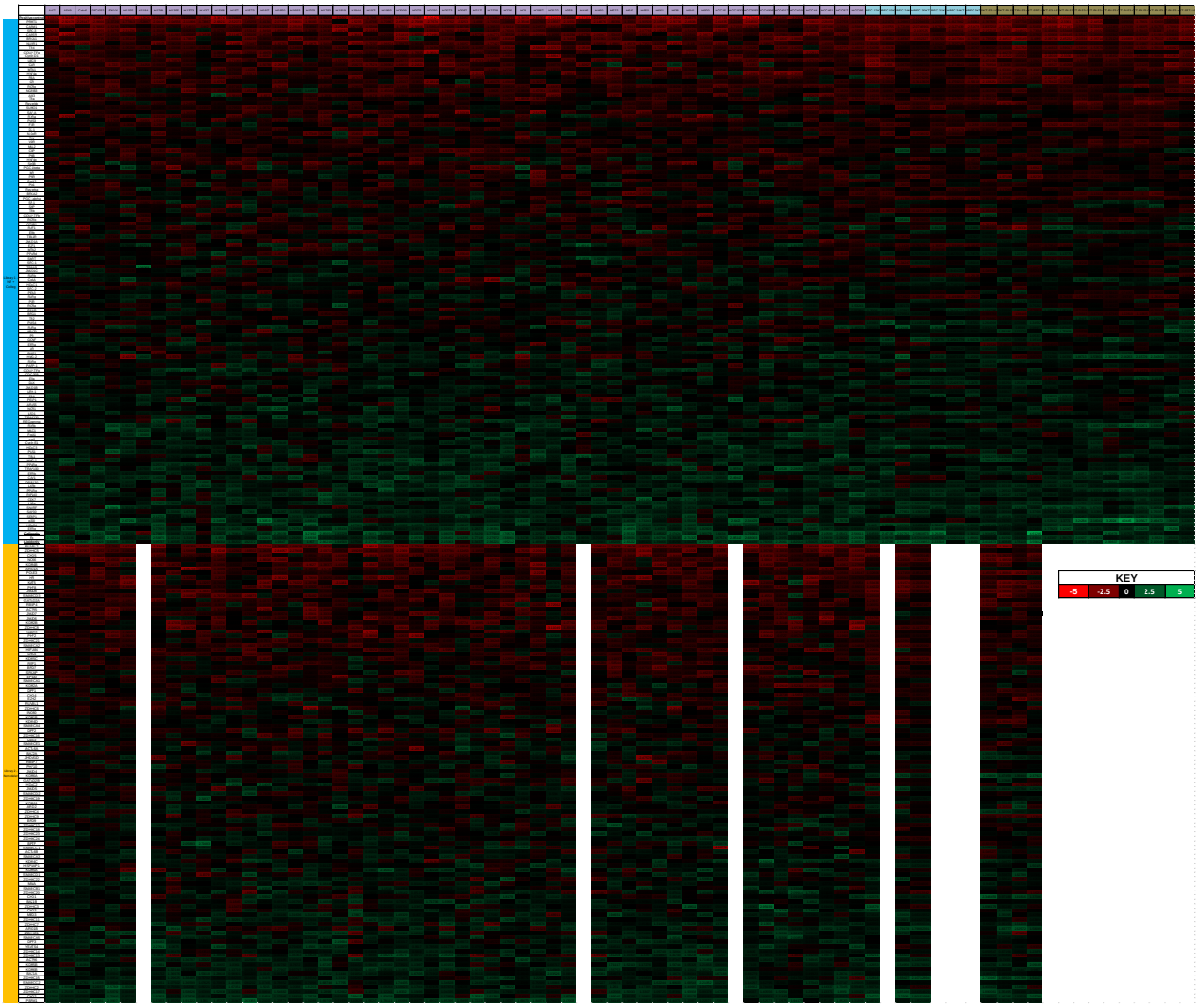


Figure 3.1. Results of Viability-Based of siRNA Screen of NR + CoRegulator (Library 1) and Remodeler (Library 2) in Approximately 50 NSCLC Cell Lines and HBECs. A variable number of cells and amount of lipid (see **Table 1**) was using to reverse transfect various cell lines with siRNAs against indicated genes. Cell viability by MTS assay was determined after 5 days using a plate reader. Heat mapped values shown are z-scores, where a negative (red) score indicates cell viability loss and a positive (green) score indicates cell viability gain. Each column represents a cell line and each row represents a gene targeted by a pool of four siRNAs. Blue and yellow coloring (far left) represent siRNAs present in NR+CoReg or Remodeler screen, respectively. Purple, blue and tan coloring (top) represent NSCLC cell lines, HBECs, and HBECs with oncogenic manipulations, respectively.

were also siRNAs that specifically killed cancer, but not HBECs, as well as siRNAs that tended to kill certain lineages (for instance, adenocarcinoma rather than squamous cell carcinoma). Furthermore, there were molecular correlates to these siRNA-induced phenotypes, such as siRNAs that specifically killed KEAP1 mutant cell lines. Thus, these siRNAs phenotypes

provided a wealth of information. However, prior to following up on these hits, a secondary screen to validate these hits using a more reliable RNAi technology, endoribonuclease-prepared siRNAs (esiRNAs) (Kittler et al., 2004; Kittler et al., 2007), was performed to determine if these hits were true positives or false positives.

3.2.2 Validation of the siRNA Screen of NRs, Their Coregulators and Chromatin Remodelers using esiRNAs

Although not frequently discussed and underappreciated, most RNAi technologies, such as siRNAs and shRNAs, have a propensity to downregulate 100-200 non-target or off-target transcripts (i.e. genes that we not intended to be downregulated) (Kittler et al., 2007). These off-target effects can produce cellular phenotypes, such as loss of viability (Fedorov et al., 2006), and therefore confound screens. Thus, every siRNA phenotype needs to be replicated with multiple, independent RNAi reagents, orthogonal approaches (CRISPR or pharmacological inhibition) or ideally, the gold standard, genetic rescue studies. Since CRSIPR had not yet been invented, small molecules against all targets in our library do not exist (and it should be noted that small molecules generally also have hundreds to thousands of off-targets), and genetic rescues are not feasible in medium- to high-throughput setting yet, a secondary screen utilizing a slightly orthogonal and more reliable RNAi reagent, esiRNAs (Kittler et al., 2007) was performed. Like chemically produced siRNAs, these are generally 21-25 nucleotide double-stranded RNA molecules with 3' overhangs. However, unlike chemically synthesized siRNAs, esiRNAs consist of a pool of thousands of unique siRNAs, produced by digestion of a 500bp dsRNA fragment randomly by an endonuclease. Compared to siRNAs, these reagents have a reduced propensity to downregulate off-target transcripts (Kittler et al., 2007).

Library	Gene name	Forward primer (5'-3')	Reverse primer (5'-3')
Library 1 - NR+CoReg	AR	TCACTATAGGGAGAGCTGTGCAAGTGCCCAAGAT	TCACTATAGGGAGACAAACTTCCCGTGGCATAAGA
Library 1 - NR+CoReg	NR1I3	TCACTATAGGGAGAGTGCTTAGATGCTGGCATGA	TCACTATAGGGAGACCGCAGAGGAAGTTTTGTGT

Library 1 - NR+CoReg	NR2F1	TCACTATAGGGAGAGCCTCTCTCCCTCCTCTCCTC	TCACTATAGGGAGACTCTCGCTGCCTTCTTCTTTC
Library 1 - NR+CoReg	NR2F2	TCACTATAGGGAGAGTCAACTGCCACTCGTACCTG	TCACTATAGGGAGACGCTTTCCACATGGGCTACAT
Library 1 - NR+CoReg	NR2F6	TCACTATAGGGAGAGGTTGAGAGCCTGCAGGAGAA	TCACTATAGGGAGACCCTAGGATTGGACCCTCCAT
Library 1 - NR+CoReg	NR0B1	TCACTATAGGGAGAGCTTGCAGTTCGAGACTGTGG	TCACTATAGGGAGACATGATGGGCCTGAAGAACAG
Library 1 - NR+CoReg	ESR1	TCACTATAGGGAGAGAGCACCCTGAAGTCTCTGGA	TCACTATAGGGAGACATGAAGTAGAGCCCGCAGTG
Library 1 - NR+CoReg	ESR2	TCACTATAGGGAGAGATAAAAACCGGCGCAAGAG	TCACTATAGGGAGACCCAACTTGGTCAGGGACATC
Library 1 - NR+CoReg	ESRRA	TCACTATAGGGAGAGGCCAGAGTCTCCCAGTG	TCACTATAGGGAGACAAAACCAAAAGCGGTTTCTC
Library 1 - NR+CoReg	ESRRB	TCACTATAGGGAGAGTCAGAGAGCAGCCCATACCT	TCACTATAGGGAGACGCGTCACAAACTCCTCCTTC
Library 1 - NR+CoReg	ESRRG	TCACTATAGGGAGAGCCGTGCAGCATTTCTACAAC	TCACTATAGGGAGACAAAGAAAGAAGGCAGGCAGA
Library 1 - NR+CoReg	NR1H4	TCACTATAGGGAGAGTTTGGACCATGAAGACCAGA	TCACTATAGGGAGACAGCGTGGTGATGATTGAATG
Library 1 - NR+CoReg	NR6A1	TCACTATAGGGAGAGTTCTGCGAGCTCTCAATCAA	TCACTATAGGGAGACGGCACATTCACCATCTTTCC
Library 1 - NR+CoReg	NR3C1	TCACTATAGGGAGAGCCCTACCCTGGTGTCACTGT	TCACTATAGGGAGACGGCTCTTCAGACCGTCCTTA
Library 1 - NR+CoReg	HNF4A	TCACTATAGGGAGAGGCCAAGTACATCCCAGCTTT	TCACTATAGGGAGACTGGATCTGCTCGATCATCTG
Library 1 - NR+CoReg	HNF4g	TCACTATAGGGAGAGGGTCTCGCCAGATCTCAGTC	TCACTATAGGGAGACGCTTAGCCCTTTTGCATCTG
Library 1 - NR+CoReg	NR5A2	TCACTATAGGGAGAGTGCGTGGAGGAAGGAATAAG	TCACTATAGGGAGACGCTGGAGAGCTCGTCTGGTA
Library 1 - NR+CoReg	NR1H3	TCACTATAGGGAGAGCCCTTCAGAACCCACAGAGA	TCACTATAGGGAGACCTTCTCGATCATGCCCAGTT
Library 1 - NR+CoReg	NR1H2	TCACTATAGGGAGAGCAGCAGCAGGAGTCACAGTC	TCACTATAGGGAGACGTGGAAGTCGTCCTTGCTGT
Library 1 - NR+CoReg	NR3C2	TCACTATAGGGAGAGCATTCATGTTCAGGCACCTC	TCACTATAGGGAGACGACCGGATACCCATCACTTC
Library 1 - NR+CoReg	NR4A1	TCACTATAGGGAGAGACCTTCATGGACGGCTACAC	TCACTATAGGGAGACTGAAGGAAAAGAAGGCTGGA
Library 1 - NR+CoReg	NR4A3	TCACTATAGGGAGAGAAGAGACGTCGAAACCGATG	TCACTATAGGGAGACTGAAGTCGATGCAGGACAAG
Library 1 - NR+CoReg	NR4A2	TCACTATAGGGAGAGCCCAGTGGAGGGTAAACTCA	TCACTATAGGGAGACGAGCTGAGACTGCTCACACG
Library 1 - NR+CoReg	NR2E3	TCACTATAGGGAGAGCACTTCATGGCCAGCCTTAT	TCACTATAGGGAGACCTGGCTTGAAGAGGACCAAG
Library 1 - NR+CoReg	PPARa	TCACTATAGGGAGAGGCCTCAGGCTATCATTACG	TCACTATAGGGAGACAGCCATACACAGTGTCTCCA
Library 1 - NR+CoReg	PPARd	TCACTATAGGGAGAGAGCCAGTACAACCCACAGGT	TCACTATAGGGAGACGCGTTGAACTTGACAGCAAA
Library 1 - NR+CoReg	PPARg	TCACTATAGGGAGAGTGAATGTGAAGCCCATTGAA	TCACTATAGGGAGACTGGAAGAAGGGAAATGTTGG
Library 1 - NR+CoReg	PGR	TCACTATAGGGAGAGTTCCACCACTGATCAACCTG	TCACTATAGGGAGACAGCCCTTCCAAAGGAATTGT
Library 1 - NR+CoReg	NR1I2	TCACTATAGGGAGAGTGTGTCTCTGCATCCATTTGA	TCACTATAGGGAGACTGATTGTCAGCGTAGCCTTG
Library 1 - NR+CoReg	RARa	TCACTATAGGGAGAGCCTTGCTTTGTCTGTCAGG	TCACTATAGGGAGACTTGGCGAACTCCACAGTCT
Library 1 - NR+CoReg	RARb	TCACTATAGGGAGAGTCAAAATGATTTACCCCTGGTT	TCACTATAGGGAGACCTGGCAGTTACACTGATACAGAA
Library 1 - NR+CoReg	RARg	TCACTATAGGGAGAGCCGCGACAAAAACTGTATCA	TCACTATAGGGAGACGCAGAGTGATCTGGTCAGCA
Library 1 - NR+CoReg	NR1D1	TCACTATAGGGAGAGTGTATGCAGCCCCAGAAG	TCACTATAGGGAGACGCTTCTCGCTGAAGTCGAAC
Library 1 - NR+CoReg	NR1D2	TCACTATAGGGAGAGTGGACAGTTCAAAGGGAGGA	TCACTATAGGGAGACTAATGATGCGAACCGTACCA
Library 1 - NR+CoReg	RORa	TCACTATAGGGAGAGCGTGCCTTTGACTCTCAGAAC	TCACTATAGGGAGACGCATTGCTGGCTCAAATTCT
Library 1 - NR+CoReg	RORB	TCACTATAGGGAGAGCCCCTTCTTCCTCATCTTCC	TCACTATAGGGAGACTTCATGGCACTCTGCATCTC

Library 1 - NR+CoReg	RORC	TCACTATAGGGAGAGGAGGAAGTCCATGTGGGAGA	TCACTATAGGGAGACAAGGCCAGCTCCAGATTGTA
Library 1 - NR+CoReg	RXRa	TCACTATAGGGAGAGCATCTTTGACAGGGTGCTGA	TCACTATAGGGAGACGCTAGTTCTTGCCACGAAGG
Library 1 - NR+CoReg	RXRb	TCACTATAGGGAGAGAGGTCAGGCAGCTGACAAACAG	TCACTATAGGGAGACCCTGCTGCTCAGGGTACTTC
Library 1 - NR+CoReg	RXRg	TCACTATAGGGAGAGAGGACATCAAGCCCTTACCA	TCACTATAGGGAGACGGTTCAACAGCAAGTTCAGC
Library 1 - NR+CoReg	NR5A1	TCACTATAGGGAGAGATGGTCTTCAAGGAGCTGGA	TCACTATAGGGAGACTGGAGTATGTGGCTTGGACA
Library 1 - NR+CoReg	NR0B2	TCACTATAGGGAGAGAGGGACCATCCTCTTCAACC	TCACTATAGGGAGACGTCCAAACCAAGGAAGTCCA
Library 1 - NR+CoReg	NR2E1	TCACTATAGGGAGAGTGAATGGGACCCCAATGTAT	TCACTATAGGGAGACGCATTCCGGAAACTTCTCAG
Library 1 - NR+CoReg	NR2C1	TCACTATAGGGAGAGAAGGACCTTCGTAGCCCATTA	TCACTATAGGGAGACGGTGTACACTTCCTTCCATGC
Library 1 - NR+CoReg	NR2C2	TCACTATAGGGAGAGCAGCAGCCTTTGATACGTGA	TCACTATAGGGAGACTGCACGTTGAGGTACTCTGG
Library 1 - NR+CoReg	THRA	TCACTATAGGGAGAGCCAGATGGAAAGCGAAAAAG	TCACTATAGGGAGACCTCTTCAGGAGTGGGCTCTG
Library 1 - NR+CoReg	THRB	TCACTATAGGGAGAGAAGGCTGCAAGGGTTTCTTT	TCACTATAGGGAGACGGGCATTGACTATTGGTGCT
Library 1 - NR+CoReg	VDR	TCACTATAGGGAGAGCCAGTTCGTGTGAATGATGG	TCACTATAGGGAGACGCTCCTCCTCATGCAAGTTC
Library 1 - NR+CoReg	NCOA1	TCACTATAGGGAGAGCAGTGGGCTTTCTCCTCAAG	TCACTATAGGGAGACAGGAATTGTTTGGCATCCTG
Library 1 - NR+CoReg	NCOA2	TCACTATAGGGAGAGTTGCAGTCCTGCTTGATTTG	TCACTATAGGGAGACTCAGATCCGGATTCATCACA
Library 1 - NR+CoReg	NCOA3	TCACTATAGGGAGAGTTAGTGTCACCAGCCCCTCT	TCACTATAGGGAGACTCCAAGTCTCCAGATCCCTCT
Library 1 - NR+CoReg	CARM1	TCACTATAGGGAGAGCCATGGGCTACATGCTCTTC	TCACTATAGGGAGACTGAAAGCAACGTCAAACCAG
Library 1 - NR+CoReg	CREBBP	TCACTATAGGGAGAGACGTCTGGCTCATGTTCAA	TCACTATAGGGAGACTCGAGGTCTGCCAGTTTTCT
Library 1 - NR+CoReg	EP300	TCACTATAGGGAGAGATACCGAACCAAAGCCCTCT	TCACTATAGGGAGACCAGAACATTGGGCCAGAAAT
Library 1 - NR+CoReg	RBM14	TCACTATAGGGAGAGGTACCCTGACTGTCCCTCTG	TCACTATAGGGAGACGAAAGATGGCAGGCTAGCAG
Library 1 - NR+CoReg	RBM39	TCACTATAGGGAGAGGCAAAAGCCGTGAAAGAAAG	TCACTATAGGGAGACCGACGAACTCCACATAAGCA
Library 1 - NR+CoReg	NCOR1	TCACTATAGGGAGAGCCACCAGAACCCATTTCTA	TCACTATAGGGAGACAACCGCAGGTTCTGTGTTTC
Library 1 - NR+CoReg	NCOR2	TCACTATAGGGAGAGGCACGAGGTGTCAGAGATCA	TCACTATAGGGAGACTTCCTTGTCGTTCTCCACCT
Library 1 - NR+CoReg	PHB2	TCACTATAGGGAGAGCAAGAACCCTGGCTACATC	TCACTATAGGGAGACTGAGAAATCACGCACTGTCC
Library 1 - NR+CoReg	PHB	TCACTATAGGGAGAGGGCTGAGCAACAGAAAAAGG	TCACTATAGGGAGACAGCTGGTTTGCATAGGCACT
Library 1 - NR+CoReg	PSME3	TCACTATAGGGAGAGGCTGAAGGTGGATCAGGAAG	TCACTATAGGGAGACTGGGAATCAGGAGCTGTACC
Library 1 - NR+CoReg	KDM3A	TCACTATAGGGAGAGTCCTATTCATGATCAAAGCTGGT	TCACTATAGGGAGACGGAATCCTGCCTGAAGAGTTT
Library 1 - NR+CoReg	KDM3B	TCACTATAGGGAGAGCCCTGATCATGACCCAATTC	TCACTATAGGGAGACTGCCGTTCCCTGTTAAGTGT
Library 1 - NR+CoReg	JMJD1C	TCACTATAGGGAGAGTGGACGGACTATGCCTAACA	TCACTATAGGGAGACTTCTTCAAAACCATCCCAGAA
Library 1 - NR+CoReg	NCOA6	TCACTATAGGGAGAGATGAGGGAAGCACCAACATC	TCACTATAGGGAGACGTGCTTGGCTGTGATCCTTT
Library 1 - NR+CoReg	NRIP1	TCACTATAGGGAGAGAGCTCGGGAAAGTGTCTGAA	TCACTATAGGGAGACTTGGGTGACAAGCTGTTGAG
Library 1 - NR+CoReg	SRA1	TCACTATAGGGAGAGCCACACAAGGAAGCAGGTA	TCACTATAGGGAGACAAGGGAGCCAAGTGACAGAA
Library 1 - NR+CoReg	SIN3B	TCACTATAGGGAGAGTCTGGACCAGGTGAAGATCC	TCACTATAGGGAGACTGCTCCTTCTGGTACGTGTG
Library 1 - NR+CoReg	MTA1	TCACTATAGGGAGAGAAGGATTTCACGGACATTCA	TCACTATAGGGAGACATCTAACCGGGTTGGCATTT
Library 1 - NR+CoReg	MTA2	TCACTATAGGGAGAGATGTGGAGGCAAAGGTTGTC	TCACTATAGGGAGACCTCCATCTTCTGCTGGTTCC

Library 1 - NR+CoReg	PPARGC 1A	TCACTATAGGGAGAGGTGACATCGAGTGTG CTGCT	TCACTATAGGGAGACTAGCTGAGTGTTGGCTGG TG
Library 1 - NR+CoReg	PPARGC 1B	TCACTATAGGGAGAGTCAAAATCTCTCCAG CGACA	TCACTATAGGGAGACTATTGGAAGGGCCTTGTC TG
Library 1 - NR+CoReg	PIN1	TCACTATAGGGAGAGCAGATGCAGAAGCCA TTTGA	TCACTATAGGGAGACCTGACCAGGCCTTCTCTT TG
Library 1 - NR+CoReg	BRCA1	TCACTATAGGGAGAGCTTCCCTGCTTCCAA CACTT	TCACTATAGGGAGACCAACTCCCTGGCTTTCAG AC
Library 1 - NR+CoReg	BRCA2	TCACTATAGGGAGAGTTCCTCTGCCCTTAT CATCG	TCACTATAGGGAGACAGATTCCATGGCCTTCCT A
Library 1 - NR+CoReg	MLL2	TCACTATAGGGAGAGATGCAGGACATGTGT GTGGT	TCACTATAGGGAGACGCATGACAGATAGGGCA GGT
Library 1 - NR+CoReg	TRRAP	TCACTATAGGGAGAGGCTCAGCATGAAGCA CTCTG	TCACTATAGGGAGACTCAAGGCCCTTTCATTTG AC
Library 1 - NR+CoReg	SMARCA 4	TCACTATAGGGAGAGAAGTGGCAGCGAAGA AGAC	TCACTATAGGGAGACGCGAGTCTGACCTGTCCA AT
Library 1 - NR+CoReg	PARP1	TCACTATAGGGAGAGCACTCATGCAACCAC ACACA	TCACTATAGGGAGACGTTTTGCCCAAACCTTTG AC
Library 1 - NR+CoReg	PIAS1	TCACTATAGGGAGAGCTCACTTGTCCGACT GTCCA	TCACTATAGGGAGACAGCTCAAGCATCCATCGA CT
Library 1 - NR+CoReg	KDM1A	TCACTATAGGGAGAGCTATGGCTGTGGTCA GCAAA	TCACTATAGGGAGACAGATCCCTGTGTTTGCTT TT
Library 1 - NR+CoReg	PELP1	TCACTATAGGGAGAGATGCTGCTGTCCTCA GA	TCACTATAGGGAGACCTGCACCCACAGCTCTAA T
Library 1 - NR+CoReg	MUC1	TCACTATAGGGAGAGAGTTCAGGCCAGGAT CTGTG	TCACTATAGGGAGACCAGCTGCCCGTAGTTCTT TC
Library 1 - NR+CoReg	MED24	TCACTATAGGGAGAGCTTGACAAGTGCCAA AATGG	TCACTATAGGGAGACAGCTCAGACGGTCACAAA A
Library 1 - NR+CoReg	MED23	TCACTATAGGGAGAGGGAGTGGATTACAAG GGTGT	TCACTATAGGGAGACATCCCTGGAATAAGGCTG CT
Library 1 - NR+CoReg	MED1	TCACTATAGGGAGAGAGCACCTTAAGGGCC TTGTT	TCACTATAGGGAGACAGGGGTGCATAAGTTGGT TG
Library 1 - NR+CoReg	HDAC1	TCACTATAGGGAGAGCGAATCCGCATGACT CATAA	TCACTATAGGGAGACTGTACAGCACCCTCTGGT GA
Library 1 - NR+CoReg	HDAC3	TCACTATAGGGAGAGGAGCTGACTCTCTGG GCTGT	TCACTATAGGGAGACCAGCCTCATCAGTCCTGT CA
Library 1 - NR+CoReg	HDAC4	TCACTATAGGGAGAGCCTCCAAACCTTACC TGCAA	TCACTATAGGGAGACATGTAGTCCATCCGCTCT CG
Library 1 - NR+CoReg	SAP30	TCACTATAGGGAGAGGCTTCAGCAAGAGGA TCCAG	TCACTATAGGGAGACCCACGTCTCCTAGTGAAC ACC
Library 1 - NR+CoReg	HMGB1	TCACTATAGGGAGAGTCGGGAGGAGCATAA GAAGA	TCACTATAGGGAGACGCATCAGGCTTTCCTTTA GC
Library 1 - NR+CoReg	HMGB2	TCACTATAGGGAGAGAAAGCTGTGGTGATT CGTCA	TCACTATAGGGAGACGGCTCTGGGAGTTGAATC TG
Library 1 - NR+CoReg	HNRNPU	TCACTATAGGGAGAGGAGGAAGAGCATCCT ATGG	TCACTATAGGGAGACATGGCTTTTCCTTCTGAC CA
Library 1 - NR+CoReg	NCOA4	TCACTATAGGGAGAGGAGCAGCCTTTCTGC TGATT	TCACTATAGGGAGACACCCACAGCAAGAGAAG CAT
Library 1 - NR+CoReg	TGFB1I1	TCACTATAGGGAGAGGCTAGATCGGTTGCT TCAGG	TCACTATAGGGAGACTTATTGCAGGAGCCACAG AG
Library 1 - NR+CoReg	RNF4	TCACTATAGGGAGAGTAACCAGAGGGCATG AAAGG	TCACTATAGGGAGACTCCCTGGACAACTCCTCA TC
Library 1 - NR+CoReg	TBL1Y	TCACTATAGGGAGAGCACACAGGAGAAGCC AAACA	TCACTATAGGGAGACAGACACCTTGCTCCACAT CC
Library 1 - NR+CoReg	TBL1X	TCACTATAGGGAGAGGTAACCTGGCCAGCA CCTTA	TCACTATAGGGAGACAGCCTGAAGATCATGGAT GC
Library 1 - NR+CoReg	PIAS3	TCACTATAGGGAGAGTCGGACGGAATTACT CCTTG	TCACTATAGGGAGACCCTCAGATGCCTCCTTCT TG
Library 1 - NR+CoReg	PIAS4	TCACTATAGGGAGAGGCCGGAGTAAGAGT GGACTG	TCACTATAGGGAGACGACCTGCACGGCTTTAAC TC
Library 1 - NR+CoReg	UBE2I	TCACTATAGGGAGAGACGCTTGTAATCCCA GCACT	TCACTATAGGGAGACATCTCGGCTCACTGCAAC TT
Library 1 - NR+CoReg	UBE3A	TCACTATAGGGAGAGAAACTGCCTTTCTCA ATGCAC	TCACTATAGGGAGACGCAACAATGGCATCATCA TC
Library 1 - NR+CoReg	SUMO1	TCACTATAGGGAGAGTCAAAGACAGGGTGT TCCAA	TCACTATAGGGAGACGCCTGAAAATGCAATGTC CT
Library 1 - NR+CoReg	SENP1	TCACTATAGGGAGAGCTTTTGGGGAAAGAC CACCT	TCACTATAGGGAGACTGCTTTGGTCTGTACAAA GTCTG

Library 1 - NR+CoReg	OTUB1	TCACTATAGGGAGAGCGACTCCGAAGGTGTTAACTG	TCACTATAGGGAGACGAGGTCTGCTTCTCCACCTG
Library 1 - NR+CoReg	CAV1	TCACTATAGGGAGAGGAGCTGAGCGAGAAGCAAGT	TCACTATAGGGAGACGATGCGGACATTGCTGAATA
Library 1 - NR+CoReg	CCND1	TCACTATAGGGAGAGAACTACCTGGACCGCTTCCT	TCACTATAGGGAGACTGAGGCGGTAGTAGGACAGG
Library 1 - NR+CoReg	CCNE1	TCACTATAGGGAGAGATCCTCCAAAGTTGCACCAG	TCACTATAGGGAGACTCCCCGTCTCCCTTATAACC
Library 1 - NR+CoReg	CDC25B	TCACTATAGGGAGAGCCGAGAGCTGATTGGAGATT	TCACTATAGGGAGACGCCGCCTTTCAGGATATACA
Library 1 - NR+CoReg	CDK7	TCACTATAGGGAGAGTGCTGACACCATCACACATC	TCACTATAGGGAGACAAGTCGTCTCCTGCTGCACT
Library 1 - NR+CoReg	PRMT1	TCACTATAGGGAGAGCGCCTCTTGAAGAAGTGTCC	TCACTATAGGGAGACGCATAGAGCACGGTGTTGAG
Library 1 - NR+CoReg	PARK7	TCACTATAGGGAGAGACTGAAGGAGCAGGAAAACC	TCACTATAGGGAGACAAGGACAGCGACTTCTGAACA
Library 1 - NR+CoReg	PUS1	TCACTATAGGGAGAGTCCCTCTCACATTCGGATTC	TCACTATAGGGAGACGGCATAACCCTTCACAATGG
Library 1 - NR+CoReg	RAF1	TCACTATAGGGAGAGCCAGAGTGCTGTGCAGTGTT	TCACTATAGGGAGACAACAGGCATCCTGGAAACAG
Library 1 - NR+CoReg	RB1	TCACTATAGGGAGAGTGCATGGCTCTCAGATTCAC	TCACTATAGGGAGACGGTCCAAATGCCTGTCTCTC
Library 1 - NR+CoReg	FOXA1	TCACTATAGGGAGAGGACTCCAGCCTCCTCAACTG	TCACTATAGGGAGACATGGCTATGCCAGACAAACC
Library 1 - NR+CoReg	FOXA2	TCACTATAGGGAGAGAAACAGAGGGCCACACAGAT	TCACTATAGGGAGACCCTTGCAGCCAGAATACACA
Library 1 - NR+CoReg	E2F1	TCACTATAGGGAGAGACCCCTCTCCTCTGTCTCCA	TCACTATAGGGAGACAGAAGTGCTCTCACCGTCCT
Library 1 - NR+CoReg	SNAI1	TCACTATAGGGAGAGTTTACCTTCCAGCAGCCCTA	TCACTATAGGGAGACCCAGGCTGAGGTATTCCTTG
Library 1 - NR+CoReg	ETV4	TCACTATAGGGAGAGGGAGACATCAAGCAGGAAGG	TCACTATAGGGAGACAAGGGACTGTGTCCTCCTCA
Library 2 - Remodeler	ZDHHC1	TCACTATAGGGAGAGTTGAAGACCTGCACTGCAAC	TCACTATAGGGAGACTCGAGCTCCCTGTGAAC
Library 2 - Remodeler	ZDHHC12	TCACTATAGGGAGAGCCACCCACTCTTTGTGGTCT	TCACTATAGGGAGACTTGAAGCTCCGTTCTGG
Library 2 - Remodeler	ZDHHC22	TCACTATAGGGAGAGACTGTTTCTTCACCGGCAAC	TCACTATAGGGAGACAGGGCTCTAGCAGACAGCAG
Library 2 - Remodeler	JMJD8	TCACTATAGGGAGAGCCCTTCCAGGAGTATGTGGA	TCACTATAGGGAGACGATGAAGACGCTGGTGTCAA
Library 2 - Remodeler	KDM4A	TCACTATAGGGAGAGACTGCAGGCCAGAAAGTCAT	TCACTATAGGGAGACGCATGTCTGAGGCTACTGA
Library 2 - Remodeler	CBX4	TCACTATAGGGAGAGCGTCGGCCTGAATCTCTC	TCACTATAGGGAGACCAAAGAAGGGCTTGAACTCG
Library 2 - Remodeler	ZDHHC2	TCACTATAGGGAGAGTCTAGGTGATGGCTGCTCCT	TCACTATAGGGAGACAAGCAATGGCTTGGAGAGAA
Library 2 - Remodeler	ZDHHC13	TCACTATAGGGAGAGCTGCCATGTATGCAACTGCT	TCACTATAGGGAGACGGTGTCTTCCTGAGGGACAA
Library 2 - Remodeler	ZDHHC23	TCACTATAGGGAGAGATGTGGCATCTGTGTGAGGA	TCACTATAGGGAGACTGTCCATCATGGGTTCTCAA
Library 2 - Remodeler	KDM2B	TCACTATAGGGAGAGACGAGTGCGATGTCGAAAAT	TCACTATAGGGAGACTTTGGCTTGCACAGCTTC
Library 2 - Remodeler	KDM4B	TCACTATAGGGAGAGGAGCACCCCACTCAACTAC	TCACTATAGGGAGACTTTCCCTGCCTGGTCTGTA
Library 2 - Remodeler	CBX7	TCACTATAGGGAGAGCTCAAGTGAGGTGACCGTGA	TCACTATAGGGAGACTGCTGCGTCACTAGAGGAGA
Library 2 - Remodeler	ZDHHC3	TCACTATAGGGAGAGTGCCATCGTTACCTGGTTT	TCACTATAGGGAGACTCAAAGCAATGCAGGAAGTG
Library 2 - Remodeler	ZDHHC14	TCACTATAGGGAGAGGGTTAACCTGGGTGTCCT	TCACTATAGGGAGACGGTCCCCATCACAAAGAAGA
Library 2 - Remodeler	ZDHHC24	TCACTATAGGGAGAGTTGCTCACAGGCAGAGTGTC	TCACTATAGGGAGACGTGGAGTTGTCCAATGCAGA
Library 2 - Remodeler	KDM2A	TCACTATAGGGAGAGCAAGGCACTTGAAGGAAAGC	TCACTATAGGGAGACGCAGTACACATAGCGCTCCA
Library 2 - Remodeler	KDM4D	TCACTATAGGGAGAGAAATATGTACGGGGCAACCA	TCACTATAGGGAGACTTTGGATTCTGGGCACAGTT
Library 2 - Remodeler	CBX8	TCACTATAGGGAGAGGAGAGCGAGCGAGAGAGAAA	TCACTATAGGGAGACATCAAGGCGCCAGTAAACAC

Library 2 - Remodeler	ZDHHC4	TCACTATAGGGAGAGTCAGGAGCTGGAGTTGTCCT	TCACTATAGGGAGACATGGAGGTGTCCAAGGTC
Library 2 - Remodeler	ZDHHC15	TCACTATAGGGAGAGTTAGAGGCCTTCTGCACTCC	TCACTATAGGGAGACTTTCAATCCAACACGGTGA
Library 2 - Remodeler	KDM1B	TCACTATAGGGAGAGAACAGGCATTTCCCACAAAC	TCACTATAGGGAGACTTCCTGCTTGATTGACTTGG
Library 2 - Remodeler	JHDM1D	TCACTATAGGGAGAGCCAAAAACTTGCTGGAAA	TCACTATAGGGAGACTGTGGAGGATGGTTGGAG
Library 2 - Remodeler	KDM5A	TCACTATAGGGAGAGAAGAAGCAGGGGCCAGTTAG	TCACTATAGGGAGACTGGACAAAAGCCACATCCT
Library 2 - Remodeler	RNF2	TCACTATAGGGAGAGCACTAAGGCCAGACCCAAAC	TCACTATAGGGAGACCAACAGTGGCGTTACCAGAA
Library 2 - Remodeler	ZDHHC5	TCACTATAGGGAGAGTGGTTGAACTCTGCATCTGG	TCACTATAGGGAGACGAGGTGTGCCCTGTGTTTCT
Library 2 - Remodeler	ZDHHC16	TCACTATAGGGAGAGCTGTGCAGTTCTGTGGCACT	TCACTATAGGGAGACTCTGAGAAAAGCTGCCCTTG
Library 2 - Remodeler	JMJD7	TCACTATAGGGAGAGATGAAGAGGCCATGGAGAA	TCACTATAGGGAGACCTGGCACCTTGAGTCCTTA
Library 2 - Remodeler	PHF8	TCACTATAGGGAGAGGCTCTTTCCAGAAAGCAAA	TCACTATAGGGAGACCTTCCACCATGTCCTCATC
Library 2 - Remodeler	KDM5B	TCACTATAGGGAGAGCTTTGCCAAGACTGGAAACC	TCACTATAGGGAGACATCTTGGAGAGGCGACAG
Library 2 - Remodeler	BMI1	TCACTATAGGGAGAGTCATCCTTCTGCTGATGCTG	TCACTATAGGGAGACTGGATGAGGAGACTGCACTG
Library 2 - Remodeler	ZDHHC6	TCACTATAGGGAGAGCCATCATAGCCCTTGGTGTT	TCACTATAGGGAGACTTCACTGTGTTCCACCCAAA
Library 2 - Remodeler	ZDHHC17	TCACTATAGGGAGAGATTGGGCTGCCATCAATAAC	TCACTATAGGGAGACAGCTCCAGCTTCCAGAAGAA
Library 2 - Remodeler	HIF1AN	TCACTATAGGGAGAGGGACCTTGAATACCTGCAA	TCACTATAGGGAGACGGGTGATGAACAGGGTATGG
Library 2 - Remodeler	PHF2	TCACTATAGGGAGAGTGTGCCCAACAAAGATGTG	TCACTATAGGGAGACGGCAGCACAGCCTTCTTATC
Library 2 - Remodeler	KDM5C	TCACTATAGGGAGAGAAGGAGTTCTGGAGGCTGGT	TCACTATAGGGAGACGACAAGTTGGTGCAGGAGGT
Library 2 - Remodeler	RYBP	TCACTATAGGGAGAGCAACAAAGACCAGCGAAACA	TCACTATAGGGAGACTCCTGGCAGCATCACTAAGA
Library 2 - Remodeler	ZDHHC7	TCACTATAGGGAGAGCGTGGCTCATCAGACTGAAA	TCACTATAGGGAGACTGCTTGGAGAATCCCTGTTC
Library 2 - Remodeler	ZDHHC18	TCACTATAGGGAGAGCTGCTTCACCTGCAAGATGT	TCACTATAGGGAGACCACGAGCCTTTGATGTCTT
Library 2 - Remodeler	HSPBAP1	TCACTATAGGGAGAGCTGACCTGGAACTGTGACCA	TCACTATAGGGAGACCGCATGTCTTTGAGCTTT
Library 2 - Remodeler	HR	TCACTATAGGGAGAGCACCAGGTCTGGGTCAAGTT	TCACTATAGGGAGACGGGCTTTCTCCTGGATCTTC
Library 2 - Remodeler	JARID2	TCACTATAGGGAGAGCCCTTTTGCAATCAGCATTT	TCACTATAGGGAGACTGGGACTATTCGGCTGAGAC
Library 2 - Remodeler	PCGF1	TCACTATAGGGAGAGGGTCGCGTAGGGCCTATTAT	TCACTATAGGGAGACTTGAGCAGTGGCTGTGTCTC
Library 2 - Remodeler	ZDHHC8	TCACTATAGGGAGAGATGTGCGAGGTATCCAGGT	TCACTATAGGGAGACAGGAGTTCAGGCCTAAGGA
Library 2 - Remodeler	ZDHHC19	TCACTATAGGGAGAGCTGGTTCCTCCCTAGCCTCT	TCACTATAGGGAGACGACAGGACAAGCAGCATGAA
Library 2 - Remodeler	JMJD5	TCACTATAGGGAGAGTTGAAGCAGGACATCAGCA	TCACTATAGGGAGACAGGCCCTTTCAGCTCCTATC
Library 2 - Remodeler	KDM6B	TCACTATAGGGAGAGTGAAGCTGCGCTCACTTAG	TCACTATAGGGAGACTGGGATTTCGAGGGTCTGTA
Library 2 - Remodeler	MINA	TCACTATAGGGAGAGCTCACAGTACTGCCGGATCA	TCACTATAGGGAGACTTTCTTTCATGTGCCCGTTA
Library 2 - Remodeler	PCGF2	TCACTATAGGGAGAGCAAATACTGCCCCATGTGTG	TCACTATAGGGAGACATCCATCTTGTTGCGGAGAA
Library 2 - Remodeler	ZDHHC9	TCACTATAGGGAGAGCACCGCCTCGTATCAAGAAT	TCACTATAGGGAGACTTCTTCCCTGTCCATGATCC
Library 2 - Remodeler	ZDHHC20	TCACTATAGGGAGAGAAAAACCGCTTGTTGGACAG	TCACTATAGGGAGACTGTGATGACAGCTCATATTATAGCAA
Library 2 - Remodeler	JMJD4	TCACTATAGGGAGAGACCACCTGCTACGGACCTA	TCACTATAGGGAGACTGAAGGAGCGGAAGATGTC
Library 2 - Remodeler	KDM6A	TCACTATAGGGAGAGCGTGTCGTATCAGCAGGAAA	TCACTATAGGGAGACAGTGGACCAACATTCCAAGC

Library 2 - Remodeler	NO66	TCACTATAGGGAGAGCGAGCCAAAGACTTCATTC	TCACTATAGGGAGACTGCCTTGTTTCCAGCAAT
Library 2 - Remodeler	PCGF3	TCACTATAGGGAGAGGAAAAGGCCAGAAGGAGGAG	TCACTATAGGGAGACAAACCGTCCTGGGAGTTGAT
Library 2 - Remodeler	ZDHHC11	TCACTATAGGGAGAGCCATCCTGCTGTATGTCCT	TCACTATAGGGAGACTGAATCAGCAGGGAGCTCTT
Library 2 - Remodeler	ZDHHC21	TCACTATAGGGAGAGCTTCAGCAAGCAGGTTCTC	TCACTATAGGGAGACGGGGTTCTCAGGGAGTCTTC
Library 2 - Remodeler	JMJD6	TCACTATAGGGAGAGCGGCACAACTACTACGAGAGC	TCACTATAGGGAGACTCCCCAGCATACTGGAAAAG
Library 2 - Remodeler	KDM4C	TCACTATAGGGAGAGCAGAAGCAGCAGTGAAGCTG	TCACTATAGGGAGACTTCCACTTCCTCCTCAATGG
Library 2 - Remodeler	CBX2	TCACTATAGGGAGAGCATGGAGGAGCTGAGCA	TCACTATAGGGAGACGGGGACCCCTCTTAGCATCT
Library 2 - Remodeler	RING1	TCACTATAGGGAGAGCACCATCTACATCGCACCTG	TCACTATAGGGAGACTGAATGGGAGGGTTCTTCAC
Library 2 - Remodeler	SMARCA4	TCACTATAGGGAGAGCAGTAACGGGTAGCAGCAGA	TCACTATAGGGAGACGGTTTAATTTATTACTGTTTGACATCC
Library 2 - Remodeler	ACTL6A	TCACTATAGGGAGAGTTGCCTCAGGTTACGAGGTC	TCACTATAGGGAGACAAACCTCCGTTCCACTGTTG
Library 2 - Remodeler	MTA3	TCACTATAGGGAGAGCGACGTGATATTTCCAACACA	TCACTATAGGGAGACAGCATTTCTGGAATGTCTGCT
Library 2 - Remodeler	ACTR5	TCACTATAGGGAGAGATGGCCAGATGGATCAGTT	TCACTATAGGGAGACCTTTGGGTACCTGTCCAGA
Library 2 - Remodeler	POLE3	TCACTATAGGGAGAGTACGCCACATCCTGTGCTA	TCACTATAGGGAGACTGAGACTACTCTGCCCAGCA
Library 2 - Remodeler	MBD3	TCACTATAGGGAGAGGCCACAGGGATGTCTTTTA	TCACTATAGGGAGACGTCTTGACCAGCTCCTCAGC
Library 2 - Remodeler	SMARCA3	TCACTATAGGGAGAGCAAATGCAGTGTCTTCCAATG	TCACTATAGGGAGACGTGCATTAGCGCATTAATCT
Library 2 - Remodeler	ACTL6B	TCACTATAGGGAGAGCACGTCAAGTCTGAGCCAAA	TCACTATAGGGAGACGGAAGTCCTGGATCACCTCA
Library 2 - Remodeler	BRD7	TCACTATAGGGAGAGCGCCCCTGTGAGATTAGACT	TCACTATAGGGAGACTCTTGAAGGCGTGTGCTT
Library 2 - Remodeler	ACTR6	TCACTATAGGGAGAGTAAATGCTGGGGCTCTCA	TCACTATAGGGAGACGAAGAATTTGTTCCCCAGA
Library 2 - Remodeler	RBBP7	TCACTATAGGGAGAGTTCAGTGGCCCAGTCTTACC	TCACTATAGGGAGACAGCCTTCCTTCTGGTGACCT
Library 2 - Remodeler	RBBP4	TCACTATAGGGAGAGCAGGGCATACGGCAGTAGTAG	TCACTATAGGGAGACTGCGATCAGTACCACTGGA
Library 2 - Remodeler	SMARCA2	TCACTATAGGGAGAGTTTGACAAATGGGCTCCTTC	TCACTATAGGGAGACTCCACCCTTTCACCAGTCAT
Library 2 - Remodeler	SMARCE1	TCACTATAGGGAGAGAATCTCGCATGGAGAAAGGA	TCACTATAGGGAGACTTTCAGACCGCACAACCT
Library 2 - Remodeler	BRD9	TCACTATAGGGAGAGTGGCACCATGAAAGACAAAA	TCACTATAGGGAGACGTGGCCACAGAGCACTACCT
Library 2 - Remodeler	GATAD2A	TCACTATAGGGAGAGTGCAGAGGCAAGACCTCAAT	TCACTATAGGGAGACTATAGATCGCCATGGGAAGG
Library 2 - Remodeler	RSF1	TCACTATAGGGAGAGCATGGGAGATGGAGAAGAA	TCACTATAGGGAGACTCCATAGGCTGCTCCTCACT
Library 2 - Remodeler	EZH2	TCACTATAGGGAGAGTCATGCAACACCCAACACTT	TCACTATAGGGAGACACAACCGGTGTTTCCTCTT
Library 2 - Remodeler	SMARCB1	TCACTATAGGGAGAGGATGGCAACGATGAGAAGT	TCACTATAGGGAGACCACATGGATGTTCAGCTTG
Library 2 - Remodeler	SMARCD1	TCACTATAGGGAGAGTGTTGACCCGAATGATCAGA	TCACTATAGGGAGACTGGTGTTGTCCTTGAACCAA
Library 2 - Remodeler	INO80	TCACTATAGGGAGAGGCACTAAAGAACAAAATTTCCA	TCACTATAGGGAGACGGAGGCTTTCAGAGACAGGA
Library 2 - Remodeler	GATAD2B	TCACTATAGGGAGAGTCCAGTTCCAGAATGGAAGAA	TCACTATAGGGAGACGTGTGGAAGGGTGGTATTGG
Library 2 - Remodeler	HDAC2	TCACTATAGGGAGAGCAGTTGCTGGAGCTGTGAAG	TCACTATAGGGAGACTCTGCACCACACTGTAATACCA
Library 2 - Remodeler	PHC1	TCACTATAGGGAGAGCATCTCCTGGGCCTTTATCA	TCACTATAGGGAGACTCTTCCCTGCAAAGTCTGCT
Library 2 - Remodeler	SMARCC1	TCACTATAGGGAGAGCGGATTTCAACCAAGAATG	TCACTATAGGGAGACTGATCACCTTTGGCAGGAT
Library 2 - Remodeler	SMARCD2	TCACTATAGGGAGAGCCCTGTGGCTTTACATCAA	TCACTATAGGGAGACTCTCTGGGTCTTCAGCTGGT

Library 2 - Remodeler	RUVBL1	TCACTATAGGGAGAGAAGGGGATGTGCACAAAAAG	TCACTATAGGGAGACATCACTCGGTCCAGAAGGT
Library 2 - Remodeler	SMARCA5	TCACTATAGGGAGAGCATTCAACAAGGGAGGCTTG	TCACTATAGGGAGACGTTGTTTTGGAGGTCGAGGA
Library 2 - Remodeler	CHD1	TCACTATAGGGAGAGGATGACATTGAGTTGGAACC	TCACTATAGGGAGACCGAGTCTACCACCTGTTCG
Library 2 - Remodeler	EZH1	TCACTATAGGGAGAGCCTGTGAGTGGACACCCTTT	TCACTATAGGGAGACTTGCCTTCAATAGCATGTCG
Library 2 - Remodeler	SMARCC2	TCACTATAGGGAGAGACTGCCGATCAAATGTTTCC	TCACTATAGGGAGACGGGATCCACGTGTCGTAACT
Library 2 - Remodeler	SMARCD3	TCACTATAGGGAGAGCCTGACCCAATTGTCATCAA	TCACTATAGGGAGACAGGGCTGGTGGTAGAACTCA
Library 2 - Remodeler	RUVBL2	TCACTATAGGGAGAGCCCCTACAGCGAGAAAGACA	TCACTATAGGGAGACAGTGTCAGAACTCTGGTGGA
Library 2 - Remodeler	SMARCA1	TCACTATAGGGAGAGTGGAATTTCTGGGTCAAAGG	TCACTATAGGGAGACTTCCTCTTTTGCCAGCTTGT
Library 2 - Remodeler	CHD2	TCACTATAGGGAGAGCATCAAGTGGAAGGGTTGGT	TCACTATAGGGAGACGCTGTCAATGCAATTCTGGA
Library 2 - Remodeler	EED	TCACTATAGGGAGAGTGGAAGTCAAAGAAATGCAAA	TCACTATAGGGAGACCCTCCAAATATTGCCACCAG
Library 2 - Remodeler	PHF10	TCACTATAGGGAGAGAAGCTGCCACTCCAAGAAAA	TCACTATAGGGAGACAGTCACAAATCCAGCGACCT
Library 2 - Remodeler	PBRM1	TCACTATAGGGAGAGGGCAGACTTCTCTGTGAGC	TCACTATAGGGAGACTGGGCAATGGTCTTGAGAT
Library 2 - Remodeler	SRCAP	TCACTATAGGGAGAGCTGAGGAACAGTTGGAAGG	TCACTATAGGGAGACGCAAGTACTCCACCCCAAAA
Library 2 - Remodeler	BAZ1B	TCACTATAGGGAGAGAACGCCAAGCTGAAGAAGAA	TCACTATAGGGAGACTTCCCTGAGGGTGAAGACAG
Library 2 - Remodeler	CHD3	TCACTATAGGGAGAGAGGACACTGACGTGCAGAA	TCACTATAGGGAGACTGGAGGCAGTGGCTTATCTT
Library 2 - Remodeler	SUZ12	TCACTATAGGGAGAGCAAGGCAACAAACTGAAGCA	TCACTATAGGGAGACGCCATTCAGGATCCTTTTCA
Library 2 - Remodeler	DPF1	TCACTATAGGGAGAGTGGCCCAGAACAACTGCTAC	TCACTATAGGGAGACTGTTCTTCCTCCTGGGAATG
Library 2 - Remodeler	ARID2	TCACTATAGGGAGAGTGAAATGCATGTGGGAAGTC	TCACTATAGGGAGACTCACAGATGAACCACCCAAA
Library 2 - Remodeler	P400	TCACTATAGGGAGAGATAGGATCGGGAGATGCAA	TCACTATAGGGAGACTTCATCACACGGCATGTTC
Library 2 - Remodeler	BPTF	TCACTATAGGGAGAGGGAAGTATCGCGTCTACCA	TCACTATAGGGAGACTCGCCATATTGGTAGCATCA
Library 2 - Remodeler	CHD4	TCACTATAGGGAGAGAAGGATGAAGCCACTGATGG	TCACTATAGGGAGACCTTCCTCTGAAGCCACTGA
Library 2 - Remodeler	YY1	TCACTATAGGGAGAGGTCACCATGTGGTCCTCAGA	TCACTATAGGGAGACTGCACTGAAAGGGCTTCTCT
Library 2 - Remodeler	DPF2	TCACTATAGGGAGAGCCTGAAGGAAGTTGGAGCTG	TCACTATAGGGAGACGTGAGCTGCTCTCCCACTCT
Library 2 - Remodeler	ARID1A	TCACTATAGGGAGAGATGGGACACCCAAGACAG	TCACTATAGGGAGACCCGTTCAATCTTGCATTC
Library 2 - Remodeler	YEATS4	TCACTATAGGGAGAGCGGGAGAGTAAAGGGTGTT	TCACTATAGGGAGACTCATTGCTGTTGGGTCTTGA
Library 2 - Remodeler	BAZ2A	TCACTATAGGGAGAGACTGGCTTGGTATGCAGCTT	TCACTATAGGGAGACTGGTGAGGTTGCTGGATGTA
Library 2 - Remodeler	CHD5	TCACTATAGGGAGAGACCCACATGGGAGAGAAAA	TCACTATAGGGAGACTGGAACCCATCGGTAAAGAG
Library 2 - Remodeler	PHC2	TCACTATAGGGAGAGAATCCAAAGAGGAGGGTGCT	TCACTATAGGGAGACGAGATGGGTGACAAGGGTTC
Library 2 - Remodeler	DPF3	TCACTATAGGGAGAGTCCCTGCACTGTTTTTCCTC	TCACTATAGGGAGACGCTTGGATGGACTCTGTTCC
Library 2 - Remodeler	ARID1B	TCACTATAGGGAGAGGCGAAAGATTACCTCCAAA	TCACTATAGGGAGACAGCGATGCTGCTCTTTTCAT
Library 2 - Remodeler	KAT5	TCACTATAGGGAGAGTCAAGCCGTGGTACTTCTCC	TCACTATAGGGAGACGTTAGGATGCAGGCCACATT
Library 2 - Remodeler	BAZ1A	TCACTATAGGGAGAGCTGTGTTCGACCAAAGCTCA	TCACTATAGGGAGACTGCTCTGCTGACTCCTTGAA
Library 2 - Remodeler	MBD2	TCACTATAGGGAGAGCGGATGGAAGAAGGAGGAAG	TCACTATAGGGAGACTGCACTAAGTCCTTGTAGCCTCT
Library 2 - Remodeler	PHC3	TCACTATAGGGAGAGCTTTGGTCCAGTTGCCATTT	TCACTATAGGGAGACTCCAATCCCTCCTGAATCAC

Negative control	GFP	TCACTATAGGGAGAGACGTAAACGGCCACAAGTTC	TCACTATAGGGAGACGCGGATCTTGAAGTTCACCT
Positive control	PLK1	TCACTATAGGGAGAGCTGCACCGAAACCGAGTTAT	TCACTATAGGGAGACAGCAGCTCGTTAATGGTTGG

Table 2. Primer Sequences for esiRNA Generation.

We synthesized two esiRNAs library, the NR+CoReg library (Library 1) and the Remodeler library (Library 2), targeting the same genes as in our siRNA screen. Primer sequences for esiRNA creation can be found in **Table 2**. We performed the NR+CoReg screen (Library 1) on 15 NSCLC cell lines and 3 HBECs. We also performed the Remodeler screen (Library 2) on 20 NSCLC cell lines, with an overlap of 9 NSCLC cell lines between these two screens (H1299, H522, Calu-6, H1693, H2009, H1993, H838, HCC15 and EKVX). A heatmap of relative viability, in comparison to the non-targeting esiGFP control, is shown in **Figure 3.2**. A bright red color on the heatmap in **Figure 3.2** indicates that the knockdown of that gene results in a >50% loss of viability. The most apparent trend in the heatmap is that some cell lines appear particularly sensitive to esiRNAs, meaning that many esiRNAs appear to decrease their viability, whereas other cell lines have very few, if any, esiRNAs that decrease their viability (aside from esiPLK1, top row). For cell lines that respond to many esiRNAs, we believe this may be due to strong activation of the interferon response, as previous studies have shown that the induction of the interferon response following siRNA transfection is both cell line and siRNA length dependent (Reynolds et al., 2006). An esiRNA against RNF4 (also known as SNURF) score in many cell lines and scored especially strong in cell lines that appeared to contain many hits, which led us to believe this esiRNA was causing the interferon response. To test if this occurred, we compared the esiRNF4 (esiRNA #1) used in the screen to a second synthesis of this esiRNA (esiRNA #2) which was performed with a longer digestion step to ensure that it was properly digested. The esiRNA that was digested longer (esiRNA#2) produced similar levels of

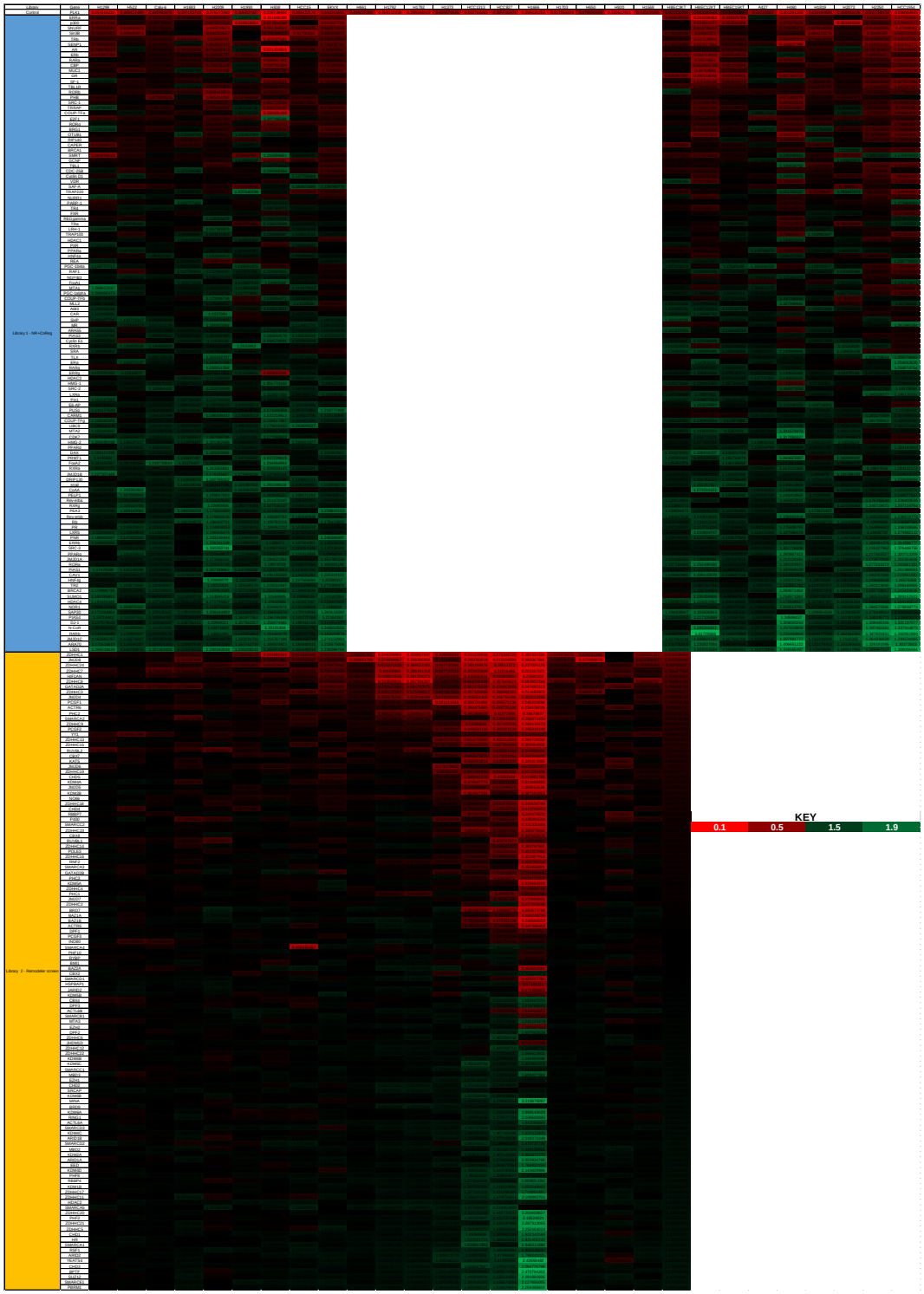


Figure 3.2. Results of Viability-Based of esiRNA Screen of NR + CoRegulator (Library 1) and Remodeler (Library 2) in Approximately 15 NSCLC Cell Lines and HBECs. Cell viability by MTS assay was determined after 5 days using a plate reader. Heat mapped values shown relative viability, in comparison to a non-targeting control (esiGFP). Each column represents a cell line and each row represents a gene targeted by a pool of four siRNAs. Blue and yellow coloring (far left) represent siRNAs present in NR+CoReg or Remodeler screen, respectively.

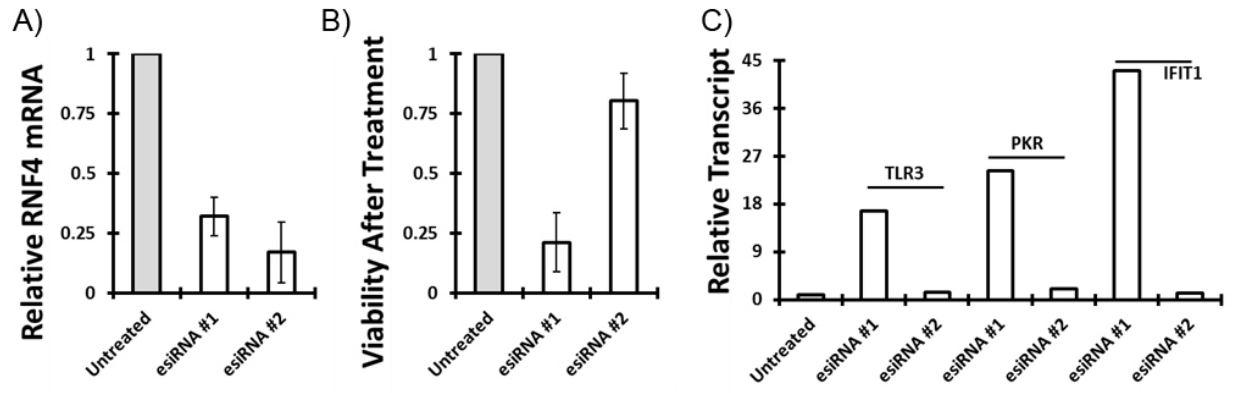


Figure 3.3. Resynthesis of esiRNF4 Shows That This esiRNA Likely Triggers Cell Death via the Interferon Response. The original esiRNF4 (also known as SNURF – labeled esiRNA #1 above) was compared to a resynthesized version of the same esiRNA (labeled esiRNA #2 above) that was made using a longer digestion step. A) Levels of RNF4 mRNA 48 hours after transfection with original esiRNF4 used in the screen (esiRNA #1) or a resynthesized version (esiRNA #2) relative to esiGFP. B) Viability of cells 5 days after being transfected with the original esiRNF4 used in the screen (esiRNA #1) or a resynthesized version (esiRNA #2) relative to esiGFP. B) Levels of mRNAs involved in the interferon response (TLR3, PKR, IFIT1) 48 hours after transfection with the original esiRNF4 used in the screen (esiRNA #1) or a resynthesized version (esiRNA #2) relative to esiGFP.

target knock down as the original esiRNA used in the screen (esiRNA #1 – **Figure 3.3A**). However, the esiRNA with increased digestion (esiRNA #2) did not produce any phenotype, whereas the original esiRNA from the screen (esiRNA #1) reduced cell growth (**Figure 3.3B**). Furthermore, the original esiRNA used in the screen (esiRNA #1) induced the expression of genes involved in the interferon response (TLR3, PKR and IFIT1), but the esiRNA that was digested longer did not (esiRNA #2 – **Figure 3.3C**). For this reason, we believe that when many esiRNAs produce a viability loss in a single cell line, this viability loss may be due to activation of the interferon response, and these interferon-response causing esiRNAs may be identified by producing this pattern in other cell lines. Aside from esiRNAs that likely scored via induction of the interferon response, most esiRNAs in this screen were fairly inert. This contrasts with the siRNA screen, where there were many siRNAs that decreased cell viability (**Figure 3.1**).

To compare the esiRNA screen to the siRNA screen in a global and unbiased manner, we performed unsupervised hierarchical clustering analysis. One would expect that, if the

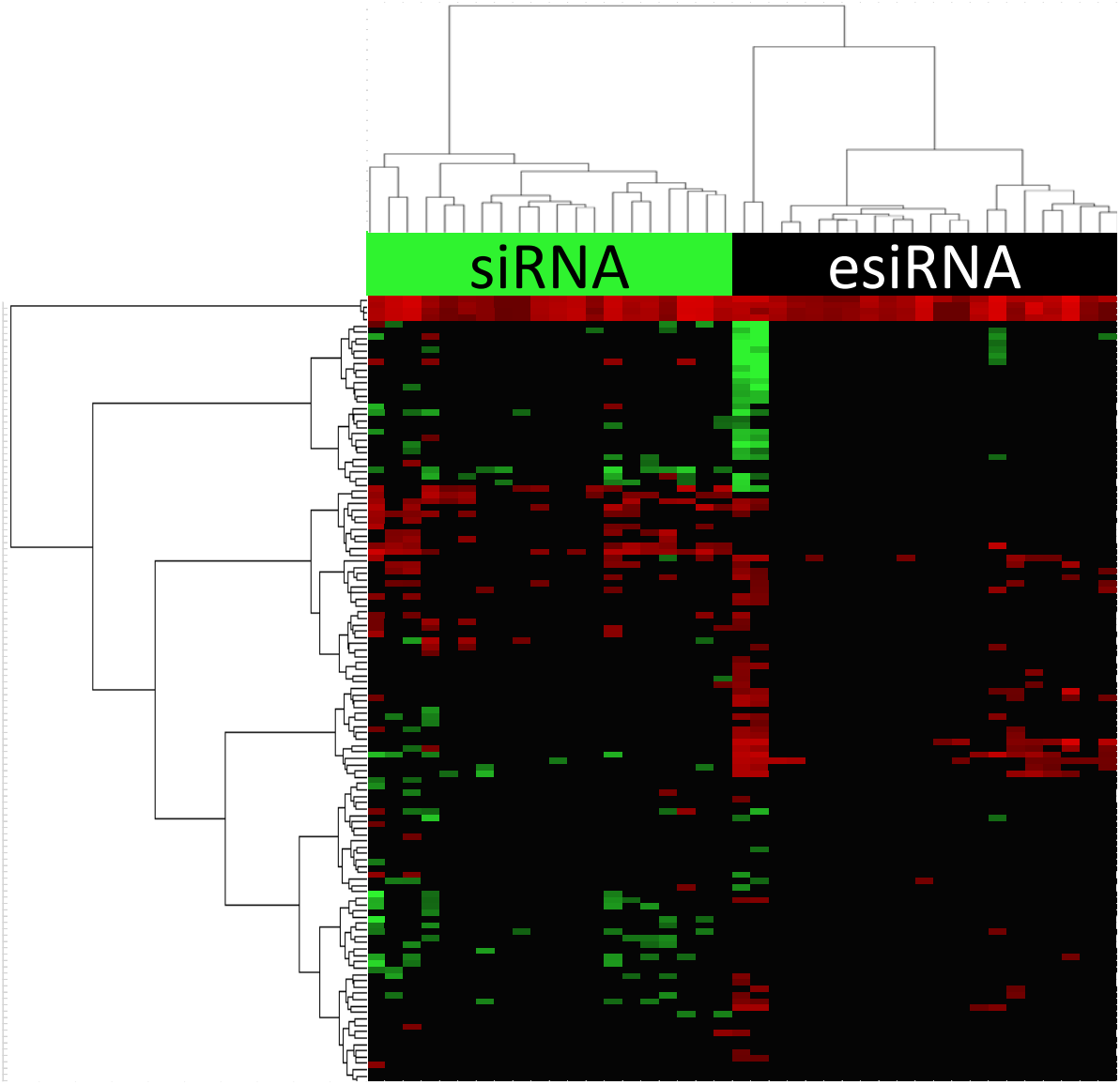


Figure 3.4. Unsupervised Hierarchical Clustering of esiRNA and siRNA Phenotypes. Clustering based upon the relative viability five days after transfection with each RNAi reagent, relative to control. Rows represent the genes targeted, whereas columns represent cell lines. To simply the heatmap visually, any relative viability between 60-140% was blacked out. Therefore, red represents < 60% viability, whereas green represents > 140% viability.

phenotypes induced by the siRNA were similar to the phenotypes induced by the esiRNA, these two RNAi reagents would cluster together by cell line, meaning that the siRNA and esiRNA produced similar phenotypes. Alternatively, if the phenotypes induced by these two RNAi reagents were very different, they would form separate clusters. Our unsupervised hierarchical clustering results showed that these two RNAi reagents formed their own clusters, suggesting

that there was very little concordance between these two reagents (**Figure 3.4**). A separate correlative analysis, where the Pearson correlation coefficients were calculated for all pairwise comparisons of all RNAi reagents from all screens clearly showed that no siRNAs or esiRNAs correlated strongly with each other (except the positive control, PLK1, **Figure 3.5**). This means that siRNAs and esiRNAs cause different phenotypes, suggesting that either some of the viability loss is due to off-target effects or that the lack of viability loss from one reagent is due to its inability to efficiently silence its target genes.

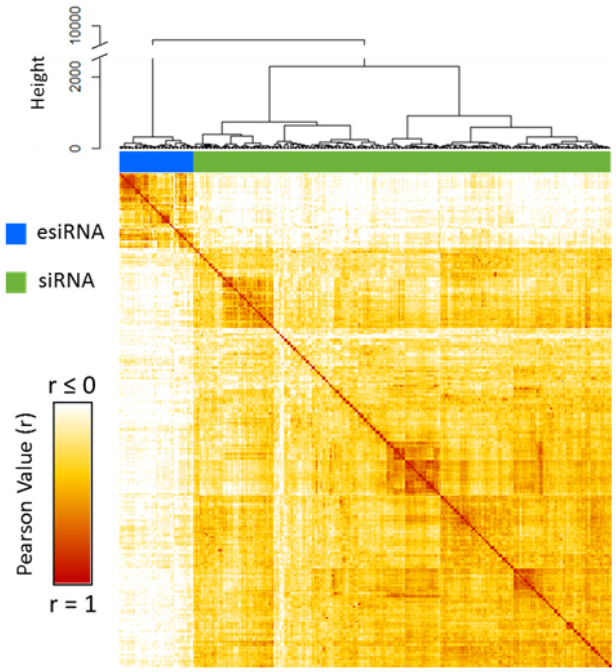


Figure 3.5. Pairwise Correlations of siRNA and esiRNA Phenotypes. The pairwise Pearson correlation for the effect two RNAi reagents had on cell viability across a panel of cell lines was calculated for all RNAi reagents, and then this matrix of correlation coefficients was clustered using hierarchical clustering. The dark red diagonal down the middle of the matrix represents the correlation between the same RNAi reagent.

The lack of concordance between these two reagents, and the dearth of non-interferon-based phenotypes induced by the esiRNAs, prompted us to test whether the esiRNAs were knocking down their target mRNAs as efficiently as the siRNAs. To do this, we transfected H2009 cells with esiRNAs or siRNAs targeting 12 different genes. We used the same RNAi

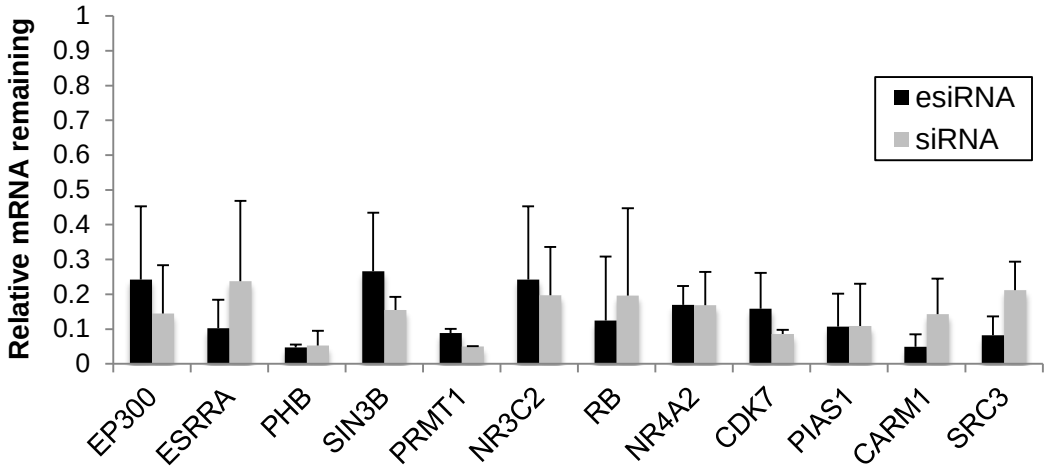


Figure 3.6. Comparison of Knock Down Efficiency of esiRNAs and siRNAs. H2009 was transfected with esiRNAs or siRNAs from the primary RNAi screen. The gene targeted is listed at the bottom. Three days after transfection, cells were lysed and mRNA levels were measured by RT-qPCR. Values shown are averages and relative to each RNAi reagents non-targeting control. Error bars represent the standard deviation between two biological replicates.

that were used in the primary viability screens, and after three days measured the amount of mRNA remaining in comparison to each RNAi reagents respective non-targeting control. This experiment showed that the esiRNAs depleted the target mRNA as good, if not better, than the siRNA (**Figure 3.6**). Many of these siRNAs caused a strong viability loss in multiple cell lines, whereas the esiRNAs did not (**Figure 3.7**). These data show that while the ability of esiRNA and siRNAs to knock-down the same targets are similar, only the siRNAs reduce cell viability. In particular, we show that siRNAs and esiRNAs targeting PRMT1, SRC3 and NR4A2 show similar levels of knockdown (**Figure 3.6**), but only the siRNAs reduce cell growth (**Figure 3.7**)

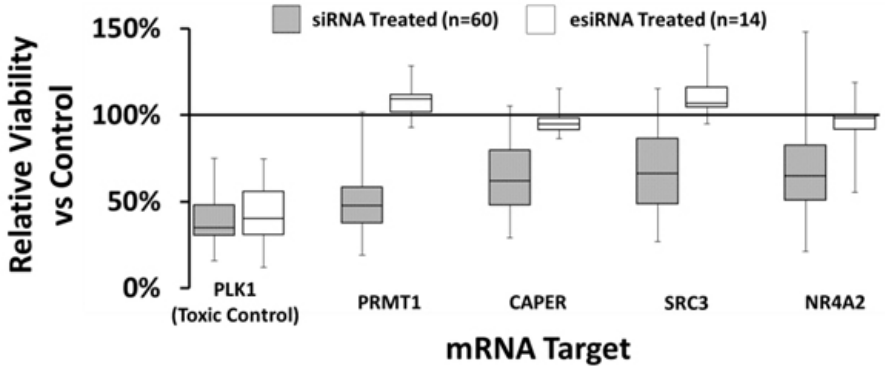


Figure 3.7. esiRNAs Targeting the Same Targets as siRNAs do not Decrease Cell Viability. From 96-well screening data (**Figure 3.1** for siRNAs, **Figure 3.2** for esiRNAs), reshown to illustrate differences between reagents. esiRNAs and siRNAs against PRMT1, SRC3 and NR4A2 were both shown to efficiently deplete target mRNAs to a similar extent (**Figure 3.6**)

Frequently when siRNA screens are performed using a pool of siRNAs, meaning that multiple siRNAs are pooled together and this pool of siRNAs is transfected, a typical way to assess if the siRNA-induced phenotype is off-target is to do what is known as a pool deconvolution analysis. In deconvolution analysis, the pool is broken down into individual siRNAs, and each of these individual siRNAs are transfected. If the majority of siRNAs against the same target give the same phenotype, it is assumed that this majority phenotype is likely due to on-target activity, as each siRNA should have its own unique off-target pattern (Jackson et al., 2006), but all should share the on-target activity. Since our siRNA screen was performed with siRNA pools, we decided to determine if we could use this type of analysis as a different way to identify on-target hits. To test this, we chose to perform deconvolution analysis on our siRNAs targeting PRMT1, as this was a strong, universally toxic hit in our siRNA screen, but showed little activity in our esiRNA screen (**Figure 3.7**), despite the fact that we validated that both RNAi reagents efficiently deplete PRMT1 (**Figure 3.6**). We first validated that all four siRNAs against PRMT1 were able to efficiently deplete PRMT1 transcript in 3 different cell lines (**Figure 3.8A**). Interestingly, we found that all four siRNAs also reduced cell viability in 3 different cell lines (**Figure 3.8B**). Thus, without our prior knowledge that esiRNAs against PRMT1 are both efficient (**Figure 3.6**) and non-toxic (**Figure 3.7**), this would have passed deconvolution analysis. We believed that even though all four siRNAs against PRMT1 caused cell death, the cells were still likely losing viability for different reasons (different off-target effects). Thus, we measured the percent of cells in each stage of the cell cycle by performing DNA content analysis on asynchronous cells four days after transfection with each individual siRNA. Here, were clearly see that these siRNAs are causing the cells to lose viability in different ways, because all four siRNAs targeting PRMT1 caused cells to arrest in different

stages of the cell cycle and/or undergo apoptosis following siRNAs transfection (**Figure 3.8C**). This indicates that the ability of these siRNAs to reduce cellular viability likely stems from different off-target activities of these siRNAs, and the deconvolution analysis, at least for a pool of 4 siRNAs, is not a reliable method to discriminate off-target from on-target effects in siRNAs screens.

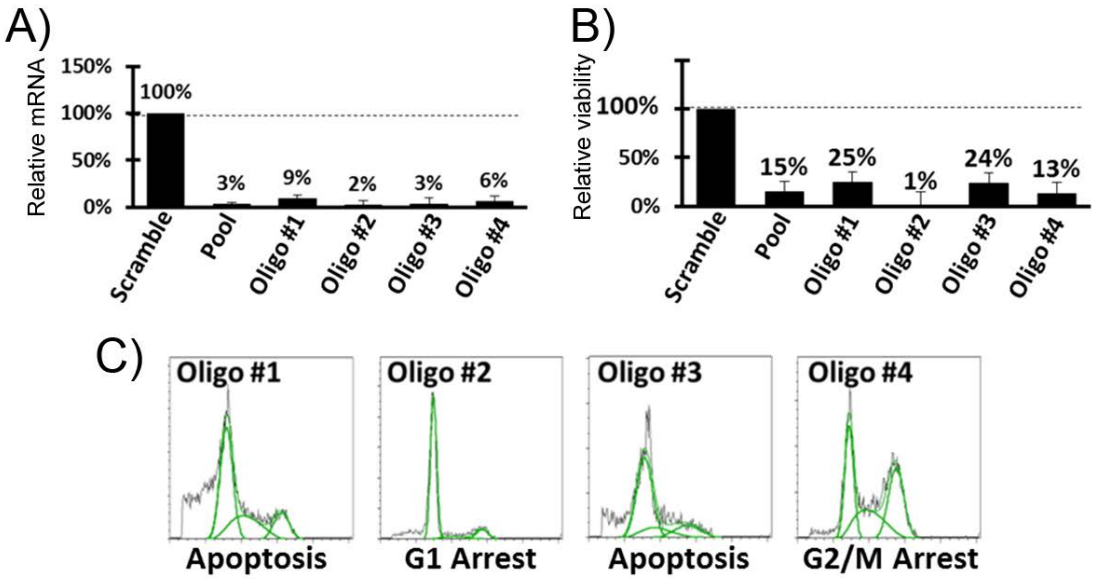


Figure 3.8. Deconvolution Analysis Fails to Identify Pools of Off-Target siRNAs. The pool of siRNAs targeting PRMT1 was deconvoluted. A) Each siRNA against PRMT1 strongly depleted PRMT1 transcript. The averages of 3 NSCLC cell lines relative to a non-targeting control are shown with standard deviations. B) Each siRNA against PRMT1 decreased cell viability. The averages of 3 NSCLC cell lines relative to a non-targeting control are shown with standard deviations. C) Each siRNA against PRMT1 induces a different cell cycle arrest as assed by DNA content. Y-axis is a histogram of cell number, X-axis is DNA content (propidium iodide).

3.3 Discussion

Prior studies have demonstrated that there may be some therapeutic utility in targeting NRs in lung cancer (Jeong et al., 2012; Jeong et al., 2010; Srivastava et al., 2014). For this reason, we decided to determine if the depletion of NRs, their coregulators, or their chromatin remodelers may hinder the viability of NSCLC cell lines using siRNAs. From this screen, we

found that many siRNA pools were able to inhibit the viability of NSCLC cell lines, and in some cases, these siRNAs had interesting molecular, clinical, or subtype associations. For instance, we identified siRNAs that specifically killed cancer cell lines, or siRNAs that specifically killed cell lines with certain mutations. In order to determine the specificity of these hits, we conducted a secondary screen targeting the same genes using esiRNAs, which have been shown to have significantly less off-target effects. In contrast to the siRNA screen, depletion of the NRs, their coregulators or chromatin remodelers using esiRNAs caused very few defects in viability. Even for the majority of esiRNAs that did decrease viability, we believe that many of these effects stem from a non-specific interferon response to esiRNAs that were not properly digested. A direct comparison of esiRNAs and siRNAs targeting the same genes that were nominated as essential for viability in the siRNA screen showed that both reagents efficiently depleted their target mRNA, but only the siRNA produced a phenotype. This strongly suggests that the ability of these siRNAs to decrease cell viability comes from their off-target activity, rather than their on-target activity. We then attempted to do siRNA pool deconvolution on one of our hits, as this is frequently done to determine if the phenotypes from pooled siRNA screens are due to on-target activity. We found that this method was not reliable, at least when four siRNAs were used, for determining if a gene was truly essential for viability.

The widespread off-target activity of siRNAs we witnessed here largely precluded their use as faithful interrogators of gene essentiality. A further study into the off-target activity of these siRNAs was conducted by Minna lab member Ryan Carstens and can be found in his 2015 thesis. In short, Ryan further confirmed by using C911 controls (Buehler et al., 2012) that the vast majority, if not all, of these siRNA-induced phenotypes stemmed from the off-target activity of the siRNA, likely via seed-mediated effects. Even siRNAs with very interesting molecular and clinical correlates, such as cancer-, mutation- and subtype-specificity, were found to reduce cell viability via off-target effects. Ryan also attempted to identify the off-target

transcripts that were responsible for these phenotypes, but because each siRNA was found to downregulate 100-200 genes, this necessitated a screen to interrogate all these transcripts, such as an siRNA or shRNA screen, setting up a circular problem. Additionally, like miRNAs, it is possible that these interesting phenotypes were driven by the cumulative knockdown of multiple transcripts, precluding their identification via simple one gene by one gene screening methods. Whether these off-target transcripts responsible for this interesting phenotype could be identified, or whether these off-target siRNAs themselves could be leveraged as RNAi-based therapies themselves, therefore, remains an open question

CHAPTER FOUR:
The Identification and Exploration of RUVBL1 and RUVBL2 as Potential Therapeutic Targets in NSCLC

4.1 Introduction

Non-small cell lung cancer (NSCLC) is a deadly disease which, despite a wealth of molecular data, intense research, and new therapeutic options, still kills the majority patients that develop this disease. Therefore, new therapeutic regiments and new therapeutic targets need to be identified to help treat NSCLC.

RUVBL1 and RUVBL2 (RUVBL1/2) are AAA+ ATPases that function as protein co-chaperones involved in the assembly and regulation of many multiprotein complexes, such as the PAQosome (Houry et al., 2018) and the INO80 family of chromatin remodelers (Feng et al., 2018; Mao and Houry, 2017). Through the PAQosome, RUVBL1/2 controls the stability of the phosphatidylinositol-3 kinase-related protein kinases (PIKKs) family, which includes ATM, ATR, DNA-PK_{cs}, MTOR, TRAPP and SMG1 (Izumi et al., 2010) and the biogenesis of the small nuclear ribonucleoproteins and small nucleolar ribonucleoproteins (Bizarro et al., 2015; McKeegan et al., 2009). Through the INO80-family of chromatin remodelers, RUVBL1/2 helps promote or repress gene expression. RUVBL1/2 are known to be essential for cellular proliferation, from yeast (Qiu et al., 1998) to man (Munoz et al., 2016), but the exact reason underlying their essentiality is unknown.

RUVBL1/2 have been implicated in many different cancer types. For instance, one early study showed that RUVBL1 was overexpressed in colorectal cancer in comparison to normal tissue at the protein level (Lauscher et al., 2007). The first study directly implicating RUVBL1/2 in cancerous growth showed that RUVBL2 was overexpressed and essential for the growth of hepatocellular carcinoma. Additionally, it was shown that the forced expression of RUVBL2

increased the growth of xenografted HuH7 cells, suggesting that RUVBL2 may be required for tumor growth, as well as a driver of tumor growth (Rousseau et al., 2007). Later studies showed that both RUVBL1 (Breig et al., 2014) and RUVBL2 (Osaki et al., 2013) expression were required for the growth of leukemias. Additionally, a later study in breast cancer showed that RUVBL1 was overexpessed, high expression was prognostic of poor overall survival, and that RUVBL1 promoted invasion and metastasis.

When we examined the concordance between our siRNA and esiRNA screen of NRs, their coregulators and chromatin remodelers in NSCLC cell lines, we noticed that one of the few RNAi reagents that consistently decreased the viability of NSCLC cell lines were RNAi reagents targeting RUVBL1 or RUVBL2. Because RUVBL1/2 have been implicated in various cancer types (as discussed above), RUVBL1/2 has been shown to regulate the assembly of the telomerase complex (Venteicher et al., 2008) and RUVBL1/2 has ATPase activity, which suggests that it could theoretically be inhibited by small molecules, we decided to examine the expression and prognostic utility of RUVBL1/2 in NSCLC. Our analyses indicated that in NSCLC RUVBL1/2 were overexpressed in comparison to adjacent normal lung and high expression of RUVBL1/2 was prognostic of NSCLC patient outcome. Because of this, we decided to further study the role of RUVBL1/2 in NSCLC. We went on to determine that NSCLC require RUVBL1/2 for their growth, and that they also require RUVBL1/2 ATPase activity. We also obtained a RUVBL1/2 ATPase inhibitor, Compound B, from Daiichi-Sankyo, and we went on to show that this inhibitor inhibits RUVBL1/2 *in vitro* and *in vivo*. To definitively show the on-target activity of Compound B, as well as gain insight into the ATPase activity of RUVBL1/2, we performed a PCR-based mutagenesis screen for mutations that relieve the growth-inhibitory effects of Compound B. This screen yielded multiple mutations that tended to cluster in the 3D structure of RUVBL1/2, strongly suggesting that Compound B kills NSCLC in an on-target manner and providing some insights into how RUVBL1/2 hydrolyze ATP and how Compound B effects this

process. Although we show that RUVBL1/2 ATPase activity are required for NSCLC growth *in vivo*, there is modest toxicity when RUVBL1/2 ATPase activity is inhibited systemically by Compound B. Therefore, we searched for clinically relevant therapeutic modalities that could enhance the efficacy of Compound B. We found that Compound B could robustly increase the efficacy of radiation in NSCLC, but not in normal cells, suggesting that combining Compound B with radiation may be the best path forward for any future preclinical development of Compound B.

4.2 Results

4.2.1 RUVBL1/2 are Overexpressed in NSCLC Patient Tumors and High Expression Correlates with Poor Overall Survival

Given the overall discordance between our siRNA and esiRNA screens, we looked for genes to further study that were hits in both siRNA and esiRNA screens, but whose knockdown only effected a subset of NSCLC cell lines. This latter criterion was used to ensure that we would not select a gene that was universally toxic to all cell lines. One of the few genes that passed this criterion was RUVBL1 and RUVBL2 (collectively referred to as RUVBL1/2) (**Figure 4.1**)

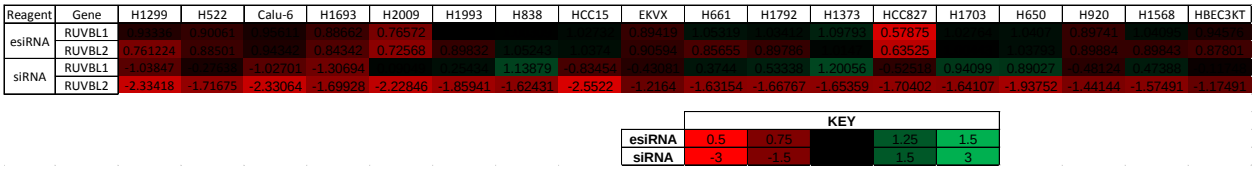


Figure 4.1. Depletion of RUVBL1 or RUVBL2 in esiRNA and siRNA Screens Consistently Caused Toxicity in Some NSCLC Cell Lines. Data from **Figure 3.1** (siRNAs) and **Figure 3.2** (esiRNAs). For both esiRNAs and siRNAs, red color indicates viability loss whereas green indicates viability gain. However, esiRNAs are expressed as percent viability relative to esiGFP, whereas siRNAs are z-scores.

Before launching a more thorough investigation into the molecular role of RUVBL1/2 in NSCLC, we wanted to determine if RUVBL1/2 may have any role in the biology of NSCLC in

patients using correlative analyses. First, we analyzed the expression of RUVBL1 or RUVBL2 mRNAs in the TCGA RNA-seq database. We found that RUVBL1 and RUVBL2, in both adenocarcinoma and squamous cell carcinoma, were upregulated in comparison to adjacent normal lung tissue (**Figure 4.2A**). To determine if this high level of expression had any association with patient outcomes, we utilized the public database and online web tool

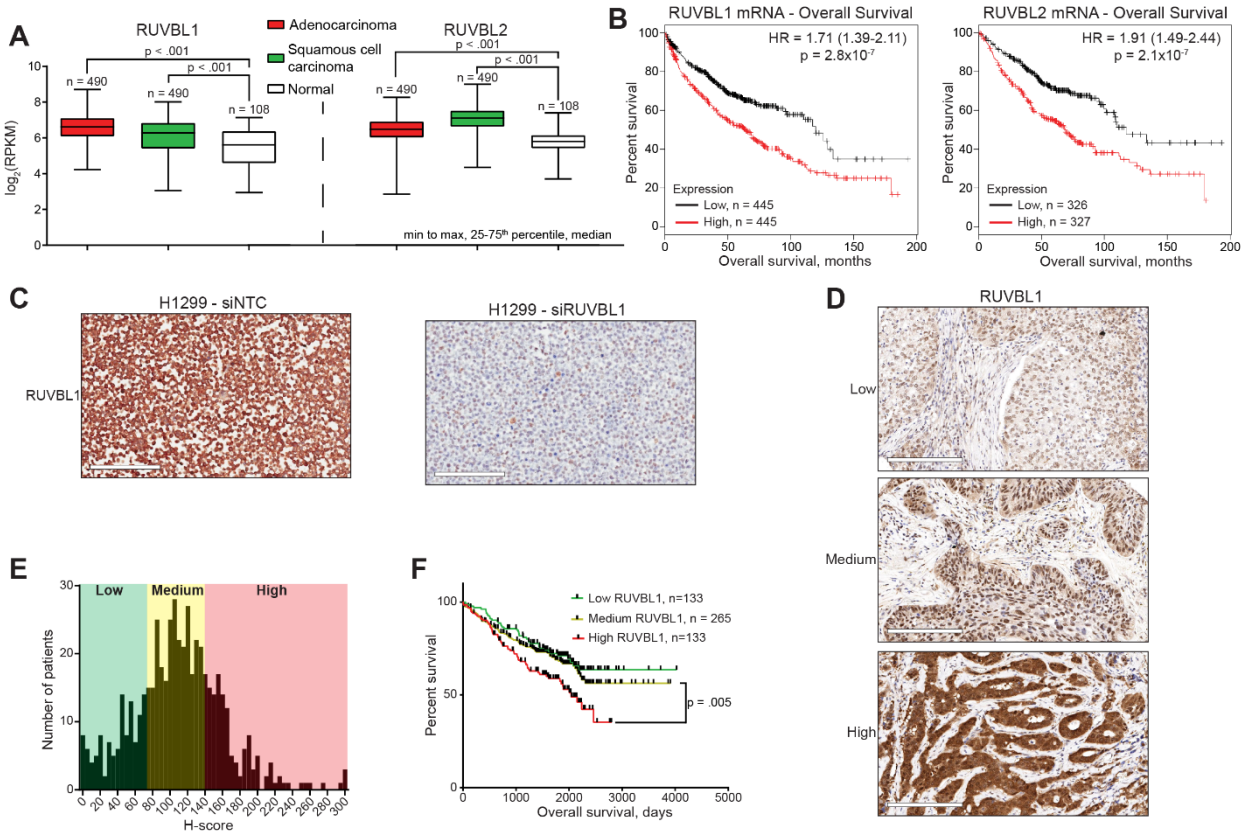


Figure 4.2. RUVBL1/2 Expression in NSCLC is Elevated and High Expression Predicts Poor Patient Survival. A) RUVBL1 (left) and RUVBL2 (right) mRNAs are overexpressed in TCGA NSCLC RNA-seq data. Whiskers represent minimum to maximum values, boxes represent 25th-75th percentile, lines represent median, and n refers to number of patients. Statistical significance was assessed with a one-way ANOVA with a post-hoc Dunnett's correction (compared to normal tissue). B) High RUVBL1 or RUVBL2 mRNA levels are associated with poor prognosis in NSCLC. Kaplan Meier plots were generated using KMPlotter (Szasz et al., 2016) on NSCLC patients with information available for histology, stage and gender and otherwise default settings. Statistical significance was assessed using the log-rank test and n represents the number of patients. High and Low groups represent patients in the top or bottom 50 percentile, respectively, for expression of RUVBL1 or RUVBL2. HR = hazard ratio. C) Validation of RUVBL1 antibody (clone 5G3-11) for immunocytochemistry. Cells were harvested 3 days after transfection. Scale bars are 200 μm. D) Examples of RUVBL1 staining in patient tumors from human NSCLC tissue microarrays. Scale bars are 200 μm. E) Histogram of RUVBL1 H-scores in 531 NSCLC patient tumors. H-score represents the intensity and percent

of tumor cells displaying staining. Low, Medium, and High groups represent the bottom 25, the middle 50, and the top 25 percentiles of RUVBL1 staining, respectively. F) Kaplan-Meier plots of the different groups (Low, Medium or High RUVBL1 protein levels) assigned in **Figure 4.2E**. Significance was assessed using the log-rank (Mantel-Cox) test and n represents the number of patients in each group.

kmplotter.com (Szasz et al., 2016). This online tool compiles multiple clinically annotated microarrays so that gene expression can be evaluated for its prognostic utility across multiple datasets. Univariate analysis of this dataset showed that, when RUVBL1 or RUVBL2 expression was divided into high and low groups (bifurcated at the mean, although other methods of bifurcation such as 25/75 also showed highly significant results), patients with higher levels of RUVBL1 or RUVBL2 expression had significantly shorter overall survival times (**Figure 4.2B**). Further multivariate analyses indicated that the prognostic utility of RUVBL1 or RUVBL2 expression was independent of tumor histology, grade and patient gender ($p = .0012$ for RUVBL1 mRNA, $p = .0004$ for RUVBL2 mRNA, Cox regression). Encouraged by these results, we decided to examine the prognostic utility of these genes at the protein level. To do this, we tested the ability of an anti-RUVBL1 antibody (clone 5G3-11) to detect RUVBL1 protein by immunocytochemistry in formalin-fixed paraffin-embedded (FFPE) cell pellets of H1299 that we transfected for three days with either a non-targeting siRNA or an siRNA against RUVBL1. RUVBL1 staining was greatly reduced in the cell pellet transfected with an siRNA against RUVBL1 (**Figure 4.3C**), indicating that this antibody could be used for immunocytochemistry and may perform well in immunohistochemistry (IHC) on human FFPE NSCLC tumor tissue.

Having validated an antibody against RUVBL1 for IHC, we collaborated with Dr. Ignacio Wistuba's lab at UT MD Anderson Cancer Center to stain two independent clinically annotated NSCLC patient tumor tissue microarrays (TMAs). Between the two NSCLC TMAs, a total of 531 patient tumor samples were evaluated for RUVBL1 expression. These tumors displayed various levels of RUVBL1 expression, from high to low, with samples of representative low, medium and

high RUVBL1 staining shown in **Figure 4.2D**. A histogram of RUVBL1 H-scores, which represents the intensity and percent of tumor cells displaying staining, in these NSCLC tumor TMAs is shown in **Figure 4.2E**, and samples are divided into low, medium or high RUVBL1 staining depending upon if they are in the bottom 25% percentile, middle 50% percentile, or top 25% percentile of RUVBL1 staining, respectively. These cuts off for low, medium or high RUVBL1 staining were then utilized to generate Kaplan-Meier plots for overall survival. This result indicated that similar to high RUVBL1 or RUVBL2 mRNA levels, patients with high RUVBL1 protein levels (average of nuclear and cytoplasmic scores) had poorer overall survival (**Figure 4.2F**). Interestingly, high nuclear staining was also prognostic ($p = .02$), while high cytoplasmic staining was not ($p = .11$) . This suggests that RUVBL1/2 may play some role in driving the poor overall survival of NSCLC patients, or alternatively, that high RUVBL1/2 levels are indicative of more aggressive NSCLC tumors.

Because these clinically annotated tissue microarrays had additional clinical information other than overall survival, we decided to analyze RUVBL1 protein expression in regard to other clinical information. There was not a strong tendency for RUVBL1 protein expression to change as tumors progress, as only stage IB and IIB had higher staining than IA (**Figure 4.3A**). There also was no association between RUVBL1 expression and the mutational status of two frequently mutated oncogenes in NSCLC, EGFR and KRAS (**Figure 4.3B**). Interestingly, patients with squamous cell carcinoma (**Figure 4.3C**) and patients with a smoking history (**Figure 3D**) tended to have higher levels of RUVBL1 expression. The latter suggests that either cigarette smoke may affect RUVBL1 expression levels, or possibly that RUVBL1 is upregulated in response to the well documented DNA damage that cigarette smoke causes to lung epithelial cells (Hopkins and Evans, 1980).

4.2.2 RUVBL1/2 ATPase Activity are Required for NSCLC Growth *In Vitro*

In order to more accurately assess the necessity of RUVBL1/2 in NSCLC for growth we synthesized additional esiRNAs against RUVBL1/2 and identified siRNAs against RUVBL1/2 that appeared to have strong on-target activity by utilizing C911 controls (Buehler et al., 2012).

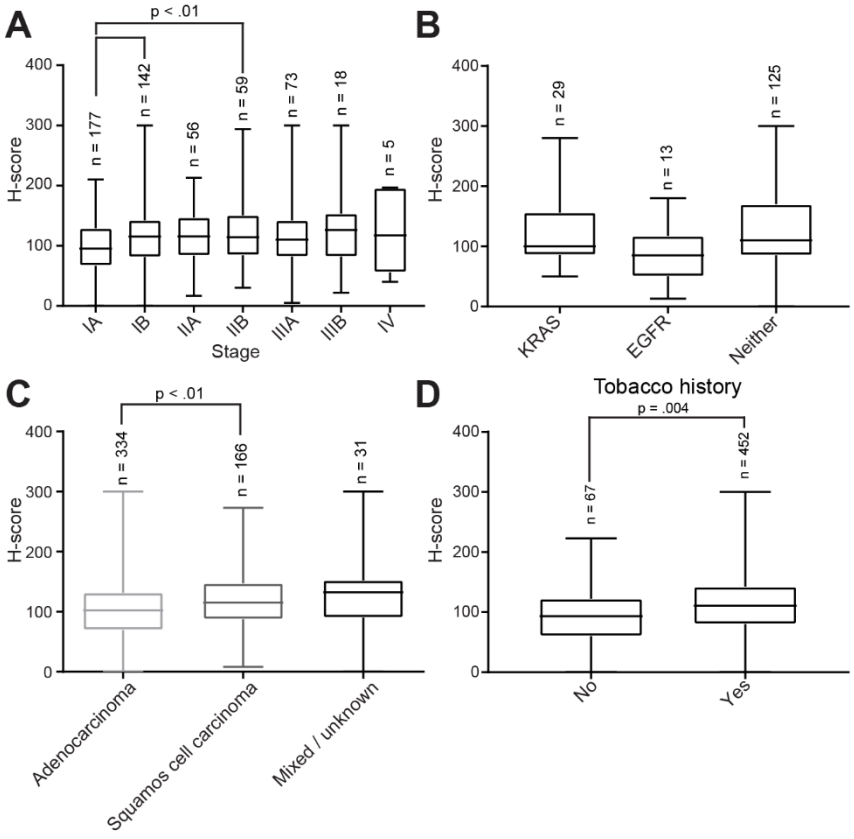


Figure 4.3. RUVBL1 Protein Expression in NSCLC is Higher in Squamous Cell Carcinoma and Patients with Smoking History. A-D) RUVBL1 protein does not significantly associate with A) tumor stage or B) KRAS or EGFR mutation, but is higher in patients with C) squamous histology D) or a smoking history. H-score represent both the intensity and the percent of cells displaying staining. Whiskers represent minimum to maximum values, boxes represent 25th-75th percentile, line represents median, and n refers to number of patients. For A-C, significance was assessed with a one-way ANOVA with post-hoc Tukey correction, whereas for D it was assessed with a two-tailed T-test. Only significant p-values are shown.

We then used these RNAi reagents to deplete RUVBL1/2 in 24 NSCLC cell lines and measured the effect this had on cell growth. Similar to the 96-well screen, the majority of NSCLC cell lines showed a reduction in cell growth following depletion of RUVBL1/2, although some were

markedly more sensitive than others (**Figure 4.4A**). Transfection of these RNAi reagents achieved similar levels of knockdown at the protein level in one of the most sensitive cell lines, H1299, as one of the most resistant cell lines, H2073, suggesting that the differential sensitivity to knockdown was not due to differences in knockdown efficiency (**Figure 4.4B**). Additionally, RT-qPCR using these reagents and conditions was performed in every cell line tested for growth inhibition following RUVBL1/2 knockdown, and there was no correlation between the level of knockdown achieved, as measured by RT-qPCR, and the relative amount of growth inhibition (**Figure 4.4C**). This strongly suggests that these differences in growth following RUVBL1/2 knockdown were due to sensitivity to RUVBL1/2 knockdown, and not the level of knockdown achieved in each cell line (**Figure 4.4C**). The NSCLC cell lines chosen to assess the necessity of RUVBL1/2 for cellular growth (n = 27) have mRNA levels of RUVBL1/2 similar to most of the NSCLC lines that the Minna lab has (n = 241), suggesting that this panel is representative of NSCLC as a whole (**Figure 4.4D**). Furthermore, by immunoblot most NSCLC cell lines had similar levels of RUVBL1/2 protein, and sensitivity to RUVBL1/2 depletion did not correlate with the total levels of RUVBL1/2 protein, further suggesting that this panel is representative and that expression of RUVBL1/2 does not dictate sensitivity to their depletion (**Figure 4.4E**).

Given our prior problems with the systemic off-target nature of RNAi, in particular siRNAs, we sought to determine whether the loss of cell viability we observed following RUVBL1/2 depletion stem from the on-target activities of these RNAi reagents. Gratifyingly, there was a strong correlation between the loss of cell viability seen after transfection of

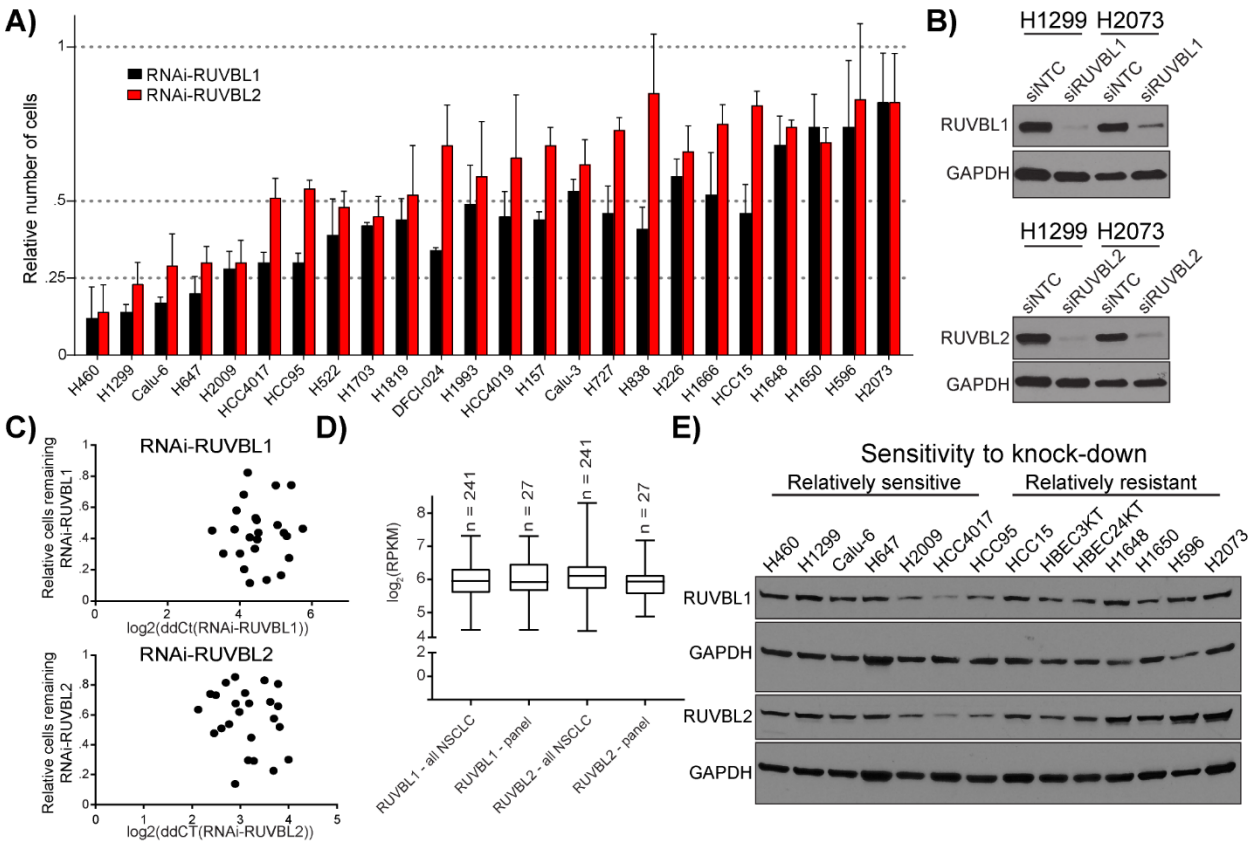


Figure 4.4 Effect of RUVBL1/2 Depletion in 24 NSCLC Cell Lines. A) Effect of RUVBL1 or RUVBL2 knockdown on the growth of different NSCLC lines. Values for RNAi-RUVBL1 or RNAi-RUVBL2 represents the average relative number of cells remaining 5 days after knockdown of RUVBL1 or RUVBL2, respectively, between an siRNA and an esiRNA, in comparison to control oligonucleotides (siNTC and esiGFP, respectively). All knockdowns were performed with ≥ 2 biological replicates, and error bars represent the standard deviation (SD) between siRNAs and esiRNAs. B) Immunoblot showing that RUVBL1/2 can be knocked down efficiently by siRUVBL1 or siRUVBL2 in one of the most resistant (H2073) or sensitive (H1299) NSCLC cell lines. C) Efficiency of RUVBL1/2 knockdown does not correlate with effects on growth. Run in parallel with viability assays shown in **Figure 4.4A**. X-axis values represent the average fold mRNA knockdown achieved with siRNAs and esiRNAs targeting RUVBL1 (top, RNAi-RUVBL1) or RUVBL2 (bottom, RNAi-RUVBL2) 2 days after transfection. Y-axis represents the average number of cells remaining after 5 days of knockdown between an esiRNA and an siRNA, normalized to their respective controls (esiGFP and siNTC). ddCt = delta delta Ct. All siRNA and esiRNA transfections were done at least twice, and each dot represents the average values for one cell line D) mRNA levels of RUVBL1 and RUVBL2 by RNA-seq in 241 NSCLC cell lines ("all NSCLC") and the panel of cell lines chosen for knockdown experiments in **Figure 4.4A** ("panel"). Whiskers represent minimum to maximum values, boxes represent 25th-75th percentile, the line represents median and n refers to the number of cell lines. E) Protein levels by immunoblot of RUVBL1 or RUVBL2 in some of the NSCLC lines chosen for RUVBL1/2 knockdown studies. Cell lines are arranged from most to least sensitive to RUVBL1/2 knockdown, left to right

esiRNAs and siRNAs targeting RUVBL1 (**Figure 4.5A**) or RUVBL2 (**Figure 4.5B**) across our panel of 24 NSCLC cell lines used in **Figure 4.4A**. Some studies have implicated RUVBL1 or RUVBL2 in certain processes (without discussing the other paralog), or have suggested that RUVBL1 and RUVBL2 could have separate, antagonistic roles (Bauer et al., 2000). At least in regard to NSCLC cell growth, we see a strong correlation between the sensitivity to RUVBL1 and RUVBL2 knockdown (**Figure 4.5C**). This makes sense as we and others have seen that the depletion of RUVBL1 results in depletion of RUVBL2 at the protein level, and vice-versa, suggesting that these paralogs depend on each other for stability (**Figure 4.5D**) (Izumi et al., 2010).

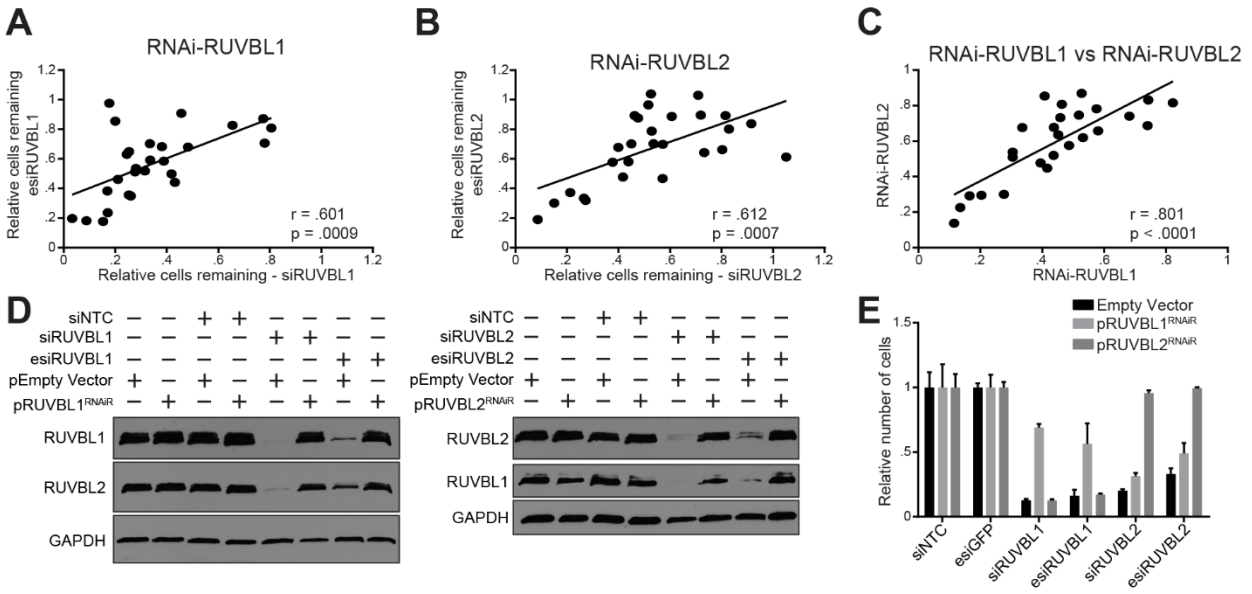


Figure 4.5. Both esiRNAs and siRNAs Targeting RUVBL1 or RUVBL2 Kill NSCLC due to On-Target Activities. A-C) Strong correlation between growth defects seen following RUVBL1 or RUVBL2 knockdown, regardless of the RNAi-reagent utilized or paralog being interrogated. A) Correlation between growth defects observed 5 days after siRUVBL1 or esiRUVBL1 transfection across 24 NSCLC cell lines. B) Correlation between growth defects observed 5 days after siRUVBL2 or esiRUVBL2 transfection across 24 NSCLC cell lines. C) Correlation between growth defects observed after depleting either RUVBL1 or RUVBL2 using multiple RNAi reagents. RNAi-RUVBL1 and RNAi-RUVBL2 represents the average growth defect observed 5 days after transfection of an esiRNA and siRNA targeting either RUVBL1 or RUVBL2, respectively, relative to each reagents control (esiGFP and siNTC, respectively). For A-C, all siRNA and esiRNA transfections were done at least twice, and each dot represents one cell line. Statistical significance was assessed using Pearson correlation. D) Stable expression of RNAi-resistant rat RUVBL1 (pRUVBL1^{RNAiR}) or RUVBL2 (pRUVBL2^{RNAiR}) cDNA in H1299 can rescue protein levels following RUVBL1/2 knockdown. Left: Constitutive expression of an RNAi-

resistant RUVBL1 rat cDNA can rescue protein depletion observed following 3 days of siRUVBL1 or esiRUVBL1 transfection in H1299 cells. Right: Constitutive expression of an RNAi-resistant RUVBL2 rat cDNA can rescue protein depletion observed following 3 days of siRUVBL1 or esiRUVBL1 transfection in H1299 cells. E) Stable expression of RNAi-resistant rat RUVBL1 (pRUVBL1^{RNAiR}) or RUVBL2 (pRUVBL2^{RNAiR}) cDNA in H1299 can rescue growth defects observed following 5 days of RUVBL1/2 knockdown. Values shown are the averages ± SD of 3 biological replicates.

To definitively determine whether the RNAi reagents we utilized targeting RUVBL1/2 killed NSCLC due to on-target activity, we performed genetic rescue experiments, where a cDNA that is resistant to knockdown (RNAi-resistant) is exogenously expressed in cell lines that are then transfected with RNAi reagents targeting the endogenous mRNA. If the phenotype of interest (in this case, the growth of NSCLC cell lines) is suppressed or reversed ("rescued") in the cell line expressing the RNAi-resistant cDNA, it is likely that the phenotype from the RNAi reagents are a consequence of the siRNA depleting it's intended target (i.e. due to on-target activity). To do this, we cloned the *Rattus norvegicus* RUVBL1 or RUVBL2 cDNA into mammalian expression vectors, further mutated synonymous sites where the siRNA binds, and then transfected these expression vectors into H1299 and selected for stable cell lines. The *Rattus norvegicus* RUVBL1/2 cDNAs were used because they have 99% protein homology to *Homo sapiens* RUVBL1/2 proteins, but only 60-70% nucleotide similarity. This difference should render the RNAi reagents targeting the human transcript ineffective against the rat RUVBL1/2 cDNA (Kittler et al., 2005b). Indeed, the exogenously expressed rat cDNAs were refractory to the human RNAi reagents, as total RUVBL1 or RUVBL2 protein levels did not change following transfection of RNAi reagents targeting RUVBL1 in a cell line expressing rat RUVBL1, or following transfection of RNAi reagents targeting RUVBL2 in a cell line expressing rat RUVBL2 (**Figure 4.5D**). Next, we tested whether these stably transfected cells were still able to proliferate after transfection with these RNAi reagents. The RNAi-resistant cDNA for RUVBL1 was able to confer resistance to RNAi reagents targeting RUVBL1, but not RUVBL2. The same was true for RUVBL2; the RUVBL2 RNAi-resistant cDNA conferred resistance to RNAi reagents targeting RUVBL2, but not RUVBL1 (**Figure 4.5E**).

Given the fact that NSCLC cells were unable to proliferate, to various extents, after depletion of RUVBL1 or RUVBL2 by RNAi reagents (**Figure 4.4A**) and this was due to on-target activity of these RNAi reagents (**Figure 4.5E**), we next wanted to determine if RUVBL1/2 required their ATPase activity to support viability. To do this, we performed rescue experiments whereby we depleted the endogenous RUVBL1 or RUVBL2 with RNAi reagents and then supplied exogenous *Rattus norvegicus* RNAi-resistant cDNAs that either retained ATPase activity (Wild-type) or cDNAs that were mutated by site-directed mutagenesis to lack ATPase activity (ATPase dead – amino acid substitutions D302N in RUVBL1 and D299N in RUVBL2).

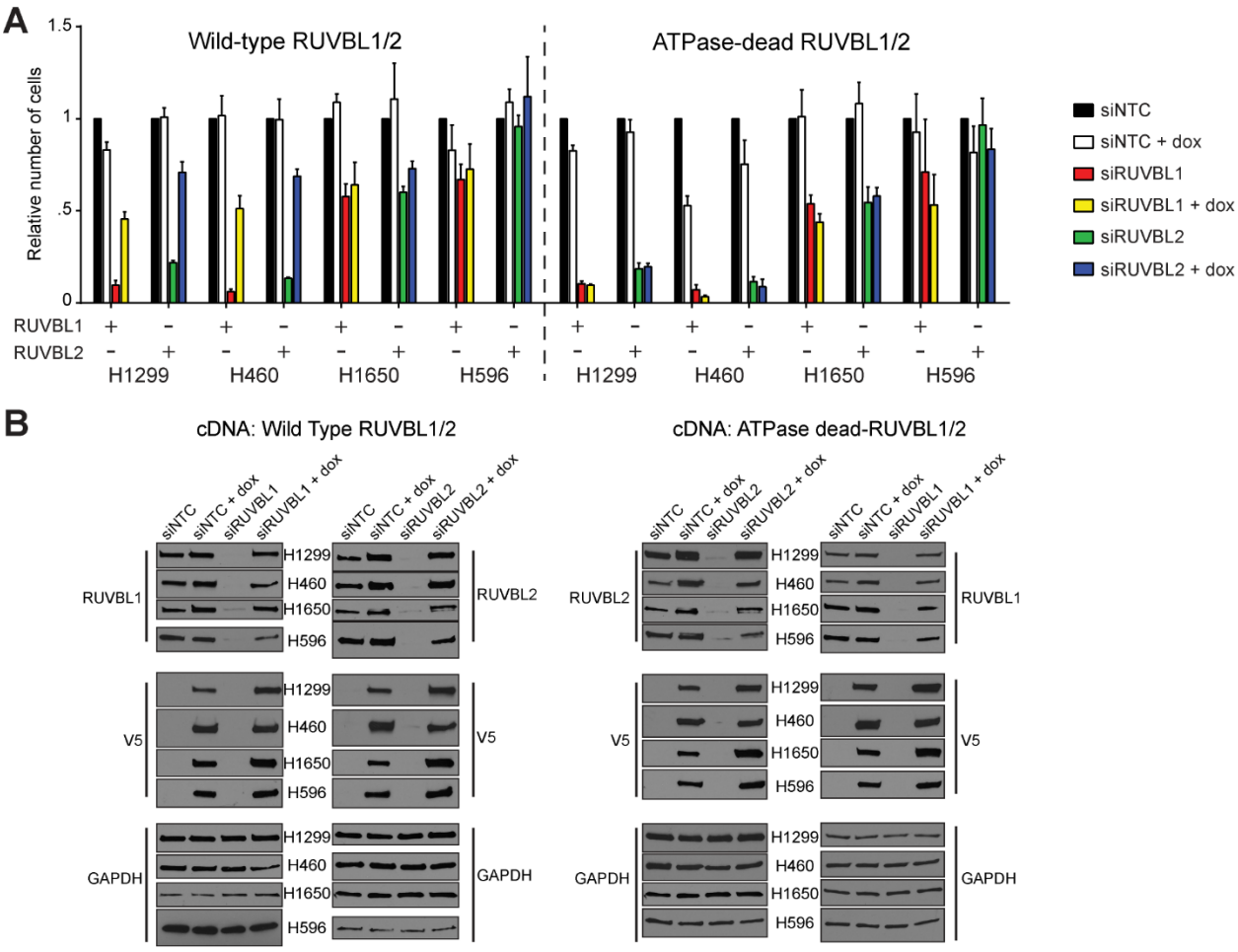


Figure 4.6. Genetic Rescue Experiments Demonstrate the Necessity of RUVBL1/2 ATPase Activity for NSCLC Cell Growth. A) Expression of wild-type doxycycline-inducible siRNA-resistant RUVBL1/2 protein can rescue the growth defect seen following 5 days of RUVBL1/2 knockdown (left) but ATPase-dead RUVBL1/2 protein cannot (right, D302N in RUVBL1 and

D299N in RUVBL2) in multiple NSCLC lines (H1299, H460, H1650 and H596, indicated below). +dox = 2 μg/mL doxycycline. Values shown are the averages ± SD of ≥ 2 biological replicates. B) Validation of RUVBL1/2 protein expression by immunoblot after depleting endogenous RUVBL1/2 and expressing doxycycline-inducible V5-tagged wild type or ATPase-dead RUVBL1/2 in 4 NSCLC lines for 3 days. Addition of doxycycline results in expression of indicated cDNA. Left: Expression of wild type V5-tagged RUVBL1/2 cDNA after depletion of RUVBL1 or RUVBL2 by siRNAs in indicated cell lines (H1299, H460, H1650, and H596). Right: Expression of ATPase-dead V5-tagged RUVBL1/2 cDNA after depletion of RUVBL1 or RUVBL2 by siRNA in indicated cell lines (H1299, H460, H1650 and H596).

Because prior studies have shown that the expression of ATPase dead RUVBL1/2 alleles can have dominant negative effects (Grigoletto et al., 2013), we expressed these cDNAs from a doxycycline-inducible vector so that they would only be present after knockdown. We transduced four cell lines, two that were relatively sensitive to RUVBL1/2 depletion (H1299 and H460) and two that were relatively resistant to RUVBL1/2 depletion (H1650 and H596), with these doxycycline-inducible vectors, depleted RUVBL1 or RUVBL2 with siRNAs, added doxycycline to induce expression of wild-type or ATPase dead cDNAs, and measured cell growth. As expected, the wild-type cDNA for RUVBL1 or RUVBL2 was able to rescue the inhibitory effects of cell growth following RUVBL1 or RUVBL2 knockdown, respectively. However, the ATPase dead cDNAs were unable to rescue cell growth (**Figure 4.6A**). This was not due to inefficient expression of the ATPase dead RUVBL1/2, as expression of either the wild-type and ATPase dead RUVBL1/2 cDNAs were able to rescue total RUVBL1/2 protein levels following knockdown (**Figure 4.6B**). Thus, these experiments indicate that RUVBL1/2 require their ATPase activity to support the growth of NSCLC.

4.2.3 Development and Validation of a RUVBL1/2 ATPase Inhibitor, Compound B

Given our prior genetic data which showed that RUVBL1/2 require their ATPase activity to support NSCLC proliferation (**Figure 4.6A**), and the fact that enzymes that hydrolyze ATP are frequently druggable, we wished to identify small molecules that inhibit the ATPase activity of RUVBL1/2. Fortuitously, only a couple years after we began working on RUVBL1/2, a pharmaceutical company, Daiichi-Sankyo, published a worldwide patent where they identified

multiple RUVBL1/2 inhibitors (Ebisawa et al., 2017). By contacting Daiichi-Sankyo we were able to start a collaboration. Daiichi-Sankyo screened 400,000 compounds for their ability to inhibit the intrinsic ATPase activity of purified RUVBL1 and RUVBL2. The lead compound from this screen was modified to yield 119 daughter molecules with structural similarity to the lead compound, and these 119 molecules were screened for their ability to inhibit purified RUVBL1/RUVBL2 and to inhibit the growth of the Ramos cell line (**Figure 4.7A**). This screen yielded Compound B and an enantiomer of Compound B, Compound C (**Figure 4.7B,** top and bottom, respectively – Compound B is Compound 40 from WO 2015/125785 A1). We refer to all daughter molecules from this screen as Compound B-like molecules for simplicity. Compound B has an IC_{50} for inhibiting the intrinsic RUVBL1/RUVBL2 ATPase activity of 59 nM *in vitro*, and inhibits Ramos cell growth at similar concentrations, whereas Compound C has an IC_{50} for inhibiting the intrinsic RUVBL1/RUVBL2 ATPase activity of >1 μM *in vitro* and inhibits Ramos cell growth at concentrations above 10 μM (**Figure 4.7A**). Given the dramatic difference in cell killing between Compound B and Compound C, and the fact that Compound C is an enantiomer of Compound B, we wanted to further determine if Compound C is inert and would therefore be a suitable control molecule for Compound B. To do this, we performed RNA-seq on cell lines treated for 24 hours with 100 nM of Compound C. This analysis showed that, in comparison to untreated cells, Compound C treatment caused minimal changes in gene expression, resulting in very few differentially expressed (DE) genes (defined as genes with $p < .01$, FDR < .05, in comparison to untreated cells) in both H2009 and H596 NSCLC cell lines (**Figure 4.7C**). Thus, when possible, we utilize Compound C as a control for Compound B. To determine if Compound B could inhibit RUVBL1/2 in cells, we treated H2009 with either Compound B or siRNAs targeting RUVBL1/2 and measured the stability of the proteins ATM, ATR, and DNA-PK_{cs}, all of which are known to be stabilized by the ATPase activity of RUVBL1/2 (Izumi et al., 2010). Both treatments decreased the total levels of ATM, ATR, and DNA-PK_{cs} (**Figure 4.7D**),

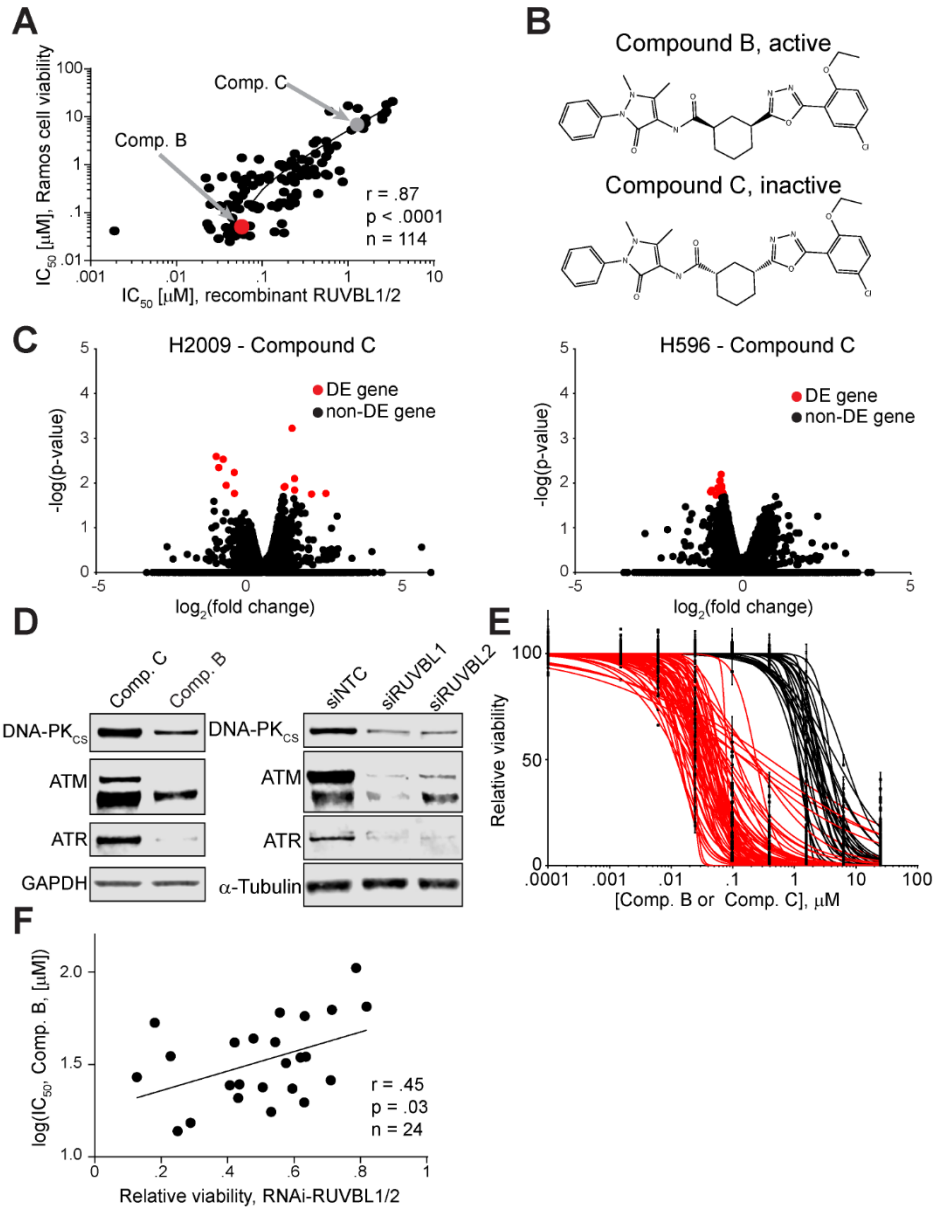


Figure 4.7. Development of Compound B, a RUVBL1/2 ATPase Inhibitor. A) Pearson correlation between the ability of Compound B-like molecules to inhibit purified RUVBL1/2 protein and inhibit the growth of the Ramos cell line. Compound B is shown in red, whereas Compound C is shown in gray. n represents the number of Compound B-like molecules and r is the Pearson correlation. B) Structure of Compound B (active RUVBL1/2 inhibitor, top) and Compound C (inactive control compound, bottom). C) Volcano plots of RNA-seq data from H2009 (left) and H596 (right) NSCLC lines treated with 100 nM Compound C for 24 hours (compared to untreated cells). Red dots represent differentially expressed genes, defined here as genes with $p < .01$, FDR < .05 with 2 biological replicates. D) Immunobloting of PIKK family members DNA-PKCS (PRKDC), ATM and ATR following 3 days of 100 nM Compound B (left, abbreviated Comp. B) or 100 nM Compound C (abbreviated Comp. C) and 4 days of siRNA-mediated RUVBL1 or RUVBL2 knockdown (right) in H2009. E) Fitted viability-based dose-response curves for cancer cell lines treated with Compound B (67 cell lines, red) or Compound C (32 cell lines, black) for 4 days. All data points represent the average ± SD and most assays have ≥ 2 biological replicates. F) Pearson correlation between the growth inhibitory response to

Compound B (IC50) and knockdown of RUVBL1/2 in 24 NSCLC cell lines. RNAi-RUVBL1/2 is the average of RNAi-RUVBL1 and RNAi-RUVBL2 (from **Figure 4.4A**). n represents the number of NSCLC cell lines analyzed.

	Compound B (nM)			Compound C (nM)		
Cell Line	**# of biological replicates**	**Average IC_{50}**	**SD**	**# of biological replicates**	**Average IC_{50}**	**SD**
A-427	2	11.2	1.4			
H1993	9	11.8	4.3	3	1100	150
ASPC-1	2	14	2.9			
HOP-62	3	14	3.2			
H647	4	14.7	3.1	3	1150	180
H2347	3	14.8	5.7			
EBC-1	2	15.3	1.5			
H1373	2	16.2	8.4			
H3122	2	16.3	0.96			
H1581	2	19	3.7			
H838	3	19.7	3.4	3	1080	180
H2009	8	20.3	13	3	1150	55
H1703	3	20.8	3.9	3	1370	230
HCC1719	2	20.8	4.3			
H1693	4	21	7.3			
H1648	3	22.7	3.4	2	1800	
DFCI 024	3	23.2	0.98	3	1420	75
H727	3	23.4	1.7	3	1400	89
HCC4017	4	24.4	3.7	4	1630	120
H522	3	24.7	2.2	3	1600	63
H1048	1	25				
HCC2814	2	25.5	2.6			
HCC78	2	25.8	2.4			
H810	3	26	7.9	2	1980	260
Mia PaCa2	2	26	2.9			
H460	3	27	5.9	2	2130	290
H2087	3	28.5	1.8			
HCC1833	3	30.2	6.7	3	1620	120
H1355	4	31.9	2.5			
Calu-3	3	32.2	3.1	3	2000	120
SK-LU-1	2	32.3	1.3			
H226	3	34.5	7	3	2080	98
HCC15	3	34.8	5.6	3	2300	600
HCC4190	2	35.3	4.6			
H1755	1	36				

HCC193	2	37.3	6.3			
Calu-6	3	37.8	6.1	2	2170	150
H1975	4	38.8	6.9			
H1437	3	39.5	8.7			
H820	2	40.8	6.9			
HCC95	3	41.5	2.6	3	2330	480
PC-3	2	41.5	3.4			
HCC4019	3	41.7	6.9	3	2550	390
HCC44	3	43.2	9.2			
H1819	4	43.9	7.3	3	3150	460
OVCAR5	2	45	5.1			
H1155	7	45.9	13	3	2370	100
DU 145	3	46.5	5.3			
H2882	2	46.5	8.7			
H2126	2	48.5	7			
HCC827	2	51.5	1.9			
H1299	4	54.8	4.7	3	3320	280
HCC1195	1	57.5				
H1666	4	57.8	21	4	2750	600
H661	3	58.8	34			
H157	4	60.3	12	4	3610	450
H1650	3	62.5	9	3	3280	1000
H2073	5	65.2	18	4	1850	180
H358	1	69				
H2030	2	82.3	21			
H1944	1	91				
Calu-1	3	93.8	100			
H596	6	103	14	4	5900	500
H2085	2	106	63			
PANC-1	2	123	75			
A549	5	127	27			
H1792	3	198	23			

Table 3. IC_{50}'s of Compound B and Compound C in Viability-based Assays.

strongly suggesting that Compound B can inhibit RUVBL1/2 in cells. The ability of Compound B to inhibit cellular viability was then tested in a panel of 67 cell lines, which consisted primarily of NSCLC but also pancreatic, breast, and prostate cancer cell lines (**Figure 4.7E**). All cell lines responded to Compound B, with IC_{50}'s ranging from 11-198 nM (**Table 3**). In line with Compound B being able to inhibit RUVBL1/2 and cause on-target cell death, for cell lines

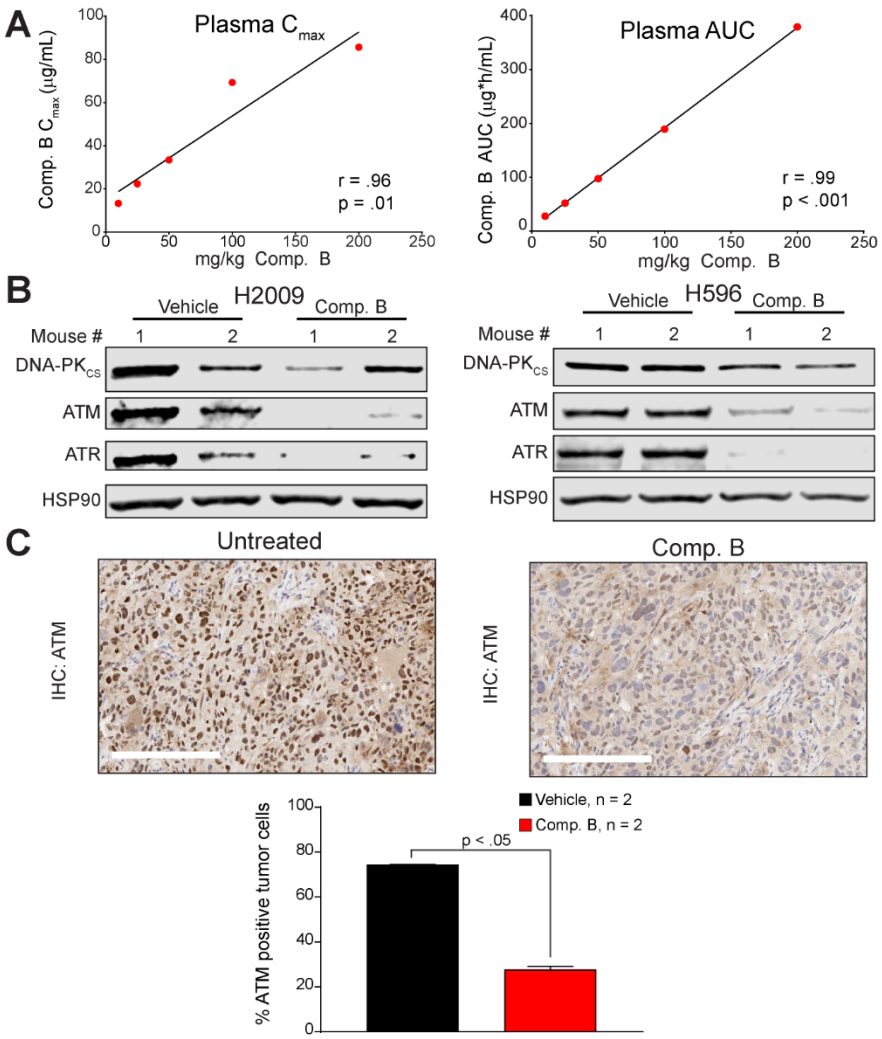


Figure 4.8. Compound B can be Administered Orally. A) Increasing doses of Compound B via oral gavage results in linear accumulation of Compound B in the plasma of BALB/C mice. Left: maximal plasma concentration (C_{max}) of Compound B administered orally at various doses. Right: area under the curve (AUC) values of Compound B plasma levels after oral gavage at various doses. Each data point represents one mouse and r is the Pearson correlation. B and C) Orally delivered Compound B can inhibit RUVBL1/2 in tumors *in vivo*. B) Immunoblot of tumor protein extracts from mice bearing H2009 (left) or H596 (right) NSCLC cell lines xenografted subcutaneously into NOD/SCID mice and treated with vehicle or 175 mg/kg/day Compound B by oral gavage for 3 days. Each number represents an independent mouse. C) Part of the tumors from H2009 xenografts (**Figure 4.8B**) were analyzed for tumor-cell specific levels of ATM by IHC. Values represent the average ± SD of the percent of ATM positive tumor cells in 2 mice. Scale bars are 200 μM.

screened for both sensitivity to RUVBL1/2 depletion and Compound B sensitivity, there existed a modest correlation between the sensitivity of these cell lines to these two perturbations (**Figure 4.7F**).

The efficacy of Compound B to inhibit RUVBL1/2 ATPase activity *in vitro* lead us to investigate the ability of Compound B to inhibit RUVBL1/2 ATPase activity *in vivo*, where molecules are subject to increased metabolism and excretion. To first test the stability and oral bioavailability of Compound B in mice, increasing doses of Compound B was orally gavaged into separate male BALB/C mice and the plasma concentration of Compound B was determined by mass spectrometry. This experiment showed that Compound B's maximal plasma concentration (C_{max}) and time-dependent plasma concentration (AUC) increased in a linear manner with increasing doses (**Figure 4.8A**), suggesting that Compound B could be orally delivered.

Encouraged by this finding, we tested the ability of Compound B to inhibit RUVBL1/2 ATPase activity in established NSCLC tumors. H2009 and H596 NSCLC cell lines were injected subcutaneously into the rear flank of female NOD/SCID mice, tumors were established, and then mice were treated either with vehicle or 175 mg/kg/day for 3 days. After 3 days, tumor tissue protein lysate was made, and a piece of the tumor was also fixed in formalin for IHC. We first tested the tumor tissue protein lysate for the total levels of ATM, ATR, and DNA-PK_{cs} as our previous data showed these are destabilized by Compound B treatment *in vitro* (**Figure 4.7D**). Immunoblot for these proteins indicated that, relative to vehicle treated tumors, Compound B treated tumors had lower levels of all three of these proteins, both in H2009 and H596 xenografts (**Figure 4.8B**). Because these tumors likely have some normal mouse stroma and innate immune cells, we wanted to determine if Compound B could deplete the level of these proteins (ATM, ATR and DNA-PK_{cs}) specifically in tumor cells. To do this, we performed IHC for ATM and looked at the amount of nuclear ATM signal specifically in tumor cells. This analysis demonstrated that ATM protein could be depleted specifically in tumor cells by Compound B (**Figure 4.8C**), strongly suggesting that orally delivered Compound B at this dose was sufficient to inhibit RUVBL1/2 in established xenografts.

4.2.4 Validating the On-Target Activity of Compound B

While we clearly demonstrated the ability of Compound B to inhibit RUVBL1/2 ATPase activity, both *in vitro* and *in vivo*, this does not necessarily mean the phenotypes resulting from Compound B (for instance, decreased cellular proliferation) are due to the inhibition of RUVBL1/2. This is because small molecule inhibitors frequently target many proteins (i.e. off-targets), and sometimes the inhibition of these off-targets can produce a phenotype, while inhibition of the intended target (i.e. the on-target) does not produce this phenotype (Huang et al., 2017), or produces a phenotype in addition to the off-targets.

Some of our prior data argued that Compound B was inhibiting cellular growth in an on-target manner. For instance, for the Compound B-like molecules we synthesized, as chemical modifications increased their ability to inhibit purified RUVBL1/2, these modifications also increased the cell killing activity of these molecules in a linear manner (**Figure 4.7A**), suggesting that these two effects are linked. Additionally, there was a correlation between the sensitivity (regarding growth) of NSCLC cell lines to genetic depletion of RUVBL1/2 and Compound B (**Figure 4.7F**). We also wanted to determine the ability of Compound B to inhibit kinases, as we assumed Compound B may inhibit RUVBL1/2 by binding the ATP-binding pocket, and kinases also hydrolyze ATP and have ATP-binding pockets. We screened 1 μM of Compound B across 97 kinases using KINOMEscan scanEDGE by DiscoverX. In this assay, the ability of a compound to displace a kinase from its substrate, relative to a control compound, is measured. This assay showed that Compound B did not appear to significantly inhibit the activity of any of the 97 kinases tested (**Figure 4.9A**), suggesting that Compound B does not have significant off-target activity against kinases.

To definitively determine whether Compound B kills cancer cells in an on-target manner, as well as to gain insight into how ATP hydrolysis might affect the structure of RUVBL1/2, we

sought to exhaustively identify mutations in RUVBL1 or RUVBL2 that may confer resistance to Compound B. To do this, we performed a screen where we used PCR with error-prone Taq polymerase to mutagenize RUVBL1 or RUVBL2 cDNAs, cloned these cDNAs into a doxycycline-inducible expression vector, and then expressed these mutagenized cDNAs in H2009 cells in the presence of 500 nM of Compound B, a concentration that normally kills >99% of cells. Cells that were able to grow in the presence of doxycycline and Compound B were pooled, their genomic DNA isolated, the stably integrated RUVBL1 or RUVBL2 cDNA was amplified via PCR, sequenced using Illumina sequencing, and the frequency of single nucleotide variants (SNVs) that resulted from point mutations in RUVBL1 or RUVBL2 between parental and surviving cells was compared (**Figure 4.9B**). We found 14 nonsynonymous SNVs in RUVBL1 and 6 nonsynonymous SNVs in RUVBL2 that were enriched >10 fold in comparison to parental cells in H2009 (**Table 4**).

These resistance-conferring mutations do not obviously cluster in the 2D structure of RUVBL1/2 (**Figure 4.9C**), however, when mapped to the 3D RUVBL1/RUVBL2 structure, they cluster predominantly at the interfaces between RUVBL1/RUVBL2 and RUVBL2/RUVBL1 (**Figure 4.9D**, 12 mutations), which is also where ADP/ATP binds. Comparison of the ATP and ADP bound states reveal the presence of mutations in and surrounding a flexible switch loop in both RUVBL1 and RUVBL2 that interacts at this interface (**Figure 4.9E**, 9 mutations). This switch loop adopts nucleotide-dependent conformations, which is interesting given that a recently published, structurally similar daughter molecule of Compound B (Assimon et al., 2019) binds only to ATP-bound RUVBL1/2. Similarly, two of the remaining mutations from RUVBL1 map near the flexible N-terminus of RUVBL2 (**Figure 4.9F**), which is reported to act as a gatekeeper to allow nucleotide exchange in the presence of R2TP (Munoz-Hernandez et al., 2019). Thus, most putative resistance-conferring mutations that could be mapped to the RUVBL1/RUVBL2 structure (15 out of 18) map to the RUVBL1/RUVBL2/RUVBL1 interfaces or

position flexible interface loops whose orientation are dependent on the nucleotide bound state of the complex. We believe multiple mechanisms may explain how these mutations confer resistance to Compound B. It is possible that some of these mutations disfavor the ATP-bound state to which the drug presumably binds, as some resistance-conferring mutations (such as RUVBL1-E110K and RUVBL1-K265E) form hydrogen bonds in the ATP bound state not present in the ADP bound state, and these may destabilize the ATP-bound conformation. Alternatively, some solvent exposed mutations (such as RUVBL1-P296S and RUVBL1-G63E) may alter the physical binding site of Compound B.

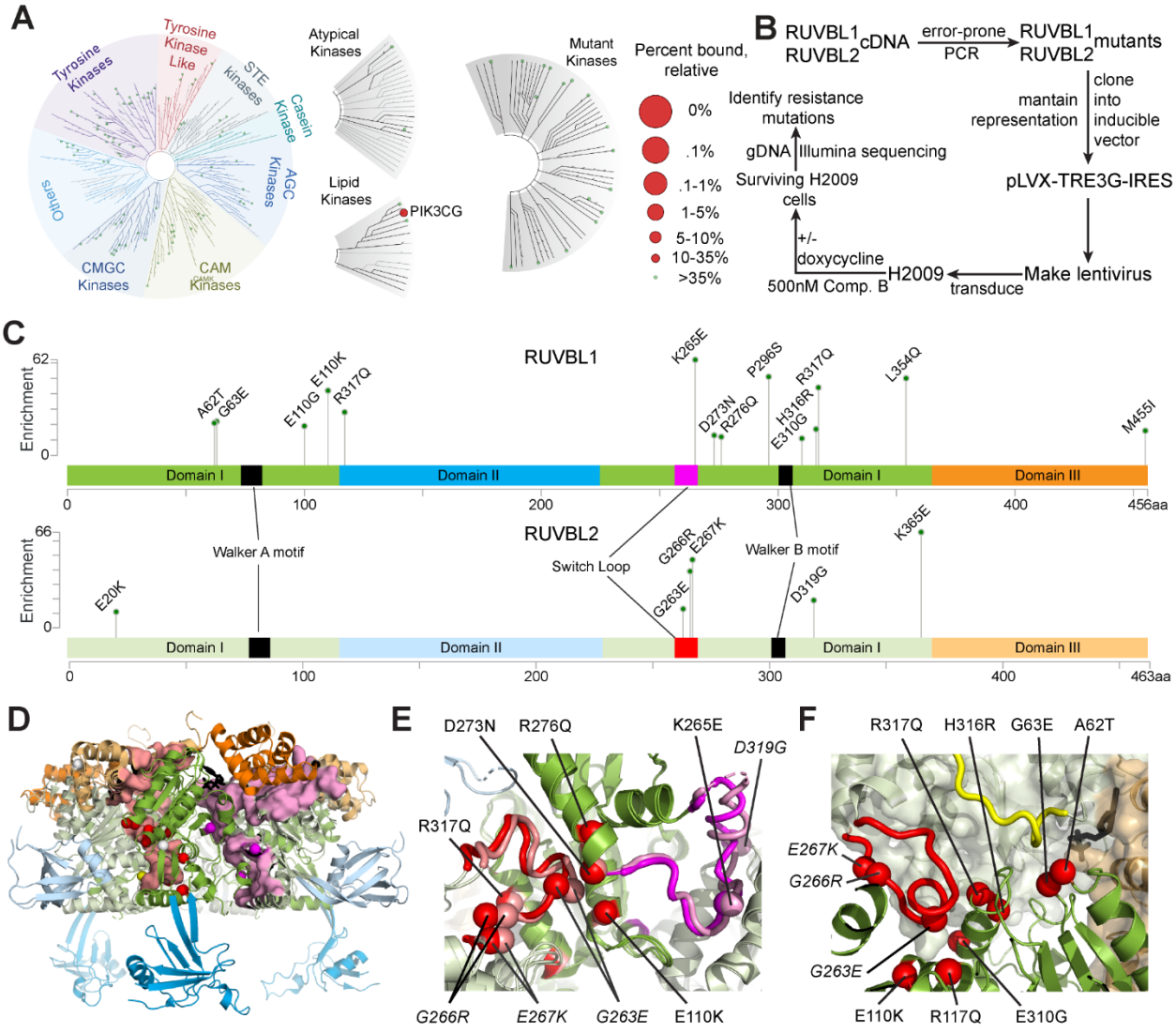


Figure 4.9 Compound B Inhibits RUVBL1/2 in an On-Target Manner and Resistance Mutations Cluster on the 3D Structure of RUVBL1/2. A) Compound B does not inhibit kinases. 1 μM of Compound B was screened for its ability to displace 97 kinases from their substrate using KINOMEscan scanEDGE by DiscoverX. Percent bound represents the percent of kinase displaced from its substrate, in comparison to control, and larger red circles represent greater kinase displacement (see key). B) Representation of how putative Compound B resistance-conferring mutations were identified by PCR mutagenesis. RUVBL1- and RUVBL2-RNAiR cDNAs (as used in **Figure 4.5D** and **Figure 4.5E**) were amplified by PCR using 30 cycles of an error-prone Taq polymerase, then these products were cloned into the lentiviral doxycycline-inducible pLVX-TRE3G-IRES plasmid, ensuring that enough transformants were made such that each nucleotide was mutated at least once. Lentivirus was made from these mutant plasmids, then H2009 cells were infected and treated with 500 nM of Compound B, which normally kills >99% of the cells, with or without doxycycline. Colonies formed only in the presence of doxycycline, and these surviving cells were collected, genomic DNA isolated, and the RUVBL1 or RUVBL2 open reading frame amplified via PCR. These PCR products were then assembled into next generation sequencing libraries and sequenced on an Illumina machine. C) PCR-mutagenesis identifies amino acid substitutions in RUVBL1 or RUVBL2 that confer resistance to Compound B. Lollipop diagrams were generated using cBioPortal (https://www.cbioportal.org/mutation_mapper) and known RUVBL1/2 domains were overlaid. Enrichment refers to the frequency a residue was mutated in cells surviving Compound B in comparison to the parental population. Only substitutions >10 fold enriched between 2 biological replicates are shown. See also **Table 4**. D) Compound B resistance-conferring mutations cluster at RUVBL1/2 interfaces. RUVBL1/RUVBL2 from *Chaetomium thermophilum* (PDB: 4wvy). Domains are depicted in cartoon and colored as in **Figure 4.9C**, with ATP depicted in black stick and resistance-conferring mutations in colored spheres. The RUVBL2/RUVBL1 interaction surface (RUVBL2 surface depicted in salmon) includes 9 resistance-conferring mutations (depicted as red spheres), while RUVBL1/RUVBL2 interaction surface (RUVBL2 surface depicted in pink) includes 3 resistance-conferring mutations (depicted as red spheres). Remaining resistance-conferring mutations are white. E) Superposition of the ATP/apo (PDB:4wvy) and ADP/ADP (PDB:4ww4) bound states of the RUVBL1/RUVBL2 interface highlights nucleotide-dependent switch loop conformations in RUVBL1 (magenta/pink thick loops for ATP/ADP states, respectively) and RUVBL2 (red/salmon thick loops for apo/ADP states, respectively) that span both interfaces. Compound B resistance-conferring mutations in or near the switch loops are labeled. F) A flexible RUVBL2 N-terminal gatekeeper (yellow thick loop) from human RUVBL1/RUVBL2 bound to R2TP (PDB:6qi8) is revealed by superposition of RUVBL1/RUVBL2 heterodimers from the nucleotide bound (ordered switch and gatekeeper loops) and apo (ordered elements in transparent surface with disordered loops) states. The ordered N-terminus completes the RUVBL1/RUVBL2 interaction surface and Compound B resistance-conferring mutations are labeled.

Gene	Mutation	Enrichment	Verified?	Fold IC_{50} increase, viability, H2009	Location in 3D structures		
					Mapping to partial or non-human proteins		Location
					PDB: 2xsz	PDB: wvy	
RUVBL1	A62T	21.04	Yes	1530.6	A76	A63	surface II[5]
RUVBL1	G63E	21.72	Yes	1923.1	G77	G64	surface II[5]

RUVBL1	E100G	19.17	No		E114	E101	surface I[4]
RUVBL1	E110K	28.48	Yes	1953.1	E124	E111	ring surface[3]
RUVBL1	R117Q	28.13	No		R131	R118	surface II[3]
RUVBL1	K265E	61.91	No		missing	K266	surface I[4]
RUVBL1	D273N	13.11	Yes	90.7	D184	D274	surface II[3]
RUVBL1	R276Q	11.71	No		R187	R277	surface II[3]
RUVBL1	P296S	50.69	No		P207	P297	surface
RUVBL1	E310G	11.01	No		E221	E311	surface II
RUVBL1	H316R	16.57	No		H227	N317[1]	surface II
RUVBL1	R317Q	44.19	Yes	1088.9	R228	K318[1]	surface II[3]
RUVBL1	L354Q	50.15	No		L265	F355[1]	core
RUVBL1	M455I	15.75	No		missing	missing	na
RUVBL2	E20K	10.57	Yes	28.1	missing	missing	na
RUVBL2	G263E	12.52	No		missing	G262	surface II[3]
RUVBL2	G266R	38.64	Yes	25.9	missing	G265	loop near II[3]
RUVBL2	G267K	46.57	No		missing	E266	loop near II[3]
RUVBL2	D319G	19.12	No		D234	D318	surface I[4]
RUVBL2	K365E	66.54	No		K283	R367[1]	surface

Table 4. List of Putative Compound B Resistance Conferring Mutations Identified by a PCR-based Mutagenesis Screen. Enrichment refers to the frequency this substitution was identified in the surviving cells in comparison to the frequency of this substitution in the parental population. Verified means that the substitution was independently cloned and shown to confer resistance to Compound B. [1]Conservative amino acid substitution in fungi. [2]Within 5Å of interface in ADP state only. [3]RUVBL2 switch loop conformation. [4]RUVBL1 switch loop conformation. [5]RUVBL2 N-terminal gatekeeper conformation.

To experimentally validate if these identified mutations can confer resistance to Compound B, we introduced some of these mutations into wild type RUVBL1 or RUVBL2 cDNAs by site-directed mutagenesis. We introduced two mutations into RUVBL1, purified mutant RUVBL1 protein and found that these mutants, when mixed with wild-type RUVBL2, were able to rescue the intrinsic in vitro ATPase activity of RUVBL1/2 after Compound B

treatment (**Figure 4.10A**). To test whether these mutations could rescue the cell growth defect seen following Compound B treatment, we cloned five of the identified mutations in RUVBL1 and two of the identified mutations in RUVBL2 into doxycycline-inducible vectors, transduced them into H2009 cells, and then measured sensitivity to Compound B with or without doxycycline. All these mutations in RUVBL1 (**Figure 4.10B**) or RUVBL2 (**Figure 4.10C**) were able to rescue the growth defect seen following Compound B treatment in the NSCLC cell line H2009. We tested the ability of these mutations in RUVBL1 (**Figure 4.10D**) and RUVBL2 (**Figure 4.10E**) to rescue the growth defect seen following Compound B treatment in an additional NSCLC cell line, H1993. These data demonstrate that the ability of Compound B to hinder cancer cell growth is due to the inhibition of RUVBL1/2 and it is likely that most of the other identified resistance mutations confer resistance to Compound B.

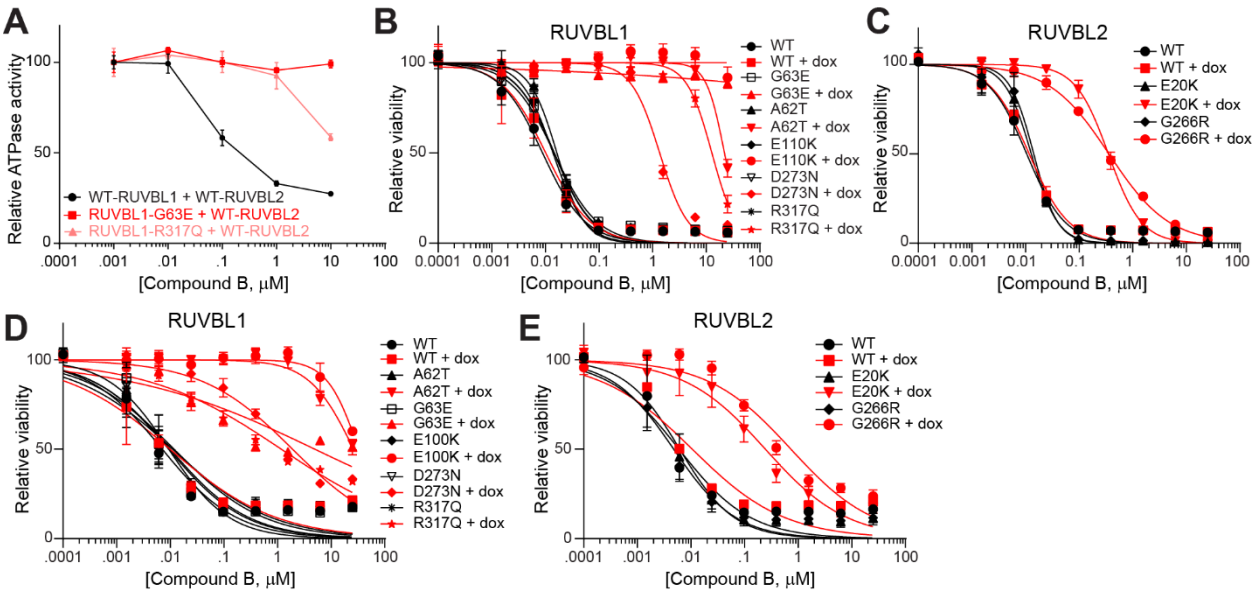


Figure 4.10. Mutations in RUVBL1/2 Identified in PCR-based Mutagenesis Screen as Compound B Resistance Mutations Confer Resistance to Compound B. A) Identified resistance-conferring mutations in RUVBL1 can rescue the ability of Compound B to inhibit the intrinsic ATPase activity of RUVBL1/2 *in vitro*. Values represent the average ± SD of 3 biological replicates. B) Doxycycline-inducible expression of Compound B resistance-conferring mutations in RUVBL1 causes resistance to Compound B in viability-based assays in H2009. Values represent the average ± SD of 3 biological replicates. C) Doxycycline-inducible expression of Compound B resistance-conferring mutations in RUVBL2 causes resistance to Compound B in viability-based assays in H2009. Values represent the average ± SD of 3 biological replicates. D) Doxycycline-inducible expression of Compound B resistance mutations in RUVBL1 causes resistance to Compound B in viability-based assays in H1993. Values represent the average ±

SD of 3 biological replicates. E) Doxycycline-inducible expression of Compound B resistance mutations in RUVBL2 causes resistance to Compound B in viability-based assays in H1993. Values represent the average ± SD of 3 biological replicates.

4.2.5 Many of RUVBL1/2's Cellular Functions Likely Require ATPase Activity

Previous studies have shown that RUVBL1/2 require their ATPase activity for some (Izumi et al., 2010; Zaarur et al., 2015) but not all (Jha et al., 2013; Jonsson et al., 2004) of their molecular functions. Thus, the global effects of RUVBL1/2 depletion versus the inhibition of RUVBL1/2's ATPase activity is unknown. Our results (**Figure 4.6A**) and the results of others have shown that globally, cells require RUVBL1/2 ATPase activity to survive, but it is not known if all of the functions of RUVBL1/2, especially in the cell as opposed to *in vitro*, require RUVBL1/2 ATPase activity. To assess the importance of RUVBL1/2 ATPase activity in its cellular functions at a global level, we analyzed the transcriptomic effects of RUVBL1 genetic depletion by siRNAs or RUVBL1/2 ATPase inhibition by Compound B via RNA-seq in two NSCLC cell lines, H2009 and H596. We chose these two cell lines as H2009 is relatively sensitive to Compound B (IC_{50} = 20 nM, **Table 3**) whereas H596 is relatively resistant to Compound B (IC_{50} = 103 nM, **Table 3**). These results are mirrored in our genetic knockdown studies as well (**Figure 4.4A**). Interestingly, treatment of H596 with Compound B or siRUVBL1 caused fewer genes to be differentially expressed (DE – defined here as RPKM > 1, $p < .01$, false discovery rate < .05, fold change > 2, **Appendix B**) than each respective treatment in H2009 (**Figure 4.11A**). Regardless, we found considerable overlap in DE genes, both between siRUVBL1 and Compound B in H2009 (**Figure 4.11B**), or between H2009 and H596 following treatment with Compound B (**Figure 4.11C**). This suggests that many cellular functions of RUVBL1/2 require ATPase activity, but does not rule out the possibility of there being ATPase independent functions.

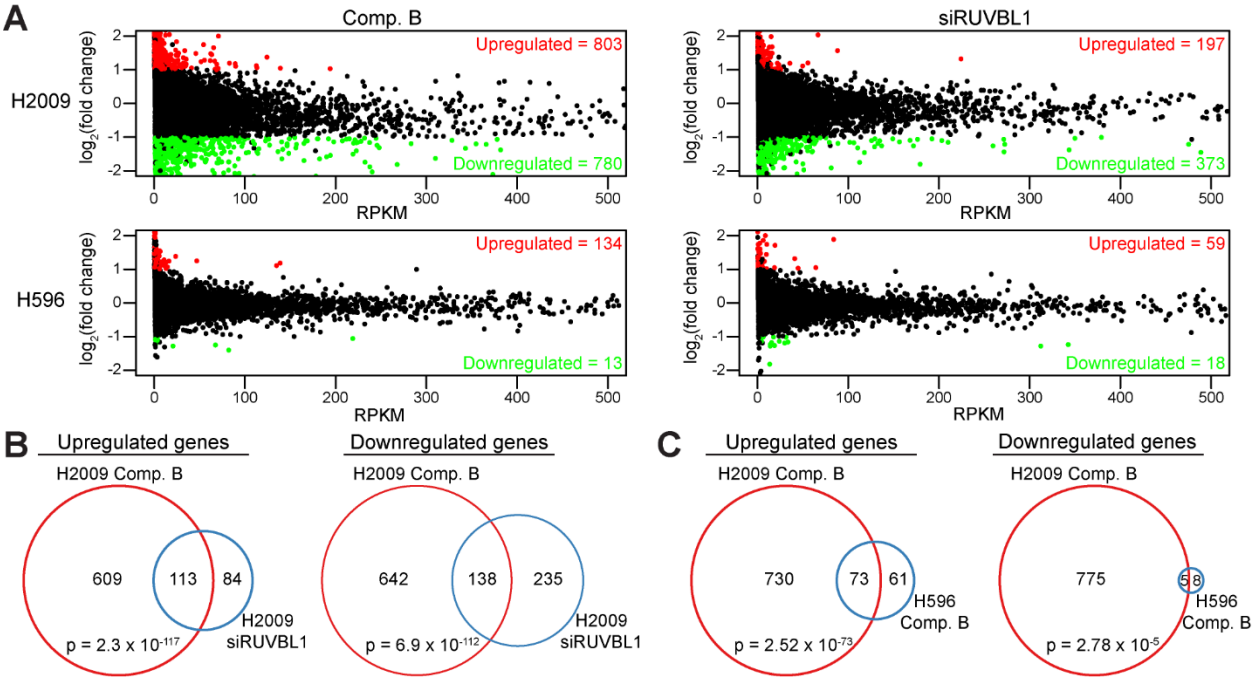


Figure 4.11. RNA-seq Profiling Suggests Many of RUVBL1/2's Cellular Functions Likely Require ATPase Activity. A) MA plots of RNA-seq data from H2009 (top two panels) and H596 (bottom two panels) treated with Compound B for 24 hours (left 2 panels) or siRUVBL1 for 3 days (right two panels). Colored dots represent differentially expressed (DE) genes, defined here as genes with RPKM > 1, p < .01, false discovery rate (FDR) < .05 and fold change > 2. Upregulated DE genes are shown in red, downregulated DE genes are shown in green. Values are averages of 2 biological replicates. B) Venn Diagrams of DE genes (upregulated genes left panel, downregulated genes right panel) from **Figure 4.11A** illustrating overlap of DE genes after Compound B and siRUVBL1 treatment in H2009. Significance of overlap was assessed by hypergeometric test. C) Venn Diagrams of DE genes (upregulated genes left panel, downregulated genes right panel) from **Figure 4.11A** illustrating overlap of DE genes after Compound B treatment in H2009 and H596. Significance of overlap was assessed by hypergeometric test.

4.2.6. Acute Inhibition of RUVBL1/2 ATPase Activity Inhibits PAQosome Maturation but not the INO80-family of Chromatin Remodelers

Because RUVBL1/2 interact with and are required for the function of many multiprotein complexes, we sought to interrogate the effects of acute RUVBL1/2 ATPase inhibition on the formation of RUVBL1/2-containing protein complexes at a global level. To do this, we treated H2009 cells that stably express a V5-tagged RUVBL1 with 100 nM Compound B or Compound C for 12 hours, immunoprecipitated RUVBL1-V5, and then subjected coimmunoprecipitating

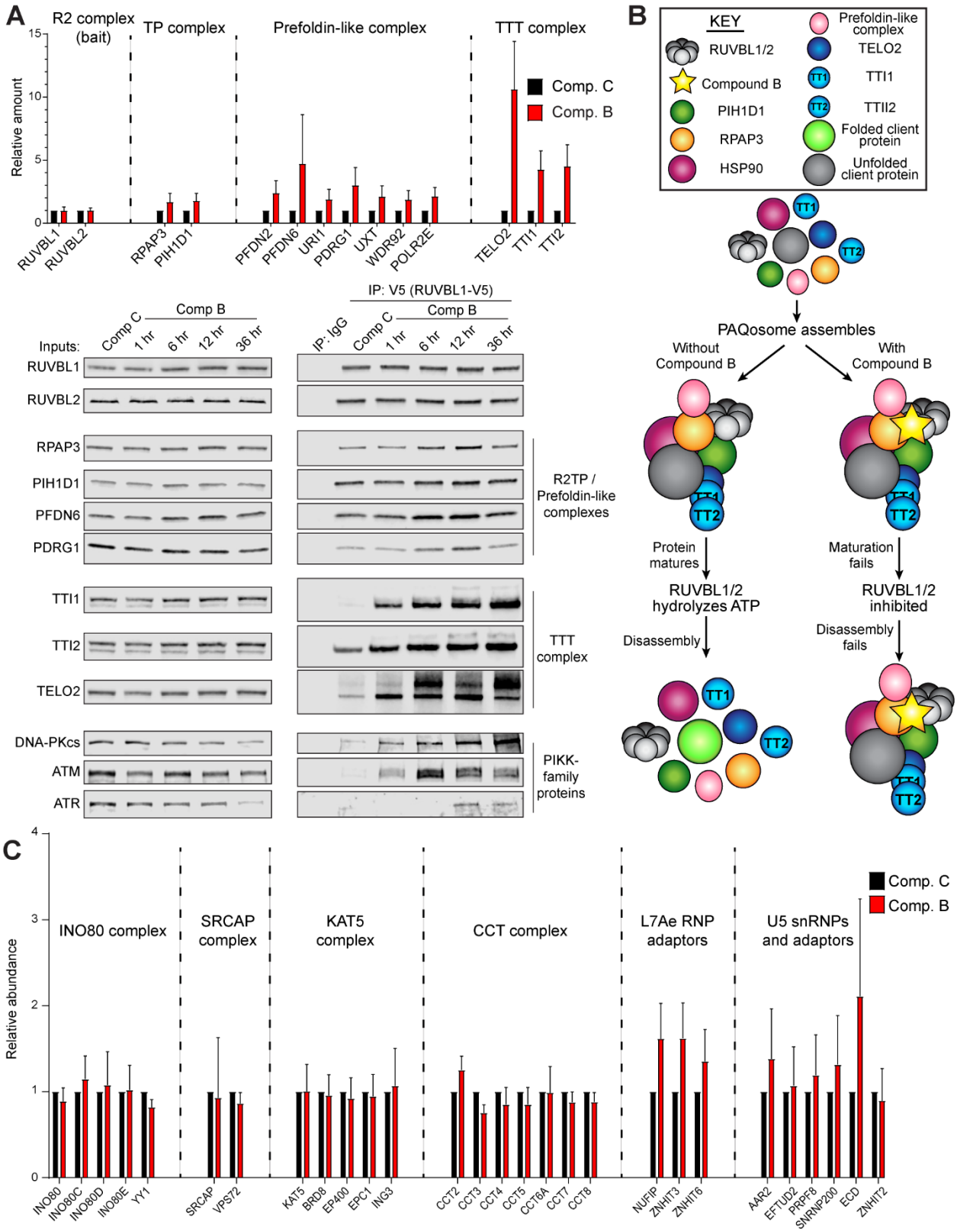


Figure 4.12. Inhibition of RUVBL1/2 ATPase Activity Causes Accumulation of PAQosome Components but not INO80-family of Chromatin Remodelers. A) Inhibition of RUVBL1/2 ATPase increases amount of PAQosome components associated with RUVBL1/2. Top: H2009

cells that stably express a RUVBL1-V5 cDNA were treated with 100nM of Compound B or Compound C for 12 hours, RUVBL1-V5 was immunoprecipitated and identity/abundance of coimmunoprecipitated proteins was determined by mass spectrometry. Values represent the average relative amount of protein between Compound B and Compound C treatment ± SD of 3 biological replicates. Bottom: validation of immunoprecipitation-mass spectrometry data by independent immunoprecipitation-immunoblotting after indicated time of Compound B treatment. B) Proposed cartoon model illustrating how RUVBL1/2 ATPase activity may affect maturation and/or disassembly of the PAQosome complex. C) Inhibition of RUVBL1/2 does not cause increased binding with INO80-family of chromatin remodelers but does increase binding to L7Ae RNPs and snRNP adaptors. Relative abundances from mass spectrometry of RUVBL1 co-immunoprecipitated proteins after Compound B treatment relative to Compound C treatment. Values represent the average ± SD of 3 biological replicates.

proteins to mass spectrometry (**Appendix C**). We found that components of the PAQosome complex, such as RPAP3, PIH1D1, the Prefoldin-like complex, and the TTT complex (TELO2, TTI1, TTI2) all had increased interactions with RUVBL1 after Compound B treatment (**Figure 4.12A**, top). This suggests that the PAQosome can assemble after the inhibition of RUVBL1/2 ATPase activity, but is unable to dissociate and/or mature. While Compound B increases the binding of PAQosome components, as well as some PAQosome substrates such as the L7Ae RNP and U5 snRNP adaptors, to RUVBL1/2, it does not affect the binding of the INO80-family of chromatin remodelers (INO80, SRCAP and TIP60) to RUVBL1/2 (**Figure 4.12C**). Thus, RUVBL1/2 ATPase activity likely serves different purposes within these complexes. This does not mean that the INO80-family of chromatin remodelers do not require RUVBL1/2 ATPase activity in cells for their functions, but it does strongly suggest that it is not required for complex assembly or disassembly. Independent immunoprecipitation of RUVBL1-V5 after various lengths of Compound B treatment followed by immunoblotting of PAQosome components confirmed these mass spectrometry-based findings and showed that this effect occurred in a time-dependent manner (**Figure 4.12A**, bottom). Additionally, we found that PIKK family proteins, such as DNA-PKcs, ATM and ATR, which require the PAQosome for their stability, increased binding to RUVBL1/2 and likely the PAQosome complex in a time-dependent manner, while conversely being depleted from total cellular lysate after Compound B treatment (**Figure**

4.12A, bottom). We propose that RUVBL1/2 ATPase activity is necessary for the proper maturation and/or dissociation of the PAQosome complex and its client proteins, such as the PIKK family proteins, as illustrated in a cartoon model (**Figure 4.12B**).

4.2.7 NSCLC Primarily Require RUVBL1/2 for Viability for Efficient DNA Replication

We sought to understand the mechanisms underlying the essential role of RUVBL1/2 for cellular viability, specifically in NSCLC. Because RUVBL1/2 have been implicated in numerous cellular processes, many of which are essential for viability such as splicing, transcription and rRNA biogenesis, we first decided to conduct unbiased analyses to nominate which pathways may be the most integral to the role RUVBL1/2 plays in supporting cellular viability in NSCLC. First, we performed gene set enrichment analysis (GSEA) (Subramanian et al., 2005) on the RNA-seq data following Compound B or siRUVBL1 treatment in H2009 NSCLC cells to identify pathways that may underlie the essential role of RUVBL1/2 for cellular growth. Of interest, transcripts involved in DNA replication were frequently downregulated after genetic or pharmacological inhibition of RUVBL1/2 (**Figure 4.13A**). Next, we assessed the potential function of RUVBL1/2 in NSCLC patient tumors by gene coexpression analysis. This type of analysis can infer putative gene function because genes that are coexpressed often act within the same pathway (Lee et al., 2004). To this end, we determined the Pearson correlation between the expression levels of RUVBL1 or RUVBL2 to those of every gene in the TCGA NSCLC RNA-seq dataset (adenocarcinoma and squamous cell carcinoma combined). GSEA analysis of this rank ordered list revealed a highly significant enrichment for both RUVBL1 and RUVBL2 to be coexpressed in NSCLC patient tumors with genes involved in DNA replication (**Figure 4.13B**). As a final correlative analysis, we compared the pattern of sensitivity, in regard to cellular growth, of RUVBL1/2 depletion to the pattern of sensitivity to depletion of other genes in lung cancer. To do this, we correlated the RSA score of RUVBL1/2 in a large shRNA-based

drop-out screen, Project DRIVE (McDonald et al., 2017), to the score of every other gene tested (7726) in 63 lung cancer cell lines. We then rank ordered this list and analyzed it with GSEA so

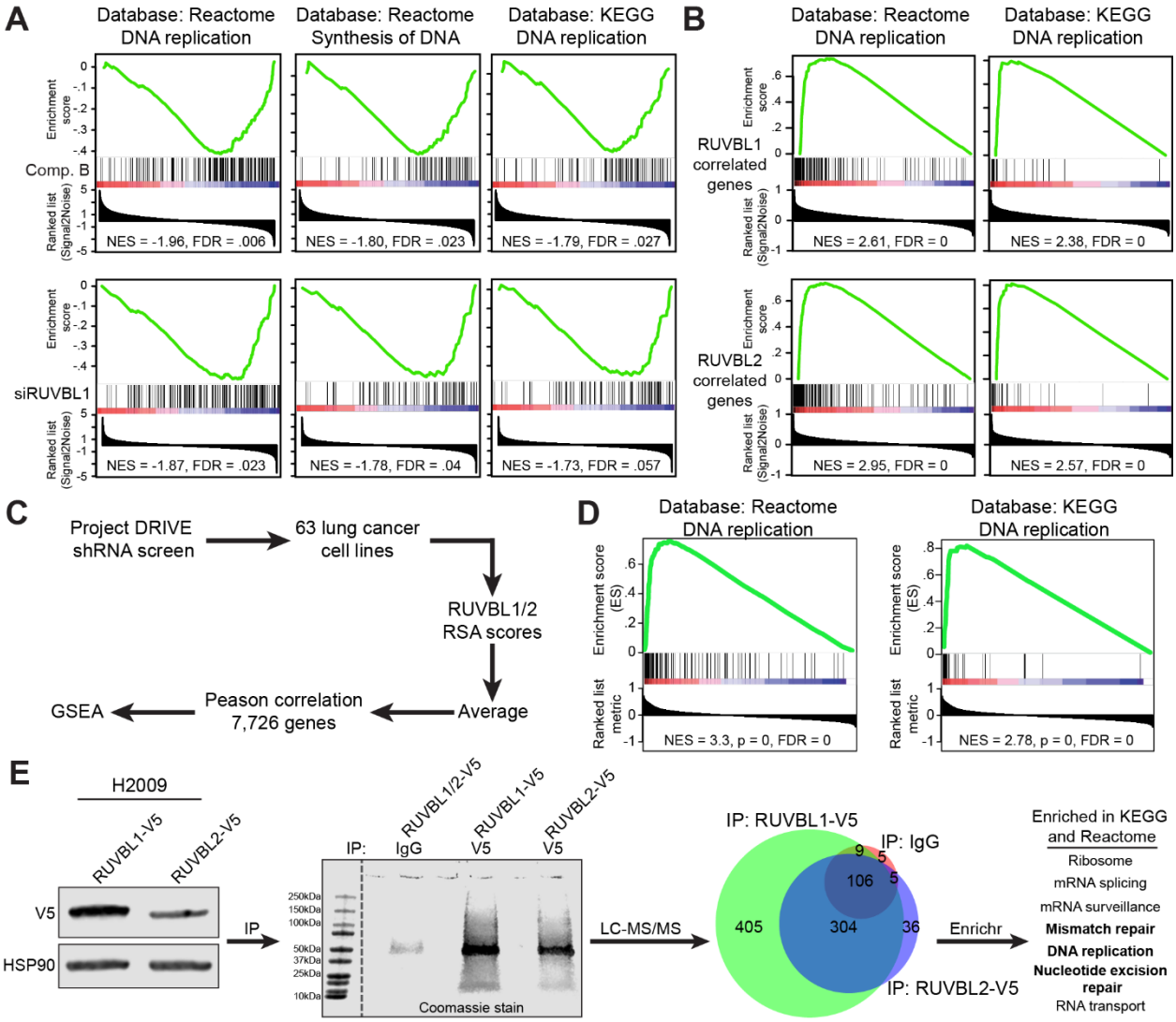


Figure 4.13. Correlative Analyses Implicate RUVBL1/2 in DNA Replication in NSCLC. A) GSEA of RNA-seq data following Compound B treatment (top panels) or RUVBL1 knockdown (bottom panels) in H2009 shows that mRNAs involved in DNA replication are downregulated. NES = normalized enrichment score, FDR = false discovery rate. B) RUVBL1/2 are co-expressed with DNA replication genes in NSCLC patient tumors. GSEA of the Pearson correlation between RUVBL1 (top) or RUVBL2 (bottom) mRNA expression and the mRNA expression of every gene in the TCGA NSCLC (adenocarcinoma and squamous cell carcinoma combined) RNA-seq dataset. C) Outline of scheme used to determine inhibition of what cellular processes inhibits the growth of lung cancer in a manner similar to RUVBL1/2 depletion. D) The pattern of sensitivity of lung cancer cell lines to knockdown of RUVBL1/2 correlates with sensitivity to the knockdown of DNA replication factors. GSEA of the Pearson correlation between the average RSA score of RUVBL1 and RUVBL2 and the RSA score of every gene tested in 63 lung cancer cell lines in the project DRIVE shRNA drop-out screen.

that we could identify what types of cellular processes inhibited cellular growth in a pattern similar to RUVBL1/2 inhibition (**Figure 4.13C**). We found that the pattern of sensitivity to RUVBL1/2 knockdown in lung cancer cell lines strongly correlated with the pattern of sensitivity to knockdown of DNA replication factors (**Figure 4.13D**). This means that cell lines that are more sensitive to depletion of RUVBL1/2 are also more sensitive to depletion of DNA replication factors, but not other essential processes, suggesting that the primary phenotypic consequence of RUVBL1/2 depletion in lung cancer may be the inhibition of DNA replication. Additionally, by immunoprecipitating RUVBL1-V5 or RUVBL2-V5 and performing mass spectrometry on coimmunoprecipitating proteins, we find an enrichment of replication factors in the proteins that coimmunoprecipitate with RUVBL1/2 (**Figure 4.13E**, **Appendix D**).

Because our unbiased correlative analyses implicated RUVBL1/2 in DNA replication, we sought to determine if defects with DNA replication and/or S-phase progression may arise following RUVBL1/2 inhibition or depletion. DNA content analysis of asynchronously proliferating cells 48 hours after 100 nM Compound B treatment showed that NSCLC cell lines that were more sensitive to Compound B displayed delayed S-phase progression or S-phase arrest (**Figure 4.14A**). This phenomenon was not unique to RUVBL1/2 ATPase inhibition, as genetic depletion of RUVBL1 also resulted in in impaired S-phase progression (**Figure 4.14B**). We confirmed that cells displaying delayed S-phase progression (or arrest) did not progress to mitosis, as these cells had decreased levels of phosphorylated histone H3 (S10), a marker of mitosis, by immunoblotting and immunofluorescent microscopy after Compound B treatment (**Figure 4.14C** and **4.14D**). Because loss of RUVBL1/2 impaired S-phase progression, we measured the levels of phosphorylated H2AX (S139, referred to as γH2AX), a general marker of DNA damage or replication stress, by immunoblotting. Compound B treatment increased the total level of γH2AX, but only after 48 hours of treatment in cell lines that displayed S-phase

arrest (H2009, **Figure 4.14E**). Similar results were seen when RUVBL1/2 was depleted using siRNAs (**Figure 14.4F**). When we analyzed the distribution of γH2AX in nuclei by immunofluorescent microscopy, we did not find a dramatic increase in the number of γH2AX or 53BP1 foci, both of which are generally indicative of DNA double strand breaks (DSBs) (**Figure 4.14G**). However, in cell lines with impaired S-phase progression there was a significant increase in the number of cells displaying nuclear pan-positive γH2AX staining (H2009, **Figure 4.14H**), which is generally indicative of cells undergoing replicative stress (Toledo et al., 2011). The S-phase arrest following Compound B treatment eventually culminates in apoptosis, as indicated by the sub-G1 population in DNA content analysis (see, for instance, H2009, **Figure 4.14A**) and cleaved PARP1 in immunoblots (**Figure 4.14E**). Similarly, knockdown of RUVBL1/2 in H2009 cells resulted in cells with sub-G1 DNA content (**Figure 4.14B**), increased total γH2AX levels, and increased cleavage of PARP1 (**Figure 4.14F**).

To further demonstrate that RUVBL1/2 inhibition impairs DNA replication, we synchronized H2009 cells at the late G1/early S-phase boundary by double thymidine block, pre-treated cells with Compound B or Compound C, and released them from this block in the presence of Compound B or Compound C. We then monitored the progression of cells through S-phase by flow cytometric analysis of BrdU incorporation and DNA content. Initially cells treated with Compound B replicated most of their DNA at a rate similar to Compound C treated cells (see the 6-hour time point, **Figure 4.15**). However, Compound B treated cells ultimately continued to synthesize DNA and stay in S-phase for a longer period of time than Compound C treated cells (see the 12- and 18-hour time points, **Figure 4.15**). The finding that Compound B did not inhibit bulk DNA replication, but kept cells in S-phase for a longer period of time, suggests that replication forks may stall or not fire properly at regions of the genome that are difficult or late to replicate when RUVBL1/2 ATPase activity is inhibited. Determining exactly

where these replication forks are stalled, or what causes their stalling, remains an open question.

Considering our finding that RUVBL1/2 inhibition or depletion impedes DNA replication, we sought to characterize changes at the DNA replication fork that occur after Compound B treatment in an unbiased manner. To do this, we treated cells with 100 nM of Compound B or Compound C for 12 hours and then performed isolation of proteins on nascent DNA (iPOND) (Sirbu et al., 2012), a technique where active replisomes and associated proteins are purified. We then identified and quantified purified replisome components by mass spectrometry and compared the abundance of these proteins between Compound B and Compound C treated cells. Similar to hydroxyurea treatment (Dungrawala et al., 2015), we found that 12 hours of 100 nM Compound B treatment caused the majority of replisome components, such as the CMG complex and the RFC complex, to dissociate from the replication fork (**Figure 4.16A**, see also **Appendix E**). However, while the lagging strand DNA polymerases alpha and delta (POLA1, POLA2, POLD1, POLD2 and POLD3) dissociated from replication forks, the leading strand DNA polymerase epsilon (POLE, POLE2) remained bound to replication forks, suggesting that the decrease in replisome components was not a general phenomenon and Compound B treatment preferentially affected the lagging strand. However, unlike hydroxyurea treatment, we did not see recruitment of DNA replication stress proteins to these replication forks, such as the RPA complex, ATR, the Fanconi Anemia Complex or other various replication stress factors. Instead, Compound B treatment decreased the amount of these factors at replication forks (**Figure 4.16B**). It is unlikely that this decrease in replisome components and stress response factors at the replication fork was due to differences in purification efficiency between treatments, as Coomassie staining of purified proteins prior to mass spectrometry showed similar total protein abundances in all conditions and replicates (**Figure 4.16C**).

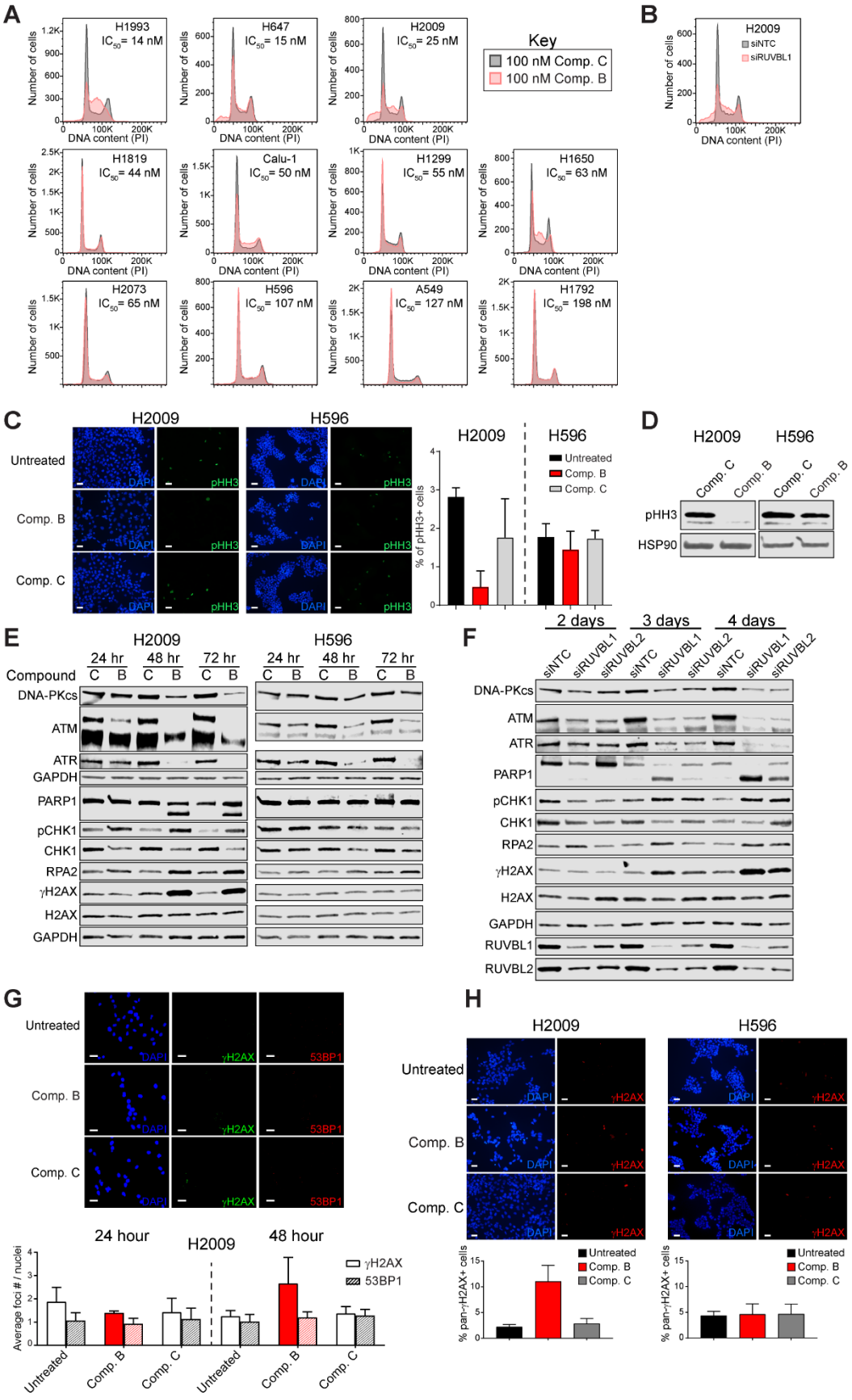

A
H1993
IC50= 14 nM
H647
IC50= 15 nM
H2009
IC50= 25 nM
Key
100 nM Comp. C
100 nM Comp. B
H1819
IC50= 44 nM
Calu-1
IC50= 50 nM
H1299
IC50= 55 nM
H1650
IC50= 63 nM
H2073
IC50= 65 nM
H596
IC50= 107 nM
A549
IC50= 127 nM
H1792
IC50= 198 nM
Number of cells
DNA content (PI)
B
H2009
siNTC
siRUVBL1
C
H2009
H596
Untreated
Comp. B
Comp. C
DAPI
pHH3
% of pHH3+ cells
D
H2009
H596
Comp. C
Comp. B
pHH3
HSP90
E
H2009
H596
24 hr
48 hr
72 hr
Compound
C
B
DNA-PKcs
ATM
ATR
GAPDH
PARP1
pCHK1
CHK1
RPA2
γH2AX
H2AX
F
2 days
3 days
4 days
siNTC
siRUVBL1
siRUVBL2
DNA-PKcs
ATM
ATR
PARP1
pCHK1
CHK1
RPA2
γH2AX
H2AX
GAPDH
RUVBL1
RUVBL2
G
Untreated
Comp. B
Comp. C
DAPI
γH2AX
53BP1
24 hour
H2009
48 hour
Average foci # / nuclei
H
H2009
H596
Untreated
Comp. B
Comp. C
DAPI
γH2AX
% pan-γH2AX+ cells

Figure 4.14 Inhibition or Depletion of RUVBL1/2 Interferes with S-phase Progression in NSCLC That are Sensitive to Compound B. A) Cell cycle analysis by DNA content (PI staining) in various NSCLC cell lines, arranged most sensitive to most resistant (top left to bottom right) after 48 hours of 100 nM Compound B or Compound C. Each plot contains ≥10,000 cells and images are representative of at least 2 biological replicates. B) Cell cycle analysis by DNA content (PI staining) in H2009 cells 4 days after siRUVBL1 transfection. Each plot contains 10,000 cells and is representative of 3 biological replicates. C) Immunofluorescent microscopy of phospho-Histone H3 (pHH3, Serine10) in NSCLC lines that arrest in S-phase (H2009) or do not (H596) after 48 hours of 100 nM Compound B or 100 nM Compound C treatment. Left: representative single-color images. Blue = DAPI (DNA), green = pHH3. Scale bars are 20 μm. Right: Quantification of immunofluorescent images. Values represent the average ± SD of 2 biological replicates. D) Immunoblot of phospho-Histone H3 (pHH3, Serine10) after 48 hours of 100 nM Compound B or 100 nM Compound C treatment in cell lines that arrest in S-phase (H2009) or do not (H596). E) Time course of the effects of 100 nM Compound B on various proteins by immunoblot in H2009 (left) and H596 (right). F) Immunoblot of various proteins after indicated siRNA treatments in H2009 cells. G) Immunofluorescent microscopy of γH2AX and 53BP1 in H2009 cells after 24 or 48 hours of 100 nM Compound B treatment. Top: representative images. Blue = DAPI (DNA), green = γH2AX, red = 53BP1. Scale bars are 20 μm. Bottom: quantification of the number of γH2AX or 53BP1 foci within nuclei of immunofluorescent images. Values represent the average ± SD of 3 biological replicates. H) Top: Representative images from immunofluorescent microscopy of H2009 (left) and H596 (right) cells treated with 100 nM Compound B or Compound C for 48 hours, then fixed and stained for DAPI (blue) or γH2AX (red). Bottom: Quantification of pan-γH2AX positive cells, defined as nuclei covered in γH2AX staining, where values represent averages ± SD from 3 biological replicates. Scale bars are 20 μm.

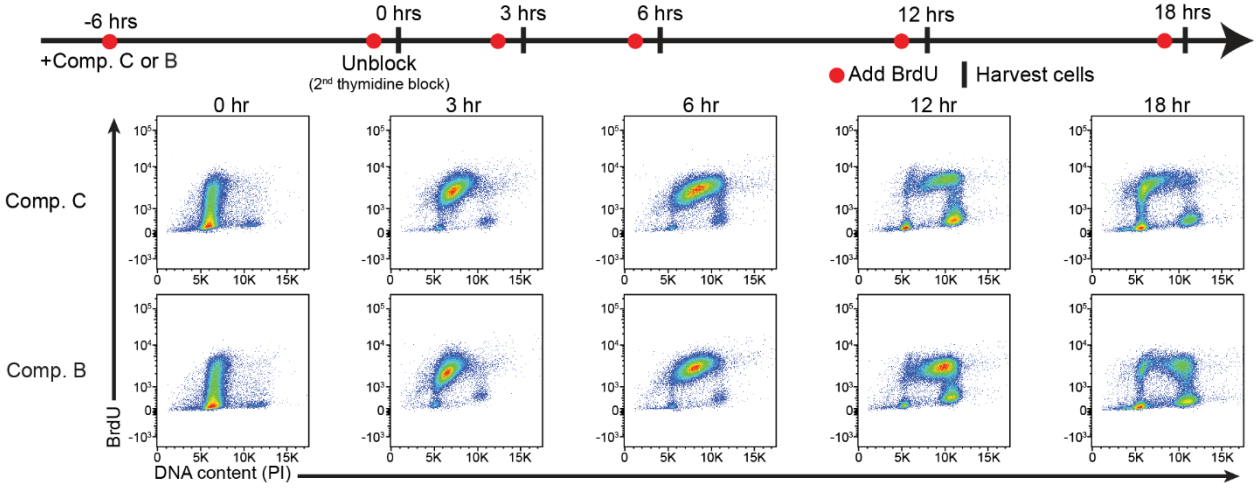


Figure 4.15. Compound B Hinders S-phase Progression. Compound B slows progression through S-phase after release from a double thymidine block. Top: schematic of experiment outline. Bottom: flow cytometric analysis of BrdU incorporation and DNA content (PI, propidium iodide) in H2009 cells following release into S-phase from a double thymidine block. Plots display 30,000 cells and are representative of 3 biological replicates.

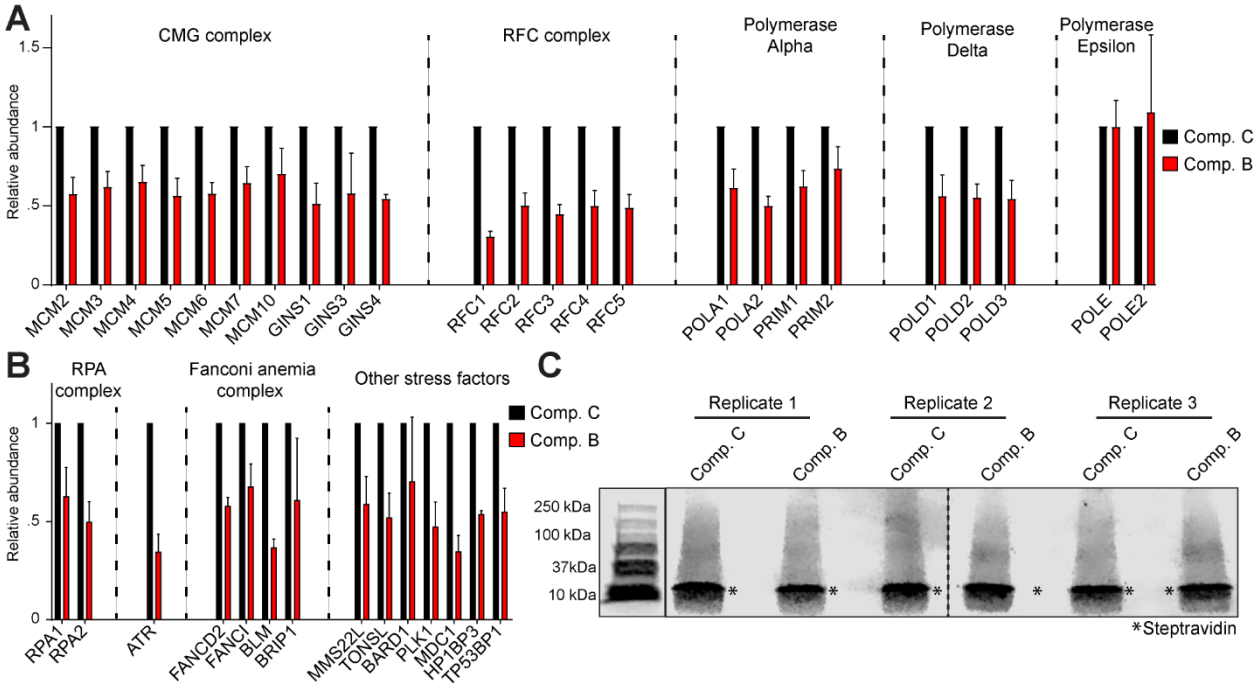


Figure 4.16 Compound B Treatment Dissociates Most Replisome Components, but not Polymerase Epsilon, Without Recruiting Replication Stress Factors. A) Isolation of proteins on nascent DNA (iPOND) followed by mass spectrometry reveals disassembly of replisome components but sparing of polymerase epsilon (POLE). H2009 was treated with 100 nM of Compound C or Compound B for 12 hours, active replisomes were purified by iPOND, and eluted proteins were analyzed by mass spectrometry. Only core replisome components are shown. Values shown are averages ± standard error of the mean (SEM) from 3 biological replicates. See also **Appendix E.** B) Replication stress factors are not recruited to stalled replisomes after Compound B treatment. iPOND-mass spectrometry data from **Figure 4.16A**. Only replication stress factors are shown. Values shown are averages ± SEM from 3 biological replicates. See also **Appendix E**. C) Similar amount of total protein was purified for iPOND-mass spectrometry in all conditions. Eluates from 3 biological replicates of iPOND were ran on an SDS-gel, Coomassie stained and imaged with a Licor Odyssey Fc prior to submission for mass spectrometry. Prominent bands with an asterisk represent the streptavidin protein.

We were intrigued by the depletion of RPA from these replication forks after Compound B treatment as its absence could potentially explain the collapse of the lagging strand polymerase and the failure to recruit replication stress proteins to these disassembled replication forks. This is because RPA serves as a platform to help recruit key replication factors to the DNA lagging strand, such as the DNA polymerase delta (but not DNA polymerase epsilon) and the endonucleases FEN1 and DNA2 (Bae et al., 2001; Chilkova et al., 2007).

Additionally, during times of replication stress, RPA also recruits and activates replication stress proteins at replication forks (Zou and Elledge, 2003). To validate our findings of perturbed RPA loading using a different technique, we transiently permeabilized H2009 cells, fixed them, and then analyzed chromatin bound RPA2 by flow cytometry. Similar to our iPOND results, after 24 hours of Compound B treatment, RPA2 was underloaded onto chromatin (**Figure 4.17A**), despite there being a slight increase in total RPA2 levels by immunoblotting (**Figure 4.14E**). In contrast, by 48 hours, RPA2 was hyperloaded onto chromatin (**Figure 4.17A**). We noticed that at 48 hours, when RPA2 becomes hyperloaded onto chromatin, the PIKK-family member protein ATR, which is a guardian of replication forks and the major sensor of replication stress (Zeman and Cimprich, 2014), is dramatically depleted (**Figure 4.14E**). Thus we hypothesized that the following scenario occurs: after 24 hours of Compound B treatment, the majority of cells are arrested in late S-phase with stalled/disassembled replication forks; after 48 hours, when ATR is depleted, unfired and/or suppressed origins fire aberrantly due to the near complete loss of ATR, and their subsequent arrest results in the hyperloading of RPA. This phenomenon, where replication fork stalling and subsequent ATR inhibition results in RPA hyperloading and apoptosis, has been termed replication catastrophe (Toledo et al., 2013). To test this hypothesis, we treated cells for 24 hours with Compound B (a time point when RPA2 is normally underloaded), then added 80 nM of the ATR inhibitor VE-822 for 2 hours. This transient addition of an ATR inhibitor to cells treated with Compound B for 24 hours induced a level of RPA2 hyperloading nearly identical to 48 hours of Compound B treatment (**Figure 4.17B**). Transient treatment with 100 nM of the CHEK1 inhibitor LY2603618 produced nearly identical effects on RPA hyperloading (**Figure 4.17C**) and co-treatment of Compound B with a CHEK1 inhibitor was able to induce premature apoptosis (**Figure 4.17D**). These results strongly suggest that RUVBL1/2 inhibition initially causes replisome stalling/dissociation, and subsequent loss of the ATR/CHEK1 signaling axis causes replication catastrophe.

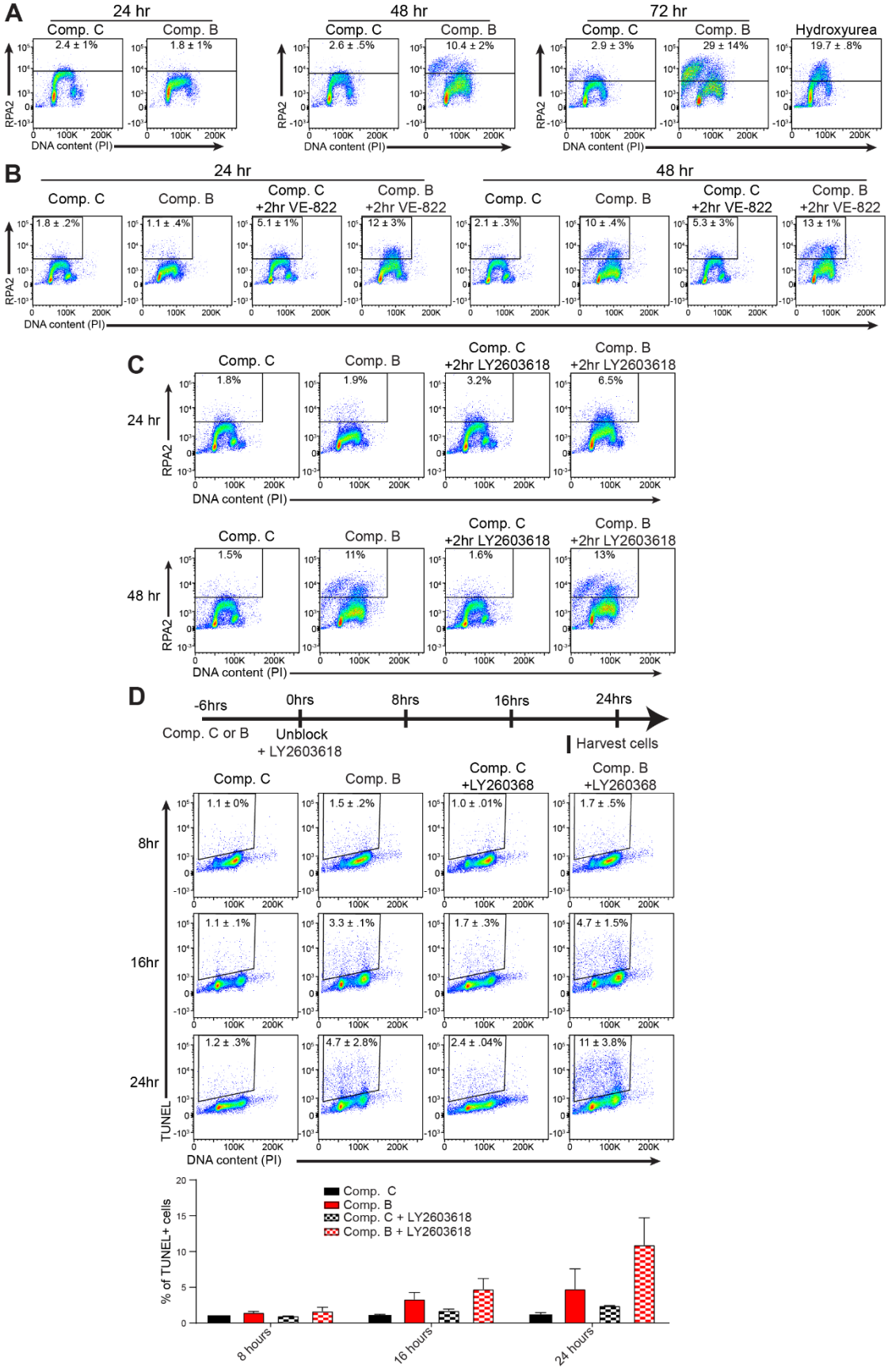

A
24 hr
48 hr
72 hr
Comp. C
Comp. B
Hydroxyurea
2.4 ± 1%
1.8 ± 1%
2.6 ± .5%
10.4 ± 2%
2.9 ± 3%
29 ± 14%
19.7 ± .8%
RPA2
DNA content (PI)
B
24 hr
48 hr
Comp. C
Comp. B
Comp. C +2hr VE-822
Comp. B +2hr VE-822
1.8 ± .2%
1.1 ± .4%
5.1 ± 1%
12 ± 3%
2.1 ± .3%
10 ± .4%
5.3 ± 3%
13 ± 1%
C
Comp. C +2hr LY2603618
Comp. B +2hr LY2603618
24 hr
48 hr
1.8%
1.9%
3.2%
6.5%
1.5%
11%
1.6%
13%
D
-6hrs
0hrs
8hrs
16hrs
24hrs
Comp. C or B
Unblock
+ LY2603618
Harvest cells
Comp. C +LY260368
Comp. B +LY260368
8hr
16hr
24hr
TUNEL
1.1 ± 0%
1.5 ± .2%
1.0 ± .01%
1.7 ± .5%
1.1 ± .1%
3.3 ± .1%
1.7 ± .3%
4.7 ± 1.5%
1.2 ± .3%
4.7 ± 2.8%
2.4 ± .04%
11 ± 3.8%
% of TUNEL+ cells
Comp. C
Comp. B
Comp. C + LY2603618
Comp. B + LY2603618
8 hours
16 hours
24 hours

Figure 4.17. RPA Hyperloading and Replication Catastrophe Occurs After Compound B Treatment due to ATR Loss. A) RPA is initially underloaded, then hyperloaded, after Compound B treatment in sensitive NSCLC cells. H2009 cells were pre-extracted and analyzed for chromatin bound RPA2 and DNA content (PI) by flow cytometry after 100 nM of Compound B or Compound C treatment for indicated times. Hydroxyurea (2 mM for 2 hours, far right) serves as a positive control. Numbers shown indicate the percentage of RPA hyperloaded cells (gated populations) and represent the average ± SD of 3 biological replicates. Plots display 30,000 cells and images are representative of 3 biological replicates. B) Complete loss of ATR causes RPA hyperloading and replication catastrophe after RUVBL1/2 inhibition. H2009 cells were pre-extracted and analyzed for chromatin bound-RPA2 and DNA content (PI) by flow cytometry after being treated with 100 nM of Compound B, 100 nM Compound C or 80 nM VE-822 (ATR inhibitor) for indicated times. Percentages for gated populations (RPA hyperloaded cells) represent the average ± SD of 3 biological replicates with ≥ 30,000 cells per replicate. C) Loss of CHEK1 signaling causes RPA hyperloading and replication catastrophe after RUVBL1/2 inhibition. H2009 cells were pre-extracted and analyzed for chromatin bound-RPA2 and DNA content (PI) by flow cytometry after being treated with 100 nM of Compound B, 100 nM Compound C or 100 nM LY2603618 (CHEK1 inhibitor) for indicated times. Percentages for gated populations (RPA hyperloaded cells) represent the average ± SD of 3 biological replicates with ≥ 30,000 cells per replicate. D) Compound B + LY2603618 (CHEK1 inhibitor) synergistically increases apoptotic cell death in H2009, primarily as cell progress from S phase to G2/mitosis. Top: experimental outline. Middle: Representative plots where H2009 cells were synchronized at G1/S boundary by double thymidine block, pre-treated for 6 hours with 100 nM Compound B or Compound C, then released from the block in the presence of 100 nM Compound B or Compound C, with or without 100 nM LY2603618. At indicated times, cells were harvested and analyzed for terminal deoxynucleotidyl transferase dUTP nick end labeling (TUNEL) and DNA content (PI staining) by flow cytometry. Numbers in gates represent the average percent of cells ± SD with TUNEL staining greater than ~99% of control cells in 2 biological replicates. Bottom: Quantification of gated TUNEL positive cells. Values represent the average ± SD of 2 biological replicates.

To better understand the mechanism underlying the diminished loading of RPA onto chromatin during DNA replication we inspected our mass spectrometry data of RUVBL1 coimmunoprecipitating proteins after Compound B treatment (**Appendix C**). Interestingly, we found that Compound B treatment dramatically increased binding of RUVBL1/2 to RPA3, one of the subunits of heterotrimeric RPA complex (**Figure 4.18A**). We confirmed that this interaction occurred in a time-dependent manner by immunoprecipitating RUVBL1 after various lengths of Compound B treatment and analyzing RPA3 binding by immunoblotting (**Figure 4.18B**). We next sought to determine if Compound B treatment inhibited the formation of the RPA complex, either under steady state conditions or during replication stress. To do this, we

immunoprecipitated RPA2 after 24 hours of Compound B or Compound C treatment, with or without 1 hour of 2 mM hydroxyurea (HU) treatment to induce replication stress, and analyzed levels of RPA1 or RPA3 bound to RPA2 by immunoblotting. Equal levels of RPA1 and RPA3 associated with RPA2 after all treatments (**Figure 4.18C**), suggesting that while Compound B affects loading of the RPA complex onto DNA during replication, Compound B does not inhibit RPA complex formation.

Compared to normal cells, cancer cells have been shown to, in general, have higher levels of replication stress, potentially due to their increased mutational load, increased proliferation rate, or their abnormal genomes, and it has been suggested that this property could be a therapeutic target. For this reason, and because Compound B inhibits NSCLC proliferation

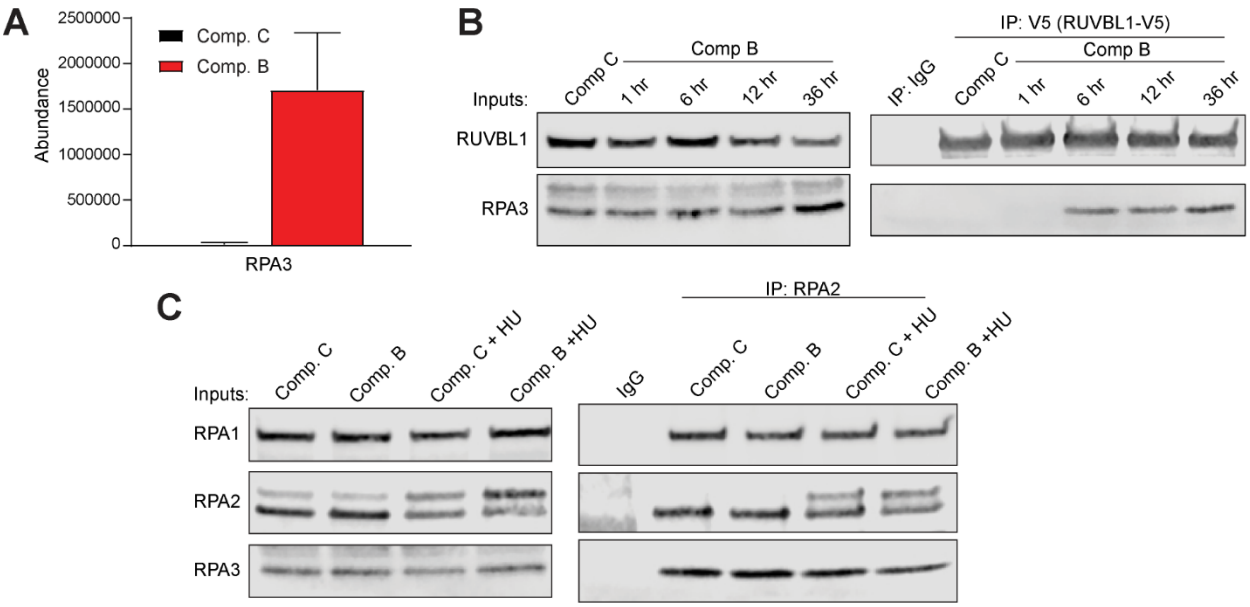


Figure 4.18. RUVBL1/2 Binds RPA3 After Compound B Treatment but does not Disturb RPA Complex Formation. A) RUVBL1 binds RPA3 after Compound B treatment. Immunoprecipitation followed by mass spectrometry data same as in **Figure 4.12A**. See also **Appendix C**. B) Validation of immunoprecipitation followed by mass spectrometry data from **Figure 4.18A** by independent immunoprecipitation-immunoblot. C) Compound B does not disturb the formation of the heterotrimeric RPA complex. H2009 cells were pretreated with 100 nM of Compound C or Compound B for 24 hours, treated with or without 2 mM or hydroxyurea (HU) for 1 hour, RPA2 was immunoprecipitated, and RPA components were examined by immunoblot.

in vitro, we decided to test the efficacy of Compound B in NSCLC xenografts. First, we tested the necessity of RUVBL1/2 *in vivo* using genetic knockdown studies. H1299 cells that were transduced either with a doxycycline-inducible shRNA that did not target a sequence present in humans (shNTC) or targeting RUVBL1 (shRUVBL1) were implanted into NOD/SCID mice subcutaneously. Once tumor volumes reached 150mm^3, 2 mg/mL doxycycline was added to the mice drinking water to induce expression of the shRNAs, and tumor volume was measured over time. These shRNAs were able to reduce RUVBL1/2 protein levels *in vivo* (**Figure 4.19A,** right) and able to significantly delay tumor growth, in comparison to the non-targeting control (**Figure 4.19A**, left). While this is encouraging, this system is unlike systemic drug treatment, which is how humans would be treated, as RUVBL1/2 is only depleted in tumor cells. A more relevant preclinical model involves systemic inhibition of RUVBL1/2. Systemic treatment can determine if the treatment can have the desired effect without unacceptable toxicities (i.e. if there is a therapeutic window). This is especially important for targets that have roles in normal cell physiology, such as RUVBL1/2.

To see if Compound B would provide an ample therapeutic window in multiple NSCLC models, H2009 and H596 NSCLC cell lines were injected subcutaneously into NOD/SCID mice, and mice were randomized to receive either vehicle or 175 mg/kg Compound B, the maximum tolerated dose, via oral gavage once their tumors reached ~150 mm^3. Treatment with Compound B significantly reduced tumor growth in both models (**Figure 4.19B and 4.19D**), but had a larger effect in H2009 tumors, which were also more sensitive to Compound B and RUVBL1/2 knockdown in vitro (**Figure 4.4A** and **Table 3**). H2009 tumors treated with Compound B displayed morphological changes, with evidence of stressed and vacuolated nuclei by H&E staining (**Figure 4.19D**, bottom). While Compound B was able to reduce tumor growth, it caused mild and transient bodyweight loss in mice following four days of administration at 175 mg/kg/day (**Figure 4.19C**), despite there being no marked changes in the

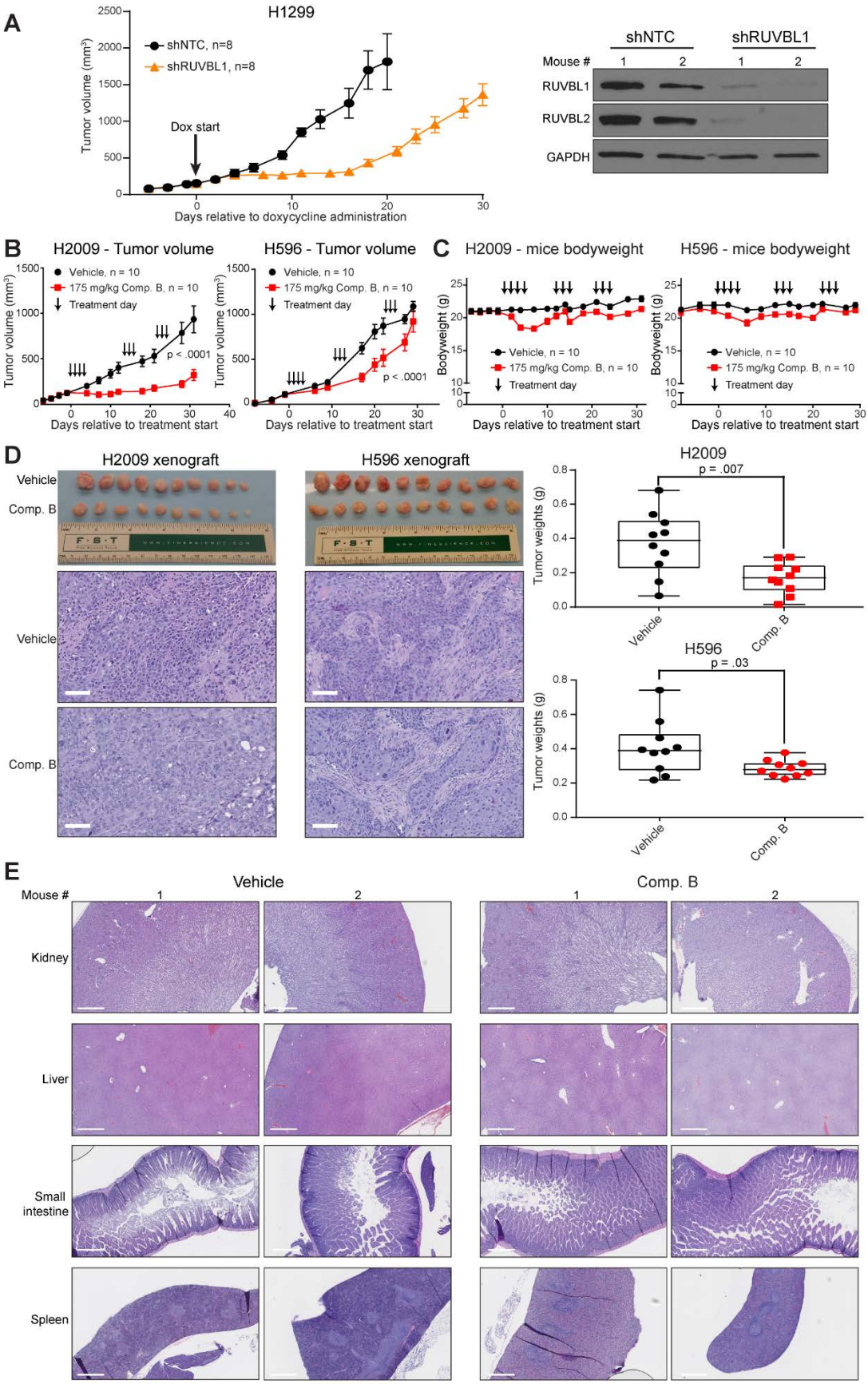

A
H1299
shNTC, n=8
shRUVBL1, n=8
Tumor volume (mm³)
Dox start
Days relative to doxycycline administration
shNTC
shRUVBL1
Mouse #
RUVBL1
RUVBL2
GAPDH
B
H2009 - Tumor volume
H596 - Tumor volume
Vehicle, n = 10
175 mg/kg Comp. B, n = 10
Treatment day
p < .0001
Days relative to treatment start
C
H2009 - mice bodyweight
H596 - mice bodyweight
Bodyweight (g)
D
H2009 xenograft
H596 xenograft
Vehicle
Comp. B
H2009
p = .007
H596
p = .03
Tumor weights (g)
E
Mouse #
Kidney
Liver
Small intestine
Spleen

Figure 4.19. RUVBL1/2 are Required for NSCLC Growth *In Vivo* but Afford a Small Therapeutic Window. A) Depletion of RUVBL1 by doxycycline-inducible shRNAs in vivo results in delayed tumor growth. H1299 cells transduced with doxycycline-inducible shNTC or shRUVBL1 were implanted subcutaneously into the flanks of female NOD/SCID mice. Once tumor volumes reached ~150 mm^3, 2 mg/mL doxycycline (Dox start) was added to mice drinking water for the duration of the experiment. Left: Tumor volumes are shown as averages ± SEM, with 8 mice in each group (n=8). Right: immunoblotting of tumor protein extracts 14 days after doxycycline administration shows that doxycycline-inducible shRUVBL1 depletes RUVBL1/2 proteins in vivo. B) Orally delivered Compound B can inhibit NSCLC tumor growth *in vivo*. NSCLC lines that were relatively sensitive (H2009, left) or relatively resistant (H596, right) *in vitro* to Compound B were implanted subcutaneously into NOD/SCID mice. Once tumor volumes reached ~150 mm^3, mice were randomized to receive 175 mg/kg Compound B (red) or vehicle (PEG 200, black) and tumor volume was measured over time. Arrows represent treatment days, and values shown are averages ± SEM. Statistical significance was assessed with two-way repeated measures ANOVA. n represents the number of mice in each group. C) Body weight of NOD/SCID mice bearing H2009 (left) or H596 (right) NSCLC lines xenografted subcutaneously and treated with 175 mg/kg Compound B (red) or vehicle (PEG 200, black). Arrows represent treatment days and n represents the number of mice in each group and values shown are averages ± SEM. D) Compound B decreases tumor size and weight *in vivo*. Top left: picture of tumors from mice in **Figure 4.19B**. Bottom left: H&E staining of H2009 (left) or H596 (right) tumors treated for 3 days with 175 mg/kg/day Compound B or vehicle (PEG 200). Scale bars are 100 μM. Right: tumor weights from mice bearing H2009 (top) or H596 (bottom) cells xenografted subcutaneously into NOD/SCID mice and treated with Compound B or vehicle from mice in **Figure 4.19B**. Whiskers represent minimum to maximum values, boxes represent 25th-75th percentile, the line represents the median and n refers to the number of mice. Significance was assessed with a two-tailed T-test. E) Representative H&E staining of mouse tissue from 2 NOD/SCID mice treated with vehicle (left) or 175 mg/kg/day Compound B for 3 days (right). Images are representative of 4 mice. Scale bars are 500 μm.

tissue architecture or cell morphology of the kidney, liver, spleen or small intestine from these mice (**Figure 4.19E**). These results suggest that Compound B inhibits NSCLC tumor growth in vivo but may only offer a moderate therapeutic window as a monotherapy in a subset of NSCLCs.

Because only some NSCLC cell lines had an acceptable therapeutic response to Compound B, we attempted to identify pre-treatment biomarkers that would predict sensitivity to Compound B. This is necessary as our data suggests that Compound B, if used clinically, would work in a subset of NSCLC patients, thus it is important to identify this subset. The Minna lab has exome- and RNA-sequencing on the vast majority of the 60 NSCLC cell lines that were tested for their sensitivity, in regard to cell viability, to Compound B. In a collaboration with

Elizabeth McMillian, a former graduate student at Michael White's former lab at UT Southwestern, we leveraged this data to attempt to identify biomarkers that could predict sensitivity or resistance to Compound B (IC_{50} values ranged from 11-198 nM). Despite running both regularized machine learning algorithms such as elastic net and probability-based metrics such as a scanning Kolmogorv-Smirnov test, we were unable to find satisfactory simple (i.e. 1-10 gene) solutions that explain the sensitivity of NSCLC cell lines to Compound B. This does not necessarily mean that there are not biomarkers that could predict sensitivity to Compound B. However, given the current dataset and methods we were unable to identify reliable biomarkers that could predict sensitivity or resistance to Compound B.

4.2.8 Inhibition of the ATPase Activity of RUVBL1/2 Radiosensitizes NSCLC, but not Normal Cells

Given the lack of reliable response biomarkers, the modest therapeutic window afforded by Compound B and the fact that some cell lines (and likely patients) would be resistant to Compound B, it is possible that Compound B may not be superior to other treatments already FDA-approved NSCLC treatments, such as chemotherapy, at least as a monotherapy. We therefore decided to search for clinically relevant therapies to combine with RUVBL1/2 inhibition to improve this therapeutic window. GSEA analysis of our RNA-seq data following Compound B treatment or RUVBL1 knockdown showed that cell cycle genes that were upregulated after IR were downregulated following Compound B treatment, as well as genes involved in base excision repair (**Figure 4.20A**), an integral pathway in the recovery from IR (Chaudhry, 2007). In addition, our proteomic analysis suggested that RUVBL1/2 interacting proteins were enriched for proteins involved in nucleotide excision repair (**Figure 4.13E**). Furthermore, the INO80-family of chromatin modelers, which require RUVBL1/2 (Jha et al., 2013; Jonsson et al., 2004), are important for the DNA damage response (Dong et al., 2014; Ikura et al., 2000; Morrison et al., 2004) and RUVBL1/2 have been shown to regulate the abundance of the Fanconi anemia

core complex (Rajendra et al., 2014), which regulates the repair of interstrand DNA crosslinks and recovery from IR (Walden and Deans, 2014). Thus, we speculated that RUVBL1/2 may be required for efficient DNA repair and the survival of NSCLC in response to IR, which is frequently used to treat patients with NSCLC.

To test if RUVBL1/2 affects the response to IR in NSCLC, we first examined the ability of RUVBL1/2 depleted cells to survive IR. Knockdown of RUVBL1 or RUVBL2 using doxycycline-inducible shRNAs synergistically decreased the clonogenic potential of cells following IR in two NSCLC cell lines (**Figure 4.20B**). Utilizing the maximum dose of Compound B that did not inhibit the clonogenic potential of each cell line, we extended these findings to 8 NSCLC cell lines (**Figure 4.20C**) and 2 non-transformed human bronchial epithelial cell lines (HBECs) that were immortalized by CDK4 and hTERT overexpression (**Figure 4.20D**). Importantly, while all NSCLC tumor cell lines were radiosensitized by Compound B, our two models of non-transformed lung epithelial cells, HBEC3KT and HBEC30KT, were not radiosensitized. Of note, HCC4017, an NSCLC cell line that was radiosensitized, was derived from the same patient as HBEC30KT, a normal bronchial epithelial cell line that was not radiosensitized, demonstrating that Compound B broadly and therapeutically synergizes (i.e. synergizes in cancerous, but not normal cells) with IR in NSCLC.

To better understand the differential ability of Compound B to radiosensitize NSCLC, but not HBECs, we treated both H2009 and HBEC3KT with the same dosing strategy as used for clonogenic assays (**Figure 4.20C** and **4.20D**), administered 10 Gy of radiation and then monitored the activation of DNA repair proteins by immunoblotting over time. In H2009, 12.5 nM of Compound B was able to lower the total levels of DNA-PK_{cs} and ATM proteins, as well as

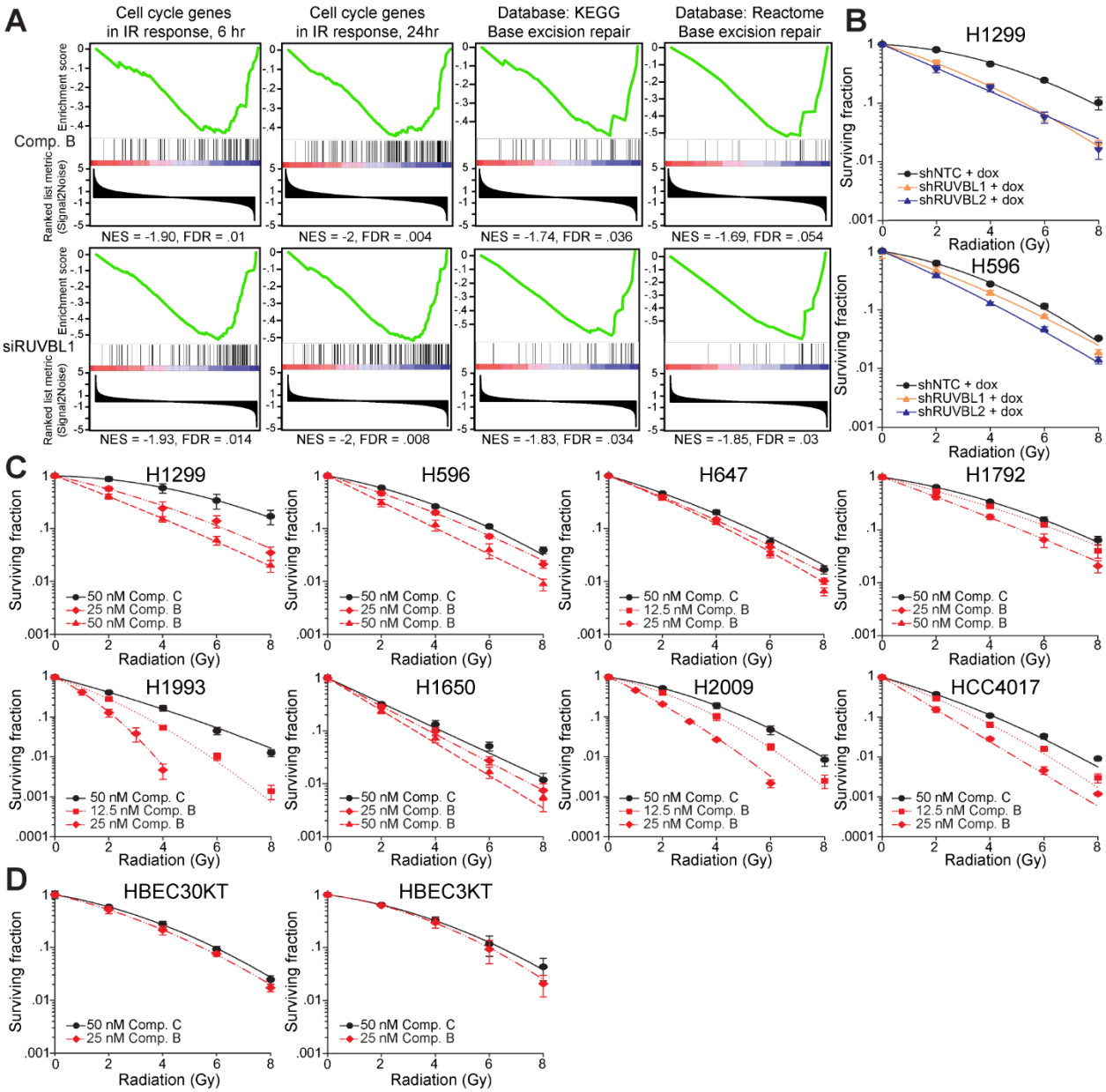


Figure 4.20. RUVBL1/2 Inhibition or Depletion Enhances the Cell Killing Effect of Radiation *In Vitro*. A) GSEA analysis of the RNA-seq data following Compound B (top) or siRUVBL1 (bottom) treatment in H2009 (from **Figure 4.11A**) shows downregulation of gene sets that are important in the response to IR. B) Doxycycline-inducible shRNAs against RUVBL1 or RUVBL2 radiosensitize NSCLC in clonogenic assays. Cells were treated for 3 days with 62.5 ng/mL doxycycline (+ dox), plated as single cells, irradiated at various doses, and left in the presence of 62.5 ng/mL doxycycline until colonies (~50 cells/colony) were formed, stained and counted. Values represent the average ± SD of 2 biological replicates. C) Compound B radiosensitizes NSCLC lines in clonogenic assays. Cells were treated for 3 days with the indicated doses of Compound B or Compound C, plated as single cells, irradiated at various doses, and left in the presence of Compound B or Compound C until colonies (~50 cells/colony) were formed, stained and counted. Values represent the average ± SD of 2 biological replicates.

D) Compound B does not radiosensitize normal human bronchial epithelial cells (HBECs). Assay performed as in **Figure 4.20E**.

their subsequent activation, as measured by decreased phosphorylation following IR (**Figure 4.21A**). In contrast, HBEC3KT maintained total DNA-PK_{cs} and ATM protein levels and was able to activate these proteins equally between Compound C and Compound B treatments (**Figure 4.21B**). Titration of Compound B on H2009 and models of normal cells such as HBEC3KT, HBEC30KT and IMR-90 showed that key DNA repair proteins like DNA-PK_{cs} and ATM are modestly more sensitive to Compound B in H2009 than HBEC3KT (**Figure 4.21C**). This may, in part, explain why these cells lines are differentially radiosensitized (**Figure 4.20C** and **4.20D**).

We next studied the ability of NSCLCs and normal lung epithelial cells pretreated with Compound B or Compound C to repair DSBs resulting from 2 Gy IR by monitoring the appearance and resolution of γH2AX and 53BP1 foci by immunofluorescent microscopy. Regardless of the cell line or reagent used, all cells displayed a similar number of DSBs 15 minutes after 2 Gy IR (**Figure 4.21D**). However, whereas RUVBL1/2 inhibition did not delay DSB repair kinetics in normal lung epithelial cells (HBEC3KT), it delayed repair kinetics in all NSCLC lines tested (**Figures 4.21E and 4.21F**). Additionally, genetic depletion or pharmacological inhibition of RUVBL1/2 delayed DSB repair kinetics to nearly identical rates following 2 Gy IR in H1299 cells, suggesting that these effects are mediated specifically by loss of RUVBL1/2 ATPase activity (**Figure 4.21G** and **4.21H**).

In order to evaluate the therapeutic potential of RUVBL1/2 inhibition for radiosensitization, we tested the effects of IR and Compound B *in vivo* using a clinically relevant dosing schedule of 2 Gy of radiation delivered for 5 consecutive days. For this purpose, we implanted H1299 cells subcutaneously into nude mice, and once tumors reached a volume of

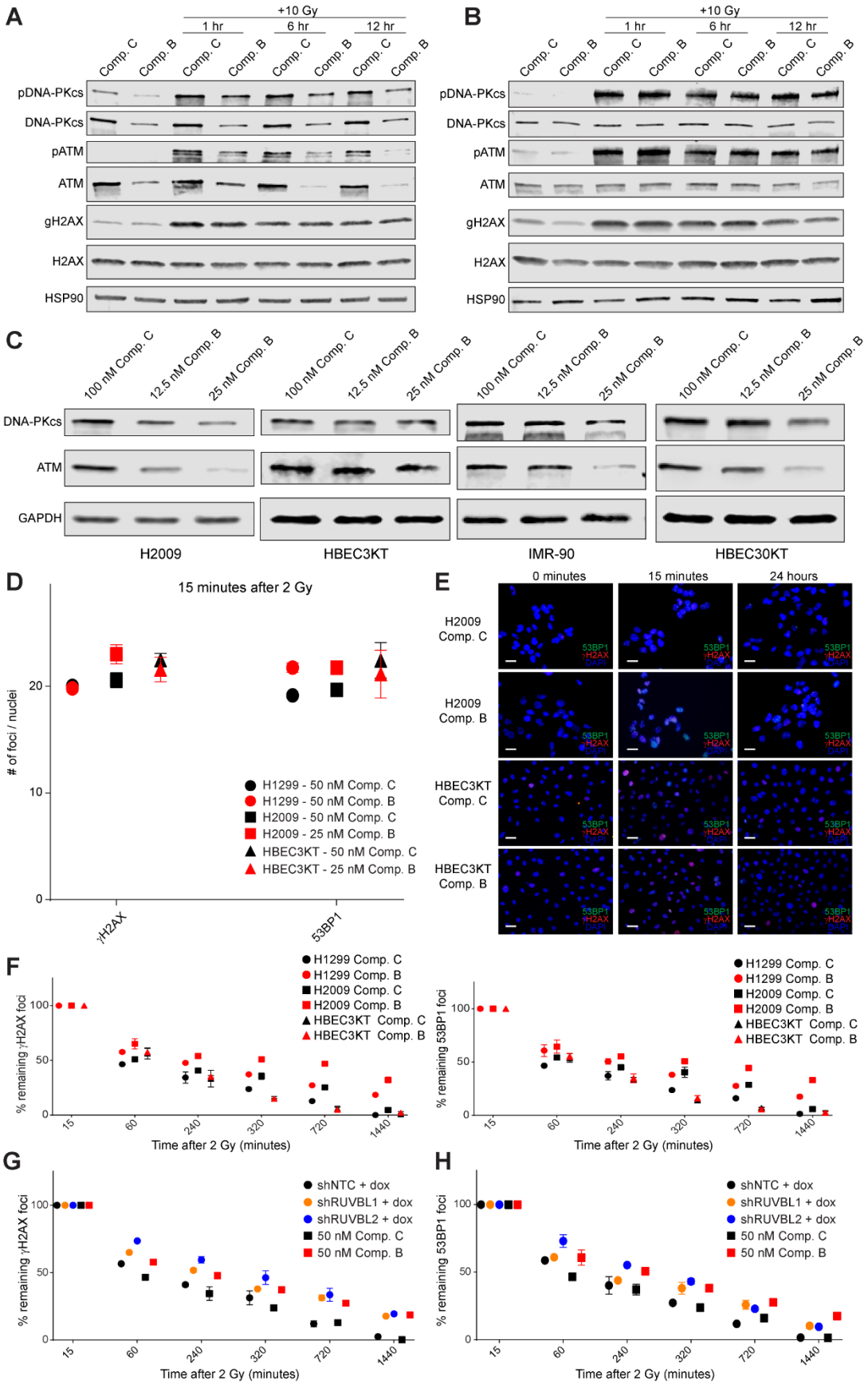

A
+10 Gy
1 hr
6 hr
12 hr
Comp. C
Comp. B
pDNA-PKcs
DNA-PKcs
pATM
ATM
gH2AX
H2AX
HSP90
B
C
100 nM Comp. C
12.5 nM Comp. B
25 nM Comp. B
DNA-PKcs
ATM
GAPDH
H2009
HBEC3KT
IMR-90
HBEC30KT
D
15 minutes after 2 Gy
of foci / nuclei
H1299 - 50 nM Comp. C
H1299 - 50 nM Comp. B
H2009 - 50 nM Comp. C
H2009 - 25 nM Comp. B
HBEC3KT - 50 nM Comp. C
HBEC3KT - 25 nM Comp. B
γH2AX
53BP1
E
0 minutes
15 minutes
24 hours
H2009 Comp. C
H2009 Comp. B
HBEC3KT Comp. C
HBEC3KT Comp. B
F
% remaining γH2AX foci
% remaining 53BP1 foci
H1299 Comp. C
H1299 Comp. B
H2009 Comp. C
H2009 Comp. B
HBEC3KT Comp. C
HBEC3KT Comp. B
Time after 2 Gy (minutes)
G
H
shNTC + dox
shRUVBL1 + dox
shRUVBL2 + dox
50 nM Comp. C
50 nM Comp. B

Figure 4.21 Compound B Delays the Resolution of DSBs in NSCLC, but not Normal Cells, *In Vitro*. A) Compound B treatment blunts activation of ATM and DNA-PK_{cs} following IR in H2009, an NSCLC line. Cells were treated for 3 days with 12.5 nM Compound B or Compound C, irradiated with 10 Gy, harvested at indicated times post-radiation, and the levels of phosphorylated (activated) and total DNA repair proteins were examined by immunoblot. B) Compound B treatment does not affect ATM or DNA-PK_{cs} activation following IR in HBEC3KT, a normal lung epithelial cell line. Cells were treated as in **Figure 4.21A**. C) PIKK family proteins, such as ATM and DNA-PK_{cs}, are destabilized at lower concentrations of Compound B in H2009 than in models of normal cells, such as HBEC3KT, HBEC30KT and IMR-90. Cells were treated for 3 days with the indicated concentrations then harvested for immunoblot. D-F) Inhibition of RUVBL1/2 delays DSB resolution in NSCLC but not in HBECs. Cell lines were treated for 3 days with indicated drug concentrations, irradiated with 2 Gy, grown in the presence of drug until indicated time points, then fixed and prepared for immunofluorescent microscopy. D) Similar number of DSBs are evident immediately after 2 Gy radiation, regardless of cell line or treatment used. All values shown represent the average ± SD of 2 biological replicates. E) Representative immunofluorescent microscopy images before (0 minutes) or after (15 minutes, 24 hours) 2 Gy radiation in H2009 and HBEC3KT treated with 25 nM Compound B or 50 nM Compound C. Blue = DNA, green = 53BP1, red = γH2AX. Scale bars are 20 μm. F) Left: Quantification of the percent remaining γH2AX foci at various time points after 2 Gy radiation. Right: percent remaining 53BP1 foci at various time points after 2 Gy radiation. For percent remaining foci, all values are normalized to the number of foci observed 15 minutes after 2 Gy radiation, and all values shown represent the average ± SD of 2 biological replicates. G) Genetic depletion of RUVBL1/2 delays DSB repair to a similar extent as Compound B. H1299 cells that harbor stable integrations of doxycycline-inducible shRNAs were pretreated with 62.5 ng/mL doxycycline for 3 days to induce knockdown, irradiated with 2 Gy, then cells were fixed and prepared for immunofluorescent microscopy for γH2AX at the indicated time points. Data from H1299 treated with Compound B is from **Figures 4.21D-F** and shown here for comparison. Number of foci is normalized to the 15-minute post-IR timepoint and all values shown represent the average ± SD of 2 biological replicates. H) Same as in **Figure 4.21G** except cells were stained for 53BP1.

~150 mm^3, mice were randomized to either receive (i) vehicle, (ii) vehicle and 2 Gy radiation for 5 days, (iii) 125 mg/kg Compound B or (iv) 125 mg/kg Compound B and 2 Gy radiation for 5 days. For these experiments, 125 mg/kg of Compound B was chosen as it produced no changes in mice bodyweight (**Figure 4.22C**, right panel), but was able to lower total ATM protein levels in xenografted H1299 tumor cells (**Figure 4.22A** and **4.22B**). Treatment with Compound B at this reduced dose as a single agent had no effect on H1299 tumor growth. However, Compound B significantly potentiated the effects of IR, without measurable toxicity (**Figure 4.22C**, bottom left and right panels). These results suggest that RUVBL1/2 inhibition can enhance the therapeutic window afforded by IR.

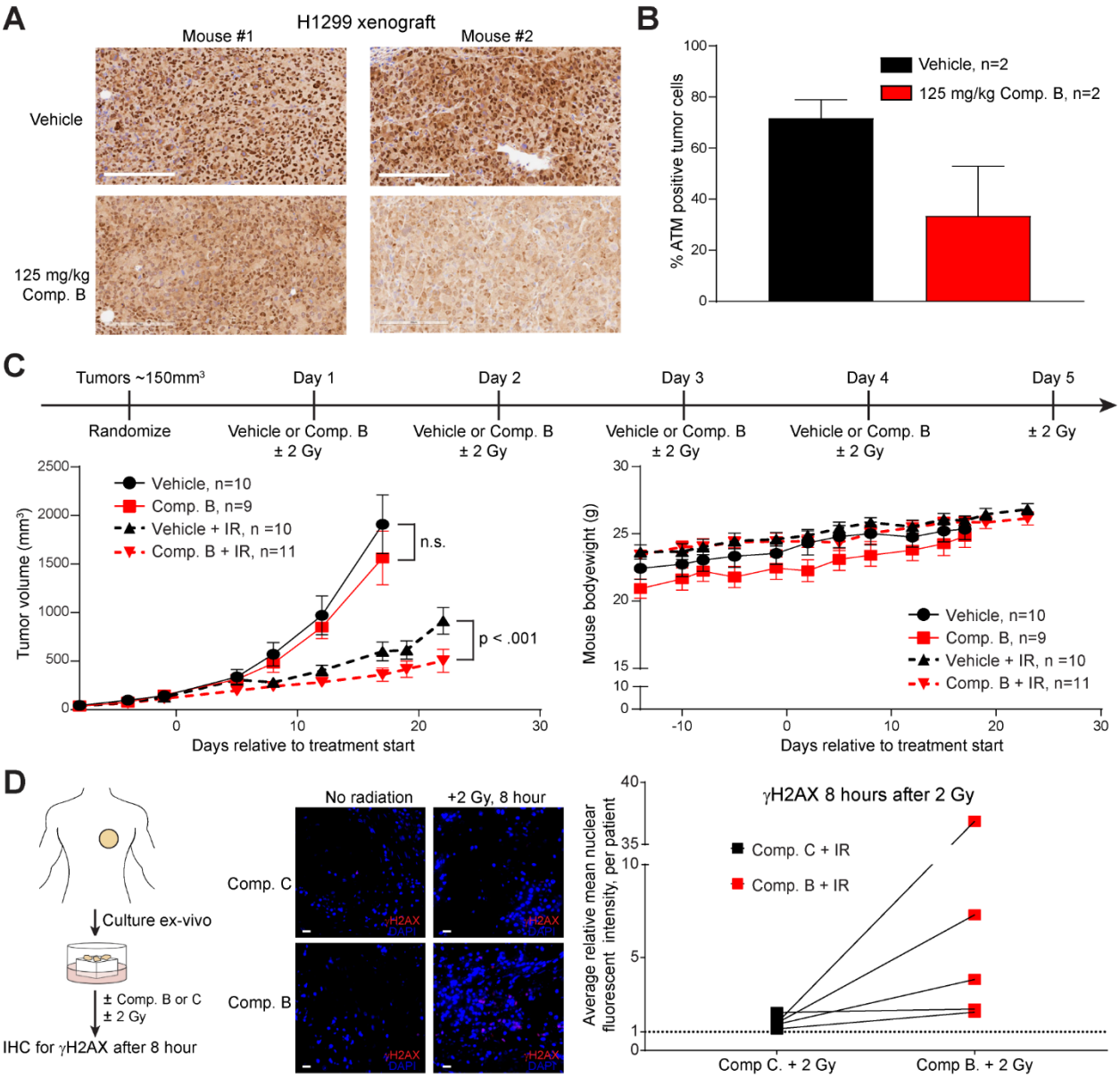


Figure 4.22. Compound B can Radiosensitize Xenografted Tumors and Patient-Derived Explant Models. A) Non-toxic doses of Compound B can lower ATM protein levels *in vivo*. Representative images of IHC for ATM in xenografts of H1299 cells. Mice were treated for 3 days with 125 mg/kg Compound B or vehicle, then tumors were harvested for IHC. Scale bars are 200 μm. B) Quantification of **Figure 4.22A**. n represents the number of mice, and values shown are averages ± SD. C) Inhibition of RUVBL1/2 potentiates radiation *in vivo* without toxicity. Top: experiment outline. Bottom: H1299 was xenografted subcutaneously into female Nude mice and once tumor volumes reached ~150 mm^3 mice were randomized to receive indicated treatments. Bottom left: Tumor volumes of mice treated as indicated. Numbers represent averages ± SEM, n refers to number of mice in each group and n.s. = not significant. Statistical significance between Vehicle and Compound B and between Vehicle + IR and Compound B + IR was assessed using 2-way repeated measures ANOVA. Bottom right: body weight of mice treated as indicated. Values represent the average ± SEM and n indicates the number of mice in each group. D) NSCLC patient derived explants (PDExs) are radiosensitized by Compound B. Left: experiment outline. NSCLC patient tumors were taken from surgical

resections, diced into small pieces, grown on a gelatin sponge, treated for 3 days with 150 nM Compound C or Compound B, irradiated with 2 Gy, and after 8 hours were fixed and prepared for IHC. Middle: representative γH2AX staining for one patient tumor explant. Blue = DAPI, red = γH2AX. Scale bars are 20 μm. Right: quantification of γH2AX staining in tumor cells from 5 patient explants. Mean fluorescent intensity in samples that received radiation was normalized to their respective drug treated, no radiation control sample, and lines connect samples from the same patient.

To extend these findings to a more relevant pre-clinical model, we utilized patient-derived explant (PDEx) models, where primary tumor tissue specimens are obtained directly from NSCLC patients undergoing surgical resection and grown *ex vivo* for a short period of time (Centenera et al., 2013). Tumor tissue obtained directly from five different NSCLC patients was treated with 150 nM of Compound B or Compound C for three days, irradiated with 2 Gy, and after 8 hours was fixed and prepared for γH2AX IHC analysis. Relative to their respective drug treatments, all five human tumor NSCLC explants treated with Compound B + IR had more residual γH2AX staining than explants treated with Compound C + IR, demonstrating that Compound B impairs the recovery from IR at therapeutic doses in primary NSCLC patient tumors (**Figure 4.22D**). Taken together, these findings suggest that RUVBL1/2 inhibition radiosensitizes NSCLC and may thus present an opportunity for combination therapy of local and locally advanced NSCLC.

4.3 Discussion

Our initial RNAi screens to determine if NSCLC cell lines required NRs, their coregulators, or their chromatin remodelers for viability was fraught with unexpected off-target effects. Before beginning this screen, we believed that off-targets would have minimal effects in our siRNA screen. Additionally, after finishing the siRNA screen, but before beginning the esiRNA screen, we were encouraged by the fact that these siRNAs produced interesting phenotypes, such as cancer- and subtype-specificity and that some siRNAs had mutation biomarkers, as we did not believe these could stem from off-target effects. After the esiRNA and

siRNA screens were performed and compared and we found little overlap, our subsequent literature search showed that siRNAs and shRNAs could have extensive off-target effects which can confound screening results and produce specific, and interesting, off-target phenotypes (Schultz et al., 2011; Sudbery et al., 2010). Even in large shRNA screens, if these off-target effects are not computationally corrected, the results of these screens are highly unreliable, as shRNAs targeting the same gene tend to have very little correlation to each other, even when screened across a large panel of cell lines. These algorithms, however, have only been recently developed and require a large amount of input data, such that they are not feasible to be used for small scale screens like ours (Tsherniak et al., 2017). In our opinion, only RNAi screens utilizing a very large number of shRNAs, such as Project DRIVE, which utilized 20 shRNAs per gene (McDonald et al., 2017), produce reliable data. This is because this shRNA screen is one of the few screens that produces some of the relationships one would expect (i.e. cell type lineage genes are only essential to that cell type, non-expressed genes do not score frequently, and important oncogenes are only essential to cell lines harboring the oncogenic mutation).

One of the few reliable and interesting hits from our viability-based siRNA and esiRNA screens was RUVBL1/2. This hit was reliable because both esiRNAs and siRNAs targeting RUVBL1/2 produced defects in viability. Additionally, we were also encouraged by the fact that, at least in the esiRNA screen, esiRNAs targeting RUVBL1 and RUVBL2 produced similar phenotypes. This hit was interesting because, at least from the esiRNA screen, the NSCLC lines responded differentially to the depletion of RUVBL1/2, suggesting that there may be different degrees of dependency on RUVBL1/2, and the HBECs appeared resistant. Further studies revealed that all cell lines, including HBECs, required RUVBL1/2 for their proliferation, but that some cell lines were more sensitive or resistant to these effects. This is in line with prior data showing that RUVBL1/2 are essential from yeast (Qiu et al., 1998) to humans (Munoz et

al., 2016), but that there are differential effects on viability when RUVBL1/2 are depleted in many cell lines (McDonald et al., 2017).

After we nominated RUVBL1/2 as essential for the viability of NSCLC, we next investigated whether RUVBL1/2 expression was deregulated in NSCLC and if this deregulation had any correlation to patient outcomes. While not causative, this latter analysis is important because it can implicate certain genes as playing a role in the aggressiveness or the pathogenesis of a disease. Interestingly, while RUVBL1/2 are not frequently amplified or mutated in NSCLC, we found that both RUVBL1 and RUVBL2 mRNAs were overexpressed in a large number of NSCLC patient tumors in the TCGA database. This overexpression may have some significance, as an independent analysis using KMplot (Szasz et al., 2016), a database and analysis tool that combines and analyzes multiple, independent clinically annotated microarrays, showed that patients with high RUVBL1 or RUVBL2 mRNA levels have poor overall prognosis. We then went on to validate that patients with high RUVBL1 protein levels, similar to high RUVBL1/2 mRNAs levels, also have poor prognosis. Given the fact that there appears to be a strong association between high RUVBL1/2 and poor patient prognosis, determining if this correlation is due to a specific function of RUVBL1/2, or if this is just a mere correlation, will be interesting. Notably, cancer patients generally die of disseminated cancer, and there is evidence to suggest that RUVBL1/2 may play a role in cellular migration and metastasis (Fan et al., 2017). Additionally, our work shows that RUVBL1/2 have roles in the DNA damage response following radiation, suggesting that patients with high RUVBL1/2 levels may have poorer response to therapies that damage DNA, such as radiation and cisplatin.

We found that RUVBL1/2 and RUVBL1/2 ATPase activity are required for NSCLC proliferation and attempted to dissect the mechanisms underlying this essentiality. Similar to their interacting partner HSP90 (Trepel et al., 2010), RUVBL1/2 interact with and stabilize a diverse array of multiprotein complexes (Bizarro et al., 2015; Izumi et al., 2010; Jha et al., 2013;

Jonsson et al., 2004; McKeegan et al., 2009; Venteicher et al., 2008). This property complicates studying their role in normal and cancerous physiology, in part because their diverse sets of client proteins may have varying expression levels, importance, and roles among different cell types, cancers, or even within one cancer type. Additionally, the dearth of RUVBL1/2 ATPase inhibitors has delayed the dissection of the role of their ATPase activity in these processes. Here we present a specific, potent and orally bioavailable RUVBL1/2 inhibitor, Compound B, and have used this compound to investigate the role of the ATPase activity of RUVBL1/2 in multiprotein complex regulation, supporting the viability of NSCLC and its utility as a therapeutic target in NSCLC.

While RUVBL1/2 are essential for the formation of the PAQosome (Houry et al., 2018) and the INO80-family of chromatin remodelers (Jha et al., 2013; Jonsson et al., 2004; Nguyen et al., 2013), the role, if any, of the ATPase activity of RUVBL1/2 in these complexes was previously unknown. Utilizing Compound B, we show that acute inhibition of RUVBL1/2 ATPase activity results in the failure of the PAQosome complex to either mature client proteins and/or dissociate, without affecting the assembly or disassembly of the INO80-family of chromatin remodelers. Precisely why the PAQosome requires RUVBL1/2 ATPase activity, while the INO80-family does not, awaits further investigation. Prior in vitro systems have shown that both TIP60 and INO80 do not require RUVBL1/2 ATP hydrolysis for their functions (Jha et al., 2013; Jonsson et al., 2004), suggesting that the role of RUVBL1/2 in these complexes may be ATPase-independent.

Multiple unbiased analyses suggested that RUVBL1/2 have important roles in DNA replication in NSCLC. We found that the inhibition of RUVBL1/2 results in S-phase arrest, loss of RPA loading at replication forks and subsequent replication catastrophe, primarily in NSCLC cell lines that are sensitive to Compound B. This newly established role of RUVBL1/2 in promoting DNA replication in NSCLC, potentially by affecting RPA loading at replication forks,

may only be necessary during specific problems that can arise during replication, such as the replication of repeat sequences, secondary structures, or when dealing with replication stress due to strong proliferative signals. This is because not all NSCLC cell lines arrest in S-phase following Compound B treatment, and cells that do not arrest in S-phase do not show evidence of altered RPA loading, even after 72 hours of treatment (H596, data not shown). Thus, while our work sheds considerable light onto the role of RUVBL1/2 in DNA replication, delineating the precise role of RUVBL1/2 in this process, as well as why some NSCLC cell lines do not require RUVBL1/2 for efficient DNA replication, represents an outstanding question. As RUVBL1/2 is a highly pleiotropic protein and has roles in the cell other than DNA replication, we note that it is also possible that some cells may be more sensitive to the inhibition of other processes RUVBL1/2 are integral to, such as splicing and rRNA biogenesis, and die/arrest from the inhibition of these processes before problems with DNA replication can occur.

Because Compound B monotherapy does not produce a large therapeutic window in all NSCLC cell lines in vivo, we searched for clinically relevant treatment modalities that may be beneficial when paired with Compound B. Prior studies have suggested a role for RUVBL1/2 in DNA repair (Dong et al., 2014; Ikura et al., 2000; Rajendra et al., 2014; Raymond et al., 2015) and our GSEA analysis of RNA-seq data after RUVBL1/2 inhibition or knockdown suggested that inhibiting RUVBL1/2 may inhibit pathways integral to the response to IR. Thus, we investigated whether inhibition of RUVBL1/2 may synergize with radiation. We found that the inhibition or depletion of RUVBL1/2 delayed DSB repair and resulted in the synergistic killing of NSCLC, but not bronchial epithelial cells, *in vitro* following IR. Mechanistically, this may be because the stability of crucial DNA repair proteins such as ATM and DNA-PK_{cs} are more sensitive to PAQosome inhibition in tumor cell lines than normal cell lines, possibly due to the strained protein buffering capacity of HSP90 that is documented in cancer (Jaeger and Whitesell, 2019). In more rigorous preclinical models, Compound B was able to potentiate the

antitumor effects of IR in NSCLC xenografts and delay the repair of DSBs after IR in NSCLC patient derived explant models. The combination of Compound B and IR may be particularly attractive because Compound B alone has antitumor activity and can be administered systemically, whereas IR is only delivered locally. Thus, Compound B may provide systemic antitumor effects (for instance, at metastases) while enhancing the local effects of radiation. Mechanistically, it is interesting to note that our data suggests that the antitumor effects may stem from inhibiting DNA replication, whereas the enhancement of radiation may stem from inhibiting the PAQosome complex. Future preclinical work aimed at optimizing this combination, as well as identifying pre-treatment response biomarkers, will help illuminate the full potential of this therapeutic strategy.

CHAPTER FIVE:
Conclusions

In this study we sought to identify NRs, their coregulators, and their chromatin remodelers that are essential for the viability of NSCLC, an aggressive and highly lethal cancer that desperately needs new treatment modalities. Our prior analyses had implicated (Jeong et al., 2012; Jeong et al., 2010) or directly shown (Srivastava et al., 2014) these factors to be important for lung cancer aggressiveness and/or proliferation. To interrogate their essentiality in a medium-throughput manner in many cell lines, we first conducted an siRNA screen of NRs, their coregulators and their chromatin remodelers in >50 NSCLC cell lines as well as normal human bronchial epithelial cells. We had hoped this screen would provide us with a comprehensive annotation of the essentiality of NRs, their coregulators and chromatin remodelers in NSCLC. This map of essentiality, we had hoped, could then be used to identify both therapeutic targets and/or discover new biology. For instance, if an NR and one of its coregulators (but not its other coregulators) had similar patterns of essentiality across various NSCLC cell lines, it is possible that this NR recruits this coregulator to sustain a gene expression program conducive to viability in these NSCLC cell lines. This would discover novel biology, and by identifying drugs that disrupt this gene expression pattern, potentially new therapeutics for NSCLC. Additionally, because of the extensive molecular and clinical characterization of the NSCLC cell lines used in this study, we had hoped to identify response biomarkers and/or gain a deeper biological understanding of this essentiality.

While the siRNA screen did provide a wealth of phenotypic information and identified interesting biomarkers, our secondary screen using esiRNAs showed that the majority, if not all, of our siRNA-induced phenotypes were due to off-target effects. In contrast to the siRNA screen, the esiRNA screen suggested that very few of the 240 NRs, their coregulators, and their chromatin remodelers were essential for the viability of NSCLC. This was not because the

esiRNAs were ineffective. In fact, both esiRNAs and siRNAs provided similar levels of target depletion. These esiRNAs, however, did not reduce cellular viability, strongly suggesting that the siRNA-induced phenotypes were due to off-targets. Because many of these siRNA-induced phenotypes had very interesting molecular properties, such as the ability to kill cancer but not normal cells, or biomarkers, such as certain gene mutations that predicted their efficacy, they still might be interesting therapeutically. For instance, if one could identify the off-target transcript(s) responsible for these phenotypes, this could be therapeutically leveraged. Additionally, given the advancements of *in vivo* siRNA delivery (Tatiparti et al., 2017), it is also possible that these siRNAs themselves could be delivered for cancer therapy. Whether either of these options are tractable therapeutic options remains to be seen.

RUVBL1/2 are known to have ATPase activity and a long-standing question in the field of RUVBL1/2 biology is what role(s) this ATPase activity plays, both in regulating the structure of RUVBL1/2 itself and the many actions that RUVBL1/2 perform within the cell. Also, given the fact that we and others have found RUVBL1/2 ATPase activity to be essential for the viability of cancer cells, but RUVBL1/2 is also essential for normal proliferation, it was unknown whether targeting this enzymatic activity would provide a sufficient therapeutic window. Daiichi-Sankyo developed a RUVBL1/2 inhibitor, named Compound B, and we have shown that this molecule is a specific and potent inhibitor of RUVBL1/2, both *in vitro* and *in vivo*. We validated Compound B's specificity by developing a novel PCR-based mutagenesis approach to identify mutations in RUVBL1 or RUVBL2 that confer resistance to Compound B and this technique identified at least 20 mutations that we believe can confer resistance to Compound B. Not only does this confirm the on-target activity of Compound B, but by mapping these resistance mutations to the 3D structure of RUVBL1/RUVBL2 it shows that these mutations lie within nucleotide-sensitive switch loop regions between the RUVBL1/RUVBL2/RUVBL1 interfaces, suggesting that these switch loop regions are important to both Compound B binding and hydrolysis of ATP. We also

used Compound B to assess the therapeutic window afforded by inhibiting RUVBL1/2 ATPase activity in NSCLC. Our results suggest that while Compound B shows modest efficacy as a monotherapy, it is limited by its toxicity to normal tissue, suggesting it may not be an effective anti-cancer molecule alone. Development of predictive biomarkers, which we failed to identify, or finding other agents that enhance the therapeutic window afforded by Compound B may aid the preclinical development of RUVBL1/2 inhibitors in NSCLC.

RUVBL1/2 are known to be essential to the formation of many multiprotein complexes. However, the necessity of their ATPase activity in these processes, especially within cells under physiological conditions, is poorly understood. To address this question, we immunoprecipitated RUVBL1 after Compound B treatment and determined the abundance of RUVBL1 interacting proteins unbiasedly by mass spectrometry. Interestingly, nearly all the components of the PAQosome increased their binding to RUVBL1 after Compound B treatment, and PAQosome client proteins were depleted from total cellular lysate, strongly suggesting that the maturation/dissociation of this chaperone complex is dependent upon the ATPase activity of RUVBL1/2. In contrast, the abundance of the INO80-family of chromatin remodelers bound to RUVBL1 did not change after Compound B treatment, suggesting that these complexes do not require the ATPase activity of RUVBL1/2 for their assembly or disassembly.

Our screen and others have shown that RUVBL1/2 are essential for the growth of many cell types and organisms, but the mechanisms underlying this essentiality remain poorly defined. This is at least in part due to the pleiotropic nature of RUVBL1/2, and the fact that many of the processes controlled by RUVBL1/2, such as the biogenesis of snoRNAs (McKeegan et al., 2009) and snRNPs (Bizarro et al., 2015; Cloutier et al., 2017), the INO80-family of chromatin remodelers (Mao and Houry, 2017), and some of the PIKK-family of proteins (McDonald et al., 2017; Munoz et al., 2016), are essential for cellular viability. We sought to shed light on this question by using unbiased methods to nominate which RUVBL1/2-controlled process may be

the most integral to supporting the viability of NSCLC. These unbiased analyses nominated RUVBL1/2 as having novel roles in DNA replication, and our subsequent investigation showed that NSCLC cell lines that are the most sensitive to Compound B tend to arrest in S-phase. This is not completely surprising, given the fact that INO80 has previously been shown to have a role in DNA replication (Conaway and Conaway, 2009), but is non-obvious as RUVBL1/2 have multiple essential roles within the cell and it is unknown how RUVBL1/2 ATPase activity affects these processes. It also should be noted that we currently have no data showing that inhibiting RUVBL1/2 ATPase activity has any effect on the INO80 family of chromatin remodelers, as the INO80 complex still seems to associate following Compound B treatment and studies performed *in vitro* show that ATPase dead RUVBL2 can still support the nucleosome remodeling functions of INO80 (Jonsson et al., 2004). While cell lines that are very sensitive to Compound B appear to require RUVBL1/2 for DNA replication, we are unable to explain why some NSCLC cell lines do not appear to require RUVBL1/2 for efficient DNA replication. In fact, some of the more resistant cell lines tend to arrest in G1, or do not appear to arrest in any specific stage of the cell cycle. We suggest that this may be due to the pleiotropic role of RUVBL1/2. It is possible that in these cells that do not arrest in S-phase, they are more sensitive to the inhibition of other processes controlled by RUVBL1/2, such as snoRNP or snRNP biogenesis, and that they arrest from the inhibition of these processes prior to S-phase arrest. In the future it would be interesting to tease out the mechanisms underlying this differential effect on the cell cycle seen following the inhibition of RUVBL1/2 ATPase activity.

After discovering the S-phase arrest witnessed in some NSCLC cell lines following Compound B treatment, we sought to further characterize this DNA replication defect. Our iPOND followed by mass spectrometry analysis showed that the majority of DNA replication proteins, such as DNA polymerase alpha, DNA polymerase delta, the RPA complex, and the MCM complex, had dissociated from replication forks after 12 hours of Compound B treatment.

Interestingly, however, both POLE1 and POLE2 abundance were unchanged at the replication fork. Additionally, replication stress response proteins, such as the RPA complex, ATR and the Fanconi anemia complex, were not recruited to replication forks, as would be expected with the dissociation of the replication fork. Both of these phenomena, loss of replication proteins and a failure to recruit replication stress proteins, can potentially be explained by loss of RPA loading at the replication fork (Bae et al., 2001; Chilkova et al., 2007; Zou and Elledge, 2003), which we found to occur both in our iPOND mass spectrometry data and independently by flow cytometry for RPA2 on transient permeabilized cells. While we currently cannot explain the mechanism underlying this failure to load RPA at the replication fork, we noticed that RUVBL1 dramatically increases binding to RPA3, a subunit of RPA, but not RPA2 or RPA1, following Compound B treatment. However, this binding of RUVBL1 to RPA3 does not disturb RPA complex formation. This suggests that the defect of RPA loading onto replication forks occurs specifically during the actual loading of RPA onto DNA at the replication fork, potentially via interactions with RPA3, and is unlikely to be a consequence of problems with RPA complex formation or availability. Somewhat paradoxically, while RPA was underloaded at replication forks 12 and 24 hours after Compound B treatment, by 48 hours RPA was hyperloaded onto chromatin and NSCLC cells underwent a process known as replication catastrophe. This is likely due to the dramatic depletion of ATR after 48 hours, as ATR is known to be stabilized by RUVBL1/2 in an ATPase-dependent manner, and this RPA hyperloading phenomenon can be forced by addition of an ATR inhibition after just 24 hours of Compound B treatment (a timepoint when RPA is usually underloaded onto chromatin).

Because systemic inhibition of the ATPase activity of RUVBL1/2 *in vivo* by Compound B only produced a modest therapeutic window in some xenografted NSCLC cell lines, we searched for therapies that could enhance this therapeutic window. We found that Compound B enhanced the efficacy of radiation in NSCLC, both *in vitro* using cell lines and *in vivo* using

xenografted cell lines and patient derived explant models. Interestingly, we found that in *in vitro* assays, Compound B did not enhance the effects of radiation in normal cells. This property, whereby Compound B radiosensitizes tumor cells and not normal cells, combined with the fact that Compound B can provide systemic anti-tumor effects (for instance, at metastases) while enhancing the local effects of radiation, is an attractive property for future pre-clinical development.

Even though this study unearthed new basic and translational biology surrounding RUVBL1/2 and their ATPase activity, significant questions remain. Is the association of RUVBL1/2 with the prognosis of NSCLC patients causative or correlative? Can predictive biomarkers to Compound B monotherapy, or Compound B with radiation, be identified? What is the precise mechanism underlying the loss of RPA loading at active DNA replication forks, and why do only some NSCLC cell lines experience this phenomenon? Why do some NSCLC cell lines arrest in S-phase, whereas others arrest in G1, while others show no defect in any specific stage of the cell cycle (but still stop proliferating)? What specific step in PAQosome maturation/dissociation is affected by RUVBL1/2 ATPase activity? Do the INO80-family of chromatin remodelers require the ATPase activity of RUVBL1/2 for any of their functions? What cancer type would benefit the most from the inhibition of RUVBL1/2 ATPase activity? With the development of Compound B and the data presented here, unraveling these questions is now feasible and of high importance to better understanding the basic biology and therapeutic potential of the enigmatic AAA+ ATPases RUVBL1 and RUVBL2.

APPENDIX A
Sequence and Product ID of Qiagen siRNAs used in NR, Coregulator and Chromatin Remodeler Viability-Based Screen

Library	Entrez Gene Id	NCBI gene symbol	siRNA Target Sequence	Product Id	Product Name
Remodeler	86	ACTL6A	TACGAGGTCTTG GCACAATTA	SI00062 405	Hs_ACTL6A_1
Remodeler	86	ACTL6A	TGGCAGGAGGA AACACACTAA	SI04433 940	Hs_ACTL6A_10
Remodeler	86	ACTL6A	CAACAGTGGAAC GGAGGTTTA	SI02779 994	Hs_ACTL6A_6
Remodeler	86	ACTL6A	AAAGCTTTAACT GGCTCTATA	SI02779 987	Hs_ACTL6A_5
Remodeler	51412	ACTL6B	CACGGCCATTCC AGTACATGA	SI00114 247	Hs_ACTL6B_4
Remodeler	51412	ACTL6B	CCCACCGAGCA TGCGACTGAA	SI03076 346	Hs_ACTL6B_5
Remodeler	51412	ACTL6B	CACCTACAGCAA ACACGTCAA	SI00114 240	Hs_ACTL6B_3
Remodeler	51412	ACTL6B	CAACAGCACCAT GGAGCGCAA	SI00114 226	Hs_ACTL6B_1
Remodeler	79913	ACTR5	AACCTCGAGGT GGATGTGGTA	SI04274 998	Hs_ACTR5_6
Remodeler	79913	ACTR5	TGGCGGTGTCCT GATTATTAT	SI04362 344	Hs_ACTR5_7
Remodeler	79913	ACTR5	CAGCTACATCGC TGAGGATTA	SI04132 380	Hs_ACTR5_5
Remodeler	79913	ACTR5	ACCCACTGTATT CACGGCAAA	SI00291 648	Hs_ACTR5_4
Remodeler	64431	ACTR6	TCCGAGATAATC CTTCCGAAT	SI04233 138	Hs_ACTR6_7
Remodeler	64431	ACTR6	GACGACCTTAGT GCTGGATAA	SI04346 881	Hs_ACTR6_8
Remodeler	64431	ACTR6	AAGGGTGGAGA CTAAGCTAAT	SI04141 256	Hs_ACTR6_6
Remodeler	64431	ACTR6	TAGGTAGGTTAC TACAGTAAA	SI00291 676	Hs_ACTR6_4
Remodeler	8289	ARID1A	ATGGCGGGAAC TTGCAACCAA	SI03051 461	Hs_ARID1A_5
Remodeler	8289	ARID1A	CTCGGTATCACC GTTGATGAA	SI03091 865	Hs_ARID1A_6
Remodeler	8289	ARID1A	CAGAGTTTACTC TGTACGAAT	SI00083 727	Hs_ARID1A_4
Remodeler	8289	ARID1A	CACCTTGGTTAC ACTCGCCAA	SI00083 713	Hs_ARID1A_2
Remodeler	57492	ARID1B	ATGAGCCAGTAT GGACCACAA	SI04178 426	Hs_ARID1B_8

Remodeler	57492	ARID1B	CCCGGAGTTTAATAATTACTA	SI04189598	Hs_ARID1B_9
Remodeler	57492	ARID1B	CAGGCCCACAGCGGTATCCAA	SI04171216	Hs_ARID1B_7
Remodeler	57492	ARID1B	CAGGAAGGCTATGGAACTAGA	SI04261789	Hs_ARID1B_10
Remodeler	196528	ARID2	AGAACTCGTCTCATTACTTTA	SI04324334	Hs_ARID2_8
Remodeler	196528	ARID2	AAGCGTAGTGATTGTAAGCCA	SI04329857	Hs_ARID2_9
Remodeler	196528	ARID2	CAGCGGGTACTTCAGATTGCA	SI04216471	Hs_ARID2_7
Remodeler	196528	ARID2	ACCTCGAAAGCTGGGCATTAA	SI04165798	Hs_ARID2_6
Remodeler	11177	BAZ1A	CACAAGTTAGATTGCCAGTTA	SI00102354	Hs_BAZ1A_3
Remodeler	11177	BAZ1A	ACCTTGGATCGTAGCGTGATA	SI03040828	Hs_BAZ1A_5
Remodeler	11177	BAZ1A	CAGCTAGACCAGCTTATTGAA	SI00102347	Hs_BAZ1A_2
Remodeler	11177	BAZ1A	AACGAGGAAGACCACAAGTTA	SI00102340	Hs_BAZ1A_1
Remodeler	9031	BAZ1B	AAGAACGAATACGGAAGCACA	SI03030909	Hs_BAZ1B_5
Remodeler	9031	BAZ1B	ATGCCTGTATCAAGTGGGATA	SI03050089	Hs_BAZ1B_6
Remodeler	9031	BAZ1B	CAGATGCTCAGTATCCTATTA	SI00134967	Hs_BAZ1B_4
Remodeler	9031	BAZ1B	AGGAGATAGTTCGATACTTTA	SI00134960	Hs_BAZ1B_3
Remodeler	11176	BAZ2A	CCCGCAGTGACGGCCAGTAAA	SI00102382	Hs_BAZ2A_3
Remodeler	11176	BAZ2A	CACTGAGAAGGCTAAGACTAA	SI00102389	Hs_BAZ2A_4
Remodeler	11176	BAZ2A	CACCACTACAGAGATATCATA	SI00102375	Hs_BAZ2A_2
Remodeler	11176	BAZ2A	CTCGGTAGCTTTGAATCTTAA	SI00102368	Hs_BAZ2A_1
Remodeler	2186	BPTF	AACGCCTTATGATGAATCTAA	SI00064022	Hs_FALZ_3
Remodeler	2186	BPTF	GAGGGTGGAATTAAGGGTATA	SI00064029	Hs_FALZ_4
Remodeler	2186	BPTF	AAGGTCCAACTTGCAGAATTA	SI00064015	Hs_FALZ_2
Remodeler	2186	BPTF	AAGCATAATGCTGTAATAGAA	SI00064008	Hs_FALZ_1
Remodeler	29117	BRD7	TCCATGATCATTAAACACCCA	SI04320204	Hs_BRD7_8
Remodeler	29117	BRD7	AAGCACGTATGGAGTTCGAAA	SI04352138	Hs_BRD7_9

Remodeler	29117	BRD7	CAAGTCGGACAAACACCTCTA	SI04168059	Hs_BRD7_7
Remodeler	29117	BRD7	CAGGGCGTTTGGACTCCAGTA	SI04134088	Hs_BRD7_6
Remodeler	65980	BRD9	TAGGACGCTCTTCCAGCTGAA	SI04158609	Hs_BRD9_7
Remodeler	65980	BRD9	CAGGCGGAGACCACTCTAGGA	SI04234153	Hs_BRD9_9
Remodeler	65980	BRD9	TAGGCCAGATACCGTGTACTA	SI03228498	Hs_BRD9_6
Remodeler	65980	BRD9	CACGCTGGGCTTCAAAGACGA	SI05169465	Hs_BRD9_12
Remodeler	79697	C14orf169	CAGATTCTAAGGATCCGCGAA	SI00136710	Hs_C14orf169_3
Remodeler	79697	C14orf169	TAAGATGCCTCTAGCCCTAAA	SI03107580	Hs_C14orf169_6
Remodeler	79697	C14orf169	AAGCAGCTGCGAAGTGTTGTA	SI03032876	Hs_C14orf169_5
Remodeler	79697	C14orf169	GAGGTCCAGGAAGATACGAAA	SI00136703	Hs_C14orf169_2
Remodeler	1105	CHD1	AAGATTCCGATGACTCATCAA	SI03032519	Hs_CHD1_5
Remodeler	1105	CHD1	TGGACGCATCATCAGACCAAA	SI03119445	Hs_CHD1_6
Remodeler	1105	CHD1	GCGGTTTATCAAGAGCTATAA	SI00024535	Hs_CHD1_4
Remodeler	1105	CHD1	ATGCAGAAATTAGGCGGTTTA	SI00024528	Hs_CHD1_3
Remodeler	1106	CHD2	GACCACGATTTGTAGCTTTAA	SI03215989	Hs_CHD2_7
Remodeler	1106	CHD2	GAGCCCGAATATCTATGTAAA	SI04164993	Hs_CHD2_8
Remodeler	1106	CHD2	CAGTCGGAATCTGAGAGCGAA	SI03178343	Hs_CHD2_6
Remodeler	1106	CHD2	CAAGAGGAGGACAGTTCGCTA	SI03156944	Hs_CHD2_5
Remodeler	1107	CHD3	CTGAAGGGCGTAGACAGTCAA	SI00345562	Hs_CHD3_4
Remodeler	1107	CHD3	CAGGCCATAAGAGGCGGAGTA	SI03070319	Hs_CHD3_6
Remodeler	1107	CHD3	AGCGACAAGCGTAAAGTGAAA	SI00345555	Hs_CHD3_3
Remodeler	1107	CHD3	CCGGACCGGGTCGGAAACGAA	SI02777341	Hs_CHD3_5
Remodeler	1108	CHD4	CGGGTATTGAATGGTTACTCA	SI00024563	Hs_CHD4_4
Remodeler	1108	CHD4	CAGCAAGAAGATCTAGCCCGA	SI03065265	Hs_CHD4_5
Remodeler	1108	CHD4	TAAGTTCTTCCGGGTATTGAA	SI00024556	Hs_CHD4_3

Remodeler	1108	CHD4	CATGAAGGTTATAAATACGAA	SI00024549	Hs_CHD4_2
Remodeler	26038	CHD5	ACGGTACATGATCCTCAACGA	SI04279961	Hs_CHD5_7
Remodeler	26038	CHD5	CCACACGGTGATGTATCGCAA	SI04305581	Hs_CHD5_8
Remodeler	26038	CHD5	AAAGTTGGATGACGTATGGAA	SI04194372	Hs_CHD5_6
Remodeler	26038	CHD5	CACGGTCAAGTTCGACAAGCA	SI04193476	Hs_CHD5_5
Remodeler	8193	DPF1	CCGCATGACCTCGAGGTGGAA	SI00066542	Hs_DPF1_3
Remodeler	8193	DPF1	CAGGGCCAAAGGAAAGGCATA	SI04951338	Hs_DPF1_8
Remodeler	8193	DPF1	ACCATTATGGACTGTCAGAAA	SI00066535	Hs_DPF1_2
Remodeler	8193	DPF1	CCCGGGACAGATTTACACGTA	SI00066528	Hs_DPF1_1
Remodeler	5977	DPF2	CCGGAGTAGCCCAGAGCAATT	SI03081904	Hs_DPF2_5
Remodeler	5977	DPF2	GACCTCGATGATGAAGACTAT	SI03101742	Hs_DPF2_6
Remodeler	5977	DPF2	ATCCATCTTGCCTCCAATTTA	SI00086716	Hs_DPF2_4
Remodeler	5977	DPF2	CTGTATTCTAAACATTAGTAA	SI00086695	Hs_DPF2_1
Remodeler	8110	DPF3	AACAGACTCTCTGGGCAATTA	SI04200259	Hs_DPF3_8
Remodeler	8110	DPF3	AAGAAACGTATCAATACCCAT	SI04348771	Hs_DPF3_9
Remodeler	8110	DPF3	AAGAGGATATTCCCAAGCGAA	SI04161808	Hs_DPF3_7
Remodeler	8110	DPF3	AAGGGAAATCAAAGAAATCGA	SI04159610	Hs_DPF3_6
Remodeler	57634	EP400	TCCGTGCAGAGCGAATCGCAA	SI04231871	Hs_EP400_7
Remodeler	57634	EP400	CAGCATGGAGTATGTCTACGA	SI04277840	Hs_EP400_8
Remodeler	57634	EP400	CACGGCTAACTTGCCACCGCA	SI04205103	Hs_EP400_6
Remodeler	57634	EP400	AACGAGCGGCGCTGTTCTCAA	SI03125542	Hs_EP400_5
Remodeler	2146	EZH2	CAGACGAGCTGATGAAGTAAA	SI00063966	Hs_EZH2_3
Remodeler	2146	EZH2	TTCGAGCTCCTCTGAAGCAAA	SI00063973	Hs_EZH2_4
Remodeler	2146	EZH2	AAGCAAATTCTCGGTGTCAAA	SI00063959	Hs_EZH2_2
Remodeler	2146	EZH2	AACCATGTTTACAACTATCAA	SI02665166	Hs_EZH2_7

Remodeler	54815	GATAD2A	CATGGCGATCTATAAGTTGAA	SI04255867	Hs_GATAD2A_3
Remodeler	54815	GATAD2A	CCGCGTCGCCAATGTTCCCAA	SI04318636	Hs_GATAD2A_4
Remodeler	54815	GATAD2A	CAACACCAGCCTGCTCGTCAA	SI04255370	Hs_GATAD2A_2
Remodeler	54815	GATAD2A	TTGCGGCAGAGTCAAATACAA	SI04151658	Hs_GATAD2A_1
Remodeler	57459	GATAD2B	CCGACTGGTCCTGTTAAAGAA	SI00676641	Hs_P66beta_3
Remodeler	57459	GATAD2B	CTGGGCCGTGTAGACACTAAA	SI00676648	Hs_P66beta_4
Remodeler	57459	GATAD2B	CACAAGTTGGGTGGACATAAA	SI00676634	Hs_P66beta_2
Remodeler	57459	GATAD2B	CCCGGTCTATATCGCAGTCCA	SI04336822	Hs_GATAD2B_1
Remodeler	3066	HDAC2	TCCCAATGAGTTGCCATATAA	SI00434966	Hs_HDAC2_3
Remodeler	3066	HDAC2	GACCCATAACTTGCTGTTAAA	SI00434973	Hs_HDAC2_4
Remodeler	3066	HDAC2	CTGGGTTGTTTCAATCTAACA	SI00434959	Hs_HDAC2_2
Remodeler	3066	HDAC2	ACGGTCAATAAGACCAGATAA	SI00434952	Hs_HDAC2_1
Remodeler	55662	HIF1AN	AACACATAGGCTTGCGTCTTA	SI00436324	Hs_HIF1AN_1
Remodeler	55662	HIF1AN	CACTGTGAACTTCTGGTATAA	SI00436345	Hs_HIF1AN_4
Remodeler	55662	HIF1AN	CACCCACAAGTTCTTGTACTA	SI00436338	Hs_HIF1AN_3
Remodeler	55662	HIF1AN	CAAGCTCAAGCCATACATAAA	SI02778090	Hs_HIF1AN_5
Remodeler	6596	HLTF	AGGCGTGATATCTGGATGGAA	SI04437188	Hs_HLTF_3
Remodeler	6596	HLTF	AACAAGTGAATTGCCGCAGAA	SI04437195	Hs_HLTF_4
Remodeler	6596	HLTF	ACGGGAGTAGTTAATAATAAT	SI02665740	Hs_SMARCA3_7
Remodeler	6596	HLTF	AACAATGTGAATGGAAATCAA	SI02665733	Hs_SMARCA3_6
Remodeler	55806	HR	ACCCAGCGAGGAAGTGAACAA	SI03039078	Hs_HR_5
Remodeler	55806	HR	CCGGGACTTCAGGACATACCA	SI03082457	Hs_HR_7
Remodeler	55806	HR	CCAGGCCTTGTTCATACTCTT	SI03075366	Hs_HR_6
Remodeler	55806	HR	TCGGAGCAGTTTGAATGTCCA	SI00072933	Hs_HR_1
Remodeler	79663	HSPBAP1	TACGTAGAAGCTACACTCGAA	SI03225901	Hs_HSPBAP1_6

Remodeler	79663	HSPBAP1	CAGTCAACTGTTGCTACTTAA	SI04247187	Hs_HSPBAP1_8
Remodeler	79663	HSPBAP1	CTGGGCTTATGCTGACTATAA	SI04152792	Hs_HSPBAP1_7
Remodeler	79663	HSPBAP1	CACTGGTGGCATTACGTAGAA	SI03166030	Hs_HSPBAP1_5
Remodeler	54617	INO80	TTCACCTGCGTCTACACTTAA	SI04298875	Hs_INOC1_4
Remodeler	54617	INO80	TCGCGGAATTGAGTTTCGATA	SI04324075	Hs_INOC1_5
Remodeler	54617	INO80	CCCAGACTCTCTGGTCCGGAA	SI04289838	Hs_INOC1_3
Remodeler	54617	INO80	TTCCTTCGCTTTATTGATATA	SI04246319	Hs_INOC1_2
Remodeler	3720	JARID2	AGCGAGGAATATCATGAGCAT	SI04202373	Hs_JARID2_6
Remodeler	3720	JARID2	CTGCGGCAAAGTGTCTGGTAA	SI04302452	Hs_JARID2_8
Remodeler	3720	JARID2	CAGCAGGTCAACACGGGAGAA	SI04283797	Hs_JARID2_7
Remodeler	3720	JARID2	TCGGATTTATTTCAAGGCGAA	SI00449624	Hs_JARID2_1
Remodeler	80853	JHDM1D	ATGGCAGTAACCATGAGGTTA	SI00460383	Hs_KIAA1718_2
Remodeler	80853	JHDM1D	TACGAGGTGTAAGAGCTATAA	SI00460397	Hs_KIAA1718_4
Remodeler	80853	JHDM1D	CAGAGTGTCGCTGGTAAATAA	SI00460390	Hs_KIAA1718_3
Remodeler	80853	JHDM1D	ACTGCTAGGCATAATTATCAA	SI00460376	Hs_KIAA1718_1
Remodeler	65094	JMJD4	CAGGGACTTTCCGGTGGAGGA	SI04210283	Hs_JMJD4_1
Remodeler	65094	JMJD4	CACCATCTCCATCAACCACAA	SI04308213	Hs_JMJD4_3
Remodeler	65094	JMJD4	CTCGTCCGACTGGCTGAATGA	SI04286912	Hs_JMJD4_2
Remodeler	65094	JMJD4	CTCCTTCAGCTGGTCTGTCAA	SI00392217	Hs_FLJ12517_1
Remodeler	79831	JMJD5	CTGGTGGTCGTAGCCAGGATA	SI05142410	Hs_JMJD5_4
Remodeler	79831	JMJD5	CTGGCCAGAGAAGGCACTTTA	SI05166021	Hs_JMJD5_7
Remodeler	79831	JMJD5	CAGCGAGGTGATCCTGGACTA	SI05142417	Hs_JMJD5_5
Remodeler	79831	JMJD5	CTCCTGCCGCACAGTAAAGAA	SI04375693	Hs_JMJD5_3
Remodeler	23210	JMJD6	ACGAAGCTATTACCTGGTTTA	SI00109865	Hs_PTDSR_3
Remodeler	23210	JMJD6	CCCGGCGGCCGTGGCGGATAA	SI03078593	Hs_PTDSR_6

Remodeler	23210	JMJD6	CAGCTATGGTGAACACCCTAA	SI03068037	Hs_PTDSR_5
Remodeler	23210	JMJD6	CCCGCCGTATGTGAAGGAGTA	SI04953998	Hs_JMJD6_1
Remodeler	100137047	JMJD7	CAGGCCGTGCATTATCCGCAA	SI04857538	Hs_LOC100137047_2
Remodeler	100137047	JMJD7	CAGCTGCTGCCTGATCTGGAA	SI04857552	Hs_LOC100137047_4
Remodeler	100137047	JMJD7	CTGCGTGGTCTCAGGAGAGAA	SI04857545	Hs_LOC100137047_3
Remodeler	100137047	JMJD7	AAGGTAGCTGTGAGTCGTAAA	SI04857531	Hs_LOC100137047_1
Remodeler	339123	JMJD8	CGGGTACTCAGAAGTGATCTA	SI00498491	Hs_LOC339123_2
Remodeler	339123	JMJD8	CCGACCGCTGGTGGCATGCTA	SI04179266	Hs_LOC339123_5
Remodeler	339123	JMJD8	CACCGCCAACACCTACTCCTA	SI00498498	Hs_LOC339123_3
Remodeler	339123	JMJD8	AAAGCCTTCGATAAACGCTAA	SI00498484	Hs_LOC339123_1
Remodeler	10524	KAT5	CACCCGGATGAAGAACATTGA	SI00162981	Hs_HTATIP_5
Remodeler	10524	KAT5	CTGATCGAGTTCAGCTATGAA	SI02637383	Hs_HTATIP_6
Remodeler	10524	KAT5	CGGCGGAACCAGGACAACGAA	SI00088053	Hs_HTATIP_2
Remodeler	10524	KAT5	CACCACATTGCCTGTCCTCTA	SI02780897	Hs_HTATIP_8
Remodeler	221656	KDM1B	TTGGGTGATAGGACACTTTAA	SI00297213	Hs_AOF1_3
Remodeler	221656	KDM1B	CGGGTACTCGGTGATAATTGA	SI03087231	Hs_AOF1_5
Remodeler	221656	KDM1B	AACCTATTTCATCACTCTAAA	SI00297220	Hs_AOF1_4
Remodeler	221656	KDM1B	ATCGATGCGGTATGAAACCAA	SI00297199	Hs_AOF1_1
Remodeler	22992	KDM2A	AAGCCAGACTGAATCAACAAA	SI00099204	Hs_FBXL11_2
Remodeler	22992	KDM2A	TTGGAGATGCAGTACCCTAAA	SI03024651	Hs_FBXL11_5
Remodeler	22992	KDM2A	CTCACTGGAGTTCCTATAGTA	SI00099218	Hs_FBXL11_4
Remodeler	22992	KDM2A	ACCCATTTCGTTGCTACCCAA	SI00099197	Hs_FBXL11_1
Remodeler	84678	KDM2B	AGGAGTGGACTAGAAGTTTAA	SI00143794	Hs_FBXL10_3
Remodeler	84678	KDM2B	ACCGCGGGACCCAGCACCGAA	SI03040093	Hs_FBXL10_5
Remodeler	84678	KDM2B	CAGATCTAACAAAGTAGGCTA	SI00143801	Hs_FBXL10_4

Remodeler	84678	KDM2B	CCGGCAAGACCGGGAAACAAA	SI00143787	Hs_FBXL10_2
Remodeler	9682	KDM4A	ACGAGTTATCAACTCAAGATA	SI00107492	Hs_JMJD2A_2
Remodeler	9682	KDM4A	AGGCCAGAAAGTCATTAGCAA	SI00107506	Hs_JMJD2A_4
Remodeler	9682	KDM4A	TAGGACTTAGCTTCATAACTA	SI00107499	Hs_JMJD2A_3
Remodeler	9682	KDM4A	CACCGAGTTTGTCTTGAAATA	SI00107485	Hs_JMJD2A_1
Remodeler	23030	KDM4B	CCCGGCCACATTACCCTCCAA	SI00449785	Hs_JMJD2B_4
Remodeler	23030	KDM4B	CTGCTACGAAGTGAACTTCGA	SI03095757	Hs_JMJD2B_6
Remodeler	23030	KDM4B	CAGCGGCTCTTTGTATGATGA	SI03067421	Hs_JMJD2B_5
Remodeler	23030	KDM4B	CACCTGACAAATCCTAGCGAA	SI00449764	Hs_JMJD2B_1
Remodeler	23081	KDM4C	TCCCAGAAGTTCGATTCACTA	SI00109312	Hs_JMJD2C_4
Remodeler	23081	KDM4C	CCCGAAGCTTCCAGTGTGCTA	SI05163977	Hs_KDM4C_1
Remodeler	23081	KDM4C	TACATCGGAGGGAAAGACTAA	SI03108336	Hs_JMJD2C_5
Remodeler	23081	KDM4C	CAGATATTAATGGGAGCATAT	SI00109305	Hs_JMJD2C_3
Remodeler	55693	KDM4D	CTGGTAGATCCTGCTACCTCA	SI04254551	Hs_JMJD2D_7
Remodeler	55693	KDM4D	CTGGAAGAACCGCATCTATAA	SI04335198	Hs_JMJD2D_9
Remodeler	55693	KDM4D	CACAGATTATCCACCCGTCAA	SI04317796	Hs_JMJD2D_8
Remodeler	55693	KDM4D	CCGGTACTGCGTGGACGGAAA	SI04187239	Hs_JMJD2D_6
Remodeler	5927	KDM5A	AAGGAATGGTATCACAGTCTA	SI02634317	Hs_JARID1A_5
Remodeler	5927	KDM5A	GCGGACGTTTCTTAAGAAGAA	SI00071974	Hs_JARID1A_4
Remodeler	5927	KDM5A	CAGATGCTTAATTGAGCTCTA	SI02634324	Hs_JARID1A_6
Remodeler	5927	KDM5A	CGGCAAGTAAAGAATCTGCTA	SI00071960	Hs_JARID1A_2
Remodeler	10765	KDM5B	TCGTCCTAACATAACACTAAA	SI00090314	Hs_JARID1B_3
Remodeler	10765	KDM5B	CTCATAGAACTTGTTACACGA	SI03089009	Hs_JARID1B_6
Remodeler	10765	KDM5B	AGGGAGATGCACTTCGATATA	SI03045623	Hs_JARID1B_5
Remodeler	10765	KDM5B	ACGCACCAAGCCGAAAGTAAA	SI00090300	Hs_JARID1B_1

Remodeler	8242	KDM5C	CTCCGCCGTTGCAATGAACTA	SI05165223	Hs_KDM5C_2
Remodeler	8242	KDM5C	CAGCGGCTTCAACCAAGGCTA	SI03067428	Hs_SMCX_5
Remodeler	8242	KDM5C	CTGGATGAGGTGAAACGCACA	SI05165965	Hs_KDM5C_3
Remodeler	8242	KDM5C	CAGCCACACTTGAGGCCATAA	SI05162276	Hs_KDM5C_1
Remodeler	7403	KDM6A	TTGGTCTACTTCCATTATAAT	SI04206426	Hs_UTX_7
Remodeler	7403	KDM6A	CAGCGAAACGCACTCACTCTA	SI04314303	Hs_UTX_9
Remodeler	7403	KDM6A	CAAGTGCGGAGTGTCAACCAA	SI04306743	Hs_UTX_8
Remodeler	7403	KDM6A	CTCCGCGCAAATAGAAATAAT	SI04202079	Hs_UTX_6
Remodeler	23135	KDM6B	CCTCGTCATCTCAGTTCTCTA	SI04133836	Hs_JMJD3_6
Remodeler	23135	KDM6B	CCAGCTGGCCCTGGAACGATA	SI04349800	Hs_JMJD3_8
Remodeler	23135	KDM6B	AAGATCCGGCTCATCAAGGTA	SI04236365	Hs_JMJD3_7
Remodeler	23135	KDM6B	CCAGCCGAATTCAAGATCCTA	SI03181136	Hs_JMJD3_5
Remodeler	8932	MBD2	TACCTGGGAAATACTGTTGAT	SI03109246	Hs_MBD2_11
Remodeler	8932	MBD2	TGGAAAGATGATGCCTAGTAA	SI02632280	Hs_MBD2_7
Remodeler	8932	MBD2	CGAAACGATCCTCTCAATCAA	SI03083605	Hs_MBD2_10
Remodeler	8932	MBD2	AAGATGATGCCTAGTAAATTA	SI02663787	Hs_MBD2_8
Remodeler	53615	MBD3	CCAGACGGCGTCCATCTTCAA	SI00057855	Hs_MBD3_3
Remodeler	53615	MBD3	CGGGAAGAAGTTCCGCAGCAA	SI00057862	Hs_MBD3_4
Remodeler	53615	MBD3	CCCGGAGATGGAGCACGTCTA	SI00057848	Hs_MBD3_2
Remodeler	53615	MBD3	GCCGGTGACCAAGATTACCAA	SI02664886	Hs_MBD3_5
Remodeler	84864	MINA	AAGGGCAACGATTCAGTTTCA	SI03035907	Hs_MINA_5
Remodeler	84864	MINA	ATGGGTCCCTGTTCAAGCTAA	SI03051888	Hs_MINA_7
Remodeler	84864	MINA	AAGTTTAATCTCGCCCATCAA	SI03037258	Hs_MINA_6
Remodeler	84864	MINA	CTGTTGCTACAAGACGATTAA	SI00144256	Hs_MINA_2
Remodeler	57504	MTA3	CACCTAATATGCAGTGTAGAT	SI04147542	Hs_MTA3_6

Remodeler	57504	MTA3	ATCATTGACTAG CATCATTGA	SI04174 653	Hs_MTA3_7
Remodeler	57504	MTA3	CTCGCAGATAAG CATGCTAAA	SI00650 797	Hs_MTA3_3
Remodeler	57504	MTA3	ACGGCCGTTTGT TGCTATTAA	SI00650 790	Hs_MTA3_2
Remodeler	55193	PBRM1	CAGTTAGGAGTT GTCGGAATA	SI03073 413	Hs_PB1_5
Remodeler	55193	PBRM1	TCAGGACGTCTC ATTAGCGAA	SI03112 984	Hs_PB1_6
Remodeler	55193	PBRM1	TCCCAGGTTTAT AATGATGCA	SI00120 932	Hs_PB1_4
Remodeler	55193	PBRM1	CAAGGATGCAAA TTCAATTAA	SI00120 925	Hs_PB1_3
Remodeler	55274	PHF10	TCCAGGGAAGA CAGAAATCAA	SI00121 268	Hs_PHF10_4
Remodeler	55274	PHF10	AACGAATTACAG ACCATTATA	SI03029 292	Hs_PHF10_6
Remodeler	55274	PHF10	CGGACAGTTCCA GGAATATTA	SI00121 261	Hs_PHF10_3
Remodeler	55274	PHF10	ATGGCAGTGTAT GGAATGTAA	SI02778 006	Hs_PHF10_5
Remodeler	5253	PHF2	AGGACCGCTTAT TCCACTTTA	SI04310 747	Hs_PHF2_5
Remodeler	5253	PHF2	TTCATAGAATGT AGCGTGTAA	SI04374 930	Hs_PHF2_7
Remodeler	5253	PHF2	CCGCATCGTCTC CAAACAACA	SI04322 486	Hs_PHF2_6
Remodeler	5253	PHF2	CTGGATTTGTTT CTCAGGCAA	SI00683 830	Hs_PHF2_2
Remodeler	23133	PHF8	TCGGCGAACCA AGATAGCAAA	SI00109 613	Hs_PHF8_3
Remodeler	23133	PHF8	CAGGTGATGGA AGACGAATTT	SI03072 139	Hs_PHF8_6
Remodeler	23133	PHF8	CAGCCTTAACAT CGAGATGCA	SI03066 630	Hs_PHF8_5
Remodeler	23133	PHF8	CCGGAGACAGT GCGAACCGTA	SI00109 599	Hs_PHF8_1
Remodeler	54107	POLE3	CAGGAATCTAAC TCTCCCTAA	SI04955 545	Hs_POLE3_8
Remodeler	54107	POLE3	CTGACTAGAAAT ACCGTCAAA	SI04955 552	Hs_POLE3_9
Remodeler	54107	POLE3	AAGAGGGATTCT GAACGACTA	SI04185 328	Hs_POLE3_6
Remodeler	54107	POLE3	TCCCTAAACCAT CCTCTTTAA	SI00688 828	Hs_POLE3_4
Remodeler	5928	RBBP4	CACAGACTTAAC GTTGAAATT	SI03055 990	Hs_RBBP4_10
Remodeler	5928	RBBP4	ACGAGTGATCAA CGAGGAATA	SI00079 513	Hs_RBBP4_3

Remodeler	5928	RBBP4	CAGCTATCCCTCTATATAATA	SI02653420	Hs_RBBP4_8
Remodeler	5928	RBBP4	AAGACTCCTTCCAGTGATGTT	SI00301658	Hs_RBBP4_5
Remodeler	5931	RBBP7	TTGAATGTAATGCTACATGAA	SI00045444	Hs_RBBP7_3
Remodeler	5931	RBBP7	TGCGTACTGTATCATATTGTA	SI00045451	Hs_RBBP7_4
Remodeler	5931	RBBP7	CCGACGCAAGATGGCGAGTAA	SI02664466	Hs_RBBP7_6
Remodeler	5931	RBBP7	GCGGATAAGACCGTAGCTTTA	SI02664459	Hs_RBBP7_5
Remodeler	51773	RSF1	CCGGACGTCGGCAACGGAGAA	SI00117012	Hs_HBXAP_4
Remodeler	51773	RSF1	AAGAGCGTGCCGAACGAAGAA	SI03031833	Hs_RSF1_1
Remodeler	51773	RSF1	CACCGAGTCGTGTACCATGAA	SI00117005	Hs_HBXAP_3
Remodeler	51773	RSF1	CAGCCAATTGGTCGAGACAAA	SI00116991	Hs_HBXAP_1
Remodeler	8607	RUVBL1	GGAGATGTGATTTACATTGAA	SI04174296	Hs_RUVBL1_8
Remodeler	8607	RUVBL1	ACCATTAGCCATGTGATCATA	SI04348582	Hs_RUVBL1_9
Remodeler	8607	RUVBL1	CAGAGCTAACTCCGTGTGAGA	SI03168193	Hs_RUVBL1_5
Remodeler	8607	RUVBL1	TGGCGTCATAGTAGAATTAAT	SI00709240	Hs_RUVBL1_4
Remodeler	10856	RUVBL2	AACCGTTACAGCCACAACCAA	SI00709261	Hs_RUVBL2_3
Remodeler	10856	RUVBL2	CCAGGACGCCTTCCTCTTCAA	SI00709268	Hs_RUVBL2_4
Remodeler	10856	RUVBL2	CACGCAGTACATGAAGGAGTA	SI00709254	Hs_RUVBL2_2
Remodeler	10856	RUVBL2	CCGGAGATCCGTGATGTAACA	SI00709247	Hs_RUVBL2_1
Remodeler	6594	SMARCA1	ATGGACAAGATGCGACTCTTA	SI04289054	Hs_SMARCA1_7
Remodeler	6594	SMARCA1	TGCAACGAGAATGGTATACAA	SI04301395	Hs_SMARCA1_8
Remodeler	6594	SMARCA1	TTCGTGAGTTCAAGTCGACTA	SI04216051	Hs_SMARCA1_6
Remodeler	6594	SMARCA1	CTGCTGGAGACTACCGCCATA	SI04154451	Hs_SMARCA1_5
Remodeler	6595	SMARCA2	AAGGATGACGCTGAAGTAGAA	SI00726761	Hs_SMARCA2_3
Remodeler	6595	SMARCA2	AAGCCCATCGATGGTATACAT	SI03033191	Hs_SMARCA2_5
Remodeler	6595	SMARCA2	GCCCGCATAGCTCATAGGATA	SI00726754	Hs_SMARCA2_2

Remodeler	6595	SMARCA2	AGGCGTCTACATAAGGTGTTA	SI00726747	Hs_SMARCA2_1
Remodeler	6597	SMARCA4	CTGGGCGTACGAGTTTGACAA	SI03098998	Hs_SMARCA4_6
Remodeler	6597	SMARCA4	CCGCGCTACAACCAGATGAAA	SI00047579	Hs_SMARCA4_1
Remodeler	6597	SMARCA4	CCCGTGGACTTCAAGAAGATA	SI02630208	Hs_SMARCA4_5
Remodeler	6597	SMARCA4	TCACTGGATGTCAAACAGTAA	SI00047586	Hs_SMARCA4_2
Remodeler	8467	SMARCA5	TGGGTACAAGGTACCTCGAAA	SI04291133	Hs_SMARCA5_6
Remodeler	8467	SMARCA5	AGGGAATGGTATACTCGGATA	SI04366082	Hs_SMARCA5_7
Remodeler	8467	SMARCA5	AACCAGGGCGCCCACGAATAA	SI04206377	Hs_SMARCA5_5
Remodeler	8467	SMARCA5	CAGAGGAGATGTAATACCTTA	SI00726796	Hs_SMARCA5_4
Remodeler	6598	SMARCB1	TCCGAGGTTCTCTGTACAAGA	SI04237457	Hs_SMARCB1_6
Remodeler	6598	SMARCB1	CTGTGACGATCTGGATTTGAA	SI04297762	Hs_SMARCB1_7
Remodeler	6598	SMARCB1	TGGCAACGATGAGAAGTACAA	SI04226180	Hs_SMARCB1_5
Remodeler	6598	SMARCB1	GCGCGTCATCATCAAGCTGAA	SI00726810	Hs_SMARCB1_2
Remodeler	6599	SMARCC1	CAGCGGATTTCAACCAAGAAT	SI04214637	Hs_SMARCC1_7
Remodeler	6599	SMARCC1	ATGCGGATGCTCCTACCAATA	SI04364276	Hs_SMARCC1_8
Remodeler	6599	SMARCC1	AAGCATCAGCTAATGCTCGAA	SI04163768	Hs_SMARCC1_6
Remodeler	6599	SMARCC1	ATGATTGACACGTATCGTCTA	SI03151953	Hs_SMARCC1_5
Remodeler	6601	SMARCC2	CGCCGCCGCAGTGAAAGCTAA	SI04173169	Hs_SMARCC2_7
Remodeler	6601	SMARCC2	CACCGTGACCCAGTTCGACAA	SI04277560	Hs_SMARCC2_8
Remodeler	6601	SMARCC2	GAAGTCCTTGGTGCAGAATAA	SI04135383	Hs_SMARCC2_6
Remodeler	6601	SMARCC2	CAGGTGGATGCTGAGAGTCGA	SI04134466	Hs_SMARCC2_5
Remodeler	6602	SMARCD1	AGGGATGGATCAGTCCCGCAA	SI04152645	Hs_SMARCD1_7
Remodeler	6602	SMARCD1	AAGGTGCAGCAGAGACGACAA	SI04261628	Hs_SMARCD1_8
Remodeler	6602	SMARCD1	TCCGTTCAGCATGGGCTCTAA	SI04152505	Hs_SMARCD1_6
Remodeler	6602	SMARCD1	TAGGACCTCTAGATAGTGTTA	SI03228162	Hs_SMARCD1_5

Remodeler	6603	SMARCD2	CTGGGAATTCGCCTGACCTAA	SI04168640	Hs_SMARCD2_5
Remodeler	6603	SMARCD2	CATGATGGATCCATTCCGAAA	SI04272422	Hs_SMARCD2_6
Remodeler	6603	SMARCD2	CCGGATCGACAAATCCCGGAA	SI00726922	Hs_SMARCD2_2
Remodeler	6603	SMARCD2	GCGGGAGTACATCAACTGCAA	SI00726915	Hs_SMARCD2_1
Remodeler	6604	SMARCD3	CTCAAGGTGATGACAGATGTA	SI00047628	Hs_SMARCD3_4
Remodeler	6604	SMARCD3	ACGGACGGCTTCCAGGTGAAA	SI03041451	Hs_SMARCD3_5
Remodeler	6604	SMARCD3	GTGGCAGTATGTGAAGACCAA	SI00047621	Hs_SMARCD3_3
Remodeler	6604	SMARCD3	CAGGACTCCCATGACAAGGAA	SI00047607	Hs_SMARCD3_1
Remodeler	6605	SMARCE1	CAGAATAGATCACAAAGCTCA	SI04143454	Hs_SMARCE1_13
Remodeler	6605	SMARCE1	TTGGAGACTAGAAGCAAGATA	SI04255167	Hs_SMARCE1_14
Remodeler	6605	SMARCE1	CCCGCGTACCTTGCTTACATA	SI02655107	Hs_SMARCE1_6
Remodeler	6605	SMARCE1	AAGTTGTGGGAGATTGGCAAG	SI00301840	Hs_SMARCE1_1
Remodeler	10847	SRCAP	ATGGGTCGATTTGACCTTATT	SI04309858	Hs_SRCAP_6
Remodeler	10847	SRCAP	CAAGTGGAAGCTGCCCGCAAA	SI04370093	Hs_SRCAP_7
Remodeler	10847	SRCAP	ACCCGGGATGTCCACATATAT	SI04279681	Hs_SRCAP_5
Remodeler	10847	SRCAP	CACGCCAACCTTGTCCCTAAA	SI00732921	Hs_SRCAP_3
Remodeler	8089	YEATS4	AAAGCTATGGCAATCCTTTAA	SI03026716	Hs_YEATS4_5
Remodeler	8089	YEATS4	TACGGTAATGTTGCTCGGTAT	SI03109862	Hs_YEATS4_6
Remodeler	8089	YEATS4	AAAGGGTGTTACTATCGTTAA	SI00089355	Hs_YEATS4_3
Remodeler	8089	YEATS4	TTGGTAGTAAGCTAAACTGAA	SI00089348	Hs_YEATS4_2
Remodeler	29800	ZDHHC1	CCGGCCTGACTCTCTATGCAA	SI00766409	Hs_ZDHHC1_3
Remodeler	29800	ZDHHC1	ATCTACTATGTACAAGATGAA	SI04282005	Hs_ZDHHC1_6
Remodeler	29800	ZDHHC1	ACCGGCTGTGATGCTCCAATA	SI04139863	Hs_ZDHHC1_5
Remodeler	29800	ZDHHC1	CAGCACGCACATGTCATTGAA	SI00766402	Hs_ZDHHC1_2
Remodeler	79844	ZDHHC11	CAGACTTCTTATCTTAGTAGA	SI04223275	Hs_ZDHHC11_6

Remodeler	79844	ZDHHC11	CCGGCCGACTCCAATGTCAGA	SI04367755	Hs_ZDHHC11_8
Remodeler	79844	ZDHHC11	CGCGTGGAAATACATTGCCTA	SI04365914	Hs_ZDHHC11_7
Remodeler	79844	ZDHHC11	CCCAGAAGCCATACTCAATAA	SI00766444	Hs_ZDHHC11_4
Remodeler	84885	ZDHHC12	CCCACTCTTTGTGGTCTACCT	SI04131953	Hs_ZDHHC12_5
Remodeler	84885	ZDHHC12	AACGGAGCTTCAAGTCAGACA	SI04300891	Hs_ZDHHC12_7
Remodeler	84885	ZDHHC12	CACGATACCGAGCTGCGGCAA	SI04175094	Hs_ZDHHC12_6
Remodeler	84885	ZDHHC12	CAGATACTGCCTGGTGCTGCA	SI00766472	Hs_ZDHHC12_4
Remodeler	54503	ZDHHC13	TAGATTGGACATCACAGTACA	SI04141851	Hs_ZDHHC13_5
Remodeler	54503	ZDHHC13	AAGGTTCTTCGCTCAGTATGA	SI04297167	Hs_ZDHHC13_7
Remodeler	54503	ZDHHC13	TGGATTATGGACTTACCTCAA	SI04213076	Hs_ZDHHC13_6
Remodeler	54503	ZDHHC13	CAGCATAGTAGCCTTTCTATA	SI00766493	Hs_ZDHHC13_3
Remodeler	79683	ZDHHC14	ACGCTTGTGGCCAGACTGCAA	SI03141201	Hs_ZDHHC14_6
Remodeler	79683	ZDHHC14	ATGAGGTCTCGTGTTGAGATA	SI04366705	Hs_ZDHHC14_9
Remodeler	79683	ZDHHC14	CTGGGTGTCCTCGGCAAAGTT	SI03213420	Hs_ZDHHC14_8
Remodeler	79683	ZDHHC14	ACCTGAGTGCTTTGACAACAA	SI03139934	Hs_ZDHHC14_5
Remodeler	158866	ZDHHC15	TCAGTAAGACATCTACCTAAA	SI05146750	Hs_ZDHHC15_12
Remodeler	158866	ZDHHC15	TACGACAGTCTTCAGCTATTT	SI04275677	Hs_ZDHHC15_7
Remodeler	158866	ZDHHC15	GACAACGAGGATGACAACCAA	SI04199615	Hs_ZDHHC15_6
Remodeler	158866	ZDHHC15	ATGCTTGTTGATATGGCCAAA	SI05143194	Hs_ZDHHC15_10
Remodeler	84287	ZDHHC16	CTCGGGTGCTCTTACCTTCTA	SI00766577	Hs_ZDHHC16_3
Remodeler	84287	ZDHHC16	CGCCACCGTCTCCATCTGTAA	SI04227566	Hs_ZDHHC16_6
Remodeler	84287	ZDHHC16	AAGGGAGCACAAATAAAGGTA	SI04160380	Hs_ZDHHC16_5
Remodeler	84287	ZDHHC16	TAGCATCGAAAGGCACATCAA	SI00766570	Hs_ZDHHC16_2
Remodeler	23390	ZDHHC17	CAGTACCTGTTTGATACGAAA	SI00110558	Hs_ZDHHC17_2
Remodeler	23390	ZDHHC17	CAGCACATGGGACATAGTCAA	SI00110572	Hs_ZDHHC17_4

Remodeler	23390	ZDHHC17	CAGATCCTAGACCAATGTAAA	SI00110565	Hs_ZDHHC17_3
Remodeler	23390	ZDHHC17	CCGGATGAGTACGATACCGAA	SI00110551	Hs_ZDHHC17_1
Remodeler	84243	ZDHHC18	CACGTGCACTGGTCACGAGAA	SI04195324	Hs_ZDHHC18_5
Remodeler	84243	ZDHHC18	CACGTACCTCGTCGCCTCCAA	SI04295284	Hs_ZDHHC18_7
Remodeler	84243	ZDHHC18	AAGGCTCGTGGTCCAGCAAGA	SI04266262	Hs_ZDHHC18_6
Remodeler	84243	ZDHHC18	AAGCCTGATGCCAGCATGGTA	SI00766612	Hs_ZDHHC18_4
Remodeler	131540	ZDHHC19	CTCGGCCGACCGCACCTACAA	SI04207028	Hs_ZDHHC19_5
Remodeler	131540	ZDHHC19	TGGGCCTTTCCTGTTATCACA	SI04364794	Hs_ZDHHC19_7
Remodeler	131540	ZDHHC19	AAGACCCTCAATGCCCATTAA	SI04342702	Hs_ZDHHC19_6
Remodeler	131540	ZDHHC19	GACCCTGGCATCTTACATCAA	SI00766640	Hs_ZDHHC19_4
Remodeler	51201	ZDHHC2	TAAGAATTCCTAATAGGTCAA	SI04235966	Hs_ZDHHC2_6
Remodeler	51201	ZDHHC2	CAGGAAGTTCTTAGGCGAGCA	SI04341246	Hs_ZDHHC2_8
Remodeler	51201	ZDHHC2	AATGGCCTACCTGATACTCAA	SI04294388	Hs_ZDHHC2_7
Remodeler	51201	ZDHHC2	TAGCTACTGCTAGAAGTCTTA	SI04215974	Hs_ZDHHC2_5
Remodeler	253832	ZDHHC20	TACCTGTTATGAGTTGCTATA	SI03225124	Hs_ZDHHC20_1
Remodeler	253832	ZDHHC20	ATCGTCAAATCAGGTGTATGA	SI04362484	Hs_ZDHHC20_3
Remodeler	253832	ZDHHC20	AACCGCTTGTTGGACAGTGAA	SI04152267	Hs_ZDHHC20_2
Remodeler	253832	ZDHHC20	CAGCATTGACTTAGAGCTACA	SI00403956	Hs_FLJ25952_2
Remodeler	340481	ZDHHC21	CACCTTCTTATAGTATAGGTA	SI04196850	Hs_ZDHHC21_6
Remodeler	340481	ZDHHC21	GTGGGACTAATACAAGATCTA	SI04297461	Hs_ZDHHC21_8
Remodeler	340481	ZDHHC21	TTATAGGAAGCTACTACTAAA	SI04200021	Hs_ZDHHC21_7
Remodeler	340481	ZDHHC21	AAGCGTAATTTGGACCTCTTT	SI04196038	Hs_ZDHHC21_5
Remodeler	283576	ZDHHC22	TGGGTTCATTTATGCCCTATA	SI04273493	Hs_ZDHHC22_6
Remodeler	283576	ZDHHC22	CCCTAGAGAGCTAATGTAGTA	SI04306533	Hs_ZDHHC22_8
Remodeler	283576	ZDHHC22	CTGGCGCAAGAACTTACAAGA	SI04288795	Hs_ZDHHC22_7

Remodeler	283576	ZDHHC22	CCCGCTGATAGCTGCGCAACA	SI04236722	Hs_ZDHHC22_5
Remodeler	254887	ZDHHC23	CTGCGAGTACATAGATCGGAA	SI03208513	Hs_ZDHHC23_5
Remodeler	254887	ZDHHC23	AAGGGTGTGATCGATGGATTA	SI04209884	Hs_ZDHHC23_7
Remodeler	254887	ZDHHC23	CTGAACGGTTAGTGAAGACAA	SI04188926	Hs_ZDHHC23_6
Remodeler	254887	ZDHHC23	AAGGATCAGGATTGCATGAAA	SI00766745	Hs_ZDHHC23_3
Remodeler	254359	ZDHHC24	CTGGTCCGTTGGCCAGATCAA	SI00488187	Hs_LOC254359_2
Remodeler	254359	ZDHHC24	CCGCTGCGTGGGCTTCGGCAA	SI04329675	Hs_ZDHHC24_1
Remodeler	254359	ZDHHC24	ACACCTAGACTCAGTAAGGAA	SI00488194	Hs_LOC254359_3
Remodeler	254359	ZDHHC24	CAGGGCTTGGGCCGTGACTTA	SI00488180	Hs_LOC254359_1
Remodeler	51304	ZDHHC3	ACCACTCGCATGAGAACTTAA	SI04955202	Hs_ZDHHC3_10
Remodeler	51304	ZDHHC3	CATCGAGAGTTTACAGTTGAA	SI03073742	Hs_ZDHHC3_6
Remodeler	51304	ZDHHC3	CAGTATGGACAGAATAGCTTA	SI04955209	Hs_ZDHHC3_11
Remodeler	51304	ZDHHC3	TCCGTTCTCATGAATGTTTAA	SI02777642	Hs_ZDHHC3_5
Remodeler	55146	ZDHHC4	ATGGATTGCTTCATTACCTTT	SI04266689	Hs_ZDHHC4_7
Remodeler	55146	ZDHHC4	CACCTGGGAAGTATTTGGCTA	SI04913867	Hs_ZDHHC4_9
Remodeler	55146	ZDHHC4	TTGAGCTGTAGTTCCCGTTTA	SI04273185	Hs_ZDHHC4_8
Remodeler	55146	ZDHHC4	AAGAACCATGTCCGGCAGCTA	SI04148508	Hs_ZDHHC4_6
Remodeler	25921	ZDHHC5	ACCACCATTGCCAGACTACAA	SI04159694	Hs_ZDHHC5_6
Remodeler	25921	ZDHHC5	CTTGGCCTAGCTCAAACAATA	SI04372683	Hs_ZDHHC5_8
Remodeler	25921	ZDHHC5	CACCTCGGCTTGGCTACTAAT	SI04329717	Hs_ZDHHC5_7
Remodeler	25921	ZDHHC5	AGGGATTAGAGTGTGCTCCTA	SI03147186	Hs_ZDHHC5_5
Remodeler	64429	ZDHHC6	CCGAGAGGTGCTCGGCTTGTA	SI04228427	Hs_ZDHHC6_6
Remodeler	64429	ZDHHC6	GAGGTTTACGATACTGGTTAT	SI04363345	Hs_ZDHHC6_8
Remodeler	64429	ZDHHC6	TGGGTACGTTCTGTTCGGTTA	SI04318167	Hs_ZDHHC6_7
Remodeler	64429	ZDHHC6	AAGGCTAAAGATCGAATTCAG	SI04165784	Hs_ZDHHC6_5

Remodeler	55625	ZDHHC7	CAGCAGGGCGTTTACATAGAA	SI00766857	Hs_ZDHHC7_3
Remodeler	55625	ZDHHC7	TTCGGGTTATTACATGGGTTA	SI04299610	Hs_ZDHHC7_7
Remodeler	55625	ZDHHC7	ACCCACGGCACAGGTGATAAA	SI04282117	Hs_ZDHHC7_6
Remodeler	55625	ZDHHC7	CCCGTGGTTACTATGAATGTA	SI00766850	Hs_ZDHHC7_2
Remodeler	29801	ZDHHC8	CCGGGCTCCGCTGTACAAGAA	SI00766885	Hs_ZDHHC8_3
Remodeler	29801	ZDHHC8	CGCGCCGTGTCTGATGTGTCA	SI04141277	Hs_ZDHHC8_5
Remodeler	29801	ZDHHC8	CGCCAGGCTACTCCTAACTAA	SI00766892	Hs_ZDHHC8_4
Remodeler	29801	ZDHHC8	CCGCCTTTCCTTAGGCCTGAA	SI00766871	Hs_ZDHHC8_1
Remodeler	51114	ZDHHC9	CAGGAATAGCAGGCAACGTGA	SI04152967	Hs_ZDHHC9_7
Remodeler	51114	ZDHHC9	ATCGTCTATGTGGCCCTCAAA	SI04295018	Hs_ZDHHC9_9
Remodeler	51114	ZDHHC9	TACACTCTTCTTCGCCTTTGA	SI04173351	Hs_ZDHHC9_8
Remodeler	51114	ZDHHC9	CTCAACCAGACAACCAATGAA	SI04132513	Hs_ZDHHC9_6
NR+CoReg	142	PARP1	ACCCAAGGGCTAATAGTAATA	SI04433982	Hs_PARP1_11
NR+CoReg	142	PARP1	ACGGTGATCGGTAGCAACAAA	SI02662996	Hs_PARP1_6
NR+CoReg	142	PARP1	CAGGGAGACCCAATAGGCTTA	SI04433989	Hs_PARP1_12
NR+CoReg	142	PARP1	CCGAGAAATCTCTTACCTCAA	SI02662989	Hs_PARP1_5
NR+CoReg	190	NR0B1	ATCGAACTTAATAGTACCCTT	SI00010227	Hs_NR0B1_3
NR+CoReg	190	NR0B1	ATGCTCTGTACAAAGATATAA	SI00010220	Hs_NR0B1_2
NR+CoReg	190	NR0B1	ATGGATGATATGATGCTGGAA	SI00010234	Hs_NR0B1_4
NR+CoReg	190	NR0B1	CAGCATGCTGACGAGCGCAAA	SI03066014	Hs_NR0B1_5
NR+CoReg	367	AR	AAGGAACTCGATCGTATCATT	SI02757265	Hs_AR_6
NR+CoReg	367	AR	CACAAACGTTTACTTATCTTA	SI04434171	Hs_AR_10
NR+CoReg	367	AR	CACGGGAAGTTTAGAGAGCTA	SI02757258	Hs_AR_5
NR+CoReg	367	AR	CCCAAGATCCTTTCTGGGAAA	SI04434178	Hs_AR_11
NR+CoReg	595	CCND1	AACACCAGCTCCTGTGCTGCG	SI02654540	Hs_CCND1_5

NR+CoReg	595	CCND1	AAGGCCAGTATGATTTATAAA	SI00147812	Hs_CCND1_1
NR+CoReg	595	CCND1	ATGCATGTAGTCACTTTATAA	SI00147819	Hs_CCND1_2
NR+CoReg	595	CCND1	GCCCTCGGTGTCCTACTTCAA	SI02654547	Hs_CCND1_6
NR+CoReg	672	BRCA1	AACCTATCGGAAGAAGGCAAG	SI00299495	Hs_BRCA1_9
NR+CoReg	672	BRCA1	ACCATACAGCTTCATAAATAA	SI02664368	Hs_BRCA1_15
NR+CoReg	672	BRCA1	CAGCAGTTTATTACTCACTAA	SI02654575	Hs_BRCA1_13
NR+CoReg	672	BRCA1	CAGGAAATGGCTGAACTAGAA	SI02664361	Hs_BRCA1_14
NR+CoReg	675	BRCA2	CAGCGTTTGTGTATCGGGCAA	SI00000966	Hs_BRCA2_1
NR+CoReg	675	BRCA2	CAGGACACAATTACAACTAAA	SI02653434	Hs_BRCA2_6
NR+CoReg	675	BRCA2	TACGTACTCCAGAACATTTAA	SI00000980	Hs_BRCA2_3
NR+CoReg	675	BRCA2	TTGGAGGAATATCGTAGGTAA	SI02653595	Hs_BRCA2_7
NR+CoReg	857	CAV1	AAATTAAGAGCTTCCTGATTG	SI02654617	Hs_CAV1_13
NR+CoReg	857	CAV1	AACTAAACACCTCAACGATGA	SI00299621	Hs_CAV1_7
NR+CoReg	857	CAV1	AAGCAAGTGTACGACGCGCAC	SI00299642	Hs_CAV1_10
NR+CoReg	857	CAV1	CACCTTCACTGTGACGAAATA	SI00299614	Hs_CAV1_6
NR+CoReg	898	CCNE1	AAGGCAAACGTGACCGTTTTT	SI00299691	Hs_CCNE1_5
NR+CoReg	898	CCNE1	AAGGCCCTTAAGTGGCGTTTA	SI03035319	Hs_CCNE1_7
NR+CoReg	898	CCNE1	ACCGGGTTTACCCAAACTCAA	SI02625693	Hs_CCNE1_6
NR+CoReg	898	CCNE1	CAGGGTATCAGTGGTGCGACA	SI00024024	Hs_CCNE1_2
NR+CoReg	994	CDC25B	CAGGAGGCTGAGGAACCTAAA	SI02652916	Hs_CDC25B_8
NR+CoReg	994	CDC25B	CCCAGTCTGTTGAGTTAGTTA	SI02659272	Hs_CDC25B_10
NR+CoReg	994	CDC25B	CGCCGAGAGCTTCCTACTGAA	SI02659279	Hs_CDC25B_11
NR+CoReg	994	CDC25B	TTGGGTTAATACCAGCTTAAA	SI02653616	Hs_CDC25B_9
NR+CoReg	1022	CDK7	AACCGCCTTAAGAGAGATAAA	SI02759442	Hs_CDK7_10
NR+CoReg	1022	CDK7	CCGGATGGCTCTGGACGTGAA	SI00287392	Hs_CDK7_5

NR+CoReg	1022	CDK7	GAGGCTTTAAGGTAGCTTTAA	SI00287399	Hs_CDK7_6
NR+CoReg	1022	CDK7	TTGGACATAGATCAGAAGCTA	SI02664795	Hs_CDK7_9
NR+CoReg	1387	CREBBP	AACGGAGGTCGCGTTTACATA	SI02633085	Hs_CREBBP_6
NR+CoReg	1387	CREBBP	CCCGATCCTGGTGAATCCAAA	SI02633092	Hs_CREBBP_7
NR+CoReg	1387	CREBBP	CCCGCATTGTCGAACCATGAA	SI02622648	Hs_CREBBP_2
NR+CoReg	1387	CREBBP	CTGCCAGTGAATCGCATGCAA	SI02633099	Hs_CREBBP_8
NR+CoReg	1869	E2F1	AACTCCTCGCAGATCGTCATC	SI00300083	Hs_E2F1_5
NR+CoReg	1869	E2F1	ACGCTATGAGACCTCACTGAA	SI02664410	Hs_E2F1_6
NR+CoReg	1869	E2F1	CAGATGGTTATGGTGATCAAA	SI00073990	Hs_E2F1_3
NR+CoReg	1869	E2F1	CAGGACCTTCGTAGCATTGCA	SI00073976	Hs_E2F1_1
NR+CoReg	2033	EP300	ACCAAGGGTTGCAAACGGAAA	SI03038259	Hs_EP300_9
NR+CoReg	2033	EP300	CACCGATAACTCAGACTTGAA	SI02622592	Hs_EP300_3
NR+CoReg	2033	EP300	CCCGGTGAACTCTCCTATAAT	SI03078761	Hs_EP300_10
NR+CoReg	2033	EP300	TTGGACTACCCTATCAAGTAA	SI02626267	Hs_EP300_7
NR+CoReg	2063	NR2F6	AAGGCCAATAATAAAGACATT	SI00074172	Hs_NR2F6_1
NR+CoReg	2063	NR2F6	CAGACACTACATGATGACTCA	SI00074186	Hs_NR2F6_3
NR+CoReg	2063	NR2F6	CGCGGTGCTGGGCATCGACAA	SI03085320	Hs_NR2F6_5
NR+CoReg	2063	NR2F6	TTAAATGATCATGAAACCAAA	SI02634744	Hs_NR2F6_4
NR+CoReg	2099	ESR1	CAGCAGCAAGCCCGCCGTGTA	SI03065615	Hs_ESR1_10
NR+CoReg	2099	ESR1	CCGGCATGCATCCAACACCAA	SI00002506	Hs_ESR1_1
NR+CoReg	2099	ESR1	GAGACTTGAATTAATAAGTGA	SI02781401	Hs_ESR1_8
NR+CoReg	2099	ESR1	TCCGAGTATGATCCTACCAGA	SI03114979	Hs_ESR1_11
NR+CoReg	2100	ESR2	CACGAATCTTTGAGAACATTA	SI00025970	Hs_ESR2_4
NR+CoReg	2100	ESR2	CAGCTACAAATCAGTGTACAA	SI00025963	Hs_ESR2_3
NR+CoReg	2100	ESR2	CCTGACCAAGTTGGCCGACAA	SI03083269	Hs_ESR2_6

NR+CoReg	2100	ESR2	CTGGTCGTGTGAAGGATGTAA	SI02626295	Hs_ESR2_5
NR+CoReg	2101	ESRRA	AGAGGAGTATGTTCTACTAAA	SI02633295	Hs_ESRRA_2
NR+CoReg	2101	ESRRA	CCGAGAGATTGTGGTCACCAT	SI00063917	Hs_ESRRA_1
NR+CoReg	2101	ESRRA	CTGGCCTTCGCTGAGGACTTA	SI03098074	Hs_ESRRA_5
NR+CoReg	2101	ESRRA	TGCGTGGGAGGCAGAAACCTA	SI03119088	Hs_ESRRA_6
NR+CoReg	2103	ESRRB	ACCAAGATTGTCTCATACCTA	SI03038217	Hs_ESRRB_5
NR+CoReg	2103	ESRRB	ACGCAGGTACAAGAAGCTCAA	SI00063931	Hs_ESRRB_2
NR+CoReg	2103	ESRRB	CAGCACTTCTATAGCGTCAAA	SI00063924	Hs_ESRRB_1
NR+CoReg	2103	ESRRB	CATGGAGGACTCGGCCATCAA	SI03073980	Hs_ESRRB_6
NR+CoReg	2104	ESRRG	CTGTAGTGTGATTCTAGATAA	SI00025998	Hs_ESRRG_4
NR+CoReg	2104	ESRRG	GACGATTATATAATGGACGAA	SI03101987	Hs_ESRRG_5
NR+CoReg	2104	ESRRG	TGCATTATAGCCAGTAGTAAA	SI00025991	Hs_ESRRG_3
NR+CoReg	2104	ESRRG	TTGAACAATTACGAACAATAA	SI00025977	Hs_ESRRG_1
NR+CoReg	2118	ETV4	ACCGGAGTCATTGGGAAGGAA	SI02627485	Hs_ETV4_7
NR+CoReg	2118	ETV4	ATGGGCTATGGCTATGAGAAA	SI00030954	Hs_ETV4_1
NR+CoReg	2118	ETV4	CACCGGGTGCGCATCAATGTA	SI00030961	Hs_ETV4_2
NR+CoReg	2118	ETV4	CCGCTCGCTCCGATACTATTA	SI03081393	Hs_ETV4_8
NR+CoReg	2494	NR5A2	ACCCGAGTCCATAATGGGCTA	SI00056392	Hs_NR5A2_1
NR+CoReg	2494	NR5A2	ACGACAGGAGCTGATAAGCAA	SI00056406	Hs_NR5A2_3
NR+CoReg	2494	NR5A2	ACGCATGTTAATCTATGCAAA	SI00056399	Hs_NR5A2_2
NR+CoReg	2494	NR5A2	CTCGACCACATTTACCGACAA	SI00056413	Hs_NR5A2_4
NR+CoReg	2516	NR5A1	AAGGATAACCGAGTTTGCTAA	SI00070469	Hs_NR5A1_1
NR+CoReg	2516	NR5A1	ACGCAGGTGCATGGTCTTCAA	SI00070476	Hs_NR5A1_2
NR+CoReg	2516	NR5A1	CCGCAACAACCTGCTCATCGA	SI03080441	Hs_NR5A1_5
NR+CoReg	2516	NR5A1	CTGGAATAAATTTCGCAATTA	SI00070483	Hs_NR5A1_3

NR+CoReg	2649	NR6A1	AAGCGGAGCATTTGCAACAAA	SI00146139	Hs_NR6A1_1
NR+CoReg	2649	NR6A1	CACGCCCATGTTGATTGAAGA	SI00146153	Hs_NR6A1_3
NR+CoReg	2649	NR6A1	CTGGAACAATTGAATAAACGA	SI02626358	Hs_NR6A1_6
NR+CoReg	2649	NR6A1	GAGGAGTATGCTTGCATGAAA	SI02626351	Hs_NR6A1_5
NR+CoReg	2908	NR3C1	AAGCTTTCCTGGAGCAAATAT	SI02654757	Hs_NR3C1_5
NR+CoReg	2908	NR3C1	AAGTGCAAACCTGCTGTGTTT	SI02654764	Hs_NR3C1_6
NR+CoReg	2908	NR3C1	CAGACTCAACTTGGAGGATCA	SI00003752	Hs_NR3C1_2
NR+CoReg	2908	NR3C1	GAGGATCATGACTACGCTCAA	SI00003745	Hs_NR3C1_1
NR+CoReg	3065	HDAC1	CACAGCGATGACTACATTAAA	SI00070609	Hs_HDAC1_1
NR+CoReg	3065	HDAC1	CACCCGGAGGAAAGTCTGTTA	SI02663472	Hs_HDAC1_6
NR+CoReg	3065	HDAC1	CCACAGCGATGACTACATTAA	SI00070623	Hs_HDAC1_3
NR+CoReg	3065	HDAC1	CGGGATTGATGACGAGTCCTA	SI00070630	Hs_HDAC1_4
NR+CoReg	3146	HMGB1	AACCTTTACATGAGGACTCTA	SI02627835	Hs_HMGB1_3
NR+CoReg	3146	HMGB1	AAGAGTAATCAATCTACTCAA	SI02627828	Hs_HMGB1_2
NR+CoReg	3146	HMGB1	AAGGATATTGCTGCATATCGA	SI03650374	Hs_HMGB1_6
NR+CoReg	3146	HMGB1	TCCTTTCATATAGTTAGCTAA	SI02627842	Hs_HMGB1_4
NR+CoReg	3148	HMGB2	AAAGGAGAAGTCGAAGTTTGA	SI04949322	Hs_HMGB2_6
NR+CoReg	3148	HMGB2	AGGAATTAGTATCAATAGTAA	SI00033040	Hs_HMGB2_2
NR+CoReg	3148	HMGB2	CTGCAAAGAAATTGGGTGAAA	SI04949329	Hs_HMGB2_7
NR+CoReg	3148	HMGB2	TTGCTAAGAATGTGAATTCAA	SI00033047	Hs_HMGB2_3
NR+CoReg	3164	NR4A1	CACAGGAGAGTTTGACACCTT	SI03056221	Hs_NR4A1_5
NR+CoReg	3164	NR4A1	CAGCACCTTCATGGACGGCTA	SI00033138	Hs_NR4A1_4
NR+CoReg	3164	NR4A1	CAGCATTATGGTGTCCGCACA	SI00033117	Hs_NR4A1_1
NR+CoReg	3164	NR4A1	CTCCAGTGGCTCTGACTACTA	SI03089576	Hs_NR4A1_6
NR+CoReg	3169	FOXA1	CAAACCGTCAACAGCATAATA	SI04159330	Hs_FOXA1_7

NR+CoReg	3169	FOXA1	CCAGACGGGTTTCATTATTAT	SI04154010	Hs_FOXA1_6
NR+CoReg	3169	FOXA1	CGGCGACGCCAAGACGTTCAA	SI04217038	Hs_FOXA1_8
NR+CoReg	3169	FOXA1	CTCCTCCGTCCCGGTCAGCAA	SI04311888	Hs_FOXA1_9
NR+CoReg	3170	FOXA2	CACGTTCTATATAAGGAGGAA	SI00420525	Hs_FOXA2_4
NR+CoReg	3170	FOXA2	CAGAACCAGAGGGTTGTACTA	SI04190599	Hs_FOXA2_6
NR+CoReg	3170	FOXA2	CAGAGACGCAAGGGAGAAGAA	SI04357654	Hs_FOXA2_7
NR+CoReg	3170	FOXA2	TTGCAGGGAAGTCTTACTTAA	SI03243653	Hs_FOXA2_5
NR+CoReg	3172	HNF4A	CAAGAGATCCATGGTGTTCAA	SI03053785	Hs_HNF4A_6
NR+CoReg	3172	HNF4A	CGAGCAGATCCAGTTCATCAA	SI03083773	Hs_HNF4A_7
NR+CoReg	3172	HNF4A	CGGCATGGCCAAGATTGACAA	SI03086125	Hs_HNF4A_8
NR+CoReg	3172	HNF4A	CGGCGACATTCGGGCGAAGAA	SI03086286	Hs_HNF4A_9
NR+CoReg	3174	HNF4G	AAGCACTGACATAAACGTTAA	SI00060095	Hs_HNF4G_1
NR+CoReg	3174	HNF4G	AGGGCTAAGCGATCCAGTAAA	SI03046001	Hs_HNF4G_5
NR+CoReg	3174	HNF4G	CAACTATGTTATTCACCGCAA	SI03053267	Hs_HNF4G_6
NR+CoReg	3174	HNF4G	CACCGGATGGATTCTGATGAA	SI00060116	Hs_HNF4G_4
NR+CoReg	3192	HNRNPU	AGGATATTATTGAATACCCAA	SI02780540	Hs_HNRPU_5
NR+CoReg	3192	HNRNPU	CTGGCCGTGGTAGTTACTCAA	SI02781002	Hs_HNRPU_6
NR+CoReg	3192	HNRNPU	TCGGGAGTCATTGTCACAATA	SI00064477	Hs_HNRPU_1
NR+CoReg	3192	HNRNPU	TTGGCTGGTCACTAACTACAA	SI04435361	Hs_HNRNPU_1
NR+CoReg	3276	PRMT1	CACCAACGCCTGCCTCATAAA	SI00441840	Hs_HRMT1L2_1
NR+CoReg	3276	PRMT1	CACCATCGACCTGGACTTCAA	SI02663493	Hs_HRMT1L2_7
NR+CoReg	3276	PRMT1	CCCGTTCTGCCTGCAAGTGAA	SI00441861	Hs_HRMT1L2_4
NR+CoReg	3276	PRMT1	CCGGCAGTACAAAGACTACAA	SI02663500	Hs_HRMT1L2_8
NR+CoReg	4306	NR3C2	CAGCAATTAATTAGATCAACA	SI00018081	Hs_NR3C2_1
NR+CoReg	4306	NR3C2	CAGCCCTTCGAACACTAATAA	SI03066322	Hs_NR3C2_5

NR+CoReg	4306	NR3C2	CCACGAGGAAG CAGCAATTAA	SI00018 102	Hs_NR3C2_4
NR+CoReg	4306	NR3C2	CCAGACCTAGTC TTTAATGAA	SI00018 095	Hs_NR3C2_3
NR+CoReg	4582	MUC1	CAGCACCGACTA CTACCAAGA	SI04949 826	Hs_MUC1_10
NR+CoReg	4582	MUC1	CAGCAGCCTCTC TTACACAAA	SI02780 673	Hs_MUC1_7
NR+CoReg	4582	MUC1	CCCGGGATACCT ACCATCCTA	SI00038 143	Hs_MUC1_4
NR+CoReg	4582	MUC1	TGAGAAGGTTTC TGCAGGTAA	SI04949 833	Hs_MUC1_11
NR+CoReg	4929	NR4A2	CAGACACTATGT AGTCTGTTA	SI00085 316	Hs_NR4A2_2
NR+CoReg	4929	NR4A2	CTCCGGGTCGG TTTACTACAA	SI00085 309	Hs_NR4A2_1
NR+CoReg	4929	NR4A2	CTGGATTTAGAA CATGGACTA	SI00085 323	Hs_NR4A2_3
NR+CoReg	4929	NR4A2	TACGACACTGTC CACCTTTAA	SI00085 330	Hs_NR4A2_4
NR+CoReg	5241	PGR	AAGGAGCCGCG TGTCACTAAA	SI00018 690	Hs_PGR_2
NR+CoReg	5241	PGR	CACAGCGTTTCT ATCAACTTA	SI00018 683	Hs_PGR_1
NR+CoReg	5241	PGR	CCCGAACTTCCC GAAGATCCA	SI00018 697	Hs_PGR_3
NR+CoReg	5241	PGR	CTGCCTCTCAAT CACGCCTTA	SI00018 704	Hs_PGR_4
NR+CoReg	5245	PHB	AAAGCCAGCTTC CTCGCATCT	SI00301 168	Hs_PHB_5
NR+CoReg	5245	PHB	CCCAGAAATCAC TGTGAAATT	SI00301 175	Hs_PHB_6
NR+CoReg	5245	PHB	CCCAGTGGAATT CCAACTTGA	SI00040 733	Hs_PHB_2
NR+CoReg	5245	PHB	TGGGAAGGAAA CAAATGTGTA	SI00040 747	Hs_PHB_4
NR+CoReg	5300	PIN1	CAGGCCGAGTG TACTACTTCA	SI02636 921	Hs_PIN1_3
NR+CoReg	5300	PIN1	CAGTATTTATTG TTCCCACAA	SI02662 667	Hs_PIN1_6
NR+CoReg	5300	PIN1	CGGCTACATCCA GAAGATCAA	SI02636 928	Hs_PIN1_4
NR+CoReg	5300	PIN1	GACCGCCAGATT CTCCCTTAA	SI02662 128	Hs_PIN1_5
NR+CoReg	5465	PPARA	AAGCTTTGGCTT TACGGAATA	SI03034 108	Hs_PPARA_5
NR+CoReg	5465	PPARA	CAAGAGAATCTA CGAGGCCTA	SI03053 757	Hs_PPARA_6
NR+CoReg	5465	PPARA	CAGTGGAGCATT GAACATCGA	SI03073 189	Hs_PPARA_7

NR+CoReg	5465	PPARA	TCGGCGAACGATTCGACTCAA	SI03116918	Hs_PPARA_8
NR+CoReg	5467	PPARD	CAGGTTACCCTTCTCAAGTAT	SI03072412	Hs_PPARD_6
NR+CoReg	5467	PPARD	CAGTGATATCATTGAGCCTAA	SI00086058	Hs_PPARD_3
NR+CoReg	5467	PPARD	CCCACAGGTGGCCGACCTGAA	SI05383420	Hs_PPARD_16
NR+CoReg	5467	PPARD	TAAGTTTGAATTTGCTGTCAA	SI04950288	Hs_PPARD_12
NR+CoReg	5468	PPARG	CAGACAAATCACCATTCGTTA	SI00071680	Hs_PPARG_2
NR+CoReg	5468	PPARG	CAGCGACTTGGCAATATTTAT	SI02634275	Hs_PPARG_5
NR+CoReg	5468	PPARG	GAGGGCGATCTTGACAGGAAA	SI00071673	Hs_PPARG_1
NR+CoReg	5468	PPARG	TCCGGAGAACAATCAGATTGA	SI03115266	Hs_PPARG_7
NR+CoReg	5469	MED1	AAGTTTAAGGGCAATAACCAA	SI00068278	Hs_PPARBP_3
NR+CoReg	5469	MED1	CAGAGTCTCGTTTCAGCGTAT	SI03064355	Hs_PPARBP_5
NR+CoReg	5469	MED1	CAGTGTTTCGTTCTAAATCTA	SI00068264	Hs_PPARBP_1
NR+CoReg	5469	MED1	CCCGCCTTTAGAGTTAAATAT	SI00068285	Hs_PPARBP_4
NR+CoReg	5894	RAF1	AAGACGTTCCTGAAGCTTGCC	SI00301623	Hs_RAF1_5
NR+CoReg	5894	RAF1	CAGATCTTAGTAAGCTATATA	SI02223032	Hs_RAF1_6
NR+CoReg	5894	RAF1	GTGGATGTTGATGGTAGTACA	SI00045157	Hs_RAF1_2
NR+CoReg	5894	RAF1	TGGGAAATAGAAGCCAGTGAA	SI02223039	Hs_RAF1_7
NR+CoReg	5914	RARA	CACTGAGATCTACTGGATAAA	SI03062318	Hs_RARA_5
NR+CoReg	5914	RARA	CAGGAAATGTTGGAGAACTCA	SI03068821	Hs_RARA_6
NR+CoReg	5914	RARA	CCACATCTTCATCACCAGCAA	SI00019376	Hs_RARA_3
NR+CoReg	5914	RARA	CTCCACCAAGTGCATCATTAA	SI00019369	Hs_RARA_2
NR+CoReg	5915	RARB	ATGGAATAGTCAAGACATCAA	SI00019390	Hs_RARB_1
NR+CoReg	5915	RARB	CTCCGTAGCATCAGTGCTAAA	SI00019397	Hs_RARB_2
NR+CoReg	5915	RARB	CTGCCAGTTCAGTTAATCAAA	SI00019404	Hs_RARB_3
NR+CoReg	5915	RARB	GAGCGTGTAATTACCTTGAAA	SI00019411	Hs_RARB_4

NR+CoReg	5916	RARG	AACAGGAACACTAGAGACCAA	SI04950547	Hs_RARG_13
NR+CoReg	5916	RARG	CAGGCCCGATGCCTCCCTTAA	SI00019432	Hs_RARG_3
NR+CoReg	5916	RARG	CCCGTCCTTGTGCCAGGTCAA	SI00019439	Hs_RARG_4
NR+CoReg	5916	RARG	GAGCCTGGGTTTGGACTCTAA	SI04950540	Hs_RARG_12
NR+CoReg	5925	RB1	AAGGACCGAGAAGGACCAACT	SI00301651	Hs_RB1_5
NR+CoReg	5925	RB1	AAGGTTCAACTACGCGTGTAA	SI00007091	Hs_RB1_1
NR+CoReg	5925	RB1	CAGGGTTGTGTCGAAATTGGA	SI02653931	Hs_RB1_8
NR+CoReg	5925	RB1	CGCGTGTAAATTCTACTGCAA	SI02653819	Hs_RB1_7
NR+CoReg	6047	RNF4	AAGACTGTTTCGAAACCAACA	SI04167828	Hs_RNF4_8
NR+CoReg	6047	RNF4	CCCTGTTTCCTAAGAACGAAA	SI03187310	Hs_RNF4_5
NR+CoReg	6047	RNF4	TAGGCCGAGCTTTGCGGGAAA	SI03228512	Hs_RNF4_6
NR+CoReg	6047	RNF4	TCCCATCTGCATGGACGGATA	SI03231438	Hs_RNF4_7
NR+CoReg	6095	RORA	CACCGAGAAGATGGAATACTA	SI02630047	Hs_RORA_5
NR+CoReg	6095	RORA	CACCGTGTACTTTGATGGGAA	SI02630061	Hs_RORA_7
NR+CoReg	6095	RORA	CAGGTCTTGATATCAATGGAA	SI02630068	Hs_RORA_8
NR+CoReg	6095	RORA	CCCGACGTCTTCAAATCCTTA	SI02630054	Hs_RORA_6
NR+CoReg	6096	RORB	ATGCATCACCATTAAGACAAA	SI00093184	Hs_RORB_3
NR+CoReg	6096	RORB	CAGATCACTCACGCCATCCAA	SI03064635	Hs_RORB_5
NR+CoReg	6096	RORB	CAGGCTCTCTTCTATGATTTA	SI00093170	Hs_RORB_1
NR+CoReg	6096	RORB	CAGGGATAACCATGACTGAAA	SI00093177	Hs_RORB_2
NR+CoReg	6097	RORC	AAGGAGCTCTTCAGCACTGAA	SI00072030	Hs_RORC_4
NR+CoReg	6097	RORC	CCGGGCCTACAATGCTGACAA	SI00072023	Hs_RORC_3
NR+CoReg	6097	RORC	CGGGTTCATCTGAGTAAACAT	SI00072009	Hs_RORC_1
NR+CoReg	6097	RORC	TAGGATGTGCCGGGCCTACAA	SI00072016	Hs_RORC_2
NR+CoReg	6256	RXRA	CTCATCGGCCTTGTAGTTGTA	SI00046151	Hs_RXRA_4

NR+CoReg	6256	RXRA	GCGCGCCATCG TCCTCTTTAA	SI03105 242	Hs_RXRA_5
NR+CoReg	6256	RXRA	TCCGTACGATTG TCTCTGAAA	SI00046 144	Hs_RXRA_3
NR+CoReg	6256	RXRA	TTCGTGTAAGCA AGTACATAA	SI00046 130	Hs_RXRA_1
NR+CoReg	6257	RXRB	ACGGGCTTAATT CGACCCAAT	SI00131 957	Hs_RXRB_1
NR+CoReg	6257	RXRB	AGGGATCTGCTT GATATCCCA	SI00131 964	Hs_RXRB_2
NR+CoReg	6257	RXRB	CTGGCAAACGG CTATGTGCAA	SI00131 971	Hs_RXRB_3
NR+CoReg	6257	RXRB	GAGGGCAATCAT TCTGTTTAA	SI00131 978	Hs_RXRB_4
NR+CoReg	6258	RXRG	CAGGAGAGGAA CATGAACTGA	SI03069 479	Hs_RXRG_5
NR+CoReg	6258	RXRG	CGGCAGCATTAT GCGTGATTA	SI03086 055	Hs_RXRG_6
NR+CoReg	6258	RXRG	GACGAGTAAACA TGTATGGAA	SI00093 247	Hs_RXRG_4
NR+CoReg	6258	RXRG	TAGAGGCAGATT CCTGACTAA	SI03110 618	Hs_RXRG_7
NR+CoReg	6597	SMARCA4	CCCGTGGACTTC AAGAAGATA	SI02630 208	Hs_SMARCA4_ 5
NR+CoReg	6597	SMARCA4	CCGCGCTACAA CCAGATGAAA	SI00047 579	Hs_SMARCA4_ 1
NR+CoReg	6597	SMARCA4	CTGGGCGTACG AGTTTGACAA	SI03098 998	Hs_SMARCA4_ 6
NR+CoReg	6597	SMARCA4	TCACTGGATGTC AAACAGTAA	SI00047 586	Hs_SMARCA4_ 2
NR+CoReg	6615	SNAI1	ACACTGGTATTT ATATTTCAA	SI00083 419	Hs_SNAI1_4
NR+CoReg	6615	SNAI1	CAGCGAGCTGC AGGACTCTAA	SI03066 875	Hs_SNAI1_6
NR+CoReg	6615	SNAI1	CCGAATGTCCCT GCTCCACAA	SI02636 424	Hs_SNAI1_5
NR+CoReg	6615	SNAI1	GAGGTGTGACTA ACTATGCAA	SI00083 398	Hs_SNAI1_1
NR+CoReg	6907	TBL1X	CAGCCTGCGGC CGCAAGCAAA	SI04175 528	Hs_TBL1X_5
NR+CoReg	6907	TBL1X	CATGACGTCCCG AGTAACAAA	SI04370 884	Hs_TBL1X_8
NR+CoReg	6907	TBL1X	TGCGTTAGAGTG TACTCTGAA	SI04329 514	Hs_TBL1X_7
NR+CoReg	6907	TBL1X	TGGCGCGTAGTA AGTGCTTTA	SI04296 544	Hs_TBL1X_6
NR+CoReg	7025	NR2F1	AAGAGAGAGGG CTAAACTTAA	SI00079 891	Hs_NR2F1_3
NR+CoReg	7025	NR2F1	CCGGCGTGAATT ATCCCGTAT	SI00079 877	Hs_NR2F1_1

NR+CoReg	7025	NR2F1	CTGGCCTTACATGTCCATCCA	SI03098067	Hs_NR2F1_5
NR+CoReg	7025	NR2F1	TCCGCAGGAACTTAACTTACA	SI00079884	Hs_NR2F1_2
NR+CoReg	7026	NR2F2	CCGCTTAGTTCTTGAATTGTT	SI03649065	Hs_NR2F2_6
NR+CoReg	7026	NR2F2	CGGGCAGTTCGCGCTGACCAA	SI04437300	Hs_NR2F2_10
NR+CoReg	7026	NR2F2	CTGGCCGTATATGGCAATTCA	SI00128814	Hs_NR2F2_1
NR+CoReg	7026	NR2F2	GTGGAATTTATTGGCAGCCAA	SI03649156	Hs_NR2F2_7
NR+CoReg	7041	TGFB1I1	AACGGCCCAGCCAGACCTAAA	SI02641765	Hs_TGFB1I1_5
NR+CoReg	7041	TGFB1I1	ACCGGTGGTGAGCTCCACAAA	SI00112630	Hs_TGFB1I1_2
NR+CoReg	7041	TGFB1I1	CACAGATGAAATCATGTCTCA	SI04951114	Hs_TGFB1I1_6
NR+CoReg	7041	TGFB1I1	TCGGTTGCTTCAGGAACTTAA	SI00112623	Hs_TGFB1I1_1
NR+CoReg	7067	THRA	CAGCGAGTTTACCAAGATCAT	SI00049805	Hs_THRA_3
NR+CoReg	7067	THRA	CCCGATGACATTGGCCAGTCA	SI00049798	Hs_THRA_2
NR+CoReg	7067	THRA	TCCCACCTATTCCTGCAAATA	SI03114041	Hs_THRA_5
NR+CoReg	7067	THRA	TCGCCGCACAATCCAGAAGAA	SI03116470	Hs_THRA_6
NR+CoReg	7068	THRB	AAGTGAGACTTTAACCTTGAA	SI02662352	Hs_THRB_6
NR+CoReg	7068	THRB	CTGGGTGTCATTTCATTCCAT	SI00010101	Hs_THRB_3
NR+CoReg	7068	THRB	TCCAGAATGATTACTAACCTA	SI02662919	Hs_THRB_7
NR+CoReg	7068	THRB	TTGGACTAGCTCAATATTCCA	SI00010094	Hs_THRB_2
NR+CoReg	7101	NR2E1	CCGGTTGATGCTAACACTCTA	SI00050099	Hs_NR2E1_1
NR+CoReg	7101	NR2E1	TACGTTATGTTGGAGCATTTA	SI00050113	Hs_NR2E1_3
NR+CoReg	7101	NR2E1	TCCCGTTAACATAGTGCTGAA	SI00050106	Hs_NR2E1_2
NR+CoReg	7101	NR2E1	TCGGACGTCCACCATCCGCAA	SI03116701	Hs_NR2E1_5
NR+CoReg	7181	NR2C1	AACGGTGATGTTTCAAGGGCA	SI00050330	Hs_NR2C1_4
NR+CoReg	7181	NR2C1	AAGGAAGTGTACACCTAATCA	SI03034269	Hs_NR2C1_5
NR+CoReg	7181	NR2C1	AAGGACCTTCGTAGCCCATTA	SI00050309	Hs_NR2C1_1

NR+CoReg	7181	NR2C1	ACCCATTGAAGTATCACGAGA	SI03039162	Hs_NR2C1_6
NR+CoReg	7182	NR2C2	ATGTTTCGATAGACAGCATAA	SI03052441	Hs_NR2C2_5
NR+CoReg	7182	NR2C2	CACACGTCACATTTAAGCTAA	SI00661332	Hs_NR2C2_4
NR+CoReg	7182	NR2C2	CCCACGTTTGTGGCAGACAAA	SI00661325	Hs_NR2C2_3
NR+CoReg	7182	NR2C2	TACCTTAGCTAAAGCACTTAA	SI00661311	Hs_NR2C2_1
NR+CoReg	7329	UBE2I	AAGGGATTGGTTTGGCAAGAA	SI00754551	Hs_UBE2I_1
NR+CoReg	7329	UBE2I	AAGGGTCCGAGCACAAGCCAA	SI04368420	Hs_UBE2I_9
NR+CoReg	7329	UBE2I	ACCACCATTATTTCACCCGAA	SI04185937	Hs_UBE2I_8
NR+CoReg	7329	UBE2I	CAAGAAGTTTGCGCCCTCATA	SI03156699	Hs_UBE2I_6
NR+CoReg	7337	UBE3A	CAGACTGTGGTCTAAATACAA	SI02623502	Hs_UBE3A_5
NR+CoReg	7337	UBE3A	CCAGATTGCTCTCTAATGAAA	SI02623509	Hs_UBE3A_6
NR+CoReg	7337	UBE3A	CTCGAGCTTTATAAGATTAAT	SI00149919	Hs_UBE3A_1
NR+CoReg	7337	UBE3A	TTCCATATTGTGATAAGGTAA	SI02623516	Hs_UBE3A_7
NR+CoReg	7341	SUMO1	CAGGTTGAAGTCAAGATGACA	SI00051121	Hs_SUMO1_2
NR+CoReg	7341	SUMO1	CAGTTACCTAATCATGTTGAA	SI00051135	Hs_SUMO1_4
NR+CoReg	7341	SUMO1	CTGAAGTGCCTTCTGAATCAA	SI00051128	Hs_SUMO1_3
NR+CoReg	7341	SUMO1	CTGAATCAAGGATTTAATTAA	SI00051114	Hs_SUMO1_1
NR+CoReg	7376	NR1H2	ATCGTGGACTTCGCTAAGCAA	SI00094794	Hs_NR1H2_2
NR+CoReg	7376	NR1H2	CAGCGGCTCAAGAACTAATGA	SI03067407	Hs_NR1H2_5
NR+CoReg	7376	NR1H2	CAGGGCAACAGGAGTAGTTCA	SI00094801	Hs_NR1H2_3
NR+CoReg	7376	NR1H2	CCGGAAGAAGAAGATTCGGAA	SI00094787	Hs_NR1H2_1
NR+CoReg	7421	VDR	CCGCGTCAGTGACGTGACCAA	SI00008211	Hs_VDR_1
NR+CoReg	7421	VDR	CTCAATGTGAATCAGACCCTA	SI04437489	Hs_VDR_12
NR+CoReg	7421	VDR	TACCACTGATTTGGAGATATT	SI03649163	Hs_VDR_8
NR+CoReg	7421	VDR	TCAGACTCCATTTGTATTATA	SI03649177	Hs_VDR_9

NR+CoReg	8013	NR4A3	AAGAAGTTGTCCGTACAGATA	SI03031161	Hs_NR4A3_5
NR+CoReg	8013	NR4A3	ACCGATGTCAGTACTGTCGAT	SI03039939	Hs_NR4A3_6
NR+CoReg	8013	NR4A3	CAGTACCTTCGTGGAGGGCTA	SI03072685	Hs_NR4A3_7
NR+CoReg	8013	NR4A3	CTCGAGCAACTACGAACTCAA	SI00093541	Hs_NR4A3_2
NR+CoReg	8031	NCOA4	AAGAGAAGTGGTTATATCGAA	SI00077217	Hs_NCOA4_4
NR+CoReg	8031	NCOA4	ACCGACTAAGCAAATAGGCAA	SI02780806	Hs_NCOA4_5
NR+CoReg	8031	NCOA4	CCCACGTTAGTTCTACATTAT	SI00077210	Hs_NCOA4_3
NR+CoReg	8031	NCOA4	CTGGTCAATAGTGATTACCAA	SI00077196	Hs_NCOA4_1
NR+CoReg	8085	MLL2	CACCAGCATGTCTAAGGCATA	SI00052465	Hs_MLL2_4
NR+CoReg	8085	MLL2	CCCGTTGAGTCCCATAGGGAA	SI00052451	Hs_MLL2_2
NR+CoReg	8085	MLL2	CGGCCGGAGTTTGTAATCAAA	SI00052444	Hs_MLL2_1
NR+CoReg	8085	MLL2	CTCGGAGTGGTTTGAGAACTA	SI00052458	Hs_MLL2_3
NR+CoReg	8202	NCOA3	AAGGTTGTCAATATAGATACA	SI00089376	Hs_NCOA3_2
NR+CoReg	8202	NCOA3	CAGGAGGAGATTATAATACTT	SI00089369	Hs_NCOA3_1
NR+CoReg	8202	NCOA3	CAGGATTATATGGACAGACAT	SI00089383	Hs_NCOA3_3
NR+CoReg	8202	NCOA3	CCGACAGGCACTTGAATTGAA	SI00089390	Hs_NCOA3_4
NR+CoReg	8204	NRIP1	AACCAACCCAATACTATATTA	SI00052570	Hs_NRIP1_3
NR+CoReg	8204	NRIP1	AACCGATAGGTATGATTGATA	SI03028725	Hs_NRIP1_6
NR+CoReg	8204	NRIP1	AAGAATGGTCTGCTAAGTCGA	SI03031245	Hs_NRIP1_7
NR+CoReg	8204	NRIP1	AAGCGTGCTAACGATAAAGAA	SI00052563	Hs_NRIP1_2
NR+CoReg	8295	TRRAP	AAGATTCGACAGCAAGTTAAA	SI00052584	Hs_TRRAP_1
NR+CoReg	8295	TRRAP	ATCGAGGAAATACTTAGCCAA	SI00052605	Hs_TRRAP_4
NR+CoReg	8295	TRRAP	CAGACCTTTGTAACAAGTGTA	SI00052598	Hs_TRRAP_3
NR+CoReg	8295	TRRAP	CTGGCGCACATTATCGCCAAA	SI00052591	Hs_TRRAP_2
NR+CoReg	8431	NR0B2	AAGGAATATGCCTGCCTGAAA	SI02757678	Hs_NR0B2_6

NR+CoReg	8431	NR0B2	AGGCTGCTTATTGGACCAGAA	SI00131838	Hs_NR0B2_4
NR+CoReg	8431	NR0B2	CCCGGTGCCCAGCATACTCAA	SI00131831	Hs_NR0B2_3
NR+CoReg	8431	NR0B2	TCCTATCGACTTTATACAGAA	SI02644964	Hs_NR0B2_5
NR+CoReg	8554	PIAS1	AAGCACGGACGCAAACACGAA	SI02641968	Hs_PIAS1_6
NR+CoReg	8554	PIAS1	AGGCTCCATATGAACACCTTA	SI02641975	Hs_PIAS1_7
NR+CoReg	8554	PIAS1	CCGGATCATTCTAGAGCTTTA	SI00113974	Hs_PIAS1_1
NR+CoReg	8554	PIAS1	TTGGGCACCGATGAGATCAAA	SI03025274	Hs_PIAS1_8
NR+CoReg	8648	NCOA1	CAGCAGCTACTGACTGAATAA	SI02631797	Hs_NCOA1_16
NR+CoReg	8648	NCOA1	CAGCGGGAACTGTACAGTCAA	SI00055342	Hs_NCOA1_1
NR+CoReg	8648	NCOA1	CCCGAGTAAATCCCTCGGTCA	SI03077669	Hs_NCOA1_17
NR+CoReg	8648	NCOA1	CTCCTAATATTTCGACATTAA	SI02631783	Hs_NCOA1_14
NR+CoReg	8819	SAP30	AAAGCACAACTTGTTGAGATA	SI00710605	Hs_SAP30_3
NR+CoReg	8819	SAP30	CCAGAGGTTGATTTATACCAA	SI00710591	Hs_SAP30_1
NR+CoReg	8819	SAP30	GACGTGGAATTGAGACTAATA	SI00710598	Hs_SAP30_2
NR+CoReg	8819	SAP30	TCGGGAGCTCGGAGACATGAA	SI00710612	Hs_SAP30_4
NR+CoReg	8841	HDAC3	CACCCGCATCGAGAATCAGAA	SI03057901	Hs_HDAC3_6
NR+CoReg	8841	HDAC3	CAGCCGGTTATCAACCAGGTA	SI00057316	Hs_HDAC3_1
NR+CoReg	8841	HDAC3	CAGGTAGTGGACTTCTACCAA	SI00057323	Hs_HDAC3_2
NR+CoReg	8841	HDAC3	GACCATGACAATGACAAGGAA	SI00057337	Hs_HDAC3_4
NR+CoReg	8856	NR1I2	CAGGAGCAATTCGCCATTACT	SI03069535	Hs_NR1I2_5
NR+CoReg	8856	NR1I2	CAGGAGGGCCATGAAACGCAA	SI00057456	Hs_NR1I2_1
NR+CoReg	8856	NR1I2	CAGGAGTTGTTCGGCATCACA	SI03069745	Hs_NR1I2_6
NR+CoReg	8856	NR1I2	CTGGCTATCACTTCAATGTCA	SI03098298	Hs_NR1I2_7
NR+CoReg	9112	MTA1	CAGCATCATTGAGTACTACTA	SI00067130	Hs_MTA1_1
NR+CoReg	9112	MTA1	CAGGGTCGGAGACTACGTCTA	SI02633736	Hs_MTA1_5

NR+CoReg	9112	MTA1	GCGCATCTTGTTGGACATATT	SI02757699	Hs_MTA1_6
NR+CoReg	9112	MTA1	TTGGACATATTGGAAGAAATA	SI00067151	Hs_MTA1_4
NR+CoReg	9219	MTA2	ACGCCAGTTCTCAGAAATAAA	SI00067774	Hs_MTA2_1
NR+CoReg	9219	MTA2	ACGGCCTTATGCTCCTATCAA	SI00067781	Hs_MTA2_2
NR+CoReg	9219	MTA2	CAGCCAAGCGTCAGAAACTAA	SI02780834	Hs_MTA2_5
NR+CoReg	9219	MTA2	TAGACGGATTGAGGAGCTCAA	SI00067788	Hs_MTA2_3
NR+CoReg	9439	MED23	AAGGGTGTTCGAGATCTCTTA	SI00068943	Hs_CRSP3_2
NR+CoReg	9439	MED23	CCGCGCATTTCTCAAACGAAA	SI00068936	Hs_CRSP3_1
NR+CoReg	9439	MED23	CTGGATCATCTAGGAGGCTTA	SI00068950	Hs_CRSP3_3
NR+CoReg	9439	MED23	TTCCAGTATTTGATATAGTAA	SI00112847	Hs_CRSP3_5
NR+CoReg	9572	NR1D1	CAGCGTCATAACGAGGCCCTA	SI00130928	Hs_NR1D1_1
NR+CoReg	9572	NR1D1	CTCCGTTGCCTCAACGTCCAA	SI00130935	Hs_NR1D1_2
NR+CoReg	9572	NR1D1	GAGGTGGTAGAGTTTGCCAAA	SI03104269	Hs_NR1D1_5
NR+CoReg	9572	NR1D1	TGCTTCGTTGTTCAACGTGAA	SI03119214	Hs_NR1D1_6
NR+CoReg	9584	RBM39	AGAGAACCTATTGATAATTTA	SI04213741	Hs_RBM39_2
NR+CoReg	9584	RBM39	CAGACCAGGGATGTAATGTTT	SI03167367	Hs_RNPC2_5
NR+CoReg	9584	RBM39	CAGCAGCAATCTCTTCCCGAA	SI04166771	Hs_RBM39_1
NR+CoReg	9584	RBM39	CCTGAAGATGTTTAAACGTGA	SI04371885	Hs_RBM39_3
NR+CoReg	9611	NCOR1	ACCGCAGTATTGTCCAAATTA	SI02780862	Hs_NCOR1_5
NR+CoReg	9611	NCOR1	AGGCAATTCAGTGGACTATAA	SI00087304	Hs_NCOR1_2
NR+CoReg	9611	NCOR1	CCCGCTCACCAGGGAGTATAA	SI00087297	Hs_NCOR1_1
NR+CoReg	9611	NCOR1	CCCGGTGGTTTCCTAGAAACA	SI00087318	Hs_NCOR1_4
NR+CoReg	9612	NCOR2	AACGAGATTGCTGGAAACCAA	SI00087325	Hs_NCOR2_1
NR+CoReg	9612	NCOR2	AAGGGCCACGTCATCTACGAA	SI03035970	Hs_NCOR2_6
NR+CoReg	9612	NCOR2	CACCCGCTCAATGGCTAATGA	SI03057936	Hs_NCOR2_7

NR+CoReg	9612	NCOR2	CAGAATGAATTC GATGCGTAT	SI00087 339	Hs_NCOR2_3
NR+CoReg	9759	HDAC4	ACGGTTTATTCT GATTGAGAA	SI02636 536	Hs_HDAC4_5
NR+CoReg	9759	HDAC4	CCGGCGTGGGT TTCAACGTCA	SI03082 282	Hs_HDAC4_7
NR+CoReg	9759	HDAC4	TTCCAATGTATT CCAAGCTAA	SI00083 951	Hs_HDAC4_3
NR+CoReg	9759	HDAC4	TTGCGTCTTATT GAACTTATT	SI00083 958	Hs_HDAC4_4
NR+CoReg	9862	MED24	AACCTTATGGCT AAGCGCAAA	SI04384 842	Hs_THRAP4_8
NR+CoReg	9862	MED24	ATCGAGCATTCT CTCTTGAAA	SI00108 297	Hs_THRAP4_1
NR+CoReg	9862	MED24	CACCGCGAAGA CATTGAGGAT	SI03058 419	Hs_THRAP4_7
NR+CoReg	9862	MED24	CGGCGTCTACTG GTTCTGCAA	SI00108 304	Hs_THRAP4_2
NR+CoReg	9970	NR1I3	AACACCTGTGCA ACTGAGTAA	SI03027 479	Hs_NR1I3_5
NR+CoReg	9970	NR1I3	CACACACTTCGC AGACATCAA	SI00072 709	Hs_NR1I3_1
NR+CoReg	9970	NR1I3	GCGGGCCTCTT CGCTACACAA	SI04951 947	Hs_NR1I3_9
NR+CoReg	9970	NR1I3	TGCAGGTGACAT GCTGCCTAA	SI03117 905	Hs_NR1I3_6
NR+CoReg	9971	NR1H4	AAGTGTCAAGAG TGTCGACTA	SI03037 055	Hs_NR1H4_5
NR+CoReg	9971	NR1H4	CCGACTTATCCT AATGCGAAA	SI00072 737	Hs_NR1H4_1
NR+CoReg	9971	NR1H4	CTGGGTCGCCT GACTGAATTA	SI03099 208	Hs_NR1H4_6
NR+CoReg	9971	NR1H4	GACAAGTGACCT CGACAACAA	SI03101 224	Hs_NR1H4_7
NR+CoReg	9975	NR1D2	ATGGTACGGTTC GCATCATTA	SI03051 965	Hs_NR1D2_6
NR+CoReg	9975	NR1D2	TGCCAGATCTTC GATCTTTAA	SI00072 814	Hs_NR1D2_4
NR+CoReg	9975	NR1D2	TTCGTGCACTAA GGACCTTAA	SI03023 216	Hs_NR1D2_5
NR+CoReg	9975	NR1D2	TTGGTGGGACAC TGTTGATTA	SI05146 771	Hs_NR1D2_10
NR+CoReg	10002	NR2E3	CACGGAGTTTGC CTGCATGAA	SI00115 577	Hs_NR2E3_1
NR+CoReg	10002	NR2E3	CACTTCATGGCC AGCCTTATA	SI03062 521	Hs_NR2E3_8
NR+CoReg	10002	NR2E3	CAGCAGCAGCG GGAAGCACTA	SI03065 629	Hs_NR2E3_9
NR+CoReg	10002	NR2E3	CTGAAGGATCCT GAGCACGTA	SI03092 901	Hs_NR2E3_10

NR+CoReg	10011	SRA1	CAGGCGCTCGC TGCTTACCAA	SI02785 510	Hs_SRA1_2
NR+CoReg	10011	SRA1	CAGGGAAACGA ACAAGAGTCA	SI04248 853	Hs_SRA1_6
NR+CoReg	10011	SRA1	CAGGGCCCTGA TGGTTCATTA	SI02785 517	Hs_SRA1_3
NR+CoReg	10011	SRA1	CCCGACGGTTGT GAACCAGCA	SI04298 511	Hs_SRA1_7
NR+CoReg	10062	NR1H3	CAGGAGTGTCG GCTTCGCAAA	SI00080 430	Hs_NR1H3_4
NR+CoReg	10062	NR1H3	CATGAATGAGCT GCAACTCAA	SI00080 416	Hs_NR1H3_2
NR+CoReg	10062	NR1H3	CCCACAGAGATC CGTCCACAA	SI00080 409	Hs_NR1H3_1
NR+CoReg	10062	NR1H3	CTGCAGCACACA TATGTGGAA	SI04952 052	Hs_NR1H3_7
NR+CoReg	10197	PSME3	CACCCATGGATC GTAATGTAA	SI04339 615	Hs_PSME3_8
NR+CoReg	10197	PSME3	CACCGTGACAG AGATTGATGA	SI04263 714	Hs_PSME3_7
NR+CoReg	10197	PSME3	CCCACGAATAGT ACTCAGTAA	SI00695 093	Hs_PSME3_3
NR+CoReg	10197	PSME3	CTGGACCAGATT TCTAGATAT	SI04169 809	Hs_PSME3_6
NR+CoReg	10401	PIAS3	AAGGGTTAATAT TTAACCTCT	SI04203 682	Hs_PIAS3_8
NR+CoReg	10401	PIAS3	CAGAGCAAAGG GTATCCGGAA	SI04277 665	Hs_PIAS3_9
NR+CoReg	10401	PIAS3	TAGTGAAGCTCT CACCCATAA	SI04173 757	Hs_PIAS3_7
NR+CoReg	10401	PIAS3	TGGACTGAGTTC CCTGGATTA	SI04167 212	Hs_PIAS3_6
NR+CoReg	10432	RBM14	AACAGTTCGCCT TCGTGCACA	SI00301 665	Hs_RBM14_5
NR+CoReg	10432	RBM14	CACGCTATTCGG GCTCCTATA	SI02637 229	Hs_RBM14_6
NR+CoReg	10432	RBM14	CTCTCTGATTAC CGCCGTTTA	SI03092 467	Hs_RBM14_10
NR+CoReg	10432	RBM14	TAGGGTTACAGA TCCAGGTTA	SI02637 236	Hs_RBM14_7
NR+CoReg	10498	CARM1	AGGGTTCACCTC ACACTTGAA	SI00164 486	Hs_CARM1_3
NR+CoReg	10498	CARM1	CACAACAACCTG ATTCCTTTA	SI02663 822	Hs_CARM1_6
NR+CoReg	10498	CARM1	CAGGATAGAAAT CCCATTCAA	SI02663 815	Hs_CARM1_5
NR+CoReg	10498	CARM1	CTCGGCGGGCA TCGCCCTCTA	SI04438 658	Hs_CARM1_10
NR+CoReg	10499	NCOA2	AAGGATTGGCAT TCAGTCAAA	SI00089 516	Hs_NCOA2_2

NR+CoReg	10499	NCOA2	ACAGTGCTTCTCGGCCTACTA	SI03038049	Hs_NCOA2_5
NR+CoReg	10499	NCOA2	AGGGCTGTTAACATTAGCAAA	SI00089509	Hs_NCOA2_1
NR+CoReg	10499	NCOA2	CCAGGAATGATGGGTAATCAA	SI00089523	Hs_NCOA2_3
NR+CoReg	10891	PPARGC1A	AAGACTCTAGACAACTAGAAA	SI00101024	Hs_PPARGC1A_1
NR+CoReg	10891	PPARGC1A	ATCGAGATTTAGTAAATCCTA	SI00101031	Hs_PPARGC1A_2
NR+CoReg	10891	PPARGC1A	CTGGAAGACATGATACACCTA	SI02639833	Hs_PPARGC1A_6
NR+CoReg	10891	PPARGC1A	TAGAATAGCCATGTACTATAA	SI02639826	Hs_PPARGC1A_5
NR+CoReg	11315	PARK7	AATGGAGGTCATTACACCTAC	SI00301091	Hs_PARK7_5
NR+CoReg	11315	PARK7	CACCCTCTTGCTAAAGACAAA	SI00095956	Hs_PARK7_3
NR+CoReg	11315	PARK7	CAGGCTTGTAAACATATAACA	SI02662107	Hs_PARK7_6
NR+CoReg	11315	PARK7	TGCGACGATCACTTAGAGAAA	SI02662646	Hs_PARK7_7
NR+CoReg	11331	PHB2	AACCCAGGAATTCTCAATAAA	SI02780918	Hs_PHB2_1
NR+CoReg	11331	PHB2	CAGCCTCATCAAGGGTAAGAA	SI03066504	Hs_PHB2_2
NR+CoReg	11331	PHB2	CTGGATGATGTGGCCATCACA	SI03097633	Hs_PHB2_3
NR+CoReg	11331	PHB2	TCGCCACATCACAGAATCGTA	SI00096131	Hs_REA_4
NR+CoReg	23028	KDM1A	ACATCTTACCTTAGTCATCAA	SI00109102	Hs_AOF2_2
NR+CoReg	23028	KDM1A	AGGCCTAGACATTAAACTGAA	SI02781177	Hs_AOF2_6
NR+CoReg	23028	KDM1A	CACAGGGATCTGACCGCCCTA	SI04439043	Hs_AOF2_10
NR+CoReg	23028	KDM1A	CTGGAAATGACTATGATTTAA	SI02780932	Hs_AOF2_5
NR+CoReg	23054	NCOA6	AAGGAGCTAATGCCATTATAA	SI02640225	Hs_NCOA6_7
NR+CoReg	23054	NCOA6	CAGCGTGCGTGTGACATTCAA	SI02655485	Hs_NCOA6_8
NR+CoReg	23054	NCOA6	CCACAGATTAATATTCCTTTA	SI02640218	Hs_NCOA6_6
NR+CoReg	23054	NCOA6	CCAGTGTACGCTCGATAGTAA	SI03075744	Hs_NCOA6_10
NR+CoReg	23309	SIN3B	CAAGATGGTGTTCATCGTGAA	SI00719089	Hs_SIN3B_3
NR+CoReg	23309	SIN3B	CACGTTCGTCAGCTCCAAGAA	SI04172077	Hs_SIN3B_5

NR+CoReg	23309	SIN3B	CAGCTATGTGAA TAAGATTAA	SI00719 082	Hs_SIN3B_2
NR+CoReg	23309	SIN3B	CCGCTGCATCG CACTCTTCAA	SI00719 096	Hs_SIN3B_4
NR+CoReg	27043	PELP1	CAAGGTGTATGC GATATTAGA	SI00105 532	Hs_PELP1_1
NR+CoReg	27043	PELP1	CACGGTTCGGA CCAAGGTGTA	SI00105 539	Hs_PELP1_2
NR+CoReg	27043	PELP1	CGGGCTTGTGG TTCTCTCAAA	SI02640 498	Hs_PELP1_5
NR+CoReg	27043	PELP1	TTGGTGAGTCTC AGTAATGCA	SI00105 553	Hs_PELP1_4
NR+CoReg	29843	SENP1	AAGCATTTCGCC TGACCATTA	SI00106 743	Hs_SENP1_3
NR+CoReg	29843	SENP1	CAGAGGCGACA TGTTAGTACA	SI00106 750	Hs_SENP1_4
NR+CoReg	29843	SENP1	TCGATTTGGACT ATGAATCAA	SI00106 736	Hs_SENP1_2
NR+CoReg	29843	SENP1	TCGCCTGACCAT TACACGCAA	SI00106 729	Hs_SENP1_1
NR+CoReg	51588	PIAS4	CACCGAATTAGT CCCACAGAA	SI00684 453	Hs_PIAS4_3
NR+CoReg	51588	PIAS4	CCCGCCCAACAT CGCTGTGAA	SI00684 446	Hs_PIAS4_2
NR+CoReg	51588	PIAS4	CCGGAACTCCA GGGAACTGCA	SI04131 498	Hs_PIAS4_5
NR+CoReg	51588	PIAS4	TAGCCCTGAGCT GTTCAAGAA	SI04347 644	Hs_PIAS4_6
NR+CoReg	51780	KDM3B	ACCGAAGGGTC TAGCCTTCGA	SI04135 411	Hs_JMJD1B_5
NR+CoReg	51780	KDM3B	ATGGATAATTCA ACGCCTCAA	SI04197 172	Hs_JMJD1B_6
NR+CoReg	51780	KDM3B	CTGGGATGGTTT CGAGATCAT	SI04270 357	Hs_JMJD1B_7
NR+CoReg	51780	KDM3B	TGGAGCGGTAC CGGAAGTTTA	SI04277 385	Hs_JMJD1B_8
NR+CoReg	55611	OTUB1	CACTACGATATC CTCTACAAA	SI00676 053	Hs_OTUB1_3
NR+CoReg	55611	OTUB1	CAGCAGGACCG AATTCAGCAA	SI00676 039	Hs_OTUB1_1
NR+CoReg	55611	OTUB1	CTCCGACTACCT TGTGGTCTA	SI04168 038	Hs_OTUB1_5
NR+CoReg	55611	OTUB1	CTGCCAGGCGC TAGACATGTA	SI00676 060	Hs_OTUB1_4
NR+CoReg	55818	KDM3A	AAGATCGGAAAT ATGGAACAA	SI04343 626	Hs_JMJD1A_6
NR+CoReg	55818	KDM3A	CACGATCCTATT CATGATCAA	SI00449 715	Hs_JMJD1A_2
NR+CoReg	55818	KDM3A	CAGGAGGTTACA ATTCAACAA	SI00449 722	Hs_JMJD1A_3

NR+CoReg	55818	KDM3A	CAGGATGTAAACAGTCTTCGA	SI04139002	Hs_JMJD1A_5
NR+CoReg	80324	PUS1	CACGGGCGGGTTTAACTCCAA	SI00696143	Hs_PUS1_1
NR+CoReg	80324	PUS1	CCCGGCCATGCCGGCGTTGTA	SI04263434	Hs_PUS1_6
NR+CoReg	80324	PUS1	CTGATTGACGACATTCTAGAA	SI00696164	Hs_PUS1_4
NR+CoReg	80324	PUS1	CTGGAGATGTACTGCGAGGAA	SI04195317	Hs_PUS1_5
NR+CoReg	90665	TBL1Y	AGAGGCTGAGATAAGCATCAA	SI04265359	Hs_TBL1Y_8
NR+CoReg	90665	TBL1Y	CACGACGTCCCAAGTAATAAA	SI00740439	Hs_TBL1Y_1
NR+CoReg	90665	TBL1Y	CTGGTTCAGCCTGGAAGGCGA	SI04191460	Hs_TBL1Y_6
NR+CoReg	90665	TBL1Y	TTCTGGATCTGTGAAAGTAAA	SI04209555	Hs_TBL1Y_7
NR+CoReg	133522	PPARGC1B	AGCCGAAGTTGTACAGAACTA	SI03043306	Hs_PPARGC1B_7
NR+CoReg	133522	PPARGC1B	CACCCGTGAGAGAGACTTGAA	SI02647911	Hs_PPARGC1B_6
NR+CoReg	133522	PPARGC1B	CAGGCGATGGTGCAACTCATA	SI00150024	Hs_PPARGC1B_2
NR+CoReg	133522	PPARGC1B	GAGGGCCGTGTTCAGACAGAA	SI03104031	Hs_PPARGC1B_8
NR+CoReg	221037	JMJD1C	AAGGGCTCAGATAGCAGTATA	SI02632798	Hs_JMJD1C_6
NR+CoReg	221037	JMJD1C	CTGCTGTGAGATAGGGCCTAA	SI04908547	Hs_JMJD1C_7
NR+CoReg	221037	JMJD1C	CTGGGATTACTTAACCTTGAA	SI02632791	Hs_JMJD1C_5
NR+CoReg	221037	JMJD1C	TAGCCGGATCATCTAGTCAAA	SI04909730	Hs_JMJD1C_8

APPENDIX B
DE Genes After Compound B Treatment in H2009 and H596

DE gene	Cell Line	log2(fold_change)	p_value	q_value
MYBPH	H2009	5.0678	5.00E-05	0.00025
MAP2K6	H2009	4.07096	0.00145	0.005381
ZBED2	H2009	3.78839	0.0038	0.012649
C11orf86	H2009	3.71072	0.00015	0.000695
FGFBP1	H2009	3.59612	5.00E-05	0.00025
PWARSN,SNORD107	H2009	3.53975	5.00E-05	0.00025
MMP1	H2009	3.41185	0.00865	0.026076
GRHL3	H2009	3.39656	0.00065	0.002626
PWAR5	H2009	3.06906	5.00E-05	0.00025
BTN3A2	H2009	2.98794	5.00E-05	0.00025
C14orf23	H2009	2.96119	5.00E-05	0.00025
CAPN8	H2009	2.94104	5.00E-05	0.00025
MIR205HG	H2009	2.92369	0.0028	0.009662
MMP13	H2009	2.91933	5.00E-05	0.00025
RAB3A	H2009	2.87485	5.00E-05	0.00025
SARS2	H2009	2.8716	0.00015	0.000695
EYA1	H2009	2.86026	5.00E-05	0.00025
METTL7A	H2009	2.72078	5.00E-05	0.00025
PRICKLE1	H2009	2.71378	5.00E-05	0.00025
TJP3	H2009	2.6759	0.00885	0.026596
SPRR3	H2009	2.65743	0.0053	0.016948
PFAS	H2009	2.62878	5.00E-05	0.00025
FAM13C	H2009	2.62213	5.00E-05	0.00025
LOC102723373	H2009	2.58379	0.00035	0.001505
BTN3A1	H2009	2.49932	5.00E-05	0.00025
LY6D	H2009	2.47329	5.00E-05	0.00025
IFI44	H2009	2.4542	5.00E-05	0.00025
TMEM144	H2009	2.44823	5.00E-05	0.00025
CPA4	H2009	2.43733	5.00E-05	0.00025
MKRN2OS	H2009	2.42022	5.00E-05	0.00025
ZBTB12	H2009	2.41793	5.00E-05	0.00025
ZNF586	H2009	2.40002	5.00E-05	0.00025
OR2A4	H2009	2.38673	0.0004	0.001697
GJA1	H2009	2.38226	5.00E-05	0.00025
GPX8	H2009	2.36881	5.00E-05	0.00025
FAM178B	H2009	2.36448	0.00015	0.000695
KAT5	H2009	2.30319	0.00015	0.000695
SLITRK6	H2009	2.28686	5.00E-05	0.00025
KRT13	H2009	2.27408	5.00E-05	0.00025

DDX39A	H2009	2.27225	5.00E-05	0.00025
PCDHB5	H2009	2.238	5.00E-05	0.00025
ASB9	H2009	2.23084	5.00E-05	0.00025
EDN2	H2009	2.21207	5.00E-05	0.00025
HNRNPD	H2009	2.19009	5.00E-05	0.00025
TNFSF12	H2009	2.18752	0.00465	0.015107
ZNF784	H2009	2.1651	5.00E-05	0.00025
CCDC94	H2009	2.16063	5.00E-05	0.00025
C4orf19	H2009	2.14799	0.016	0.044598
GLYCTK	H2009	2.14113	5.00E-05	0.00025
HNRNPDL	H2009	2.13297	5.00E-05	0.00025
HNRNPA1	H2009	2.10774	5.00E-05	0.00025
CAMKK1	H2009	2.10745	5.00E-05	0.00025
IFIT3	H2009	2.10606	5.00E-05	0.00025
LOC102288414	H2009	2.10431	5.00E-05	0.00025
PRR5	H2009	2.10079	0.00705	0.021771
FUBP1	H2009	2.09427	5.00E-05	0.00025
SNHG3	H2009	2.09029	0.00125	0.004713
MRPL54	H2009	2.07366	5.00E-05	0.00025
CUTC	H2009	2.07256	0.00455	0.014823
PCDHB8	H2009	2.06544	5.00E-05	0.00025
SNHG8	H2009	2.05476	5.00E-05	0.00025
SOX2	H2009	2.05382	5.00E-05	0.00025
SNRPA	H2009	2.0537	5.00E-05	0.00025
VIM	H2009	2.05166	5.00E-05	0.00025
LINC00525	H2009	2.05158	5.00E-05	0.00025
RFXAP	H2009	2.04154	5.00E-05	0.00025
H19	H2009	2.02011	5.00E-05	0.00025
DDIT4	H2009	2.00811	5.00E-05	0.00025
SPRY1	H2009	2.00358	5.00E-05	0.00025
SNHG1	H2009	2.00171	5.00E-05	0.00025
RNF223	H2009	1.99843	5.00E-05	0.00025
SH2B2	H2009	1.99588	5.00E-05	0.00025
MIR210HG	H2009	1.98985	5.00E-05	0.00025
ZNF587B	H2009	1.98628	5.00E-05	0.00025
PRR15	H2009	1.96552	5.00E-05	0.00025
C2orf54	H2009	1.95727	5.00E-05	0.00025
SFTA3	H2009	1.95453	5.00E-05	0.00025
PTGES	H2009	1.95279	5.00E-05	0.00025
ING3	H2009	1.94986	5.00E-05	0.00025
CCDC23	H2009	1.94911	5.00E-05	0.00025
TADA1	H2009	1.94476	5.00E-05	0.00025
XKR8	H2009	1.94201	5.00E-05	0.00025

TRMT10A	H2009	1.93543	5.00E-05	0.00025
SNRNP35	H2009	1.9298	5.00E-05	0.00025
C10orf91	H2009	1.9194	5.00E-05	0.00025
DTWD2	H2009	1.91776	5.00E-05	0.00025
SAP25	H2009	1.91645	5.00E-05	0.00025
NKX2-1	H2009	1.91642	5.00E-05	0.00025
DFFB	H2009	1.91308	5.00E-05	0.00025
LOC100506178	H2009	1.90471	5.00E-05	0.00025
TMEM126A	H2009	1.90283	5.00E-05	0.00025
FCHO1	H2009	1.89627	5.00E-05	0.00025
RASSF10	H2009	1.89358	5.00E-05	0.00025
RPP40	H2009	1.89161	5.00E-05	0.00025
UTP18	H2009	1.88597	5.00E-05	0.00025
TBCE	H2009	1.8816	0.0079	0.024065
SDPR	H2009	1.88068	5.00E-05	0.00025
KPTN	H2009	1.87699	5.00E-05	0.00025
IGSF9	H2009	1.86942	5.00E-05	0.00025
RBMX	H2009	1.86878	5.00E-05	0.00025
LOC101448202	H2009	1.86571	5.00E-05	0.00025
NOV	H2009	1.86483	5.00E-05	0.00025
CDPF1	H2009	1.85633	5.00E-05	0.00025
HNRNPH3	H2009	1.84792	5.00E-05	0.00025
FAM26F	H2009	1.84395	0.01825	0.04987
FXN	H2009	1.83555	5.00E-05	0.00025
PCDHB13	H2009	1.82861	5.00E-05	0.00025
HNRNPA1P10	H2009	1.82802	0.00475	0.015392
PDCD2L	H2009	1.82602	5.00E-05	0.00025
C11orf54	H2009	1.82448	5.00E-05	0.00025
CLPB	H2009	1.81875	5.00E-05	0.00025
GTF2H2B	H2009	1.81307	5.00E-05	0.00025
RASGEF1A	H2009	1.81219	5.00E-05	0.00025
LOC101927446	H2009	1.8115	5.00E-05	0.00025
ACP5	H2009	1.81077	5.00E-05	0.00025
ZBTB22	H2009	1.80558	5.00E-05	0.00025
JDP2	H2009	1.80282	5.00E-05	0.00025
PDK1	H2009	1.80273	5.00E-05	0.00025
COQ3	H2009	1.80262	5.00E-05	0.00025
LOC101927934	H2009	1.79984	0.00065	0.002626
TFAP4	H2009	1.79693	5.00E-05	0.00025
NTHL1	H2009	1.78951	5.00E-05	0.00025
PEMT	H2009	1.78917	5.00E-05	0.00025
EMG1	H2009	1.77861	5.00E-05	0.00025
ARNTL	H2009	1.77851	5.00E-05	0.00025

TMBIM4	H2009	1.76871	5.00E-05	0.00025
BMP4	H2009	1.75915	5.00E-05	0.00025
PARP2	H2009	1.75841	5.00E-05	0.00025
ROR1	H2009	1.75302	5.00E-05	0.00025
SMIM11	H2009	1.75046	5.00E-05	0.00025
FUT3	H2009	1.74741	5.00E-05	0.00025
LINC01214	H2009	1.74723	0.0021	0.007487
DBP	H2009	1.7405	5.00E-05	0.00025
CIART	H2009	1.73985	5.00E-05	0.00025
TUBB2B	H2009	1.7386	5.00E-05	0.00025
PRSS1	H2009	1.72647	0.0014	0.005217
EXOSC8	H2009	1.72628	0.0002	0.000905
PAK1IP1	H2009	1.7144	5.00E-05	0.00025
RBMXL1	H2009	1.71101	5.00E-05	0.00025
TIMP4	H2009	1.70859	0.0003	0.001308
KHK	H2009	1.70765	0.01295	0.037085
UBXN8	H2009	1.70622	5.00E-05	0.00025
PDE9A	H2009	1.70582	5.00E-05	0.00025
CHEK2	H2009	1.70457	5.00E-05	0.00025
ZNF692	H2009	1.70114	5.00E-05	0.00025
SLC27A2	H2009	1.70035	5.00E-05	0.00025
SMIM7	H2009	1.6993	5.00E-05	0.00025
TOP1MT	H2009	1.6974	5.00E-05	0.00025
IPW	H2009	1.69701	5.00E-05	0.00025
TNFAIP8L1	H2009	1.69663	5.00E-05	0.00025
LINC00704	H2009	1.6952	5.00E-05	0.00025
KIAA0020	H2009	1.69197	5.00E-05	0.00025
ECSIT	H2009	1.69021	5.00E-05	0.00025
TBL1X	H2009	1.68776	5.00E-05	0.00025
TSEN2	H2009	1.67658	5.00E-05	0.00025
TSEN15	H2009	1.67423	5.00E-05	0.00025
ZBTB26	H2009	1.67323	5.00E-05	0.00025
DDX39B	H2009	1.66914	5.00E-05	0.00025
ANKRD1	H2009	1.66893	5.00E-05	0.00025
MIS18BP1	H2009	1.66867	5.00E-05	0.00025
ZNF628	H2009	1.66774	5.00E-05	0.00025
SAP30	H2009	1.66657	5.00E-05	0.00025
HS3ST1	H2009	1.66525	5.00E-05	0.00025
BDNF	H2009	1.65018	5.00E-05	0.00025
SYNE4	H2009	1.64594	5.00E-05	0.00025
HNRNPL	H2009	1.64099	5.00E-05	0.00025
UBE2D4	H2009	1.64008	0.00025	0.001109
TRIM16L	H2009	1.63789	5.00E-05	0.00025

ALX1	H2009	1.6351	0.0002	0.000905
TSPAN15	H2009	1.63356	5.00E-05	0.00025
MRPL27	H2009	1.63056	5.00E-05	0.00025
NKX2-8	H2009	1.62911	5.00E-05	0.00025
ALPP	H2009	1.62736	5.00E-05	0.00025
SLC7A11	H2009	1.62589	5.00E-05	0.00025
CST7	H2009	1.62554	5.00E-05	0.00025
S100A14	H2009	1.62187	5.00E-05	0.00025
DDRGK1	H2009	1.62116	5.00E-05	0.00025
IFIT1	H2009	1.61842	5.00E-05	0.00025
ZNF772	H2009	1.61402	5.00E-05	0.00025
SLC16A4	H2009	1.60871	0.00015	0.000695
UNK	H2009	1.60778	5.00E-05	0.00025
ATAD3B	H2009	1.6076	5.00E-05	0.00025
RASD2	H2009	1.60502	5.00E-05	0.00025
BCL9	H2009	1.60197	5.00E-05	0.00025
CCDC28B	H2009	1.59739	5.00E-05	0.00025
PUS7	H2009	1.59013	5.00E-05	0.00025
ZFP36L2	H2009	1.58767	5.00E-05	0.00025
KIF20B	H2009	1.58318	5.00E-05	0.00025
CLDN3	H2009	1.58009	5.00E-05	0.00025
PQBP1	H2009	1.57953	5.00E-05	0.00025
RGCC	H2009	1.57785	5.00E-05	0.00025
MMP9	H2009	1.57778	5.00E-05	0.00025
COQ7	H2009	1.57206	5.00E-05	0.00025
TBC1D30	H2009	1.57201	5.00E-05	0.00025
MRPL48	H2009	1.57092	5.00E-05	0.00025
MED11	H2009	1.57025	0.00025	0.001109
ADORA1	H2009	1.56665	5.00E-05	0.00025
CCDC58	H2009	1.56283	5.00E-05	0.00025
ZBTB8B	H2009	1.56262	5.00E-05	0.00025
TMEM53	H2009	1.56256	5.00E-05	0.00025
KRT16P3	H2009	1.55552	5.00E-05	0.00025
MTERFD1	H2009	1.55458	5.00E-05	0.00025
CEP135	H2009	1.55409	5.00E-05	0.00025
PLEKHA2	H2009	1.55207	5.00E-05	0.00025
LOC101927750	H2009	1.55127	0.0019	0.006852
TPTEP1	H2009	1.54758	0.0004	0.001697
RAC3	H2009	1.5471	5.00E-05	0.00025
TMEM223	H2009	1.5455	0.0001	0.000478
HILPDA	H2009	1.54462	5.00E-05	0.00025
RBBP8NL	H2009	1.53916	5.00E-05	0.00025
ANKMY2	H2009	1.53822	5.00E-05	0.00025

SP140	H2009	1.53801	0.0054	0.017231
CGREF1	H2009	1.52552	5.00E-05	0.00025
SOX12	H2009	1.5224	5.00E-05	0.00025
ZFAND4	H2009	1.52203	0.00015	0.000695
FGF11	H2009	1.52028	5.00E-05	0.00025
PCGF1	H2009	1.51625	0.001	0.003864
TMEM251	H2009	1.51403	5.00E-05	0.00025
CWC22	H2009	1.5139	5.00E-05	0.00025
PRDM1	H2009	1.50617	5.00E-05	0.00025
KRT16P1	H2009	1.50235	5.00E-05	0.00025
HSD3B7	H2009	1.50214	5.00E-05	0.00025
NUBP1	H2009	1.50184	5.00E-05	0.00025
LINC00960	H2009	1.50143	0.00075	0.002984
EXOC6	H2009	1.50108	5.00E-05	0.00025
KLHL35	H2009	1.5001	5.00E-05	0.00025
AKAP5	H2009	1.50002	5.00E-05	0.00025
ZNF608	H2009	1.49492	5.00E-05	0.00025
C1orf210	H2009	1.49445	5.00E-05	0.00025
PROCR	H2009	1.49319	5.00E-05	0.00025
C3orf33	H2009	1.48786	5.00E-05	0.00025
EMP3	H2009	1.48564	5.00E-05	0.00025
HBQ1	H2009	1.47556	0.0014	0.005217
DLEU2L	H2009	1.47218	0.00195	0.00701
EXOSC3	H2009	1.47033	5.00E-05	0.00025
TMEM125	H2009	1.46954	5.00E-05	0.00025
MPHOSPH10	H2009	1.46771	5.00E-05	0.00025
APOO	H2009	1.46473	5.00E-05	0.00025
SUOX	H2009	1.46023	5.00E-05	0.00025
PRG1	H2009	1.45702	0.0031	0.010574
SLC18B1	H2009	1.45597	5.00E-05	0.00025
DCTN6	H2009	1.45328	0.0104	0.030628
MRPS28	H2009	1.45254	5.00E-05	0.00025
RCC1	H2009	1.45243	5.00E-05	0.00025
FAM162A	H2009	1.45119	5.00E-05	0.00025
PITX2	H2009	1.45107	5.00E-05	0.00025
SLC25A10	H2009	1.44863	5.00E-05	0.00025
ELF3	H2009	1.44702	5.00E-05	0.00025
FAM195A	H2009	1.44699	5.00E-05	0.00025
TMC5	H2009	1.44386	5.00E-05	0.00025
HK2	H2009	1.44352	5.00E-05	0.00025
COIL	H2009	1.44043	5.00E-05	0.00025
NOL7	H2009	1.43706	5.00E-05	0.00025
MTFR2	H2009	1.433	5.00E-05	0.00025

ZFAT	H2009	1.43113	5.00E-05	0.00025
POLM	H2009	1.43053	5.00E-05	0.00025
NCF2	H2009	1.42903	5.00E-05	0.00025
KRT16P2	H2009	1.4286	5.00E-05	0.00025
MCRS1	H2009	1.42587	5.00E-05	0.00025
OVOL2	H2009	1.42365	5.00E-05	0.00025
TEX19	H2009	1.42278	5.00E-05	0.00025
TMEM39B	H2009	1.42057	5.00E-05	0.00025
FPGT	H2009	1.41873	5.00E-05	0.00025
SGK3	H2009	1.41803	0.01795	0.049164
ST6GALNAC4	H2009	1.41615	5.00E-05	0.00025
MYB	H2009	1.41582	5.00E-05	0.00025
ZNF300	H2009	1.4139	5.00E-05	0.00025
MAZ	H2009	1.41077	5.00E-05	0.00025
BARX1	H2009	1.41028	5.00E-05	0.00025
RABGGTA	H2009	1.4101	5.00E-05	0.00025
ZNF414	H2009	1.40684	5.00E-05	0.00025
ZNF880	H2009	1.40464	5.00E-05	0.00025
SAMD1	H2009	1.40459	5.00E-05	0.00025
PDCL3	H2009	1.40088	5.00E-05	0.00025
HSPA9	H2009	1.40043	5.00E-05	0.00025
DNAJB12	H2009	1.40015	5.00E-05	0.00025
ZNF114	H2009	1.39849	5.00E-05	0.00025
G2E3	H2009	1.39773	5.00E-05	0.00025
MSL3P1	H2009	1.39353	5.00E-05	0.00025
GSTZ1	H2009	1.39193	5.00E-05	0.00025
STX10	H2009	1.3876	5.00E-05	0.00025
CPPED1	H2009	1.38697	5.00E-05	0.00025
TRA2B	H2009	1.38647	5.00E-05	0.00025
PTBP1	H2009	1.38631	5.00E-05	0.00025
ING5	H2009	1.38531	5.00E-05	0.00025
DTWD1	H2009	1.38522	5.00E-05	0.00025
DEPDC1B	H2009	1.3845	5.00E-05	0.00025
PPP1R14B	H2009	1.38279	5.00E-05	0.00025
DHODH	H2009	1.3815	5.00E-05	0.00025
ZSCAN2	H2009	1.38118	0.00105	0.004037
SRSF1	H2009	1.38037	5.00E-05	0.00025
MEX3D	H2009	1.37989	5.00E-05	0.00025
EZH1	H2009	1.37949	5.00E-05	0.00025
DAZAP1	H2009	1.37847	5.00E-05	0.00025
HMBS	H2009	1.37768	5.00E-05	0.00025
EPN3	H2009	1.37705	5.00E-05	0.00025
SPX	H2009	1.37251	0.0122	0.035209

KIAA0895L	H2009	1.37196	0.0048	0.015533
KRTCAP3	H2009	1.37171	5.00E-05	0.00025
ALKBH8	H2009	1.37073	5.00E-05	0.00025
HAUS7	H2009	1.37069	5.00E-05	0.00025
FAM127C	H2009	1.3689	5.00E-05	0.00025
KIAA1462	H2009	1.36816	5.00E-05	0.00025
DANCR	H2009	1.36751	5.00E-05	0.00025
ZNF883	H2009	1.36607	5.00E-05	0.00025
RRS1	H2009	1.36565	5.00E-05	0.00025
HMOX1	H2009	1.36227	5.00E-05	0.00025
BNIP1	H2009	1.3611	5.00E-05	0.00025
BHLHA15	H2009	1.3593	0.0081	0.024604
SFPQ	H2009	1.35852	5.00E-05	0.00025
HSPA8	H2009	1.35566	0.0002	0.000905
RPL23	H2009	1.35425	5.00E-05	0.00025
PIGO	H2009	1.35123	5.00E-05	0.00025
NCAPH	H2009	1.35081	5.00E-05	0.00025
CHMP4A	H2009	1.35058	5.00E-05	0.00025
MRPL42	H2009	1.35016	5.00E-05	0.00025
PRDM13	H2009	1.34951	5.00E-05	0.00025
ALG14	H2009	1.34884	5.00E-05	0.00025
ZNF391	H2009	1.34799	5.00E-05	0.00025
IL18	H2009	1.34533	5.00E-05	0.00025
NPM1	H2009	1.34394	5.00E-05	0.00025
HNRNPH1	H2009	1.3437	5.00E-05	0.00025
ZSCAN26	H2009	1.34264	5.00E-05	0.00025
TNIK	H2009	1.33884	5.00E-05	0.00025
MPHOSPH9	H2009	1.33808	5.00E-05	0.00025
NECAP1	H2009	1.33718	5.00E-05	0.00025
PHACTR3	H2009	1.33489	5.00E-05	0.00025
ZNF511	H2009	1.33486	0.00775	0.023667
LHX6	H2009	1.3347	5.00E-05	0.00025
EPHA6	H2009	1.33423	0.00105	0.004037
PEX2	H2009	1.33397	5.00E-05	0.00025
RNF216P1	H2009	1.32991	5.00E-05	0.00025
FUT10	H2009	1.32874	5.00E-05	0.00025
CD177	H2009	1.32731	5.00E-05	0.00025
AP5S1	H2009	1.32698	5.00E-05	0.00025
LANCL2	H2009	1.3262	5.00E-05	0.00025
SDHAF2	H2009	1.32584	5.00E-05	0.00025
ILVBL	H2009	1.32398	5.00E-05	0.00025
ANKLE1	H2009	1.32375	5.00E-05	0.00025
GJB7	H2009	1.32255	0.0011	0.004209

ARHGEF19	H2009	1.32186	5.00E-05	0.00025
SLC27A5	H2009	1.32144	5.00E-05	0.00025
MPZL2	H2009	1.31762	5.00E-05	0.00025
GAB2	H2009	1.31591	5.00E-05	0.00025
GAR1	H2009	1.31534	5.00E-05	0.00025
ADSL	H2009	1.3102	5.00E-05	0.00025
TRAF5	H2009	1.3096	0.0004	0.001697
DNAJC19	H2009	1.30846	5.00E-05	0.00025
DLEU1	H2009	1.30788	0.0002	0.000905
MRPL3	H2009	1.30633	5.00E-05	0.00025
ZNF14	H2009	1.30526	5.00E-05	0.00025
PWP1	H2009	1.3048	5.00E-05	0.00025
SURF2	H2009	1.30387	5.00E-05	0.00025
PWWP2B	H2009	1.3028	5.00E-05	0.00025
ALDH16A1	H2009	1.3026	5.00E-05	0.00025
PLK1	H2009	1.30232	5.00E-05	0.00025
PACSIN3	H2009	1.30044	5.00E-05	0.00025
ZNF787	H2009	1.29985	5.00E-05	0.00025
UTP6	H2009	1.29855	5.00E-05	0.00025
RABEPK	H2009	1.29796	5.00E-05	0.00025
ARNT	H2009	1.29756	5.00E-05	0.00025
BCAT1	H2009	1.29685	5.00E-05	0.00025
DENND1B	H2009	1.29646	5.00E-05	0.00025
B9D2	H2009	1.29399	0.0008	0.003162
42430	H2009	1.29366	5.00E-05	0.00025
ANXA1	H2009	1.29334	5.00E-05	0.00025
TPRKB	H2009	1.29272	5.00E-05	0.00025
MPP7	H2009	1.29244	5.00E-05	0.00025
FBXO44	H2009	1.29233	0.00265	0.009207
POLR3E	H2009	1.28843	5.00E-05	0.00025
ARTN	H2009	1.28771	0.0002	0.000905
SULT2B1	H2009	1.28498	5.00E-05	0.00025
C17orf58	H2009	1.28282	5.00E-05	0.00025
YEATS4	H2009	1.28196	5.00E-05	0.00025
STEAP3	H2009	1.2795	5.00E-05	0.00025
KRT19	H2009	1.27755	5.00E-05	0.00025
FAM221A	H2009	1.27701	0.00015	0.000695
SPATA24	H2009	1.27695	5.00E-05	0.00025
SLC25A12	H2009	1.27309	5.00E-05	0.00025
ZFP64	H2009	1.27272	5.00E-05	0.00025
VPS36	H2009	1.27259	5.00E-05	0.00025
GRAMD3	H2009	1.27117	5.00E-05	0.00025
MB	H2009	1.27099	5.00E-05	0.00025

UNC119	H2009	1.26559	5.00E-05	0.00025
ACTR5	H2009	1.2651	5.00E-05	0.00025
CYB5A	H2009	1.2647	5.00E-05	0.00025
THG1L	H2009	1.26444	5.00E-05	0.00025
MTIF2	H2009	1.2628	5.00E-05	0.00025
NAT10	H2009	1.26076	5.00E-05	0.00025
CDCA7	H2009	1.2603	5.00E-05	0.00025
CPT1B	H2009	1.26006	0.00895	0.026855
RAB19	H2009	1.25967	0.01625	0.045197
IFI35	H2009	1.25722	5.00E-05	0.00025
CHCHD5	H2009	1.25616	5.00E-05	0.00025
BCL11A	H2009	1.25595	5.00E-05	0.00025
ZNF30	H2009	1.25512	5.00E-05	0.00025
GAS5	H2009	1.25423	5.00E-05	0.00025
TAF6L	H2009	1.25399	5.00E-05	0.00025
RIOK1	H2009	1.25288	5.00E-05	0.00025
CRTAP	H2009	1.24882	5.00E-05	0.00025
NDUFS2	H2009	1.24805	5.00E-05	0.00025
SLC39A4	H2009	1.248	5.00E-05	0.00025
GTF3C2	H2009	1.24782	5.00E-05	0.00025
PHLDA3	H2009	1.24692	0.00065	0.002626
HAUS1	H2009	1.2453	5.00E-05	0.00025
GIN1	H2009	1.24454	5.00E-05	0.00025
EEF2	H2009	1.24431	5.00E-05	0.00025
DNMT3A	H2009	1.24409	5.00E-05	0.00025
FEZF1-AS1	H2009	1.24331	0.00175	0.006369
CHD1L	H2009	1.24221	5.00E-05	0.00025
ZFP37	H2009	1.24023	5.00E-05	0.00025
PLEKHF1	H2009	1.23834	5.00E-05	0.00025
STEAP1	H2009	1.23787	5.00E-05	0.00025
MTHFD1L	H2009	1.23628	5.00E-05	0.00025
IL7R	H2009	1.23447	5.00E-05	0.00025
SEMA3B	H2009	1.23383	5.00E-05	0.00025
RANGRF	H2009	1.23305	5.00E-05	0.00025
LRIG3	H2009	1.23304	5.00E-05	0.00025
ELFN1-AS1	H2009	1.23238	0.00035	0.001505
GEMIN2	H2009	1.23187	5.00E-05	0.00025
DCAF16	H2009	1.22994	5.00E-05	0.00025
RDH13	H2009	1.22778	5.00E-05	0.00025
CTU1	H2009	1.22647	5.00E-05	0.00025
C6orf223	H2009	1.22644	5.00E-05	0.00025
PNRC2	H2009	1.22612	5.00E-05	0.00025
PDIK1L	H2009	1.22464	5.00E-05	0.00025

CDCA7L	H2009	1.2226	5.00E-05	0.00025
JUND	H2009	1.22143	5.00E-05	0.00025
ZNF280D	H2009	1.22036	5.00E-05	0.00025
FAM175A	H2009	1.21897	0.0066	0.020539
RING1	H2009	1.21805	5.00E-05	0.00025
TMEM160	H2009	1.21715	5.00E-05	0.00025
ANKRD39	H2009	1.21605	5.00E-05	0.00025
GYLTL1B	H2009	1.21582	0.0002	0.000905
IKBIP	H2009	1.21421	5.00E-05	0.00025
NPM3	H2009	1.21407	5.00E-05	0.00025
ZNF585A	H2009	1.21405	0.0045	0.014681
TATDN1	H2009	1.21263	0.00225	0.007962
EHMT2	H2009	1.21226	5.00E-05	0.00025
TAF1A	H2009	1.2122	5.00E-05	0.00025
MIIP	H2009	1.21053	5.00E-05	0.00025
SNRNP40	H2009	1.21024	5.00E-05	0.00025
GNA15	H2009	1.20691	5.00E-05	0.00025
ASPSCR1	H2009	1.2044	5.00E-05	0.00025
HAUS8	H2009	1.20424	5.00E-05	0.00025
C11orf74	H2009	1.2039	0.0006	0.002445
GMPR	H2009	1.20367	5.00E-05	0.00025
TTC27	H2009	1.20237	5.00E-05	0.00025
POLR1A	H2009	1.20229	5.00E-05	0.00025
ZNF771	H2009	1.20197	0.00025	0.001109
LPCAT1	H2009	1.20063	5.00E-05	0.00025
PMPCB	H2009	1.20014	0.0003	0.001308
SFXN4	H2009	1.19969	5.00E-05	0.00025
SREBF1	H2009	1.19933	0.00015	0.000695
EXD2	H2009	1.199	5.00E-05	0.00025
POLG2	H2009	1.19859	5.00E-05	0.00025
COA6	H2009	1.19745	5.00E-05	0.00025
N6AMT1	H2009	1.1954	0.00035	0.001505
ZC3HAV1L	H2009	1.19534	0.00015	0.000695
CTPS1	H2009	1.19485	5.00E-05	0.00025
IGFL1	H2009	1.19286	5.00E-05	0.00025
LEPREL4	H2009	1.19259	5.00E-05	0.00025
PPARG	H2009	1.19089	5.00E-05	0.00025
SMIM3	H2009	1.18936	5.00E-05	0.00025
ZMYM1	H2009	1.18919	5.00E-05	0.00025
ASB8	H2009	1.18711	5.00E-05	0.00025
PRDM10	H2009	1.18518	5.00E-05	0.00025
AFAP1L2	H2009	1.18412	5.00E-05	0.00025
HINT3	H2009	1.18411	5.00E-05	0.00025

PIGU	H2009	1.18347	5.00E-05	0.00025
ZSCAN5A	H2009	1.18326	5.00E-05	0.00025
BCAT2	H2009	1.18192	5.00E-05	0.00025
TMEM180	H2009	1.18177	5.00E-05	0.00025
PODXL	H2009	1.1813	5.00E-05	0.00025
FUT11	H2009	1.18041	5.00E-05	0.00025
ADAT2	H2009	1.17887	5.00E-05	0.00025
POP1	H2009	1.17808	5.00E-05	0.00025
GJB5	H2009	1.17772	5.00E-05	0.00025
PARPBP	H2009	1.17589	5.00E-05	0.00025
USE1	H2009	1.17472	5.00E-05	0.00025
TRIB3	H2009	1.17301	5.00E-05	0.00025
IGSF8	H2009	1.17269	5.00E-05	0.00025
HSH2D	H2009	1.17129	0.0001	0.000478
SF3B3	H2009	1.17111	5.00E-05	0.00025
MRPS22	H2009	1.17007	5.00E-05	0.00025
ARMC6	H2009	1.16935	5.00E-05	0.00025
COA3	H2009	1.16893	5.00E-05	0.00025
INTS3	H2009	1.16831	5.00E-05	0.00025
GOLGA2P7	H2009	1.16709	0.0004	0.001697
WDR18	H2009	1.16642	5.00E-05	0.00025
MTHFD1	H2009	1.16484	5.00E-05	0.00025
FADS3	H2009	1.1635	5.00E-05	0.00025
LSM2	H2009	1.16283	5.00E-05	0.00025
SMARCB1	H2009	1.16224	5.00E-05	0.00025
TECPR1	H2009	1.16181	5.00E-05	0.00025
NBN	H2009	1.16157	5.00E-05	0.00025
ANP32E	H2009	1.16034	5.00E-05	0.00025
FAM117B	H2009	1.15972	5.00E-05	0.00025
C12orf10	H2009	1.15868	5.00E-05	0.00025
PLD6	H2009	1.15801	5.00E-05	0.00025
CENPA	H2009	1.15672	5.00E-05	0.00025
USP16	H2009	1.1563	5.00E-05	0.00025
PAFAH2	H2009	1.15586	5.00E-05	0.00025
SOCS2	H2009	1.15572	0.00025	0.001109
PPIL2	H2009	1.1546	5.00E-05	0.00025
LOC101927667	H2009	1.15437	0.00055	0.002261
PNPLA5	H2009	1.15393	5.00E-05	0.00025
PSMG1	H2009	1.15383	5.00E-05	0.00025
VKORC1	H2009	1.15327	5.00E-05	0.00025
NSRP1	H2009	1.15226	5.00E-05	0.00025
PSMG4	H2009	1.1522	5.00E-05	0.00025
PEG10	H2009	1.15122	5.00E-05	0.00025

METTL1	H2009	1.15092	5.00E-05	0.00025
IGFLR1	H2009	1.1486	0.00025	0.001109
C1QBP	H2009	1.1485	0.0002	0.000905
SNX21	H2009	1.14788	0.0001	0.000478
SFXN2	H2009	1.14717	5.00E-05	0.00025
MEIOB	H2009	1.1471	0.0008	0.003162
ARRB1	H2009	1.14706	5.00E-05	0.00025
CNKSR3	H2009	1.14694	5.00E-05	0.00025
SUV420H1	H2009	1.14552	5.00E-05	0.00025
SPG20	H2009	1.1443	5.00E-05	0.00025
AARS	H2009	1.14359	5.00E-05	0.00025
RBM28	H2009	1.14358	5.00E-05	0.00025
MLLT3	H2009	1.14134	5.00E-05	0.00025
PGM1	H2009	1.14115	5.00E-05	0.00025
PFDN2	H2009	1.14102	0.00035	0.001505
CDC20	H2009	1.13907	5.00E-05	0.00025
MGST1	H2009	1.13877	5.00E-05	0.00025
SMIM10	H2009	1.13613	0.00065	0.002626
RCN3	H2009	1.13553	5.00E-05	0.00025
TMEM170B	H2009	1.1355	0.00035	0.001505
TMEM109	H2009	1.13464	5.00E-05	0.00025
LAGE3	H2009	1.13095	5.00E-05	0.00025
LSM7	H2009	1.13071	5.00E-05	0.00025
CCDC101	H2009	1.13069	5.00E-05	0.00025
ERP27	H2009	1.12977	0.00245	0.008588
QRSL1	H2009	1.12875	5.00E-05	0.00025
AGAP2-AS1	H2009	1.12706	0.0005	0.002076
NCK1	H2009	1.12679	5.00E-05	0.00025
SMIM20	H2009	1.12596	5.00E-05	0.00025
BAG2	H2009	1.12593	5.00E-05	0.00025
DCTPP1	H2009	1.1254	5.00E-05	0.00025
ZNF232	H2009	1.12455	5.00E-05	0.00025
TMEM18	H2009	1.12395	5.00E-05	0.00025
FOXG1	H2009	1.12318	5.00E-05	0.00025
ID1	H2009	1.12292	5.00E-05	0.00025
TSKU	H2009	1.12209	5.00E-05	0.00025
C1orf220	H2009	1.12173	0.0007	0.002808
MRPL24	H2009	1.12139	5.00E-05	0.00025
NDC1	H2009	1.12057	5.00E-05	0.00025
HES7	H2009	1.12026	0.0008	0.003162
STRADA	H2009	1.11995	5.00E-05	0.00025
GPR87	H2009	1.11681	0.001	0.003864
USP18	H2009	1.11653	5.00E-05	0.00025

RPL22L1	H2009	1.11605	5.00E-05	0.00025
INTS7	H2009	1.11539	0.00245	0.008588
VEPH1	H2009	1.11422	0.00325	0.011023
MTSS1L	H2009	1.11345	5.00E-05	0.00025
PARD6A	H2009	1.11341	0.0012	0.004544
HSD11B2	H2009	1.11311	0.0008	0.003162
LYSMD2	H2009	1.1128	0.00025	0.001109
FAM104B	H2009	1.11278	0.0001	0.000478
MAGOHB	H2009	1.11195	5.00E-05	0.00025
ANP32B	H2009	1.11098	5.00E-05	0.00025
KCNMA1	H2009	1.11042	0.0004	0.001697
CASP4	H2009	1.10854	5.00E-05	0.00025
CCDC104	H2009	1.10834	5.00E-05	0.00025
C20orf96	H2009	1.10794	0.00045	0.001888
MACC1	H2009	1.10712	5.00E-05	0.00025
CASC5	H2009	1.10683	5.00E-05	0.00025
HIGD2A	H2009	1.10596	5.00E-05	0.00025
TUBB	H2009	1.10593	0.0003	0.001308
TMEM161A	H2009	1.10568	5.00E-05	0.00025
APEX1	H2009	1.1047	5.00E-05	0.00025
MLST8	H2009	1.10454	5.00E-05	0.00025
C3orf55	H2009	1.10438	0.00055	0.002261
SLC17A5	H2009	1.10405	0.00045	0.001888
NHEJ1	H2009	1.1038	5.00E-05	0.00025
CBX2	H2009	1.1031	5.00E-05	0.00025
AUTS2	H2009	1.10268	5.00E-05	0.00025
CLN6	H2009	1.10188	5.00E-05	0.00025
LDHA	H2009	1.10119	0.00065	0.002626
THADA	H2009	1.09911	5.00E-05	0.00025
CMTM8	H2009	1.09754	5.00E-05	0.00025
THOC6	H2009	1.09751	0.01475	0.041566
CCDC138	H2009	1.09694	5.00E-05	0.00025
COA7	H2009	1.09687	5.00E-05	0.00025
SPATC1L	H2009	1.09685	5.00E-05	0.00025
POLE2	H2009	1.09654	5.00E-05	0.00025
TTC5	H2009	1.09649	5.00E-05	0.00025
MRPS18A	H2009	1.09609	5.00E-05	0.00025
PCDHB3	H2009	1.09594	5.00E-05	0.00025
BAHCC1	H2009	1.09473	5.00E-05	0.00025
EWSR1	H2009	1.09259	5.00E-05	0.00025
TMPRSS13	H2009	1.09244	5.00E-05	0.00025
NIF3L1	H2009	1.09182	5.00E-05	0.00025
SYCP2L	H2009	1.08938	0.0003	0.001308

ZNF484	H2009	1.08867	0.00025	0.001109
ECI2	H2009	1.08716	5.00E-05	0.00025
C6orf132	H2009	1.08669	5.00E-05	0.00025
C9orf156	H2009	1.08532	5.00E-05	0.00025
C15orf41	H2009	1.08493	5.00E-05	0.00025
UFC1	H2009	1.08246	5.00E-05	0.00025
CECR5	H2009	1.08137	5.00E-05	0.00025
NXT1	H2009	1.08031	5.00E-05	0.00025
OSGEP	H2009	1.07982	5.00E-05	0.00025
MEST	H2009	1.07872	0.0001	0.000478
TRAPPC4	H2009	1.0782	5.00E-05	0.00025
VLDLR	H2009	1.07601	0.0001	0.000478
ITGB6	H2009	1.07517	5.00E-05	0.00025
SNW1	H2009	1.07511	5.00E-05	0.00025
FANCE	H2009	1.07508	0.0001	0.000478
ENO2	H2009	1.0733	5.00E-05	0.00025
SSB	H2009	1.07326	5.00E-05	0.00025
U2AF1	H2009	1.07292	5.00E-05	0.00025
PAF1	H2009	1.07265	5.00E-05	0.00025
CASP6	H2009	1.07141	5.00E-05	0.00025
GOLPH3L	H2009	1.07117	5.00E-05	0.00025
SRI	H2009	1.07085	5.00E-05	0.00025
PEF1	H2009	1.07075	5.00E-05	0.00025
PIR	H2009	1.06935	0.0029	0.009968
AARSD1	H2009	1.06823	5.00E-05	0.00025
BUB1B	H2009	1.06812	5.00E-05	0.00025
FIGN	H2009	1.06667	0.00065	0.002626
NUDT13	H2009	1.06664	0.00035	0.001505
RNF41	H2009	1.06647	5.00E-05	0.00025
METTL2A	H2009	1.06613	5.00E-05	0.00025
PCCB	H2009	1.06512	5.00E-05	0.00025
SNX12	H2009	1.06449	5.00E-05	0.00025
NDRG3	H2009	1.06416	5.00E-05	0.00025
IFIT2	H2009	1.06352	0.00025	0.001109
PSMD3	H2009	1.06254	5.00E-05	0.00025
GTF2H2C_2	H2009	1.06215	0.0002	0.000905
MRPL4	H2009	1.06156	5.00E-05	0.00025
DHRS11	H2009	1.06152	0.0001	0.000478
UQCRHL	H2009	1.06113	0.00105	0.004037
ATP5G2	H2009	1.06109	5.00E-05	0.00025
GALNT18	H2009	1.06073	5.00E-05	0.00025
PSMC2	H2009	1.06028	5.00E-05	0.00025
HMGXB4	H2009	1.05943	5.00E-05	0.00025

IMP4	H2009	1.05873	5.00E-05	0.00025
LIG3	H2009	1.05868	5.00E-05	0.00025
PRMT3	H2009	1.05747	5.00E-05	0.00025
OGFOD3	H2009	1.05614	0.0029	0.009968
PTRH2	H2009	1.05583	5.00E-05	0.00025
ADM5	H2009	1.05349	0.00035	0.001505
CCDC51	H2009	1.05333	5.00E-05	0.00025
DDX60	H2009	1.05216	5.00E-05	0.00025
LOC101927746	H2009	1.05198	0.0019	0.006852
ORC2	H2009	1.05149	5.00E-05	0.00025
TEX40	H2009	1.05125	0.00845	0.025543
PKN1	H2009	1.05107	5.00E-05	0.00025
KRT10	H2009	1.05037	5.00E-05	0.00025
DNAAF3	H2009	1.0503	0.00015	0.000695
CCDC12	H2009	1.04692	0.0018	0.006531
CDKN3	H2009	1.04675	5.00E-05	0.00025
MANEAL	H2009	1.04628	5.00E-05	0.00025
CCDC86	H2009	1.0459	5.00E-05	0.00025
VAV3	H2009	1.04494	0.00215	0.007645
ZNF775	H2009	1.043	0.0011	0.004209
RAB30-AS1	H2009	1.04243	0.0007	0.002808
HEBP2	H2009	1.04182	5.00E-05	0.00025
SNRPD1	H2009	1.04167	5.00E-05	0.00025
KLHDC3	H2009	1.04089	5.00E-05	0.00025
MAP3K13	H2009	1.04055	0.0001	0.000478
ZNF239	H2009	1.04018	5.00E-05	0.00025
PKP2	H2009	1.03993	5.00E-05	0.00025
TARBP1	H2009	1.03691	5.00E-05	0.00025
ANKZF1	H2009	1.03686	0.0004	0.001697
HEATR3	H2009	1.03597	5.00E-05	0.00025
SLC39A10	H2009	1.03571	5.00E-05	0.00025
LSM6	H2009	1.03527	5.00E-05	0.00025
PABPC4	H2009	1.03303	5.00E-05	0.00025
INTS10	H2009	1.03276	5.00E-05	0.00025
STK33	H2009	1.03161	0.00065	0.002626
PRSS8	H2009	1.03156	5.00E-05	0.00025
RNF187	H2009	1.03041	5.00E-05	0.00025
C7orf25	H2009	1.02961	5.00E-05	0.00025
SFXN3	H2009	1.02909	5.00E-05	0.00025
KIF20A	H2009	1.02706	0.0003	0.001308
MMADHC	H2009	1.02528	5.00E-05	0.00025
SLC25A13	H2009	1.02475	5.00E-05	0.00025
HAX1	H2009	1.02441	5.00E-05	0.00025

SLC29A2	H2009	1.02369	5.00E-05	0.00025
IFIH1	H2009	1.02266	0.00025	0.001109
RSRC1	H2009	1.02228	5.00E-05	0.00025
NOP16	H2009	1.02213	5.00E-05	0.00025
MBIP	H2009	1.02136	5.00E-05	0.00025
PPAP2C	H2009	1.02102	5.00E-05	0.00025
PTCD3	H2009	1.02083	5.00E-05	0.00025
MRM1	H2009	1.02076	5.00E-05	0.00025
SNAPC2	H2009	1.02008	0.0001	0.000478
SLITRK5	H2009	1.01915	0.0004	0.001697
AHCY	H2009	1.01894	0.0001	0.000478
TUBD1	H2009	1.01889	0.0001	0.000478
FAM92A1	H2009	1.01817	5.00E-05	0.00025
C12orf45	H2009	1.01801	0.0001	0.000478
C1orf174	H2009	1.01778	5.00E-05	0.00025
ANXA9	H2009	1.01694	0.00085	0.003341
PTPN2	H2009	1.01538	5.00E-05	0.00025
TARS2	H2009	1.01508	5.00E-05	0.00025
NFIC	H2009	1.01349	5.00E-05	0.00025
SCARB1	H2009	1.0132	5.00E-05	0.00025
TMEM209	H2009	1.01268	0.0001	0.000478
ZNF551	H2009	1.01216	5.00E-05	0.00025
ZFAND2B	H2009	1.01213	5.00E-05	0.00025
SEH1L	H2009	1.01147	5.00E-05	0.00025
MRPS10	H2009	1.01107	5.00E-05	0.00025
WDR89	H2009	1.01106	0.00025	0.001109
TTC37	H2009	1.00985	5.00E-05	0.00025
NOL12	H2009	1.00979	5.00E-05	0.00025
DTNA	H2009	1.00975	0.0006	0.002445
VEZF1	H2009	1.00975	5.00E-05	0.00025
KCNH2	H2009	1.00917	0.00175	0.006369
CRYZL1	H2009	1.00907	0.00045	0.001888
EIF2B4	H2009	1.00834	5.00E-05	0.00025
ZNF678	H2009	1.0078	0.0077	0.023529
ZNF174	H2009	1.00742	5.00E-05	0.00025
MTFP1	H2009	1.00621	5.00E-05	0.00025
RAB29	H2009	1.00553	0.0004	0.001697
PUS3	H2009	1.00492	0.0107	0.031401
HNRNPA3	H2009	1.00457	5.00E-05	0.00025
ZNF566	H2009	1.00385	0.00015	0.000695
KPNA5	H2009	1.00319	0.00125	0.004713
SRSF3	H2009	1.00234	5.00E-05	0.00025
AIG1	H2009	-1.00077	0.0001	0.000478

PPAPDC2	H2009	-1.00083	0.00015	0.000695
ZNF468	H2009	-1.00279	5.00E-05	0.00025
EXO5	H2009	-1.00302	5.00E-05	0.00025
KIAA1432	H2009	-1.00367	5.00E-05	0.00025
CD83	H2009	-1.00389	0.0002	0.000905
OPTN	H2009	-1.00505	5.00E-05	0.00025
HCN3	H2009	-1.00624	0.0006	0.002445
SLC35E4	H2009	-1.00712	0.00035	0.001505
KIF27	H2009	-1.0083	0.00105	0.004037
BICC1	H2009	-1.00844	0.00165	0.006042
RWDD2B	H2009	-1.00877	5.00E-05	0.00025
B3GALTL	H2009	-1.00928	5.00E-05	0.00025
UAP1	H2009	-1.01089	5.00E-05	0.00025
MYL12A	H2009	-1.01313	5.00E-05	0.00025
PTER	H2009	-1.01436	5.00E-05	0.00025
ZNF433	H2009	-1.01436	0.00025	0.001109
KIF13B	H2009	-1.01467	5.00E-05	0.00025
FLJ43681	H2009	-1.01474	0.00265	0.009207
CPE	H2009	-1.01478	0.0002	0.000905
SKIL	H2009	-1.01629	5.00E-05	0.00025
ZNF589	H2009	-1.01683	5.00E-05	0.00025
ZNF542P	H2009	-1.0171	5.00E-05	0.00025
BAI2	H2009	-1.01715	0.0002	0.000905
RSG1	H2009	-1.01718	0.0013	0.004883
ZNF720	H2009	-1.01728	5.00E-05	0.00025
LINC00669	H2009	-1.01785	0.00035	0.001505
SLC41A1	H2009	-1.01809	5.00E-05	0.00025
ZNF582	H2009	-1.01853	5.00E-05	0.00025
SPTY2D1	H2009	-1.02105	5.00E-05	0.00025
PRDM2	H2009	-1.02135	5.00E-05	0.00025
FZD9	H2009	-1.02343	0.0037	0.012355
PARP14	H2009	-1.02484	5.00E-05	0.00025
LAMB3	H2009	-1.02497	5.00E-05	0.00025
NETO2	H2009	-1.02617	5.00E-05	0.00025
SYNJ1	H2009	-1.02712	5.00E-05	0.00025
MAP3K7CL	H2009	-1.02724	0.00045	0.001888
ARHGEF18	H2009	-1.02756	5.00E-05	0.00025
CTSL	H2009	-1.02786	5.00E-05	0.00025
STPG1	H2009	-1.02793	0.0102	0.030113
MAST4	H2009	-1.02836	0.00015	0.000695
AKR1C3	H2009	-1.02867	0.01725	0.047519
TYRO3	H2009	-1.02871	5.00E-05	0.00025
PIM2	H2009	-1.02878	5.00E-05	0.00025

ADIPOR2	H2009	-1.02895	5.00E-05	0.00025
CPT2	H2009	-1.02986	0.0001	0.000478
THBS3	H2009	-1.03189	0.00075	0.002984
VSIG1	H2009	-1.03222	0.00275	0.00951
TMEM242	H2009	-1.03269	5.00E-05	0.00025
ASAP2	H2009	-1.03298	5.00E-05	0.00025
LINC00673	H2009	-1.03321	5.00E-05	0.00025
LEPR	H2009	-1.03388	0.01185	0.034329
OGFRP1	H2009	-1.03402	0.0025	0.008741
GAB1	H2009	-1.03426	5.00E-05	0.00025
EDN1	H2009	-1.03463	0.00045	0.001888
MSANTD2	H2009	-1.03578	0.00015	0.000695
MIR22HG	H2009	-1.03585	0.0004	0.001697
FAM86JP	H2009	-1.03685	0.01485	0.041811
LMF2	H2009	-1.03735	5.00E-05	0.00025
C6orf141	H2009	-1.03821	0.0002	0.000905
ITPR1	H2009	-1.03989	0.00025	0.001109
NPC1	H2009	-1.04017	0.0001	0.000478
C17orf100	H2009	-1.04058	0.0003	0.001308
FOSL1	H2009	-1.04075	5.00E-05	0.00025
GSAP	H2009	-1.04153	0.00065	0.002626
LRRC41	H2009	-1.04165	0.00305	0.010422
RGS2	H2009	-1.04197	0.00025	0.001109
DPY19L3	H2009	-1.0435	5.00E-05	0.00025
HSF2BP	H2009	-1.04428	0.00065	0.002626
PITHD1	H2009	-1.04516	5.00E-05	0.00025
NFKB2	H2009	-1.04558	5.00E-05	0.00025
ZNF75D	H2009	-1.04807	5.00E-05	0.00025
GTF2B	H2009	-1.04824	5.00E-05	0.00025
AHR	H2009	-1.04976	5.00E-05	0.00025
ENPEP	H2009	-1.04976	0.0005	0.002076
CACNA2D1	H2009	-1.04996	0.0001	0.000478
CCND1	H2009	-1.05028	5.00E-05	0.00025
CTBP1-AS2	H2009	-1.05124	5.00E-05	0.00025
P2RX4	H2009	-1.05272	5.00E-05	0.00025
OAT	H2009	-1.05346	5.00E-05	0.00025
DMWD	H2009	-1.05412	5.00E-05	0.00025
VPS39	H2009	-1.05552	5.00E-05	0.00025
CDK14	H2009	-1.05706	0.0001	0.000478
ISG20	H2009	-1.05714	0.0002	0.000905
CASP3	H2009	-1.06	5.00E-05	0.00025
MCAM	H2009	-1.06054	5.00E-05	0.00025
PYROXD2	H2009	-1.06128	0.00145	0.005381

HDAC9	H2009	-1.06358	0.0002	0.000905
STARD13	H2009	-1.06375	5.00E-05	0.00025
RFX8	H2009	-1.06516	0.01335	0.038082
ARHGEF9	H2009	-1.06663	5.00E-05	0.00025
LINC00999	H2009	-1.067	5.00E-05	0.00025
EMBP1	H2009	-1.06724	0.0016	0.005879
KIF3C	H2009	-1.06819	5.00E-05	0.00025
ATP11A	H2009	-1.06896	5.00E-05	0.00025
CEP89	H2009	-1.06985	5.00E-05	0.00025
CEP63	H2009	-1.07076	0.0066	0.020539
KDSR	H2009	-1.07135	5.00E-05	0.00025
STYK1	H2009	-1.07163	0.00015	0.000695
ZNF699	H2009	-1.07339	5.00E-05	0.00025
NXF1	H2009	-1.07447	0.0001	0.000478
ZNF519	H2009	-1.07596	5.00E-05	0.00025
TMEM181	H2009	-1.07686	5.00E-05	0.00025
LRRC8B	H2009	-1.07687	5.00E-05	0.00025
RSRP1	H2009	-1.07731	5.00E-05	0.00025
TLCD2	H2009	-1.07844	0.0001	0.000478
C7orf31	H2009	-1.07957	5.00E-05	0.00025
GPX3	H2009	-1.08015	5.00E-05	0.00025
ERVK13-1	H2009	-1.08021	5.00E-05	0.00025
HMGCS1	H2009	-1.08221	5.00E-05	0.00025
GNAO1	H2009	-1.08337	0.0001	0.000478
FAM214A	H2009	-1.08357	5.00E-05	0.00025
LOC100506730	H2009	-1.08526	0.00095	0.00369
IDI1	H2009	-1.08679	5.00E-05	0.00025
WDR45	H2009	-1.08741	5.00E-05	0.00025
HDAC4	H2009	-1.08751	5.00E-05	0.00025
SUCO	H2009	-1.0879	5.00E-05	0.00025
LOC100499194	H2009	-1.08907	0.00045	0.001888
RGS20	H2009	-1.09108	0.00045	0.001888
NOTCH2	H2009	-1.09129	5.00E-05	0.00025
ATP10D	H2009	-1.09241	5.00E-05	0.00025
F2RL1	H2009	-1.09258	5.00E-05	0.00025
SDCBP	H2009	-1.09272	5.00E-05	0.00025
GPR19	H2009	-1.09445	0.00095	0.00369
HEY1	H2009	-1.09545	0.00055	0.002261
ZP3	H2009	-1.09619	0.0006	0.002445
SLC8B1	H2009	-1.09703	5.00E-05	0.00025
42624	H2009	-1.09827	5.00E-05	0.00025
SNAPC1	H2009	-1.10003	5.00E-05	0.00025
EML6	H2009	-1.10031	0.00015	0.000695

CRIPAK	H2009	-1.10061	5.00E-05	0.00025
MR1	H2009	-1.10116	5.00E-05	0.00025
TRAPPC6B	H2009	-1.10171	5.00E-05	0.00025
FERMT2	H2009	-1.10189	5.00E-05	0.00025
TRAPPC6A	H2009	-1.10501	5.00E-05	0.00025
S100A13	H2009	-1.10522	0.00315	0.010725
ZNF730	H2009	-1.10726	5.00E-05	0.00025
SEMA3C	H2009	-1.10817	0.00015	0.000695
B4GALT4	H2009	-1.10876	5.00E-05	0.00025
H2AFJ	H2009	-1.10901	5.00E-05	0.00025
PGBD4	H2009	-1.10921	0.00065	0.002626
EFHC1	H2009	-1.10923	5.00E-05	0.00025
AGPAT4	H2009	-1.11007	5.00E-05	0.00025
GPCPD1	H2009	-1.11199	0.0001	0.000478
LOC100287015	H2009	-1.11231	0.00015	0.000695
SPHK1	H2009	-1.11262	5.00E-05	0.00025
SLC25A25	H2009	-1.1128	5.00E-05	0.00025
SECISBP2L	H2009	-1.11375	5.00E-05	0.00025
ETV5	H2009	-1.11388	5.00E-05	0.00025
BTG3	H2009	-1.11405	5.00E-05	0.00025
C14orf28	H2009	-1.11423	0.0062	0.019448
C6orf52	H2009	-1.11454	0.0012	0.004544
PRKCA	H2009	-1.11509	5.00E-05	0.00025
LOC101928891	H2009	-1.11917	0.00655	0.020401
DNAJC6	H2009	-1.11992	5.00E-05	0.00025
ATG16L2	H2009	-1.11999	0.0001	0.000478
SNTB2	H2009	-1.12044	5.00E-05	0.00025
CRIM1	H2009	-1.12341	5.00E-05	0.00025
FBXL8	H2009	-1.12347	0.0099	0.029335
CEACAM19	H2009	-1.12429	0.00025	0.001109
OAS3	H2009	-1.1255	5.00E-05	0.00025
SAMD4A	H2009	-1.12564	5.00E-05	0.00025
LOC100506123	H2009	-1.12663	0.002	0.007171
CHCHD7	H2009	-1.1278	5.00E-05	0.00025
GLIPR2	H2009	-1.12782	0.00015	0.000695
SLC4A7	H2009	-1.12793	5.00E-05	0.00025
CYB5D2	H2009	-1.12933	0.0001	0.000478
CDH24	H2009	-1.13121	5.00E-05	0.00025
CCDC126	H2009	-1.13183	0.00015	0.000695
FLJ37201	H2009	-1.13219	0.00355	0.01191
FAM24B	H2009	-1.13432	0.0034	0.011466
RSPH3	H2009	-1.1359	5.00E-05	0.00025
EPM2AIP1	H2009	-1.13637	5.00E-05	0.00025

TSC22D3	H2009	-1.13739	5.00E-05	0.00025
LOC100506990	H2009	-1.13836	0.0006	0.002445
TST	H2009	-1.14092	0.00865	0.026076
SH3BP4	H2009	-1.14178	5.00E-05	0.00025
ZNF83	H2009	-1.14255	5.00E-05	0.00025
UBFD1	H2009	-1.14288	5.00E-05	0.00025
RERE	H2009	-1.14423	5.00E-05	0.00025
C19orf54	H2009	-1.14538	0.0014	0.005217
KLF4	H2009	-1.14559	5.00E-05	0.00025
NEU1	H2009	-1.14655	5.00E-05	0.00025
TPST1	H2009	-1.14849	5.00E-05	0.00025
KIAA0040	H2009	-1.15032	5.00E-05	0.00025
GOLGA2P5	H2009	-1.15079	5.00E-05	0.00025
RHBDF1	H2009	-1.15086	5.00E-05	0.00025
C22orf46	H2009	-1.15103	5.00E-05	0.00025
ACBD7	H2009	-1.15116	5.00E-05	0.00025
TRAPPC9	H2009	-1.1531	5.00E-05	0.00025
DGKQ	H2009	-1.15539	5.00E-05	0.00025
KIAA1107	H2009	-1.15547	0.0002	0.000905
DLX3	H2009	-1.15574	5.00E-05	0.00025
DUSP14	H2009	-1.1567	5.00E-05	0.00025
EN2	H2009	-1.15676	0.0003	0.001308
ZNF185	H2009	-1.15702	5.00E-05	0.00025
PHLDA1	H2009	-1.15713	5.00E-05	0.00025
C2orf81	H2009	-1.15781	0.0005	0.002076
GALC	H2009	-1.16	5.00E-05	0.00025
HLA-B	H2009	-1.1617	5.00E-05	0.00025
ABTB2	H2009	-1.16206	5.00E-05	0.00025
RGL1	H2009	-1.16255	5.00E-05	0.00025
HGSNAT	H2009	-1.16407	5.00E-05	0.00025
LSR	H2009	-1.16642	5.00E-05	0.00025
TMEM194B	H2009	-1.16656	5.00E-05	0.00025
KIAA0247	H2009	-1.16767	5.00E-05	0.00025
C3orf62	H2009	-1.17074	5.00E-05	0.00025
SGCB	H2009	-1.17161	5.00E-05	0.00025
C16orf46	H2009	-1.17198	0.00025	0.001109
DNAJB9	H2009	-1.1725	0.00295	0.010117
EDEM3	H2009	-1.17338	5.00E-05	0.00025
CHST2	H2009	-1.17554	5.00E-05	0.00025
ZNF92	H2009	-1.17612	5.00E-05	0.00025
C6orf147	H2009	-1.17689	0.00375	0.012501
NQO2	H2009	-1.17731	5.00E-05	0.00025
HIST1H2BC	H2009	-1.17732	0.00025	0.001109

GLIS3	H2009	-1.179	5.00E-05	0.00025
ANKRD10	H2009	-1.17933	5.00E-05	0.00025
MMP14	H2009	-1.17949	5.00E-05	0.00025
PLAGL1	H2009	-1.18041	5.00E-05	0.00025
CDCP1	H2009	-1.18286	5.00E-05	0.00025
DPY19L2	H2009	-1.18317	0.00015	0.000695
CASP7	H2009	-1.18335	5.00E-05	0.00025
CCP110	H2009	-1.18411	5.00E-05	0.00025
SLC25A45	H2009	-1.18435	5.00E-05	0.00025
CCDC171	H2009	-1.18548	0.00025	0.001109
FAM105A	H2009	-1.18587	5.00E-05	0.00025
SAMD8	H2009	-1.18807	5.00E-05	0.00025
IRX4	H2009	-1.18874	5.00E-05	0.00025
PARP16	H2009	-1.189	5.00E-05	0.00025
SOS2	H2009	-1.19064	5.00E-05	0.00025
NMRK1	H2009	-1.1912	0.0002	0.000905
APLF	H2009	-1.19176	5.00E-05	0.00025
EPG5	H2009	-1.19404	5.00E-05	0.00025
SPPL2B	H2009	-1.19675	5.00E-05	0.00025
TNFRSF10B	H2009	-1.19678	5.00E-05	0.00025
CDIP1	H2009	-1.197	5.00E-05	0.00025
GPR3	H2009	-1.19752	0.00135	0.00505
FAM114A1	H2009	-1.19895	5.00E-05	0.00025
TMEM191A	H2009	-1.19913	0.00165	0.006042
TTC13	H2009	-1.20019	5.00E-05	0.00025
ZNF10	H2009	-1.20106	5.00E-05	0.00025
FRMD6	H2009	-1.20267	5.00E-05	0.00025
ZNF833P	H2009	-1.20284	0.003	0.01027
CDKN2D	H2009	-1.20325	5.00E-05	0.00025
FAM86EP	H2009	-1.20491	0.00015	0.000695
SEPSECS	H2009	-1.20688	5.00E-05	0.00025
WWC3	H2009	-1.20736	5.00E-05	0.00025
ATF7IP2	H2009	-1.21026	5.00E-05	0.00025
HIST1H3A	H2009	-1.212	0.0116	0.033691
TRPC1	H2009	-1.21512	5.00E-05	0.00025
ZNF28	H2009	-1.21531	5.00E-05	0.00025
UCP2	H2009	-1.2165	5.00E-05	0.00025
C6orf99	H2009	-1.21712	0.002	0.007171
RHBDD2	H2009	-1.21949	5.00E-05	0.00025
HEATR5A	H2009	-1.21978	5.00E-05	0.00025
SERTAD4-AS1	H2009	-1.22204	0.01815	0.049642
KDM7A	H2009	-1.22229	5.00E-05	0.00025
SLC6A8	H2009	-1.22342	5.00E-05	0.00025

CA13	H2009	-1.22369	5.00E-05	0.00025
AOC2	H2009	-1.22427	0.0002	0.000905
LRRC56	H2009	-1.22445	5.00E-05	0.00025
ZNF878	H2009	-1.22793	5.00E-05	0.00025
MMD	H2009	-1.2288	5.00E-05	0.00025
ZEB1-AS1	H2009	-1.23149	0.00045	0.001888
NRP2	H2009	-1.23244	5.00E-05	0.00025
CCDC136	H2009	-1.23246	5.00E-05	0.00025
NOSTRIN	H2009	-1.2325	0.0077	0.023529
LOC101927797	H2009	-1.2328	0.0023	0.00812
ACSF2	H2009	-1.23534	5.00E-05	0.00025
ATP6V1E2	H2009	-1.23783	0.00015	0.000695
TMEM81	H2009	-1.23985	0.0013	0.004883
EPHA4	H2009	-1.24098	5.00E-05	0.00025
TP53	H2009	-1.24297	5.00E-05	0.00025
RAP1GAP2	H2009	-1.24451	5.00E-05	0.00025
WDR87	H2009	-1.24509	5.00E-05	0.00025
LINC01119	H2009	-1.24585	0.0001	0.000478
PLEKHM1P	H2009	-1.24969	0.0001	0.000478
FCRLB	H2009	-1.25082	0.0003	0.001308
LACC1	H2009	-1.25438	0.0001	0.000478
MICALL2	H2009	-1.25548	5.00E-05	0.00025
STS	H2009	-1.25745	5.00E-05	0.00025
ZNF550	H2009	-1.25798	5.00E-05	0.00025
RAET1K	H2009	-1.25838	5.00E-05	0.00025
GLCE	H2009	-1.25892	5.00E-05	0.00025
SRD5A1	H2009	-1.25907	5.00E-05	0.00025
MIEF2	H2009	-1.2608	5.00E-05	0.00025
CDC14A	H2009	-1.26117	5.00E-05	0.00025
IER5L	H2009	-1.26229	5.00E-05	0.00025
TAPT1	H2009	-1.26503	5.00E-05	0.00025
TCP11L1	H2009	-1.26531	5.00E-05	0.00025
ABHD16B	H2009	-1.26561	5.00E-05	0.00025
HECA	H2009	-1.26566	5.00E-05	0.00025
IFI30	H2009	-1.26684	5.00E-05	0.00025
ADAM8	H2009	-1.26896	5.00E-05	0.00025
SH3BGR	H2009	-1.27173	0.00065	0.002626
TTLL7	H2009	-1.27608	5.00E-05	0.00025
LOC101928295	H2009	-1.27761	5.00E-05	0.00025
LOC646719	H2009	-1.27786	5.00E-05	0.00025
LINC00592	H2009	-1.27821	0.0001	0.000478
PPIEL	H2009	-1.27889	0.00105	0.004037
MAP1LC3B	H2009	-1.28042	5.00E-05	0.00025

GPR126	H2009	-1.28146	5.00E-05	0.00025
SETX	H2009	-1.28174	5.00E-05	0.00025
SERPINE1	H2009	-1.28634	5.00E-05	0.00025
NIPSNAP3B	H2009	-1.28986	0.0011	0.004209
CLU	H2009	-1.29042	5.00E-05	0.00025
ARHGEF40	H2009	-1.29295	0.00035	0.001505
PAEP	H2009	-1.29325	0.0017	0.006205
ZNF763	H2009	-1.29408	0.0001	0.000478
SEPW1	H2009	-1.29439	5.00E-05	0.00025
MAP2K3	H2009	-1.29571	5.00E-05	0.00025
KLF10	H2009	-1.29699	5.00E-05	0.00025
EFNB2	H2009	-1.29823	5.00E-05	0.00025
MET	H2009	-1.30341	5.00E-05	0.00025
ZSWIM3	H2009	-1.3041	5.00E-05	0.00025
ARRDC3	H2009	-1.30471	5.00E-05	0.00025
FAM120B	H2009	-1.30493	5.00E-05	0.00025
LOC400684	H2009	-1.30596	0.00015	0.000695
NUDT6	H2009	-1.30819	5.00E-05	0.00025
THAP10	H2009	-1.30932	5.00E-05	0.00025
C21orf67	H2009	-1.30951	5.00E-05	0.00025
RND3	H2009	-1.30951	5.00E-05	0.00025
ALS2CL	H2009	-1.30976	5.00E-05	0.00025
CHKB-AS1	H2009	-1.31196	0.00015	0.000695
HLA-E	H2009	-1.31254	5.00E-05	0.00025
FOXD2-AS1	H2009	-1.31283	5.00E-05	0.00025
GS1-259H13.2	H2009	-1.313	0.0001	0.000478
UGGT2	H2009	-1.31325	5.00E-05	0.00025
ZNF606	H2009	-1.31439	5.00E-05	0.00025
APOL2	H2009	-1.31524	5.00E-05	0.00025
AADAT	H2009	-1.31535	5.00E-05	0.00025
LOC100506746	H2009	-1.31538	5.00E-05	0.00025
TACC1	H2009	-1.31616	5.00E-05	0.00025
ZNF404	H2009	-1.31706	5.00E-05	0.00025
RNMT	H2009	-1.31791	5.00E-05	0.00025
KCNJ8	H2009	-1.31868	5.00E-05	0.00025
BCORL1	H2009	-1.31964	5.00E-05	0.00025
NUDT9P1	H2009	-1.32013	0.00605	0.01904
BEX4	H2009	-1.32044	0.00025	0.001109
THSD4	H2009	-1.32065	5.00E-05	0.00025
STK17A	H2009	-1.32342	5.00E-05	0.00025
NPIPA5	H2009	-1.3238	0.00315	0.010725
SLC20A2	H2009	-1.3248	5.00E-05	0.00025
SFT2D3	H2009	-1.32666	5.00E-05	0.00025

NMNAT1	H2009	-1.32668	5.00E-05	0.00025
MORN1	H2009	-1.32698	0.00075	0.002984
GINS4	H2009	-1.32726	5.00E-05	0.00025
COL12A1	H2009	-1.32893	5.00E-05	0.00025
TBC1D9	H2009	-1.32956	5.00E-05	0.00025
TECPR2	H2009	-1.33024	5.00E-05	0.00025
PTK6	H2009	-1.33275	5.00E-05	0.00025
NKX3-1	H2009	-1.33312	5.00E-05	0.00025
TIMP2	H2009	-1.33395	5.00E-05	0.00025
ARHGAP26	H2009	-1.33591	5.00E-05	0.00025
KLHL31	H2009	-1.33743	5.00E-05	0.00025
ZNF563	H2009	-1.33886	5.00E-05	0.00025
TMEM175	H2009	-1.34064	5.00E-05	0.00025
GDF15	H2009	-1.34226	0.0012	0.004544
COL7A1	H2009	-1.34255	5.00E-05	0.00025
PHLDA2	H2009	-1.34585	5.00E-05	0.00025
ULBP3	H2009	-1.34604	5.00E-05	0.00025
FAM214B	H2009	-1.34608	5.00E-05	0.00025
ADAMTS6	H2009	-1.34642	5.00E-05	0.00025
SAMD15	H2009	-1.34688	5.00E-05	0.00025
PYGL	H2009	-1.34844	5.00E-05	0.00025
PARD6B	H2009	-1.34874	5.00E-05	0.00025
OVOL1	H2009	-1.34917	5.00E-05	0.00025
SC5D	H2009	-1.34935	5.00E-05	0.00025
KHDRBS3	H2009	-1.3515	5.00E-05	0.00025
WNT7A	H2009	-1.35382	5.00E-05	0.00025
LINC01176	H2009	-1.35514	0.0091	0.027241
LRRIQ3	H2009	-1.35703	0.0003	0.001308
ZNF296	H2009	-1.35838	5.00E-05	0.00025
HIST2H3D	H2009	-1.36017	0.0077	0.023529
RNF213	H2009	-1.36182	5.00E-05	0.00025
ZNF610	H2009	-1.36389	5.00E-05	0.00025
TMCC3	H2009	-1.36443	5.00E-05	0.00025
GPATCH2L	H2009	-1.36444	5.00E-05	0.00025
NABP1	H2009	-1.36502	5.00E-05	0.00025
SLFN12L	H2009	-1.36547	0.00095	0.00369
ITGA2	H2009	-1.3657	5.00E-05	0.00025
CCRN4L	H2009	-1.36757	5.00E-05	0.00025
CLIC3	H2009	-1.36818	0.0002	0.000905
IRAK2	H2009	-1.369	5.00E-05	0.00025
PEAK1	H2009	-1.37137	5.00E-05	0.00025
PLEKHH2	H2009	-1.37178	5.00E-05	0.00025
HS6ST1	H2009	-1.37301	5.00E-05	0.00025

C14orf79	H2009	-1.37355	5.00E-05	0.00025
OPN3	H2009	-1.37518	0.00145	0.005381
IRF1	H2009	-1.37559	5.00E-05	0.00025
SMPD1	H2009	-1.37573	5.00E-05	0.00025
CCNYL1	H2009	-1.37952	5.00E-05	0.00025
SLC31A2	H2009	-1.38016	5.00E-05	0.00025
C5orf55	H2009	-1.38183	5.00E-05	0.00025
PTK2B	H2009	-1.38399	5.00E-05	0.00025
FAM101B	H2009	-1.38439	5.00E-05	0.00025
NDST2	H2009	-1.38649	5.00E-05	0.00025
KCNAB2	H2009	-1.38821	0.0006	0.002445
MAFG	H2009	-1.38824	5.00E-05	0.00025
NOXO1	H2009	-1.38856	0.0003	0.001308
TUBA1A	H2009	-1.38869	5.00E-05	0.00025
VCL	H2009	-1.39114	5.00E-05	0.00025
ZNF251	H2009	-1.39143	5.00E-05	0.00025
NINL	H2009	-1.39248	5.00E-05	0.00025
LPAL2	H2009	-1.39259	0.0003	0.001308
ARID5A	H2009	-1.39279	5.00E-05	0.00025
SERINC5	H2009	-1.39315	5.00E-05	0.00025
YPEL3	H2009	-1.4002	5.00E-05	0.00025
RAB36	H2009	-1.40631	5.00E-05	0.00025
LOC101927204	H2009	-1.40913	5.00E-05	0.00025
LRRC37A3	H2009	-1.40927	5.00E-05	0.00025
STOX1	H2009	-1.40947	5.00E-05	0.00025
SLFN12	H2009	-1.41274	5.00E-05	0.00025
DHDH	H2009	-1.41607	0.00305	0.010422
SMCO2	H2009	-1.41967	0.00105	0.004037
IDH2	H2009	-1.42567	5.00E-05	0.00025
NES	H2009	-1.42815	5.00E-05	0.00025
ASF1B	H2009	-1.42963	5.00E-05	0.00025
CHST11	H2009	-1.43112	5.00E-05	0.00025
DHRS3	H2009	-1.43346	5.00E-05	0.00025
KCTD13	H2009	-1.43603	5.00E-05	0.00025
DHRS4L2	H2009	-1.4399	5.00E-05	0.00025
ANKRD42	H2009	-1.44038	5.00E-05	0.00025
PMAIP1	H2009	-1.4422	5.00E-05	0.00025
IFNA8	H2009	-1.44227	5.00E-05	0.00025
HSPA2	H2009	-1.44465	5.00E-05	0.00025
AMACR	H2009	-1.44505	5.00E-05	0.00025
SLFN5	H2009	-1.44559	5.00E-05	0.00025
PXDC1	H2009	-1.44802	5.00E-05	0.00025
TMC8	H2009	-1.44862	0.01295	0.037085

ZNF846	H2009	-1.44904	5.00E-05	0.00025
GAS6-AS2	H2009	-1.44921	5.00E-05	0.00025
HRH1	H2009	-1.44946	5.00E-05	0.00025
LINC00601	H2009	-1.45015	0.0007	0.002808
TRAF1	H2009	-1.45187	5.00E-05	0.00025
RPL23AP53	H2009	-1.45209	5.00E-05	0.00025
IL17D	H2009	-1.45553	5.00E-05	0.00025
GATA2	H2009	-1.4565	5.00E-05	0.00025
SLC9A1	H2009	-1.45701	5.00E-05	0.00025
TBX20	H2009	-1.46132	5.00E-05	0.00025
RABL2A	H2009	-1.46308	5.00E-05	0.00025
TRIM36	H2009	-1.46418	5.00E-05	0.00025
ENPP1	H2009	-1.46513	5.00E-05	0.00025
UBE2D1	H2009	-1.46942	5.00E-05	0.00025
FAM210A	H2009	-1.47189	5.00E-05	0.00025
SLC2A11	H2009	-1.4746	5.00E-05	0.00025
MORC4	H2009	-1.47488	5.00E-05	0.00025
RLN2	H2009	-1.48445	5.00E-05	0.00025
POLR2A	H2009	-1.48473	5.00E-05	0.00025
ARHGAP30	H2009	-1.48518	5.00E-05	0.00025
HMGCL	H2009	-1.4857	5.00E-05	0.00025
FURIN	H2009	-1.48596	5.00E-05	0.00025
MAK	H2009	-1.487	5.00E-05	0.00025
CBX4	H2009	-1.48917	5.00E-05	0.00025
LOC155060	H2009	-1.49135	5.00E-05	0.00025
IGDCC4	H2009	-1.49149	5.00E-05	0.00025
CDKL5	H2009	-1.49204	5.00E-05	0.00025
LGMN	H2009	-1.49214	5.00E-05	0.00025
FAM219B	H2009	-1.49312	5.00E-05	0.00025
LOC100130744	H2009	-1.49327	0.002	0.007171
OSMR-AS1	H2009	-1.49328	0.01045	0.030757
LINC00941	H2009	-1.49364	5.00E-05	0.00025
ADPRHL1	H2009	-1.49402	5.00E-05	0.00025
CCNA1	H2009	-1.49765	5.00E-05	0.00025
FAM167B	H2009	-1.49813	0.001	0.003864
ITPRIP	H2009	-1.49831	5.00E-05	0.00025
NR1D1	H2009	-1.49899	5.00E-05	0.00025
ELAVL2	H2009	-1.50012	5.00E-05	0.00025
KIAA1161	H2009	-1.5028	5.00E-05	0.00025
TNFAIP3	H2009	-1.50671	5.00E-05	0.00025
ELOVL7	H2009	-1.5068	5.00E-05	0.00025
SH3BGRL2	H2009	-1.50856	5.00E-05	0.00025
IL23A	H2009	-1.51078	5.00E-05	0.00025

BACH1	H2009	-1.51289	5.00E-05	0.00025
LTBP2	H2009	-1.5141	5.00E-05	0.00025
TPCN1	H2009	-1.51415	5.00E-05	0.00025
CAPN10-AS1	H2009	-1.5157	5.00E-05	0.00025
CCDC146	H2009	-1.51586	0.0001	0.000478
LOC101928103	H2009	-1.51608	0.00025	0.001109
LOC648987	H2009	-1.52106	0.0091	0.027241
LSMEM1	H2009	-1.52277	0.00185	0.006693
SLC35D1	H2009	-1.52599	5.00E-05	0.00025
OSTM1	H2009	-1.5269	5.00E-05	0.00025
CRELD1	H2009	-1.52692	5.00E-05	0.00025
CDKL3	H2009	-1.53057	5.00E-05	0.00025
TSPYL2	H2009	-1.53332	5.00E-05	0.00025
RIBC2	H2009	-1.53649	5.00E-05	0.00025
C2orf27A	H2009	-1.53658	0.0028	0.009662
TMEM38A	H2009	-1.53665	5.00E-05	0.00025
LINC00294	H2009	-1.53682	5.00E-05	0.00025
RBPMS	H2009	-1.53684	5.00E-05	0.00025
ZBED5-AS1	H2009	-1.53841	5.00E-05	0.00025
BBS1	H2009	-1.53961	5.00E-05	0.00025
LPIN2	H2009	-1.54189	5.00E-05	0.00025
ACCS	H2009	-1.54255	5.00E-05	0.00025
PCP4L1	H2009	-1.54263	5.00E-05	0.00025
ARHGAP31	H2009	-1.54266	5.00E-05	0.00025
PPP4R1L	H2009	-1.54345	5.00E-05	0.00025
GABARAPL1	H2009	-1.54357	5.00E-05	0.00025
WBSCR27	H2009	-1.54504	5.00E-05	0.00025
LRRC27	H2009	-1.54745	5.00E-05	0.00025
SGMS2	H2009	-1.54803	5.00E-05	0.00025
SMIM24	H2009	-1.55151	5.00E-05	0.00025
ATG2A	H2009	-1.55282	5.00E-05	0.00025
NTN4	H2009	-1.55555	5.00E-05	0.00025
NUP62CL	H2009	-1.56129	5.00E-05	0.00025
ZBED9	H2009	-1.56205	5.00E-05	0.00025
CEP83-AS1	H2009	-1.56383	5.00E-05	0.00025
JHDM1D-AS1	H2009	-1.5665	5.00E-05	0.00025
FAM171B	H2009	-1.57165	5.00E-05	0.00025
GUCA1B	H2009	-1.57284	5.00E-05	0.00025
MEGF8	H2009	-1.57288	5.00E-05	0.00025
NXNL2	H2009	-1.57595	0.0052	0.016666
LINC00507	H2009	-1.57603	0.0001	0.000478
ZNF844	H2009	-1.57688	5.00E-05	0.00025
ARSB	H2009	-1.57804	5.00E-05	0.00025

MGAT5	H2009	-1.58408	5.00E-05	0.00025
TNFRSF10C	H2009	-1.58731	5.00E-05	0.00025
ST3GAL3	H2009	-1.58876	5.00E-05	0.00025
PIK3IP1	H2009	-1.59138	5.00E-05	0.00025
CCDC80	H2009	-1.59163	5.00E-05	0.00025
VASN	H2009	-1.59179	5.00E-05	0.00025
RP2	H2009	-1.59193	5.00E-05	0.00025
SH2D2A	H2009	-1.59241	5.00E-05	0.00025
FBF1	H2009	-1.59243	5.00E-05	0.00025
ZNF554	H2009	-1.5938	5.00E-05	0.00025
FLJ27354	H2009	-1.5959	0.00345	0.011614
TPI1P2	H2009	-1.59729	5.00E-05	0.00025
HIST1H2AG	H2009	-1.59848	5.00E-05	0.00025
LOC100132077	H2009	-1.60117	5.00E-05	0.00025
NKX3-2	H2009	-1.60388	5.00E-05	0.00025
LOC729970	H2009	-1.60471	0.0015	0.005546
HIST1H2AC	H2009	-1.6074	5.00E-05	0.00025
IQCD	H2009	-1.61067	5.00E-05	0.00025
PPP1R15A	H2009	-1.61228	5.00E-05	0.00025
LINC00240	H2009	-1.61237	0.00925	0.027632
CCRL2	H2009	-1.61523	5.00E-05	0.00025
KLRAP1	H2009	-1.6176	5.00E-05	0.00025
PRSS22	H2009	-1.61824	5.00E-05	0.00025
RASD1	H2009	-1.61827	5.00E-05	0.00025
ADTRP	H2009	-1.61975	5.00E-05	0.00025
CSGALNACT2	H2009	-1.62186	5.00E-05	0.00025
PTGR1	H2009	-1.62251	5.00E-05	0.00025
NTRK2	H2009	-1.6269	5.00E-05	0.00025
KRCC1	H2009	-1.63112	5.00E-05	0.00025
C12orf57	H2009	-1.63136	5.00E-05	0.00025
H6PD	H2009	-1.63217	5.00E-05	0.00025
VSIG10	H2009	-1.63228	5.00E-05	0.00025
SEC31B	H2009	-1.6331	5.00E-05	0.00025
CTF1	H2009	-1.63355	5.00E-05	0.00025
SGK1	H2009	-1.637	5.00E-05	0.00025
MICU3	H2009	-1.6382	5.00E-05	0.00025
N4BP2L1	H2009	-1.6395	5.00E-05	0.00025
SELPLG	H2009	-1.64094	5.00E-05	0.00025
HIST1H4H	H2009	-1.64125	0.0043	0.014105
PELI1	H2009	-1.6435	5.00E-05	0.00025
CRIP1	H2009	-1.64385	5.00E-05	0.00025
LOC54944	H2009	-1.64466	5.00E-05	0.00025
HIST1H2AM	H2009	-1.64719	5.00E-05	0.00025

TMEM44-AS1	H2009	-1.64805	0.0004	0.001697
SHOX2	H2009	-1.65226	5.00E-05	0.00025
CCDC11	H2009	-1.65802	0.00015	0.000695
RHOV	H2009	-1.66142	5.00E-05	0.00025
ZSWIM4	H2009	-1.66455	5.00E-05	0.00025
NEDD9	H2009	-1.66998	5.00E-05	0.00025
HAPLN3	H2009	-1.68343	5.00E-05	0.00025
GAN	H2009	-1.68365	5.00E-05	0.00025
PPM1M	H2009	-1.68863	0.0002	0.000905
DDX60L	H2009	-1.69033	5.00E-05	0.00025
FAM86C2P	H2009	-1.69402	5.00E-05	0.00025
ZNF702P	H2009	-1.69426	5.00E-05	0.00025
MFGE8	H2009	-1.69547	5.00E-05	0.00025
GCH1	H2009	-1.69796	5.00E-05	0.00025
LINC00174	H2009	-1.69798	5.00E-05	0.00025
ZCCHC24	H2009	-1.70664	5.00E-05	0.00025
WDFY3-AS2	H2009	-1.72153	5.00E-05	0.00025
C21orf58	H2009	-1.72246	5.00E-05	0.00025
EPOR	H2009	-1.72799	5.00E-05	0.00025
RNF19B	H2009	-1.73882	5.00E-05	0.00025
FMO4	H2009	-1.74252	0.0011	0.004209
TFPI2	H2009	-1.74578	5.00E-05	0.00025
HIST1H2BK	H2009	-1.74749	5.00E-05	0.00025
FAHD2CP	H2009	-1.74845	0.0009	0.003515
ATP6AP1L	H2009	-1.74909	5.00E-05	0.00025
NTNG2	H2009	-1.75427	5.00E-05	0.00025
LMBRD2	H2009	-1.75483	5.00E-05	0.00025
ABHD5	H2009	-1.76182	5.00E-05	0.00025
ELOVL4	H2009	-1.76461	5.00E-05	0.00025
PPP1R3F	H2009	-1.76462	5.00E-05	0.00025
PDLIM3	H2009	-1.76576	5.00E-05	0.00025
RFTN2	H2009	-1.77145	0.00035	0.001505
DCUN1D2	H2009	-1.77313	5.00E-05	0.00025
CRYL1	H2009	-1.77371	5.00E-05	0.00025
LIPG	H2009	-1.77618	5.00E-05	0.00025
CRISPLD2	H2009	-1.7765	5.00E-05	0.00025
SMOX	H2009	-1.77762	5.00E-05	0.00025
RNF32	H2009	-1.77789	5.00E-05	0.00025
PRKAR2A-AS1	H2009	-1.78124	5.00E-05	0.00025
LINC01061	H2009	-1.78214	5.00E-05	0.00025
ETS2	H2009	-1.7826	5.00E-05	0.00025
CCDC19	H2009	-1.78715	5.00E-05	0.00025
CLDN9	H2009	-1.79934	5.00E-05	0.00025

NCEH1	H2009	-1.80208	5.00E-05	0.00025
WDR88	H2009	-1.80531	0.0005	0.002076
EPHA2	H2009	-1.80551	5.00E-05	0.00025
ZNF517	H2009	-1.80716	5.00E-05	0.00025
ENO3	H2009	-1.80933	5.00E-05	0.00025
TOB2P1	H2009	-1.81259	5.00E-05	0.00025
TMEM158	H2009	-1.81357	5.00E-05	0.00025
ERN1	H2009	-1.82343	5.00E-05	0.00025
ANTXR2	H2009	-1.82496	5.00E-05	0.00025
CCDC92	H2009	-1.83648	5.00E-05	0.00025
MAN1A1	H2009	-1.83742	5.00E-05	0.00025
KCNG3	H2009	-1.83744	5.00E-05	0.00025
CATSPER3	H2009	-1.84065	0.0004	0.001697
TOB1	H2009	-1.8432	5.00E-05	0.00025
HHLA3	H2009	-1.84466	5.00E-05	0.00025
NT5E	H2009	-1.84893	5.00E-05	0.00025
UCN2	H2009	-1.85474	5.00E-05	0.00025
HIST1H2AE	H2009	-1.85556	0.0003	0.001308
TRIM4	H2009	-1.85754	5.00E-05	0.00025
CD274	H2009	-1.86963	5.00E-05	0.00025
WDR78	H2009	-1.87114	5.00E-05	0.00025
NOP14-AS1	H2009	-1.87129	0.0079	0.024065
PIK3R3	H2009	-1.87226	5.00E-05	0.00025
HCST	H2009	-1.87499	0.0081	0.024604
CCT6B	H2009	-1.87542	0.0005	0.002076
CASC11	H2009	-1.87932	0.00465	0.015107
LBX2-AS1	H2009	-1.88099	0.00255	0.008898
CSRNP2	H2009	-1.88442	5.00E-05	0.00025
COQ10A	H2009	-1.88556	5.00E-05	0.00025
LOC158960	H2009	-1.88576	5.00E-05	0.00025
FAM86FP	H2009	-1.88642	0.0001	0.000478
GCSAM	H2009	-1.88671	5.00E-05	0.00025
CABLES2	H2009	-1.88684	5.00E-05	0.00025
RASL11B	H2009	-1.89505	5.00E-05	0.00025
GIPR	H2009	-1.89954	5.00E-05	0.00025
ZNF177	H2009	-1.90637	0.0121	0.034958
KCNK5	H2009	-1.90641	5.00E-05	0.00025
TMX4	H2009	-1.90869	5.00E-05	0.00025
SLC13A3	H2009	-1.91039	0.0004	0.001697
42432	H2009	-1.91779	5.00E-05	0.00025
TBX19	H2009	-1.93122	5.00E-05	0.00025
WDR31	H2009	-1.93163	5.00E-05	0.00025
ARL14	H2009	-1.93231	5.00E-05	0.00025

TNFRSF10D	H2009	-1.93244	5.00E-05	0.00025
TGFA	H2009	-1.93523	5.00E-05	0.00025
LOC100289361	H2009	-1.93558	5.00E-05	0.00025
GLUL	H2009	-1.93887	5.00E-05	0.00025
BFSP1	H2009	-1.93918	5.00E-05	0.00025
HIST3H2A	H2009	-1.94078	5.00E-05	0.00025
RBM26-AS1	H2009	-1.94145	5.00E-05	0.00025
CDRT4	H2009	-1.94257	0.0009	0.003515
DHRS12	H2009	-1.94273	5.00E-05	0.00025
TNFRSF6B	H2009	-1.946	0.00965	0.028691
LINC00337	H2009	-1.94634	5.00E-05	0.00025
BTG2	H2009	-1.95648	5.00E-05	0.00025
LOC100652758	H2009	-1.95661	5.00E-05	0.00025
BVES	H2009	-1.96293	5.00E-05	0.00025
TP53INP1	H2009	-1.9718	5.00E-05	0.00025
SLC12A2	H2009	-1.99049	5.00E-05	0.00025
SPRED3	H2009	-1.99751	5.00E-05	0.00025
THAP7-AS1	H2009	-2.00197	0.0064	0.019994
TSGA10	H2009	-2.00999	5.00E-05	0.00025
TAGLN	H2009	-2.01231	0.00015	0.000695
BACE1	H2009	-2.01306	5.00E-05	0.00025
TNFSF9	H2009	-2.0267	5.00E-05	0.00025
HIST2H2BF	H2009	-2.033	5.00E-05	0.00025
TNKS2-AS1	H2009	-2.03341	0.00355	0.01191
KHDC1	H2009	-2.04215	5.00E-05	0.00025
TSSK3	H2009	-2.04573	5.00E-05	0.00025
APOLD1	H2009	-2.04862	5.00E-05	0.00025
ZNF641	H2009	-2.04886	5.00E-05	0.00025
F2R	H2009	-2.05403	5.00E-05	0.00025
DDX26B	H2009	-2.05528	5.00E-05	0.00025
LOC100507634	H2009	-2.05831	5.00E-05	0.00025
FAM229A	H2009	-2.06176	0.00215	0.007645
KLHL15	H2009	-2.06341	5.00E-05	0.00025
ARSD	H2009	-2.07633	5.00E-05	0.00025
SOCS1	H2009	-2.09088	5.00E-05	0.00025
TK2	H2009	-2.09714	5.00E-05	0.00025
PLXNA3	H2009	-2.10645	5.00E-05	0.00025
LOC100129636	H2009	-2.10874	0.00355	0.01191
MICB	H2009	-2.11135	5.00E-05	0.00025
AQP7P3	H2009	-2.12687	0.00445	0.014541
WDR47	H2009	-2.13369	5.00E-05	0.00025
HEXIM1	H2009	-2.13477	5.00E-05	0.00025
IL11	H2009	-2.13826	5.00E-05	0.00025

C1QTNF1	H2009	-2.14819	5.00E-05	0.00025
PRDM8	H2009	-2.1489	5.00E-05	0.00025
PAPL	H2009	-2.15126	5.00E-05	0.00025
CNNM4	H2009	-2.15596	5.00E-05	0.00025
HIST1H2BN	H2009	-2.16728	0.0036	0.012058
KLLN	H2009	-2.16799	5.00E-05	0.00025
FLJ42969	H2009	-2.17324	5.00E-05	0.00025
SLC16A5	H2009	-2.18141	5.00E-05	0.00025
HHAT	H2009	-2.1894	5.00E-05	0.00025
CPEB4	H2009	-2.19308	5.00E-05	0.00025
HIST3H2BB	H2009	-2.19913	0.00735	0.022583
CCDC103	H2009	-2.20024	5.00E-05	0.00025
SOHLH2	H2009	-2.20148	0.0124	0.035699
PPP1R36	H2009	-2.20594	0.0005	0.002076
HELZ2	H2009	-2.2126	5.00E-05	0.00025
HSD17B6	H2009	-2.21316	5.00E-05	0.00025
LINC00936	H2009	-2.21621	5.00E-05	0.00025
SERPINI1	H2009	-2.22268	5.00E-05	0.00025
FZD7	H2009	-2.22316	5.00E-05	0.00025
SLC26A2	H2009	-2.23515	5.00E-05	0.00025
C19orf18	H2009	-2.2379	5.00E-05	0.00025
LOC100272217	H2009	-2.2412	5.00E-05	0.00025
MAN1B1-AS1	H2009	-2.24166	5.00E-05	0.00025
MIR31HG	H2009	-2.24287	5.00E-05	0.00025
DNAJA4	H2009	-2.24999	5.00E-05	0.00025
WNT3	H2009	-2.25086	5.00E-05	0.00025
GPR176	H2009	-2.25519	5.00E-05	0.00025
BTBD19	H2009	-2.25952	5.00E-05	0.00025
HIST1H2BJ	H2009	-2.2701	5.00E-05	0.00025
CTSV	H2009	-2.27929	5.00E-05	0.00025
ROS1	H2009	-2.30282	5.00E-05	0.00025
SYNM	H2009	-2.31469	5.00E-05	0.00025
FOS	H2009	-2.32608	5.00E-05	0.00025
YPEL5	H2009	-2.32722	5.00E-05	0.00025
LIPE-AS1	H2009	-2.33254	0.00375	0.012501
SCARF1	H2009	-2.33297	5.00E-05	0.00025
SNAI1	H2009	-2.33404	5.00E-05	0.00025
APLN	H2009	-2.33541	5.00E-05	0.00025
DOCK9-AS2	H2009	-2.33563	5.00E-05	0.00025
FAM86B3P	H2009	-2.33804	5.00E-05	0.00025
LOC644189	H2009	-2.35716	5.00E-05	0.00025
CAPN5	H2009	-2.35843	5.00E-05	0.00025
SNAI3-AS1	H2009	-2.36905	5.00E-05	0.00025

SMC1B	H2009	-2.37045	5.00E-05	0.00025
TP53INP2	H2009	-2.3759	5.00E-05	0.00025
LEKR1	H2009	-2.38361	5.00E-05	0.00025
DLGAP1-AS2	H2009	-2.39276	5.00E-05	0.00025
PSCA	H2009	-2.39336	5.00E-05	0.00025
TPTE2	H2009	-2.40597	5.00E-05	0.00025
HIST1H2BG	H2009	-2.41247	5.00E-05	0.00025
GBX2	H2009	-2.41527	5.00E-05	0.00025
PAQR8	H2009	-2.41652	5.00E-05	0.00025
ARC	H2009	-2.41873	5.00E-05	0.00025
AKAP12	H2009	-2.41884	5.00E-05	0.00025
MEIG1	H2009	-2.42948	0.00025	0.001109
LOC100131691	H2009	-2.44215	5.00E-05	0.00025
SLC5A4	H2009	-2.44325	5.00E-05	0.00025
CABYR	H2009	-2.4462	5.00E-05	0.00025
PDCD4-AS1	H2009	-2.44717	5.00E-05	0.00025
MARCKSL1	H2009	-2.44993	5.00E-05	0.00025
SPRY4	H2009	-2.45891	5.00E-05	0.00025
ZNF703	H2009	-2.45895	5.00E-05	0.00025
HIST2H2BA	H2009	-2.4631	5.00E-05	0.00025
EPPK1	H2009	-2.47323	5.00E-05	0.00025
PLK3	H2009	-2.48084	5.00E-05	0.00025
PGF	H2009	-2.48173	5.00E-05	0.00025
TUFT1	H2009	-2.48608	5.00E-05	0.00025
RNASE1	H2009	-2.50087	5.00E-05	0.00025
LOC101927043	H2009	-2.50198	0.00085	0.003341
CTSO	H2009	-2.5136	5.00E-05	0.00025
BST1	H2009	-2.5138	5.00E-05	0.00025
CYP1A1	H2009	-2.51416	5.00E-05	0.00025
MEIS3	H2009	-2.51463	5.00E-05	0.00025
KLHL22	H2009	-2.51909	5.00E-05	0.00025
VAMP1	H2009	-2.52444	5.00E-05	0.00025
NR4A2	H2009	-2.52927	5.00E-05	0.00025
ULBP2	H2009	-2.52931	5.00E-05	0.00025
OSGIN1	H2009	-2.5424	5.00E-05	0.00025
PON1	H2009	-2.55421	0.0014	0.005217
LOC100996324	H2009	-2.55562	5.00E-05	0.00025
FAM132B	H2009	-2.55896	5.00E-05	0.00025
HCP5	H2009	-2.56506	5.00E-05	0.00025
HAR1B	H2009	-2.58741	0.0031	0.010574
B3GALT4	H2009	-2.58942	5.00E-05	0.00025
LOC399815	H2009	-2.59417	0.0001	0.000478
FRG2	H2009	-2.59511	5.00E-05	0.00025

CEBPA	H2009	-2.60076	5.00E-05	0.00025
LOC100268168	H2009	-2.6324	5.00E-05	0.00025
KLHL29	H2009	-2.63281	5.00E-05	0.00025
LOC102723354	H2009	-2.63646	0.00065	0.002626
HIC1	H2009	-2.64481	5.00E-05	0.00025
FLJ44313	H2009	-2.64907	5.00E-05	0.00025
PLEKHO2	H2009	-2.65029	5.00E-05	0.00025
LINC01212	H2009	-2.6731	5.00E-05	0.00025
TMEM190	H2009	-2.67324	0.0044	0.014395
CDKN2B	H2009	-2.67348	5.00E-05	0.00025
PCYOX1L	H2009	-2.69295	5.00E-05	0.00025
NUP50-AS1	H2009	-2.69327	5.00E-05	0.00025
SLC16A10	H2009	-2.69419	5.00E-05	0.00025
MAP2	H2009	-2.6988	5.00E-05	0.00025
MAFF	H2009	-2.70196	5.00E-05	0.00025
SLC17A7	H2009	-2.70773	5.00E-05	0.00025
HBEGF	H2009	-2.70943	5.00E-05	0.00025
YTHDF3-AS1	H2009	-2.70972	0.00075	0.002984
LOC100506207	H2009	-2.73061	5.00E-05	0.00025
MLLT11	H2009	-2.73668	5.00E-05	0.00025
PROCA1	H2009	-2.74498	5.00E-05	0.00025
STC1	H2009	-2.74618	5.00E-05	0.00025
CBR3	H2009	-2.75532	5.00E-05	0.00025
LPXN	H2009	-2.75927	5.00E-05	0.00025
LRAT	H2009	-2.76188	5.00E-05	0.00025
HIST1H2BD	H2009	-2.77272	5.00E-05	0.00025
HIST1H3H	H2009	-2.77755	0.00345	0.011614
TMEM2	H2009	-2.77942	5.00E-05	0.00025
GALR2	H2009	-2.78375	5.00E-05	0.00025
LINC01024	H2009	-2.81226	5.00E-05	0.00025
DLX2	H2009	-2.8186	5.00E-05	0.00025
FAM46C	H2009	-2.83593	5.00E-05	0.00025
LOH12CR2	H2009	-2.83607	0.00185	0.006693
ID2	H2009	-2.84545	5.00E-05	0.00025
SORBS1	H2009	-2.85262	5.00E-05	0.00025
PGAM2	H2009	-2.87425	5.00E-05	0.00025
TMEM31	H2009	-2.88294	0.0047	0.01525
OSER1-AS1	H2009	-2.88325	5.00E-05	0.00025
OVGP1	H2009	-2.89784	5.00E-05	0.00025
FAM43A	H2009	-2.91412	5.00E-05	0.00025
NPTXR	H2009	-2.91653	5.00E-05	0.00025
ASB4	H2009	-2.92076	5.00E-05	0.00025
FAM222A	H2009	-2.926	5.00E-05	0.00025

C2orf48	H2009	-2.92627	5.00E-05	0.00025
GADD45A	H2009	-2.9353	5.00E-05	0.00025
HIST2H2BE	H2009	-2.9732	5.00E-05	0.00025
RASGRF1	H2009	-3.006	5.00E-05	0.00025
DBIL5P	H2009	-3.02006	5.00E-05	0.00025
SYTL2	H2009	-3.03553	5.00E-05	0.00025
TLE4	H2009	-3.05274	5.00E-05	0.00025
NRARP	H2009	-3.06638	5.00E-05	0.00025
LINC01125	H2009	-3.06721	0.0003	0.001308
LOC653160	H2009	-3.08512	5.00E-05	0.00025
PINLYP	H2009	-3.10555	0.00035	0.001505
ATF3	H2009	-3.15173	5.00E-05	0.00025
HIST1H2BO	H2009	-3.18345	5.00E-05	0.00025
STX11	H2009	-3.19322	5.00E-05	0.00025
CCDC147	H2009	-3.26263	5.00E-05	0.00025
ADM	H2009	-3.27904	5.00E-05	0.00025
C9orf169	H2009	-3.29436	5.00E-05	0.00025
VIPR1	H2009	-3.31239	5.00E-05	0.00025
ZNF425	H2009	-3.32344	5.00E-05	0.00025
LOC100289495	H2009	-3.32684	5.00E-05	0.00025
CTGF	H2009	-3.35704	5.00E-05	0.00025
IFI27	H2009	-3.44108	0.00075	0.002984
RND1	H2009	-3.49026	5.00E-05	0.00025
NBPF18P	H2009	-3.4974	0.01005	0.029723
C1orf61	H2009	-3.52474	5.00E-05	0.00025
WDR96	H2009	-3.5698	5.00E-05	0.00025
PCDH10	H2009	-3.59934	5.00E-05	0.00025
MYL4	H2009	-3.62031	0.01225	0.035331
USP12-AS2	H2009	-3.63245	0.0099	0.029335
RNF122	H2009	-3.68197	5.00E-05	0.00025
WEE2-AS1	H2009	-3.69188	5.00E-05	0.00025
SP6	H2009	-3.70915	5.00E-05	0.00025
LOC90246	H2009	-3.7425	5.00E-05	0.00025
ZFP2	H2009	-3.79833	5.00E-05	0.00025
ERO1LB	H2009	-3.84576	5.00E-05	0.00025
C1QL4	H2009	-3.92652	5.00E-05	0.00025
FOSB	H2009	-4.02136	5.00E-05	0.00025
C2orf78	H2009	-4.08468	5.00E-05	0.00025
FGFR3	H2009	-4.21506	5.00E-05	0.00025
TEX14	H2009	-4.68764	5.00E-05	0.00025
PIPOX	H2009	-4.72353	5.00E-05	0.00025
PLA2G4C	H2009	-4.74151	5.00E-05	0.00025
NPTX2	H2009	-4.85981	5.00E-05	0.00025

HAP1	H2009	-4.90745	5.00E-05	0.00025
NR4A3	H2009	-5.10486	5.00E-05	0.00025
NPTX1	H2009	-5.19525	5.00E-05	0.00025
LGI4	H2009	-5.19832	0.00035	0.001505
GOLGA6C	H2009	-5.20109	0.00025	0.001109
HCG26	H2009	-5.2998	0.0084	0.025405
DLL4	H2009	-5.64897	5.00E-05	0.00025
C17orf103	H2009	-5.81597	5.00E-05	0.00025
STEAP1	H596	1.54702	0.0023	0.00812
DDX39A	H596	1.50836	5.00E-05	0.00025
PLA2G2A	H596	1.36352	0.00045	0.001888
HIST1H4J	H596	1.34522	0.01775	0.048702
HIST2H2AC	H596	1.31239	5.00E-05	0.00025
HIST1H2AJ	H596	1.30941	0.00025	0.001109
TFEC	H596	1.28965	0.00055	0.002261
IL1RL1	H596	1.26759	5.00E-05	0.00025
CDH6	H596	1.24367	5.00E-05	0.00025
GJB6	H596	1.23546	0.0006	0.002445
SNRPA	H596	1.20451	5.00E-05	0.00025
HOTAIRM1	H596	1.15675	0.0146	0.041203
VIT	H596	1.14721	0.0116	0.033691
TRIM47	H596	1.12783	5.00E-05	0.00025
C4BPB	H596	1.09592	0.00385	0.012794
DLK2	H596	1.08797	0.01275	0.036582
TFAP4	H596	1.08338	5.00E-05	0.00025
ZSCAN31	H596	1.07757	5.00E-05	0.00025
RPP40	H596	1.07477	5.00E-05	0.00025
ZBED2	H596	1.05297	0.0062	0.019448
TNFAIP8L1	H596	1.05202	5.00E-05	0.00025
RPL22L1	H596	1.04921	5.00E-05	0.00025
SAMD13	H596	1.04224	0.0093	0.027764
SOCS2	H596	1.03498	0.00035	0.001505
CDC20	H596	1.03437	5.00E-05	0.00025
HAGHL	H596	1.01367	0.0024	0.008431
KRT14	H596	1.00125	0.0003	0.001308
ACKR3	H596	1.00085	0.00015	0.000695
ZNF844	H596	-1.00225	0.0001	0.000478
GMDS-AS1	H596	-1.00582	0.00585	0.018479
FAM222A	H596	-1.00816	5.00E-05	0.00025
CDC14A	H596	-1.00896	0.00195	0.00701
GRAMD1C	H596	-1.01325	0.00025	0.001109
LOC642236	H596	-1.01641	0.00485	0.015679
GABRQ	H596	-1.01948	0.0071	0.021907

SOCS1	H596	-1.02664	0.01225	0.035331
STMN3	H596	-1.02794	0.00145	0.005381
ERP27	H596	-1.02865	0.01495	0.04205
FAM214B	H596	-1.03316	0.00045	0.001888
SFTA1P	H596	-1.03463	0.01775	0.048702
GADD45B	H596	-1.03496	5.00E-05	0.00025
WDFY3-AS2	H596	-1.03583	0.0028	0.009662
FOSB	H596	-1.03725	5.00E-05	0.00025
ING4	H596	-1.03908	5.00E-05	0.00025
LOC101927204	H596	-1.04147	0.00015	0.000695
AMDHD1	H596	-1.0435	0.0077	0.023529
FANK1	H596	-1.04607	0.00395	0.013087
IRF7	H596	-1.04629	5.00E-05	0.00025
MEIS3	H596	-1.05143	0.00085	0.003341
ACBD7	H596	-1.05441	0.0029	0.009968
FLJ37201	H596	-1.06067	0.0084	0.025405
LOC400684	H596	-1.06232	0.01255	0.03608
FMO4	H596	-1.06837	0.00095	0.00369
HIST1H2BC	H596	-1.07199	5.00E-05	0.00025
LCA5L	H596	-1.07768	0.00475	0.015392
SLC2A12	H596	-1.0902	0.00075	0.002984
LRRC27	H596	-1.09042	0.0062	0.019448
ID2	H596	-1.09044	5.00E-05	0.00025
TRAPPC6A	H596	-1.10155	0.0001	0.000478
LOC158960	H596	-1.10337	0.0003	0.001308
PSG4	H596	-1.11081	5.00E-05	0.00025
KLHL7-AS1	H596	-1.11207	5.00E-05	0.00025
NUP62CL	H596	-1.11467	5.00E-05	0.00025
TSGA10	H596	-1.11479	0.00855	0.025807
CRYL1	H596	-1.11491	5.00E-05	0.00025
PAIP2B	H596	-1.12245	0.0003	0.001308
CDKL3	H596	-1.12329	0.00265	0.009207
LEKR1	H596	-1.1246	0.0023	0.00812
COQ10A	H596	-1.12559	0.00015	0.000695
CD86	H596	-1.14031	0.00035	0.001505
ZBED5-AS1	H596	-1.14404	5.00E-05	0.00025
C19orf82	H596	-1.14462	0.0031	0.010574
ATP6AP1L	H596	-1.15188	0.00165	0.006042
AKAP12	H596	-1.15389	0.0001	0.000478
ERV3-1	H596	-1.15894	0.0014	0.005217
STK4-AS1	H596	-1.16125	0.0018	0.006531
PLXNA3	H596	-1.16277	5.00E-05	0.00025
LPXN	H596	-1.16283	0.00075	0.002984

GLRB	H596	-1.16681	0.0001	0.000478
ANKRD20A12P	H596	-1.16719	0.01005	0.029723
CCT6B	H596	-1.17569	0.00025	0.001109
GLIPR2	H596	-1.17697	0.0002	0.000905
LOC399815	H596	-1.17805	0.0102	0.030113
IL1A	H596	-1.18008	0.00015	0.000695
GDF15	H596	-1.18132	5.00E-05	0.00025
CORO1A	H596	-1.18149	0.0002	0.000905
CCDC146	H596	-1.18271	0.0038	0.012649
LACC1	H596	-1.18496	0.0025	0.008741
OSER1-AS1	H596	-1.18497	5.00E-05	0.00025
HIST1H2AG	H596	-1.18598	5.00E-05	0.00025
C2orf48	H596	-1.1966	0.0041	0.013524
GALR2	H596	-1.19681	0.00395	0.013087
LOC102606465	H596	-1.19834	0.0002	0.000905
HIST1H2BD	H596	-1.20949	5.00E-05	0.00025
DKFZp434J0226	H596	-1.21011	0.0005	0.002076
BFSP1	H596	-1.21197	0.0006	0.002445
SLC30A4	H596	-1.21462	0.00065	0.002626
ERO1LB	H596	-1.21983	5.00E-05	0.00025
VAMP1	H596	-1.22428	0.00425	0.013956
ELDR	H596	-1.23093	0.0157	0.043867
HHAT	H596	-1.23961	0.0001	0.000478
LINC00888	H596	-1.2427	5.00E-05	0.00025
CABYR	H596	-1.24895	0.00015	0.000695
LOC100506476	H596	-1.25672	0.00285	0.009815
WDR31	H596	-1.25852	0.00025	0.001109
CTSO	H596	-1.25954	5.00E-05	0.00025
POLR2A	H596	-1.26963	5.00E-05	0.00025
KIAA1107	H596	-1.28051	0.0002	0.000905
PADI3	H596	-1.28091	5.00E-05	0.00025
TUBB3	H596	-1.28736	5.00E-05	0.00025
PROCA1	H596	-1.29325	0.0001	0.000478
APOLD1	H596	-1.30483	5.00E-05	0.00025
FADS2	H596	-1.31447	0.0019	0.006852
HCP5	H596	-1.31724	5.00E-05	0.00025
HIST1H2AK	H596	-1.32252	0.01345	0.038329
CDKN2B	H596	-1.33272	5.00E-05	0.00025
LOC653160	H596	-1.33341	5.00E-05	0.00025
LINC01176	H596	-1.33383	0.0062	0.019448
LINC00944	H596	-1.33481	0.00165	0.006042
CLIC2	H596	-1.33515	0.0019	0.006852
MARCKSL1	H596	-1.35104	5.00E-05	0.00025

PGAM2	H596	-1.35549	0.0017	0.006205
C2orf81	H596	-1.37528	0.00045	0.001888
HIST1H4K	H596	-1.37657	0.0106	0.031143
HIST1H2BN	H596	-1.38531	0.002	0.007171
LINC01119	H596	-1.3894	0.0009	0.003515
C11orf65	H596	-1.39565	0.00675	0.02095
TOLLIP-AS1	H596	-1.41215	0.00035	0.001505
LINC00467	H596	-1.41934	5.00E-05	0.00025
UPK2	H596	-1.43608	0.00035	0.001505
LYRM9	H596	-1.4395	0.0002	0.000905
LINC01024	H596	-1.44012	5.00E-05	0.00025
ZNF396	H596	-1.44449	0.00065	0.002626
ATF3	H596	-1.45231	5.00E-05	0.00025
ANKUB1	H596	-1.45588	5.00E-05	0.00025
ARSD	H596	-1.45817	5.00E-05	0.00025
CNGA1	H596	-1.46296	5.00E-05	0.00025
C7orf57	H596	-1.46746	0.0005	0.002076
NKX3-1	H596	-1.47485	5.00E-05	0.00025
PSG5	H596	-1.47831	5.00E-05	0.00025
PRKAR2A-AS1	H596	-1.48165	5.00E-05	0.00025
HHLA3	H596	-1.48832	5.00E-05	0.00025
HIST2H2BF	H596	-1.4983	5.00E-05	0.00025
MAPK10	H596	-1.50869	5.00E-05	0.00025
RASGRF1	H596	-1.50987	5.00E-05	0.00025
AP3B2	H596	-1.51828	5.00E-05	0.00025
LOC100506746	H596	-1.52753	5.00E-05	0.00025
ZNF610	H596	-1.55239	5.00E-05	0.00025
HIST1H2BF	H596	-1.55575	5.00E-05	0.00025
FAHD2CP	H596	-1.56395	0.0006	0.002445
CAPN5	H596	-1.58374	5.00E-05	0.00025
LRRIQ3	H596	-1.60841	0.0067	0.02081
DLGAP1-AS2	H596	-1.63564	0.0027	0.009359
STEAP4	H596	-1.64498	5.00E-05	0.00025
CALB1	H596	-1.68064	5.00E-05	0.00025
LOC100507634	H596	-1.68312	5.00E-05	0.00025
C9orf169	H596	-1.69266	5.00E-05	0.00025
C17orf103	H596	-1.71554	5.00E-05	0.00025
LOC100506860	H596	-1.71689	5.00E-05	0.00025
TP53INP2	H596	-1.72173	5.00E-05	0.00025
LOC101928767	H596	-1.72888	0.00445	0.014541
OVGP1	H596	-1.74671	5.00E-05	0.00025
ZNF833P	H596	-1.7723	0.00325	0.011023
IQCD	H596	-1.80684	0.00015	0.000695

SERPINI1	H596	-1.83629	5.00E-05	0.00025
ABCB11	H596	-1.84471	5.00E-05	0.00025
HAP1	H596	-1.96966	5.00E-05	0.00025
MYPN	H596	-2.01563	5.00E-05	0.00025
SPATA17	H596	-2.04758	5.00E-05	0.00025
ERICH2	H596	-2.04865	0.0108	0.031653
C19orf18	H596	-2.11226	0.006	0.018903
VASN	H596	-2.2064	0.00475	0.015392
WDR78	H596	-2.22796	5.00E-05	0.00025
FAM154B	H596	-2.29333	5.00E-05	0.00025
HIST1H3B	H596	-2.34424	5.00E-05	0.00025
HIST4H4	H596	-2.87217	5.00E-05	0.00025
ARNT2	H596	-2.94591	5.00E-05	0.00025
PGF	H596	-3.02072	5.00E-05	0.00025
RAB33A	H596	-3.09599	0.0015	0.005546

APPENDIX C
RUVBL1 Co-Immunoprecipitating Proteins after Compound B Treatment

Accession	Gene Symbol	Average enrichment (B/C)
H7BZW2	CEP85	200.67
P42771	CDKN2A	130.59
Q6PJW8	CNST	43.29
P35244	RPA3	41.82
P21283	ATP6V1C1	37.82
Q96P16	RPRD1A	22.52
Q13561	DCTN2	22.19
Q68D10	SPTY2D1	21.19
J3KQR7	CEP170B	19.38
Q9H9A6	LRRC40	19.32
Q9BYB4	GNB1L	17.07
Q7Z3B4	NUP54	13.84
O15084	ANKRD28	13.47
Q9NQG5	RPRD1B	12.44
Q9UID3	VPS51	11.73
P57076	CFAP298	11.18
J3KR72	TAF6	10.94
Q9H410	DSN1	10.93
Q9Y244	POMP	10.90
Q9Y4R8	TELO2	10.56
Q9H7N4	SCAF1	9.63
Q13546	RIPK1	9.58
O00443	PIK3C2A	9.38
O75170	PPP6R2	8.43
O94762	RECQL5	8.43
Q9NYL9	TMOD3	7.35
O95104	SCAF4	5.43
Q9P086	MED11	5.34
Q96TA1	FAM129B	5.32
O15212	PFDN6	5.20
Q96HY6	DDRGK1	5.13
P16402	HIST1H1D	5.09
Q15468	STIL	5.09
Q9UPN7	PPP6R1	5.00
Q8N3X6	LCORL	4.98
P24928	POLR2A	4.94
Q5VT52	RPRD2	4.83

Q5H9R7	PPP6R3	4.74
O94913	PCF11	4.56
P78527	PRKDC	4.53
Q9P1Y6	PHRF1	4.51
Q6NXR4	TTI2	4.43
Q8IXW5	RPAP2	4.16
Q9HCN4	GPN1	4.15
O43156	TTI1	4.14
Q8NEY8	PPHLN1	4.06
P0CAP2	POLR2M	3.95
Q9UHW5	GPN3	3.93
Q9BTC0	DIDO1	3.90
O00743	PPP6C	3.88
Q9BWH6	RPAP1	3.65
Q9UI30	TRMT112	3.62
Q8WV41	SNX33	3.59
P52434	POLR2H	3.49
A0A0X1KG71		3.38
P53803	POLR2K	3.37
O95402	MED26	3.24
P13804	ETFA	3.23
P37198	NUP62	3.07
M0R0P8	MYO9B	3.03
Q9NUG6	PDRG1	2.99
L0R819	ASDURF	2.95
O75330	HMMR	2.94
P49354	FNTA	2.93
A0A096LPC5	WASHC2C	2.74
Q96GC5	MRPL48	2.72
Q96Q15	SMG1	2.67
O00178	GTPBP1	2.65
Q99590	SCAF11	2.64
P19387	POLR2C	2.61
A0A0G2JQH2	RPS18	2.60
P30876	POLR2B	2.54
Q7L3T8	PARS2	2.48
A0A0G2JPP5	SCRIB	2.45
Q9UHV9	PFDN2	2.44
O75691	UTP20	2.39
P00367	GLUD1	2.39
A0A087WU53	MAGT1	2.36
B1AHD1	SNU13	2.36
P12273	PIP	2.27

P18615	NELFE	2.24
Q02539	HIST1H1A	2.24
P32780	GTF2H1	2.24
Q9C0B7	TANGO6	2.21
Q05469	LIPE	2.17
A0A0C4DGG9	CHD4	2.16
Q9UBK9	UXT	2.13
H0Y9Z5	CNOT6L	2.13
Q2NL82	TSR1	2.12
P19388	POLR2E	2.12
G8JLG2	CDSN	2.11
Q5JWT2	MED23	2.08
Q9Y6V7	DDX49	2.08
P62891	RPL39	2.08
Q9P0M6	H2AFY2	2.08
Q8NCA5	FAM98A	2.04
Q14676	MDC1	2.03
P81605	DCD	2.03
Q8WY22	BRI3BP	2.01
P05387	RPLP2	1.97
A8MXP9	MATR3	1.97
O95905	ECD	1.95
P82933	MRPS9	1.94
Q14690	PDCD11	1.92
Q8N201	INTS1	1.89
P50750	CDK9	1.88
Q9UDY4	DNAJB4	1.87
P28799	GRN	1.87
Q86YZ3	HRNR	1.85
Q86W42	THOC6	1.84
A0A0B4J1W0	MED24	1.84
P42766	RPL35	1.83
O94763	URI1	1.83
Q96MX6	WDR92	1.83
Q9UIG0	BAZ1B	1.81
A0A1W2PRB8		1.79
Q9NWS0	PIH1D1	1.79
Q9H944	MED20	1.79
P45880	VDAC2	1.77
Q641Q2	WASHC2A	1.76
A0A0A0MRM9	NOLC1	1.75
Q5T3I0	GPATCH4	1.75
Q68E01	INTS3	1.75

Q9UL03	INTS6	1.73
P62861	FAU	1.73
Q8NI27	THOC2	1.71
Q12768	WASHC5	1.71
Q9P232	CNTN3	1.71
P16401	HIST1H1B	1.71
P60903	S100A10	1.70
Q12788	TBL3	1.69
Q56P03	EAPP	1.69
P17480	UBTF	1.68
A0A0B4J231	IGLL5	1.67
E9PAU2	RAVER1	1.66
Q9Y4G8	RAPGEF2	1.66
O00255	MEN1	1.65
P05089	ARG1	1.65
Q13428	TCOF1	1.65
Q9H6T3	RPAP3	1.64
Q15649	ZNHIT3	1.64
O60832	DKC1	1.64
Q52LW3	ARHGAP29	1.63
Q9UHK0	NUFIP1	1.63
Q6P6C2	ALKBH5	1.63
Q86U42	PABPN1	1.62
A6NHR9	SMCHD1	1.62
Q15404	RSU1	1.61
Q02413	DSG1	1.61
Q8WXF1	PSPC1	1.61
Q13595	TRA2A	1.60
Q8NHV4	NEDD1	1.60
Q8N2K0	ABHD12	1.60
P23246	SFPQ	1.59
Q15233	NONO	1.59
Q5T749	KPRP	1.59
Q13835	PKP1	1.59
A0A1W2PPZ5	TCEA1	1.58
Q6PI26	SHQ1	1.58
H3BN98		1.58
Q13439	GOLGA4	1.58
Q86V48	LUZP1	1.57
Q9NX58	LYAR	1.56
Q08554	DSC1	1.56
Q6DT37	CDC42BPG	1.56
O43824	GTPBP6	1.55

Q9BZE4	GTPBP4	1.54
P11233	RALA	1.54
Q96CX6	LRRC58	1.54
Q96HW7	INTS4	1.53
P25685	DNAJB1	1.53
Q96HR3	MED30	1.53
O60942	RNGTT	1.53
Q96AG4	LRRC59	1.53
Q5EBL8	PDZD11	1.52
Q6I9Y2	THOC7	1.52
Q9UBU9	NXF1	1.52
Q9Y3U8	RPL36	1.51
Q12904	AIMP1	1.51
Q7Z417	NUFIP2	1.50
P08574	CYC1	1.50
Q96P63	SERPINB12	1.50
Q9H9J2	MRPL44	1.49
Q5SSJ5	HP1BP3	1.49
F8WA39	MTMR1	1.49
Q6P1L8	MRPL14	1.48
Q13895	BYSL	1.48
P25398	RPS12	1.48
Q9Y5U2	TSSC4	1.47
Q8NFD5	ARID1B	1.47
P62633	CNBP	1.47
Q9NYF8	BCLAF1	1.47
Q9Y2X3	NOP58	1.47
A0A087X2H1	HECTD1	1.46
P52435	POLR2J	1.46
Q9Y224	RTRAF	1.45
O00567	NOP56	1.45
Q93077	HIST1H2AC	1.45
H3BSH7	UTP4	1.45
P61011	SRP54	1.45
Q9Y2W1	THRAP3	1.45
Q9NVH2	INTS7	1.45
P98179	RBM3	1.44
P84090	ERH	1.44
P32519	ELF1	1.44
Q9H814	PHAX	1.44
P12270	TPR	1.43
Q53H12	AGK	1.43
Q9NWH9	SLTM	1.42

O95714	HERC2	1.42
Q2TAZ0	ATG2A	1.42
Q75QN2	INTS8	1.41
Q9H8G2	CAAP1	1.41
P04040	CAT	1.41
Q9NS86	LANCL2	1.40
Q96HN2	AHCYL2	1.40
Q9Y5B9	SUPT16H	1.40
A4D1E9	GTPBP10	1.39
C9JIF9	APEH	1.39
Q9HC52	CBX8	1.39
P58107	EPPK1	1.39
H7C3T2	ATG2A	1.39
Q9NPJ6	MED4	1.38
Q6L8Q7	PDE12	1.38
P55209	NAP1L1	1.38
O75427	LRCH4	1.37
P50914	RPL14	1.37
O60684	KPNA6	1.37
Q5D862	FLG2	1.36
Q9NWK9	ZNHIT6	1.36
Q01130	SRSF2	1.36
Q9BRR8	GPATCH1	1.36
P52292	KPNA2	1.35
Q15287	RNPS1	1.35
P62424	RPL7A	1.35
Q53GS9	USP39	1.35
P06748	NPM1	1.35
P32969	RPL9, RPL9P7, RPL9P8, RPL9P9	1.34
Q9Y312	AAR2	1.34
O60244	MED14	1.34
Q9NUQ6	SPATS2L	1.34
Q9Y2X0	MED16	1.33
H0Y9X1	TMA16	1.32
Q9P2N5	RBM27	1.32
Q8N3C0	ASCC3	1.32
P20930	FLG	1.32
D6REX3	SEC31A	1.32
J3KQ48	PTRH2	1.31
P61927	RPL37	1.31
P10155	RO60	1.31
Q7L2H7	EIF3M	1.31
P27824	CANX	1.31

Q9NYP7	ELOVL5	1.31
P09012	SNRPA	1.31
Q8NDV7	TNRC6A	1.31
O15056	SYNJ2	1.31
O00233	PSMD9	1.30
P62753	RPS6	1.30
Q15007	WTAP	1.30
Q6P9B9	INTS5	1.30
A0A087X256	WASHC4	1.29
Q9H0H5	RACGAP1	1.29
P10412	HIST1H1E	1.29
Q15018	ABRAXAS2	1.29
H7C2Q8	EBNA1BP2	1.29
Q9H307	PNN	1.29
Q9Y450	HBS1L	1.29
Q96T37	RBM15	1.28
P39023	RPL3	1.28
O75643	SNRNP200	1.28
O76021	RSL1D1	1.28
Q9UPQ9	TNRC6B	1.28
O00264	PGRMC1	1.28
Q9H6F5	CCDC86	1.28
Q9UNE7	STUB1	1.27
Q16629	SRSF7	1.27
Q13356	PPIL2	1.27
Q9HAF1	MEAF6	1.27
Q04637	EIF4G1	1.27
O43143	DHX15	1.27
Q5JPH6	EARS2	1.26
A0A1W2PPR8	HLA-B	1.26
Q13769	THOC5	1.26
Q13155	AIMP2	1.26
P57678	GEMIN4	1.26
P05198	EIF2S1	1.26
P17029	ZKSCAN1	1.26
P05109	S100A8	1.25
P11387	TOP1	1.25
P62136	PPP1CA	1.25
Q86UE4	MTDH	1.25
D6R9M0	KIF2A	1.25
Q9UKV3	ACIN1	1.25
P62995	TRA2B	1.25
P78371	CCT2	1.25

P15531	NME1	1.25
P08621	SNRNP70	1.24
Q96NW4	ANKRD27	1.24
O75947	ATP5PD	1.24
P62847	RPS24	1.24
P48634	PRRC2A	1.24
P19525	EIF2AK2	1.24
H3BLV9	SRPK1	1.23
P19338	NCL	1.23
Q8TDN6	BRIX1	1.23
J3KPP4	LUC7L3	1.22
Q9P2R6	RERE	1.22
V9GYM8	ARHGEF2	1.22
Q8WUA4	GTF3C2	1.22
Q9UN81	L1RE1	1.22
O00203	AP3B1	1.22
P62273	RPS29	1.22
Q9UL15	BAG5	1.22
Q9BY44	EIF2A	1.22
Q7Z333	SETX	1.21
A0A286YF11	MICU1	1.21
E7EQZ4	SMN1	1.21
P62750	RPL23A	1.21
Q08379	GOLGA2	1.21
J3QK89	CHERP	1.21
P30153	PPP2R1A	1.20
Q9UN86	G3BP2	1.20
Q8WUY1	THEM6	1.20
P41252	IARS	1.20
Q7Z6E9	RBBP6	1.20
P61626	LYZ	1.20
A0A087WYN9	DHX29	1.20
Q02880	TOP2B	1.20
P62304	SNRPE	1.20
Q13555	CAMK2G	1.19
Q01844	EWSR1	1.19
P17931	LGALS3	1.19
Q9GZS1	POLR1E	1.19
P07814	EPRS	1.19
Q9NYU2	UGGT1	1.19
Q16698	DECR1	1.19
Q99547	MPHOSPH6	1.19
Q5T280	SPOUT1	1.19

F8W727	RPL32	1.18
Q9H2Y7	ZNF106	1.18
O60763	USO1	1.18
A0A024R4M0	RPS9	1.18
Q96H79	ZC3HAV1L	1.18
Q9ULR0	ISY1	1.18
P09497	CLTB	1.18
P22087	FBL	1.18
E7ETY2	TCOF1	1.18
Q92526	CCT6B	1.18
P36578	RPL4	1.18
M0QYS1	RPL13A	1.18
Q6P2Q9	PRPF8	1.18
P31431	SDC4	1.18
J3KN01	AFDN	1.18
Q9Y3Y2	CHTOP	1.17
Q92804	TAF15	1.17
Q13242	SRSF9	1.17
P46087	NOP2	1.17
P25788	PSMA3	1.17
Q9NVP1	DDX18	1.17
Q9Y3B4	SF3B6	1.17
P15924	DSP	1.17
H7BY58	PCMT1	1.17
Q9BZH6	WDR11	1.17
H3BPE7	FUS	1.17
Q9UPY3	DICER1	1.17
Q9BWU0	SLC4A1AP	1.17
Q9NVX0	HAUS2	1.17
E9PB61	ALYREF	1.17
A0A0D9SEY1	MAP4K4	1.17
A0A0G2JMW4	RASSF7	1.17
P32320	CDA	1.17
Q9NZB2	FAM120A	1.16
Q92896	GLG1	1.16
B3KY94	CDIPT	1.16
Q9P2E9	RRBP1	1.16
P62805	HIST1H4A, HIST1H4B, HIST1H4C, HIST1H4D, HIST1H4E, HIST1H4F, HIST1H4H, HIST1H4I, HIST1H4J, HIST1H4K, HIST1H4L, HIST2H4A, HIST2H4B, HIST4H4	1.16
Q68CZ2	TNS3	1.16
P08240	SRPRA	1.16
O43290	SART1	1.16

P09661	SNRPA1	1.16
Q9BWJ5	SF3B5	1.16
X6RAL5		1.16
Q12769	NUP160	1.16
Q9Y5S9	RBM8A	1.16
Q7L0Y3	TRMT10C	1.16
O75940	SMNDC1	1.16
E9PRY8	EEF1D	1.15
P11182	DBT	1.15
Q9H6S0	YTHDC2	1.15
O15226	NKRF	1.15
Q14444	CAPRIN1	1.15
P84103	SRSF3	1.15
O95816	BAG2	1.15
O00139	KIF2A	1.15
Q7RTV0	PHF5A	1.15
Q49A26	GLYR1	1.14
B7Z6Z4	MYL6	1.14
Q9NQT5	EXOSC3	1.14
Q8N726	CDKN2A	1.14
Q9BQG0	MYBBP1A	1.14
O94822	LTN1	1.14
Q9P2J5	LARS	1.14
Q9Y520	PRRC2C	1.14
P05388	RPLP0	1.14
P80748	IGLV3-21	1.14
Q6PI98	INO80C	1.14
P49756	RBM25	1.14
Q92759	GTF2H4	1.14
O95486	SEC24A	1.14
Q9BRJ6	C7orf50	1.14
Q5STZ8	ABCF1	1.14
A0A0A0MR72	EP400	1.14
P49207	RPL34	1.14
O95347	SMC2	1.14
P52294	KPNA1	1.13
P26373	RPL13	1.13
O60293	ZFC3H1	1.13
Q9C0J8	WDR33	1.13
Q8N9N2	ASCC1	1.13
P62917	RPL8	1.13
P18124	RPL7	1.13
P46777	RPL5	1.13

P07305	H1F0	1.13
Q9UH99	SUN2	1.13
Q01085	TIAL1	1.13
Q92615	LARP4B	1.13
P04083	ANXA1	1.13
P46778	RPL21	1.13
O94992	HEXIM1	1.13
Q86UP2	KTN1	1.12
O00165	HAX1	1.12
P31942	HNRNPH3	1.12
F6VRR5	POLDIP3	1.12
Q9P013	CWC15	1.12
Q52LJ0	FAM98B	1.12
Q9NW64	RBM22	1.12
Q8TBM8	DNAJB14	1.12
Q969X5	ERGIC1	1.11
Q8IY37	DHX37	1.11
Q9GZR7	DDX24	1.11
P0C0S8	HIST1H2AG, HIST1H2AI, HIST1H2AK, HIST1H2AL, HIST1H2AM	1.11
Q13283	G3BP1	1.11
P62888	RPL30	1.11
A0A0A0MT49	SMARCA4	1.11
P08579	SNRPB2	1.11
Q8WVM0	TFB1M	1.11
Q9BTV4	TMEM43	1.11
O15042	U2SURP	1.11
P62899	RPL31	1.11
O14545	TRAFD1	1.11
P07910	HNRNPC	1.11
E5KLJ9	OPA1	1.11
P62857	RPS28	1.11
Q8N9G1	SEC16A	1.10
O95793	STAU1	1.10
K7ES00	H3F3B	1.10
P78406	RAE1	1.10
P15880	RPS2	1.10
Q6UXN9	WDR82	1.10
Q13247	SRSF6	1.10
Q13619	CUL4A	1.10
Q12874	SF3A3	1.10
O15344	MID1	1.10
P48651	PTDSS1	1.10

K7EJ20	GPX4	1.10
P53992	SEC24C	1.10
P62081	RPS7	1.10
Q92925	SMARCD2	1.09
Q08AF3	SLFN5	1.09
O60508	CDC40	1.09
P30405	PPIF	1.09
O00541	PES1	1.09
O43353	RIPK2	1.09
Q7KZF4	SND1	1.09
P30050	RPL12	1.09
K7ELC2	RPS15	1.09
J3QLS3	MRPS7	1.09
Q9Y484	WDR45	1.09
Q9UHB9	SRP68	1.09
O60318	MCM3AP	1.09
Q15650	TRIP4	1.09
Q9NXR8	ING3	1.09
P05423	POLR3D	1.09
P62241	RPS8	1.09
Q9NR12	PDLIM7	1.09
P22626	HNRNPA2B1	1.09
P62277	RPS13	1.09
Q08945	SSRP1	1.09
P09429	HMGB1	1.08
Q9UKM9	RALY	1.08
O75367	H2AFY	1.08
P62906	RPL10A	1.08
Q08AM6	VAC14	1.08
P26368	U2AF2	1.08
P56182	RRP1	1.08
O94964	SOGA1	1.08
Q05707	COL14A1	1.08
A0A0A0MSY4	DOCK9	1.08
P47755	CAPZA2	1.08
P62244	RPS15A	1.08
E7ENQ6		1.08
Q7KZI7	MARK2	1.08
Q9BVG4	PBDC1	1.08
O43395	PRPF3	1.08
Q3ZCM7	TUBB8	1.08
O75340	PDCD6	1.07
Q8NB90	SPATA5	1.07

O75446	SAP30	1.07
P61513	RPL37A	1.07
Q8NFW8	CMAS	1.07
Q92922	SMARCC1	1.07
P47914	RPL29	1.07
C9JFV4	PELP1	1.07
P61254	RPL26	1.07
P23458	JAK1	1.07
B2R5W2	HNRNPC	1.07
Q5RKV6	EXOSC6	1.07
P14868	DARS	1.07
Q9NWT1	PAK1IP1	1.07
Q8TAQ2	SMARCC2	1.07
O75175	CNOT3	1.07
Q7L2J0	MEPCE	1.07
Q13523	PRPF4B	1.07
P52272	HNRNPM	1.07
B4DJL6	INTS14	1.06
A0A087WW87	IGKV2-40	1.06
Q9BYG3	NIFK	1.06
Q5BKZ1	ZNF326	1.06
Q9NUL3	STAU2	1.06
A6NEM2	HCFC1	1.06
P46783	RPS10	1.06
Q9NZN8	CNOT2	1.06
A5YKK6	CNOT1	1.06
J3QQ67	RPL18	1.06
Q86TJ2	TADA2B	1.06
O14965	AURKA	1.06
Q9UKV8	AGO2	1.06
Q5VZU9	TPP2	1.06
Q02543	RPL18A	1.06
Q9H972	C14orf93	1.06
Q9NR30	DDX21	1.05
O43324	EEF1E1	1.05
Q52LR7	EPC2	1.05
H0YKD8	RPL28	1.05
Q9BQ75	CMSS1	1.05
P35579	MYH9	1.05
P39019	RPS19	1.05
Q96PK6	RBM14	1.05
H0Y5K5	ERGIC3	1.05
Q9HAU4	SMURF2	1.05

O75165	DNAJC13	1.05
Q9H1I8	ASCC2	1.05
Q13868	EXOSC2	1.05
P10515	DLAT	1.04
Q5C9Z4	NOM1	1.04
Q13148	TARDBP	1.04
P41091	EIF2S3	1.04
Q53TQ3	INO80D	1.04
Q14165	MLEC	1.04
Q86U38	NOP9	1.04
Q9Y5M8	SRPRB	1.04
P46776	RPL27A	1.04
Q9H0A0	NAT10	1.04
Q04917	YWHAH	1.04
Q02878	RPL6	1.04
Q9Y6W5	WASF2	1.04
P62701	RPS4X	1.04
Q8NI36	WDR36	1.03
P20839	IMPDH1	1.03
P62851	RPS25	1.03
J3KQN4	RPL36A	1.03
P51114	FXR1	1.03
P61353	RPL27	1.03
Q08211	DHX9	1.03
O43818	RRP9	1.03
P50416	CPT1A	1.03
Q8WWM7	ATXN2L	1.03
Q15029	EFTUD2	1.03
Q03252	LMNB2	1.03
P84098	RPL19	1.03
O95239	KIF4A	1.03
Q07021	C1QBP	1.03
Q13751	LAMB3	1.03
P54136	RARS	1.03
E9PLN8		1.03
A0A0A6YYL6	RPL17-C18orf32	1.03
P49720	PSMB3	1.03
Q01469	FABP5	1.03
Q9BQ67	GRWD1	1.02
Q92734	TFG	1.02
O75607	NPM3	1.02
P19447	ERCC3	1.02
Q6IN84	MRM1	1.02

P55265	ADAR	1.02
Q9H6R4	NOL6	1.02
O43809	NUDT21	1.02
A0A0U1RQC9	TP53	1.02
O60231	DHX16	1.02
P06733	ENO1	1.02
Q13888	GTF2H2	1.02
P38159	RBMX	1.02
P09132	SRP19	1.02
P46013	MKI67	1.01
Q15046	KARS	1.01
Q92993	KAT5	1.01
Q9Y2U8	LEMD3	1.01
Q9Y4P3	TBL2	1.01
Q96EY1	DNAJA3	1.01
Q15024	EXOSC7	1.01
Q5LJA5	UCHL5	1.01
Q8NBZ0	INO80E	1.01
O14497	ARID1A	1.01
P83731	RPL24	1.01
Q9Y5X2	SNX8	1.01
P61247	RPS3A	1.01
F5H5P2		1.01
U3KQK0	HIST1H2BN	1.01
P53621	COPA	1.01
O75533	SF3B1	1.00
Q14684	RRP1B	1.00
Q03701	CEBPZ	1.00
F1T0I1	SEC16A	1.00
P06899	HIST1H2BJ	1.00
Q05BQ5	MBTD1	1.00
Q13889	GTF2H3	1.00
Q9HAU0	PLEKHA5	1.00
P47897	QARS	1.00
Q9Y4C8	RBM19	1.00
O95487	SEC24B	1.00
O15127	SCAMP2	1.00
P20700	LMNB1	1.00
Q15393	SF3B3	0.99
P38919	EIF4A3	0.99
Q96J84	KIRREL1	0.99
Q9P2I0	CPSF2	0.99
Q8N1G4	LRRC47	0.99

Q15717	ELAVL1	0.99
O00411	POLRMT	0.99
Q9BVI4	NOC4L	0.99
P63010	AP2B1	0.99
O75436	VPS26A	0.99
P34932	HSPA4	0.99
J3KTL2	SRSF1	0.99
A0A075B716	RPS17	0.99
P23526	AHCY	0.99
Q15424	SAFB	0.99
Q13535	ATR	0.99
Q9Y230	RUVBL2	0.99
P26640	VARS	0.99
Q13813	SPTAN1	0.99
Q00577	PURA	0.98
P16989	YBX3	0.98
Q9BQ39	DDX50	0.98
Q9Y3F4	STRAP	0.98
I3L4C2	BAIAP2	0.98
Q14966	ZNF638	0.98
Q10570	CPSF1	0.98
J3KNN5	DDX41	0.98
P51991	HNRNPA3	0.98
P54652	HSPA2	0.98
A0A0U1RRM4	PTBP1	0.98
P78347	GTF2I	0.98
O14979	HNRNPDL	0.98
F2Z2U4	TRRAP	0.98
Q8IY81	FTSJ3	0.98
Q14008	CKAP5	0.98
A0A0A6YYJ8	LUC7L2	0.98
O14818	PSMA7	0.98
P62266	RPS23	0.98
P62854	RPS26	0.98
Q9Y265	RUVBL1	0.98
P39656	DDOST	0.97
P20290	BTF3	0.97
Q9UFW8	CGGBP1	0.97
Q9Y2R4	DDX52	0.97
P35268	RPL22	0.97
H7C127	BRD8	0.97
O95373	IPO7	0.97
P09211	GSTP1	0.97

Q96HA1	POM121	0.97
Q2TAY7	SMU1	0.97
P11388	TOP2A	0.97
Q01650	SLC7A5	0.97
Q14558	PRPSAP1	0.97
O75400	PRPF40A	0.97
J3KQ70	INO80B-WBP1	0.97
Q9BX40	LSM14B	0.97
O43390	HNRNPR	0.97
X6R4W8	ZNF207	0.97
P62913	RPL11	0.97
O00425	IGF2BP3	0.97
Q5T653	MRPL2	0.97
Q8TCT9	HM13	0.97
Q8N3U4	STAG2	0.96
Q9Y3B2	EXOSC1	0.96
Q99700	ATXN2	0.96
A0A087WY31	YTHDF3	0.96
A0A0G2JK23	BAG6	0.96
P18077	RPL35A	0.96
Q9UHX1	PUF60	0.96
A0A0C4DFX9	NELFA	0.96
P62140	PPP1CB	0.96
Q13838	DDX39B	0.96
Q9H0D6	XRN2	0.96
Q9H2F5	EPC1	0.96
Q3YBR2	TBRG1	0.96
Q7Z2W4	ZC3HAV1	0.96
Q13243	SRSF5	0.96
Q9Y2K7	KDM2A	0.96
Q9P270	SLAIN2	0.96
Q13435	SF3B2	0.96
Q6NZY4	ZCCHC8	0.96
P30048	PRDX3	0.96
J3KTA4	DDX5	0.96
Q96RF0	SNX18	0.96
Q8TDD1	DDX54	0.96
Q08188	TGM3	0.96
P32119	PRDX2	0.96
Q32MZ4	LRRFIP1	0.96
Q9NXV6	CDKN2AIP	0.96
Q96GC9	VMP1	0.95
Q15014	MORF4L2	0.95

Q9NTI5	PDS5B	0.95
P48729	CSNK1A1	0.95
P09651	HNRNPA1	0.95
P06576	ATP5F1B	0.95
G5E975	SMARCB1	0.95
P35606	COPB2	0.95
Q07666	KHDRBS1	0.95
P62316	SNRPD2	0.95
Q92900	UPF1	0.95
O43172	PRPF4	0.95
Q9NV56	MRGBP	0.95
Q9BSJ2	TUBGCP2	0.95
H3BS72	HACD3	0.95
Q09161	NCBP1	0.95
Q9NW13	RBM28	0.95
J3KMZ8	DPF2	0.95
Q92572	AP3S1	0.95
P51648	ALDH3A2	0.95
P40227	CCT6A	0.95
Q9H147	DNTTIP1	0.95
P48047	ATP5PO	0.95
Q9H0S4	DDX47	0.95
Q92979	EMG1	0.95
O60524	NEMF	0.95
A0A087WVQ6	CLTC	0.95
P55735	SEC13	0.95
Q96L91	EP400	0.95
Q01780	EXOSC10	0.94
O15230	LAMA5	0.94
Q9UGP8	SEC63	0.94
Q96B26	EXOSC8	0.94
O15355	PPM1G	0.94
Q12905	ILF2	0.94
O60925	PFDN1	0.94
P42285	MTREX	0.94
Q9Y295	DRG1	0.94
A0A087WUZ3	SPTBN1	0.94
O95470	SGPL1	0.94
Q3KQU3	MAP7D1	0.94
P30049	ATP5F1D	0.94
Q9BUJ2	HNRNPUL1	0.94
Q13310	PABPC4	0.94
Q9NVM9	INTS13	0.94

P61106	RAB14	0.94
P61964	WDR5	0.94
P78325	ADAM8	0.94
P51116	FXR2	0.94
P61313	RPL15	0.94
P67809	YBX1	0.94
A0A0A0MS59	SRCAP	0.93
F8WF69	CLTA	0.93
P32239	CCKBR	0.93
Q5JTH9	RRP12	0.93
Q9BXP5	SRRT	0.93
M0QYZ2	AP2S1	0.93
Q13151	HNRNPA0	0.93
Q9Y2Z0	SUGT1	0.93
A0A0D9SF53	DDX3X	0.93
Q9Y3D0	CIAO2B	0.93
P24752	ACAT1	0.93
P13995	MTHFD2	0.93
F8W930	IGF2BP2	0.93
Q9UQ35	SRRM2	0.93
P06702	S100A9	0.93
Q9Y3B7	MRPL11	0.93
Q9UHI6	DDX20	0.92
Q12906	ILF3	0.92
P50402	EMD	0.92
Q53GA4	PHLDA2	0.92
Q12789	GTF3C1	0.92
Q8WU90	ZC3H15	0.92
O95251	KAT7	0.92
P49711	CTCF	0.92
E9PFW3	AP2M1	0.92
P62306	SNRPF	0.92
H0Y4W2	TRRAP	0.92
O43819	SCO2	0.92
P25786	PSMA1	0.92
Q9BW92	TARS2	0.92
Q86VZ6	JAZF1	0.92
O94874	UFL1	0.92
Q92817	EVPL	0.92
Q9P0L0	VAPA	0.92
Q92598	HSPH1	0.92
Q96P11	NSUN5	0.92
Q96MG2	JSRP1	0.92

P11940	PABPC1	0.92
O60306	AQR	0.91
Q9NVV4	MTPAP	0.91
Q9UKZ1	CNOT11	0.91
P62269	RPS18	0.91
O60506	SYNCRIP	0.91
P55072	VCP	0.91
Q9NQW6	ANLN	0.91
Q96EE3	SEH1L	0.91
P35869	AHR	0.91
J3KQ40	TBC1D8	0.91
Q9HCS7	XAB2	0.91
P55060	CSE1L	0.91
Q6WKZ4	RAB11FIP1	0.91
Q8WXG6	MADD	0.91
Q96RN5	MED15	0.91
Q92688	ANP32B	0.91
Q16342	PDCD2	0.91
Q9ULX3	NOB1	0.90
Q9ULW0	TPX2	0.90
O75534	CSDE1	0.90
Q99459	CDC5L	0.90
P57088	TMEM33	0.90
P62979	RPS27A	0.90
P60866	RPS20	0.90
D6RBZ0	HNRNPAB	0.90
Q14764	MVP	0.90
Q9H2G4	TSPYL2	0.90
P26196	DDX6	0.90
P14678	SNRPB	0.90
Q9H6T0	ESRP2	0.90
Q7LBC6	KDM3B	0.90
G3V3A4	SNW1	0.90
O75475	PSIP1	0.90
Q15291	RBBP5	0.90
B0QY89	EIF3L	0.90
Q9Y3I0	RTCB	0.90
Q14669	TRIP12	0.90
O15091	KIAA0391	0.90
P28482	MAPK1	0.90
Q9BTT6	LRRC1	0.90
Q9BVC5	C2orf49	0.90
Q06265	EXOSC9	0.90

Q9Y3D9	MRPS23	0.90
Q9Y446	PKP3	0.90
O43707	ACTN4	0.89
P27635	RPL10	0.89
P62263	RPS14	0.89
Q9H5Z1	DHX35	0.89
O76094	SRP72	0.89
P62318	SNRPD3	0.89
Q00403	GTF2B	0.89
Q9HCE1	MOV10	0.89
A1L0T0	ILVBL	0.89
Q9NZI8	IGF2BP1	0.89
P26639	TARS	0.89
Q9NUL7	DDX28	0.89
P60891	PRPS1	0.89
O60884	DNAJA2	0.89
Q12797	ASPH	0.89
P0C0S5	H2AFZ	0.89
O60563	CCNT1	0.89
Q9NTJ3	SMC4	0.89
Q8NC51	SERBP1	0.89
Q5TGY3	AHDC1	0.89
B7Z645	SYNCRIP	0.89
P10809	HSPD1	0.89
P18583	SON	0.89
M0R0R2	RPS5	0.89
C9IZQ1	SSR1	0.89
Q8N5A5	ZGPAT	0.89
P32322	PYCR1	0.89
Q96SI9	STRBP	0.89
Q9NTJ5	SACM1L	0.89
P35251	RFC1	0.88
Q6P4R8	NFRKB	0.88
A0A087WWS1	THOC1	0.88
A0A0G2JMX7	MAPT	0.88
P55084	HADHB	0.88
Q15020	SART3	0.88
Q96GQ7	DDX27	0.88
Q9BZJ0	CRNKL1	0.88
Q9C0D5	TANC1	0.88
Q9UNQ2	DIMT1	0.88
P24539	ATP5PB	0.88
Q658Y4	FAM91A1	0.88

Q15637	SF1	0.88
A0A1B0GU03		0.88
O95782	AP2A1	0.88
Q9ULU4	ZMYND8	0.88
Q99832	CCT7	0.88
O60437	PPL	0.88
A0A1W2PQ51	DDX17	0.88
Q969G3	SMARCE1	0.88
Q99615	DNAJC7	0.88
P50990	CCT8	0.88
P09874	PARP1	0.88
P21333	FLNA	0.88
P28070	PSMB4	0.88
Q13085	ACACA	0.88
E5RHQ5	NPIPB11	0.88
Q05048	CSTF1	0.88
A0A1B0GTL5	RAB11FIP5	0.88
O43660	PLRG1	0.88
Q12962	TAF10	0.88
Q9H4K7	MTG2	0.88
K7ERV3	TK1	0.88
Q9ULG1	INO80	0.87
Q9NSD9	FARSB	0.87
Q15262	PTPRK	0.87
P38646	HSPA9	0.87
Q16630	CPSF6	0.87
B1AK88	CAPZB	0.87
Q92552	MRPS27	0.87
P52907	CAPZA1	0.87
Q96EZ8	MCRS1	0.87
Q15906	VPS72	0.87
Q04837	SSBP1	0.87
P62249	RPS16	0.87
P62314	SNRPD1	0.87
Q9Y5K5	UCHL5	0.87
Q7Z6M4	MTERF4	0.87
P30530	AXL	0.87
O95168	NDUFB4	0.87
P25686	DNAJB2	0.87
Q8NAP3	ZBTB38	0.87
P35249	RFC4	0.87
A0A0G2JIW1	HSPA1B	0.87
P0C1Z6	TFPT	0.87

P04899	GNAI2	0.87
P98175	RBM10	0.87
Q9NQT4	EXOSC5	0.87
P16070	CD44	0.87
P20042	EIF2S2	0.87
Q9BVP2	GNL3	0.87
Q9H2U1	DHX36	0.86
H7BYT1	CSNK1D	0.86
Q14258	TRIM25	0.86
Q9UHR6	ZNHIT2	0.86
Q99653	CHP1	0.86
O00629	KPNA4	0.86
Q01081	U2AF1	0.86
Q96KR1	ZFR	0.86
Q9NVR2	INTS10	0.86
P68400	CSNK2A1	0.86
O60264	SMARCA5	0.86
P22234	PAICS	0.86
P02545	LMNA	0.86
Q96I24	FUBP3	0.86
P51398	DAP3	0.86
O15160	POLR1C	0.86
Q13185	CBX3	0.86
Q9P258	RCC2	0.86
Q8NE71	ABCF1	0.86
Q9UBU8	MORF4L1	0.86
G5E9Q6	PFN2	0.86
P04406	GAPDH	0.86
Q86Y07	VRK2	0.86
Q8N7H5	PAF1	0.86
A0A0C4DG17	RPSA	0.86
P62879	GNB2	0.86
A0A1W2PP35	HNRNPU	0.86
Q9Y2T2	AP3M1	0.86
Q9Y5X1	SNX9	0.86
O14776	TCERG1	0.85
P63220	RPS21	0.85
Q8N163	CCAR2	0.85
O94887	FARP2	0.85
P14866	HNRNPL	0.85
P23284	PPIB	0.85
D3DQV9	EIF4G2	0.85
Q6ZNB6	NFXL1	0.85

P56537	EIF6	0.85
Q96FJ2	DYNLL2	0.85
Q92499	DDX1	0.85
O75223	GGCT	0.85
E9PI41	EXOSC4	0.85
P13473	LAMP2	0.85
Q8WUF5	PPP1R13L	0.85
P62937	PPIA	0.85
A0A0C4DFX4		0.85
Q14331	FRG1	0.85
O75563	SKAP2	0.85
Q9NWV8	BABAM1	0.85
Q5SRN5	HLA-A	0.85
Q13724	MOGS	0.85
P50991	CCT4	0.85
Q99873	PRMT1	0.85
Q8IZH2	XRN1	0.85
Q8N6R0	EEF1AKNMT	0.85
O94851	MICAL2	0.84
O00505	KPNA3	0.84
P46060	RANGAP1	0.84
Q5UIP0	RIF1	0.84
P40937	RFC5	0.84
Q00839	HNRNPU	0.84
Q86XN7	PROSER1	0.84
P62280	RPS11	0.84
Q13510	ASAH1	0.84
Q9NW08	POLR3B	0.84
P23443	RPS6KB1	0.84
Q8IXI2	RHOT1	0.84
P07900	HSP90AA1	0.84
O75934	BCAS2	0.84
P48643	CCT5	0.84
P11047	LAMC1	0.84
O00391	QSOX1	0.84
Q8NBJ5	COLGALT1	0.84
E7EVA0	MAP4	0.84
Q1KMD3	HNRNPUL2	0.84
Q8TEQ6	GEMIN5	0.84
P53396	ACLY	0.84
O75369	FLNB	0.83
Q15369	ELOC	0.83
O15427	SLC16A3	0.83

Q14103	HNRNPD	0.83
Q5SRQ6	CSNK2B	0.83
Q15428	SF3A2	0.83
P21964	COMT	0.83
A0A0G2JPT5	RAD17	0.83
Q08J23	NSUN2	0.83
Q9UPT5	EXOC7	0.83
P11142	HSPA8	0.83
P13674	P4HA1	0.83
C9JJ19	MRPS34	0.83
Q9Y4W2	LAS1L	0.83
Q96P47	AGAP3	0.83
Q06587	RING1	0.83
P35659	DEK	0.82
Q15019	43710	0.82
P29317	EPHA2	0.82
Q13061	TRDN	0.82
P37108	SRP14	0.82
Q9ULV4	CORO1C	0.82
Q9UMS4	PRPF19	0.82
Q6PD62	CTR9	0.82
P42704	LRPPRC	0.82
Q14974	KPNB1	0.82
G8JLB6	HNRNPH1	0.82
P25490	YY1	0.82
Q8ND24	RNF214	0.82
Q15773	MLF2	0.82
Q9Y2S7	POLDIP2	0.82
O43257	ZNHIT1	0.82
Q9H5V8	CDCP1	0.82
P31948	STIP1	0.82
Q14694	USP10	0.82
P56192	MARS	0.82
J3KPD3	RBM7	0.82
Q9Y4W6	AFG3L2	0.82
Q9NRL2	BAZ1A	0.82
Q93008	USP9X	0.82
Q9H845	ACAD9	0.82
P02786	TFRC	0.82
O95757	HSPA4L	0.82
Q96HS1	PGAM5	0.82
P45973	CBX5	0.81
B5MBZ0	EML4	0.81

P09382	LGALS1	0.81
P60468	SEC61B	0.81
A0A087WTP3	KHSRP	0.81
Q06330	RBPJ	0.81
P12081	HARS	0.81
Q05639	EEF1A2	0.81
Q96A33	CCDC47	0.81
Q9NRX2	MRPL17	0.81
Q9H0H0	INTS2	0.81
Q9NPF5	DMAP1	0.81
Q01804	OTUD4	0.81
Q15427	SF3B4	0.81
Q9HCM4	EPB41L5	0.81
O95619	YEATS4	0.81
P16278	GLB1	0.80
Q9Y6D6	ARFGEF1	0.80
P16615	ATP2A2	0.80
B7ZLQ5	SMARCA1	0.80
Q99613	EIF3C	0.80
P23396	RPS3	0.80
Q8ND56	LSM14A	0.80
Q9UBM7	DHCR7	0.80
P17028	ZNF24	0.80
P31153	MAT2A	0.80
Q16513	PKN2	0.80
Q9Y4C2	TCAF1	0.80
Q8WWI1	LMO7	0.80
O95248	SBF1	0.80
E7EQR4	EZR	0.80
Q6DD88	ATL3	0.80
A0A024R4E5	HDLBP	0.80
P52597	HNRNPF	0.80
Q8IXB1	DNAJC10	0.80
P11021	HSPA5	0.80
Q8NHQ9	DDX55	0.80
O95159	ZFPL1	0.80
Q96ST3	SIN3A	0.80
J3KPF3	SLC3A2	0.80
Q99470	SDF2	0.80
P51148	RAB5C	0.80
Q9Y5Q9	GTF3C3	0.80
Q29RF7	PDS5A	0.80
Q5SRE5	NUP188	0.80

Q15366	PCBP2	0.79
O14578	CIT	0.79
A3KMH1	VWA8	0.79
G3XAI2	LAMB1	0.79
Q13123	IK	0.79
O75962	TRIO	0.79
Q5T9A4	ATAD3B	0.79
P07237	P4HB	0.79
Q13501	SQSTM1	0.79
P49748	ACADVL	0.79
P42166	TMPO	0.79
Q8WWY3	PRPF31	0.79
Q9NYH9	UTP6	0.79
Q8N9T8	KRI1	0.79
M0R2B7	POLD1	0.79
Q8NBQ5	HSD17B11	0.79
P21359	NF1	0.79
P26641	EEF1G	0.79
S4R369	MRPL37	0.79
Q9GZS3	WDR61	0.78
O43684	BUB3	0.78
E7EX17	EIF4B	0.78
P40938	RFC3	0.78
P08238	HSP90AB1	0.78
P04844	RPN2	0.78
P40939	HADHA	0.78
Q9UEE9	CFDP1	0.78
Q9UKL0	RCOR1	0.78
P35749	MYH11	0.78
Q6NZI2	CAVIN1	0.78
Q9HD45	TM9SF3	0.78
P33992	MCM5	0.78
A0AV96	RBM47	0.78
Q9P206	KIAA1522	0.78
O95292	VAPB	0.78
P35250	RFC2	0.78
P04792	HSPB1	0.78
Q15459	SF3A1	0.78
Q9UQE7	SMC3	0.77
Q15022	SUZ12	0.77
Q9UG63	ABCF2	0.77
Q6PJT7	ZC3H14	0.77
Q96N67	DOCK7	0.77

A0A1W2PQ47	FDFT1	0.77
Q6UN15	FIP1L1	0.77
P33981	TTK	0.77
O14773	TPP1	0.77
P05023	ATP1A1	0.77
Q9UKX7	NUP50	0.77
Q96DF8	ESS2	0.77
J3KQE5	RAN	0.77
O15371	EIF3D	0.77
Q66K74	MAP1S	0.77
P55795	HNRNPH2	0.77
Q8N490	PNKD	0.77
Q15334	LLGL1	0.77
H0Y2W2	ATAD3A	0.77
Q6YN16	HSDL2	0.77
Q15436	SEC23A	0.77
P61978	HNRNPK	0.77
Q9UJ70	NAGK	0.77
Q3BDU5	LMNA	0.77
Q9Y619	SLC25A15	0.77
Q5JWF2	GNAS	0.77
O60216	RAD21	0.76
Q9Y6K0	CEPT1	0.76
Q15392	DHCR24	0.76
P82650	MRPS22	0.76
Q15149	PLEC	0.76
Q9Y676	MRPS18B	0.76
Q09666	AHNAK	0.76
Q96T17	MAP7D2	0.76
Q13131	PRKAA1	0.76
Q9UNL2	SSR3	0.76
Q9Y6K9	IKBKG	0.76
Q53GQ0	HSD17B12	0.76
P17858	PFKL	0.76
Q8WVC0	LEO1	0.76
P49792	RANBP2	0.76
Q99575	POP1	0.76
Q86U86	PBRM1	0.76
Q9NZ01	TECR	0.76
Q15648	MED1	0.76
Q86SQ4	ADGRG6	0.76
Q14980	NUMA1	0.76
P52799	EFNB2	0.76

J3QS41	HELZ	0.76
Q8IVS2	MCAT	0.76
B4DUT8	CNN2	0.76
P49368	CCT3	0.75
P41250	GARS	0.75
P07858	CTSB	0.75
Q9UJF2	RASAL2	0.75
Q3ZCQ8	TIMM50	0.75
Q93009	USP7	0.75
P07355	ANXA2	0.75
P13639	EEF2	0.75
Q9P287	BCCIP	0.75
P63104	YWHAZ	0.75
Q15437	SEC23B	0.75
Q9NR50	EIF2B3	0.75
P31321	PRKAR1B	0.75
Q06830	PRDX1	0.75
Q8WTW3	COG1	0.75
Q92621	NUP205	0.75
Q7Z2T5	TRMT1L	0.75
O95864	FADS2	0.75
Q9H3P7	ACBD3	0.75
Q9BWF3	RBM4	0.75
E9PAV3	NACA	0.75
P43121	MCAM	0.75
P62258	YWHAE	0.75
Q15365	PCBP1	0.74
Q9BTD8	RBM42	0.74
E7ERS3	ZC3H18	0.74
Q6PKG0	LARP1	0.74
P49327	FASN	0.74
P42167	TMPO	0.74
Q96A26	FAM162A	0.74
Q13753	LAMC2	0.74
O43852	CALU	0.74
Q9UFC0	LRWD1	0.74
P14618	PKM	0.74
P51571	SSR4	0.74
Q9HBH1	PDF	0.74
Q15582	TGFBI	0.74
P63244	RACK1	0.74
P17987	TCP1	0.74
O75676	RPS6KA4	0.74

P00403	MT-CO2	0.74
Q92973	TNPO1	0.74
Q8WXX5	DNAJC9	0.74
P31689	DNAJA1	0.73
Q9UKN8	GTF3C4	0.73
P11274	BCR	0.73
Q14498	RBM39	0.73
O15198	SMAD9	0.73
P27708	CAD	0.73
Q03001	DST	0.73
P49915	GMPS	0.73
P62873	GNB1	0.73
Q86UL3	GPAT4	0.73
Q99733	NAP1L4	0.73
Q14683	SMC1A	0.73
Q6P158	DHX57	0.73
A0A087X117	NOMO1	0.73
A0A087WYT3	PTGES3	0.73
I3L504	EIF5A	0.73
Q96GM5	SMARCD1	0.73
P61962	DCAF7	0.73
P12268	IMPDH2	0.73
J3KQY1	MRPL22	0.73
Q92576	PHF3	0.73
Q01813	PFKP	0.73
Q92575	UBXN4	0.73
P43490	NAMPT	0.73
P35613	BSG	0.72
Q92599	43716	0.72
Q13887	KLF5	0.72
Q8N5I9	C12orf45	0.72
Q16531	DDB1	0.72
Q9UNP9	PPIE	0.72
P29401	TKT	0.72
Q99623	PHB2	0.72
A0A0J9YXF2	PON2	0.72
O14976	GAK	0.72
Q86W92	PPFIBP1	0.72
Q16543	CDC37	0.72
Q9UGM3	DMBT1	0.72
P61981	YWHAG	0.72
Q9NWW5	CLN6	0.72
Q6P1J9	CDC73	0.72

Q9BSJ8	ESYT1	0.72
P31946	YWHAB	0.72
Q9H0U9	TSPYL1	0.72
P57078	RIPK4	0.72
A0A024QZP7	CDK1	0.72
Q14119	VEZF1	0.72
Q9H857	NT5DC2	0.71
Q99570	PIK3R4	0.71
J3KN66	TOR1AIP1	0.71
I1E4Y6	GIGYF2	0.71
I3L0E3	hCG_1984214	0.71
P82673	MRPS35	0.71
A0A087WX23	PEG10	0.71
Q9UKF6	CPSF3	0.71
O43175	PHGDH	0.71
Q96AQ6	PBXIP1	0.71
Q13547	HDAC1	0.71
P49406	MRPL19	0.71
B1APK8	ZNF678	0.71
Q5VZL5	ZMYM4	0.71
P36542	ATP5F1C	0.71
Q53EU6	GPAT3	0.71
Q9C0C2	TNKS1BP1	0.71
Q8WX93	PALLD	0.71
Q9HC07	TMEM165	0.71
Q9UJX3	ANAPC7	0.71
P63167	DYNLL1	0.71
D6RBW1	EIF4E	0.71
A0A087WXI5	CDH1	0.71
Q9Y5Q8	GTF3C5	0.71
P60842	EIF4A1	0.70
P04843	RPN1	0.70
Q92665	MRPS31	0.70
P08754	GNAI3	0.70
O75396	SEC22B	0.70
P08237	PFKM	0.70
P21796	VDAC1	0.70
A0A0B4J1V9	HELLS	0.70
P20337	RAB3B	0.70
P60228	EIF3E	0.70
P61758	VBP1	0.70
A0A0A0MSG2	FHL2	0.70
Q8NBM4	UBAC2	0.70

P62993	GRB2	0.70
Q9UIV1	CNOT7	0.70
Q92769	HDAC2	0.70
Q27J81	INF2	0.70
A8MWD9	SNRPGP15	0.70
Q02338	BDH1	0.70
Q9BW19	KIFC1	0.70
Q9HAW4	CLSPN	0.70
P33991	MCM4	0.70
P14923	JUP	0.70
O00483	NDUFA4	0.70
O00267	SUPT5H	0.69
O96000	NDUFB10	0.69
P30291	WEE1	0.69
Q96NB3	ZNF830	0.69
Q9UHD8	43717	0.69
H0Y368	DPM1	0.69
A0A1W2PNX8	UNC45A	0.69
Q9Y678	COPG1	0.69
Q09028	RBBP4	0.69
X6RAY8	MRPL4	0.69
J3KPS0	DNAJB12	0.69
Q9Y305	ACOT9	0.69
Q02978	SLC25A11	0.69
Q7L576	CYFIP1	0.69
O95171	SCEL	0.69
Q8N122	RPTOR	0.69
Q13263	TRIM28	0.69
O75694	NUP155	0.69
Q00059	TFAM	0.69
O00268	TAF4	0.69
Q92616	GCN1	0.68
Q8WUK0	PTPMT1	0.68
P28074	PSMB5	0.68
O15294	OGT	0.68
Q9Y2L1	DIS3	0.68
P49790	NUP153	0.68
O95573	ACSL3	0.68
Q7L2E3	DHX30	0.68
P52701	MSH6	0.68
P51153	RAB13	0.68
Q969V3	NCLN	0.68
M0R2Z9	SUGP2	0.68

Q9HBH0	RHOF	0.68
Q96K37	SLC35E1	0.68
P46977	STT3A	0.68
P25705	ATP5F1A	0.68
A0A087WXK8	FAM83D	0.68
Q5SVZ6	ZMYM1	0.68
Q96R06	SPAG5	0.68
P02768	ALB	0.68
P50281	MMP14	0.68
Q14315	FLNC	0.68
O14646	CHD1	0.67
Q9UKK3	PARP4	0.67
O60645	EXOC3	0.67
Q9BRK5	SDF4	0.67
K7ER00	FARSA	0.67
P61163	ACTR1A	0.67
P09543	CNP	0.67
P20339	RAB5A	0.67
Q02447	SP3	0.67
O94842	TOX4	0.67
Q5TDF0	NTPCR	0.67
E9PDI4	LAD1	0.67
O95817	BAG3	0.67
Q6ZRV2	FAM83H	0.67
Q86XI2	NCAPG2	0.67
A0A0G2JPQ2	NLRP2	0.67
O95202	LETM1	0.67
Q96A65	EXOC4	0.67
E9PI68	SPCS2	0.66
O00148	DDX39A	0.66
O75190	DNAJB6	0.66
Q00325	SLC25A3	0.66
O75616	ERAL1	0.66
A0A140TA86	MICOS13	0.66
P49815	TSC2	0.66
Q99714	HSD17B10	0.66
H3BQK9	MACF1	0.66
Q8NBX0	SCCPDH	0.66
D6W592	HNRNPLL	0.66
P05141	SLC25A5	0.66
P07195	LDHB	0.66
P49750	YLPM1	0.66
O43823	AKAP8	0.66

Q9NP72	RAB18	0.66
Q8NI60	COQ8A	0.66
Q9UBB4	ATXN10	0.66
P17812	CTPS1	0.66
Q9H223	EHD4	0.66
Q9BRX2	PELO	0.66
O00303	EIF3F	0.66
P23258	TUBG1	0.66
Q96S55	WRNIP1	0.66
P11166	SLC2A1	0.66
P68104	EEF1A1	0.65
P53007	SLC25A1	0.65
Q9P2R7	SUCLA2	0.65
A0A1B0GTU4	PXN	0.65
P18031	PTPN1	0.65
Q8WUQ7	CACTIN	0.65
Q8TEM1	NUP210	0.65
Q14318	FKBP8	0.65
Q01196	RUNX1	0.65
Q15061	WDR43	0.65
P35232	PHB	0.65
P00338	LDHA	0.65
Q96EY7	PTCD3	0.65
O60341	KDM1A	0.65
Q5JVF3	PCID2	0.65
Q9HCC0	MCCC2	0.65
P0DOY2	IGLC2	0.65
P49411	TUFM	0.64
Q9UKM7	MAN1B1	0.64
P63173	RPL38	0.64
P21127	CDK11B	0.64
Q9Y697	NFS1	0.64
Q15293	RCN1	0.64
B0YIW6	ARCN1	0.64
A0A087X2I1	PSMC6	0.64
Q96QK1	VPS35	0.64
P43246	MSH2	0.64
O60716	CTNND1	0.64
Q15645	TRIP13	0.64
Q9ULC5	ACSL5	0.64
H0YMV8	RPS27L	0.64
Q14157	UBAP2L	0.64
P25205	MCM3	0.64

P78346	RPP30	0.64
Q9Y5A9	YTHDF2	0.64
A0A0A0MTH9	BTAF1	0.64
P55263	ADK	0.64
P11413	G6PD	0.64
Q96TA2	YME1L1	0.64
Q8IUR7	ARMC8	0.64
Q8NDX5	PHC3	0.63
Q9P0J1	PDP1	0.63
Q13049	TRIM32	0.63
A2AEA2	HLA-C	0.63
Q5T4U5	ACADM	0.63
P12004	PCNA	0.63
Q16576	RBBP7	0.63
P36957	DLST	0.63
P19784	CSNK2A2	0.63
P62829	RPL23	0.63
P40222	TXLNA	0.63
Q9UHD2	TBK1	0.63
P38117	ETFB	0.63
F8VYN9	ARL1	0.63
O00487	PSMD14	0.63
P51665	PSMD7	0.63
O75821	EIF3G	0.63
Q15084	PDIA6	0.63
P43699	NKX2-1	0.63
Q8IZU2	WDR17	0.63
O75925	PIAS1	0.63
O14929	HAT1	0.63
O75157	TSC22D2	0.63
P18085	ARF4	0.63
Q8N5K1	CISD2	0.63
Q7Z5L9	IRF2BP2	0.62
P38432	COIL	0.62
Q9UNM6	PSMD13	0.62
P01834	IGKC	0.62
P52948	NUP98	0.62
Q15118	PDK1	0.62
H7BXI1	ESYT2	0.62
Q6ISB3	GRHL2	0.62
Q13363	CTBP1	0.62
Q9H2P0	ADNP	0.62
Q15008	PSMD6	0.62

Q15166	PON3	0.62
P42677	RPS27	0.62
Q9BPW8	NIPSNAP1	0.62
Q8NC54	KCT2	0.62
A0A0J9YWL0	CRYBG1	0.62
P13010	XRCC5	0.62
Q9Y314	NOSIP	0.62
P53618	COPB1	0.62
P51530	DNA2	0.61
Q9H6R7	WDCP	0.61
Q8NCL4	GALNT6	0.61
Q9H9B4	SFXN1	0.61
P12236	SLC25A6	0.61
A0A0C4DGQ5	CAPNS1	0.61
M0R2C6		0.61
J3KNA0	OXA1L	0.61
O15269	SPTLC1	0.61
P46940	IQGAP1	0.61
A0A087WU02	ERGIC2	0.61
Q9BQT8	SLC25A21	0.61
F5H2F4	MTHFD1	0.61
Q9UKI2	CDC42EP3	0.61
Q8IXI1	RHOT2	0.61
H0YL70	TLE3	0.60
Q9BTE3	MCMBP	0.60
Q16401	PSMD5	0.60
Q5VUA4	ZNF318	0.60
Q06203	PPAT	0.60
P12956	XRCC6	0.60
Q96S59	RANBP9	0.60
H0YGM0	CLPB	0.60
H3BQK0	DDX19B	0.60
P41212	ETV6	0.60
Q14257	RCN2	0.60
P52789	HK2	0.60
P31040	SDHA	0.60
Q9H9Y6	POLR1B	0.60
Q92600	CNOT9	0.60
Q9UBS4	DNAJB11	0.60
Q14204	DYNC1H1	0.59
P20020	ATP2B1	0.59
A0A0G2JPQ3	HLA-G	0.59
P08559	PDHA1	0.59

Q96JM3	CHAMP1	0.59
P17980	PSMC3	0.59
P33527	ABCC1	0.59
O76031	CLPX	0.59
Q9BV38	WDR18	0.59
P48556	PSMD8	0.59
Q9UPR3	SMG5	0.59
P55036	PSMD4	0.59
Q16186	ADRM1	0.59
P11177	PDHB	0.59
P24666	ACP1	0.59
P42345	MTOR	0.59
Q9Y287	ITM2B	0.59
O94776	MTA2	0.58
P30837	ALDH1B1	0.58
O43291	SPINT2	0.58
P08047	SP1	0.58
P46734	MAP2K3	0.58
Q9H7D7	WDR26	0.58
Q8NF37	LPCAT1	0.58
Q8NE86	MCU	0.58
C9J2C0	TUBA8	0.58
P54886	ALDH18A1	0.58
Q13200	PSMD2	0.58
Q96SK2	TMEM209	0.58
P35998	PSMC2	0.58
Q5SQP8	CTBP2	0.58
P27348	YWHAQ	0.58
Q9ULX6	AKAP8L	0.57
Q00535	CDK5	0.57
Q8WWC4	MAIP1	0.57
O75376	NCOR1	0.57
O14681	EI24	0.57
Q99567	NUP88	0.57
Q99650	OSMR	0.57
Q9H8H0	NOL11	0.57
Q9Y3Z3	SAMHD1	0.57
Q08380	LGALS3BP	0.57
H3BVG0	NUP93	0.57
O00231	PSMD11	0.57
Q96CS3	FAF2	0.57
Q5VV42	CDKAL1	0.57
O95163	ELP1	0.56

O94906	PRPF6	0.56
Q96EP5	DAZAP1	0.56
Q5JQQ2	DPCD	0.56
O14980	XPO1	0.56
Q13509	TUBB3	0.56
Q14152	EIF3A	0.56
E5RJR5	SKP1	0.56
P46821	MAP1B	0.56
Q13948	CUX1	0.56
Q9Y6G9	DYNC1LI1	0.56
Q9UBW7	ZMYM2	0.56
Q04721	NOTCH2	0.56
B4DR61	SEC61A1	0.56
Q9HCN8	SDF2L1	0.56
A0A087WUB9	CTNNBL1	0.56
Q9UNF1	MAGED2	0.56
Q8NFH5	NUP35	0.56
E9PK25	CFL1	0.55
Q8TEY7	USP33	0.55
Q15390	MTFR1	0.55
I3L0M9	ELOB	0.55
P35658	NUP214	0.55
Q8IVF2	AHNAK2	0.55
O76071	CIAO1	0.55
Q13608	PEX6	0.55
O00299	CLIC1	0.55
Q12983	BNIP3	0.55
O15231	ZNF185	0.55
Q13951	CBFB	0.55
P40692	MLH1	0.55
Q8TB37	NUBPL	0.54
Q96GD4	AURKB	0.54
P04049	RAF1	0.54
O94915	FRYL	0.54
P33993	MCM7	0.54
Q8N8Z6	DCBLD1	0.54
Q7Z6Z7	HUWE1	0.54
Q9H5Q4	TFB2M	0.54
P62191	PSMC1	0.54
P43686	PSMC4	0.54
P05067	APP	0.54
Q9Y6Y8	SEC23IP	0.54
A0A087WZ40	MAP7	0.53

Q86UW6	N4BP2	0.53
O75306	NDUFS2	0.53
P60604	UBE2G2	0.53
A0A087WW66	PSMD1	0.53
O75179	ANKRD17	0.53
Q96CW5	TUBGCP3	0.53
Q9UN37	VPS4A	0.53
Q9H936	SLC25A22	0.53
P67775	PPP2CA	0.52
Q2NKX8	ERCC6L	0.52
Q9Y4B6	DCAF1	0.52
Q15758	SLC1A5	0.52
O95391	SLU7	0.52
Q9NWZ5	UCKL1	0.52
O15379	HDAC3	0.52
Q9Y679	AUP1	0.52
Q9BUQ8	DDX23	0.52
O75489	NDUFS3	0.52
Q9Y618	NCOR2	0.51
Q9UBB6	NCDN	0.51
Q9HCM1	RESF1	0.51
P35221	CTNNA1	0.51
P62195	PSMC5	0.51
A0A0D9SF58	CHTF18	0.51
O43242	PSMD3	0.51
P49721	PSMB2	0.51
Q9P015	MRPL15	0.51
Q9NU22	MDN1	0.51
O75832	PSMD10	0.51
Q9BUF5	TUBB6	0.51
A0A0J9YXC7	LIMS4	0.51
Q86VP6	CAND1	0.51
P07437	TUBB	0.50
Q9P0U3	SENP1	0.50
O43379	WDR62	0.50
Q13347	EIF3I	0.50
Q9H4A3	WNK1	0.50
P68366	TUBA4A	0.50
Q5SRD1	TIMM23B	0.50
Q14527	HLTF	0.49
O95400	CD2BP2	0.49
P54619	PRKAG1	0.49
Q9NRA8	EIF4ENIF1	0.49

Q15386	UBE3C	0.49
P17612	PRKACA	0.49
H7BXF4	SMPD4	0.49
Q96RT1	ERBIN	0.49
A0A1P0AYU5	SFXN3	0.49
P10644	PRKAR1A	0.49
O43237	DYNC1LI2	0.48
Q969F9	HPS3	0.48
Q8WYP5	AHCTF1	0.48
Q8IY17	PNPLA6	0.48
P51617	IRAK1	0.48
Q9NV96	TMEM30A	0.48
A6QL64	ANKRD36	0.48
P04626	ERBB2	0.48
Q6P3X3	TTC27	0.48
O00469	PLOD2	0.48
P48552	NRIP1	0.48
P55884	EIF3B	0.48
P57740	NUP107	0.48
Q71U36	TUBA1A	0.48
Q6UXY8	TMC5	0.48
P00533	EGFR	0.48
P53350	PLK1	0.47
Q14247	CTTN	0.47
X6R8A1	CTSA	0.47
O95602	POLR1A	0.47
Q14697	GANAB	0.47
Q96DI7	SNRNP40	0.47
P68371	TUBB4B	0.47
Q8IUC4	RHPN2	0.47
Q9UMZ2	SYNRG	0.47
Q86XL3	ANKLE2	0.47
Q5T160	RARS2	0.47
Q6ZRP7	QSOX2	0.47
O95758	PTBP3	0.46
Q6NXG1	ESRP1	0.46
Q8IV08	PLD3	0.46
Q9Y2X9	ZNF281	0.46
Q13042	CDC16	0.46
Q92538	GBF1	0.46
Q9BVA1	TUBB2B	0.46
A0A286YEU2	RBFOX1	0.46
Q9UJX4	ANAPC5	0.46

Q8WVX9	FAR1	0.46
Q9H3S7	PTPN23	0.46
Q16891	IMMT	0.46
F6S8M0	GNS	0.46
O14734	ACOT8	0.46
Q6R327	RICTOR	0.46
O00232	PSMD12	0.45
Q02086	SP2	0.45
Q9BT22	ALG1	0.45
Q9BZK7	TBL1XR1	0.45
O43592	XPOT	0.45
H3BND4	PDXDC1	0.45
Q9Y3T9	NOC2L	0.45
O15031	PLXNB2	0.44
Q9BYJ9	YTHDF1	0.44
Q9NRG9	AAAS	0.44
P35222	CTNNB1	0.44
Q9UKA4	AKAP11	0.44
H0Y966	CEP192	0.44
P08581	MET	0.43
F8WAR4	CHCHD3	0.43
Q13885	TUBB2A	0.43
P30260	CDC27	0.43
F5H0C4	PAAF1	0.43
P16144	ITGB4	0.43
O60701	UGDH	0.42
B5MCA4	EPCAM	0.42
H0Y8C6	IPO5	0.41
Q92609	TBC1D5	0.41
Q06210	GFPT1	0.41
P11717	IGF2R	0.41
Q9UJS0	SLC25A13	0.41
Q9BQE3	TUBA1C	0.41
Q4V339	CBWD6	0.41
O60476	MAN1A2	0.41
Q8IWZ3	ANKHD1	0.41
Q13409	DYNC1I2	0.41
Q9H1A4	ANAPC1	0.41
A0A1B0GVY1	NEDD4L	0.41
Q96KP1	EXOC2	0.40
Q9BW27	NUP85	0.40
Q93063	EXT2	0.40
O95831	AIFM1	0.40

P10586	PTPRF	0.40
P61221	ABCE1	0.39
Q96II5	ARAF	0.39
Q86YV9	HPS6	0.39
A0A0U1RR27	DENND4A	0.39
O95071	UBR5	0.39
O14744	PRMT5	0.38
P14625	HSP90B1	0.38
P22695	UQCRC2	0.38
Q9UJX2	CDC23	0.38
Q96T76	MMS19	0.38
Q14435	GALNT3	0.37
Q13495	MAMLD1	0.37
Q9UBX3	SLC25A10	0.36
Q5W0B1	RNF219	0.36
Q6P2E9	EDC4	0.36
Q3V6T2	CCDC88A	0.36
Q9BZG1	RAB34	0.36
Q9BPZ7	MAPKAP1	0.35
Q9NW81	DMAC2	0.35
O94808	GFPT2	0.35
O75822	EIF3J	0.35
Q9Y5G9	PCDHGA4	0.34
P08670	VIM	0.34
Q06190	PPP2R3A	0.34
Q9BVM2	DPCD	0.34
Q8IWI9	MGA	0.34
P29590	PML	0.33
Q68DQ2	CRYBG3	0.33
P63151	PPP2R2A	0.33
Q7Z4F1	LRP10	0.33
Q2KHR3	QSER1	0.33
Q8IVT5	KSR1	0.33
Q14671	PUM1	0.32
Q86YA3	ZGRF1	0.32
O75746	SLC25A12	0.32
Q7Z5K2	WAPL	0.32
K7ELX0	CEP192	0.32
Q99519	NEU1	0.32
Q9Y5G0	PCDHGB5	0.32
Q8NEV8	EXPH5	0.31
Q9NQX7	ITM2C	0.31
Q658P3	STEAP3	0.31

Q5T5P2	KIAA1217	0.31
Q8NG31	KNL1	0.30
Q8NDG6	TDRD9	0.30
P42224	STAT1	0.29
Q9Y4D1	DAAM1	0.29
Q68D06	SLFN13	0.29
O43524	FOXO3	0.29
O14802	POLR3A	0.29
A0A0A0MTH3	ILK	0.28
Q6ULP2	AFTPH	0.28
P04150	NR3C1	0.27
Q9Y5W7	SNX14	0.27
Q9BY89	KIAA1671	0.26
Q6P444	MTFR2	0.26
Q9C0C7	AMBRA1	0.25
P51587	BRCA2	0.25
P22223	CDH3	0.25
Q13444	ADAM15	0.24
Q8TDJ6	DMXL2	0.23
Q00587	CDC42EP1	0.23
H0Y4R2	POR	0.23
Q9P003	CNIH4	0.22
P18074	ERCC2	0.19
Q9Y2Z2	MTO1	0.18

APPENDIX D
RUVBL1/2 Co-Immunoprecipitating Proteins

Gene ID	Quantity (MIC Sin)			
	IgG	RUVBL1	RUVBL2	RUVBL1/2 (average)
DDX3Y	3.62E-06			0
EIF4A2	3.3E-06			0
GTF2I	4.45E-07			0
PCBP2	3E-06			0
ZIM2	3.97E-07			0
KRT6C	8.48E-05	1.8E-07		0.001059736
TUBB4B	9.67E-07	1.76E-08		0.009110651
KRT16	0.000116	2.76E-06	3.77E-08	0.01207006
TIA1	3.32E-06	1.99E-07		0.029927667
SYNCRIP	1.19E-05	1.29E-06		0.054043871
PEF1	4.12E-06		5.04E-07	0.061159631
TFG	5.98E-05	4.72E-06	4.27E-06	0.075178828
RPSAP58	1.3E-05		1.95E-06	0.075405405
KHDRBS1	5.21E-05	2.82E-06	5.97E-06	0.08420982
DARS	7.46E-06	7.1E-07	5.67E-07	0.085495109
RPS28	0.000211	2.47E-05	1.8E-05	0.101065341
HSPA9	9.92E-05	7.21E-06	1.37E-05	0.105491481
EEF1A1	7.45E-05	6.96E-06	9.11E-06	0.107824477
TAF15	1.81E-05	4.74E-07	3.59E-06	0.112117537
KRT14	6.4E-05	1.15E-05	5E-06	0.128541064
DLD	1.95E-06	1.93E-07	3.15E-07	0.130539846
DDX17	1.3E-05	2.2E-06	1.37E-06	0.13703262
EIF3G	2.81E-06	3E-07	4.73E-07	0.13745105
HNRNPA2B1	5.44E-05	3.43E-06	1.25E-05	0.146182146
HNRNPK	4.11E-05	4.41E-06	9.39E-06	0.167862874
HSPA1A	4.97E-05	3.7E-06	1.4E-05	0.17845132
KRT1	0.002322	0.000393	0.000536	0.199926778
RPS19	0.000441	8.73E-05	9.04E-05	0.201699285
PSMA1	5.2E-06	2.22E-06		0.213477675
EEF1B2	7.18E-06	2.97E-06	2.84E-07	0.226225285
RPS16	0.000146	2.53E-05	4.1E-05	0.226418319
HSPA8	0.000126	1.57E-05	4.51E-05	0.240900636
PDHA1	1.25E-06	2.77E-07	3.83E-07	0.263407821
IGLC2	3.19E-05	6.76E-06	1.02E-05	0.26533877
KIF5B	1.16E-07	6.2E-08		0.267891098
TUBA1C	3E-05	1.11E-05	5.31E-06	0.273921307
RBM4	5.36E-06	2.04E-06	9.37E-07	0.277252378

HNRNPAB	2.67E-06	3.59E-07	1.31E-06	0.312303665
TIAL1	4.29E-06	5.03E-07	2.18E-06	0.313477246
RPL30	0.000251	9.28E-05	6.83E-05	0.320511938
CCT8	5.13E-06	1.74E-06	1.59E-06	0.324415205
G3BP1	4.73E-06	1.67E-06	1.41E-06	0.325702624
CLTB	5.71E-06	1.76E-06	2.03E-06	0.33099405
KRT80	1.01E-06	2.5E-07	4.23E-07	0.331508876
LDHA	2.18E-06	1.45E-06		0.332234432
KRT18	2.32E-05	8.22E-06	7.4E-06	0.336428941
XRCC6	1.13E-05	3.55E-06	4.11E-06	0.338840746
EEF1G	4.5E-06	1.08E-06	2.02E-06	0.344659116
ATP5A1	1.15E-05	4.15E-06	3.81E-06	0.346730602
PDIA6	1.19E-06	1.38E-07	7.63E-07	0.379058032
RPS14	0.000189	7.76E-05	6.7E-05	0.381909139
RPS25	0.000327	0.000129	0.000124	0.387496179
HNRNPC	7.11E-06		5.53E-06	0.388654576
PSMB6	3.76E-06	2.95E-06		0.392315873
KRT7	1.44E-05	3.43E-06	8.28E-06	0.405270083
TUBB	3.86E-06	8.5E-07	2.33E-06	0.412561576
KRT8	1.26E-05	4.12E-06	6.37E-06	0.417024662
HSPD1	3.21E-05	7.82E-06	1.96E-05	0.427026867
KRT9	0.000434	0.000177	0.000194	0.427640561
FLNB	4.48E-06		3.85E-06	0.430085995
HSP90AB1	2.66E-05	7.5E-06	1.59E-05	0.440327684
TARDBP	3.14E-06	1.22E-06	1.58E-06	0.446246819
GAPDH	3.34E-05	6.83E-06	2.32E-05	0.449856244
CLTC	2.78E-05	1.63E-05	9.47E-06	0.462265914
RPLP2	0.000291	0.000184	0.000102	0.492604059
PSMC2	4.29E-06	1.76E-06	2.46E-06	0.492653918
ILF2	7.16E-06	2.85E-06	4.4E-06	0.506420994
HNRNPA1	1.13E-05	4.26E-06	8.12E-06	0.547259063
ATP5B	6.16E-06	4.81E-06	2.1E-06	0.561272521
ACTB	3.37E-05	1.47E-05	2.37E-05	0.570313985
TPR	1.69E-06	1.38E-06	6.56E-07	0.601365248
ENO1	2.36E-06	2.06E-06	8.37E-07	0.614915218
LANCL1	2.89E-06	1.37E-06	2.26E-06	0.626641327
NPM1	5.72E-05	2.42E-05	4.77E-05	0.627498253
ASPH	1.76E-06	1.64E-06	6.96E-07	0.662664325
EIF2S2	3.18E-06	1.61E-06	2.66E-06	0.669535176
SNRNP70	4.66E-06	2.97E-06	3.29E-06	0.671632013
RPL22	0.000182	8.79E-05	0.000167	0.700154585
YBX1	1.91E-06	1.61E-06	1.19E-06	0.733132845
AHNAK	1.98E-05	1.23E-05	1.76E-05	0.756025215

ANXA2	1.08E-05	3.91E-06	1.33E-05	0.796665434
SERBP1	3.83E-06	4.59E-06	2.06E-06	0.868315927
KHSRP	4.24E-06	2.54E-06	5.15E-06	0.907087264
HNRNPU	2.21E-05	2.24E-05	1.79E-05	0.911286974
HSPA5	4.65E-06	1.83E-06	6.68E-06	0.915244034
FLNC	4.26E-06	4.32E-06	4.6E-06	1.047859474
KRT5	1.32E-05	1.8E-05	1.03E-05	1.073745247
RPS3	7.13E-05	8.55E-05	6.77E-05	1.074716611
LGALS3BP	1.63E-06	2.38E-06	1.18E-06	1.095299619
PSMA7	1.59E-06	1.27E-06	2.26E-06	1.109459459
EIF2S3	3.37E-06	4.63E-06	3.15E-06	1.153914591
NCL	0.000104	0.000138	0.000111	1.199023076
FLNA	8.56E-06	1.23E-05	1.16E-05	1.396319664
KRT19	1.78E-06	1.34E-06	4.23E-06	1.562780269
PKM	2.52E-06	6.41E-06	1.67E-06	1.600952003
EIF2A	2.51E-06	8.32E-06		1.658090873
ILF3	1.94E-06	2.66E-06	3.98E-06	1.714894221
HSPA4	1.76E-06	5.78E-06	5.91E-07	1.814513375
HRNR	5.17E-07	7.37E-07	1.2E-06	1.875453666
VCP	9.39E-07	2.7E-06	8.33E-07	1.879709296
C7orf50	1.38E-06		5.41E-06	1.963352685
HADHB	5.28E-07	6.05E-07	1.5E-06	1.988642817
RPL17	3.04E-05	5.41E-05	6.86E-05	2.016770799
DYNC1H1	9.39E-07	3.71E-06	1.82E-07	2.07271841
HIST1H1E	2.24E-05	8.45E-05	8.95E-06	2.088035658
SPTAN1	7.66E-07	2.17E-06	1.2E-06	2.203602193
LRRC59	4.02E-06	1.12E-05	8.42E-06	2.438369781
SPTBN1	9.34E-07	3.02E-06	1.77E-06	2.56070166
RPL11	2.16E-05	0.000102	6.18E-05	3.779112754
TRIM28	9.42E-07	4.58E-06	2.83E-06	3.934491085
RPL12	3.45E-05	0.000152	0.000128	4.048978079
XRCC5	1.47E-06	8.47E-06	4.18E-06	4.310694823
RPL4	2.11E-06	1.24E-05	6.11E-06	4.40617284
MAP4	1.35E-06	1.02E-05	3.59E-06	5.136693908
RPS2	3.62E-06	2.93E-05	1.11E-05	5.582798673
PLEC	1.8E-06	1.11E-05	9.72E-06	5.769690067
RPS4X	1.1E-05	7.61E-05	5.51E-05	5.941136775
RPL10A	1.03E-05	9.3E-05	8.9E-05	8.869088694
MYH9	1.51E-07	3.62E-06		11.98311899
DHX9	5.79E-07	1.29E-05	9.13E-06	19.0590273
RUVBL2	2.05E-06	0.000606	0.000962	382.9301172
RUVBL1	6.51E-07	0.001188	0.000636	1401.832283
KRT10		0.000167		

EP400		2.83E-05	2.15E-05	
DPCD		0.000191	6.78E-05	
TRRAP		9.14E-06	6.06E-06	
SRCAP		1.39E-05	8.81E-06	
C12orf45		8.88E-05	4.41E-05	
PRKDC		6.94E-06	1.42E-06	
RPAP3		1.21E-05	5.18E-05	
PCMT1		0.000128		
RPS8		5.84E-05	5.55E-05	
HNRNPM		5.21E-06	6.47E-06	
CDC5L		2.04E-05	9.96E-07	
SNRNP200		1.14E-05	2.7E-06	
EFTUD2		2.06E-05	9.31E-06	
NFRKB		9.97E-06	6.82E-06	
PRPF8		9.26E-06	1.88E-06	
NOP58		1.39E-05	1.26E-06	
DDX21		1.36E-05	1.34E-05	
HIST1H1B		4.78E-05	1.23E-05	
ZNHIT6		9.74E-06	4.98E-07	
RPLP0		8.97E-05	0.000111	
URI1		2.06E-05	4.82E-05	
RPL18		6.63E-05	3.26E-05	
HIST1H4A		7.88E-05		
RPL13A		5.22E-05	2.13E-05	
RPL13		3.57E-05	9.32E-06	
RPL7A		4.64E-05	8.95E-06	
PRPF19		2.35E-05	1.41E-06	
TOP2A		8.18E-06	3.36E-06	
RPS11		8.38E-05	3.55E-05	
RPS18		3.09E-05	1.43E-05	
KPNA2		1.09E-05	1.17E-06	
RPS15A		0.000101		
RPL27		0.000124	0.000104	
MKI67		1.79E-06		
POLR2A		3.58E-06	9.95E-07	
MDC1		4.78E-06	1.82E-06	
RPL31		7.23E-05	3.87E-05	
DMAP1		5.1E-06	9.43E-06	
TOP1		8.43E-06	1.27E-06	
POLR2B		6.64E-06	3.23E-06	
ACTL6A		7.27E-06	1.38E-05	
RPS13		3.65E-05	3E-05	
PTBP1		7.61E-06	1.19E-05	

DHX15		4.84E-06	2.02E-06	
RPS3A		1.5E-05	1.42E-05	
SND1		6.9E-06	1.67E-06	
PFDN2		3.24E-05	0.000101	
RPL24		3.84E-05	2.71E-05	
SNU13		3.43E-05		
SRRM2		2.47E-06	8.01E-07	
NUMA1		1.92E-06	1.13E-06	
SFPQ		7.25E-06		
ZNHIT3		3.44E-05		
STIP1		2.09E-06	3.17E-06	
EEF2		4.35E-06	7.85E-07	
RPS5		4.83E-05	2.89E-05	
EPC2		4.61E-06	1.96E-06	
DDX3X		2.41E-06	2.34E-06	
HSP90AA1		3.21E-06	3.89E-06	
UBB		0.000106	5.87E-05	
RPL7		2.65E-05	2.03E-05	
SMC3		3.63E-06		
PABPC1		4.57E-06		
RPL23		3E-05	1.49E-05	
RPL23A		4.19E-05	3.85E-05	
RPL5		3.71E-06	2.14E-06	
RPS10		1.65E-05	1.37E-05	
DKC1		2.68E-06	3.63E-06	
PIH1D1		2.09E-06	8.53E-06	
BRD8		1.2E-05	1.4E-05	
ZNHIT2		4.28E-06	2.93E-06	
RPL6		2.06E-05	5.53E-06	
EIF2S1		1.73E-05	2.48E-06	
NONO		1.15E-06	9.77E-07	
RRBP1		2.45E-06	7.75E-07	
ACTN4		2.91E-06	1.36E-06	
DHX30		9.61E-06		
RPL14		3.87E-05		
RPS6		1.81E-05	2.41E-06	
TMPO		4.89E-06	6.41E-07	
ATP2A2		5.86E-06	1.54E-06	
DDX5		6.66E-06	6.05E-06	
MACF1		5.9E-07		
H2AFV		0.00015	8.17E-05	
DSP		1.09E-06	7.25E-07	
FASN		1.93E-06	5.13E-07	

INO80		1.92E-06	5.62E-07	
VARS		3.68E-06	1.1E-06	
SF3B3		2.42E-06	1.98E-06	
RPL3		1.6E-06	2.34E-06	
ACTR5		3.08E-06	2.04E-06	
RPL18A		2.03E-05	5.85E-06	
SF3B1		6.19E-06	8.15E-07	
CAPRIN1		1.55E-05	2.31E-06	
CAD		2.63E-06	6.23E-07	
CKAP5		3.73E-06		
LRPPRC		1.49E-06	5.46E-07	
VPS72		2.82E-06	7.05E-06	
KPNB1		3.05E-06	4.13E-06	
ACTR8		2.32E-06	1.43E-06	
TUBA4A		1.23E-06	5.28E-07	
NUP153		2.42E-06		
PARP1		8.33E-06	4.87E-07	
PRPF6		2.25E-06	1.2E-06	
HADHA		1.78E-06	1.93E-06	
HNRNPF		2.15E-06	1.47E-06	
NUFIP1		9.83E-06		
RTCB		8.37E-07	7.35E-07	
SRSF1		6.27E-06	8.25E-06	
RIPK2		2.64E-06	2.3E-06	
WDR92		6.07E-06	1.72E-05	
INO80E		8.37E-06	6.95E-06	
USP7		2.1E-06	5.56E-07	
TCP1		1.01E-06	7.81E-07	
HNRNPR		1.21E-06	2.91E-06	
AQR		1.55E-06		
HLTF		1.91E-06	1.31E-06	
HMGA1		8.63E-06	1.6E-05	
POLR2E		2.09E-05	9.59E-05	
SEC16A		4.69E-06	3.43E-06	
ZC3HAV1		2.02E-06	4.52E-07	
EWSR1		1.79E-06	3.55E-06	
ABCF1		1.99E-06		
RPL9		2.14E-05		
EZR		9.48E-07	2.18E-07	
RPL26L1		1.81E-05	1.1E-05	
SKIV2L2		2.41E-06		
MYBBP1A		2.06E-06		
ACLY		1.58E-06	4E-07	

EXOSC10		2.41E-06	6.83E-07	
WDCP		6.59E-07	1.41E-06	
RPL8		2.59E-05	3.09E-05	
SF3B2		1.78E-06	1.42E-06	
DEK		2.56E-06	8.7E-07	
HDLBP		1.28E-06		
DDX18		4.25E-07		
PA2G4		2.1E-06	7.85E-07	
STAU1		1.86E-06	6.32E-07	
KTN1		1.31E-06	9.41E-07	
PSMC3		2.64E-06	9.93E-07	
YWHAG		7.78E-06	4.01E-06	
IGF2BP3		7.01E-07	1.29E-06	
SART1		1.64E-06	8.27E-07	
SUPT16H		1.17E-06		
THRAP3		2.38E-06		
PSMD3		5E-07	8.43E-07	
HNRNPL		1.13E-06	5.02E-06	
CCT2		1.6E-06	1.26E-06	
PUF60		2.49E-06	2.8E-06	
ATG2A		1.53E-06	7.07E-07	
CCT4		9.35E-07	1.31E-06	
PCBP1		2.36E-06	2.18E-06	
HCFC1		1.02E-06	3.76E-07	
MATR3		1.75E-06	1.33E-06	
PLRG1		7.92E-07		
PSMC5		1.52E-06	1.24E-06	
ATAD3A		3.83E-07	1.59E-06	
KRT6A		2.38E-06	2.12E-06	
SMARCA5		2.19E-06		
EIF3A		1.26E-06		
HIST1H1C		1.27E-05	1.13E-05	
PPL		6.72E-07		
RPL34		2.72E-05	2.21E-05	
RPN1		2.59E-06	4.91E-07	
SRSF2		5.67E-06	1.72E-06	
TPX2		2.23E-06	5.93E-07	
RBM14		3.75E-07		
UBAP2L		1.49E-06	8.47E-07	
RPSA		6.55E-06		
GTF2I		1.72E-06	8.39E-07	
TCOF1		2.3E-06	3.82E-07	
CCT7		5.32E-06	1.24E-06	

CCT3		2.96E-06	6.26E-07	
AHNAK2		5.3E-07	1.05E-06	
DDX1		5.81E-07	1.26E-06	
DDX47		1.08E-06	5.67E-07	
DDX6		2.18E-06	4.79E-07	
DRG1		5.6E-07	6.28E-07	
ERH		2.06E-05		
PPIF		7.44E-06	4.51E-05	
RFC1		1.16E-06	4.09E-07	
SEC24C		1.73E-06	1.07E-06	
SMC2		1.24E-06		
TUFM		1.31E-06	4.22E-06	
TJP1		7.65E-07		
MTDH		6.4E-07	6.84E-07	
RANBP2		4.9E-07		
SHQ1		8.54E-07		
RAVER1		8.85E-07	2.3E-06	
SEC31A		2.14E-06		
BUB3		1.04E-06	1.85E-06	
TOP2B		1.89E-06		
PPP2R1A		3.71E-07	6.16E-07	
RFC4		9.79E-07	8.33E-07	
NOP2		1.82E-06		
POLR3A		1.45E-06	5.81E-07	
CDC73		3.89E-07	6.28E-07	
EIF5B		8.64E-07		
HIST1H1D		3.55E-06	2.02E-06	
IGF2BP1		2.61E-07	2.74E-07	
LMNB1		4.67E-07	1.47E-06	
RPS9		1.06E-05		
RRP9		7.33E-07	2.84E-07	
SMC4		1.3E-06		
SRPRA		1.26E-06		
MBTD1		1.72E-06	5.27E-07	
MVP		2.58E-06		
PSMC1		1.98E-06	3.04E-07	
PSMD11		7.81E-07	1.1E-06	
NAT10		1.22E-06		
MOGS		8.77E-07		
NOP56		3.43E-07		
CCT6A		5.4E-07	7.58E-07	
SEC13		1.54E-05	3.25E-06	
HNRNPH2		8.7E-07	1.82E-06	

YEATS4		4.44E-06	1.42E-05	
RARS		3.8E-07	2.7E-07	
SEC23A		4.95E-07	3.14E-07	
RBMX		7.07E-07	3.36E-06	
AAR2		6.87E-07		
C7orf55		3.67E-06		
DDX23		3.28E-06		
DHX16		9.69E-07		
FUS		4.43E-07		
H3F3A		2.94E-05		
HSPH1		9.62E-07		
IGF2BP2		2.07E-07	7.61E-07	
ING3		6.6E-07	7.16E-07	
NSUN2		1.99E-06		
PDRG1		1.43E-05	4.41E-05	
PSIP1		7.63E-07	4.42E-07	
SSRP1		7.59E-07		
MORF4L2		1.53E-06	3.32E-06	
RECQL		7.96E-07	5.14E-07	
ACTR6		2.01E-06	3.87E-06	
CCT5		6.78E-07	5.28E-07	
EIF4G1		1.22E-06		
HNRNPH1		1.92E-06		
ADAR		1.43E-06		
AHCY		6.47E-07		
ANXA1		1.17E-06	4.56E-07	
DDX46		2.22E-06		
EMG1		2.55E-06	3.15E-06	
EML4		1.18E-06		
EPRS		8.01E-07	2.42E-07	
FAM98B		1.95E-06	4.11E-07	
HNRNPA0		6.43E-07	2.41E-06	
HSP90B1		1.39E-06	1.97E-07	
PDS5B		6.32E-07		
PRRC2A		1.1E-06		
RAD50		1.2E-06		
RPAP2		5.51E-07	8.06E-07	
TBL2		6.44E-07	8.73E-07	
TJP2		7.93E-07		
UBR5		3.86E-07		
ZFR		1.01E-06	4.05E-07	
EIF3D		3.59E-07		
LRRFIP1		1.84E-06		

RPL35A		6.37E-06		
KAT5		4.54E-07	9.87E-07	
PSMC6		5.93E-07	3.33E-07	
PSMD12		2.29E-07	4.01E-07	
RAD21		1.95E-06		
RPA1		6.98E-07		
RPL10		7.63E-06		
SRRT		1.48E-06	6.41E-07	
LARP1		1.14E-06	7.63E-07	
SMARCA4		1.84E-06	2.62E-06	
CCAR2		8.81E-07	3.99E-07	
AIFM1		2.5E-07	9.77E-07	
CCAR1		7.16E-07		
DST		1.24E-07		
ECD		6E-07		
PEG10		7.53E-07		
POLR1A		5.2E-07	2.6E-07	
SMARCC2		7.69E-07	2.58E-06	
ALYREF		8.95E-07		
ARHGEF2		9.25E-07	3.77E-07	
BAIAP2L1		8.47E-07		
COPA		2.01E-06		
DNAJB11		7.06E-07		
EIF3CL		7.27E-07		
EIF4A3		4.31E-07		
HIST1H1A		8.42E-07	1.84E-07	
HMGA2		7.37E-06		
NUFIP2		1.38E-07		
RPL19		1.36E-05		
RPL28		1.42E-05		
RPLP1		2.4E-05	2.19E-05	
RPS26		1.17E-05	1.58E-05	
SMC1A		6.04E-07		
SNRNP40		3.45E-07	1.75E-07	
SRP72		4.67E-07		
USP10		8.24E-07		
CAP1		1.59E-07		
CLASP1		5.95E-07		
CPSF7		2.65E-07	7.53E-07	
SSB		2.81E-07	6.06E-07	
AIM1		5.83E-07		
GPI		2.12E-07		
INO80B		5.39E-07		

MCM3		1.9E-06		
MRE11A		1.61E-07		
POLR1C		2.98E-07	8.03E-07	
SHMT2		1.21E-06		
SRSF6		2.42E-06	1.91E-06	
ACIN1		3.86E-07		
P4HB		3.34E-07		
PGK1		6.59E-07		
EIF3E		3.81E-07	1.09E-06	
KPNA6		3.71E-07		
PRPF31		2.7E-07	6.18E-07	
SF1		2.03E-07	2.31E-06	
SMARCD1		1.5E-07		
RFC5		4.59E-07	4.8E-07	
UTP4		8.15E-07		
HNRNPH3		2.69E-06	1.12E-06	
SEPT9		2.38E-07	7.25E-07	
FMR1		6.7E-07		
ADNP		4.94E-07		
ANLN		4.68E-07	3.63E-07	
ATXN2L		1.03E-06	2.37E-07	
BCAS2		4.55E-06		
BCLAF1		1.62E-06		
EBNA1BP2		3.98E-07	6.34E-07	
EIF3F		3.58E-07	1.16E-06	
EIF3I		3.11E-07	1.09E-06	
FUBP3		8.2E-07	4.82E-07	
GLG1		4.95E-07		
HDAC1		4.04E-07		
KARS		1.58E-07		
KDM2A		1.88E-07		
MARK2		1.6E-07		
MSH2		1.16E-06		
NKX2-1		2.15E-07		
ORC2		1.32E-07		
PDCD11		3.85E-07		
PKP3		4.65E-07		
POLR2C		2.59E-07		
PSMC4		2.12E-06	3.46E-07	
RCC1		5.56E-07	6.62E-07	
RFC3		1.72E-06	6.37E-07	
RIF1		5.35E-07		
RNPC2		1.22E-06	1.53E-07	

RPN2		1.85E-07		
SCEL		2.86E-07		
SKAP2		4.82E-07		
TPP2		6.63E-07		
U2AF2		4.49E-07	6.45E-07	
YTHDF3		1.62E-07	5.7E-07	
ATXN10		1.17E-07		
GRSF1		2.11E-07	1.38E-06	
LDHB		5.94E-07	5.59E-07	
MAP7D1		1.07E-06	3.93E-07	
DPF2		2.85E-07	3.03E-07	
GTPBP4		5.25E-07	1.5E-07	
MED17		7.58E-07		
SF3A1		4.55E-06		
ACOT9		2.85E-07	5.82E-07	
CLTA		1.57E-06	5.9E-07	
POLDIP3		2E-07	4.31E-07	
RFC2		5.28E-07	8.77E-07	
YBX3		1.22E-07	2.79E-07	
CNOT1		2.81E-07		
DAZAP1		2.91E-07	6.19E-07	
DYNC1I2		6.81E-07		
JUP		6.58E-07		
ASUN		1.24E-07		
DLAT		4.09E-07	1.04E-06	
RANGAP1		5.48E-07		
SON		3.05E-07		
SEC24A		3.15E-07		
SEC24B		4.38E-07		
BAZ1A		1.69E-07		
C14orf166		1.55E-06		
CD3EAP		1.22E-07		
CLASP2		2.93E-07		
CSDE1		3.9E-07		
CSTF2		2.72E-07	3.56E-07	
DKFZP586J0619		2.16E-07		
DNAJA1		3.11E-07		
DNAJA3		2.46E-07	3.82E-07	
EIF3B		3.03E-06	1.92E-06	
FDFT1		1.16E-07	5.15E-07	
HNRNPA3		2.09E-06	4.78E-07	
KPNA3		3.35E-07		
LAD1		1.09E-07		

NACA		8.17E-08		
NKRF		6.95E-07		
PAF1		4.12E-07		
PSMD1		1.01E-06	5.96E-07	
PSMD13		3.64E-07	4.71E-07	
PSMD2		1.66E-06	4.88E-07	
PTRF		3.25E-07	2.04E-07	
PURA		5.27E-07		
RCC2		1.31E-07		
RRP1		1.28E-07	3.41E-07	
RRP1B		6.6E-07		
SLAIN2		1.64E-07		
SMU1		2.48E-07		
SRP14		3.4E-06		
TANGO6		1.01E-06		
TFPT		5.56E-07	7.61E-07	
TSR1		6.23E-07		
TTI1		5.16E-07		
UTP20		7.51E-07		
UXT		3.08E-06	7.44E-06	
VPS35		1.37E-07		
XAB2		5.09E-07		
YTHDF1		2.67E-07	3.21E-07	
ZMYM2		2.68E-07		
ZNF830		1.19E-07		
CFL1		8.79E-06		
YY1		2.73E-07	6.36E-07	
CMAS		7.14E-07	7.11E-07	
MTHFD1L		7.09E-07		
NIFK		1.43E-07		
RBM26		3.53E-07		
RNMT		1.88E-07		
U2AF1		4.14E-07	2.08E-06	
RACGAP1		1.58E-07		
TCEA1		2.31E-07		
ACTR1A		2.23E-07		
DECR1		3.81E-07		
FIP1L1		9.25E-08	2.49E-07	
GPN1		6.39E-07	6.22E-07	
MCRS1		2.54E-07	3.13E-07	
NMT1		5.92E-07		
PES1		1.52E-07		
PSMD4		2.6E-07		

QARS		2.19E-07		
RBM42		5.3E-07		
RPL36A		3.24E-06	4.66E-06	
SEPT2		1.94E-07		
U2SURP		4.33E-07		
WHSC2		2.3E-07		
TUBB4B		3.49E-07	1.67E-06	
TUBB6		1.69E-07	8.76E-07	
GATAD2B		5.24E-07	2.97E-07	
RBBP7		7.88E-07		
BOD1L1		2.68E-07		
CAST		2.49E-06		
CDC123		1.3E-07		
CHERP		3.49E-07		
COPB2		3.02E-07		
CPSF1		3.37E-07		
CPSF6		2.11E-07	5.28E-07	
CSTF1		1.03E-07	4.61E-07	
CSTF3		7.79E-08	2.22E-07	
DDX24		4.35E-07		
DDX50		5.51E-08		
DHX29		3.96E-07		
DLST		2.92E-07	4.13E-07	
EED		1.45E-07		
FAM83D		4.69E-08		
GTPBP1		6.64E-08		
GYG1		4.93E-06		
HELLS		4.93E-07		
INTS10		2.92E-07		
IRF2BP2		1.02E-07		
KIFC1		7.71E-08		
LARP4B		5.86E-07		
LMNB2		2.7E-07		
MED16		2.4E-07	4.22E-07	
MORC2		2.78E-07		
MTA2		7.03E-08		
MTHFD1		4.35E-07		
NCDN		1E-07	1.99E-07	
PAK1IP1		1.21E-07		
PDHB		2.27E-07	8.86E-07	
PDIA3		1.35E-07	4.01E-07	
PLOD2		5.93E-07		
POP1		3.56E-07		

PSMD14		8.15E-07	8.31E-07	
RBM27		2.9E-07		
SMURF2		1.88E-07		
SNW1		1.01E-07		
SPRR2E		2.4E-06		
SRSF5		1.55E-07		
TRIP4		1.04E-07		
TRMT1L		2.84E-06		
TSSC4		1.59E-06	2.22E-06	
TUBB3		4.44E-08		
UBAP2		4.72E-07	2.89E-07	
VCL		2.88E-07		
WDR33		2.4E-07		
WDR5		2.12E-07		
ZC3H15		5.05E-07		
DDX52		2.3E-07		
H2AFY		1.78E-07		
KIF4A		3.25E-07		
PABPN1		4.52E-07		
SMN2		8.35E-07		
DOCK9		3.77E-07		
EIF3H		9.03E-07	7.13E-07	
HP1BP3		1.23E-07		
HSD17B4		8.24E-08		
KPNA1		6.27E-08		
PSMD6		1.67E-07		
SNRPA		5.38E-07	2.86E-06	
SRRM1		6.78E-07	1.54E-06	
STAG2		5.08E-07		
DDX41		6.32E-08		
DNAJB6		2.97E-07		
EIF4B		1.17E-07		
HNRNPDL		2.86E-07	2.29E-07	
INO80C		6.42E-06		
MORF4L1		1.33E-07	2.53E-07	
NUMB		2.77E-07		
RPS20		1.01E-05		
RSL1D1		1.61E-07		
TP53		2.68E-07		
ZC3H18		8.02E-07		
DNMT1		1.48E-07		
PPP1CB		7.83E-07	1.25E-06	
PYM1		5.11E-07		

ADRM1		6.12E-08	3.23E-07	
AIMP1		5.1E-08		
AKAP8		9.34E-07		
ARRDC1		2.43E-07		
BYSL		5.19E-08		
CAPZA1		1.16E-07	3.34E-07	
CCNK		1.06E-07		
CEBPZ		4.78E-07		
COLGALT1		5.23E-08		
CORO1C		1.99E-07		
CPNE3		5.29E-08		
CTBP2		5.81E-08	9.14E-07	
CTNNB1		1.33E-07		
DDX28		3.91E-08		
DDX43		5.81E-08		
DHX8		2.28E-07		
DIDO1		1.77E-07		
DNAJA2		1.51E-07	9.9E-07	
DNAJB1		2.49E-07		
DNAJB12		1.06E-07	2.57E-07	
DSG1		3.03E-07		
DYNC1LI1		7.31E-08		
EIF2AK2		1.09E-07		
ELAVL1		1.47E-07		
EMD		2.22E-07	1.21E-06	
EXOSC7		7.97E-08		
FLII		9.3E-06		
GEMIN5		1.28E-07		
GFPT1		1.83E-07		
GRWD1		2.12E-07	3.51E-07	
GTF2H2C		1.17E-06		
GTF3C4		8.39E-08		
HUWE1		1.31E-07		
IK		2E-07		
IMPDH2		2.3E-07	5.21E-07	
JSRP1		1.04E-07		
KAT7		2.33E-08		
LETM1		5.11E-08		
LPCAT1		3.42E-08		
LRRC47		4.44E-08		
LRWD1		3.92E-08		
LYAR		1.09E-07		
MAP1B		3.01E-07	2.62E-07	

MED14		7E-07		
MEN1		6.88E-08		
MINA		2.67E-07		
MRGBP		4.73E-07	2.76E-07	
MRPS22		7.29E-08		
MRPS31		6.43E-08		
MRPS9		1.22E-07		
NCAPG		2.97E-07		
NCBP1		3.65E-07		
NCKAP1		1.82E-07		
NELFB		7.58E-08		
NELFE		7.02E-08		
NOM1		2.99E-07		
P4HA1		5.95E-08	9.23E-08	
PAK4		1.71E-07		
PALLD		2.86E-08		
PDS5A		1.79E-07	2.24E-07	
POLDIP2		9.34E-08		
PPIE		4.39E-07		
PPIL4		1.15E-07		
PPM1G		8.09E-08		
PPP1CA		9.37E-07		
PSPC1		1.27E-06		
PTCD3		3.66E-08	3.78E-07	
PURB		6.26E-08		
RALY		2.39E-07		
RBM10		3.77E-07		
RBM22		1.48E-07		
RBM28		3.36E-07		
RPL37		6.06E-06		
RPP38		1.11E-06		
RPS23		1.52E-06		
RPS7		1.35E-05	3.7E-05	
SEC23B		2.67E-08	1.9E-07	
SGPL1		4.13E-07		
SIN3A		3.22E-07		
SMARCA1		3.74E-07		
SMARCD1		2.58E-08		
SNRPN		1.17E-06		
SNX9		6.75E-08		
ST13		3.04E-07		
TAF4		2.21E-07	1.55E-07	
TBRG1		7.18E-07		

TFB2M		1.42E-07		
TFRC		4.18E-07		
TMEM109		1.02E-06	2.04E-06	
TPM3		3.48E-06		
TRIM25		4.5E-08		
TTI2		4.46E-08		
TUBG1		1.87E-07		
TXLNA		6.95E-08		
TXLNG		5.18E-08		
UBTF		5.16E-07		
UGP2		1.39E-07		
USP39		4.84E-08	5.01E-07	
UTP15		5.99E-08		
VPS26A		1.06E-07		
VRK1		1.12E-07		
WDR1		8.05E-08		
WDR11		1.85E-07		
WDR82		5.11E-08		
XPNPEP3		9.94E-08	1.42E-06	
XRCC1		7.12E-08		
ZNF326		3.97E-08		
ARID1A		1.49E-07		
AUP1		2.78E-08		
AURKA		9.25E-08		
CDKN2AIP		2.03E-08		
CLP1		8.59E-08		
EPC1		2.96E-07	1.21E-06	
ESRP1		5.79E-08		
ESYT1		1.64E-07		
GTF3C5		7.03E-08	1.71E-07	
HSPA4L		2.6E-07		
LSM14A		1.63E-07		
MAP7		4.79E-07		
NXF1		4.75E-07		
PLEKHA5		2.87E-07		
PRRC2C		8.08E-08		
SAMHD1		3.62E-08		
SMARCC1		3.44E-07	3.42E-07	
TMEM214		1.67E-07		
VIM		7.1E-08		
AP1B1		6.45E-07		
CPSF3L		1.11E-07		
CS		8.52E-08		

DYNC1LI2		8.39E-08		
ERCC2		6.08E-08		
EXOSC9		2.39E-07		
FBL		4.41E-07	8.4E-07	
GPN3		9.94E-08		
LSM14B		7.76E-08		
MCF2L		1.69E-07		
MED24		1.89E-07		
NOL11		1.94E-07		
POLR1B		3.06E-07		
RBPJ		1.19E-07		
SARS2		2.49E-08		
SART3		2.81E-07		
SEC61A1		8.58E-08	2.45E-07	
SMARCB1		1.61E-07	3.29E-07	
TWF1		9.28E-07		
TXNL1		8.48E-07		
WDR45		3.01E-07	4.41E-07	
YTHDF2		9.83E-08	4.68E-08	
ZNF638		5.99E-07		
CDK9		3.17E-07		
TUBB2A		4.26E-08	1.3E-07	
ACTBL2		9.01E-08	8.95E-07	
AP2A1		1.66E-07		
BAG3		2.82E-08		
CD2BP2		1.03E-07		
CDC23		3.2E-08		
CPSF2		2.62E-07		
DBR1		6.16E-08		
DDOST		1.39E-07		
DROSHA		5.65E-08		
EEFSEC		2.92E-08		
EIF3M		6.7E-07		
ERCC5		8.19E-08		
EXOSC8		4.97E-08		
FRG1		2.55E-07		
G3BP2		2.3E-07		
GPKOW		2.29E-08		
HK2		6.93E-08		
HSPA1L		1.47E-08		
HSPB1		1.27E-06		
IGF2R		5.13E-08		
IMPDH1		3.72E-08		

IQSEC2		6.38E-08		
KPNA4		2.03E-08		
KRT79		1.27E-07		
MED13		5.63E-08		
MSN		2.63E-07		
NOL6		3.23E-07		
PCID2		4.24E-08		
PLOD1		5.04E-08		
PPAN		7.65E-09		
PPP1CC		1.51E-07		
RAE1		2.65E-08		
RBBP4		5.36E-08		
TERF2		3.71E-08		
TOP1MT		2.87E-08		
VASP		1.02E-07		
YBX2		2.55E-08		
CCT6B		4.45E-08		
CDK1		1.52E-07		
KRT17		2.82E-08	1.38E-07	
PTBP3		5.72E-08	7.69E-08	
STRBP		1.95E-08		
H2AFJ		0.000127		
HIST1H2AB		9E-05		
ACSL3			6.04E-07	
ASNSD1			1.04E-05	
BCAP31			3.53E-06	
CHAF1B			7.95E-08	
EEF1D			2.54E-06	
EIF3L			4.61E-07	
GLUD1			5.63E-07	
GMPS			1.66E-07	
GNAS			3.33E-07	
HDAC2			2.61E-07	
HTATSF1			1.58E-07	
INO80B-WBP1			9.44E-07	
KIF2A			4.59E-07	
KLF16			2.01E-06	
KRT13			9.18E-06	
KRT3			2.05E-07	
KRT4			1.62E-06	
KRT77			3.53E-08	
LMNA			4.75E-06	
MRPL12			4.58E-06	

MTG2			2.41E-07	
NSUN5			2.14E-07	
P4HA2			9.02E-07	
PFDN6			5.69E-05	
PRKAR2A			4.14E-07	
PRPF4			1.66E-07	
RACK1			3.06E-07	
RPS17			1.11E-05	
RPS21			3.86E-06	
SEPT7			3.19E-07	
SNRPD2			2.37E-05	
SPATS2L			5.06E-07	
TIMM50			5.34E-07	
YWHAZ			5.92E-07	

APPENDIX E
List of Proteins Identified by iPOND-Mass Spec After Compound B Treatment

UniProt Accession	Gene symbol	Relative Amount (Compound B / Compound C), average 3 replicates
Q9H1E3	NUCKS1	0.03699
Q9BWT1	CDCA7	0.05694
P0DPD5	ZNF723	0.06587
P35789	ZNF93	0.0698
Q3SY52	ZIK1	0.0919
Q9UEG4	ZNF629	0.09364
O60765	ZNF354A	0.09409
P13682	ZNF35	0.11456
A6NHB5	ZMYM3	0.11808
Q9Y4B4	RAD54L2	0.13194
P17026	ZNF22	0.14133
P17028	ZNF24	0.14174
Q9UBW7	ZMYM2	0.14258
P62633	CNBP	0.14443
Q96GN5	CDCA7L	0.14493
Q9P255	ZNF492	0.14654
Q99697	PITX2	0.14699
Q9H2P0	ADNP	0.15719
Q9NRG0	CHRAC1	0.15751
Q92766	RREB1	0.16458
P54198	HIRA	0.16483
Q8N257	HIST3H2BB	0.16786
P46100	ATRX	0.17085
P10412	HIST1H1E	0.17097
Q9NTM9	CUTC	0.17269
O75820	ZNF189	0.17627
P17036	ZNF3	0.1775
Q8ND82	ZNF280C	0.17912
Q96Q89	KIF20B	0.18274
Q9NX24	NHP2	0.18575
J3KQN4	RPL36A	0.18752
O75928	PIAS2	0.19058
Q8IWY8	ZSCAN29	0.19658
P40692	MLH1	0.19664
Q2TB10	ZNF800	0.19989
Q99986	VRK1	0.2008

P55735	SEC13	0.20131
Q6IQ21	ZNF770	0.20134
Q15022	SUZ12	0.20195
Q9H4L7	SMARCAD1	0.20222
Q9BTC8	MTA3	0.20613
P54277	PMS1	0.20649
P16401	HIST1H1B	0.20699
Q9NRL2	BAZ1A	0.20713
A0A0B4J1V9	HELLS	0.20721
P41223	BUD31	0.21051
P61956	SUMO2	0.21741
Q68E01	INTS3	0.22001
A8MU27	SUMO3	0.22093
P09429	HMGB1	0.22123
P68431	HIST1H3A, HIST1H3B, HIST1H3C, HIST1H3D, HIST1H3E, HIST1H3F, HIST1H3G, HIST1H3H, HIST1H3I, HIST1H3J	0.22314
O96028	NSD2	0.22492
Q96KM6	ZNF512B	0.22573
Q8TF20	ZNF721	0.22639
A0A087WT20	DCAF13	0.22798
P16403	HIST1H1C	0.2304
Q96JM2	ZNF462	0.2316
Q8N2W9	PIAS4	0.23202
Q96EI5	TCEAL4	0.23475
Q8WUA4	GTF3C2	0.23591
P31151	S100A7	0.23629
A0A087WYT3	PTGES3	0.2369
P25398	RPS12	0.23896
A0A0U1RRH6	PHF14	0.23905
Q9UQ84	EXO1	0.24245
Q9NXK8	FBXL12	0.24281
Q9Y483	MTF2	0.24314
Q96G46	DUS3L	0.24418
Q8IUF8	RIOX2	0.24691
Q7Z5J4	RAI1	0.2473
P84243	H3F3A, H3F3B	0.24948
P98179	RBM3	0.25056
A0A0G2JK44	BRD2	0.25128
O60281	ZNF292	0.25193
F8W727	RPL32	0.25269
A0A0C4DGG9	CHD4	0.2542
Q9HCM9	TRIM39	0.25604

P26583	HMGB2	0.25675
Q02539	HIST1H1A	0.25706
D6W592	HNRNPLL	0.2571
G3V3A4	SNW1	0.25713
Q5VZL5	ZMYM4	0.25891
D6RGC2	ZNF721	0.25995
P16402	HIST1H1D	0.26037
P54278	PMS2	0.2609
P83916	CBX1	0.26156
D6RBW1	EIF4E	0.26162
P35268	RPL22	0.26227
Q9UIF9	BAZ2A	0.2626
A0A0A0MRM9	NOLC1	0.26279
P25490	YY1	0.26342
P49711	CTCF	0.26346
Q9BYK1	RPS21	0.26361
Q9BQ61	TRIR	0.26542
F6R0L0	SIMC1	0.26604
Q14149	MORC3	0.26672
Q92769	HDAC2	0.26724
Q8IX21	SLF2	0.26822
Q9UBU8	MORF4L1	0.26874
P23284	PPIB	0.26891
Q9UKL0	RCOR1	0.26921
Q13185	CBX3	0.27098
Q9UER7	DAXX	0.27122
Q9NS91	RAD18	0.27348
Q15937	ZNF79	0.27589
A0A0A0MSG2	FHL2	0.2787
O95218	ZRANB2	0.27927
P78347	GTF2I	0.27996
P35659	DEK	0.28104
Q96DI7	SNRNP40	0.2812
Q96T23	RSF1	0.28168
A0A087WVZ6	ZMYND8	0.28181
O00479	HMGN4	0.28202
A0A087WTW0	UHRF1	0.28221
Q9UGU0	TCF20	0.28581
A9Z1X7	SRRM1	0.28597
P37108	SRP14	0.28785
Q9ULI0	ATAD2B	0.28794
Q15059	BRD3	0.2884
P62318	SNRPD3	0.28929

P09012	SNRPA	0.28955
Q96RR1	TWNK	0.2902
P05114	HMGN1	0.29075
A0A0B4J220		0.29288
O60814	HIST1H2BK	0.29317
P17096	HMGA1	0.29436
Q66PJ3	ARL6IP4	0.29442
O75925	PIAS1	0.29446
Q96QE3	ATAD5	0.29466
Q02543	RPL18A	0.29734
O15347	HMGB3	0.29788
O75531	BANF1	0.30048
Q8TF68	ZNF384	0.30122
Q8N884	CGAS	0.30166
P05204	HMGN2	0.30254
P35251	RFC1	0.30322
P61513	RPL37A	0.30336
Q9UKD2	MRTO4	0.30384
Q9NP66	HMG20A	0.30449
P63173	RPL38	0.30499
P62805	HIST1H4A, HIST1H4B, HIST1H4C, HIST1H4D, HIST1H4E, HIST1H4F, HIST1H4H, HIST1H4I, HIST1H4J, HIST1H4K, HIST1H4L, HIST2H4A, HIST2H4B, HIST4H4	0.30665
O95251	KAT7	0.30713
Q96FC9	DDX11	0.30902
Q9Y3U8	RPL36	0.31102
B8ZZN6	SUMO1	0.31121
Q5T3J3	LRIF1	0.31261
Q8TAF3	WDR48	0.31362
P13051	UNG	0.31428
Q9Y6I4	USP3	0.31635
O60884	DNAJA2	0.31804
Q9NPF5	DMAP1	0.31839
Q969T4	UBE2E3	0.31866
P62888	RPL30	0.31929
Q6FI13	HIST2H2AA3, HIST2H2AA4	0.3199
A0A1P0AZG4	LCOR	0.32071
A0A024R216	HDGFRP3	0.3214
Q8N7H5	PAF1	0.32175
Q9NVM9	INTS13	0.32177
A0A0A0MT49	SMARCA4	0.32185
Q9P258	RCC2	0.32194

Q8NFW8	CMAS	0.32242
P51948	MNAT1	0.32261
P45973	CBX5	0.32416
O94888	UBXN7	0.32499
O60341	KDM1A	0.32508
Q7L2H7	EIF3M	0.32557
Q96PU4	UHRF2	0.32674
P25789	PSMA4	0.32858
Q7Z4V5	HDGFL2	0.32884
Q9NWT1	PAK1IP1	0.32965
Q702N8	XIRP1	0.3297
P07305	H1F0	0.32989
P62851	RPS25	0.33155
O75937	DNAJC8	0.33169
Q96RL1	UIMC1	0.33266
P62857	RPS28	0.33316
Q12830	BPTF	0.33339
Q9H307	PNN	0.33388
Q15014	MORF4L2	0.334
Q9NZ63	C9orf78	0.33409
Q9BY42	RTF2	0.33421
Q9Y281	CFL2	0.33511
Q6UX04	CWC27	0.33512
P13640	MT1G	0.3352
P08134	RHOC	0.33567
Q96L73	NSD1	0.33603
Q02241	KIF23	0.33613
F5H423		0.33628
P52701	MSH6	0.33654
Q9H582	ZNF644	0.33801
P46782	RPS5	0.33822
P39687	ANP32A	0.33832
Q92541	RTF1	0.3384
Q9NUQ6	SPATS2L	0.33892
Q8WVC0	LEO1	0.33998
Q13263	TRIM28	0.34012
Q15648	MED1	0.34152
Q14011	CIRBP	0.34276
Q8IXQ4	GPALPP1	0.34339
Q7Z3K3	POGZ	0.34346
O43150	ASAP2	0.34351
Q15417	CNN3	0.34386
P04908	HIST1H2AB, HIST1H2AE	0.34391

A0A0B4J1V8	PPAN-P2RY11	0.34452
Q13535	ATR	0.3457
Q14676	MDC1	0.34591
Q6P2Q9	PRPF8	0.34739
P62266	RPS23	0.34754
Q02880	TOP2B	0.34764
Q8WWQ0	PHIP	0.34781
Q9Y5S9	RBM8A	0.3479
P78346	RPP30	0.34812
H0YE88	TEAD1	0.34907
Q15257	PTPA	0.3492
K7ELC2	RPS15	0.3494
Q8WWI1	LMO7	0.34973
Q9HAF1	MEAF6	0.35201
O75530	EED	0.35284
Q12789	GTF3C1	0.35423
P78549	NTHL1	0.35453
A6NHR9	SMCHD1	0.3547
B1AHD1	SNU13	0.35531
Q9NYH9	UTP6	0.35644
P46778	RPL21	0.35717
Q13907	IDI1	0.35754
P53999	SUB1	0.35881
Q5SRQ6	CSNK2B	0.35889
P62280	RPS11	0.35905
P18077	RPL35A	0.35954
O60264	SMARCA5	0.36004
F5H6H0	HMGA2	0.36073
O60885	BRD4	0.36085
Q9NZJ0	DTL	0.36169
O14979	HNRNPDL	0.36325
Q9BZZ5	API5	0.36365
Q9UEE9	CFDP1	0.36408
P61964	WDR5	0.36413
O94782	USP1	0.36465
Q96PZ0	PUS7	0.36536
P54132	BLM	0.36622
Q96JM3	CHAMP1	0.36663
Q13642	FHL1	0.36676
Q15651	HMGN3	0.36727
Q5QJE6	DNTTIP2	0.36831
Q9NXF7	DCAF16	0.36851
Q6PL18	ATAD2	0.36871

Q9UPP1	PHF8	0.36894
O75940	SMNDC1	0.36921
Q8WXI9	GATAD2B	0.36924
Q7Z6I8	C5orf24	0.36998
Q9UQ80	PA2G4	0.37062
Q9BTE7	DCUN1D5	0.37102
Q14320	FAM50A	0.37112
Q52LJ0	FAM98B	0.37207
Q96B01	RAD51AP1	0.37261
Q8IWI9	MGA	0.37308
O75822	EIF3J	0.37322
Q9UFC0	LRWD1	0.37331
Q969Q0	RPL36AL	0.37341
Q9Y4A5	TRRAP	0.37395
O14602	EIF1AY	0.37431
O94776	MTA2	0.37436
O15164	TRIM24	0.37544
P78527	PRKDC	0.37582
Q14241	ELOA	0.37589
Q9H967	WDR76	0.37625
Q8N684	CPSF7	0.37644
Q9UBB5	MBD2	0.37681
O14646	CHD1	0.37682
Q9H6F5	CCDC86	0.37686
P0C0S5	H2AFZ	0.377
Q4G0S7	CCDC152	0.37731
P26358	DNMT1	0.37741
O15060	ZBTB39	0.37758
Q13547	HDAC1	0.37809
A0A1W2PPZ5	TCEA1	0.37913
Q14103	HNRNPD	0.37941
P10588	NR2F6	0.37988
Q96ME7	ZNF512	0.38282
P06702	S100A9	0.38302
Q9BRJ6	C7orf50	0.3833
Q92522	H1FX	0.3845
B7ZLQ5	SMARCA1	0.38526
Q86YP4	GATAD2A	0.38661
Q92917	GPKOW	0.38685
Q9UIG0	BAZ1B	0.38751
O14770	MEIS2	0.38887
Q9UPN9	TRIM33	0.3889
P62913	RPL11	0.38917

O00148	DDX39A	0.38921
Q14527	HLTF	0.38949
O95453	PARN	0.38956
P11387	TOP1	0.38991
P18754	RCC1	0.39045
P60866	RPS20	0.39157
P42166	TMPO	0.39211
Q86U86	PBRM1	0.39264
P13984	GTF2F2	0.3932
Q86WJ1	CHD1L	0.39358
Q9UHV9	PFDN2	0.39391
Q96IZ0	PAWR	0.39425
Q7Z5L9	IRF2BP2	0.39425
H3BLV9	SRPK1	0.3943
O75367	H2AFY	0.39445
P61254	RPL26	0.39474
Q9NPA3	MID1IP1	0.39533
P30050	RPL12	0.39536
P62829	RPL23	0.39543
Q7Z7K6	CENPV	0.39545
Q8NAP3	ZBTB38	0.39549
Q9Y5B9	SUPT16H	0.39574
H0YHG0		0.39636
Q14669	TRIP12	0.39645
M0QYS1	RPL13A	0.39682
P21291	CSRP1	0.39724
A0A1B0GTU4	PXN	0.39755
F8VRH0	PCBP2	0.3994
P27695	APEX1	0.39999
P35269	GTF2F1	0.40116
Q5T5X7	BEND3	0.40131
E9PK25	CFL1	0.4014
Q96RE7	NACC1	0.40146
Q15910	EZH2	0.40203
Q96ST2	IWS1	0.40221
P18615	NELFE	0.40297
Q01658	DR1	0.40354
P43699	NKX2-1	0.40385
O60934	NBN	0.40524
J3KQE5	RAN	0.40584
O14965	AURKA	0.40607
Q13330	MTA1	0.40608
Q8WW12	PCNP	0.40662

P62241	RPS8	0.40783
F8VXC8	SMARCC2	0.40902
Q13151	HNRNPA0	0.40945
Q9UKN8	GTF3C4	0.40954
P15153	RAC2	0.40974
P68036	UBE2L3	0.41011
P09874	PARP1	0.41067
Q92922	SMARCC1	0.41095
Q9Y232	CDYL	0.41121
Q9P016	THYN1	0.41132
P40425	PBX2	0.41196
Q5SQP8	CTBP2	0.41234
P51991	HNRNPA3	0.4124
Q9Y2X3	NOP58	0.41273
P20290	BTF3	0.41385
O75475	PSIP1	0.41419
P46777	RPL5	0.41445
P11388	TOP2A	0.4148
Q9Y2K7	KDM2A	0.41513
H3BSH7	UTP4	0.41544
O60869	EDF1	0.41592
P62316	SNRPD2	0.41604
P42766	RPL35	0.41642
Q2NL82	TSR1	0.41649
P62891	RPL39	0.4167
Q8N1G0	ZNF687	0.41741
P61758	VBP1	0.41749
Q9Y2L1	DIS3	0.41761
Q8WXX5	DNAJC9	0.41782
K7EQZ3		0.41901
P46779	RPL28	0.41929
P24928	POLR2A	0.41974
P62263	RPS14	0.41997
P49916	LIG3	0.42071
Q01831	XPC	0.42099
P62854	RPS26	0.42106
Q14331	FRG1	0.42106
P43246	MSH2	0.42113
O95696	BRD1	0.42119
Q9ULW0	TPX2	0.42275
P48443	RXRG	0.42314
P24666	ACP1	0.42401
Q15287	RNPS1	0.42407

A0A0G2JIR1	EHMT2	0.42428
Q9GZU8	FAM192A	0.42479
O60942	RNGTT	0.42491
Q9UPW0	FOXJ3	0.42543
Q9NW64	RBM22	0.42602
Q00403	GTF2B	0.4264
A0A087WX23	PEG10	0.42699
Q99575	POP1	0.42735
F6WQW2	RANBP1	0.42752
Q9BQ75	CMSS1	0.42794
K7ELG9	LSM12	0.42828
Q96ST3	SIN3A	0.42838
Q9Y4W2	LAS1L	0.42857
Q9Y224	RTRAF	0.42927
Q05D32	CTDSPL2	0.42929
O60306	AQR	0.42951
P62979	RPS27A	0.43021
Q08945	SSRP1	0.43056
Q9H0S4	DDX47	0.43068
Q9UBD5	ORC3	0.43116
P49207	RPL34	0.4314
P31942	HNRNPH3	0.43187
P38159	RBMX	0.43189
P21281	ATP6V1B2	0.43211
Q9UJA5	TRMT6	0.43243
Q8N5C6	SRBD1	0.43274
P49915	GMPS	0.43276
P48729	CSNK1A1	0.43353
Q9NZL4	HSPBP1	0.43383
Q9Y4B6	DCAF1	0.43404
Q96FZ2	HMCES	0.4343
P27635	RPL10	0.43438
Q8IXT5	RBM12B	0.43444
P46063	RECQL	0.43488
Q92979	EMG1	0.43602
Q9HCD5	NCOA5	0.4363
Q9BQ67	GRWD1	0.43674
P14678	SNRPB	0.43681
J3KTL2	SRSF1	0.43681
Q13356	PPIL2	0.43723
P39023	RPL3	0.43744
Q9Y5Q8	GTF3C5	0.43832
H3BQK9	MACF1	0.43878

P62753	RPS6	0.43905
Q5T1Z8	PUM1	0.43915
P19525	EIF2AK2	0.44101
Q9BXP5	SRRT	0.44173
Q9H501	ESF1	0.44202
P37837	TALDO1	0.4424
A0A087WU03	HNRNPDL	0.44241
Q8IYL3	C1orf174	0.44244
Q9Y6A4	CFAP20	0.44265
P22626	HNRNPA2B1	0.44287
Q9Y4E5	ZNF451	0.44302
P42677	RPS27	0.44341
P40938	RFC3	0.44371
P30876	POLR2B	0.4439
Q1KMD3	HNRNPUL2	0.44429
Q9UBT2	UBA2	0.44431
J3KPP4	LUC7L3	0.44448
Q13049	TRIM32	0.44462
O43172	PRPF4	0.44581
F8W0W8	PPP1CC	0.44619
Q9NQT4	EXOSC5	0.44626
Q9UQR1	ZNF148	0.44691
A0A0A6YYL6	RPL17-C18orf32	0.44753
O15294	OGT	0.44754
Q9NTI5	PDS5B	0.44782
Q13888	GTF2H2	0.44792
Q15004	PCLAF	0.44825
O60832	DKC1	0.44827
P62081	RPS7	0.44865
P61247	RPS3A	0.4488
Q8IUE6	HIST2H2AB	0.4488
Q6PJP8	DCLRE1A	0.44904
J3QQ67	RPL18	0.44912
Q8WVM7	STAG1	0.44929
O15446	CD3EAP	0.4501
O43447	PPIH	0.45033
O60684	KPNA6	0.45041
A0A0B4J2C3	TPT1	0.45066
Q9NX58	LYAR	0.45074
P62136	PPP1CA	0.45101
Q9Y570	PPME1	0.4513
Q9Y5M8	SRPRB	0.45134
Q99549	MPHOSPH8	0.45135

P49903	SEPHS1	0.45143
Q01844	EWSR1	0.45185
A0A0A0MQX8	MBNL1	0.45188
O95239	KIF4A	0.45195
Q9H0C8	ILKAP	0.45252
P63244	RACK1	0.45277
P17480	UBTF	0.45285
Q13428	TCOF1	0.45291
O00255	MEN1	0.45315
Q9NXG2	THUMPD1	0.45328
P18858	LIG1	0.45368
Q9NYB0	TERF2IP	0.45385
P46013	MKI67	0.45402
P62906	RPL10A	0.45415
Q9NS86	LANCL2	0.45525
P83731	RPL24	0.4563
P84098	RPL19	0.45679
Q99747	NAPG	0.45683
P25685	DNAJB1	0.45714
Q9Y2W1	THRAP3	0.45728
O00505	KPNA3	0.4574
Q8NBQ5	HSD17B11	0.45755
P09651	HNRNPA1	0.45765
H0YL70	TLE3	0.45771
B4DJL6	INTS14	0.45775
X6RAL5		0.45967
Q9BTE3	MCMBP	0.45981
E9PAU2	RAVER1	0.45995
O75676	RPS6KA4	0.46049
Q99873	PRMT1	0.46057
E9PB61	ALYREF	0.46097
Q13416	ORC2	0.46176
O43809	NUDT21	0.46253
Q9NRN7	AASDHPPT	0.46256
Q9NVP2	ASF1B	0.4631
Q9Y314	NOSIP	0.46323
C9JA08	NMD3	0.46325
O43684	BUB3	0.46399
Q9NY12	GAR1	0.46448
Q13363	CTBP1	0.46479
P14866	HNRNPL	0.46487
A0A0A6YYG9	ARPC4-TTLL3	0.46531
P46783	RPS10	0.46547

Q15061	WDR43	0.46571
Q9NQZ2	UTP3	0.4658
Q9HC52	CBX8	0.46587
Q9Y277	VDAC3	0.46644
Q9HCE6	ARHGEF10L	0.46665
Q9BRD0	BUD13	0.46674
P49959	MRE11	0.46674
Q9Y3B9	RRP15	0.4668
Q5SRE5	NUP188	0.46709
Q9UIS9	MBD1	0.4674
Q96P70	IPO9	0.4683
I3L504	EIF5A	0.46891
Q13618	CUL3	0.46921
P23497	SP100	0.46953
H3BPE7	FUS	0.46972
J3QQJ0	SAP30BP	0.47064
Q15554	TERF2	0.47099
Q9NQR4	NIT2	0.47192
X6R4W8	ZNF207	0.47194
Q9UNE7	STUB1	0.47231
P62244	RPS15A	0.47235
P60981	DSTN	0.47242
Q69YH5	CDCA2	0.47269
P28288	ABCD3	0.47273
Q9UKI8	TLK1	0.47276
P53350	PLK1	0.47292
P62277	RPS13	0.47354
O15042	U2SURP	0.47389
P35568	IRS1	0.47449
P52789	HK2	0.4746
Q6P6C2	ALKBH5	0.47477
Q9BWH6	RPAP1	0.4749
P51858	HDGF	0.47622
Q04323	UBXN1	0.47637
K7ELC7	RPL27	0.4765
Q7Z417	NUFIP2	0.47651
Q9NXV6	CDKN2AIP	0.47652
Q7Z5K2	WAPL	0.47656
P62249	RPS16	0.47666
A0A0A0MSI8	EXOC5	0.47675
O95400	CD2BP2	0.47698
O14908	GIPC1	0.47704
Q15843	NEDD8	0.47752

E5RJR5	SKP1	0.47753
Q13148	TARDBP	0.47768
P18887	XRCC1	0.47783
Q9H9B1	EHMT1	0.47787
Q9UKV3	ACIN1	0.47802
O75362	ZNF217	0.47815
Q01780	EXOSC10	0.4784
Q15561	TEAD4	0.47882
Q5VTR2	RNF20	0.47905
Q9H4A6	GOLPH3	0.47932
P08559	PDHA1	0.47942
Q9Y3T9	NOC2L	0.47954
P21796	VDAC1	0.47972
Q13242	SRSF9	0.47981
Q14739	LBR	0.48006
Q15942	ZYX	0.48021
Q7L0Y3	TRMT10C	0.48063
O43776	NARS	0.48169
Q56VL3	OCIAD2	0.48176
P42285	MTREX	0.48218
Q9BQA1	WDR77	0.48291
P55036	PSMD4	0.48297
Q13868	EXOSC2	0.48301
P48507	GCLM	0.48342
M0QXA7	WIZ	0.48386
Q16630	CPSF6	0.48386
P14174	MIF	0.48392
O75340	PDCD6	0.48442
P05386	RPLP1	0.48445
O95456	PSMG1	0.4845
P40937	RFC5	0.48459
Q01105	SET	0.48469
O96008	TOMM40	0.48483
Q9UBQ5	EIF3K	0.48494
Q13162	PRDX4	0.48495
O75494	SRSF10	0.48531
Q9UG63	ABCF2	0.48545
Q9H147	DNTTIP1	0.48545
Q86UV5	USP48	0.48602
M0R2Z9	SUGP2	0.48624
Q9NW82	WDR70	0.48657
Q6P1J9	CDC73	0.48737
J3KTA4	DDX5	0.48768

Q9UKY7	CDV3	0.48813
Q9BRP8	PYM1	0.48826
Q9Y5Q9	GTF3C3	0.48878
G5E975	SMARCB1	0.48949
Q9Y3A5	SBDS	0.4896
Q99496	RNF2	0.48975
Q13951	CBFB	0.48978
P62424	RPL7A	0.48998
Q8NCF5	NFATC2IP	0.49044
Q15388	TOMM20	0.49066
P62306	SNRPF	0.49079
Q96GD4	AURKB	0.49107
P06748	NPM1	0.49108
F8W8D3	SLBP	0.49185
Q9H444	CHMP4B	0.49187
Q9BTT0	ANP32E	0.49255
Q96JP5	ZFP91	0.49284
Q9NWH9	SLTM	0.49343
P32969	RPL9, RPL9P7, RPL9P8, RPL9P9	0.49495
P29590	PML	0.49519
Q13442	PDAP1	0.49552
Q14181	POLA2	0.49591
Q9H0A0	NAT10	0.49598
Q12972	PPP1R8	0.49613
P35249	RFC4	0.49627
Q5FWF4	ZRANB3	0.4963
Q9HAV4	XPO5	0.49637
Q13426	XRCC4	0.49651
Q9HB71	CACYBP	0.49714
P15927	RPA2	0.49766
O95983	MBD3	0.49767
O00267	SUPT5H	0.49799
P62937	PPIA	0.4982
P29372	MPG	0.49829
Q6NXE6	ARMC6	0.49852
Q09028	RBBP4	0.49869
P35250	RFC2	0.49956
Q9NSI2	FAM207A	0.4996
P13489	RNH1	0.49964
Q9BZE4	GTPBP4	0.49966
Q49A26	GLYR1	0.49973
O60231	DHX16	0.49982
O00299	CLIC1	0.50055

P31689	DNAJA1	0.50093
O14964	HGS	0.50136
P30043	BLVRB	0.50158
Q9Y4X5	ARIH1	0.50176
A0A0C4DFX9	NELFA	0.50204
O00762	UBE2C	0.50204
Q9Y383	LUC7L2	0.5026
O43929	ORC4	0.50299
Q12874	SF3A3	0.50302
Q96RS6	NUDCD1	0.50339
Q5VV89	MGST3	0.50347
P62942	FKBP1A	0.50397
P34932	HSPA4	0.50416
Q8NB37	GATD1	0.50424
Q14684	RRP1B	0.50437
Q8WWY3	PRPF31	0.50498
C9JEJ2	PCYT1A	0.50545
Q8WXB4	ZNF606	0.50632
P53007	SLC25A1	0.50645
J3KNN5	DDX41	0.50649
Q86XP3	DDX42	0.50683
Q99426	TBCB	0.50684
P54727	RAD23B	0.50839
A0A024R4M0	RPS9	0.50841
P62714	PPP2CB	0.50842
Q92878	RAD50	0.50863
R4GMW8	BIVM-ERCC5	0.50864
Q00839	HNRNPU	0.50865
Q9Y2U8	LEMD3	0.50895
Q3ZCQ8	TIMM50	0.50902
O95071	UBR5	0.50906
P20585	MSH3	0.50916
Q5VUJ9	EFCAB2	0.50942
Q03701	CEBPZ	0.50974
Q8WXF1	PSPC1	0.50979
Q05048	CSTF1	0.51031
Q15021	NCAPD2	0.51037
Q01130	SRSF2	0.51046
Q13409	DYNC1I2	0.51055
Q14691	GINS1	0.51069
Q9UMY1	NOL7	0.51092
Q86UE8	TLK2	0.51172
P05455	SSB	0.51173

Q15365	PCBP1	0.51229
Q99615	DNAJC7	0.5127
C9JCC6	DRAP1	0.5131
P41091	EIF2S3	0.51313
Q8N0X7	SPART	0.51348
Q71U36	TUBA1A	0.51354
Q9NTZ6	RBM12	0.51445
E9PN81	RNASEH2C	0.51472
P50552	VASP	0.51487
Q08J23	NSUN2	0.51507
Q06330	RBPJ	0.51513
P61313	RPL15	0.51581
P62269	RPS18	0.51596
Q8WTT2	NOC3L	0.51623
P13010	XRCC5	0.51631
Q16204	CCDC6	0.5167
O75533	SF3B1	0.51703
P22087	FBL	0.51712
P36578	RPL4	0.5174
Q96JN0	LCOR	0.51742
A0A0A0MSW4	PITPNB	0.51771
O43143	DHX15	0.51887
F8VXU5	VPS29	0.51909
O75150	RNF40	0.5191
P49821	NDUFV1	0.51911
G5E9Q6	PFN2	0.51913
Q00059	TFAM	0.51949
Q9BWF3	RBM4	0.51999
Q96HA7	TONSL	0.52035
Q5TBB1	RNASEH2B	0.52077
Q9Y5J1	UTP18	0.52088
Q14683	SMC1A	0.52132
P19388	POLR2E	0.52138
O95163	ELP1	0.52158
P14550	AKR1A1	0.52161
P29401	TKT	0.52221
Q15637	SF1	0.52237
Q8IY18	SMC5	0.52311
Q8NEF9	SRFBP1	0.52329
A0A087WUB9	CTNNBL1	0.5233
P78417	GSTO1	0.52355
P19338	NCL	0.52356
Q9UQE7	SMC3	0.52399

Q8NC51	SERBP1	0.52416
O75643	SNRNP200	0.52421
P62701	RPS4X	0.52423
Q9NR30	DDX21	0.52444
P09661	SNRPA1	0.52447
P68400	CSNK2A1	0.52484
Q6PD62	CTR9	0.52509
Q99436	PSMB7	0.5251
Q4G0J3	LARP7	0.52537
P39748	FEN1	0.52595
Q12906	ILF3	0.52604
B4DUT8	CNN2	0.52638
Q13620	CUL4B	0.52639
K7ELB1	DNMT1	0.52658
Q9Y265	RUVBL1	0.52659
Q9GZS1	POLR1E	0.5266
Q9NXH9	TRMT1	0.52666
Q9NVN8	GNL3L	0.52733
Q04917	YWHAH	0.52747
P60174	TPI1	0.52757
A0A0C4DG89	DDX46	0.5276
Q07021	C1QBP	0.52775
P55265	ADAR	0.5279
Q9Y5B8	NME7	0.52817
Q29RF7	PDS5A	0.52822
Q6PCE3	PGM2L1	0.52827
P08579	SNRPB2	0.52856
O94906	PRPF6	0.52857
Q14690	PDCD11	0.53009
Q53GS9	USP39	0.53015
P23396	RPS3	0.53017
Q5JVF3	PCID2	0.53017
Q13347	EIF3I	0.53018
Q8TEQ6	GEMIN5	0.53042
Q9NQS7	INCENP	0.53092
Q9NYF8	BCLAF1	0.53112
Q13838	DDX39B	0.53159
Q14966	ZNF638	0.53211
Q3B726	TWISTNB	0.53258
Q8NEZ5	FBXO22	0.5326
Q07666	KHDRBS1	0.53261
P05141	SLC25A5	0.53263
Q5T3I0	GPATCH4	0.53317

Q96QC0	PPP1R10	0.53329
P40222	TXLNA	0.53337
O43663	PRC1	0.53349
Q09161	NCBP1	0.53384
Q8WX93	PALLD	0.53441
D6RBZ0	HNRNPAB	0.53546
Q9NR12	PDLIM7	0.53562
Q86W56	PARG	0.53564
Q9UNL2	SSR3	0.53587
A0A1W2PQ51	DDX17	0.53587
O95373	IPO7	0.5362
Q13616	CUL1	0.5363
Q16629	SRSF7	0.53655
Q13310	PABPC4	0.53662
Q8WU90	ZC3H15	0.5367
P05387	RPLP2	0.53676
Q5SSJ5	HP1BP3	0.53706
Q92499	DDX1	0.53729
O94762	RECQL5	0.53735
P78316	NOP14	0.53741
Q5T9B7	AK1	0.53761
Q6PJG6	BRAT1	0.53771
Q96CT7	CCDC124	0.5387
E9PI41	EXOSC4	0.53974
Q8WYP5	AHCTF1	0.53975
O95747	OXSR1	0.53999
Q9BY44	EIF2A	0.54003
Q8NFH3	NUP43	0.54017
Q15054	POLD3	0.54043
Q8N726	CDKN2A	0.54085
Q9BRT9	GINS4	0.54089
Q9UGI8	TES	0.5415
Q2NKX8	ERCC6L	0.542
Q9BYG3	NIFK	0.54206
Q9Y6V7	DDX49	0.54243
A6NEM2	HCFC1	0.543
Q58FF6	HSP90AB4P	0.54302
Q14980	NUMA1	0.54316
O95376	ARIH2	0.54324
Q8NE71	ABCF1	0.54377
O14818	PSMA7	0.54428
O43148	RNMT	0.54464
O75792	RNASEH2A	0.5453

P43897	TSFM	0.54534
P60953	CDC42	0.54552
Q7KZ85	SUPT6H	0.54571
O95365	ZBTB7A	0.54578
P45880	VDAC2	0.54584
Q9Y230	RUVBL2	0.5467
P11940	PABPC1	0.5472
P19447	ERCC3	0.54775
Q6UN15	FIP1L1	0.54828
O15397	IPO8	0.54833
P55795	HNRNPH2	0.54851
P49005	POLD2	0.54888
Q15019	SEPT2	0.54889
P60228	EIF3E	0.54899
P62917	RPL8	0.5491
O43390	HNRNPR	0.54956
J3QRS3	MYL12A	0.54962
A0A087WYR3	TPD52L2	0.54978
Q12888	TP53BP1	0.55002
Q9H583	HEATR1	0.55002
Q7Z406	MYH14	0.55003
O75534	CSDE1	0.55008
Q96T60	PNKP	0.55016
Q13435	SF3B2	0.55026
P09211	GSTP1	0.55041
Q9H1B7	IRF2BPL	0.55145
P62995	TRA2B	0.55146
Q14498	RBM39	0.55216
P05023	ATP1A1	0.55262
Q06265	EXOSC9	0.55275
O43818	RRP9	0.55368
Q9NUQ3	TXLNG	0.55426
Q15029	EFTUD2	0.55433
P57088	TMEM33	0.55471
O60870	KIN	0.55493
P62879	GNB2	0.55502
P46821	MAP1B	0.55502
Q06323	PSME1	0.55534
P09960	LTA4H	0.55549
E9PL17	CLP1	0.5555
B4DR61	SEC61A1	0.55552
O75131	CPNE3	0.55578
P02768	ALB	0.55602

P62140	PPP1CB	0.55603
P20618	PSMB1	0.5565
D6RAX7	COPS4	0.55672
Q6L8Q7	PDE12	0.55701
P30085	CMPK1	0.55706
Q12904	AIMP1	0.55706
P30153	PPP2R1A	0.55715
Q8TDN6	BRIX1	0.55735
P62195	PSMC5	0.5574
Q01081	U2AF1	0.5576
O43709	BUD23	0.55834
Q04837	SSBP1	0.55855
P50613	CDK7	0.55861
O60216	RAD21	0.55862
A0A0U1RQC9	TP53	0.55867
O95396	MOCS3	0.55877
O00442	RTCA	0.55881
P49321	NASP	0.55888
M0R2B7	POLD1	0.55905
Q14318	FKBP8	0.55915
O76094	SRP72	0.55961
P33992	MCM5	0.56023
P42167	TMPO	0.56025
Q5RKV6	EXOSC6	0.56026
O75151	PHF2	0.56135
P54920	NAPA	0.56144
P85037	FOXK1	0.56147
Q9BUJ2	HNRNPUL1	0.56148
Q53HL2	CDCA8	0.56201
Q15020	SART3	0.56206
P42771	CDKN2A	0.56236
P05388	RPLP0	0.56238
Q9UKM9	RALY	0.56261
O15371	EIF3D	0.56362
Q9Y508	RNF114	0.56382
P08621	SNRNP70	0.5639
Q8N3U4	STAG2	0.56477
O95573	ACSL3	0.56504
Q96ME1	FBXL18	0.56507
P50914	RPL14	0.56535
P43034	PAFAH1B1	0.56542
O15355	PPM1G	0.56547
Q9UMS4	PRPF19	0.56568

P05198	EIF2S1	0.56578
P31948	STIP1	0.5658
Q13895	BYSL	0.56593
P00338	LDHA	0.56609
P15880	RPS2	0.5663
P49589	CARS	0.5668
P52209	PGD	0.56696
Q92665	MRPS31	0.56738
P61011	SRP54	0.56774
P29474	NOS3	0.56788
P23526	AHCY	0.56795
O15264	MAPK13	0.56812
Q9HCS7	XAB2	0.56859
Q86U38	NOP9	0.56875
O75190	DNAJB6	0.56922
Q969G3	SMARCE1	0.5693
P54136	RARS	0.56941
Q86VP6	CAND1	0.56945
P55039	DRG2	0.56958
Q96KR1	ZFR	0.56994
Q13501	SQSTM1	0.57013
Q9H9Y6	POLR1B	0.57061
Q9NP79	VTA1	0.57065
Q5JTH9	RRP12	0.57068
O00151	PDLIM1	0.57107
Q96P11	NSUN5	0.57113
P12956	XRCC6	0.57127
O43747	AP1G1	0.57263
Q86U42	PABPN1	0.57289
P49736	MCM2	0.57295
Q14847	LASP1	0.57377
P28074	PSMB5	0.574
Q14247	CTTN	0.5744
Q14566	MCM6	0.57448
Q15269	PWP2	0.57481
Q9HC98	NEK6	0.57483
Q9UHD8	SEPT9	0.57506
Q9UKX7	NUP50	0.57524
Q9BRX5	GINS3	0.57528
H3BMV3	JPT2	0.57595
Q9NWV4	CZIB	0.57611
G3V5Z7	PSMA6	0.57643
E7ESC6	XPO7	0.57658

Q01167	FOXK2	0.57681
Q13247	SRSF6	0.57681
Q9Y6G9	DYNC1LI1	0.57718
Q9BXS6	NUSAP1	0.57725
Q15233	NONO	0.57766
Q9NTJ3	SMC4	0.57769
Q9Y3I0	RTCB	0.57805
E9PEB5	FUBP1	0.5783
Q8NHQ9	DDX55	0.57884
A8MXP9	MATR3	0.57968
Q9BXW9	FANCD2	0.57981
Q16576	RBBP7	0.57997
O14980	XPO1	0.58018
Q13495	MAMLD1	0.58051
Q96B26	EXOSC8	0.58051
Q9Y3Y2	CHTOP	0.58057
P04083	ANXA1	0.58108
P32519	ELF1	0.58159
B2R5W2	HNRNPC	0.58167
P12004	PCNA	0.5817
Q7LBC6	KDM3B	0.58216
C9J470	NCAPH	0.58221
Q16531	DDB1	0.58253
Q9NYL9	TMOD3	0.58271
Q2TAL8	QRICH1	0.58281
P25788	PSMA3	0.583
Q9NZL9	MAT2B	0.58302
P61289	PSME3	0.58306
Q15024	EXOSC7	0.58307
P49792	RANBP2	0.58315
O43592	XPOT	0.58322
H0Y368	DPM1	0.58326
P26373	RPL13	0.58331
Q9P2N5	RBM27	0.58332
P49790	NUP153	0.58335
Q6P1N0	CC2D1A	0.5836
Q9NVP1	DDX18	0.58368
P31930	UQCRC1	0.58374
P47914	RPL29	0.58374
P18124	RPL7	0.58387
Q9UNQ2	DIMT1	0.58389
H0Y858		0.58491
P23246	SFPQ	0.58531

Q9UHX1	PUF60	0.58554
Q99590	SCAF11	0.5863
P18846	ATF1	0.58673
G8JLB6	HNRNPH1	0.58733
B0QY89	EIF3L	0.58804
P60903	S100A10	0.58831
Q6ZRQ5	MMS22L	0.58832
Q9H972	C14orf93	0.58966
P84103	SRSF3	0.58974
E7ERS3	ZC3H18	0.59014
Q8NI36	WDR36	0.59043
Q13243	SRSF5	0.59053
O60506	SYNCRIP	0.59053
O75717	WDHD1	0.59055
O00541	PES1	0.59132
Q9BRX2	PELO	0.59194
D6REX3	SEC31A	0.59234
O60488	ACSL4	0.59289
A0A0A0MRI2	SNX6	0.59296
Q9Y4P3	TBL2	0.59304
O95801	TTC4	0.59359
P31946	YWHAB	0.59397
Q6PKG0	LARP1	0.59409
P12236	SLC25A6	0.59461
Q04446	GBE1	0.5951
P61978	HNRNPK	0.59528
Q16658	FSCN1	0.59589
P24534	EEF1B2	0.59598
Q86W42	THOC6	0.59632
Q9NRX1	PNO1	0.59645
P40763	STAT3	0.5965
Q53EL6	PDCD4	0.59659
O75694	NUP155	0.59747
Q9Y2W2	WBP11	0.5975
P20042	EIF2S2	0.59806
Q9C0J8	WDR33	0.59838
O15305	PMM2	0.59842
P68366	TUBA4A	0.59905
Q92844	TANK	0.59926
Q9BWF2	TRAIP	0.59968
Q15691	MAPRE1	0.5998
O14776	TCERG1	0.59999
E7EX17	EIF4B	0.60004

P33981	TTK	0.60008
Q92620	DHX38	0.60011
Q8IZH2	XRN1	0.60017
P62847	RPS24	0.60098
B5MCA4	EPCAM	0.60152
Q15291	RBBP5	0.60177
Q9NQW6	ANLN	0.60178
Q08752	PPID	0.60187
P39656	DDOST	0.60198
F6VRR5	POLDIP3	0.60205
K7ER00	FARSA	0.60215
K7ERV3	TK1	0.60264
O95602	POLR1A	0.60284
Q8WUA2	PPIL4	0.60295
P46776	RPL27A	0.60302
O00410	IPO5	0.60392
E9PDI4	LAD1	0.60412
Q9ULX9	MAFF	0.60421
Q13619	CUL4A	0.60435
Q14166	TTLL12	0.60437
Q08211	DHX9	0.60438
Q9UBE0	SAE1	0.60439
Q96GQ7	DDX27	0.60453
P06733	ENO1	0.60454
Q96S55	WRNIP1	0.60493
Q96EP5	DAZAP1	0.60513
Q7L9L4	MOB1B	0.60542
P21283	ATP6V1C1	0.60552
A0A024QZP7	CDK1	0.60567
F8WF69	CLTA	0.60578
Q9H8H0	NOL11	0.60632
Q5JWT2	MED23	0.60638
P26599	PTBP1	0.60712
P07814	EPRS	0.6079
A0A0C4DGB5	CAST	0.60799
P62993	GRB2	0.60817
P22102	GART	0.60844
Q9BX63	BRIP1	0.60866
P30566	ADSL	0.60884
P68104	EEF1A1	0.60938
Q8WUM4	PDCD6IP	0.6096
A0A0C4DG17	RPSA	0.60988
P53618	COPB1	0.61155

O95235	KIF20A	0.61196
A6NMQ1	POLA1	0.61203
Q96AG4	LRRC59	0.61209
Q99832	CCT7	0.61216
H7C2Q8	EBNA1BP2	0.61335
Q92621	NUP205	0.61346
P39019	RPS19	0.61347
O60437	PPL	0.6143
Q15773	MLF2	0.61566
Q68CZ2	TNS3	0.61639
O00487	PSMD14	0.61646
Q02790	FKBP4	0.61711
Q9UJW0	DCTN4	0.61716
O75794	CDC123	0.61737
Q9P2J5	LARS	0.6174
Q15813	TBCE	0.61741
Q13595	TRA2A	0.61748
P25205	MCM3	0.61754
P13639	EEF2	0.6177
Q8IX12	CCAR1	0.61771
O00139	KIF2A	0.61777
Q13098	GPS1	0.61783
O43290	SART1	0.61846
P22314	UBA1	0.61881
O14744	PRMT5	0.61889
M0QXB4	COPE	0.6199
P11142	HSPA8	0.6199
Q9NQG5	RPRD1B	0.62031
P23258	TUBG1	0.6204
Q9NW13	RBM28	0.62067
Q6P1X5	TAF2	0.62076
P48506	GCLC	0.62114
P35606	COPB2	0.62119
Q5JWF2	GNAS	0.62122
P54619	PRKAG1	0.62142
P08238	HSP90AB1	0.62161
O15160	POLR1C	0.6218
E9PAV3	NACA	0.62193
P49642	PRIM1	0.62195
P55010	EIF5	0.62217
Q15056	EIF4H	0.62229
P31153	MAT2A	0.62247
B4DUC8	MTAP	0.62298

Q6DN03	HIST2H2BC	0.62298
D6R9M0	KIF2A	0.62323
P07195	LDHB	0.6233
Q93009	USP7	0.62359
P08708	RPS17	0.62408
Q96RT1	ERBIN	0.62428
P62750	RPL23A	0.62439
O60828	PQBP1	0.62478
Q12788	TBL3	0.62518
Q04637	EIF4G1	0.62519
Q9Y6D6	ARFGEF1	0.62554
Q9NR45	NANS	0.62556
Q92804	TAF15	0.62595
Q13123	IK	0.62668
Q96T37	RBM15	0.6267
Q8NFJ5	GPRC5A	0.62675
O43242	PSMD3	0.62679
P63104	YWHAZ	0.62687
Q15717	ELAVL1	0.62693
Q13045	FLII	0.62694
P27694	RPA1	0.62699
P67809	YBX1	0.62699
A0A0G2JPQ2	NLRP2	0.62713
Q2TAY7	SMU1	0.62722
Q9HCG8	CWC22	0.62732
O14879	IFIT3	0.62751
O14929	HAT1	0.6276
Q7Z460	CLASP1	0.62803
O95171	SCEL	0.62823
Q92945	KHSRP	0.62833
Q01518	CAP1	0.62847
Q13823	GNL2	0.62854
J3KN16	ECPAS	0.62857
P00403	MT-CO2	0.62863
P49756	RBM25	0.6289
O76021	RSL1D1	0.62893
P12814	ACTN1	0.62907
P09382	LGALS1	0.62911
Q92600	CNOT9	0.62966
P53567	CEBPG	0.62996
A0A0A0MRM8	MYO6	0.63036
P56182	RRP1	0.63043
P16152	CBR1	0.63052

E7EPK1	SEPT7	0.63053
P38606	ATP6V1A	0.63067
P61626	LYZ	0.63081
Q9HCK5	AGO4	0.63105
Q9BVI4	NOC4L	0.63111
P00558	PGK1	0.63132
O00154	ACOT7	0.63147
O43396	TXNL1	0.63174
Q15428	SF3A2	0.63219
P38919	EIF4A3	0.63253
Q8TEA8	DTD1	0.63254
I3L4C2	BAIAP2	0.63272
B5ME19	EIF3CL	0.63302
Q9NWB6	ARGLU1	0.63308
F5H2F4	MTHFD1	0.63328
Q9H3S7	PTPN23	0.6335
O95757	HSPA4L	0.63371
Q8WWM7	ATXN2L	0.63373
D6RER5	SEPT11	0.63381
A0A286YEY1	IGHA1	0.6341
P22695	UQCRC2	0.6344
P51812	RPS6KA3	0.63467
Q8IY21	DDX60	0.63471
P41743	PRKCI	0.63479
Q92598	HSPH1	0.63487
O76003	GLRX3	0.63513
Q15181	PPA1	0.63561
H7BYT1	CSNK1D	0.63621
O43252	PAPSS1	0.63646
Q9NP61	ARFGAP3	0.63654
Q14807	KIF22	0.6366
Q14651	PLS1	0.63673
P61026	RAB10	0.6372
O75400	PRPF40A	0.63844
P31350	RRM2	0.63927
H7C0C1		0.63928
P28838	LAP3	0.63932
Q9BXS5	AP1M1	0.63968
Q15785	TOMM34	0.63981
P37802	TAGLN2	0.6402
P55081	MFAP1	0.64047
P21127	CDK11B	0.64081
P20248	CCNA2	0.64083

P51571	SSR4	0.64085
A3KN83	SBNO1	0.64096
A0A0G2JIW1	HSPA1B	0.64108
P55060	CSE1L	0.64118
O75153	CLUH	0.64172
O43395	PRPF3	0.64208
P25786	PSMA1	0.6422
P55263	ADK	0.64242
P33993	MCM7	0.64284
Q15050	RRS1	0.64294
Q8IU81	IRF2BP1	0.64296
P62899	RPL31	0.643
Q15366	PCBP2	0.64332
E9PRY8	EEF1D	0.6436
Q99714	HSD17B10	0.64418
Q15424	SAFB	0.64453
P07900	HSP90AA1	0.64481
Q8IY81	FTSJ3	0.64493
Q5BKZ1	ZNF326	0.64551
Q86Y91	KIF18B	0.64568
P20962	PTMS	0.64637
X6RAY8	MRPL4	0.64704
Q9BVP2	GNL3	0.64743
P53621	COPA	0.64756
Q15393	SF3B3	0.64757
Q14152	EIF3A	0.64776
P57081	WDR4	0.64834
Q9Y2Z0	SUGT1	0.64849
Q8TBC3	SHKBP1	0.64894
P41240	CSK	0.649
P61221	ABCE1	0.64903
P45974	USP5	0.6492
P33991	MCM4	0.64935
Q9Y333	LSM2	0.64976
O75436	VPS26A	0.64983
Q9HAW4	CLSPN	0.65014
A0A087WW66	PSMD1	0.65051
Q12962	TAF10	0.65074
P28331	NDUFS1	0.65131
Q5T280	SPOUT1	0.65146
Q13283	G3BP1	0.65161
O00303	EIF3F	0.65168
Q86Y56	DNAAF5	0.65171

P11177	PDHB	0.65205
Q9BQG0	MYBBP1A	0.65242
P16989	YBX3	0.65266
P17858	PFKL	0.65274
Q96GW9	MARS2	0.65291
O00425	IGF2BP3	0.65292
P15531	NME1	0.65295
Q9NVX2	NLE1	0.65296
Q92890	UFD1	0.65299
O94826	TOMM70	0.65299
Q6UXN9	WDR82	0.65362
P46060	RANGAP1	0.65371
Q03252	LMNB2	0.65406
P22234	PAICS	0.65414
P27708	CAD	0.65473
O14976	GAK	0.65489
P35611	ADD1	0.65502
Q5C9Z4	NOM1	0.65509
Q9BUI4	POLR3C	0.65536
Q12905	ILF2	0.65546
Q5T5C7	SARS	0.65569
Q9Y606	PUS1	0.65612
Q5LJA9	UCHL5	0.65643
Q15631	TSN	0.65654
P20073	ANXA7	0.65655
P50991	CCT4	0.65682
O75083	WDR1	0.65734
B5MBZ0	EML4	0.65734
Q14258	TRIM25	0.65738
P61163	ACTR1A	0.65747
J3KN67	TPM3	0.65802
Q9BXJ9	NAA15	0.65812
Q9UNM6	PSMD13	0.65886
Q96PK6	RBM14	0.65904
P49588	AARS	0.65922
Q9P287	BCCIP	0.6593
Q9UHB6	LIMA1	0.65973
Q8N5A5	ZGPAT	0.66015
P43490	NAMPT	0.66033
Q00796	SORD	0.66039
Q09666	AHNAK	0.6604
Q13111	CHAF1A	0.66042
Q7L1Q6	BZW1	0.66163

P07355	ANXA2	0.66165
Q99959	PKP2	0.66167
Q86XI2	NCAPG2	0.66194
P08243	ASNS	0.6622
P28070	PSMB4	0.66262
P12429	ANXA3	0.6634
A0A0A0MTH9	BTAF1	0.66344
P12273	PIP	0.66349
A0A1W2PNX8	UNC45A	0.66385
P12081	HARS	0.66412
Q12792	TWF1	0.66457
P09972	ALDOC	0.66495
Q9UBF2	COPG2	0.66519
B7ZM99	MTHFD1L	0.66612
D3DQV9	EIF4G2	0.66671
Q9H6Y2	WDR55	0.66672
Q9UNS2	COPS3	0.66704
P50502	ST13	0.66707
Q9Y6C9	MTCH2	0.66723
Q8NI27	THOC2	0.66735
Q9NZN8	CNOT2	0.66741
P40925	MDH1	0.66758
Q8WUM0	NUP133	0.66839
Q9H0H5	RACGAP1	0.66846
P50402	EMD	0.66849
P30520	ADSS	0.66858
Q16543	CDC37	0.66941
Q15046	KARS	0.66979
P54577	YARS	0.66999
Q13085	ACACA	0.67005
P27824	CANX	0.67025
Q9BW19	KIFC1	0.67042
F5GYJ8	OTUB1	0.6709
G3V0E4	PMPCB	0.67121
O14737	PDCD5	0.67129
Q99856	ARID3A	0.67148
Q96T51	RUFY1	0.6715
O75815	BCAR3	0.67151
P30626	SRI	0.67169
P51659	HSD17B4	0.6721
Q9Y371	SH3GLB1	0.67215
P62258	YWHAE	0.67232
P14868	DARS	0.67239

Q9UNX4	WDR3	0.67239
Q9NV31	IMP3	0.67322
P26641	EEF1G	0.67522
Q8TC12	RDH11	0.67531
Q9UBB6	NCDN	0.67562
Q9Y446	PKP3	0.67574
A0A0D9SF53	DDX3X	0.67601
P62191	PSMC1	0.67672
P48651	PTDSS1	0.67772
Q9NVI1	FANCI	0.67781
B3KS98	EIF3H	0.67785
Q16656	NRF1	0.67807
Q9Y266	NUDC	0.67814
A0A087X0X3	HNRNPM	0.67824
Q9H0D6	XRN2	0.67825
P07437	TUBB	0.67912
P63010	AP2B1	0.67925
P55072	VCP	0.67931
B0YIW6	ARCN1	0.67945
Q03001	DST	0.67956
P50990	CCT8	0.68033
O95816	BAG2	0.68061
A2A274	ACO2	0.68063
Q13155	AIMP2	0.68205
Q9Y3D9	MRPS23	0.68216
P51398	DAP3	0.68282
P67936	TPM4	0.68284
Q12769	NUP160	0.68339
Q9BUQ8	DDX23	0.68394
Q14790	CASP8	0.6841
G3V5T9	CDK2	0.68411
Q7KZF4	SND1	0.68427
P49327	FASN	0.68496
P40818	USP8	0.68511
O00170	AIP	0.6852
P26640	VARS	0.68561
J3KN66	TOR1AIP1	0.68571
Q8NFC6	BOD1L1	0.68596
Q5T4S7	UBR4	0.686
P60842	EIF4A1	0.68611
A0A0A0MTS2	GPI	0.68635
P36405	ARL3	0.68642
P50747	HLCS	0.68649

O94822	LTN1	0.68659
A0A0X1KG71		0.6866
Q8N6H7	ARFGAP2	0.68689
P53992	SEC24C	0.68693
Q9NQ29	LUC7L	0.68697
Q9BVC3	DSCC1	0.68714
F8W930	IGF2BP2	0.68719
Q15437	SEC23B	0.6877
P49368	CCT3	0.68789
O75955	FLOT1	0.68819
P02545	LMNA	0.68887
P36957	DLST	0.68904
P60510	PPP4C	0.68904
P62495	ETF1	0.68916
B5MBX0	CDCA5	0.68971
O43583	DENR	0.68974
Q9Y520	PRRC2C	0.68987
Q8TED0	UTP15	0.68988
Q14692	BMS1	0.69033
Q13112	CHAF1B	0.69061
Q9P0L0	VAPA	0.69063
M0R2C6		0.6907
Q9Y263	PLAA	0.69105
Q6DKI1	RPL7L1	0.69122
Q8IYB8	SUPV3L1	0.69125
Q14974	KPNB1	0.69129
P04075	ALDOA	0.69167
P49720	PSMB3	0.6919
A0A087WYK6	ACACA	0.69219
O43795	MYO1B	0.6922
P51608	MECP2	0.69234
B7Z596	TPM1	0.69278
P36915	GNL1	0.69312
P16615	ATP2A2	0.69338
P07737	PFN1	0.69407
Q01813	PFKP	0.6944
Q96EE3	SEH1L	0.69462
P26196	DDX6	0.6948
Q8N1G4	LRRC47	0.69515
Q99661	KIF2C	0.6952
Q9H074	PAIP1	0.69528
Q9ULV4	CORO1C	0.69558
Q12996	CSTF3	0.69595

A0A087WVQ6	CLTC	0.69602
Q9UN37	VPS4A	0.69682
P54819	AK2	0.69738
P30086	PEBP1	0.6977
E7EQR4	EZR	0.69781
O75821	EIF3G	0.6979
Q9UBU9	NXF1	0.69804
P61981	YWHAG	0.69807
M0R3H8		0.69821
P35222	CTNNB1	0.69849
Q16763	UBE2S	0.69882
Q9NV56	MRGBP	0.6989
Q86UE4	MTDH	0.69901
P48556	PSMD8	0.69913
Q9UBB4	ATXN10	0.69938
Q7L590	MCM10	0.69938
Q53GQ0	HSD17B12	0.69979
Q9C0C2	TNKS1BP1	0.6999
Q14126	DSG2	0.70009
P05109	S100A8	0.70028
P36952	SERPINB5	0.70029
O75962	TRIO	0.70076
J3KR97	TBCD	0.70093
O00231	PSMD11	0.70098
Q9BZK7	TBL1XR1	0.70136
Q96I24	FUBP3	0.70151
E7EWR4	CSTF2	0.70186
B0QZ18	CPNE1	0.70218
Q96TA1	FAM129B	0.70219
A0A1B0GW77	ALDH7A1	0.70249
P04406	GAPDH	0.70282
Q9BYT8	NLN	0.70326
Q99728	BARD1	0.70397
P30405	PPIF	0.70399
O95758	PTBP3	0.70439
E7EW49	CLASP2	0.70448
P47897	QARS	0.70528
P15170	GSPT1	0.70533
Q9Y316	MEMO1	0.70542
Q9H2U1	DHX36	0.70581
O95433	AHSA1	0.70598
Q9NR33	POLE4	0.70652
P18669	PGAM1	0.70663

P26368	U2AF2	0.70668
P57678	GEMIN4	0.70681
Q96JH7	VCPIP1	0.70699
Q9NRG9	AAAS	0.70708
Q9UQ35	SRRM2	0.70729
P52292	KPNA2	0.70791
P17931	LGALS3	0.70794
Q9BQ52	ELAC2	0.70795
P21333	FLNA	0.70815
P26639	TARS	0.70822
O43488	AKR7A2	0.70834
Q9NSE4	IARS2	0.70869
Q9Y2A7	NCKAP1	0.70961
Q14315	FLNC	0.70987
Q9NR50	EIF2B3	0.71041
P20936	RASA1	0.71053
Q92882	OSTF1	0.71061
O95347	SMC2	0.71102
C9IZQ1	SSR1	0.71121
P14625	HSP90B1	0.71127
P48643	CCT5	0.71127
Q9Y5N6	ORC6	0.7114
Q9BSJ2	TUBGCP2	0.71203
Q8IWA0	WDR75	0.71255
A0A087WUZ3	SPTBN1	0.71309
Q92552	MRPS27	0.71334
P56537	EIF6	0.71335
P57740	NUP107	0.7135
P08758	ANXA5	0.71374
O60716	CTNND1	0.71381
Q9H5H4	ZNF768	0.71413
Q8N1F7	NUP93	0.71418
P78371	CCT2	0.7144
Q969Z0	TBRG4	0.71492
A0A0A0MRE3	SYNE2	0.71516
O43707	ACTN4	0.71521
Q02750	MAP2K1	0.7153
P32119	PRDX2	0.71549
H0YFY8	DDX11	0.71594
O75691	UTP20	0.71608
O95831	AIFM1	0.71679
P52597	HNRNPF	0.71683
Q12849	GRSF1	0.7169

P20700	LMNB1	0.71744
O43237	DYNC1LI2	0.71756
Q16401	PSMD5	0.71785
G3V1L9	TJP1	0.71809
Q9Y6A5	TACC3	0.71812
O75369	FLNB	0.71887
Q99623	PHB2	0.71909
Q15149	PLEC	0.71916
A0A087X0W9	OTUD6B	0.71917
A0A024R4E5	HDLBP	0.7193
Q9Y490	TLN1	0.71943
P11802	CDK4	0.71959
Q96QK1	VPS35	0.72023
Q9Y3E7	CHMP3	0.72035
P40926	MDH2	0.72046
P35232	PHB	0.72082
Q9Y2Z4	YARS2	0.72099
B5ME97	SEPT10	0.7211
A8MWD9	SNRPGP15	0.72111
Q9BWU0	SLC4A1AP	0.72154
Q93008	USP9X	0.72178
P28066	PSMA5	0.72184
Q16881	TXNRD1	0.72224
P18031	PTPN1	0.72327
Q92616	GCN1	0.72399
Q6NXG1	ESRP1	0.72409
P12270	TPR	0.72411
J3QQX2	ARHGDIA	0.72499
P13807	GYS1	0.72508
Q9Y3F4	STRAP	0.72512
Q99541	PLIN2	0.72517
A0A087X2I1	PSMC6	0.72529
P35573	AGL	0.7253
Q14204	DYNC1H1	0.72539
Q8NCA5	FAM98A	0.72552
P49411	TUFM	0.7261
Q96KB5	PBK	0.72648
Q7Z2W4	ZC3HAV1	0.7266
Q6UWP2	DHRS11	0.72728
O14974	PPP1R12A	0.72808
Q7Z6Z7	HUWE1	0.72972
Q06830	PRDX1	0.73006
Q9Y295	DRG1	0.73044

P42704	LRPPRC	0.73063
Q92783	STAM	0.73067
Q92973	TNPO1	0.73077
Q9UJF2	RASAL2	0.7308
Q16891	IMMT	0.73145
P46087	NOP2	0.73181
P30041	PRDX6	0.73272
P46940	IQGAP1	0.73272
A0A0G2JJL1	WDR46	0.73289
Q96R06	SPAG5	0.73317
P49643	PRIM2	0.73338
H3BQK0	DDX19B	0.73379
A0A087X1N8	SERPINB6	0.73394
P40227	CCT6A	0.73411
H0Y2W2	ATAD3A	0.73444
Q9UGR2	ZC3H7B	0.73471
P50395	GDI2	0.73515
P52948	NUP98	0.73523
Q96RQ3	MCCC1	0.73533
A0A0J9YWL0	CRYBG1	0.73549
Q96PZ2	FAM111A	0.73561
P61764	STXBP1	0.73676
Q9H814	PHAX	0.73699
Q96C19	EFHD2	0.73726
A5YKK6	CNOT1	0.73727
Q9NSD9	FARSB	0.73764
P46109	CRKL	0.7379
P35221	CTNNA1	0.73804
A0A1B0GTW1	TJP2	0.73863
P49189	ALDH9A1	0.73951
P13861	PRKAR2A	0.73977
P52907	CAPZA1	0.73981
Q02878	RPL6	0.74012
Q9Y5A9	YTHDF2	0.74031
P55084	HADHB	0.7409
P04899	GNAI2	0.74121
Q6YN16	HSDL2	0.74146
Q01085	TIAL1	0.74192
P55884	EIF3B	0.742
A0A087WUT6	EIF5B	0.74218
Q9HD26	GOPC	0.74242
H3BND4	PDXDC1	0.74301
A0AVT1	UBA6	0.74317

Q13011	ECH1	0.74367
O75323	NIPSNAP2	0.74467
Q9HAU0	PLEKHA5	0.74541
Q92688	ANP32B	0.74696
Q1ED39	KNOP1	0.74787
P54886	ALDH18A1	0.74789
Q9Y2S7	POLDIP2	0.74808
Q9P2E9	RRBP1	0.74813
P10599	TXN	0.74818
Q13509	TUBB3	0.74824
P19367	HK1	0.74862
P08574	CYC1	0.74921
Q9BX40	LSM14B	0.74935
Q13813	SPTAN1	0.74986
Q7L576	CYFIP1	0.74988
Q93052	LPP	0.75018
Q9UHB9	SRP68	0.75098
J3KR12		0.751
Q13131	PRKAA1	0.75124
O15269	SPTLC1	0.75213
P17987	TCP1	0.75346
P00367	GLUD1	0.75378
P55209	NAP1L1	0.75415
A0A1W2PQ47	FDFT1	0.75421
P58546	MTPN	0.75426
Q9BV38	WDR18	0.75475
E7EVA0	MAP4	0.75594
Q8TCS8	PNPT1	0.75602
P30101	PDIA3	0.75614
Q9H2M9	RAB3GAP2	0.75616
O43264	ZW10	0.75676
Q9NYP7	ELOVL5	0.75699
P62304	SNRPE	0.75748
Q6KC79	NIPBL	0.75767
Q9UKI2	CDC42EP3	0.75776
B1AK88	CAPZB	0.75798
Q8N163	CCAR2	0.75911
Q9BW92	TARS2	0.75935
Q9BR76	CORO1B	0.75999
Q9UN86	G3BP2	0.76033
Q9UJU6	DBNL	0.76045
P17980	PSMC3	0.76178
Q12965	MYO1E	0.76197

Q9BQ39	DDX50	0.76213
Q13554	CAMK2B	0.76229
A0A087WXI5	CDH1	0.7623
Q99459	CDC5L	0.76242
P06396	GSN	0.76294
P38432	COIL	0.76307
Q3KQU3	MAP7D1	0.76365
H0UI80	NELFCD	0.76371
P51148	RAB5C	0.76375
P02786	TFRC	0.76395
Q9NY93	DDX56	0.7643
Q13200	PSMD2	0.76436
P10768	ESD	0.7657
P42224	STAT1	0.76586
Q8TDD1	DDX54	0.76597
P13804	ETFA	0.76656
P47755	CAPZA2	0.76741
Q92575	UBXN4	0.76754
Q96T76	MMS19	0.76756
E7EMK3	FLOT2	0.76784
Q8WVM8	SCFD1	0.76826
Q9H6S3	EPS8L2	0.7683
Q14008	CKAP5	0.76849
Q8TEX9	IPO4	0.76896
C9JFV4	PELP1	0.7697
P11216	PYGB	0.7698
Q10570	CPSF1	0.76997
Q06203	PPAT	0.77026
A0A0G2JH68	DIAPH1	0.77047
Q9P270	SLAIN2	0.77067
Q9BVW5	TIPIN	0.77074
Q9H7B2	RPF2	0.77108
Q9UHD2	TBK1	0.77228
Q9HCC0	MCCC2	0.77244
Q8WXA9	SREK1	0.77266
P36776	LONP1	0.77305
A0A0A0MTL5	SKP2	0.7731
P07741	APRT	0.77381
Q9H9A6	LRRC40	0.77401
Q9BUL8	PDCD10	0.77462
A0A0G2JK23	BAG6	0.77552
P35579	MYH9	0.77576
O95793	STAU1	0.77582

P04350	TUBB4A	0.77762
P50995	ANXA11	0.77801
Q14137	BOP1	0.7784
P35241	RDX	0.77865
Q14738	PPP2R5D	0.77968
O43913	ORC5	0.78067
A0A140T930	HLA-C	0.78174
Q6ZRV2	FAM83H	0.78185
F5H5D3	TUBA1C	0.78203
E9PDR0	PCCB	0.78267
Q9Y678	COPG1	0.78358
P28072	PSMB6	0.78374
O60502	OGA	0.78418
P52306	RAP1GDS1	0.78449
P49406	MRPL19	0.78477
P17655	CAPN2	0.78479
A0A0A0MS08	IGHG1	0.78509
P55809	OXCT1	0.78535
O14745	SLC9A3R1	0.78608
O43175	PHGDH	0.78622
Q14444	CAPRIN1	0.78637
Q13206	DDX10	0.78761
P55786	NPEPPS	0.79052
Q13724	MOGS	0.79072
Q9Y512	SAMM50	0.79142
P10809	HSPD1	0.79154
Q15459	SF3A1	0.79223
Q16610	ECM1	0.7923
P36543	ATP6V1E1	0.79256
Q7L2E3	DHX30	0.7928
P04844	RPN2	0.79333
Q8TEM1	NUP210	0.79364
Q9Y2X7	GIT1	0.79415
P24752	ACAT1	0.79421
Q9NXF1	TEX10	0.79443
P38646	HSPA9	0.79506
Q6P2E9	EDC4	0.79616
Q9P035	HACD3	0.79757
B7Z6Z4	MYL6	0.79758
Q14694	USP10	0.79979
Q9Y2P8	RCL1	0.79986
P35580	MYH10	0.80077
O00232	PSMD12	0.80119

Q9Y5X1	SNX9	0.80126
Q9UHI6	DDX20	0.80136
P14618	PKM	0.80153
P50750	CDK9	0.80157
Q15907	RAB11B	0.8018
Q9UNS1	TIMELESS	0.80355
O43291	SPINT2	0.80363
Q13423	NNT	0.80399
Q96A65	EXOC4	0.80432
P41252	IARS	0.80485
P31949	S100A11	0.80572
P00505	GOT2	0.80623
P10515	DLAT	0.80637
Q9UJS0	SLC25A13	0.80675
P50570	DNM2	0.80705
P49748	ACADVL	0.80786
Q69YN2	CWF19L1	0.81023
Q9BTT6	LRRC1	0.81155
C9JJ19	MRPS34	0.81197
Q86YZ3	HRNR	0.81242
Q96KP4	CNDP2	0.8127
P12277	CKB	0.81413
P05165	PCCA	0.81429
P11498	PC	0.81465
Q14146	URB2	0.81517
Q99567	NUP88	0.81695
A0A087X117	NOMO1	0.81735
P50213	IDH3A	0.81847
P11021	HSPA5	0.81864
O95292	VAPB	0.82035
P33176	KIF5B	0.82054
O00159	MYO1C	0.8213
Q92797	SYMPK	0.82142
O94874	UFL1	0.82255
P48634	PRRC2A	0.82257
Q9NZI8	IGF2BP1	0.82276
Q96S59	RANBP9	0.82506
P45984	MAPK9	0.82542
Q16186	ADRM1	0.8257
P43686	PSMC4	0.82572
P18206	VCL	0.82679
P31939	ATIC	0.82696
P51114	FXR1	0.82752

O60763	USO1	0.82767
Q14240	EIF4A2	0.82778
P09525	ANXA4	0.83053
B7ZC38	SH3GLB2	0.83148
P08237	PFKM	0.8318
Q05519	SRSF11	0.83214
Q9NZB2	FAM120A	0.83218
F8WAR4	CHCHD3	0.83273
Q5TH30	NDRG3	0.83282
P15090	FABP4	0.83296
O00203	AP3B1	0.83441
P14324	FDPS	0.8345
O96013	PAK4	0.83567
P14635	CCNB1	0.83607
Q06210	GFPT1	0.83641
Q9NVV4	MTPAP	0.83861
Q12931	TRAP1	0.84011
Q9UN81	L1RE1	0.8405
Q92817	EVPL	0.84137
Q96KP1	EXOC2	0.84427
P49721	PSMB2	0.84649
Q9GZR7	DDX24	0.84676
Q8N6T3	ARFGAP1	0.84795
Q13439	GOLGA4	0.84879
J3KQ32	OLA1	0.84981
Q9NUQ8	ABCF3	0.85081
P52294	KPNA1	0.85089
A6NFX8	NUDT5	0.85146
P51149	RAB7A	0.85147
Q53RT3	ASPRV1	0.85189
Q9NUQ9	FAM49B	0.85274
Q9H6T3	RPAP3	0.85392
O00273	DFFA	0.85514
Q9Y2D5	AKAP2	0.85558
C9JIF9	APEH	0.85587
Q9Y5K6	CD2AP	0.85642
P07384	CAPN1	0.85815
O75390	CS	0.85852
Q9UHB7	AFF4	0.85913
P05091	ALDH2	0.85951
Q92900	UPF1	0.86019
P62820	RAB1A	0.8605
Q5JXB2	UBE2NL	0.86124

B8ZZA8	GLS	0.86316
P25705	ATP5F1A	0.8632
Q5T6F2	UBAP2	0.8658
P41250	GARS	0.86653
P04792	HSPB1	0.86716
Q10567	AP1B1	0.86841
P25787	PSMA2	0.86953
P09622	DLD	0.87041
O76031	CLPX	0.87085
I1E4Y6	GIGYF2	0.87111
A0A087WYC6	DNAH11	0.87269
A0A087X211	CIP2A	0.8727
O15198	SMAD9	0.87335
Q96HC4	PDLIM5	0.87366
Q27J81	INF2	0.87404
P07237	P4HB	0.87538
A0A0A0MTH3	ILK	0.87559
Q13492	PICALM	0.87572
P16949	STMN1	0.87598
P08670	VIM	0.87709
P07954	FH	0.87867
P30084	ECHS1	0.87876
Q8IVT2	MISP	0.87908
Q9NS87	KIF15	0.87954
A0A087WWU8	TPM3	0.87998
Q14914	PTGR1	0.88002
Q8WUF5	PPP1R13L	0.88056
P50454	SERPINH1	0.88171
P14735	IDE	0.88182
Q05639	EEF1A2	0.88264
O00429	DNM1L	0.88298
P52788	SMS	0.88404
P08047	SP1	0.88526
P30419	NMT1	0.88534
P68371	TUBB4B	0.88567
O15381	NVL	0.88609
Q9Y6D9	MAD1L1	0.88633
P06703	S100A6	0.88724
A0A0D9SFE4	DNM1	0.89033
Q15833	STXBP2	0.89046
O75179	ANKRD17	0.89165
P08754	GNAI3	0.89203

Q96CW5	TUBGCP3	0.89545
P12268	IMPDH2	0.89584
P20839	IMPDH1	0.89704
Q96N67	DOCK7	0.89749
P61604	HSPE1	0.8976
P34897	SHMT2	0.90005
Q9NYY8	FASTKD2	0.90215
P56192	MARS	0.90257
Q14203	DCTN1	0.90351
P00491	PNP	0.90596
P31040	SDHA	0.90681
Q96EY1	DNAJA3	0.90842
Q8NBF2	NHLRC2	0.90866
O60701	UGDH	0.90878
Q9Y2R4	DDX52	0.90898
Q15427	SF3B4	0.90949
O75396	SEC22B	0.90983
O60664	PLIN3	0.90995
P31947	SFN	0.91273
Q9UJZ1	STOML2	0.91353
Q71RC2	LARP4	0.91526
P10644	PRKAR1A	0.9172
Q9BSJ8	ESYT1	0.92488
O95782	AP2A1	0.92885
O94925	GLS	0.92885
P23381	WARS	0.92966
Q16822	PCK2	0.9297
O14617	AP3D1	0.93014
F5GY05	FAM120B	0.93014
Q9Y6E2	BZW2	0.93337
Q96EY7	PTCD3	0.9336
P53396	ACLY	0.93373
Q96RP9	GFM1	0.93557
Q14764	MVP	0.93854
P52732	KIF11	0.93943
P29508	SERPINB3	0.94096
P68402	PAFAH1B2	0.94156
Q9Y5L0	TNPO3	0.94231
P30048	PRDX3	0.94507
Q99497	PARK7	0.94509
A0A087WYN9	DHX29	0.94628
O00567	NOP56	0.94848
H0Y2S9	MPRIP	0.94901

Q96MG7	NSMCE3	0.94935
Q9BUF5	TUBB6	0.951
P35998	PSMC2	0.95489
P11413	G6PD	0.95598
P06576	ATP5F1B	0.95672
P04181	OAT	0.95776
Q9H223	EHD4	0.9579
J3KNL6		0.9593
P08123	COL1A2	0.96697
Q9Y6E0	STK24	0.96747
Q9UGP8	SEC63	0.96997
H7C2N1	PTMA	0.97178
Q8NHV4	NEDD1	0.97429
Q0VDF9	HSPA14	0.97714
O95104	SCAF4	0.97744
O60271	SPAG9	0.98086
O94842	TOX4	0.98155
O75312	ZPR1	0.98208
E7EMB3	CALM2	0.98477
Q9UKE5	TNIK	0.98734
P18583	SON	0.99126
H0Y704	ZNF185	0.99545
Q07864	POLE	0.99636
Q9Y4C2	TCAF1	0.99688
P53367	ARFIP1	0.99728
A0A087WY31	YTHDF3	0.99996
Q9H0E2	TOLLIP	1.00477
O00763	ACACB	1.00505
F8VVA7	COPZ1	1.00626
Q8WVV4	POF1B	1.00947
P40121	CAPG	1.0179
Q96P63	SERPINB12	1.01936
Q14157	UBAP2L	1.02437
Q86TI2	DPP9	1.03027
Q04206	RELA	1.03554
P26038	MSN	1.03612
Q9NYZ3	GTSE1	1.04683
P54578	USP14	1.04693
P58107	EPPK1	1.04961
Q08379	GOLGA2	1.0659
Q8IV08	PLD3	1.06813
Q9Y4R8	TELO2	1.07126
P12955	PEPD	1.0735

E7EXA6	CHTF18	1.07848
Q14789	GOLGB1	1.08053
H7BZJ3	PDIA3	1.08385
O95817	BAG3	1.08444
P56282	POLE2	1.0893
Q13561	DCTN2	1.09019
Q13885	TUBB2A	1.09106
Q5UIP0	RIF1	1.09582
Q9P2R7	SUCLA2	1.0959
P81605	DCD	1.09948
O94992	HEXIM1	1.10063
P22735	TGM1	1.10394
Q15102	PAFAH1B3	1.11214
Q6PGP7	TTC37	1.11486
Q9UJX2	CDC23	1.11799
A3KMH1	VWA8	1.11855
P42695	NCAPD3	1.12297
P15924	DSP	1.13511
Q5T750	XP32	1.13952
Q16512	PKN1	1.13996
P43304	GPD2	1.1423
O75431	MTX2	1.14982
P21359	NF1	1.15368
Q16698	DECR1	1.15411
Q9BPX3	NCAPG	1.15573
Q969F9	HPS3	1.16533
Q15645	TRIP13	1.16584
Q9H8V3	ECT2	1.19224
Q9NVE4	CCDC87	1.19973
P01040	CSTA	1.20124
Q9P0K7	RAI14	1.20664
P50452	SERPINB8	1.21631
Q6NZI2	CAVIN1	1.21896
Q13425	SNTB2	1.22062
Q6PI48	DARS2	1.23943
Q13835	PKP1	1.25277
Q6ZVX7	NCCRP1	1.25554
Q9H845	ACAD9	1.27709
E9PCR7	OGDH	1.29192
Q92990	GLMN	1.31711
Q5T9A4	ATAD3B	1.32414
Q08188	TGM3	1.34643
P14923	JUP	1.34769

P04040	CAT	1.3577
Q03164	KMT2A	1.36055
P22528	SPRR1B	1.37138
Q9BTV4	TMEM43	1.37216
Q96QA5	GSDMA	1.37468
U3KQ56	GRHPR	1.38145
Q8NEX9	SDR9C7	1.39617
A0A0C4DGQ5	CAPNS1	1.40812
Q92820	GGH	1.4127
P56945	BCAR1	1.41326
Q86TJ2	TADA2B	1.42027
Q96B97	SH3KBP1	1.42362
E9PHI4	SUN1	1.42562
Q6DD87	ZNF787	1.43374
Q02487	DSC2	1.44128
Q9Y450	HBS1L	1.4417
Q13867	BLMH	1.44265
O00629	KPNA4	1.48552
Q16513	PKN2	1.50178
P27348	YWHAQ	1.51527
P09543	CNP	1.52147
Q15582	TGFBI	1.52813
Q8WWH5	TRUB1	1.53859
P31944	CASP14	1.54092
Q10713	PMPCA	1.5878
P05089	ARG1	1.60539
P04843	RPN1	1.62511
Q7Z2T5	TRMT1L	1.63344
O00411	POLRMT	1.65471
Q6P2H3	CEP85	1.6719
A0A0G2JQH2	RPS18	1.67266
P07339	CTSD	1.70979
B1ALK7	ARHGEF7	1.77791
P22059	OSBP	1.7788
O75223	GGCT	1.79836
G8JLG2	CDSN	1.80161
Q9HCY8	S100A14	1.80196
Q5T749	KPRP	1.80791
Q86UP2	KTN1	1.84519
P25311	AZGP1	1.84868
Q9Y617	PSAT1	1.85813
P32322	PYCR1	1.90186
A0A087WVW4	TGM5	1.99336

Q08554	DSC1	2.0059
Q9BVJ6	UTP14A	2.00999
Q05655	PRKCD	2.06696
Q5D862	FLG2	2.07647
Q6UWP8	SBSN	2.19696
Q14C86	GAPVD1	2.20584
Q02413	DSG1	2.31844
Q14574	DSC3	2.53489
Q99570	PIK3R4	2.75177
Q7Z434	MAVS	2.85817
P40939	HADHA	2.90327
Q9P0M6	H2AFY2	2.90725
P20930	FLG	3.27537
Q9UI42	CPA4	3.38758
A0A140TA62	LOC100653049	4.38558
Q9BZF1	OSBPL8	4.56967
Q01469	FABP5	5.11715
Q9NZT1	CALML5	10.8538

BIBLIOGRAPHY

Aramayo, R.J., Willhoft, O., Ayala, R., Bythell-Douglas, R., Wigley, D.B., and Zhang, X. (2018). Cryo-EM structures of the human INO80 chromatin-remodeling complex. Nature structural & molecular biology 25, 37-44.

Assimon, V.A., Tang, Y., Vargas, J.D., Lee, G.J., Wu, Z.Y., Lou, K., Yao, B., Menon, M.K., Pios, A., Perez, K.C., et al. (2019). CB-6644 Is a Selective Inhibitor of the RUVBL1/2 Complex with Anticancer Activity. ACS chemical biology.

Aza-Blanc, P., Cooper, C.L., Wagner, K., Batalov, S., Deveraux, Q.L., and Cooke, M.P. (2003). Identification of modulators of TRAIL-induced apoptosis via RNAi-based phenotypic screening. Molecular cell 12, 627-637.

Bae, S.H., Bae, K.H., Kim, J.A., and Seo, Y.S. (2001). RPA governs endonuclease switching during processing of Okazaki fragments in eukaryotes. Nature 412, 456-461.

Baker, S., Dahele, M., Lagerwaard, F.J., and Senan, S. (2016). A critical review of recent developments in radiotherapy for non-small cell lung cancer. Radiation oncology (London, England) 11, 115.

Barbie, D.A., Tamayo, P., Boehm, J.S., Kim, S.Y., Moody, S.E., Dunn, I.F., Schinzel, A.C., Sandy, P., Meylan, E., Scholl, C., et al. (2009). Systematic RNA interference reveals that oncogenic KRAS-driven cancers require TBK1. Nature 462, 108-112.

Baskar, R., Lee, K.A., Yeo, R., and Yeoh, K.W. (2012). Cancer and radiation therapy: current advances and future directions. International journal of medical sciences 9, 193-199.

Bauer, A., Chauvet, S., Huber, O., Usseglio, F., Rothbacher, U., Aragnol, D., Kemler, R., and Pradel, J. (2000). Pontin52 and reptin52 function as antagonistic regulators of beta-catenin signalling activity. The EMBO journal 19, 6121-6130.

Bauer, M.R., Jones, R.N., Baud, M.G., Wilcken, R., Boeckler, F.M., Fersht, A.R., Joerger, A.C., and Spencer, J. (2016). Harnessing Fluorine-Sulfur Contacts and Multipolar Interactions for the Design of p53 Mutant Y220C Rescue Drugs. ACS chemical biology 11, 2265-2274.

Bell, S.P., and Dutta, A. (2002). DNA replication in eukaryotic cells. Annual review of biochemistry 71, 333-374.

Bhargava, R., Onyango, D.O., and Stark, J.M. (2016). Regulation of Single-Strand Annealing and its Role in Genome Maintenance. Trends in genetics : TIG 32, 566-575.

Bizarro, J., Dodre, M., Huttin, A., Charpentier, B., Schlotter, F., Branlant, C., Verheggen, C., Massenet, S., and Bertrand, E. (2015). NUFIP and the HSP90/R2TP chaperone bind the SMN complex and facilitate assembly of U4-specific proteins. Nucleic acids research 43, 8973-8989.

Boulon, S., Marmier-Gourrier, N., Pradet-Balade, B., Wurth, L., Verheggen, C., Jady, B.E., Rothe, B., Pescia, C., Robert, M.C., Kiss, T., et al. (2008). The Hsp90 chaperone

controls the biogenesis of L7Ae RNPs through conserved machinery. The Journal of cell biology 180, 579-595.

Boulon, S., Pradet-Balade, B., Verheggen, C., Molle, D., Boireau, S., Georgieva, M., Azzag, K., Robert, M.C., Ahmad, Y., Neel, H., et al. (2010). HSP90 and its R2TP/Prefoldin-like cochaperone are involved in the cytoplasmic assembly of RNA polymerase II. Molecular cell 39, 912-924.

Breig, O., Bras, S., Martinez Soria, N., Osman, D., Heidenreich, O., Haenlin, M., and Waltzer, L. (2014). Pontin is a critical regulator for AML1-ETO-induced leukemia. Leukemia 28, 1271-1279.

Buehler, E., Chen, Y.C., and Martin, S. (2012). C911: A bench-level control for sequence specific siRNA off-target effects. PloS one 7, e51942.

Buttitta, L.A., and Edgar, B.A. (2007). Mechanisms controlling cell cycle exit upon terminal differentiation. Current opinion in cell biology 19, 697-704.

Caldecott, K.W. (2008). Single-strand break repair and genetic disease. Nature reviews Genetics 9, 619-631.

Castedo, M., Perfettini, J.L., Roumier, T., Andreau, K., Medema, R., and Kroemer, G. (2004). Cell death by mitotic catastrophe: a molecular definition. Oncogene 23, 2825-2837.

Centenera, M.M., Raj, G.V., Knudsen, K.E., Tilley, W.D., and Butler, L.M. (2013). Ex vivo culture of human prostate tissue and drug development. Nature reviews Urology 10, 483-487.

Chapman, P.B., Hauschild, A., Robert, C., Haanen, J.B., Ascierto, P., Larkin, J., Dummer, R., Garbe, C., Testori, A., Maio, M., et al. (2011). Improved survival with vemurafenib in melanoma with BRAF V600E mutation. The New England journal of medicine 364, 2507-2516.

Chaudhry, M.A. (2007). Base excision repair of ionizing radiation-induced DNA damage in G1 and G2 cell cycle phases. Cancer cell international 7, 15.

Chen, H.H.W., and Kuo, M.T. (2017). Improving radiotherapy in cancer treatment: Promises and challenges. Oncotarget 8, 62742-62758.

Cheung, K.L., Huen, J., Kakihara, Y., Houry, W.A., and Ortega, J. (2010). Alternative oligomeric states of the yeast Rvb1/Rvb2 complex induced by histidine tags. Journal of molecular biology 404, 478-492.

Chi, A., Liao, Z., Nguyen, N.P., Xu, J., Stea, B., and Komaki, R. (2010). Systemic review of the patterns of failure following stereotactic body radiation therapy in early-stage non-small-cell lung cancer: clinical implications. Radiotherapy and oncology : journal of the European Society for Therapeutic Radiology and Oncology 94, 1-11.

Chilkova, O., Stenlund, P., Isoz, I., Stith, C.M., Grabowski, P., Lundstrom, E.B., Burgers, P.M., and Johansson, E. (2007). The eukaryotic leading and lagging strand DNA polymerases are loaded onto primer-ends via separate mechanisms but have comparable processivity in the presence of PCNA. Nucleic acids research 35, 6588-6597.

Ciccia, A., and Elledge, S.J. (2010). The DNA damage response: making it safe to play with knives. Molecular cell 40, 179-204.

Cloutier, P., Poitras, C., Durand, M., Hekmat, O., Fiola-Masson, E., Bouchard, A., Faubert, D., Chabot, B., and Coulombe, B. (2017). R2TP/Prefoldin-like component RUVBL1/RUVBL2 directly interacts with ZNHIT2 to regulate assembly of U5 small nuclear ribonucleoprotein. Nature communications 8, 15615.

Cohen, M.H., Hirschfeld, S., Flamm Honig, S., Ibrahim, A., Johnson, J.R., O'Leary, J.J., White, R.M., Williams, G.A., and Pazdur, R. (2001). Drug approval summaries: arsenic trioxide, tamoxifen citrate, anastrazole, paclitaxel, bexarotene. The oncologist 6, 4-11.

Cohen, M.H., Johnson, J.R., Chen, Y.F., Sridhara, R., and Pazdur, R. (2005). FDA drug approval summary: erlotinib (Tarceva) tablets. The oncologist 10, 461-466.

Collisson EA, C.J., Brooks AN, Berger AH, Lee W, Chmielecki J, Beer DG, Cope L, Creighton CJ, Danilova L, Ding L, Getz G, Hammerman PS, Hayes DN, Hernandez B, Herman JG, Heymach JV, Jurisica I, Kucherlapati R, Kwiatkowski D, Ladanyi M, Robertson G, Schultz N, Shen R, Sinha R, Sougnez C, Tsao MS, Travis WD, Weinstein JN, Wigle DA, Wilkerson MD, Chu A, Cherniack AD, Hadjipanayis A, Rosenberg M, Weisenberger DJ, Laird PW, Radenbaugh A, Ma S, Stuart JM, Averett Byers L, Baylin SB, Govindan R, Meyerson M, Rosenberg M, Gabriel SB, Cibulskis K, Sougnez C, Kim J, Stewart C, Lichtenstein L, Lander ES, Lawrence MS, Getz, Kandoth C, Fulton R, Fulton LL, McLellan MD, Wilson RK, Ye K, Fronick CC, Maher CA, Miller CA, Wendl MC, Cabanski C, Ding L, Mardis E, Govindan R, Creighton CJ, Wheeler D, Balasundaram M, Butterfield YS, Carlsen R, Chu A, Chuah E, Dhalla N, Guin R, Hirst C, Lee D, Li HI, Mayo M, Moore RA, Mungall AJ, Schein JE, Sipahimalani P, Tam A, Varhol R, Robertson A, Wye N, Thiessen N, Holt RA, Jones SJ, Marra MA, Campbell JD, Brooks AN, Chmielecki J, Imielinski M, Onofrio RC, Hodis E, Zack T, Sougnez C, Helman E, Sekhar Pedamallu C, Mesirov J, Cherniack AD, Saksena G, Schumacher SE, Carter SL, Hernandez B, Garraway L, Beroukhim R, Gabriel SB, Getz G, Meyerson M, Hadjipanayis A, Lee S, Mahadeshwar HS, Pantazi A, Protopopov A, Ren X, Seth S, Song X, Tang J, Yang L, Zhang J, Chen PC, Parfenov M, Wei Xu A, Santoso N, Chin L, Park PJ, Kucherlapati R, Hoadley KA, Auman JT, Meng S, Shi Y, Buda E, Waring S, Veluvolu U, Tan D, Mieczkowski PA, Jones CD, Simons JV, Soloway MG, Bodenheimer T, Jefferys SR, Roach J, Hoyle AP, Wu J, Balu S, Singh D, Prins JF, Marron JS, Parker JS, Hayes DN, Perou CM, Liu J, Cope L, Danilova L, Weisenberger DJ, Maglinte DT, Lai PH, Bootwalla MS, Van Den Berg DJ, Triche T Jr, Baylin SB, Laird PW, Rosenberg M, Chin L, Zhang J, Cho J, DiCara D, Heiman D, Lin P, Mallard W, Voet D, Zhang H, Zou L, Noble MS, Lawrence MS, Saksena G, Gehlenborg N, Thorvaldsdottir H, Mesirov J, Nazaire MD, Robinson J, Getz G, Lee W, Aksoy BA, Ciriello G, Taylor BS, Dresdner G, Gao J, Gross B, Seshan VE, Ladanyi M, Reva B, Sinha R, Sumer SO, Weinhold N, Schultz N, Shen R, Sander C, Ng S, Ma S, Zhu J, Radenbaugh A, Stuart JM, Benz CC, Yau C, Haussler D, Spellman PT, Wilkerson MD, Parker JS, Hoadley KA, Kimes PK, Hayes DN, Perou CM, Broom BM, Wang J, Lu Y, Kwok Shing Ng P, Diao L, Averett Byers L, Liu W, Heymach JV, Amos CI, Weinstein JN, Akbani R, Mills GB, Curley E, Paulauskis J, Lau K, Morris S, Shelton T, Mallery D, Gardner J, Penny R, Saller C, Tarvin K, Richards WG, Cerfolio R, Bryant A, Raymond DP, Pennell NA, Farver C, Czerwinski C, Huelsenbeck-Dill L, Iacocca M, Petrelli N, Rabeno B, Brown J, Bauer T,

Dolzhanskiy O, Potapova O, Rotin D, Voronina O, Nemirovich-Danchenko E, Fedosenko KV, Gal A, Behera M, Ramalingam SS, Sica G, Flieder D, Boyd J, Weaver J, Kohl B, Huy Quoc Thinh D, Sandusky G, Juhl H, Duhig E, Illei P, Gabrielson E, Shin J, Lee B, Rodgers K, Trusty D, Brock MV, Williamson C, Burks E, Rieger-Christ K, Holway A, Sullivan T, Wigle DA, Asiedu MK, Kosari F, Travis WD, Rekhtman N, Zakowski M, Rusch VW, Zippile P, Suh J, Pass H, Goparaju C, Owusu-Sarpong Y, Bartlett JM, Kodeeswaran S, Parfitt J, Sekhon H, Albert M, Eckman J, Myers JB, Cheney R, Morrison C, Gaudioso C, Borgia JA, Bonomi P, Pool M, Liptay MJ, Moiseenko F, Zaytseva I, Dienemann H, Meister M, Schnabel PA, Muley TR, Peifer M, Gomez-Fernandez C, Herbert L, Egea S, Huang M, Thorne LB, Boice L, Hill Salazar A, Funkhouser WK, Rathmell WK, Dhir R, Yousem SA, Dacic S, Schneider F, Siegfried JM, Hajek R, Watson MA, McDonald S, Meyers B, Clarke B, Yang IA, Fong KM, Hunter L, Windsor M, Bowman RV, Peters S, Letovanec I, Khan KZ, Jensen MA, Snyder EE, Srinivasan D, Kahn AB, Baboud J, Pot DA, Mills Shaw KR, Sheth M, Davidsen T, Demchok JA, Yang L, Wang Z, Tarnuzzer R, Zenklusen JC, Ozenberger BA, Sofia HJ, Travis WD, Cheney R, Clarke B, Dacic S, Duhig E, Funkhouser WK, Illei P, Farver C, Rekhtman N, Sica G, Suh J, Tsao MS, Travis WD, Cheney R, Clarke B, Dacic S, Duhig E, Funkhouser WK, Illei P, Farver C, Rekhtman N, Sica G, Suh J, Tsao MS. (2014). Comprehensive molecular profiling of lung adenocarcinoma. Nature 511, 543-550.

Conaway, R.C., and Conaway, J.W. (2009). The INO80 chromatin remodeling complex in transcription, replication and repair. Trends in biochemical sciences 34, 71-77.

Craig, R., and Beavis, R.C. (2004). TANDEM: matching proteins with tandem mass spectra. Bioinformatics (Oxford, England) 20, 1466-1467.

Dong, S., Han, J., Chen, H., Liu, T., Huen, M.S.Y., Yang, Y., Guo, C., and Huang, J. (2014). The human SRCAP chromatin remodeling complex promotes DNA-end resection. Current biology : CB 24, 2097-2110.

Ducat, D., Kawaguchi, S., Liu, H., Yates, J.R., 3rd, and Zheng, Y. (2008). Regulation of microtubule assembly and organization in mitosis by the AAA+ ATPase Pontin. Molecular biology of the cell 19, 3097-3110.

Dungrawala, H., Rose, K.L., Bhat, K.P., Mohni, K.N., Glick, G.G., Couch, F.B., and Cortez, D. (2015). The Replication Checkpoint Prevents Two Types of Fork Collapse without Regulating Replisome Stability. Molecular cell 59, 998-1010.

Ebisawa, M., Suzuki, T., Haginoya, N., Hamada, T., Murata, T., Uoto, K., Murakami, R., and Takata, T. (2017). Aminopyrazolone derivative (U.S. Patent Application No. 15/117,701).

Elias, J.E., and Gygi, S.P. (2007). Target-decoy search strategy for increased confidence in large-scale protein identifications by mass spectrometry. Nature methods 4, 207-214.

Fan, W., Xie, J., Xia, J., Zhang, Y., Yang, M., Wang, H., Pan, Y., Zhang, M., Han, B., Wu, B., et al. (2017). RUVBL1-ITFG1 interaction is required for collective invasion in breast cancer. Biochimica et biophysica acta 1861, 1788-1800.

Fedorov, Y., Anderson, E.M., Birmingham, A., Reynolds, A., Karpilow, J., Robinson, K., Leake, D., Marshall, W.S., and Khvorova, A. (2006). Off-target effects by siRNA can induce toxic phenotype. RNA (New York, NY) 12, 1188-1196.

Feng, Y., Tian, Y., Wu, Z., and Xu, Y. (2018). Cryo-EM structure of human SRCAP complex. Cell research 28, 1121-1123.

Fire, A., Xu, S., Montgomery, M.K., Kostas, S.A., Driver, S.E., and Mello, C.C. (1998). Potent and specific genetic interference by double-stranded RNA in Caenorhabditis elegans. Nature 391, 806-811.

Flavin, P., Redmond, A., McBryan, J., Cocchiglia, S., Tibbitts, P., Fahy-Browne, P., Kay, E., Treumann, A., Perrem, K., McIlroy, M., et al. (2011). RuvBl2 cooperates with Ets2 to transcriptionally regulate hTERT in colon cancer. FEBS letters 585, 2537-2544.

Fragkos, M., Ganier, O., Coulombe, P., and Mechali, M. (2015). DNA replication origin activation in space and time. Nature reviews Molecular cell biology 16, 360-374.

Fu, J., Hagan, I.M., and Glover, D.M. (2015). The centrosome and its duplication cycle. Cold Spring Harbor perspectives in biology 7, a015800.

Fukui, K. (2010). DNA mismatch repair in eukaryotes and bacteria. Journal of nucleic acids 2010.

Gartner, W., Rossbacher, J., Zierhut, B., Daneva, T., Base, W., Weissel, M., Waldhausl, W., Pasternack, M.S., and Wagner, L. (2003). The ATP-dependent helicase RUVBL1/TIP49a associates with tubulin during mitosis. Cell motility and the cytoskeleton 56, 79-93.

Ge, X.Q., Jackson, D.A., and Blow, J.J. (2007). Dormant origins licensed by excess Mcm2-7 are required for human cells to survive replicative stress. Genes & development 21, 3331-3341.

Geer, L.Y., Markey, S.P., Kowalak, J.A., Wagner, L., Xu, M., Maynard, D.M., Yang, X., Shi, W., and Bryant, S.H. (2004). Open mass spectrometry search algorithm. Journal of proteome research 3, 958-964.

Gentili, C., Castor, D., Kaden, S., Lauterbach, D., Gysi, M., Steigemann, P., Gerlich, D.W., Jiricny, J., and Ferrari, S. (2015). Chromosome Missegregation Associated with RUVBL1 Deficiency. PloS one 10, e0133576.

George, J., Lim, J.S., Jang, S.J., Cun, Y., Ozretic, L., Kong, G., Leenders, F., Lu, X., Fernandez-Cuesta, L., Bosco, G., et al. (2015). Comprehensive genomic profiles of small cell lung cancer. Nature 524, 47-53.

Gorynia, S., Bandeiras, T.M., Pinho, F.G., McVey, C.E., Vonrhein, C., Round, A., Svergun, D.I., Donner, P., Matias, P.M., and Carrondo, M.A. (2011). Structural and functional insights into a dodecameric molecular machine - the RuvBL1/RuvBL2 complex. Journal of structural biology 176, 279-291.

Greenberg, A.K., Hu, J., Basu, S., Hay, J., Reibman, J., Yie, T.A., Tchou-Wong, K.M., Rom, W.N., and Lee, T.C. (2002). Glucocorticoids inhibit lung cancer cell growth through both the extracellular signal-related kinase pathway and cell cycle regulators. American journal of respiratory cell and molecular biology 27, 320-328.

Gribun, A., Cheung, K.L., Huen, J., Ortega, J., and Houry, W.A. (2008). Yeast Rvb1 and Rvb2 are ATP-dependent DNA helicases that form a heterohexameric complex. Journal of molecular biology 376, 1320-1333.

Grigoletto, A., Neaud, V., Allain-Courtois, N., Lestienne, P., and Rosenbaum, J. (2013). The ATPase activity of reptin is required for its effects on tumor cell growth and viability in hepatocellular carcinoma. Molecular cancer research : MCR 11, 133-139.

Gronemeyer, H., Gustafsson, J.A., and Laudet, V. (2004). Principles for modulation of the nuclear receptor superfamily. Nature reviews Drug discovery 3, 950-964.

Hammerman PS, L.M., Voet D, Jing R, Cibulskis K, Sivachenko A, Stojanov P, McKenna A, Lander ES, Gabriel S, Getz G, Sougnez C, Imielinski M, Helman E, Hernandez B, Pho NH, Meyerson M, Chu A, Chun HJ, Mungall AJ, Pleasance E, Robertson A, Sipahimalani P, Stoll D, Balasundaram M, Birol I, Butterfield YS, Chuah E, Coope RJ, Corbett R, Dhalla N, Guin R, He A, Hirst C, Hirst M, Holt RA, Lee D, Li HI, Mayo M, Moore RA, Mungall K, Nip KM, Olshen A, Schein JE, Slobodan JR, Tam A, Thiessen N, Varhol R, Zeng T, Zhao Y, Jones SJ, Marra MA, Saksena G, Cherniack AD, Schumacher SE, Tabak B, Carter SL, Pho NH, Nguyen H, Onofrio RC, Crenshaw A, Ardlie K, Beroukhim R, Winckler W, Hammerman PS, Getz G, Meyerson M, Protopopov A, Zhang J, Hadjipanayis A, Lee S, Xi R, Yang L, Ren X, Zhang H, Shukla S, Chen PC, Haseley P, Lee E, Chin L, Park PJ, Kucherlapati R, Socci ND, Liang Y, Schultz N, Borsu L, Lash AE, Viale A, Sander C, Ladanyi M, Auman T, Hoadley KA, Wilkerson MD, Shi Y, Liquori C, Meng S, Li L, Turman YJ, Topal MD, Tan D, Waring S, Buda E, Walsh J, Jones CD, Mieczkowski PA, Singh D, Wu J, Gulabani A, Dolina P, Bodenheimer T, Hoyle AP, Simons JV, Soloway MG, Mose LE, Jefferys SR, Balu S, O'Connor BD, Prins JF, Liu J, Chiang DY, Hayes D, Perou CM, Cope L, Danilova L, Weisenberger DJ, Maglinte DT, Pan F, Van Den Berg DJ, Triche T Jr, Herman JG, Baylin SB, Laird PW, Getz G, Noble M, Voet D, Saksena G, Gehlenborg N, DiCara D, Zhang J, Zhang H, Wu CJ, Liu SY, Lawrence MS, Zou L, Sivachenko A, Lin P, Stojanov P, Jing R, Cho J, Nazaire MD, Robinson J, Thorvaldsdottir H, Mesirov J, Park PJ, Chin L, Schultz N, Sinha R, Ciriello G, Cerami E, Gross B, Jacobsen A, Gao J, Aksoy B, Weinhold N, Ramirez R, Taylor BS, Antipin Y, Reva B, Shen R, Mo Q, Seshan V, Paik PK, Ladanyi M, Sander C, Akbani R, Zhang N, Broom BM, Casasent T, Unruh A, Wakefield C, Cason R, Baggerly KA, Weinstein JN, Haussler D, Benz CC, Stuart JM, Zhu J, Szeto C, Scott GK, Yau C, Ng S, Goldstein T, Waltman P, Sokolov A, Ellrott K, Collisson EA, Zerbino D, Wilks C, Ma S, Craft B, Wilkerson MD, Auman J, Hoadley KA, Du Y, Cabanski C, Walter V, Singh D, Wu J, Gulabani A, Bodenheimer T, Hoyle AP, Simons JV, Soloway MG, Mose LE, Jefferys SR, Balu S, Marron J, Liu Y, Wang K, Liu J, Prins JF, Hayes D, Perou CM, Creighton CJ, Zhang Y, Travis WD, Rekhtman N, Yi J, Aubry MC, Cheney R, Dacic S, Flieder D, Funkhouser W, Illei P, Myers J, Tsao MS, Penny R, Mallery D, Shelton T, Hatfield M, Morris S, Yena P, Shelton C, Sherman M, Paulauskis J, Meyerson M, Baylin SB, Govindan R, Akbani R, Azodo I, Beer D, Bose R, Byers LA, Carbone D, Chang LW, Chiang D, Chu A, Chun E, Collisson E, Cope L, Creighton CJ, Danilova L, Ding L, Getz G, Hammerman PS, Hayes D, Hernandez B, Herman JG, Heymach J, Ida C, Imielinski M, Johnson B, Jurisica I, Kaufman J, Kosari F, Kucherlapati R, Kwiatkowski D, Ladanyi M, Lawrence MS, Maher CA, Mungall A, Ng S, Pao W, Peifer M, Penny R, Robertson G, Rusch V, Sander C, Schultz N, Shen R, Siegfried J, Sinha R, Sivachenko A, Sougnez C,

Stoll D, Stuart J, Thomas RK, Tomaszek S, Tsao MS, Travis WD, Vaske C, Weinstein JN, Weisenberger D, Wheeler D, Wigle DA, Wilkerson MD, Wilks C, Yang P, Zhang JJ, Jensen MA, Sfeir R, Kahn AB, Chu AL, Kothiyal P, Wang Z, Snyder EE, Pontius J, Pihl TD, Ayala B, Backus M, Walton J, Baboud J, Berton DL, Nicholls MC, Srinivasan D, Raman R, Girshik S, Kigonya PA, Alonso S, Sanbhadti RN, Barletta SP, Greene JM, Pot DA, Tsao MS, Bandarchi-Chamkhaleh B, Boyd J, Weaver J, Wigle DA, Azodo IA, Tomaszek SC, Aubry MC, Ida CM, Yang P, Kosari F, Brock MV, Rodgers K, Rutledge M, Brown T, Lee B, Shin J, Trusty D, Dhir R, Siegfried JM, Potapova O, Fedosenko KV, Nemirovich-Danchenko E, Rusch V, Zakowski M, Iacocca MV, Brown J, Rabeno B, Czerwinski C, Petrelli N, Fan Z, Todaro N, Eckman J, Myers J, Rathmell W, Thorne LB, Huang M, Boice L, Hill A, Penny R, Mallery D, Curley E, Shelton C, Yena P, Morrison C, Gaudioso C, Bartlett JM, Kodeeswaran S, Zanke B, Sekhon H, David K, Juhl H, Van Le X, Kohl B, Thorp R, Nguyen VT, Nguyen VB, Sussman H, Phu BD, Hajek R, Nguyen PH, Khan KZ, Muley T, Shaw KR, Sheth M, Yang L, Buetow K, Davidsen T, Demchok JA, Eley G, Ferguson M, Dillon LA, Schaefer C, Guyer MS, Ozenberger BA, Palchik JD, Peterson J, Sofia HJ, Thomson E. (2012). Comprehensive genomic characterization of squamous cell lung cancers. Nature 489, 519-525.

Hanna, J.M., and Onaitis, M.W. (2013). Cell of origin of lung cancer. Journal of carcinogenesis 12, 6.

Hargreaves, D.C., and Crabtree, G.R. (2011). ATP-dependent chromatin remodeling: genetics, genomics and mechanisms. Cell research 21, 396-420.

Hauf, S., and Watanabe, Y. (2004). Kinetochore orientation in mitosis and meiosis. Cell 119, 317-327.

Haurie, V., Menard, L., Nicou, A., Touriol, C., Metzler, P., Fernandez, J., Taras, D., Lestienne, P., Balabaud, C., Bioulac-Sage, P., et al. (2009). Adenosine triphosphatase pontin is overexpressed in hepatocellular carcinoma and coregulated with reptin through a new posttranslational mechanism. Hepatology (Baltimore, Md) 50, 1871-1883.

Hofmann, J., Kaiser, U., Maasberg, M., and Havemann, K. (1995). Glucocorticoid receptors and growth inhibitory effects of dexamethasone in human lung cancer cell lines. European journal of cancer (Oxford, England : 1990) 31a, 2053-2058.

Hoggatt, A.F., Hoggatt, J., Honerlaw, M., and Pelus, L.M. (2010). A spoonful of sugar helps the medicine go down: a novel technique to improve oral gavage in mice. Journal of the American Association for Laboratory Animal Science : JAALAS 49, 329-334.

Hopkins, J.M., and Evans, H.J. (1980). Cigarette smoke-induced DNA damage and lung cancer risks. Nature 283, 388-390.

Houry, W.A., Bertrand, E., and Coulombe, B. (2018). The PAQosome, an R2TP-Based Chaperone for Quaternary Structure Formation. Trends in biochemical sciences 43, 4-9.

Huang, H.T., Seo, H.S., Zhang, T., Wang, Y., Jiang, B., Li, Q., Buckley, D.L., Nabet, B., Roberts, J.M., Paulk, J., et al. (2017). MELK is not necessary for the proliferation of basal-like breast cancer cells. eLife 6.

Ikura, T., Ogryzko, V.V., Grigoriev, M., Groisman, R., Wang, J., Horikoshi, M., Scully, R., Qin, J., and Nakatani, Y. (2000). Involvement of the TIP60 histone acetylase complex in DNA repair and apoptosis. Cell 102, 463-473.

Izumi, N., Yamashita, A., Iwamatsu, A., Kurata, R., Nakamura, H., Saari, B., Hirano, H., Anderson, P., and Ohno, S. (2010). AAA+ proteins RUVBL1 and RUVBL2 coordinate PIKK activity and function in nonsense-mediated mRNA decay. Science signaling 3, ra27.

Jackson, A.L., Bartz, S.R., Schelter, J., Kobayashi, S.V., Burchard, J., Mao, M., Li, B., Cavet, G., and Linsley, P.S. (2003). Expression profiling reveals off-target gene regulation by RNAi. Nature biotechnology 21, 635-637.

Jackson, A.L., Burchard, J., Schelter, J., Chau, B.N., Cleary, M., Lim, L., and Linsley, P.S. (2006). Widespread siRNA "off-target" transcript silencing mediated by seed region sequence complementarity. RNA (New York, NY) 12, 1179-1187.

Jaeger, A.M., and Whitesell, L.J.A.R.o.C.B. (2019). HSP90: Enabler of Cancer Adaptation. 3, 275-297.

Jeong, Y., Xie, Y., Lee, W., Bookout, A.L., Girard, L., Raso, G., Behrens, C., Wistuba, II, Gadzar, A.F., Minna, J.D., et al. (2012). Research resource: Diagnostic and therapeutic potential of nuclear receptor expression in lung cancer. Molecular endocrinology (Baltimore, Md) 26, 1443-1454.

Jeong, Y., Xie, Y., Xiao, G., Behrens, C., Girard, L., Wistuba, II, Minna, J.D., and Mangelsdorf, D.J. (2010). Nuclear receptor expression defines a set of prognostic biomarkers for lung cancer. PLoS medicine 7, e1000378.

Jha, S., Gupta, A., Dar, A., and Dutta, A. (2013). RVBs are required for assembling a functional TIP60 complex. Molecular and cellular biology 33, 1164-1174.

Jha, S., Shibata, E., and Dutta, A. (2008). Human Rvb1/Tip49 is required for the histone acetyltransferase activity of Tip60/NuA4 and for the downregulation of phosphorylation on H2AX after DNA damage. Molecular and cellular biology 28, 2690-2700.

Jonsson, Z.O., Jha, S., Wohlschlegel, J.A., and Dutta, A. (2004). Rvb1p/Rvb2p recruit Arp5p and assemble a functional Ino80 chromatin remodeling complex. Molecular cell 16, 465-477.

Junker, K., Wiethege, T., and Muller, K.M. (2000). Pathology of small-cell lung cancer. Journal of cancer research and clinical oncology 126, 361-368.

Kanemaki, M., Kurokawa, Y., Matsu-ura, T., Makino, Y., Masani, A., Okazaki, K., Morishita, T., and Tamura, T.A. (1999). TIP49b, a new RuvB-like DNA helicase, is included in a complex together with another RuvB-like DNA helicase, TIP49a. The Journal of biological chemistry 274, 22437-22444.

Kanemaki, M., Makino, Y., Yoshida, T., Kishimoto, T., Koga, A., Yamamoto, K., Yamamoto, M., Moncollin, V., Egly, J.M., Muramatsu, M., et al. (1997). Molecular cloning of a rat 49-kDa TBP-interacting protein (TIP49) that is highly homologous to the bacterial RuvB. Biochemical and biophysical research communications 235, 64-68.

Kazandjian, D., Suzman, D.L., Blumenthal, G., Mushti, S., He, K., Libeg, M., Keegan, P., and Pazdur, R. (2016). FDA Approval Summary: Nivolumab for the Treatment of Metastatic Non-Small Cell Lung Cancer With Progression On or After Platinum-Based Chemotherapy. The oncologist 21, 634-642.

Kittler, R., Heninger, A.K., Franke, K., Habermann, B., and Buchholz, F. (2005a). Production of endoribonuclease-prepared short interfering RNAs for gene silencing in mammalian cells. Nature methods 2, 779-784.

Kittler, R., Pelletier, L., Ma, C., Poser, I., Fischer, S., Hyman, A.A., and Buchholz, F. (2005b). RNA interference rescue by bacterial artificial chromosome transgenesis in mammalian tissue culture cells. Proceedings of the National Academy of Sciences of the United States of America 102, 2396-2401.

Kittler, R., Putz, G., Pelletier, L., Poser, I., Heninger, A.K., Drechsel, D., Fischer, S., Konstantinova, I., Habermann, B., Grabner, H., et al. (2004). An endoribonuclease-prepared siRNA screen in human cells identifies genes essential for cell division. Nature 432, 1036-1040.

Kittler, R., Surendranath, V., Heninger, A.K., Slabicki, M., Theis, M., Putz, G., Franke, K., Caldarelli, A., Grabner, H., Kozak, K., et al. (2007). Genome-wide resources of endoribonuclease-prepared short interfering RNAs for specific loss-of-function studies. Nature methods 4, 337-344.

Korach, K.S., Couse, J.F., Curtis, S.W., Washburn, T.F., Lindzey, J., Kimbro, K.S., Eddy, E.M., Migliaccio, S., Snedeker, S.M., Lubahn, D.B., et al. (1996). Estrogen receptor gene disruption: molecular characterization and experimental and clinical phenotypes. Recent progress in hormone research 51, 159-186; discussion 186-158.

Krokan, H.E., and Bjoras, M. (2013). Base excision repair. Cold Spring Harbor perspectives in biology 5, a012583.

Kuleshov, M.V., Jones, M.R., Rouillard, A.D., Fernandez, N.F., Duan, Q., Wang, Z., Koplev, S., Jenkins, S.L., Jagodnik, K.M., Lachmann, A., et al. (2016). Enrichr: a comprehensive gene set enrichment analysis web server 2016 update. Nucleic acids research 44, W90-97.

Kunkel, T.A., and Erie, D.A. (2015). Eukaryotic Mismatch Repair in Relation to DNA Replication. Annual review of genetics 49, 291-313.

Larsen, J.E., and Minna, J.D. (2011). Molecular biology of lung cancer: clinical implications. Clinics in chest medicine 32, 703-740.

Lauscher, J.C., Loddenkemper, C., Kosel, L., Grone, J., Buhr, H.J., and Huber, O. (2007). Increased pontin expression in human colorectal cancer tissue. Human pathology 38, 978-985.

Lee, H.K., Hsu, A.K., Sajdak, J., Qin, J., and Pavlidis, P. (2004). Coexpression analysis of human genes across many microarray data sets. Genome research 14, 1085-1094.

Li, Y., Zhao, L., Yuan, S., Zhang, J., and Sun, Z. (2017). Axonemal dynein assembly requires the R2TP complex component Pontin. Development (Cambridge, England).

Lieber, M.R. (2010). The mechanism of double-strand DNA break repair by the nonhomologous DNA end-joining pathway. Annual review of biochemistry 79, 181-211.

Lin, X., Morgan-Lappe, S., Huang, X., Li, L., Zakula, D.M., Vernetti, L.A., Fesik, S.W., and Shen, Y. (2007). 'Seed' analysis of off-target siRNAs reveals an essential role of Mcl-1 in resistance to the small-molecule Bcl-2/Bcl-XL inhibitor ABT-737. Oncogene 26, 3972-3979.

Lobrich, M., and Jeggo, P.A. (2007). The impact of a negligent G2/M checkpoint on genomic instability and cancer induction. Nature reviews Cancer 7, 861-869.

Lomax, M.E., Folkes, L.K., and O'Neill, P. (2013). Biological consequences of radiation-induced DNA damage: relevance to radiotherapy. Clinical oncology (Royal College of Radiologists (Great Britain)) 25, 578-585.

Lord, C.J., and Ashworth, A. (2017). PARP inhibitors: Synthetic lethality in the clinic. Science (New York, NY) 355, 1152-1158.

Lu, Y.S., Lien, H.C., Yeh, P.Y., Kuo, S.H., Chang, W.C., Kuo, M.L., and Cheng, A.L. (2006). Glucocorticoid receptor expression in advanced non-small cell lung cancer: clinicopathological correlation and in vitro effect of glucocorticoid on cell growth and chemosensitivity. Lung cancer (Amsterdam, Netherlands) 53, 303-310.

Luo, J., Emanuele, M.J., Li, D., Creighton, C.J., Schlabach, M.R., Westbrook, T.F., Wong, K.K., and Elledge, S.J. (2009). A genome-wide RNAi screen identifies multiple synthetic lethal interactions with the Ras oncogene. Cell 137, 835-848.

Magalska, A., Schellhaus, A.K., Moreno-Andres, D., Zanini, F., Schooley, A., Sachdev, R., Schwarz, H., Madlung, J., and Antonin, W. (2014). RuvB-like ATPases function in chromatin decondensation at the end of mitosis. Developmental cell 31, 305-318.

Makino, Y., Kanemaki, M., Kurokawa, Y., Koji, T., and Tamura, T. (1999). A rat RuvB-like protein, TIP49a, is a germ cell-enriched novel DNA helicase. The Journal of biological chemistry 274, 15329-15335.

Mao, Y.Q., and Houry, W.A. (2017). The Role of Pontin and Reptin in Cellular Physiology and Cancer Etiology. Frontiers in molecular biosciences 4, 58.

Masai, H., Matsui, E., You, Z., Ishimi, Y., Tamai, K., and Arai, K. (2000). Human Cdc7-related kinase complex. In vitro phosphorylation of MCM by concerted actions of Cdks and Cdc7 and that of a criticial threonine residue of Cdc7 bY Cdks. The Journal of biological chemistry 275, 29042-29052.

Masai, H., Matsumoto, S., You, Z., Yoshizawa-Sugata, N., and Oda, M. (2010). Eukaryotic chromosome DNA replication: where, when, and how? Annual review of biochemistry 79, 89-130.

Massague, J. (2004). G1 cell-cycle control and cancer. Nature 432, 298-306.

Matias, P.M., Baek, S.H., Bandeiras, T.M., Dutta, A., Houry, W.A., Llorca, O., and Rosenbaum, J. (2015). The AAA+ proteins Pontin and Reptin enter adult age: from understanding

their basic biology to the identification of selective inhibitors. Frontiers in molecular biosciences 2, 17.

Matias, P.M., Gorynia, S., Donner, P., and Carrondo, M.A. (2006). Crystal structure of the human AAA+ protein RuvBL1. The Journal of biological chemistry 281, 38918-38929.

McDonald, E.R., 3rd, de Weck, A., Schlabach, M.R., Billy, E., Mavrakis, K.J., Hoffman, G.R., Belur, D., Castelletti, D., Frias, E., Gampa, K., et al. (2017). Project DRIVE: A Compendium of Cancer Dependencies and Synthetic Lethal Relationships Uncovered by Large-Scale, Deep RNAi Screening. Cell 170, 577-592.e510.

McKeegan, K.S., Debieux, C.M., and Watkins, N.J. (2009). Evidence that the AAA+ proteins TIP48 and TIP49 bridge interactions between 15.5K and the related NOP56 and NOP58 proteins during box C/D snoRNP biogenesis. Molecular and cellular biology 29, 4971-4981.

Meyers, R.M., Bryan, J.G., McFarland, J.M., Weir, B.A., Sizemore, A.E., Xu, H., Dharia, N.V., Montgomery, P.G., Cowley, G.S., Pantel, S., et al. (2017). Computational correction of copy number effect improves specificity of CRISPR-Cas9 essentiality screens in cancer cells. Nature genetics 49, 1779-1784.

Morrison, A.J., Highland, J., Krogan, N.J., Arbel-Eden, A., Greenblatt, J.F., Haber, J.E., and Shen, X. (2004). INO80 and gamma-H2AX interaction links ATP-dependent chromatin remodeling to DNA damage repair. Cell 119, 767-775.

Munoz-Hernandez, H., Pal, M., Rodriguez, C.F., Fernandez-Leiro, R., Prodromou, C., Pearl, L.H., and Llorca, O. (2019). Structural mechanism for regulation of the AAA-ATPases RUVBL1-RUVBL2 in the R2TP co-chaperone revealed by cryo-EM. Science advances 5, eaaw1616.

Munoz, D.M., Cassiani, P.J., Li, L., Billy, E., Korn, J.M., Jones, M.D., Golji, J., Ruddy, D.A., Yu, K., McAllister, G., et al. (2016). CRISPR Screens Provide a Comprehensive Assessment of Cancer Vulnerabilities but Generate False-Positive Hits for Highly Amplified Genomic Regions. Cancer discovery 6, 900-913.

Murr, R., Loizou, J.I., Yang, Y.G., Cuenin, C., Li, H., Wang, Z.Q., and Herceg, Z. (2006). Histone acetylation by Trrap-Tip60 modulates loading of repair proteins and repair of DNA double-strand breaks. Nature cell biology 8, 91-99.

Nano, N., and Houry, W.A. (2013). Chaperone-like activity of the AAA+ proteins Rvb1 and Rvb2 in the assembly of various complexes. Philosophical transactions of the Royal Society of London Series B, Biological sciences 368, 20110399.

Nguyen, V.Q., Ranjan, A., Stengel, F., Wei, D., Aebersold, R., Wu, C., and Leschziner, A.E. (2013). Molecular architecture of the ATP-dependent chromatin-remodeling complex SWR1. Cell 154, 1220-1231.

Niewiarowski, A., Bradley, A.S., Gor, J., McKay, A.R., Perkins, S.J., and Tsaneva, I.R. (2010). Oligomeric assembly and interactions within the human RuvB-like RuvBL1 and RuvBL2 complexes. The Biochemical journal 429, 113-125.

Niida, H., Katsuno, Y., Sengoku, M., Shimada, M., Yukawa, M., Ikura, M., Ikura, T., Kohno, K., Shima, H., Suzuki, H., et al. (2010). Essential role of Tip60-dependent recruitment of ribonucleotide reductase at DNA damage sites in DNA repair during G1 phase. Genes & development 24, 333-338.

Osaki, H., Walf-Vorderwulbecke, V., Mangolini, M., Zhao, L., Horton, S.J., Morrone, G., Schuringa, J.J., de Boer, J., and Williams, O. (2013). The AAA+ ATPase RUVBL2 is a critical mediator of MLL-AF9 oncogenesis. Leukemia 27, 1461-1468.

Ostrem, J.M., and Shokat, K.M. (2016). Direct small-molecule inhibitors of KRAS: from structural insights to mechanism-based design. Nature reviews Drug discovery 15, 771-785.

Overington, J.P., Al-Lazikani, B., and Hopkins, A.L. (2006). How many drug targets are there? Nature reviews Drug discovery 5, 993-996.

Pines, J. (2006). Mitosis: a matter of getting rid of the right protein at the right time. Trends in cell biology 16, 55-63.

Pines, J., and Rieder, C.L. (2001). Re-staging mitosis: a contemporary view of mitotic progression. Nature cell biology 3, E3-6.

Planchard, D., Besse, B., Groen, H.J.M., Souquet, P.J., Quoix, E., Baik, C.S., Barlesi, F., Kim, T.M., Mazieres, J., Novello, S., et al. (2016). Dabrafenib plus trametinib in patients with previously treated BRAF(V600E)-mutant metastatic non-small cell lung cancer: an open-label, multicentre phase 2 trial. The Lancet Oncology 17, 984-993.

Puri, T., Wendler, P., Sigala, B., Saibil, H., and Tsaneva, I.R. (2007). Dodecameric structure and ATPase activity of the human TIP48/TIP49 complex. Journal of molecular biology 366, 179-192.

Qiu, X.B., Lin, Y.L., Thome, K.C., Pian, P., Schlegel, B.P., Weremowicz, S., Parvin, J.D., and Dutta, A. (1998). An eukaryotic RuvB-like protein (RUVBL1) essential for growth. The Journal of biological chemistry 273, 27786-27793.

Rajendra, E., Garaycoechea, J.I., Patel, K.J., and Passmore, L.A. (2014). Abundance of the Fanconi anaemia core complex is regulated by the RuvBL1 and RuvBL2 AAA+ ATPases. Nucleic acids research 42, 13736-13748.

Raymond, A.A., Benhamouche, S., Neaud, V., Di Martino, J., Javary, J., and Rosenbaum, J. (2015). Reptin regulates DNA double strand breaks repair in human hepatocellular carcinoma. PloS one 10, e0123333.

Ren, J., Li, W., Liu, H., Yan, L., Jiao, W., Li, D., Tang, Y., Gu, G., and Xu, Z. (2013). Overexpression of reptin in renal cell carcinoma contributes to tumor malignancies and its inhibition triggers senescence of cancer cells. Urologic oncology 31, 1358-1366.

Reynolds, A., Anderson, E.M., Vermeulen, A., Fedorov, Y., Robinson, K., Leake, D., Karpilow, J., Marshall, W.S., and Khvorova, A. (2006). Induction of the interferon response by siRNA is cell type- and duplex length-dependent. RNA (New York, NY) 12, 988-993.

Rousseau, B., Menard, L., Haurie, V., Taras, D., Blanc, J.F., Moreau-Gaudry, F., Metzler, P., Hugues, M., Boyault, S., Lemiere, S., et al. (2007). Overexpression and role of the ATPase and putative DNA helicase RuvB-like 2 in human hepatocellular carcinoma. Hepatology (Baltimore, Md) 46, 1108-1118.

Rumman, M., Dhawan, J., and Kassem, M. (2015). Concise Review: Quiescence in Adult Stem Cells: Biological Significance and Relevance to Tissue Regeneration. Stem cells (Dayton, Ohio) 33, 2903-2912.

Sancar, A., Lindsey-Boltz, L.A., Unsal-Kacmaz, K., and Linn, S. (2004). Molecular mechanisms of mammalian DNA repair and the DNA damage checkpoints. Annual review of biochemistry 73, 39-85.

Santivasi, W.L., and Xia, F. (2014). Ionizing radiation-induced DNA damage, response, and repair. Antioxidants & redox signaling 21, 251-259.

Schmittgen, T.D., and Livak, K.J. (2008). Analyzing real-time PCR data by the comparative C(T) method. Nature protocols 3, 1101-1108.

Scholl, C., Frohling, S., Dunn, I.F., Schinzel, A.C., Barbie, D.A., Kim, S.Y., Silver, S.J., Tamayo, P., Wadlow, R.C., Ramaswamy, S., et al. (2009). Synthetic lethal interaction between oncogenic KRAS dependency and STK33 suppression in human cancer cells. Cell 137, 821-834.

Schultz, N., Marenstein, D.R., De Angelis, D.A., Wang, W.Q., Nelander, S., Jacobsen, A., Marks, D.S., Massague, J., and Sander, C. (2011). Off-target effects dominate a large-scale RNAi screen for modulators of the TGF-beta pathway and reveal microRNA regulation of TGFBR2. Silence 2, 3.

Sharifi, N., Gulley, J.L., and Dahut, W.L. (2005). Androgen deprivation therapy for prostate cancer. Jama 294, 238-244.

Shaw, A.T., Kim, D.W., Nakagawa, K., Seto, T., Crino, L., Ahn, M.J., De Pas, T., Besse, B., Solomon, B.J., Blackhall, F., et al. (2013). Crizotinib versus chemotherapy in advanced ALK-positive lung cancer. The New England journal of medicine 368, 2385-2394.

Shaw, A.T., Ou, S.H., Bang, Y.J., Camidge, D.R., Solomon, B.J., Salgia, R., Riely, G.J., Varella-Garcia, M., Shapiro, G.I., Costa, D.B., et al. (2014). Crizotinib in ROS1-rearranged non-small-cell lung cancer. The New England journal of medicine 371, 1963-1971.

Siegel, R.L., Miller, K.D., and Jemal, A. (2017). Cancer Statistics, 2017. CA: a cancer journal for clinicians 67, 7-30.

Sirbu, B.M., Couch, F.B., and Cortez, D. (2012). Monitoring the spatiotemporal dynamics of proteins at replication forks and in assembled chromatin using isolation of proteins on nascent DNA. Nature protocols 7, 594-605.

Srivastava, N., Kollipara, R.K., Singh, D.K., Sudderth, J., Hu, Z., Nguyen, H., Wang, S., Humphries, C.G., Carstens, R., Huffman, K.E., et al. (2014). Inhibition of cancer cell proliferation by PPARgamma is mediated by a metabolic switch that increases reactive oxygen species levels. Cell metabolism 20, 650-661.

Subramanian, A., Tamayo, P., Mootha, V.K., Mukherjee, S., Ebert, B.L., Gillette, M.A., Paulovich, A., Pomeroy, S.L., Golub, T.R., Lander, E.S., et al. (2005). Gene set enrichment analysis: a knowledge-based approach for interpreting genome-wide expression profiles. Proceedings of the National Academy of Sciences of the United States of America 102, 15545-15550.

Sudbery, I., Enright, A.J., Fraser, A.G., and Dunham, I. (2010). Systematic analysis of off-target effects in an RNAi screen reveals microRNAs affecting sensitivity to TRAIL-induced apoptosis. BMC genomics 11, 175.

Sul, J., Blumenthal, G.M., Jiang, X., He, K., Keegan, P., and Pazdur, R. (2016). FDA Approval Summary: Pembrolizumab for the Treatment of Patients With Metastatic Non-Small Cell Lung Cancer Whose Tumors Express Programmed Death-Ligand 1. The oncologist 21, 643-650.

Symington, L.S., and Gautier, J. (2011). Double-strand break end resection and repair pathway choice. Annual review of genetics 45, 247-271.

Szasz, A.M., Lanczky, A., Nagy, A., Forster, S., Hark, K., Green, J.E., Boussioutas, A., Busuttil, R., Szabo, A., and Gyorffy, B. (2016). Cross-validation of survival associated biomarkers in gastric cancer using transcriptomic data of 1,065 patients. Oncotarget 7, 49322-49333.

Tammana, D., and Tammana, T.V.S. (2017). Human DNA helicase, RuvBL1 and its Chlamydomonas homologue, CrRuvBL1 plays an important role in ciliogenesis. Cytoskeleton (Hoboken, NJ) 74, 251-259.

Taniuchi, K., Furihata, M., Iwasaki, S., Tanaka, K., Shimizu, T., Saito, M., and Saibara, T. (2014). RUVBL1 directly binds actin filaments and induces formation of cell protrusions to promote pancreatic cancer cell invasion. International journal of oncology 44, 1945-1954.

Tatiparti, K., Sau, S., Kashaw, S.K., and Iyer, A.K. (2017). siRNA Delivery Strategies: A Comprehensive Review of Recent Developments. Nanomaterials (Basel, Switzerland) 7.

Thiagalingam, S., Lengauer, C., Leach, F.S., Schutte, M., Hahn, S.A., Overhauser, J., Willson, J.K., Markowitz, S., Hamilton, S.R., Kern, S.E., et al. (1996). Evaluation of candidate tumour suppressor genes on chromosome 18 in colorectal cancers. Nature genetics 13, 343-346.

Toledo, L.I., Altmeyer, M., Rask, M.B., Lukas, C., Larsen, D.H., Povlsen, L.K., Bekker-Jensen, S., Mailand, N., Bartek, J., and Lukas, J. (2013). ATR prohibits replication catastrophe by preventing global exhaustion of RPA. Cell 155, 1088-1103.

Toledo, L.I., Murga, M., Zur, R., Soria, R., Rodriguez, A., Martinez, S., Oyarzabal, J., Pastor, J., Bischoff, J.R., and Fernandez-Capetillo, O. (2011). A cell-based screen identifies ATR inhibitors with synthetic lethal properties for cancer-associated mutations. Nature structural & molecular biology 18, 721-727.

Torreira, E., Jha, S., Lopez-Blanco, J.R., Arias-Palomo, E., Chacon, P., Canas, C., Ayora, S., Dutta, A., and Llorca, O. (2008). Architecture of the pontin/reptin complex, essential in

the assembly of several macromolecular complexes. Structure (London, England : 1993) 16, 1511-1520.

Tosi, A., Haas, C., Herzog, F., Gilmozzi, A., Berninghausen, O., Ungewickell, C., Gerhold, C.B., Lakomek, K., Aebersold, R., Beckmann, R., et al. (2013). Structure and subunit topology of the INO80 chromatin remodeler and its nucleosome complex. Cell 154, 1207-1219.

Trepel, J., Mollapour, M., Giaccone, G., and Neckers, L. (2010). Targeting the dynamic HSP90 complex in cancer. Nature reviews Cancer 10, 537-549.

Trudgian, D.C., and Mirzaei, H. (2012). Cloud CPFP: a shotgun proteomics data analysis pipeline using cloud and high performance computing. Journal of proteome research 11, 6282-6290.

Trudgian, D.C., Ridlova, G., Fischer, R., Mackeen, M.M., Ternette, N., Acuto, O., Kessler, B.M., and Thomas, B. (2011). Comparative evaluation of label-free SINQ normalized spectral index quantitation in the central proteomics facilities pipeline. Proteomics 11, 2790-2797.

Tsherniak, A., Vazquez, F., Montgomery, P.G., Weir, B.A., Kryukov, G., Cowley, G.S., Gill, S., Harrington, W.F., Pantel, S., Krill-Burger, J.M., et al. (2017). Defining a Cancer Dependency Map. Cell 170, 564-576.e516.

Venteicher, A.S., Meng, Z., Mason, P.J., Veenstra, T.D., and Artandi, S.E. (2008). Identification of ATPases pontin and reptin as telomerase components essential for holoenzyme assembly. Cell 132, 945-957.

Vermeulen, K., Van Bockstaele, D.R., and Berneman, Z.N. (2003). The cell cycle: a review of regulation, deregulation and therapeutic targets in cancer. Cell proliferation 36, 131-149.

Walden, H., and Deans, A.J. (2014). The Fanconi anemia DNA repair pathway: structural and functional insights into a complex disorder. Annual review of biophysics 43, 257-278.

Waldman, T., Kinzler, K.W., and Vogelstein, B. (1995). p21 is necessary for the p53-mediated G1 arrest in human cancer cells. Cancer research 55, 5187-5190.

Wang, G., and Fersht, A.R. (2017). Multisite aggregation of p53 and implications for drug rescue. Proceedings of the National Academy of Sciences of the United States of America 114, E2634-e2643.

Watkins, N.J., Lemm, I., Ingelfinger, D., Schneider, C., Hossbach, M., Urlaub, H., and Luhrmann, R. (2004). Assembly and maturation of the U3 snoRNP in the nucleoplasm in a large dynamic multiprotein complex. Molecular cell 16, 789-798.

Woo, R.A., and Poon, R.Y. (2003). Cyclin-dependent kinases and S phase control in mammalian cells. Cell cycle (Georgetown, Tex) 2, 316-324.

Wu, S., Shi, Y., Mulligan, P., Gay, F., Landry, J., Liu, H., Lu, J., Qi, H.H., Wang, W., Nickoloff, J.A., et al. (2007). A YY1-INO80 complex regulates genomic stability through homologous recombination-based repair. Nature structural & molecular biology 14, 1165-1172.

Yang, D., Buchholz, F., Huang, Z., Goga, A., Chen, C.Y., Brodsky, F.M., and Bishop, J.M. (2002). Short RNA duplexes produced by hydrolysis with Escherichia coli RNase III

mediate effective RNA interference in mammalian cells. Proceedings of the National Academy of Sciences of the United States of America 99, 9942-9947.

Yeh, S., Tsai, M.Y., Xu, Q., Mu, X.M., Lardy, H., Huang, K.E., Lin, H., Yeh, S.D., Altuwaijri, S., Zhou, X., et al. (2002). Generation and characterization of androgen receptor knockout (ARKO) mice: an in vivo model for the study of androgen functions in selective tissues. Proceedings of the National Academy of Sciences of the United States of America 99, 13498-13503.

Zaarur, N., Xu, X., Lestienne, P., Meriin, A.B., McComb, M., Costello, C.E., Newnam, G.P., Ganti, R., Romanova, N.V., Shanmugasundaram, M., et al. (2015). RuvbL1 and RuvbL2 enhance aggresome formation and disaggregate amyloid fibrils. The EMBO journal 34, 2363-2382.

Zappa, C., and Mousa, S.A. (2016). Non-small cell lung cancer: current treatment and future advances. Translational lung cancer research 5, 288-300.

Zeman, M.K., and Cimprich, K.A. (2014). Causes and consequences of replication stress. Nature cell biology 16, 2-9.

Zhao, L., Yuan, S., Cao, Y., Kallakuri, S., Li, Y., Kishimoto, N., DiBella, L., and Sun, Z. (2013). Reptin/Ruvbl2 is a Lrrc6/Seahorse interactor essential for cilia motility. Proceedings of the National Academy of Sciences of the United States of America 110, 12697-12702.

Zhou, C.Y., Stoddard, C.I., Johnston, J.B., Trnka, M.J., Echeverria, I., Palovcak, E., Sali, A., Burlingame, A.L., Cheng, Y., and Narlikar, G.J. (2017). Regulation of Rvb1/Rvb2 by a Domain within the INO80 Chromatin Remodeling Complex Implicates the Yeast Rvbs as Protein Assembly Chaperones. Cell reports 19, 2033-2044.

Zou, L., and Elledge, S.J. (2003). Sensing DNA damage through ATRIP recognition of RPA-ssDNA complexes. Science (New York, NY) 300, 1542-1548.